EUROPEAN
JOURNAL OF
BIOLOGY

OFFICIAL JOURNAL OF ISTANBUL UNIVERSITY'S SCIENCE FACULTY

ISTANBUL
UNIVERSITY
PRESS

Indexing and Abstracting

SCOPUS
TUBITAK ULAKBIM TR Index
Zoological Record - Clarivate Analytics
CAB Abstracts
DOAJ
CABI
- AgBiotechNet Database
- Animal Science Database
- VetMed Resource
- Environmental Impact Database
- Horticultural Science Database
- Nutrition and Food Sciences Database
Chemical Abstracts Service (CAS)
EBSCO Central & Eastern European Academic Source
SOBIAD
Cabells Journalytics

Authors bear responsibility for the content of their published articles.

The publication language of the journal is English.

This is a scholarly, international, peer-reviewed and open-access journal published biannually in June and December.

Publication Type: Periodical

EDITORIAL BOARD

AIMS AND SCOPE

European Journal of Biology (Eur J Biol) is an international, scientific, open access periodical published in accordance with independent, unbiased, and double-blinded peer-review principles. The journal is the official publication of Istanbul University Faculty of Science and it is published biannually on June and December. The publication language of the journal is English. European Journal of Biology has been previously published as IUFS Journal of Biology. It has been published in continuous publication since 1940.

European Journal of Biology aims to contribute to the literature by publishing manuscripts at the highest scientific level on all fields of biology. The journal publishes original research and review articles, and short communications that are prepared in accordance with the ethical guidelines in all fields of biology and life sciences.

The scope of the journal includes but not limited to; animal biology and systematics, plant biology and systematics, hydrobiology, ecology and environmental biology, microbiology, cell and molecular biology, biochemistry, biotechnology and genetics, physiology, toxicology, cancer biology, developmental and stem cell biology.

The target audience of the journal includes specialists and professionals working and interested in all disciplines of biology.

The editorial and publication processes of the journal are shaped in accordance with the guidelines of the International Committee of Medical Journal Editors (ICMJE), World Association of Medical Editors (WAME), Council of Science Editors (CSE), Committee on Publication Ethics (COPE), European Association of Science Editors (EASE), and National Information Standards Organization (NISO). The journal is in conformity with the Principles of Transparency and Best Practice in Scholarly Publishing (doaj.org/bestpractice).

European Journal of Biology is currently indexed SCOPUS, TUBITAK ULAKBIM TR Index, Zoological Record - Clarivate Analytics, CAB Abstracts, DOAJ, CABI, Chemical Abstracts Service (CAS), EBSCO Central & Eastern European Academic Source, SOBIAD, Cabells Journalytics.

Processing and publication are free of charge with the journal. No fees are requested from the authors at any point throughout the evaluation and publication process. All manuscripts must be submitted via the online submission system, which is available at dergipark. gov.tr/iufsjb. The journal guidelines, technical information, and the required forms are available on the journal's web page.

All expenses of the journal are covered by the Istanbul University.

Statements or opinions expressed in the manuscripts published in the journal reflect the views of the author(s) and not the opinions of the Istanbul University Faculty of Science, editors, editorial board, and/or publisher; the editors, editorial board, and publisher disclaim any responsibility or liability for such materials.

All published content is available online, free of charge at https://dergipark.org.tr/tr/pub/iufsjb. Printed copies of the journal are distributed free of charge.

OPEN ACCESS

Editor in Chief: Prof. Dr. Fusun OZTAY
Address: Istanbul University, Faculty of Science, Department of Biology, 34134 Vezneciler, Fatih, Istanbul, Turkiye
Phone: +90 212 4555700 (Ext. 20319)
Fax: +90 212 5280527
E-mail: fusoztay@istanbul.edu.tr; ejb@istanbul.edu.tr

INSTRUCTIONS TO AUTHORS

European Journal of Biology (Eur J Biol) is an international, scientific, open access periodical published in accordance with independent, unbiased, and double-blinded peer-review principles. The journal is the official publication of Istanbul University Faculty of Science and it is published biannually on June and December. The publication language of the journal is English. European Journal of Biology has been previously published as IUFS Journal of Biology. It has been published in continuous publication since 1940.

European Journal of Biology aims to contribute to the literature by publishing manuscripts at the highest scientific level on all fields of biology. The journal publishes original research and review articles, and short communications that are prepared in accordance with the ethical guidelines in all fields of biology and life sciences.

The scope of the journal includes but not limited to; animal biology and systematics, plant biology and systematics, hydrobiology, ecology and environmental biology, microbiology, cell and molecular biology, biochemistry, biotechnology and genetics, physiology, toxicology, cancer biology, developmental and stem cell biology.

The editorial and publication processes of the journal are shaped in accordance with the guidelines of the International Council of Medical Journal Editors (ICMJE), the World Association of Medical Editors (WAME), the Council of Science Editors (CSE), the Committee on Publication Ethics (COPE), the European Association of Science Editors (EASE), and National Information Standards Organization (NISO). The journal conforms to the Principles of Transparency and Best Practice in Scholarly Publishing (doaj.org/bestpractice).

Originality, high scientific quality, and citation potential are the most important criteria for a manuscript to be accepted for publication. Manuscripts submitted for evaluation should not have been previously presented or already published in an electronic or printed medium. Manuscripts that have been presented in a meeting should be submitted with detailed information on the organization, including the name, date, and location of the organization.

Manuscripts submitted to European Journal of Biology will go through a double-blind peer-review process. Each submission will be reviewed by at least three external, independent peer reviewers who are experts in their fields in order to ensure an unbiased evaluation process. The editorial board will invite an external and independent editor to manage the evaluation processes of manuscripts submitted by editors or by the editorial board members of the journal. The Editor in Chief is the final authority in the decision-making process for all submissions.

An approval of research protocols by the Ethics Committee in accordance with international agreements (World Medical Association Declaration of Helsinki "Ethical Principles for Medical Research Involving Human Subjects," amended in October 2013, www.wma.net) is required for experimental, clinical, and drug studies. If required, ethics committee reports or an equivalent official document will be requested from the authors.

For manuscripts concerning experimental research on humans, a statement should be included that shows the written informed consent of patients and volunteers was obtained following a detailed explanation of the procedures that they may undergo. Information on patient consent, the name of the ethics committee, and the ethics committee approval number should also be stated in the Materials and Methods section of the manuscript. It is the authors' responsibility to carefully protect the patients' anonymity. For photographs that may reveal the identity of the patients, signed releases of the patient or of their legal representative should be enclosed.

European Journal of Biology requires experimental research studies on vertebrates or any regulated invertebrates to comply with relevant institutional, national and/or international guidelines. The journal supports the principles of Basel Declaration (basel-declaration.org) and the guidelines published by International Council for Laboratory Animal Science (ICLAS) (iclas.org). Authors are advised to clearly state their compliance with relevant guidelines.

European Journal of Biology advises authors to comply with IUCN Policy Statement on Research Involving Species at Risk of Extinction and the Convention on the Trade in Endangered Species of Wild IUCN Policy Statement on Research Involving Species at Risk of Extinction and the Convention on the Trade in Endangered Species of Wild Fauna and Flora.

All submissions are screened by a similarity detection software (iThenticate by CrossCheck).

In the event of alleged or suspected research misconduct, e.g., plagiarism, citation manipulation, and data falsification/fabrication, the Editorial Board will follow and act in accordance with COPE guidelines.

Each individual listed as an author should fulfil the authorship criteria recommended by the International Committee of Medical Journal Editors (ICMJE - www.icmje.org).

European Journal of Biology
DECEMBER 2023,
VOLUME 82, NUMBER 2

İSTANBUL
UNIVERSITY
——— P R E S S ———

The ICMJE recommends that authorship be based on the following 4 criteria:

1. Substantial contributions to the conception or design of the work; or the acquisition, analysis, or interpretation of data for the work; AND

2. Drafting the work or revising it critically for important intellectual content; AN

3. Final approval of the version to be published; AND

4. Agreement to be accountable for all aspects of the work in ensuring that questions related to the accuracy or integrity of any part of the work are appropriately investigated and resolved.

In addition to being accountable for the parts of the work he/she has done, an author should be able to identify which co-authors are responsible for specific other parts of the work. In addition, authors should have confidence in the integrity of the contributions of their co-authors.

All those designated as authors should meet all four criteria for authorship, and all who meet the four criteria should be identified as authors. Those who do not meet all four criteria should be acknowledged in the title page of the manuscript.

European Journal of Biology requires corresponding authors to submit a signed and scanned version of the authorship contribution form (available for download through the journal's web page) during the initial submission process in order to act appropriately on authorship rights and to prevent ghost or honorary authorship. If the editorial board suspects a case of "gift authorship," the submission will be rejected without further review. As part of the submission of the manuscript, the corresponding author should also send a short statement declaring that he/she accepts to undertake all the responsibility for authorship during the submission and review stages of the manuscript.

European Journal of Biology requires and encourages the authors and the individuals involved in the evaluation process of submitted manuscripts to disclose any existing or potential conflicts of interests, including financial, consultant, and institutional, that might lead to potential bias or a conflict of interest. Any financial grants or other supports received for a submitted study from individuals or institutions should be disclosed to the Editorial Board. To disclose a potential conflict of interest, the ICMJE Potential Conflict of Interest Disclosure Form should be filled and submitted by all contributing authors. Cases of a potential conflict of interest of the editors, authors, or

reviewers are resolved by the journal's Editorial Board within the scope of COPE and ICMJE guidelines.

The Editorial Board of the journal handles all appeal and complaint cases within the scope of COPE guidelines. In such cases, authors should get in direct contact with the editorial office regarding their appeals and complaints. When needed, an ombudsperson may be assigned to resolve cases that cannot be resolved internally. The Editor in Chief is the final authority in the decision-making process for all appeals and complaints.

When submitting a manuscript to European Journal of Biology, authors accept to assign the copyright of their manuscript to Istanbul University Faculty of Science. If rejected for publication, the copyright of the manuscript will be assigned back to the authors. European Journal of Biology requires each submission to be accompanied by a Copyright Transfer Form (available for download at the journal's web page). When using previously published content, including figures, tables, or any other material in both print and electronic formats, authors must obtain permission from the copyright holder. Legal, financial and criminal liabilities in this regard belong to the author(s).

Statements or opinions expressed in the manuscripts published in European Journal of Biology reflect the views of the author(s) and not the opinions of the editors, the editorial board, or the publisher; the editors, the editorial board, and the publisher disclaim any responsibility or liability for such materials. The final responsibility in regard to the published content rests with the authors.

MANUSCRIPT SUBMISSION

European Journal of Biology endorses ICMJE-Recommendations for the Conduct, Reporting, Editing, and Publication of Scholarly Work in Medical Journals (updated in December 2015 - http:/ / www.icmje.org/ icmje-r ecommendations.pdf). Authors are required to prepare manuscripts in accordance with the CONSORT guidelines for randomized research studies, STROBE guidelines for observational original research studies, STARD guidelines for studies on diagnostic accuracy, PRISMA guidelines for systematic reviews and meta-analysis, ARRIVE guidelines for experimental animal studies, TREND guidelines for non-randomized public behaviour, and COREQ guidelines for qualitative research.

Manuscripts can only be submitted through the journal's online manuscript submission and evaluation system, available at the journal's web page. Manuscripts submitted via any other medium will not be evaluated.

Manuscripts submitted to the journal will first go through

a technical evaluation process where the editorial office staff will ensure that the manuscript has been prepared and submitted in accordance with the journal's guidelines. Submissions that do not conform to the journal's guidelines will be returned to the submitting author with technical correction requests.

During the initial submission, authors are required to submit the following:

- Copyright Agreement Form,
- Author Contributions Form, and

ICMJE Potential Conflict of Interest Disclosure Form (should be filled in by all contributing authors). These forms are available for download at the journal's web page.

Preparation of the Manuscript

Title page: A separate title page should be submitted with all submissions and this page should include:

- The full title of the manuscript as well as a short title (running head) of no more than 50 characters,
- Name(s), affiliations, and highest academic degree(s) of the author(s),
- Grant information and detailed information on the other sources of support,
- Name, address, telephone (including the mobile phone number) and fax numbers, and email address of the corresponding author,
- Acknowledgment of the individuals who contributed to the preparation of the manuscript but who do not fulfil the authorship criteria.

Abstract: Abstract with subheadings should be written as structured abstract in submitted papers except for Review Articles and Letters to the Editor. Please check Table 1 below for word count specifications (250 words).

Keywords: Each submission must be accompanied by a minimum of three to a maximum of six keywords for subject indexing at the end of the abstract. The keywords should be listed in full without abbreviations.

Manuscript Types

Original Articles: This is the most important type of article since it provides new information based on original research. A structured abstract is required with original articles and it should include the following subheadings: Objective, Materials and Methods, Results and Conclu-

sion. The main text of original articles should be structured with Introduction, Materials and Methods, Results, Discussion, and Conclusion subheadings. Please check Table 1 for the limitations of Original Articles. Statistical analysis to support conclusions is usually necessary. Statistical analyses must be conducted in accordance with international statistical reporting standards. Information on statistical analyses should be provided with a separate subheading under the Materials and Methods section and the statistical software that was used during the process must be specified. Units should be prepared in accordance with the International System of Units (SI).

Short Communications: Short communication is for a concise, but independent report representing a significant contribution to Biology. Short communication is not intended to publish preliminary results. But if these results are of exceptional interest and are particularly topical and relevant will be considered for publication. Short Communications should include an abstract and should be structed with the following subheadings: "Introduction", "Materials and Methods", "Results and Discussion".

Editorial Comments: Editorial comments aim to provide a brief critical commentary by reviewers with expertise or with high reputation in the topic of the research article published in the journal. Authors are selected and invited by the journal to provide such comments. Abstract, Keywords, and Tables, Figures, Images, and other media are not included.

Review Articles: Reviews prepared by authors who have extensive knowledge on a particular field and whose scientific background has been translated into a high volume of publications with a high citation potential are welcomed. These authors may even be invited by the journal. Reviews should describe, discuss, and evaluate the current level of knowledge of a topic in clinical practice and should guide future studies. The main text should contain Introduction, Experimental and Clinical Research Consequences, and Conclusion sections. Please check Table 1 for the limitations for Review Articles.

Letters to the Editor: This type of manuscript discusses important parts, overlooked aspects, or lacking parts of a previously published article. Articles on subjects within the scope of the journal that might attract the readers' attention, particularly educative cases, may also be submitted in the form of a "Letter to the Editor." Readers can also present their comments on the published manuscripts in the form of a "Letter to the Editor." Abstract, Keywords, and Tables, Figures, Images, and other media should not be included. The text should be unstructured. The

European Journal of Biology
DECEMBER 2023,
VOLUME 82, NUMBER 2

İSTANBUL
UNIVERSITY
—— P R E S S ——

manuscript that is being commented on must be properly cited within this manuscript.

Tables

Tables should be included in the main document, presented after the reference list, and they should be numbered consecutively in the order they are referred to within the main text. A descriptive title must be placed above the tables. Abbreviations used in the tables should be defined below the tables by footnotes (even if they are defined within the main text). Tables should be created using the "insert table" command of the word processing software and they should be arranged clearly to provide easy reading. Data presented in the tables should not be a repetition of the data presented within the main text but should be supporting the main text.

Figures and Figure Legends

Figures, graphics, and photographs should be submitted as separate files (in TIFF or JPEG format with 1200 dpi for graphic and 600 dpi for colour images) through the submission system. The files should not be embedded in a Word document or the main document. When there are figure subunits, the subunits should be labeled merged to form a single image. Each subunit should be submitted separately through the submission system. Images should be labeled (a, b, c, etc.) to indicate figure subunits.

Thick and thin arrows, arrowheads, stars, asterisks, and similar marks can be used on the images to support figure legends. Like the rest of the submission, the figures too should be blind. Any information within the images that may indicate an individual or institution should be blinded. The minimum resolution of each submitted figure should be 300 DPI. To prevent delays in the evaluation process, all submitted figures should be clear in resolution and large in size (minimum dimensions: 100 × 100 mm). Figure legends should be listed at the end of the main document.

All acronyms and abbreviations used in the manuscript should be defined at first use, both in the abstract and in the main text. The abbreviation should be provided in parentheses following the definition.

When a drug, chemical, product, hardware, or software program is mentioned within the main text, product information, including the name of the product, the producer of the product, and city and the country of the company (including the state if in USA), should be provided in parentheses in the following format: "Discovery St PET/CT scanner (General Electric, Milwaukee, WI, USA)"

All references, tables, and figures should be referred to within the main text, and they should be numbered consecutively in the order they are referred to within the main text.

Limitations, drawbacks, and the shortcomings of original articles should be mentioned in the Discussion section before the conclusion paragraph.

References

European Journal of Biology uses the **AMA citation style.** In the paper, you are writing, materials are cited using superscript numerals. The first reference used in a written document is listed as 1 in the reference list, and a 1 is inserted into the document immediately next to the fact, concept, or quotation being cited. If the same reference is used multiple times in one document, use the same number to refer to it throughout the document.

Example:

Finding treatments for breast cancer is a major goal for scientists.[1,2] Some classes of drugs show more promise than others. Gradishar evaluated taxanes as a class.[3] Other scientists have investigated individual drugs within this class, including Andre and Zielinski[2] and Joensuu and Gligorov.[4] Mita et al's investigation of cabazitaxel 5 seems to indicate a new role for this class of drugs.

While citing publications, preference should be given to the latest, most up to date publications. If an ahead of print publication is cited, the DOI number should be provided. Authors are responsible for the accuracy of references. Journal titles should be abbreviated in accordance with the journal abbreviations in Index Medicus/ MEDLINE/PubMed. When there are six or fewer authors, all authors should be listed. If there are seven or more authors, the first six authors should be listed followed by "et al."

At the end of the document, include a reference list with full citations to each item. The reference styles for different types of publications are presented in the following examples.

Print journal article with six or fewer authors:

Kayalar O, Oztay F, Ongen HG. Gastrin-releasing peptide induces fibrotic response in MRC5s and proliferation in A549s. *Cell Commun Signal.* 2020;18(1):96-107.

Kazerouni NN, Currier RJ, Hodgkinson C, Goldman S, Lorey F, Roberson M. Ancillary benefits of prenatal maternal serum screening achieved in the California program. *Prenat Diagn.* 2010;30 (10):981-987.

İSTANBUL
UNIVERSITY
— P R E S S —

Table 1. Limitations for each manuscript type

Type of manuscript	Word limit	Abstract word limit	Reference limit	Table limit	Figure limit
Original Article	4500	250 (Structured)	No limit	6	Maximum 10
Short Communication	2500	200	30	3	4
Review Article	5500	250	No limit	5	6
Letter to the Editor	500	No abstract	5	No tables	No media

Print journal article with more than six authors:

Baba Y, Yoshida N, Kinoshita K, et al. Clinical and prognostic features of patients with esophageal cancer and multiple primary cancers: A retrospective single-institution study. *Ann Surg.* 2018;267(3):478-483.

Online journal article:

Florez H, Martinez R, Chakra W, Strickman-Stein M, Levis S. Outdoor exercise reduces the risk of hypovitaminosis D in the obese. *J Steroid Biochem Mol Bio.* 2007;103(3-5):679-681. doi:10.1016/j.jsbmb.2006.12.032.

Journal article with no named author or group name:

Centers for Disease Control and Prevention (CDC). Licensure of a meningococcal conjugate vaccine (Menveo) and guidance for use-Advisory Committee on Immunization Practices (ACIP), 2010. *MMWR Morb Mortal Wkly Rep.* 2010;59(9):273

Book:

Brownson RC. *Evidence-based Public Health.* 2nd ed. New York, N.Y.: Oxford University Press; 2011.

Book Chapter:

Guyton JL, Crockarell JR. Fractures of acetabulum and pelvis. In: Canale ST, ed. *Campbell's Operative Orthopaedics.* 10th ed. Philadelphia, PA: Mosby, Inc; 2003:2939-2984.

Webpage:

Fast facts. National Osteoporosis Foundation website. http://www.nof.org/osteoporosis/diseasefacts.htm. Accessed August 27, 2007.

Official organization report published on a webpage:

Office of Women's Health, California Department of Public Health. California Adolescent Health 2009. http://www.cdph.ca.gov/pubsforms/Pubs/OWH-AdolHealthReport09.pdf. Accessed January 5, 2011.

Conference Proceedings:

Fritz TC, Soni MG. Use of dietary supplements in sports drinks: Consumption and safety determinations for regulatory compliance. Poster presented at: *Annual International Society of Sports Nutrition Conference and Expo*; June 16-18, 2005; New Orleans, LA.

Thesis

Yildirim M. The determination of effective long non-coding RNA on human pulmonary fibrosis in an in vitro model. Istanbul University, Science Institute, Master Thesis, 2018.

REVISIONS

When submitting a revised version of a paper, the author must submit a detailed "Response to the reviewers" that states point by point how each issue raised by the reviewers has been covered and where it can be found (each reviewer's comment, followed by the author's reply and line numbers where the changes have been made) as well as an annotated copy of the main document. Revised manuscripts must be submitted within 30 days from the date of the decision letter. If the revised version of the manuscript is not submitted within the allocated time, the revision option may be cancelled. If the submitting author(s) believe that additional time is required, they should request this extension before the initial 30-day period is over. Accepted manuscripts are copy-edited for grammar, punctuation, and format. Once the publication process of a manuscript is completed, it is published online on the journal's webpage as an ahead-of-print publication before it is included in its scheduled issue. A PDF proof of the accepted manuscript is sent to the corresponding author and their publication approval is requested within 2 days of their receipt of the proof.

Editor in Chief: Prof. Dr. Fusun OZTAY
Address: Istanbul University, Faculty of Science, Department of Biology,
34134 Vezneciler, Fatih, Istanbul, Turkiye
Phone: +90 212 4555700 (Ext. 20319)
Fax: +90 212 5280527
E-mail: fusoztay@istanbul.edu.tr

CONTENTS

İSTANBUL
UNIVERSITY
— P R E S S —

CONTENTS

İSTANBUL
UNIVERSITY
— P R E S S —

CONTENTS

Investigation of Anti-Mycobacterial Activity of Orientin and Vitexin on the Six *Mycobacterium tuberculosis* Strains

Tulin Askun[1]

[1] University of Balikesir, Faculty of Sciences and Arts, Department of Biology, Balikesir, Turkiye

ABSTRACT

Objective: Tuberculosis is an infectious disease caused by *Mycobacterium tuberculosis*, which causes disease in all organs, 80% of which are in the lungs, and can sometimes spread to other organs. It can lead to death in untreated or inadequately treated patients. Treatment of tuberculosis is very difficult due to the resistance of mycobacteria to many chemicals and disinfectants, antibiotics, and chemotherapeutics, especially in immunocompromised patients (HIV, Human Immunodeficiency Virus); this disease is very common. Therefore, in recent years, the search for new drugs to be used to treat tuberculosis has increased worldwide. We aim to determine the effect of orientin and vitexin on *M. tuberculosis* strains.

Materials and Methods: In this study, the effects of orientin and vitexin against *M. tuberculosis* standard strains (*M. tuberculosis* H37Ra and *M. tuberculosis* H37Rv) and six-clinical *M. tuberculosis* strains. The inoculum was prepared using a positive BACTEC "Mycobacteria Growth Indicator Tube" containing 7H9 Broth. Microplate Presto Blue Method and rifampicin were used as standard antibiotics in the anti-mycobacterial assay.

Results: Orientin and vitexin showed a mycobactericidal effect on tuberculosis strains depending on the concentration. Orientin and vitexin have not been tested on current clinical strains of *M. tuberculosis* before. In this respect, it is the first report describing the anti-mycobacterial activity of both orientin and vitexin.

Conclusion: These results indicate that orientin and vitexin may be helpful for further investigations into their role in inhibiting *M. tuberculosis*. They have a possibility of new anti-mycobacterial drug candidates in the near future.

Keywords: *Mycobacterium tuberculosis*, orientin, vitexin, anti-mycobacterial activity, MIC, MBC.

INTRODUCTION

Tuberculosis (TB) is a chronic bacterial disease caused by a bacterium called *Mycobacterium tuberculosis* (MT), which can primarily attack the lungs and affect other organs. The bacteria that cause tuberculosis are spread from one person to another through tiny droplets released into the air through coughing and sneezing. TB is one of the top 10 causes of death worldwide. In 2016, 10.4 million people contracted the disease and 1.7 million died from the disease (including 0.4 million people with HIV). Over 95% of TB deaths occur in low- and middle-income countries.[1] In 2019, there were 1.2 million TB deaths among HIV-negative people and an additional 209,000 TB deaths among HIV-positive people. There has been an increase in tuberculosis deaths in poor countries where access to tuberculosis diagnosis and treatment has decreased.[2] In 2021, the burden of drug-resistant TB was estimated to increase to 450,000 new cases of rifampicin-resistant-TB.[3]

Resistance to rifampicin (RR-TB) burden, 450,000 new cases of rifampicin resistance were detected between 2020 and 2021. Especially, between 2019 and 2020, there was a decrease in the number of people treated for RR-TB[4] and multidrug-resistant TB (MDR-TB) due to the COVID-19 outbreak.[5] Nowadays, drug-resistant TB remains a public health threat. RR-TB, the most effective first-line drug, is a cause for concern. Resistance to rifampicin and isoniazid is defined as MDR-TB. Both RR-TB and MDR-TB require treatment with second-line drugs. Globally, the estimated number of people who develop MDR-TB or RR-TB each year was relatively stable between 2015 and 2020 but increased in 2021. According to The World Health Organization (WHO) 2022 Global Tuberculosis Report, it is stated that the reason for this increase is the negative impact of the COVID-19 pandemic on TB detection. Added to this is the decline in global spending on essential TB services, and economic and financial barriers to access to health care to diagnose and treat TB.[1]

Orientin ($C_{21}H_{20}O_{11}$) is a water-soluble flavonoid synonymously known as -β-D-Glucopyranosyl-3,4,5,7 - tetrahydroxyflavone, Luteolin 8-C-β-D-glucopyranoside, Luteolin-8-glucoside or Lutexin (Figure 1A). Its molecular formula is $C_{21}H_{20}O_{11}$ and its molecular weight is 448.3769 g/mol.[6] Vitexin is a water-soluble flavonoid (Figure 1B). Its molecular formula is $C_{21}H_{20}O_{10}$ and its molecular weight is 432.381 g/mol.[7]

Orientin, is a flavonoid component, has been isolated from many medicinal plants. Among them, *Ocimum sanctum, Trollius chinensis, Phyllostachys pubescens*,[8] and *Passiflora incarnate*.[7] The properties of orientin have only just begun to be studied. Li et al.[9] investigated the effects of orientin on cardiac tissue remodelling after myocardial infarction and determined that orientin supplementation reduced oxidative stress in cardiac tissue and cardiomyocytes exposed to hypoxia. They also reported that orientin treatment increased hypoxia-induced neonatal rat cardiomyocyte apoptosis and cell viability in animal experiments. Endothelial nitric oxide synthase (eNOS signalling) regulates blood pressure via vascular smooth muscle contraction[10] and blood vessel vasodilation.[11] It was suggest that orientin is a promising neuroprotective agent suitable for the treatment of neuropathic pain.[12,13] Using Western blot analysis in their research, they showed that the Toll-like receptor mediates inhibition of the nuclear factor kappa-B signaling pathway. Orientin has been observed to protect heart and cardiomyocyte damage by regulating autophagy.[14–16]

In addition, orientin was also shown to inhibit the expression of matrix metalloproteinase-9 and interleukin-8. Orientin inhibits migratory and invasive responses by suppressing metalloproteinase-9 and interleukin-8 expression. Kim et al.[17] suggested that orientin inhibits tumour invasion and is applicable as a possible therapeutic agent for the treatment of cancer metastasis. Orientin, a C-glycosyl dietary flavone abundantly found in Rooibos tea and passion fruit, has received great attention for its multiple pharmacological potentials. Thangaraj et al.[18] investigated the antiproliferative and anti-inflammatory effects of orientin in rats with 1,2-dimethyl hydrazine (DMH)-induced colorectal cancer. In this study, they showed that orientin inhibited the overexpression of inflammatory cytokines induced by 1,2-dimethyl hydrazine, thus revealing its anti-proliferative and anti-inflammatory potentials.

Various plants have also been used to isolate orientin. Of these, *Trollius chinensis* is known as the "Golden Queen".[8,19] Regarding other biological activities, Yoo et al.[20] reported their anti-oxidant, anti-viral, anti-inflammatory activities to Wang et al.[21], and Xiao et al.[22] investigated their anti-glycation, anti-cancer and anti-thrombus activities.

Chen at al.[23] developed the ultrasonic circulatory extraction (UCE) approach for the effective removal of orientin and vitexin from flowers of *T. chinensis* and investigated some parameters that potentially affect the yield of orientin and vitexin.

The flowers of T. chinensis are a rich source of flavone-C-glycosides such as orientin and vitexin, and the most abundant bioactive flavonoid among flowers is orientin.[23,24] There are also various plants in which the orientin is determined. Arugula plant, *Eruca sativa* Mill, which is widely used to treat various diseases as a component of salads, as well as a folk remedy. Among the (*Brassicaceae*) flavonoids, orientin was found to be the main compound.[25]

Achillea species, one of the medicinal plants with many activities and used since ancient times, *Achillea nobilis* L. subsp. *neilreichii* orientin and vitexin were found in studies on ethyl acetate and ethanol extracts.[26]

Vitexin is, also known as apigenin flavone glycoside,[7] present in many plants and plant parts such as fruits mung beans trees and seeds, bamboo,[27] *Crataegus pinnatifida*,[28] pigeon-pea leaves (*Cajanus cajan*),[29] and *Passiflora cristalina*.[30]

Some glycosylated flavonoids have a direct bond between the sugar and the anomeric carbon (O-C bond), while others, such as vitexin, have a sugar bond at C6 or C8 (C-C bond).[31] Vitexin and isovitexin are active ingredients in many traditional Chinese medicines. Vitexin (apigenin-8-C-glucoside) is receiving increasing attention due to its neuroprotective effects,[32] anti-inflammatory, antihypertensive,[30] anti-oxidant, anti-cancer,[29] and anti-tumor and anti-angiogenesis effects against cervical cancer cells.[33] Bhat et al.[34] reported that vitexin proved to be an effective inhibitor of hypoxia-inducible factor 1α (HIF-1α) in chondrocytes during osteoarthritis. New research suggests that vitexin may be potential alternative medicines or ancillary health products that can be used in various diseases.

In this study, we investigated the efficacy of orientin and vitexin against tuberculosis, which is one of the leading causes of death worldwide until the coronavirus (COVID-19) pandemic and is on top of human immunodeficiency virus/ acquired immunodeficiency syndrome (HIV/AIDS) caused by a single infectious agent.

Kim et al.[35] studied seven flavonoids and showed that vitexin and orientin inhibited triglyceride accumulation the highest (approximately 40% and 33% at 100 µm respectively). They reported that other flavonoids (luteolin, chrysoeriol, cosmosin, apigenin, and luteolin-7-O-β-D-glucoside) showed lower levels of inhibition.

Drug-resistant TB remains a public health threat over the world. In this study, our aim is to investigate the effectiveness of orientin and vitexin against the tuberculosis agent *M. tuberculosis*, which is very difficult to treat due to its resistance to many chemicals, disinfectants, chemotherapeutics and antibiotics.
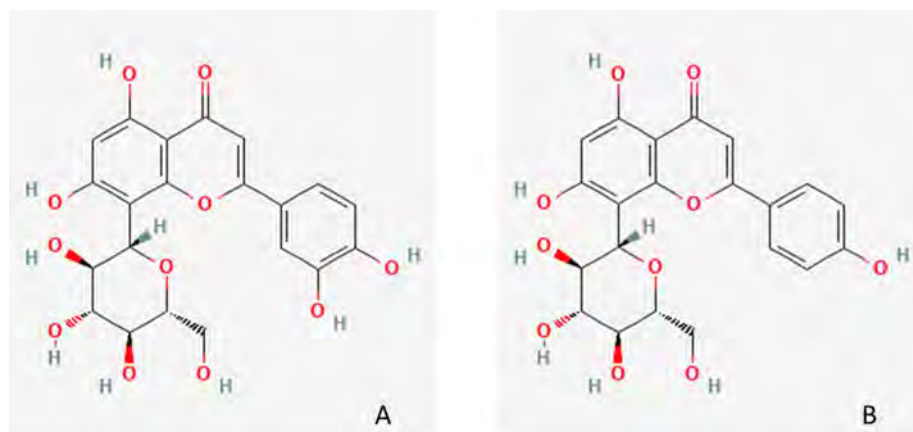
Figure 1. Chemical structure of orientin (A) and vitexin (B).

MATERIALS AND METHODS

Preparation of the Samples, Solutions, Microorganism and Inoculum Anti-Mycobacterial Assay

The compounds, orientin, (Sigma-Aldrich 55736) and vitexin (Sigma-Aldrich 49513), were obtained from Sigma-Aldrich. Ten mg were taken from the samples and dissolved in 0.5 ml dimethyl sulfoxide (DMSO). The stock solution concentration was 20 mg/mL. All stock solutions were stored in a deepfreeze at -20 ℃. To prepare 10 mL (1280 µg/mL concentration) solution, 0.64 mL of stock solution was taken and 9.36 mL of DMSO was added. Therefore, the final solution concentrations were 1280 µg/mL. The range of working solution concentrations in the wells was between 640-1.25 µg/mL. The extracts were tested against avirulent MT H37Ra (MT-Ra, ATCC 25177) and virulent MT H37 Rv (MT-Rv, ATCC 25618) from the American Type Culture Collection. Six other strains (PS-1 to PS-6) were obtained from the Balıkesir Chest Diseases Hospital tuberculosis laboratory. Anti-mycobacterial activity tests were performed in two series.

Aseptically added OADC (oleic acid, albumin, dextrose, and catalase-0.5 mL) and PANTA (polymyxin-B, amphotericin-B, nalidixic acid, trimethoprim, azlocillin-0.1 mL) antibiotic mixture into the MGIT (Mycobacteria Growth Indicator Tube-4 mL), containing modified MGIT tubes were incubated at 37 ℃. Inoculum made from a positive BACTEC MGIT tube was used one day after the tube became positive (Day1) and up to the fifth day (Day5). Day1 and Day2 positives were used directly for susceptibility testing, while Day3-Day5 positives were diluted 1:5 (1 ml positive broth into 4 ml sterile saline) and used for inoculum.[36−39] MGIT (4 mL), containing modified Middlebrook 7H9 Broth Base (MBB) was used to grow the strains at 37 ℃. Blood agar was used for each test to control the growth of suspicious bacteria other than MT. For this, the vials were

tested daily, starting from the second day of incubation, using a MicroMGIT Fluorescent reader with long-wave UV light.

Minimum Inhibition Concentration (MIC) and Minimum Bactericidal Concentration (MBC)

Determination of MIC for anti-mycobacterial assay, the microdilution method was achieved according to the CLSI, Susceptibility Testing of *Mycobacteria, Nocardia*, and Other Aerobic *Actinomycetes* guidelines.[40] The medium in MGIT tubes prepared as mentioned above was put into each well (100µL), and a sample (100 µL) at the concentration of 1280 µg/mL was added to the first well only. The volume of the first tube is 200 µL (sample solution and medium), while the others are 100 µL (only medium). 100 µL volume of the solution is transferred from the first well to the second well, by mixing three times with an automatic pipette. The volume of the first well is halved, but the concentration remains the same. In the second well, its volume doubled and its concentration was halved and this procedure included the 10th well.

After the solution in the first well was mixed three times with an automatic pipette, the dilution was repeated from the first row to the 10th row. The experiments also included positive and negative controls. Row 11 was positive and row 12 was the negative control. A 15 µL of MT suspension as inoculum was added to all wells except row 12. Then the tubes were incubated at 37 ℃. After the start day, the tubes were read daily. The day for positive was 8-12 days for MT. Results were evaluated using Presto Blue, a non-toxic, resazurin-based solution, that indicator which is a cell viability indicator. Metabolically active cells as pink and inhibited cells as blue were observed. For MBC determination, the inoculum was taken from the MIC wells and higher concentration wells and then added to wells containing fresh and sterile 7H9 medium. The plates were incubated at 37 ℃. Colour change in positive and negative control wells was

Table 1. The MIC and MBC values of orientin (µg/mL).

Anti-mycobacterial activity of orientin and vitexin (µg/mL)					Antibiotic (µg/mL)	
		Orientin	Vitexin			Rifampicin
Microorganisms	MIC	MBC	MIC	MBC	MIC	MBC
MT-Ra	160	640	80	320	0.64	5.12
MT-Rv	320	640	80	320	0.32	2.56
PS-1	160	160	80	80	-	-
PS-2	160	160	80	160	-	-
PS-3	320	640	160	>640	-	-
PS-4	640	640	320	320	-	-
PS-5	320	320	160	320	-	-

MIC:Minimum Inhibition Concentration MBC:Minimum Bactericidal Concentration PS: Patient strain
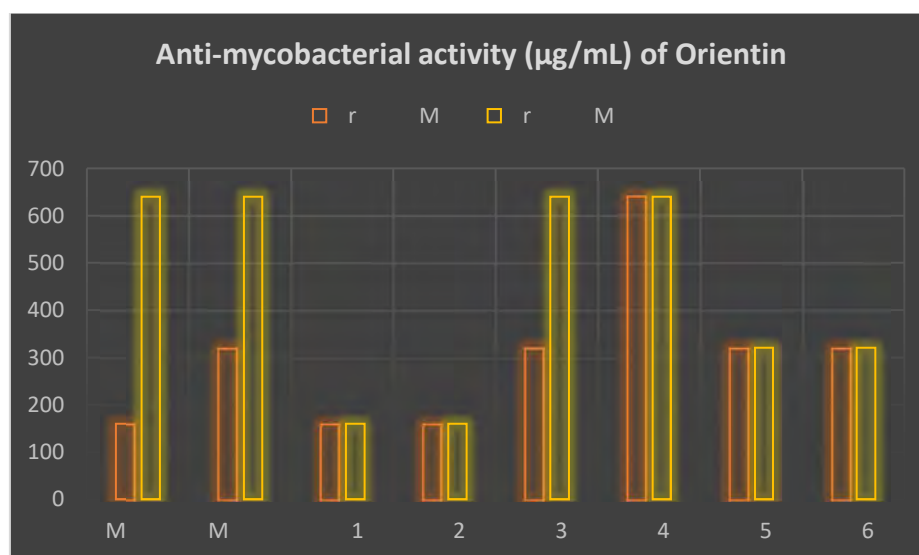
Figure 2. Anti-mycobacterial activity of orientin (µg/mL).

RESULTS

Orientin and vitexin stock solution and working solution (1280 µg/mL) were prepared. The concentration ranges from well-plate 1 to well 10 were adjusted as 640-1.25 µg/mL by serial dilution. Eight bacteria were used the determine the anti-mycobacterial activity of orientin and vitexin. Two of them were MT-Ra and MT-Rv standard bacteria, and the six clinical MT patient strains, (PS-1, PS-2, PS-3, PS-4, PS-5, and PS-6) were used as test organisms for MIC and MBC tests.

In our assays, the lowest MIC values determined for orientin checked with Presto blue indicator. The lowest concentration without bacterial growth was accepted as MBC.

were found against MT-Ra, PS-1, and PS-2 (MICs value were 160 µg/mL), and the MBCs were 640, 160, and 160 µg/mL, respectively. PS-1 and PS-2 showed the minimum MBC values. They have the same MIC and MBC values. On the other hand, the highest MIC and MBC value determined was PS-4 at 640 µg/mL. On the other hand, the highest MIC and MBC value determined PS-4 as 640 µg/mL. Depending on the concentration, orientin showed a mycobactericidal effect on tuberculosis strains (Table 1, Figure 2).

The lowest MIC values determined for vitexin were found against MT-Ra, MT-Rv, PS-1, and PS-2 (MIC values were 80 µg/mL). The MBCs were 320, 320, 80, and 160 µg/mL, respectively. MIC values obtained for vitexin were lower than that of orientin. The lowest MIC values of 80 µg/mL were observed in
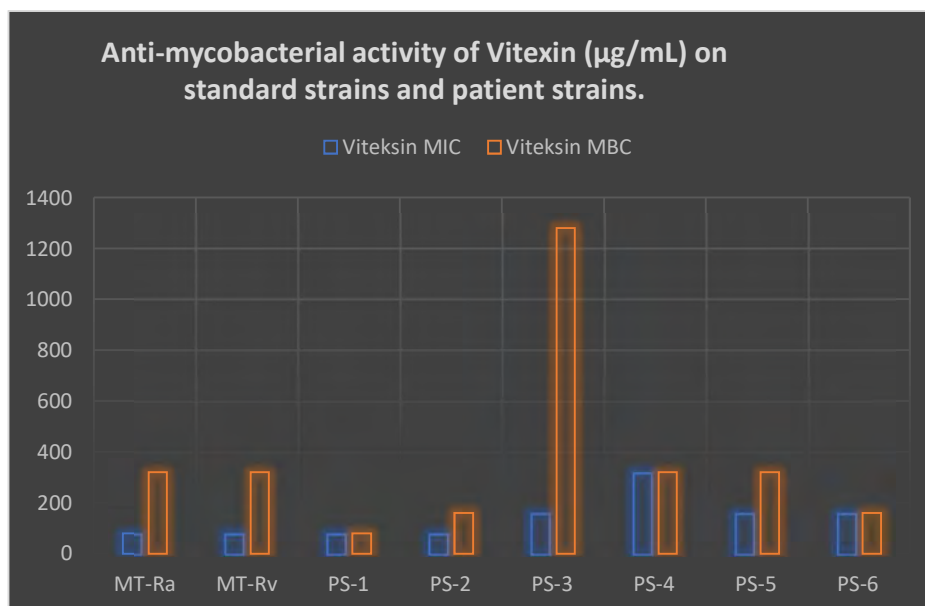
Figure 3. Anti-mycobacterial activity of vitexin (µg/mL).
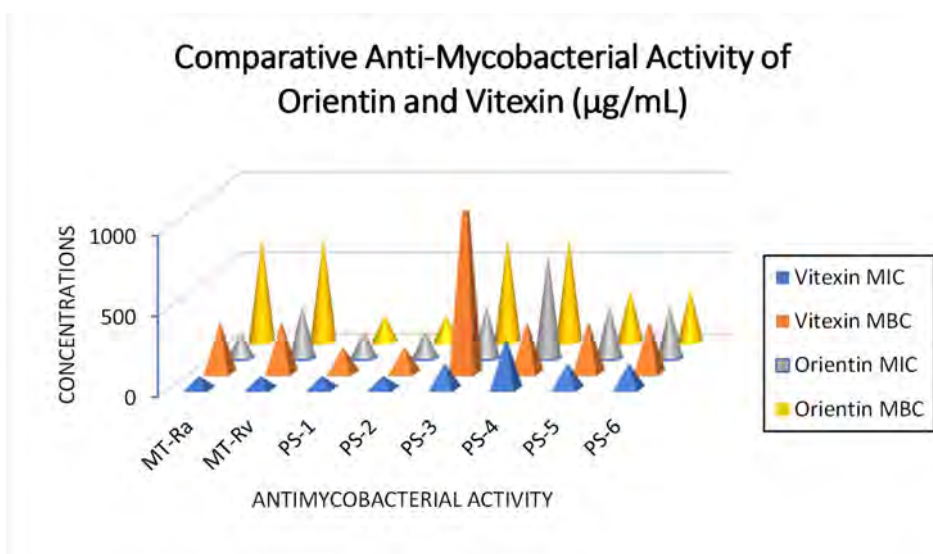
Figure 4. The comparative anti-mycobacterial activity of orientin and vitexin (µg/mL).

MT-Ra, MT-Rv, PS-1, and PS-2. While the MBC value for PS-1 was the same as the MIC value, the MBCs were 160 µg/mL for PS-2 and 320 µg/mL for MT-Ra and MT-Rv. Also, the highest MBC was found at PS-3 (MBC>640 µg/mL). The effects of vitexin on microorganisms are given in Table 1, Figure 3.

The comparative anti-mycobacterial activity of orientin and vitexin (µg/mL) is given in Figure 4. We found vitexin is more effective against Mycobacteria at lower concentrations than orientin.

DISCUSSION

There are no studies on the effects of orientin and vitexin on TB patient strains. Therefore, the antimycobacterial effect on patient strains is of great importance in terms of the potential drug substance. As a result of our research, we found that both orientin and vitexin (excluding PS-4, MBC>640 µg/mL) were highly effective against MT strains and showed mycobactericidal activity. When comparing the anti-mycobacterial activity (µg/mL) of orientin versus vitexin,

we determined that flavonoids vitexin was more effective at lower concentrations than orientin. Rifampicin, also recognized as rifampin, has a bactericidal effect on both extracellular and intracellular on Mycobacteria. We preferred to use rifampicin as the standard substance (antibiotic) because of its below-mentioned properties and because it is the most potent first-line anti-tuberculosis drug. It inhibits the RNA polymerase enzyme of Mycobacteria.[41] Rifampicin is a broad-spectrum semi-synthetic antibiotic obtained by fermentation of *Nocardia mediterranei*. It is an antimycobacterial agent that is effective at low concentrations against Mycobacteria.[42−43] Rifampicin stops bacterial growth by inhibiting RNA synthesis. The sensitivity of RNA polymerase is in good agreement with MIC values in Gram-positive bacteria. The higher MIC values observed in Gram-negative bacteria are due to less penetration of rifampicin into the outer membrane of these organisms.[44] The development of resistance is slower than in other bacteria. It has been shown to have the longest post-antibiotic effect.[45]

A study in the literature investigating the effect of orientin and isoorientin on macrophage cells was performed by Jesus et al.[44] In this study, the effects of orientin and isoorientin obtained in *Vitex polygamma* dichloromethane fraction on macrophage cells were examined. In their research, they investigated the antimycobacterial effect of orientin against the intracellular and extracellular growth of MT- H37Rv. In conclusion, they reported that it was able to reduce the growth of virulent MT-H37Rv and hypervirulent MT-M299. Besides, orientin presented a higher antimycobacterial activity. The antimycobacterial activity results of orientin on patient strains and standard strains in our study are in line with the results of Jesus et al.[46] They stated that the position of the C-glycosylation of the luteolin A-ring of orientin was effective in the action against *Mycobacterium*. Apart from Jesus et al.[46] there is no reported article on the antimycobacterial activity of orientin and vitexin in the literature. The effect of orientin and vitexin has not been tested on patient strains before. Therefore, our study is unique and fills the gap in this field.

Adamczak et al.[47] reported moderate antibacterial activities of orientin and vitexin against *Staphylococcus aureus, Enterococcus faecalis, Escherichia coli* and *Pseudomonas aeruginosa* (MIC 500–1000 µg/mL). In this respect, MIC values and tested concentrations for the bacteria mentioned above are consistent with our results.

Song et al.[48] stated that the main antibacterial mechanisms of these flavonoids from *Trollius chinensis* Bunge due to the components (4'-methoxy-2"-O-(2-methylbutyryl) and 2-O-(3-methoxycaffeoyl) for vitexin and the component of 4'-methoxy-2"-O-(2-methylbutyryl) for orientin. They noted that the antibacterial mechanism of these components is through binding to DNA.[48]

Coumarins are also known to have moderate activity against *M. tuberculosis* and this activity is attributed to prenyl at the

C-8 position.[49] However, the antimycobacterial activities of C-glycoside flavonoids (orientin and vitexin) on patient strains have not been studied.

In our study, the antimycobacterial activities of orientin and vitexin were tested on reference strains and patient strains. When the anti-mycobacterial activity of orientin and vitexin was compared, it was found that vitexin showed higher activity than orientin on MT strains. To the best of our knowledge, this study is the first report describing the anti-mycobacterial activity of orientin and vitexin against strains obtained from MT patients. However, more detailed studies are needed in areas such as pharmacology, toxicology, drug development, pharmacokinetics, pharmaceutical chemistry, drug release and clinic in order to use vitexin as a potential active drug substance. The fact that these above-mentioned stages have not yet been carried out creates a limitation in terms of demonstrating the effectiveness of orientin and vitexin.

CONCLUSION

Orientin and vitexin are bioactive compounds that can be isolated from medicinal plants and are promising flavonoids, which inhibit current strains of *M. tuberculosis*. Orientin and vitexin, rich sources of flavone-C-glycosides and the most abundant bioactive flavonoids among flowers, can potentially be promising compounds for further studies to treat MDR-TB. However, these studies require a lot of time, labour, and resources. Studies on some of their biological properties are reported. However, there is a need for a better understanding of pathways and mechanisms of action for vitexin and orientin to develop highly effective drugs with fewer side effects.

ORCID IDs of the author

Tulin Askun   0000-0002-2700-1965

REFERENCES

1. World Health Organisation. WHO-2022 [Internet]. Vol. 4, Global tuberculosis report. 2557. Available from: https://www.who.int/teams/global-tuberculosis-programme/tb-reports accessed 24 January 2023.

2. Chakaya J, Khan M, Ntoumi F, et al. Global Tuberculosis Report 2020-Reflections on the Global TB burden, treatment and prevention efforts. *Int J Infect Dis*. 2021;113(Suppl 1): S7-S12.

3. Mohr-Holland E, Daniels J, Reuter A, et al. Early mortality during rifampicin-resistant TB treatment. *Int J Tuberc Lung Dis*. 2022;26(2):150-157.

4. Chakaya J, Petersen E, Nantanda R, et al. The WHO Global Tuberculosis 2021 Report-not so good news and turning the tide back to End TB. *Int J Infect Dis*. 2022;124(1):26-29.

5. Motta I, Centis R, D'Ambrosio L, et al. Tuberculosis, COVID-19 and migrants: Preliminary analysis of deaths occurring in 69 patients from two cohorts. *Pulmonology*. 2020;26(4):233-240.

6. National Center for Biotechnology Information. 2023. PubChem Compound Summary for CID 5281675, Orientin. accessed 2 January 2023 from https://pubchem.ncbi.nlm.nih.gov/compound/Orientin.

7. National Center for Biotechnology Information. 2023. PubChem Compound Summary for CID 5280441, Vitexin. Retrieved January 12, 2023, from https://pubchem.ncbi.nlm.nih.gov/compound/Vitexin.

8. Prakash V, Jaiswal N, Srivastava M. A review on medicinal properties of Centella asiatica. *Asian J Pharm Clin Res*. 2017;10(10):69. https://doi.org/10.22159/ajpcr.2017.v10i10.20760

9. Pang Y, Wu S, He Y, et al. Plant-derived compounds as promising therapeutics for vitiligo. *Front Pharmacol*. 2021; 12:685116. doi:10.3389/fphar.2021.685116

10. Sandoo A, van Zanten JJ, Metsios GS, Carroll D, Kitas GD. The endothelium and its role in regulating vascular tone. *Open Cardiovasc Med J*. 2010; 4:302-312.

11. Li F, Zong J, Zhang H, et al. Orientin reduces myocardial infarction size via eNOS/NO signaling and thus mitigates adverse cardiac remodeling. *Front Pharmacol*. 2017;8:926. doi:10.3389/fphar.2017.00926

12. Guo D, Hu X, Zhang H, Lu C, Cui G, Luo X. Orientin and neuropathic pain in rats with spinal nerve ligation. *Int Immunopharmacol*. 2018;58:72-79.

13. Tian T, Zeng J, Zhao G, Zhao W, Gao S, Liu L. Neuroprotective effects of orientin on oxygen-glucose deprivation/reperfusion-induced cell injury in primary culture of rat cortical neurons. *Exp Biol Med (Maywood)*. 2018;243(1):78-86. doi:10.1177/1535370217737983

14. Fu XC, Wang MW, Li SP, Wang HL. Anti-apoptotic effect and the mechanism of orientin on ischaemic/reperfused myocardium. *J Asian Nat Prod Res*. 2006;8(3):265-272.

15. Lu N, Sun Y, Zheng X. Orientin-induced cardioprotection against reperfusion is associated with attenuation of mitochondrial permeability transition. *Planta Med*. 2011;77(10):984-991.

16. Liu L, Wu Y, Huang X. Orientin protects myocardial cells against hypoxia-reoxygenation injury through induction of autophagy. *Eur J Pharmacol*. 2016;776:90-98.

17. Kim SJ, Pham TH, Bak Y, Ryu HW, Oh SR, Yoon DY. Orientin inhibits invasion by suppressing MMP-9 and IL-8 expression via the PKCα/ ERK/AP-1/STAT3-mediated signaling pathways in TPA-treated MCF-7 breast cancer cells. *Phytomedicine*. 2018;50:35-42.

18. Thangaraj K, Vaiyapuri M. Orientin, a C-glycosyl dietary flavone, suppresses colonic cell proliferation and mitigates NF-κB mediated inflammatory response in 1,2-dimethylhydrazine induced colorectal carcinogenesis. *Biomed Pharmacother*. 2017;96:1253-1266.

19. Mohr-Holland E, Daniels J, Reuter A, et al. Early mortality during rifampicin-resistant TB treatment. *Int J Tuberc Lung Dis*. 2022;26(2):150-157.

20. Yoo H, Ku SK, Lee T, Bae JS. Orientin inhibits HMGB1-induced inflammatory responses in HUVECs and in murine polymicrobial sepsis. *Inflammation*. 2014;37(5):1705-1717.

21. Wang R, Wu X, Liu L, An Y. Activity directed investigation on anti-inflammatory fractions and compounds from flowers of *Trollius chinensis*. *Pak J Pharm Sci*. 2014;27(2):285-288.

22. Xiao Q, Qu Z, Zhao Y, Yang L, Gao P. Orientin ameliorates LPS-induced inflammatory responses through the inhibitory of the NF-κB pathway and NLRP3 inflammasome. *Evid Based Complement Alternat Med*. 2017;2017:2495496. doi:10.1155/2017/2495496

23. Chen F, Zhang Q, Liu J, Gu H, Yang L. An efficient approach for the extraction of orientin and vitexin from *Trollius chinensis* flowers using ultrasonic circulating technique. *Ultrason Sonochem*. 2017;37:267-278.

24. Chen F, Zhang Q, Mo K, Fei S, Gu H, Yang L. Optimization of ionic liquid-based homogenate extraction of orientin and vitexin from the flowers of *Trollius chinensis* and its application on a pilot scale. *Sep Purif Technol*. 2017;175:147-157.

25. Taviano MF, Melchini A, Filocamo A, et al. Contribution of the glucosinolate fraction to the overall antioxidant potential, cytoprotection against oxidative insult and antimicrobial activity of *Eruca sativa* Mill. leaves extract. *Pharmacogn Mag*. 2017;13(52):738-743.

26. Taşkın D, Taşkın T, Rayaman E. Phenolic composition and biological properties of *Achillea nobilis L*. subsp. *neilreichii* (Kerner) Formanek. *Ind Crops Prod*. 2018; 111:555-562.

27. He M, Min JW, Kong WL, He XH, Li JX, Peng BW. A review on the pharmacological effects of vitexin and isovitexin. *Fitoterapia*. 2016;115:74-85.

28. Han F, Guo Y, Gu H, Li F, Hu B, Yang L. Application of alkyl polyglycoside surfactant in ultrasonic-assisted extraction followed by macroporous resin enrichment for the separation of vitexin-2-O-rhamnoside and vitexin from *Crataegus pinnatifida* leaves. *J Chromatogr B Analyt Technol Biomed Life Sci*. 2016;1012-1013:69-78.

29. Fu Y, Zu Y, Liu W, et al. Preparative separation of vitexin and isovitexin from pigeonpea extracts with macroporous resins. *J Chromatogr A*. 2007;1139(2):206-213.

30. Yang H, Huang J, Mao Y, Wang L, Li R, Ha C. Vitexin alleviates interleukin-1β-induced inflammatory responses in chondrocytes from osteoarthritis patients: Involvement of HIF-1α pathway. *Scand J Immunol*. 2019;90(2):e12773. doi:10.1111/sji.12773

31. Ling T, Lang W, Feng X, et al. Novel vitexin-inspired scaffold against leukemia. *Eur J Med Chem*. 2018; 146:501-510.

32. Chen L, Zhang B, Shan S, Zhao X. Neuroprotective effects of vitexin against isoflurane-induced neurotoxicity by targeting the TRPV1 and NR2B signaling pathways. *Mol Med Rep*. 2016;14(6):5607-5613.

33. Wang Q, Zhang J, Ye J, Guo J. Vitexin exerts anti-tumor and anti-angiogenesis effects on cervical cancer through VEGFA/VEGFR2 pathway. *Eur J Gynaecol Oncol*. 2022;43(4):86-91.

34. Bhat A, Yadav J, Thakur K, et al. Exosomes from cervical cancer cells facilitate pro-angiogenic endothelial reconditioning through transfer of Hedgehog-GLI signaling components. *Cancer Cell Int*. 2021;21(1):319. doi:10.1186/s12935-021-02026-3

35. Kim J, Lee I, Seo J, et al. Vitexin, orientin and other flavonoids from *Spirodela polyrhiza* inhibit adipogenesis in 3T3-L1 cells. *Phytother Res*. 2010;24(10):1543-1548.

36. BD, Becton, Dickinson and Company Newsletter BD (2002). Bactec MGIT 960 SIRE kit now FDA-cleared for susceptibility testing of *Mycobacterium tuberculosis*. *Microbiology News & Ideas 13*, 4-4.

37. Palaci M, Ueki SY, Sato DN, Da Silva Telles MA, Cur-

cio M, Silva EA. Evaluation of mycobacteria growth indicator tube for recovery and drug susceptibility testing of *Mycobacterium tuberculosis* isolates from respiratory specimens. *J Clin Microbiol*. 1996;34(3):762-764.

38. Reisner BS, Gatson AM, Woods GL. Evaluation of mycobacteria growth indicator tubes for susceptibility testing of *Mycobacterium tuberculosis* to isoniazid and rifampin. *Diagn Microbiol Infect Dis*. 1995;22(4):325-329. doi:10.1016/0732-8893(95)00147-7

39. Walters SB, Hanna BA. Testing of susceptibility of *Mycobacterium tuberculosis* to isoniazid and rifampin by textit Mycobacterium growth indicator tube method. *J Clin Microbiol*. 1996;34(6):1565-1567.

40. CLSI. Susceptibility Testing of *Mycobacteria, Nocardiae*, and Other Aerobic Actinomycetes; Approved Standard—Second Edition. CLSI document M24-A2. Wayne, PA: Clinical and Laboratory Standards Institute; 2011.

41. Howard P, Twycross R, Grove G, Charlesworth S, Mihalyo M, Wilcock A. Rifampin (INN Rifampicin). *J Pain Symptom Manage*. 2015;50(6):891-895.

42. Sensi P, Margalith P, Timbal MT. Rifomycin, a new antibiotic; preliminary report. *Farmaco Sci.* 1959;14(2):146-147.

43. Maggi N, Pasqualucci CR, Ballotta R, Sensi P. Rifampicin: A new orally active rifamycin. *Chemotherapy*. 1966;11(5):285-292.

44. Wehrli W. Rifampin: Mechanisms of action and resistance. *Rev Infect Dis.* 1983;5(3):S407-S411

45. Horgen L, Legrand E, Rastogi N. Postantibiotic effect of amikacin, rifampin, sparfloxacin, clofazimine and clarithromycin against *Mycobacterium avium. Res Microbiol.* 1997;148(8):673-681.

46. Jesus CCM, Araújo MH, Simão TLBV, et al. Natural products from *Vitex polygama* and their antimycobacterial and anti-inflammatory activity. *Nat Prod Res.* 2022;36(5):1337-1341.

47. Adamczak A, Ożarowski M, Karpiński TM. Antibacterial activity of some flavonoids and organic acids widely distributed in plants. *J Clin Med.* 2019;9(1):109. doi:10.3390/jcm9010109

48. Song Z, Wang H, Ren B, Zhang B, Hashi Y, Chen S. On-line study of flavonoids of *Trollius chinensis* Bunge binding to DNA with ethidium bromide using a novel combination of chromatographic, mass spectrometric and fluorescence techniques. *J Chromatogr A.* 2013;1282:102-112.

49. Xu Y, Hu ZB, Feng SC, Fan GJ. Studies on the anti-tuberculosis principles from *Lysionotus pauciflora* Maxim. I. Isolation and identification of nevadensin. *Yao Xue Xue Bao*. 1979;14(7):447-448.

How to cite this article

İSTANBUL UNIVERSITY PRESS

RESEARCH ARTICLE

Solvation Methods Affect the Amount of Active Components in the Extract of Propolis as well as Its Anti-Inflammatory Activity in THP-1 Cells

Burak Durmaz[1], Latife Merve Oktay Celebi[2], Hikmet Memmedov[3], Nur Selvi Gunel[2], Hatice Kalkan Yildirim[4], Eser Yildirim Sozmen[1]

[1]Ege University Faculty of Medicine, Department of Medical Biochemistry, Izmir, Turkiye
[2]Ege University, Faculty of Medicine, Department of Medical Biology, Izmir, Turkiye
[3]Azerbaijan University of Medicine; Department of Medical Biochemistry, Baku, Azerbaijan
[4]Ege University, Faculty of Engineering, Department of Food Engineering, Izmir, Turkiye

ABSTRACT

Objective: : Propolis has been found to have various effects, including antioxidant and anti-inflammatory properties, according to studies. In this recent research, we discovered that reducing allergenic compounds in propolis through biotransformation using specific *Lactobacillus plantarum* strains enhanced its anti-inflammatory qualities. The study aimed to identify the extraction methods and solvents that had the most significant anti-inflammatory effects and assess how *L. plantarum* strains biotransformation of propolis affected these qualities in THP-1 cell line cultures.

Materials and Methods: Propolis samples were biotransformed with different concentrations (1.5%, 2.5%, 3.5%) of several *L. plantarum* strains (ISLG-2, ATCC®8014, visbyvac) before extraction using various solvents (ethanol, polyethylene glycol-PEG, water) and ultrasound treatments (300 W/40 Hz for 5, 10, 15 min). Liquid chromatography-mass spectrometer/mass spectrometry was used for phenolic analysis of the samples. ELISA test kits were employed to assess NF-kβ, IL-1α, IL-1β, IL-6, IL-10, TNF-α, IFN-γ , COX-1 in the cell culture supernatant.

Results: : Results showed that, except for NF-kβ, all cytokine levels decreased in four separate propolis samples. Caffeic acid, kaempferol, ferulic acid, quercetin, pelargonin, and naringenin were the key physiologically active components associated with the anti-inflammatory activity of propolis. The biotransformation process to reduce allergen compounds did not alter propolis's anti-inflammatory properties.

Conclusion: In samples that were dissolved in water, dissolved in ethanol+biotransformed with *L. plantarum* ATCC®8014, dissolved in water+biotransformed with *L. plantarum* ATCC®8014, and dissolved in water+sonicated for 15 min and biotransformed with *L. plantarum* ATCC®8014, the maximum anti-inflammatory effect of propolis was assessed.

Keywords: LPS, inflammation, propolis, biotransformation, extraction

INTRODUCTION

The inflammatory process is expressed with the migration of phagocytes, accumulation of neutrophils, monocytes, and macrophages, and, subsequently, loss of tissue function. At the beginning of the inflammatory process, macrophages are activated by different stimuli, such as cytokines from T and natural killer cells, and lipopolysaccharides (LPS) from G-negative bacteria cell wall.[1] Upon activation, macrophages differentiate into two phenotypes. Classical activation by LPS results in the M1 phenotype, which is involved in phagocytosis, se-

cretion of inflammatory cytokines, reactive oxygen species, and nitric oxide enzymes.[1,2] During the inflammatory process, proinflammatory cytokines, such as interleukin (IL)-6, IL-1 and tumor necrosis factor-alpha (TNF-α) were released by M1 macrophages [3] M2 phenotype produces regulatory cytokines (such as IL-10) and get involved in tissue repair and regeneration.[4] While the inflammatory process is protective against pathogens, the resulting inflammatory activity can also contribute to the development of various diseases, including cardiovascular diseases, diabetes, arthritis, and inflammatory bowel disease.[5]

Honeybees create propolis as a means of safeguarding their hives against bacterial, viral, and fungal invasions. Propolis contains over 300 active components.[6] Many active molecules such as flavonoids, flavones, flavanones, and flavonols have been identified in propolis. Some molecules from these groups have anti-cancer, anti-oxidant and anti-inflammatory effects.[6−10] It was observed that the anti-inflammatory effect of propolis in cell culture is closely associated with its phenolic content and solvation methods.[1,10−12]

As an alternative, it has been noted that about 10% of people have propolis sensitivity.[11,13] Caffeic acid esters, 1,1-dimethyl allyl caffeic acid ester (DMEA), benzyl caffeates, geranyl caffeate, similar compounds, and cinnamic acid esters are among the main allergens in propolis.[11−16] 1,1-dimethylallyl caffeic acid ester and its isomers make up the majority of the propolis (87%) and are the most prevalent molecules. 63% of these isomers were shown to be connected to DMEA.[15] Caffeic acid phenethyl esters (phenethyl caffeate; CAPE), a second allergen molecule, exhibit allergic effects comparable to those of DMEA.[15]

It was stated that the less allergenic propolis form might be produced by biotransformation and using lactic acid bacteria. Previous research has demonstrated that specific strains of *Lactobacillus helveticus* and *Lactobacillus plantarum* with cinnamoyl esterase activity can reduce the allergenic molecules in propolis (Patent No: TR2015 16914B, dated 2018/07/23).[16,17] It was proven that employing *L. plantarum* to properly extract and biotransform propolis lowered the concentration of allergenic compounds, specifically DMEA and CAPE molecules.[18,19]

Our aim in this study was to identify the extraction methods and solvents that had the largest anti-inflammatory effects, as well as to assess how *L. plantarum* strains biotransformation of propolis in the human monocyte cell line (THP-1 cells) culture affected those anti-inflammatory qualities. In this research, THP-1 cells were used as an inflammatory model, which was induced by LPS. The main inflammatory cytokine levels were measured in the supernatant of cell culture to detect possible protective effects of propolis. The relationships between the propolis extracted by different solvents/extraction methods and biotransformed by different *L. plantarum* strains and anti-inflammatory activity were evaluated.

MATERIALS AND METHODS

Propolis Sample Preparation

We sourced the propolis from a local Turkish company as raw material. The samples were taken in July from the Sarkikaraagac neighborhood of Isparta city, which is located in Turkey's Mediterranean region (coordinates: 38.8040 N, 3182100 E).

To remove unwanted rough particles, the samples underwent a milling process using conventional machines at the beginning of the experiments. Particle size was determined as 35 mesh (0.5 mm) using sieve analysis. After this physical treatment, the treated samples were mixed in order to homogenize them.

Biotransformation was carried out using different *L. plantarum* strains (ISLG-2, ATCC®8014 and Visbyvac) at different concentrations (1.5%, 2.5%, and 3.5%). All lactic acid bacteria were taken from stock culture collections (Ege University Food Engineering Department, Prof. Dr. Hatice Kalkan Yıldırım collection) stored at –80°C and containing 20% glycerol.

The frozen cultures were reactivated by growing at MRS broth containing media (9 mL MRS broth/10 mL tubes). The prepared media was sterilized at 121°C for 15 min. After allowing the media to cool up to room temperature, the inoculation was done aseptically. The prepared double samples were incubated at 30°C for 24 h. In order to eliminate the effect of glycerol solution used during storage at –80°C, the cultures were grown, and the activation process was performed consecutively two times. In such a way, the pure cultures were obtained for the next step of inoculation used during biotransformation.[18]

Before bioconversion, the propolis samples (w/v:1/1) were subjected by to various solvents or exaction methods. During the experiment, the extraction solvents were treated with 10% ethanol, 40% polyethylene glycol (PEG), and water. Another solvation method that was applied was ultrasound treatment (40 Hz and 300 W) for 5, 10, and 15 min.

The choice of water as a solvent was for control purposes. The upper values of ultrasonication treatment time (15 min) were determined by a preliminary study (5, 10, 15, 20, 30 min with propolis) (unpublished data). According to the study, increasing the duration time more than 15 min led to heating of food and consequently to possible loss of nutritional values, especially active phenolic molecules. Each extraction solvent and method was applied in duplicate for each culture and inoculum concentration. After aseptic inoculation of propolis samples with pure culture at different concentrations (1.5%, 2.5%, and 3.5%), the incubation was carried out at anaerobic conditions of 30 °C for 72 h.

Following the biotransformation process, the resulting bioproducts (biologically converted propolis) were treated with 70 mL of ethyl acetate and incubated at room temperature for 10 min. The mixture was then centrifuged at 1500 x g for 5 min. The solid particles were separated from the mixture and another 70 mL of ethyl acetate was added. The procedure was repeated under similar conditions (centrifugation at 1500 × g for 5 min). The solid extracts obtained were dried and dissolved in 100 mL methanol. The supernatants obtained after the final centrifugation at 4000 x g for 1 min were used for analyses.[19]

Analysis of Phenolic Content

A Waters Xevo ACQUITYTM TQD tandem quadrupole UPLCMS/MS instrument was used to evaluate the phenolic content of all propolis samples. This study was conducted with reference to the method we previously applied.[20]

Cell Culture Experiments

Cell culture experiments were conducted using the human monocyte cell line THP-1, which was cultured in Roswell Park Memorial Institute 1640 medium RPMI 1640) supplemented with 10% heat-inactivated fetal bovine serum, and 100 unit/mL penicillin, 100 µg/mL streptomycin at 37ºC with 5% CO_2. The cells were seeded at a density of 4×10^4 cells/well in 96-well plates and treated with propolis samples at concentrations ranging from 25–1500 µg/mL for 24, 48, and 72 h. Propolis samples were applied to these cells three times. The WST-8 assay was used to assess cell viability and any potential cytotoxicity.

For this purpose, after the end of 24, 48, and 72 h, 10 µL of water-soluble tetrazolium salt (WST) solution was added into the suspension containing 100 µL of cells and propolis. Then, absorbance values were measured at 450 nm with a reference wavelength at 620 nm using a microplate reader between 30 min and 4 h. In line with the results obtained by the WST-8 assay, the dose-effect graphs were drawn and IC_{50} values were calculated using CalcuSyn v2.1 software. In the experiments performed in this study, the IC_{50} doses and the time interval determined in the cytotoxicity study, were used. For the induction experiments with LPS, the THP-1 cells were seeded into 24-well plates so as to be 2×10^5 cells per well.

The propolis samples for which the IC_{50} values were determined in the previous cytotoxicity assay (as shown in Table 2) were added to the cell culture and incubated for 1 h. Subsequently, 2000 ng/mL LPS was added to induce inflammation following a previously established protocol.[21] The aim of this study was to examine the potential protective effect of propolis against inflammation. To achieve this, these cells were treated with propolis extract for 1 h, followed by the induction of inflammation by adding LPS at a concentration of 2000 ng/mL. After 2 h incubation at 37ºC, the supernatants were collected and centrifuged at 2000 x g for 5 min to measure cytokine levels. The experiment was performed independently three times to ensure reproducibility and reliability of the results.

Biochemical Analysis

In order to determine the appropriate concentration and incubation time that will yield the highest induction, LPS samples in different concentrations (0.1, 0.5, 1 and 2 µg/mL) were added into THP-1 cells and the TNF-α levels were determined in different time intervals (1, 2, 3, 4, 6, 18 and 24 h).[22]

Before induction with LPS, THP-1 cells were treated with propolis in a dose which was previously determined. The LPS-induced cell without propolis was used as the positive control and THP-1 cells treated with PBS (without LPS) was used as the negative control. After 24 h of incubation, the cell culture medium was removed and fresh LPS-containing medium (2 µg/mL) was added for 2 h.

Nuclear factor kappa B (NF-kβ) , IL-1α, IL-1β, IL-6, IL-10, TNF-α, interferon-gamma (IFN-γ) and cyclooxygenase (COX)-1 assays in a supernatant of cell culture were performed using a commercially available ELISA assay kit.

Statistical Analysis

Graphs of % cytotoxicity values in cell culture were plotted in the Graphpad v5 program. The results were analyzed using a two-way ANOVA test and a Bonferroni test as post test. IC_{50} values were calculated using CalcuSyn v2.0 (Biosoft) software.

The results were evaluated using the SPSS 22.0 statistical program. Phenolic content quantification, *in vitro* antioxidant, anti-inflammatory activity, and cytokine analysis tests were performed at least 3 times for each propolis sample. Results were calculated as mean and standard deviation. The least significant differences (LSD) test was used for significance between means. In addition, a Kruskall Wallis test was used for multiple comparisons and an LSD test was used as a post hoc test.

Spearman's Rho test was used for correlations between parameters.

RESULTS

Phenolic Content

Table 1 shows the quantities of phenolic compounds present in the propolis extracts added to cell culture. In general, the propolis extracts contained the highest amounts of trans-cinnamic acid, followed by ferulic acid, kaempferol, and quercetin as determined by the quantitative analysis of phenolic content. According to solvents, extracted amounts of phenolic molecules including the allergens (DMEA caffeic acid, Caffeic acid phenyl ester) were higher in extracts of propolis dissolved in water plus treated with ultrasound for 10 to 15 min, compared to those dissolved in other solvents. The biotransformation process depleted the allergen molecule content in all samples.

Cell Viability

The IC_{50} levels of propolis extracts at 24, 48, and 72 h changed between 166 µg/mL and 1012 µg/mL (Table 2). When propolis samples dissolved in water (untransformed) and dissolved in water and inoculated with 2.5% *L. plantarum* ATCC 8014 strain (transformed) were compared, significant differences

Table 1. Phenolic compounds detected in propolis samples added to cell culture.

	Ethanol	E+L2	PEG	PEG+L2	Water	W+L2	W+L3	W-US5+L2	W-US5+L2	W-US10	W-US1D+L1	W-US10+L3	W-US15	W-US15+L2
Added Prapolis	500.00	500.00	500.00	500.00	500.00	500.00	500.00	500.00	500.00	500.00	500.00	500.00	500.00	500.00
Ferulic acid ng/mL	31.31	35.07	7.52	6.59	77.62	81.66	25.18	138.71	58.53	110.65	60.99	18.44	122.10	57.45
Caffeic add ng/mL	5.01	4.49	0.95	1.34	10.35	15.64	3.99	18.60	6.94	15.41	8.61	2.70	18.59	10.60
Kampherol ng/mL	11.33	6.32	8.03	9.04	13.85	20.62	5.48	35.82	10.54	26.33	11.63	3.54	26.84	12.04
Miricetine ng/mL	4.09	1.17	8.34	0.98	4.86	1.25	0.99	10.91	4.57	7.32	4.39	0.94	8.67	0.96
Trans-sinnamic acid ng/mL	299.63	0.00	84.15	0.00	144.21	137.96	9.72	1091.89	34.85	412.57	62.28	0.00	435.00	28.79
Ellagic acid ng/mL	6.25	0.89	10.64	7.19	4.08	17.08	0.00	22.56	4.84	13.30	0.75	0.00	12.60	5.97
CAPE ng/mL	5.44	2.00	1.87	0.87	3.73	4.83	1.49	9.17	2.95	6.84	2.61	1.45	6.92	2.70
DMEA ng/mL	15.90	0.00	0.00	0.00	7.70	15.62	0.00	46.41	0.00	26.95	2.51	0.00	27.28	0.14
Naringenin ng/mL	4.18	0.10	0.08	0.47	0.91	0.82	18.10	31.29	17.60	14.10	0.00	26.11	8.62	0.80
Quercetine ng/mL	8.91	7.31	19.82	14.38	10.88	19.02	4.00	26.41	10.15	17.19	9.69	2.54	20.66	9.47
Rutin ng/mL	0.07	0.08	0.36	0.68	0.01	0.11	0.00	0.15	0.05	0.00	0.15	0.00	0.07	0.01
4-Hydroxy Benzole acid	1.87	1.89	1.48	9.10	1.07	3.49	0.76	0.64	0.51	1.97	0.36	1.21	0.74	0.47
Salydlic add ng/mL	0.05	0.05	0.03	0.26	0.03	0.03	0.03	0.05	0.02	0.03	0.05	0.03	0.03	0.03
Gentlsic acid ng/mL	0.00	0.01	0.00	0.20	0.00	0.03	0.01	0.06	0.01	0.01	0.04	0.01	0.01	0.01
Procatechoic acid ng/mL	0.00	0.00	0.00	0.24	0.00	0.01	0.00	0.06	0.01	0.00	0.03	0.00	0.00	0.00
Paracoumaric acid ng/mL	0.00	0.00	0.00	0.00	0.06	2.42	0.00	2.51	0.00	1.62	0.18	0.00	1.65	0.00
Vanillc Acid ng/mL	0.50	0.57	0.75	4.16	0.45	0.99	0.26	0.78	0.59	0.47	0.92	0.54	1.40	0.86
Chlorogenic Acid ng/mL	0.00	1.00	1.07	54.31	1.04	1.15	0.09	0.52	2.07	0.80	0.70	0.00	0.75	0.77

Propolis samples with a weight-to-volume ratio of 1:1 were treated with different Solutions, including ethanol (10%)=E. poly-ethylene glycol (40%)=PEG and water=w, and subjected to ultrasonication= US at a frequency of 40 Hz (5, 10 and 15 min) for samples dissolved in water. Biotransformation was carried out using *L. plantarum* strains= L1 (ISLG-2), L2 (ATCC®8014), and L3 (Visbyvac).

were found at concentrations of 250, 500, and 1500 µg/mL at 24 h, 250 and 500 µg/mL at 48 h, and 500 µg/mL at 72 h. When water-dissolved propolis samples (untransformed) and water-dissolved propolis samples (transformed) inoculated with 3.5% *L. plantarum* visbyvac strain were compared at 24, 48, and 72 h, the concentrations were 250–1500 g/mL, 250–500 g/mL, and 50–500 g/mL, respectively. Significant differences were discovered when propolis samples inoculated with 2.5% *L. plantarum* ATCC®8014 strain (transformed) and 3.5% *L. plantarum* visbyvac strain (transformed) dissolved in water were examined. When 3.5% *L. plantarum* visbyvac strain-inoculated propolis samples were compared, a significant difference was reported at concentrations of 500 g/mL at 24 h, 100-500 g/mL at 48 h, and 50 g/mL at 72 h. At 24 h, the cytotoxic effect value of the propolis sample inoculated with 3.5% *L. plantarum* visbyvac strain at a concentration of 500 µg/mL was 2.59 times higher than that of the sample inoculated with 2.5% *L. plantarum* ATCC®8014 strain. At 100 and 250 µg/mL concentrations, the propolis sample inoculated with 2.5% *L. plantarum* ATCC®8014 strain was 3.12 and 1.8 times more cytotoxic than the sample inoculated with 3.5% *L. plantarum* visbyvac strain.

Anti-Inflammatory Effects of Propolis Extracts

In this study, allopurinol and gossypol were used as standard molecules to investigate anti-inflammatory response. TNF-α levels increased up to 20 times compared to control samples upon administration of LPS. While IFN-γ levels elevated 5 times compared to the controls, IL-1α, IL-1β, and IL-6 levels showed elevation two times and more than those of the control cells (p<0.01). IL-10 slightly increased (p<0.05), but NF-kβ did not show any statistically significant change upon LPS in-

duction. None of the propolis samples affected NF-kβ levels (Figure 1).

As can be seen in the Figure 1, all propolis samples significantly decreased TNF-α levels, in particular, propolis samples solvated in "water (W)," in "water + sonicated 15 min (W+US15)," and in "water+sonicated 15 min+biotransformed with *L. plantarum* ATCC®8014 (W+US15+L2)" returned TNF-α to normal levels.

Four extract types (dissolved in water, in ethanol biotransformed with *L. plantarum* ATCC®8014 (L2), in water biotransformed with *L. plantarum* ATCC®8014 and in "water and sonicated for 15 min, biotransformed with *L. plantarum* ATCC®8014) decreased all cytokine levels except NF-kβ. Two extract types dissolved in water and sonicated 15 min and in water+sonicated for 10 min and biotransformed with *L. plantarum* visbyvac (L3) decreased all cytokine levels except IL-6 and NF-kβ. Propolis samples dissolved in ethanol and biotransformed with *L. plantarum* ATCC®8014, water and sonicated for 15 min, biotransformed with *L. plantarum* ATCC®8014, in water+ biotransformed with *L. plantarum* visbyvac and in water+biotransformed with *L. plantarum* ATCC®8014 returned IL-6 to normal levels (p<0.01; Figure 1)

Two extract types dissolved in PEG and biotransformed with *L. plantarum* ATCC®8014 (L2) and in water and biotransformed with *L. plantarum* visbyvac (L3) decreased all cytokine levels except IL-1β and NF-kβ (Figure 1).

While 3 extract types (dissolved in "ethanol (E)," in "water +biotransformed with *L. plantarum* ATCC®8014 (W+L2)," and in "water+sonicated for 10 min+biotransformed with *L. plantarum* ISLG-2 (W+US10+L1)") did not show any effect

Table 2. The IC$_{50}$ levels of propolis on THP-1 cell line were determined at the 24th, 48th, and 72nd h. Biotransformation was performed using *L. plantarum* strains, including L1 (ISLG-2), L2 (ATCC®8014) and L3 (Visbyvac).

Propolis samples	IC$_{50}$ values (concentration range, pg/mL)		
	24 h	48 h	72 h
Water + 40 kHz/5 min US	363.89 (250-1500 pg/mL)	290.89*** (50-1500 pg/mL)	166.49 (25-1500 pg/mL)
Dissolved in water, 40 kHz/5 min ultrasound application and 1.5% *L. plantarum* L2 strain inoculated propolis	398.98 (100-1500 pg/mL)	378.87 (100-1500 pg/mL)	402.17 (100-1500 pg/mL)
Dissolved in water and 40 kHz/15 min propolis with ultrasound application	427.96 (100-1500 pg/mL)	337.14 (100-1500 pg/mL)	347.65 (100-1500 pg/mL)
Dissolved in water, 40 kHz/15 min ultrasound application and 2.5% *L. plantarum* L2 strain inoculated propolis	598.69 (100-1500 pg/mL)	304.63*** (25-1500 pg/mL)	426.77 (100-1500 pg/mL)
Dissolved in water and 40 kHz/10 min propolis with ultrasound application	309.47 (25-1500 pg/mL)	417.92 (250-1500 pg/mL)	264.19 (25-1500 pg/mL)
Dissolved in water, 40 kHz/10 min ultrasound application and 2.5% of *L. plantarum* L1 strain inoculated propolis	262.59** (50-1500 pg/mL)	272.19* (50-1500 pg/mL)	205.45*** (25-1500 pg/mL)
Dissolved in water, 40 kHz/10 min ultrasound application and 3.5% *L. plantarum* L3 strain inoculated propolis	1012.26 (50-1500 pg/mL)	577.98 (50-1500 pg/mL)	947.66 (250-1500 pg/mL)
Propolis dissolved in water	429.91 (100-1500 pg/mL)	298.36*** (25-1500 pg/mL)	216.88 (100-1500 pg/mL)
Propolis dissolved in water and inoculated with 2.5% *L. plantarum* L2 strain	673.77 (50-1500 pg/mL)	352.13** (25-1500 pg/mL)	519.31 (100-1500 pg/mL)
Propolis dissolved in water and inoculated with 3.5% *L. plantarum* L3 strain	668.83 (100-1500 pg/mL)	480.62* (25-1500 pg/mL)	452.46 (100-1500 pg/mL)
Propolis dissolved in 10% ethyl alcohol	446.31 (25-1500 pg/mL)	468.68 (100-1500 pg/mL)	276.24 (25-1500 pg/mL)
Dissolved in 10% ethyl alcohol, 2.5% *L. plantarum* Culture-1 inoculated propolis	675.49 (50-1500 pg/mL)	526.85 (25-1500 pg/mL)	618.68 (25-1500 pg/mL)
Propolis dissolved in 50% PEG	303.14** (100-1500 pg/mL)	358.41 (100-1500 pg/mL)	405.82 (100-1500 pg/mL)
Dissolved in 50% PEG and 3.5% *L. plantarum* Culture-2 inoculated propolis	731.34 (100-1500 pg/mL)	356.59 (25-1500 pg/mL)	491.38 (25-1500 pg/mL)
Gossypol	5.98 pM	2.77 pM***	3.6 pM
Allopurinol	---	---	374.1 pM

*p<0.05, *p<0.01 and *p<0.001 according to control.

on IL-10 levels, all other propolis samples decreased IL-10 levels.

While two extract types of propolis (dissolved in "PEG" and in "water+sonicated 5 min") did not show any effect on IFN-γ levels, all other propolis samples decreased IFN-γ levels.

Ferulic acid and caffeic acid content of propolis extracts were inversely correlated with TNF-α levels (r=-0.479, p=0.001 and r=-0.485, p=0.001, respectively) of LPS induced THP-1 cells. The highest levels of ferulic acid and caffeic acid were found in propolis samples dissolved in "water+sonicated 5/10/15 min" and in propolis samples dissolved in "water+biotransformed with *L. plantarum* ATCC®8014".

COX-1 levels in LPS induced THP-1 cells were inversely correlated with pelargonin (r=-0.734, p=0.003) and naringenin (r=-0.483, p=0.08) levels in propolis samples.

NF-kβ levels in the propolis-added THP-1 cells (with LPS) were inversely correlated with ferulic acid (r=-0.295, p=0.005), trans-cinnamic acid (r=-0.395, p=0.01), and CAPE (r=-0.354, p=0.021). TNF-α levels showed negative correlations with trans-cinnamic acid (r=-0.395, p=0.01), CAPE (r=-0.415, p=0.006), kaempferol (r=-0.426, p=0.005), and DMEA
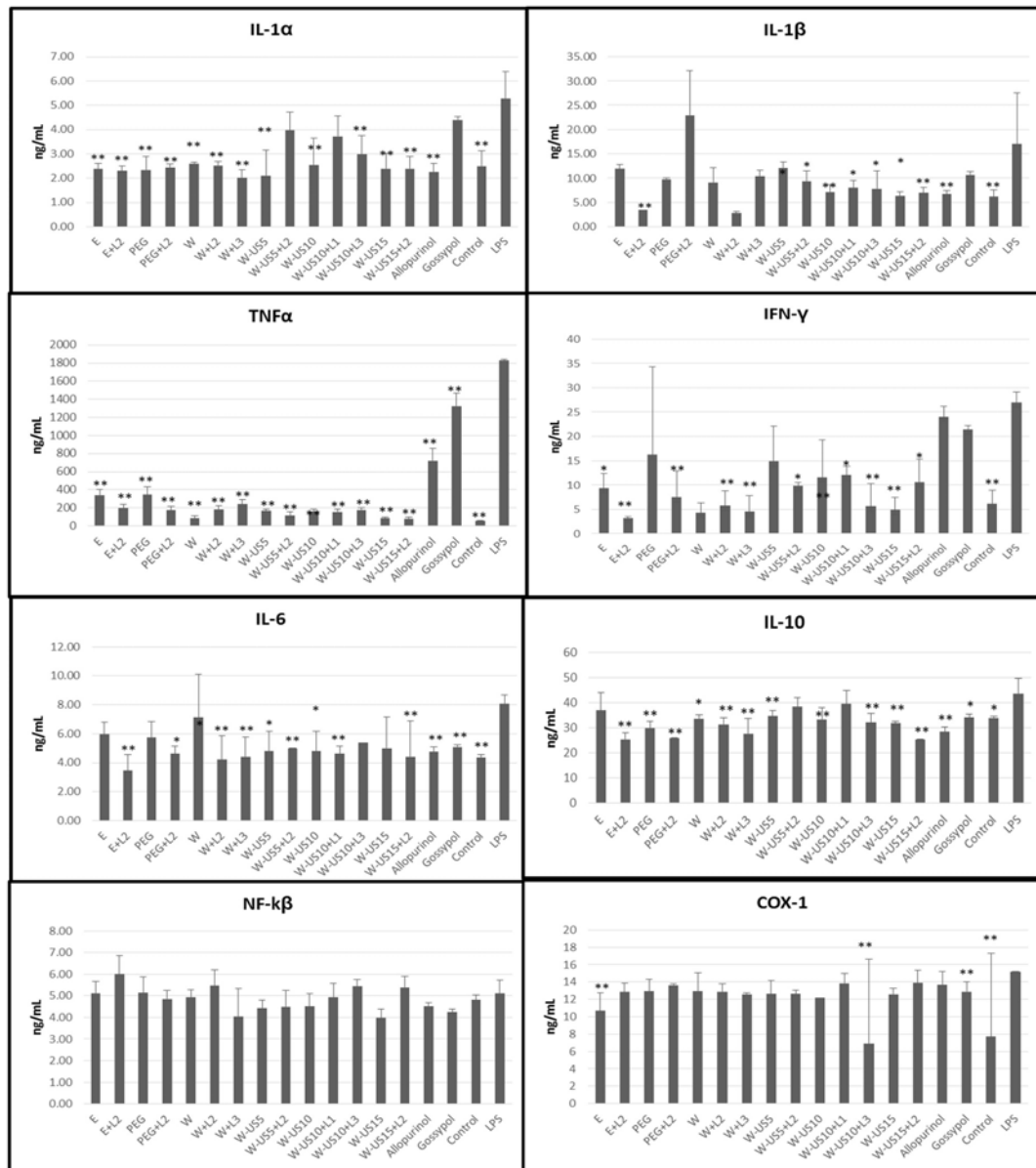
Figure 1. NF-kβ, IL-1α, IL-1β, IL-6, IL-10, TNF-α, IFN-γ, and COX-1 levels in supernatant of propolis-added THP-1 cells. (*p<0.05 and **p<0.01) *Comparisons were made versus only LPS-added cell-line. Propolis (w/v:1/1) were extracted with different solutions (ethanol (10%)=E, poly-ethylene glycol (40%)=PEG, and water=w) and ultrasonication= US was applied at 40 Hz (5, 10, and 15 min) for samples that were dissolved in water. *L. plantarum* strains= L1, L2, L3 (ISLG-2, ATCC®8014, and Visbyvac, respectively) were used for biotransformation.

caffeic acid (r=-0.338, p=0.029) levels. There is an inverse correlation between IL-1α levels and ferulic acid (r=-0.428, p=0.005), caffeic acid (r=-0.391, p=0.01), and CAPE (r=-0.349, p=0.023) levels. In the present work, the first two principal components with eigenvalues 7.1 and 2.5 accounted for 44.4% and 15.7% of the dataset. The first principal component (PC1) is correlated positively with the phenols (kaempferol, DMEA-CA, cafeic acid, CAPE, trans-cinnamic acid, ferulic acid, myricetin, quercetin, and naringenin) and PC2 is correlated with TNF-α, IFN-γ, IL-6, IL1α, IL-1β, and COX-1.

As can be seen from Figure 2, kaempferol, DMEA-CA, Cafeic acid, CAPE, trans-cinnamic acid, ferulic acid, myricetin, quercetin, and naringenin are presented on the positive side of Figure-2. TNF-α, IL-1α, IL-1β and NF-kβ are on the left side of the Figure 2. Similarly to our correlation analysis, PCA showed that TNF-α, IL-1α, NF-kβ, and IL-1β were inversely correlated with ferulic acid, CAPE, DMEACA, caffeic acid, kaemferol, and trans-cinnamic acid. It was also shown that IFN-γ, COX-1, and IL-6 were clustered in the same area and inversely correlated with naringenin and pelargonium.
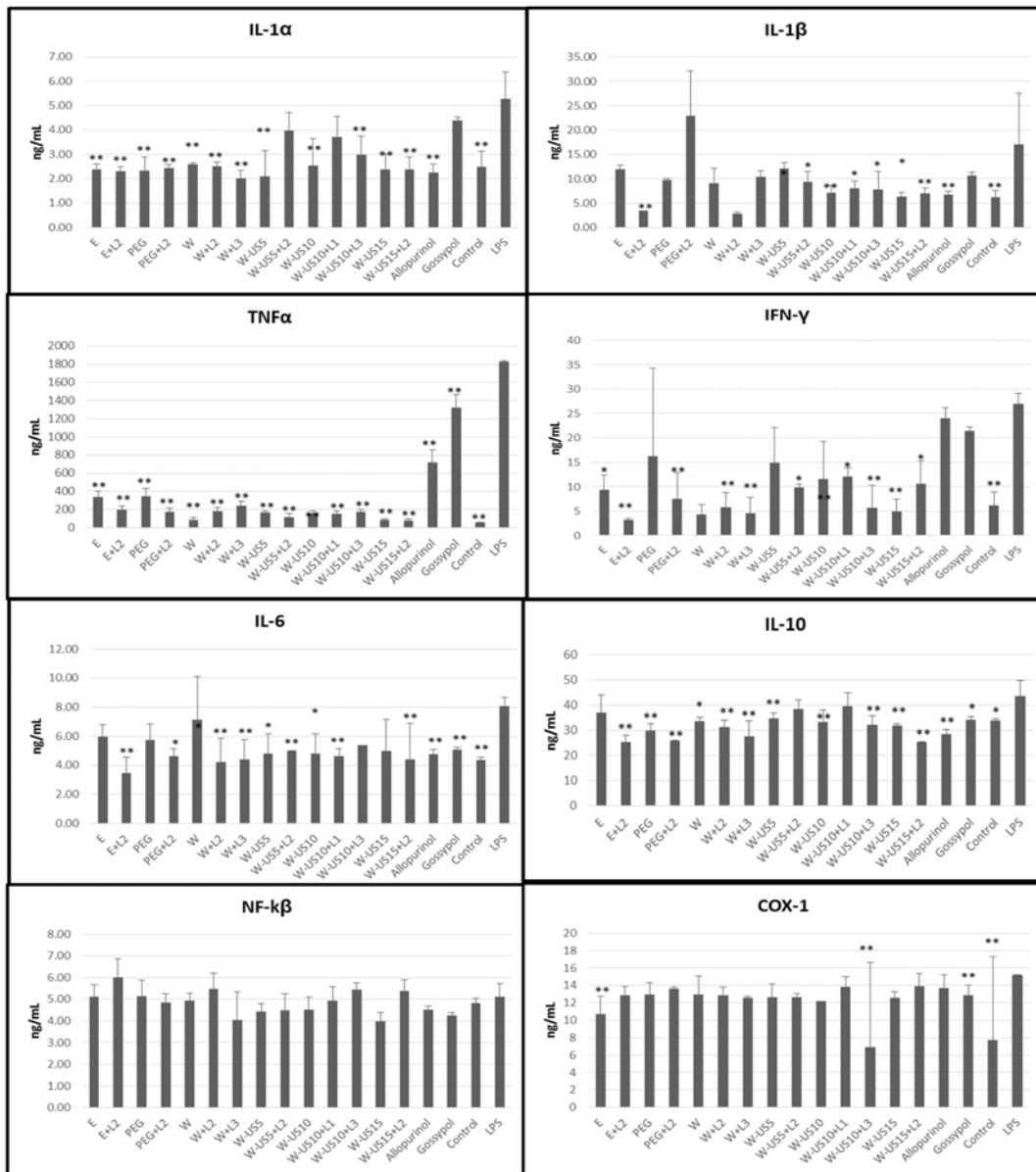
Figure 2. PC1 and PC2 correlation between phenolic compounds of propolis and inflammation markers *The first Principal component (PC1) is correlated positively with the phenols (kaempferol, DMEA-CA, cafeic acid, CAPE, trans-cinnamic acid, ferulic acid, miricetin, quercetin, and naringenin) and PC2 correlated is correlated with TNF-α, IFN-γ, IL-6, IL-1α, IL-1β, and COX-1.

DISCUSSION

When we evaluated the phenolic content, we observed that phenolic content of propolis from lowest to highest are as follows: Water+US10min+*L.plantarum* visbyvac < Ethanol+*L.plantarum* ATCC®8014 < Water+*L.plantarum* visbyvac < PEG+*L. plantarum* ATCC®8014 < Water+US15min+*L.plantarum* ATCC®8014. The highest phenolic content was in W+US5min, W+US10min, and W+US15min. Biologically transformed samples have had slightly lower total phenolic content due to a decrease in caffeic acid and DMEA by transformation process. Biologically trans-

formed samples have had slightly lower total phenolic content due to a decrease in caffeic acid and DMEA by the transformation process.

Propolis is one the most studied natural compounds due to its antioxidant, anti-inflammatory, and cytotoxic effects in many cell lines.[8,12,23−25] The authors observed that the phenolic content, antioxidant, and anti-cancer effects of propolis samples varied according to different factors including solvents used, preliminary extraction process, and collected regions.[26] In this study, we investigated the effect of the solvation procedure and biotransformation on the anti-inflammatory effect

of propolis in THP-1 cells. Generally, extraction procedures, i.e., solvents used, culture strains, and inoculum concentrations of *L. plantarum* affect the extracted amount of phenolic content and its anti-inflammatory activity, which has been shown by determining the levels of inflammatory cytokines in cell supernatants.

The IC_{50} levels of propolis samples changed between 160 µg/mL and 1000 µg/mL in the 24th h. The THP-1 cell line is commonly used as *in vitro* model in investigations on inflammatory processes.[3] It is well known that monocytes in a lesion area differentiate into macrophages, which release inflammatory cytokines. *In vitro* studies showed that THP-1 cells become activated by LPS and/or pro-inflammatory molecules. Chanput et al. observed that LPS-induced THP-1 cells released the cytokines such as IL-1β, IL-6, IL-8, IL-10, and TNF-α associated with inflammation.[3,27] THP-1 monocytes are transformed to macrophages in response to LPS induction, which is more effective than PMA induction.[27] It has been observed that propolis-treated LPS-activated macrophages were polarized to M1 phenotype, which has a role in producing pro-inflammatory cytokines and mediators (TNF-β, IL-1β, IL-6, IL-8, and IL-12) for immune defense against microorganisms.[1,3] In accordance with this data, elevation in different ratios of TNF-α, IL-1α, IL-1β, and IL-6 levels upon induction with LPS were determined in our study. All extracts of propolis decreased TNF-α levels to normal levels. Bueno-Silva et al. showed that Brazilian Propolis reduced the production of proinflammatory factors such as NO, IL-12, IL-1β, and GM-CSF, compared to only LPS-treated control macrophages.[28]

We observed a negative correlation between the TNF-α levels in cell line and the caffeic acid and ferulic acid content of propolis. Touzani et al. showed that propolis in a similar dose (250 µg/mL) to our study inhibited the TNF-α and IL-6 secretion down to control levels.[12] Girgin, et al. also assessed that propolis inhibited production of proinflammatory cytokines (IFN-γ and TNF-β).[29] Ethanolic extract of propolis suppressed production of IL-1α, IL-1β, IL-6, IL-12, and TNF-α in the J774A.1 macrophage cell line.[30,31] In our study, 4 extracts of propolis (dissolved in "water," in "ethanol+biotransformed with *L. plantarum* ATCC®8014," in "water+biotransformed with *L. plantarum* ATCC®8014," and in "water+sonicated 15 min+ biotransformed with *L. plantarum* ATCC®8014") were found to be the most effective in reducing all cytokine levels. Because of their phenolic content in terms of trans-cinnamic acid, kaempferol, ferulic acid, quercetin, and caffeic acid levels. These 4 extracts of propolis were found to be higher than those of other propolis samples (Figure 1).

Many authors have suggested that the main phenolic molecules, such as caffeic acid, caffeic acid phenyl ester, chrysin, kaempferol, quercetin, cinnamic acid, ferulic acid, and chlorogenic acid, in propolis are responsible for its anti-inflammatory activity.[15,25,32,33] According to our results, these

molecules might inhibit NFk-β pathway, NO signaling pathway, and COX-1/COX-2 expression. Although CAPE and phenyl esters of caffeic acid were asserted as the main anti-inflammatory molecules in propolis, they might lead to allergic reactions in susceptible subjects. Our data evidenced that propolis samples with lowered CAPE and/DMEA-caffeic acid levels by biological transformation showed anti-inflammatory activity in the same ratio with non-transformed propolis samples.

Bueno-Silva et al. proposed that propolis inhibited different pathways in inflammatory process: a) down regulation of IL-1β resulting in inhibition of IL-1β pathway and subsequent inhibition of NF-kβ pathway; b) reduced activation of MAPK pathway resulting in the reduction of IL-12 levels c) depletion of activation of PI3K/AKT pathway; d) inhibition of NO pathway resulting in low NO production and e) down-regulation of the expression of genes related to Toll-like receptor (TLR) response (Cd14, Elk1, Pik3cg, Tirap, and Tlr4).[28] In our study, propolis samples decreased the IL-1β levels but had no effect on NF-kβ, which has some the following logical explanations.[1] Exposure time to LPS and propolis and timing of sample collection might be important, because NF-kβ is produced in the early stages of inflammation and the studies showed that the peak of degradation occurred in the 30th min [9,31], so its level in the 2nd h of induction might decreased.[2] Nakayama et al. showed that TNF-like weak inducer of apoptosis (TWEAK) expression, which induces signaling cascades including the NF-kβ, MAPK, and AKT pathways, did not increase upon stimulation with LPS but increased with IFN-γ.[33] This observation might explain the non-effectiveness of LPS on NF-kβ levels in our study. It has been shown that ethanolic extract of propolis suppressed production and transcription of IL-1β and IL-6 by depletion in mRNA levels of IL-1β and IL-6 induced by LPS in RAW 264.7 cells and J744A.1 cells.[34,35] These effects of propolis are dependent on time and dose. It has been shown that pro-IL-1β levels increased 90 min after stimulation by LPS and ATP, and were released from cells in the 2nd h.[33] IL-1β induced production of IL-8, IL-6, TNF-α, and prostaglandin E2. In this study, IL1β levels increased up to 2 times accompanied by increases in TNF-α and IL-6 levels.

In our study, almost all propolis samples decreased IL-6 and IL-1β in the 2nd h, however, 4 of the propolis extracts (1. dissolved in Ethanol+biotransformed with *L. plantarum* ATCC®8014;" 2. "dissolved in water+sonicated 15 min and biotransformed with *L. plantarum* ATCC®8014;" 3. "dissolved in water and biotransformed with *L. plantarum* visbyvac;" and 4. "Dissolved in water and biotransformed with *L. plantarum* ATCC®8014") that returned IL-6 to normal levels were proposed as the most effective samples. It has been noted that IL-10 has an anti-inflammatory effect by inhibiting pro-inflammatory cytokines and by blocking NF-kβ activity.[33] The effect of propolis on IL-10 levels were conflicting in the literature due to the dose used and duration of treatment.[33,36]

In some studies, an increase was observed upon stimulation by LPS.[12,25] In accordance with these observations, we found a slight increase in IL-10 levels upon stimulation by LPS. The three extracts (1. dissolved in ethanol, 2. dissolved in water+biotransformed with *L. plantarum* ATCC®8014, and 3. dissolved in water+sonicated 10 min+biotransformed with *L. plantarum* ISLG-2 did not show any effect on IL-10 levels. All of these extracts of propolis have had a low concentration of naringenin followed by pelargonin, ellagic acid, vanillic acid, and myricetin. IL-10 levels showed negative correlation with trans-cinnamic acid (r=-0.495, p=0.072) and DMEA caffeic acid (r=-0.538, p=0.047) levels. Although there is no clear evidence on the suppressive effect of DMEA caffeic acid on IL-10, this correlation might suggest an inhibitory effect of DMEA caffeic acid. In regard to this explanation, low levels of DMEA caffeic acid in biologically transformed propolis samples might be an advantage to protect IL-10 levels while pro-inflammatory cytokine levels are decreasing. Touzani et al. also showed that treatment with propolis at concentrations of 125 µg/mL and 250 µg/mL increased the secretion of IL-10 compared to LPS-stimulated cells and suggested that the effect mechanism of propolis on IL-6 and TNF-α is mediated through by induction of IL-10 production.[12]

Two extracts of propolis (dissolved in PEG and dissolved in water+sonicated 5 min) did not show any effect on IFN-γ levels. All of these propolis samples have had a low concentration of naringenin followed by caffeic acid and ellagic acid. The negative correlation between naringenin levels and IFN-γ levels supported the inhibitory effect of naringenin during inflammation. In accordance with this, propolis dissolved in PEG (with or without biotransformation) has the lowest anti-inflammatory effect due to their low phenolic content, especially caffeic acid, pelargonidin, and naringenin.

Our study and the others showed that the anti-inflammatory activity of propolis is closely associated with its biologically active constituent, especially caffeic acid, kaempferol, ferulic acid, quercetin, and naringenin, which are found in different concentrations.[30,36,37] Although concentrations and type of active molecules in propolis samples varied with solvents and extraction procedures as well as collection season and region, it has been proposed that the anti-inflammatory activity of propolis is exacerbated with the synergistic and/or antagonistic effects of all these molecules.[10] Our study has also demonstrated for the first time that, biologically, transformation of propolis did not affect its anti-inflammatory activity in LPS-induced THP-1 cells.

CONCLUSION

We proposed that extracts of propolis (1) dissolved in water, (2) dissolved in ethanol+biotransformed with *L. plantarum* ATCC®8014, (3) dissolved in water+biotransformed with *L.*

plantarum ATCC®8014, (4) dissolved in water+sonicated 15 min, and biotransformed with *L. plantarum* ATCC®8014 have the highest anti-inflammatory activity. Since the biotransformation process did not affect propolis's anti-inflammatory activity, it can be used as a reliable agent for allergic subjects. It should be noted that it is crucially important to determine the biologically active molecule content to get the beneficial effect on health.

ORCID IDs of the authors

Burak Durmaz	0000-0002-5285-3641
Latife Merve Oktay Celebi	0000-0002-7110-3379
Hikmet Memmedov	0000-0002-8012-0445
Nur Selvi Gunel	0000-0003-0612-2263
Hatice Kalkan Yildirim	0000-0001-9698-9682
Eser Yildirim Sozmen	0000-0002-6383-6724

REFERENCES

1. Tan HY, Wang, N Lis, Hong M, Wang, X, Feng Y. The reactive oxygen species in macrophage polarization: Reflecting its dual role in progression and treatment of human diseases. *Oxid Med Cell Longev*. 2016;2795090. doi:10.1155/2016/2795090

2. Hausen BM, Wollenweber E, Senff H, Post B. The sensitizing properties of 1,1-dimethylallyl caffeic acid ester. *Propolis Aller (II)*. 1987;17(3):171-177.

3. Chanput W, Mes J, Vreeburg RAM, Savelkoul HFJ, Wichers HJ. Transcription profiles of LPS-stimulated THP-1 monocytes and macrophages: A tool to study inflammation modulating effects of food-derived compounds. *Food Funct*. 2010;1(3):254–261.

4. De Mendonca ICG, Porto ICC de M, do Nascimento TG, de Souza NS, Oliveira JM, Arruda RE dos S. Brazilian red propolis: Phytochemical screening, antioxidant activity and effect against cancer cells. *BMC Complement Altern Med*. 2015;15:357. doi:10.1186/s12906-015-0888-9

5. Chen L, Deng H, Cui H, et al. Inflammatory responses and inflammation-associated diseases in organs. *Oncotarget*. 2018;9(6):7204-7218.

6. Italiani P, Boraschi D. From monocytes to M1/M2 macrophages: Phenotypical vs. functional differentiation. *Front Immunol*. 2014;5:514. doi:10.3389/fimmu.2014.00514

7. Ahn MR, Kunimasa K, Kumazawa S, et al. Correlation between antiangiogenic activity and antioxidant activity of various

components from propolis. *Molecular Nut Food Res.*2009;53(5): 643–651.

8. Bankova V, Popova M, Trusheva B. Propolis volatile compounds: Chemical diversity and biological activity: A review. *Chem Cent J.* 2014;8:28. doi:10.1186/1752-153X-8-28

9. Sabbione AC, Luna-Vital D, Scilingo A, Añónb MC, Mejía EG. Amaranth peptides decreased the activity and expression of cellular tissue factor on LPS activated THP-1 human monocytes. *Food Funct.* 2018;9:3823-3834.

10. Walgrave SE, Warshaw EM, Glesne LA. Allergic contact dermatitis from propolis. *Dermatitis.* 2015;16:209–215.

11. Chanput W, Mes JJ., Wichers HJ. THP-1 cell line: An in vitro cell model for immune modulation approach. *Int Immunopharmacol.* 2014;23:37–45.

12. Touzani S, Embaslat W, Imtara H, et al. *In vitro* evaluation of the potential use of propolis as a multitarget therapeutic product: Physicochemical properties, chemical composition, and immunomodulatory, antibacterial, and anticancer properties. *Biomed Res Int.* 2019;2019:4836378. doi:10.1155/2019/4836378

13. Basista-Sołtys K. Allergy to propolis in beekeepers-A literature review. *Occup Med Health Aff.* 2013;1-105.

14. Alliboni A, D'Andrea A, Massanisso P. Propolis specimens from different locations of central Italy: Chemical profiling and gas chromatography-mass spectrometry (GC-MS) quantitative analysis of the allergenic esters benzyl cinnamate and benzyl salicylate. *J Agric Food Chem.* 2011;59(1):282–288.

15. Borrelli F, Maffia P, Pinto L, et al. Phytochemical compounds involved in the anti-inflammatory effect of propolis extract. *Fitoterapia.* 2002;73:53-63.

16. Galeotti F, Maccari F, Fachini A., Volpi N. Chemical composition and antioxidant activity of propolis prepared in different forms and in different solvents useful for finished products. *Foods.* 2018;7(3):41. doi:10.3390/foods7030041

17. Chanput W, Mes JJ, Wichers HJ. THP-1 cell line: An in vitro cell model for immune modulation approach. *Inter Immunopharmaco.* 2014;23:37–45.

18. Memmedov H., Oktay LM., Durmaz B. et al. Propolis prevents inhibition of apoptosis by potassium bromate in CCD 841 human colon cell. *Cell Biochem Func.* 2020; 38(4):510-519.

19. Aldemir O, Yıldırım HK, Sozmen, EY. Antioxidant and antiinflammatory effects of biotechnologically transformed propolis. *J Food Process Preserv.* 2018;42(6):e13642. doi:10.1111/jfpp.13642

20. Woo KJ, Jeong YJ, Inoue H, Parka JW, Kwon TK. Chrysin suppresses lipopolysaccharide-induced cyclooxygenase-2 expression through the inhibition of nuclear factor for IL-6 (NF-IL6) DNA-binding activity. *FEBS Letters*. 2005;579:705–711.

21. Yıldırım HK, Canbay E, Öztürk Ş, Aldemir O, Sözmen EY. Biotransformation of propolis phenols by L. plantarum as a strategy for reduction of allergens. *Food Sci Biotechnol.* 2018;27(6):1727-1733.

22. Öztürk Ş, Durmaz B, Memmedov, H, et al. Effect of ferulic acid on cytokine release in human leukemia monocytic cells induced with lipopolysaccharides. *Ege J Med.* 2021:60(1):39-50.

23. Memmedov H, Oktay LM, Durmaz B, Günel NS, Yıldırım HK, Sözmen EY. Propolis prevents inhibition of apoptosis by potassium bromate in CCD 841 human colon cell. *Cell Biochem Func.* 2020;38(4):510-519.

24. Ferreres F, Gomes NGM, Valentão P. Leaves and stem bark from Allophylus africanus P. Beauv: An approach to anti-inflammatory properties and characterization of their flavonoit profile. *Food Chem Toxicol.* 2018;118:430-438.

25. Rajendran P, Rengarajan T, Natarajan N, Rajendran P, Yutaka N, Ikuo N. Kaempferol, a potential cytostatic and cure for inflammatory disorders. *Eur J Med Chem.* 2014;86:103-112.

26. Touzani S, Embaslat W, Imtara H, et al. In vitro evaluation of the potential use of propolis as a multitarget therapeutic product: Physicochemical properties, chemical composition, and immunomodulatory, antibacterial, and anticancer properties. *BioMed Res Int.* 2019;2019:4836378. doi:10.1155/2019/4836378

27. Lund ME, To J, O'Brien BA, Donnelly S. The choice of phorbol 12-myristate 13-acetate differentiation protocol influences the response of THP-1 macrophages to a pro-inflammatory stimulus. *J Immunol Methods.* 2016;430:64-70.

28. Bueno-Silva B, Kawamoto D Ando-Suguimoto E, et al. Brazilian red propolis attenuates inflammatory signaling cascade in LPS activated macrophages. *Plos One.* 2015;10(12): e0144954. doi.org/10.1371/journal.pone.0144954

29. Castro C, Mura F, Valenzuela G, et al. Identification of phenolic compounds by HPLC-ESI-MS/MS and antioxidant activity from Chilean propolis. *Food Res Int.* 2014:64:873-879.

30. Giambartolomei GH, Dennis VA, Lasater BL, Murthy PK, Philipp M.T. Autocrine and exocrine regulation of interleukin-10 production in THP-1 cells stimulated with *Borrelia burgdorferi* lipoproteins. *Infect Immun.* 2002;70(4):1881–1888.

31. Bachiega TF, Orsatti CL, Pagliarone AC, Sforcin JM. The effects of propolis and its isolated compounds on cytokine production by murine macrophages. *Phytother Res.* 2012;26:1308–1313.

32. Silva JC, Rodrigues S, Fes X, Estevinho LM. Antimicrobial activity, phenolic profile and role in the inflammation of propolis. *Food Chem Toxicol.* 2012;50(5):1790–1795.

33. Nakayama M, Kayagaki N, Yamaguchi N, Okumura K, Yagita H. Involvement of TWEAK in interferon gamma-stimulated monocyte cytotoxicity. *J Exp Med.* 2000:192(9):1373–1380.

34. Ribeiro MNS, Nascimento FRF. Mechanisms of action underlying the anti- inflammatory and immunomodulatory effects of propolis: A brief review. *Braz J Pharmacogn.* 2012;22(1):208–219.

35. Paracatu LC, Quinello CM, Faria G. Caffeic acid phenethyl ester: Consequences of its hydrophobicity in the oxidative functions and cytokine release by leukocytes. *Evid Based Complement Alternat Med.* 2014;2014:793629. doi:10.1155/2014/793629

36. Szliszka E, Kucharska AZ, Sokół-Łtowska A, Mertas A, Czuba ZP, Król W. Chemical composition and anti-inflammatory effect of ethanolic extract of Brazilian green propolis on activated J774A.1 macrophages. *Evid Based Complement Alternat Med.* 2013;2013:976415. doi:10.1155/2013/976415

37. Burdock GA. Review of the biological properties and toxicity of bee propolis (propolis). *Food Chem Toxicol.*1998;36:347-363.

How cite this article

İSTANBUL
UNIVERSITY
— P R E S S —

RESEARCH ARTICLE

The Effect of Culture Dimensionality and Brain Extracellular Matrix in Neuronal Differentiation

Duygu Turan Sorhun[1], Ece Ozturk[1,2]

[1]Koç University, Research Center for Translational Medicine (KUTTAM), Engineered Cancer and Organ Models Laboratory, Istanbul, Turkiye
[2]Koç University, Faculty of Medicine, Department of Medical Biology, Istanbul, Turkiye

ABSTRACT

Objective: Neuroblastoma cells are frequently used in neuroscience studies due to their human origin and ability of extensive propagation compared to animal-derived primary neuron cultures. Although they are tumor-derived, they exhibit neuronal differentiation capability in the presence of several agents including retinoid acid. Several studies have quested for successful differentiation protocols and faithful representation of neuronal characteristics. However, they predominantly pursued conventional two-dimensional (2D) cultures where the role of three-dimensional (3D) tissue microenvironment and cell-matrix interactions remained unknown. In this study, we investigated the effect of culture dimensionality and native brain extracellular matrix (ECM) on neuronal differentiation of neuroblastoma cells.

Materials and Methods: Decellularized brain ECM hydrogels offer a physiologically relevant *in vitro* 3D culture platform with the representation of key biochemical and biophysical aspects of the native tissue microenvironment for modeling cellular processes. We cultured SH-SY5Y cells on 2D or as encapsulated in 3D decellularized brain ECM hydrogels and assessed them for morphological shift, neurite extension, and expression of neuronal, synaptic, astrocytic, cholinergic, stemness, proto-oncogene and neuropathological markers.

Results: Our findings demonstrate that the 3D brain ECM microenvironment distinctly affects the differentiation process compared to conventional culturing. In 3D ECM, neuronal differentiation occurred as in 2D, with upregulation of neuronal markers, change in cell morphology, and promotion of neurite extension. However, during differentiation, maintenance of stemness was observed in a 3D-specific manner. Furthermore, 3D differentiation promoted significant upregulation of astrocytic and synaptic markers which was not observed in 2D.

Conclusion: This study highlights the importance of physio-mimetic 3D brain models.

Keywords: Neuronal differentiation, extracellular matrix, brain tissue engineering, decellularization, hydrogels

INTRODUCTION

The extracellular matrix (ECM) is the primary non-cellular component in all tissues.[1] Three-dimensional (3D) tissue models with the capability of representing the native ECM offer advantages over conventional, two-dimensional (2D) culturing and enable cell-matrix interactions. Decellularization is a widely used technique for the fabrication of 3D tissue models with the preservation of native ECM composition.[2] In the process, cellular content is efficiently removed and the remaining ECM is solubilized with enzymatic digestion which allows for temperature and pH-induced reconstitution into hydrogel form.[3,4] Decellularization of native brain tissues has been successfully demonstrated from sources including porcine and human for use in neuroscience and brain tissue engineering fields.[5,6] Lack of brain ECM ligands in 2D culture models has been emphasized for the insufficient responses in modeling processes such as neuronal differentiation, maturation, and synaptogenesis.[7,8] ECM-instructed cell signaling is known to modulate cell behavior in neurodevelopment, homeostasis, and neurodegeneration.[9–11] Therefore, understanding the role of cell-matrix interactions in neural cell behavior is still a viable aspiration in the field.

The human neuroblastoma cell line, SH-SH5Y, is a subcloned epithelial cell line from SK-N-SH, which originated in 1970 from a metastatic bone tumor retrieved from a 4-year-old female patient.[12] SH-SH5Y is frequently used in *in vitro* neu-

roscience studies due to its human origin, ease of expansion, and neuronal differentiation capability.[13] Optimal neuronal differentiation requires obtaining a homogeneous cell population with moderate levels of neurotransmitter production.[5] Cellular proliferation is an important sign of immature phenotype and proliferation is expected to decrease significantly following differentiation.[14] For this purpose, one of the main approaches in differentiation protocols is the gradual decrease of serum in the growth medium from 10% to generally 2.5%.[15] On the other hand, starved cells are mostly supported with neurotrophic elements such as N2, B-27, retinoic acid (RA), brain-derived neurotrophic factor (BDNF), and potassium chloride (KCl).[16] RA, a form of vitamin A, has a key role in the differentiation of neuroblastoma cells into dopaminergic neurons by its interplay in the arrest of the cell cycle, elevated levels of cyclin-dependent kinase (CDK) inhibitors and anti-apoptotic proteins, and its promoting role in PI3K/AKT signaling cascade.[17] N2 supplement contains compounds such as insulin, transferrin, and selenium, which are formulated as 'Bottenstein's N-1 formulation' [18] and it promotes differential signaling at early stages. B-27 protects neuronal cells with the promotion of cell survival and inhibition of glycolysis.[19] The combination of these, including deprivation of serum and administration of neurotrophic factors, results in the negative selection of epithelial cells from the population, while differentiated mature neurons are expanded. According to the differentiation regime applied, different neuronal subtypes can be achieved including adrenergic, cholinergic, and dopaminergic neurons.[20] Differentiated neuroblastoma cells, which are phenotypically closer to primary neurons, have reduced proliferation rate, polarized cell structure, and long extended axons in connection with surrounding cells.[16]

Several molecular markers take an important role in the assessment of neuronal differentiation. Microtubule-associated protein family members play essential roles in both neuromorphogenic processes and neurodegenerative disease progression. Microtubule-associated protein 2 (MAP2) is responsible for stabilizing dendrites during neurogenesis, as well as guiding the coordination for the reconstruction of microtubules and F-actin proteins during neurite initiation.[21] While MAP2 is localized to the cell soma and dendrites, another microtubule-associated protein, TAU, is found in axonal regions, with both proteins having similar functions in promoting microtubule rigidity during dynamic cellular events within neuronal cells.[22] Class III beta-tubulin (TUBB3), also known as Tuj1, is another marker localized in the neuronal cytoskeleton and increased expression of TUBB3 is present in the early stages of neuronal differentiation with implications in axonal maturation. [23]

NEUN, a neuronal nuclei marker, is localized within the postmitotic neuronal nuclei and perinuclear cytoplasm beyond the previously mentioned cytoskeletal markers. Its expression is pronounced in neuronal nuclear areas, where low chromatin density with loosely packed DNA is present.[24] Synaptophysin (SYP), an integral membrane protein, was one of the first mark-

ers used to detect a neuronal cell. It regulates synaptic vesicle endocytosis and neurotransmitter release, which are crucial for neuronal cell communication within an organism.[25,26] The most prevalent neuronal differentiation marker retrieved from a stem cell perspective is SRY-box transcription factor 2 (SOX2). Studies have shown that the constitutive expression of SOX2 prevents terminal neuronal differentiation, resulting in intact progenitor features. Concordantly, downregulation of SOX2 expression is necessary during neuronal differentiation.[27] Ret proto-oncogene (RET) is an unusual marker of early neuronal differentiation and has an impact on neural crest development. Studies have shown that RET is upregulated during differentiation following RA treatment.[14,28,29]

Apart from the neuronal maturation markers, there are also genes and proteins which regulate the formation of neuronal subtypes, including dopaminergic, cholinergic, serotonergic, etc. neurons. Choline O-acetyltransferase (CHAT) is a gene required for the production of enzymes that synthesize the neurotransmitter acetylcholine, which completes the functionality of the cholinergic neurons.[30] In addition to neuronal markers, other markers regarding oligodendrocytes or glial cells are also important for the characterization of differentiated cells. Glial fibrillary acidic protein (GFAP) is an intermediate filament-III protein and is present in astrocytes in the central nervous system, non-myelinating Schwann cells in the peripheral nervous system, and enteric glial cells.[31]

Amyloid-beta precursor protein (APP) and presenilin 1 (PSEN1) are mostly studied for their pathological role in Alzheimer's disease and their physiological role is not completely understood. However, APP has been suggested to play an important role in synaptic plasticity and brain development. In particular, it guides the growth of axons, regulates dendritic morphology, and promotes early nervous system development.[32] PSEN1 is a component of the gamma-secretase enzyme responsible for the cleavage of APP with a possible role in calcium metabolism and signaling of Notch, and β-catenin along with APP.[33]

In this study, we aimed to investigate the role of culture dimensionality and brain ECM in neuronal differentiation of SH-SH5Y cells. To create a 3D brain tissue model, we fabricated decellularized brain ECM (db-ECM) hydrogels from bovine donors which we encapsulated with neuroblastoma cells. We compared the differentiation of cells in 3D db-ECM hydrogels to conventional 2D culturing regarding changes in morphology and expression of the abovementioned molecular markers.

MATERIALS AND METHODS

Decellularization

Fresh bovine brains removed from calves were delivered in a sealed container and placed on ice during transportation

from a local slaughterhouse. The brains were rinsed with 2% Penicillin-Streptomycin (P/S) containing distilled water (dH$_2$O) and the cerebellum was carefully disjoined. The cortex was meticulously sliced into small pieces (1×1×1cm^3) using a scalpel and scissors.

DeQuach et al.'s decellularization method was adapted for the decellularization of bovine brain tissues with minor modifications.[5] The dissected brain cortex tissues were treated with 0.1% (w/v) sodium dodecyl sulfate (SDS) in phosphate-buffered saline (PBS) solution containing 1% P/S placed in a beaker on a magnetic stirrer for 4 days. The solution was renewed each day. Followingly, 40 U/ml DNAse was applied for 2 h in 10 mM magnesium chloride (MgCl$_2$) buffer (pH 7.5). The viscous slurry was subdivided into falcon tubes and sequentially centrifuged at 10,000 rpm for 5 min before being rinsed with dH$_2$O in each centrifugation step. The leftover tissue pieces were kept at -80°C until lyophilization and a fragment of the decellularized tissue was saved for histological investigation. The tissue samples underwent lyophilization until they were dried entirely.

db-ECM Hydrogel Generation

Brain tissues that had been decellularized and lyophilized were cryo-milled into powder form. Then, 1 mg/ml pepsin in 0.1M hydrochloric acid (HCl) was used to digest powdered db-ECM for 24 h at room temperature at constant rotation. The total digest solution was then centrifuged at 13,000 rpm for 10 min to collect the solubilized form. The pH was then brought up to 7.4±0.2 by neutralizing the solubilized db-ECM on ice with sodium hydroxide. Hydrogel formation was achieved by incubating the neutralized and solubilized db-ECM at 37 °C for 40 min.

Histological Examination

The preserved wet tissue samples were used for histological and nuclear content examination. 3.7% formaldehyde solution was used to fix native and decellularized brain tissues overnight at 4°C. Before cryo-sectioning, the fixed samples were covered with OCT and frozen. Then, 10 µm cryo-sections were collected on glass slides. To indicate nuclear content, slides were first hydrated, then stained with 1 µg/ml Hoechst solution (Invitrogen) in PBS for 15 min. DNA content was visualized with fluorescence microscopy. To examine the structural changes between decellularized and native bovine brain tissues, Haematoxylin & Eosin staining was applied. First, slides were hydrated, then stained with Mayer's Haematoxylin for 3 min, and washed for 3 min with tap water. Slides were then treated with 95% ethanol for 45 sec and stained with Eosin alcoholic solution. All slides were dehydrated, mounted, and closed with a coverslip before being examined under a light microscope.

Cell Culture

The human neuroblastoma cell line SH-SY5Y (ATCC, CRL-2266TM) was grown in Dulbecco's Modified Eagle Medium (DMEM) containing 4.5 g/L glucose, 10% heat-inactivated fetal bovine serum (FBS), and 1% P/S. Cells were incubated at 37°C and 5% CO$_2$, passaged when they reached sufficient confluency (80%), and the growth medium was replaced every other day.

Phalloidin/DAPI Staining of Neuroblastoma Cells Encapsulated in db-ECM

SH-SY5Y cells were harvested and embedded in decellularized brain hydrogels at a concentration of 5x10^5 cells/ml, and after 5 days of incubation, fixation was done with 4% paraformaldehyde (Sigma). The gels were permeabilized by treating them with 0.1% Triton X-100 in PBS for 1 h at room temperature. After that, blocking was carried out with a 1% solution of bovine serum albumin (BSA) (Sigma, A2153) containing 10% goat serum for 2 h. The samples were stained with Phalloidin-FITC (Abcam) and 4',6-diamidino-2-phenylindole (DAPI, Sigma), and imaging was performed with Leica DMI8/SP8 laser scanning confocal microscope. Images were exported from the LAS X program (Leica, Wetzlar, Germany).

Neuronal Differentiation

For 2D experiments , SH-SY5Y cells were seeded onto a 6-well plate at a density of 30,000 cells/well. For 3D experiments, cells were encapsulated into db-ECM hydrogels at a density of 1.6 x 10^5 cells/ml. For this purpose, lyophilized db-ECM digest was thawed in DMEM high glucose medium with 1% PSA and 50 µg/ml Fungin. Cells were resuspended in a complete medium and mixed thoroughly with db-ECM by pipetting. Immediately, the pre-gel was plated on a 24-well plate and incubated at 37°C for 45 min to allow gelation. Then, 600 µl complete medium was carefully added into each well. During differentiation, FBS content was gradually decreased from 10% to 2.5%, and 10 µM RA (Sigma, #R2625) with 2 mM L-Glutamine (Biowest, #X0550-100) was added to the medium. After reaching day 9, the differentiation medium was switched to neurobasal medium (GibCo, #A35829-01) containing 2.5% FBS, 1% P/S, 10 µM RA, 2 mM L-Glutamine, 1X N-2 (Gibco, #17502), 1X B-27 Plus supplement (Gibco, #A35828-01) and 20 mM KCl (Sigma, P9333). At the end of the differentiation procedure, hydrogels were either collected for the extraction of RNA or fixed with 4% paraformaldehyde for immunostaining.

RNA Isolation and cDNA Synthesis

RNA extraction was applied following the manufacturer's instructions led by the NucleoSpin®-RNA isolation kit (Macherey-Nagel). For 3D samples, gels were homogenized in

RA1 buffer supplied by the kit and were centrifuged at 14,000 xg for 5 min to remove the debris. Ethanol was added to the supernatant and mixed well by vortexing followed by centrifugation at 14,000 xg for 10 min at 4°C. Supernatant was discarded and the pellet was air-dried. After resuspension of the pellet, the instructions were followed accordingly which include RNA binding, membrane desalting, DNA digestion, purification, and elution. The quantity and quality of the eluted RNA were evaluated with NanoDrop Spectrophotometer (Thermo Scientific 2000c, USA). The purified RNA was then reverse-transcribed into cDNA. First, random hexamer, 1 µg RNA, 10 mM dNTP-mix, and distilled water were mixed. After incubation at 65°C for 5 min, the second mixture including 5x First strand buffer, 100 mM DTT, and Ribonuclease Inhibitor (40 U/µl) were added to each sample. The samples were incubated at 37°C for 2 min and M-MLV RT enzyme (200 U) was added. The incubation steps for synthesis were as following: 25°C for 10 min, 37°C for 50 min, and 70°C for 15 min. The synthesized cDNA was then diluted 1:5 in RNase-free H_2O.

Gene Expression Analysis

Neuronal development-related gene expressions were quantified relatively by qRT-PCR. The primers were designed using Primer™ and sequences are shown in Table 1. QuantiNova SYBR Green PCR Master Mix (Qiagen, #172034345), forward and reverse primers, cDNA sample, and PCR grade H_2O were mixed for the reaction of each experimental group and transferred to the PCR plate. Reaction cycles were carried out by Roche's LightCycler 480 Instrument II. The mRNA expression levels (depicted as Cq values) of the related genes were normalized to a housekeeping control gene (GAPDH), and fold change was calculated using the $2^{-\triangle\triangle Ct}$ method.

Immunostaining with Neuronal Markers

SH-SY5Y cells encapsulated in db-ECM hydrogels at a concentration of $5x10^5$ cells/ml and 2D cultured cells for both undifferentiated control and the differentiated group were fixed with 4% paraformaldehyde (Sigma, 158127-500G) at day 15. Similarly, permeabilization with 0.1% Triton X-100 in PBS was done for 1 h at room temperature for 3D culture and 15 min for 2D culture. Then, blocking was carried out with 1% BSA solution including 22.52 mg/ml glycine in PBS-T for 2 h for 3D culture and 30 min for 2D culture. Primary antibodies anti-NEUN (Abcam, ab177487) and anti-Beta-Tubulin III (Biolegend, #801213) were used for immunostaining. After overnight incubation at 4°C in constant rotation, secondary antibodies Alexa Fluor 488 goat anti-mouse IgG (H+L) (Invitrogen, A11029) and Alexa Fluor 594 goat anti-rabbit (Invitrogen, R37117) were applied in dark. Nuclear counterstaining was done with DAPI and images were taken with Leica DMI8/SP8 laser scanning confocal microscope. Images were exported from the LAS X program (Leica, Wetzlar, Germany).

Image analysis was achieved using ImageJ software (National Institutes of Health, USA).

Statistical Analysis

The quantitative data was stated as mean±S.D values resulting from minimum n=3 replicates. One sample t-test was applied to the experimental data using Graph-Pad Prism 8 software. P values smaller than 0.05 were considered statistically significant ($p<0.0001$=extremely significant (****), $0.0001<p<0.001$=extremely significant (***), $0.001<p<0.01$=very significant (**), and $0.01<p<0.05$=significant (*)).

RESULTS

Generation of Decellularized Brain ECM Hydrogels

The cortex of the bovine brain was cut into small pieces and treated with SDS and DNase to achieve decellularization. After decellularization, the wet tissue was lyophilized and cryomilled. Then, the powder form of the db-ECM was solubilized through digestion with the pepsin enzyme. The soluble part of the digest was neutralized, and gelation was achieved through temperature-induced crosslinking (Figure 1a). As shown in Figure 1b, the decellularization process resulted in changes in the tissue composition, and decellularized tissue represented fiber-like structures when compared to native tissue. Decellularization was validated with Hoechst staining, while nuclear elimination was completely achieved in the decellularized tissue. To encapsulate SH-SY5Y cells in db-ECM hydrogels, cells were blended with neutralized brain ECM digest at designated concentrations and incubated at 37°C (Figures 1c and d). Upon gelation, db-ECM hydrogels with SH-SY5Y cells were cultured for 5 days to assess the cytocompatibility of the reconstituted native matrix. Phalloidin/DAPI staining demonstrated optimal cell growth in 3D and typical morphology of SH-SY5Y cells (Figure 1c).

Differentiation of Neuroblastoma in 2D and 3D Conditions

Differentiation protocol was applied to neuroblastoma cells for 17 days and the procedure included two differentiation phases (Figures 2a and b). In the first phase, serum content was gradually decreased within the DMEM high glucose medium containing RA, while in the second phase, the cells were cultured in a neurobasal medium containing various indicated neurotrophic factors (Figure 2b). Cellular morphology was carefully monitored with brightfield microscopy during the differentiation protocol optimization. The brightfield images taken at the end of differentiation, on day 17, were shown in Figure 2c. Significant reduction in cell growth was observed in differentiated cells both in 2D and 3D conditions, a well-established indication for differentiated neuroblastoma.[14,34] Apart from reduced cell proliferation, the morphology of the cells remarkably changed in

Table 1. Gene-specific primers used in qRT-PCR.

Gene	Forward primer (5'-3')	Reverse primer (5'-3')
APP	ATGGTAATGCTGGCCTGCTG	GAATCCCACTTCCCATTCTG
CHAT	GAGGAGCAGTTCAGGAAGAG	CCAGGAGTTTCTGCTGCAGG
GAPDH	CTGACTTCAACAGCGACACC	GTGGTCCAGGGGTCTTACTC
GFAP	CCAGTTATCAGGAGGCGCTG	TCCTGGTACTCCTGCAAGTG
MAP2	CTGTAGCAGTCCTGAAAGGTG	CTGTTCTGAGGCAGGTGATG
MAP1	TTAGCAACGTCCAGTCCAAG	TCAGGTCAACTGGTTTGTAG
PSENİ	AGTATCCTCGCTGGTGAAGAC	ACGAAACAGGCTATGGTTGTG
RET	ACCATGGGCGACCTCATCTC	CTGCCAAGTCCCGATGAACG
S0X2	CTTTTATGAGAGAGATCCTG	ACCGTACCACTAGAACTTT
SYP	GCTGTGTTCGCCTTCATGTG	AATGTTCTCTGGGTCTGTGG
TUBB3	GAGCGGATCAGCGTCTACTAC	GCGGACACTGTCCATGGTTC

2D and 3D conditions. In 2D, differentiated cells displayed elongated axons creating a synaptic network, while the cell body became smaller in size. In 3D culture, the encapsulated naïve cells in the control group were inclined to form round cell clump masses. On the other hand, differentiated cells in 3D tended to form neurites towards nearby cells across the hydrogel without forming cell clusters (Figure 2c).

Gene Expression in Differentiated Neuroblastoma

Next, we assessed the gene expression profile of differentiating neuroblastoma with qRT-PCR for 2D (Figure 3) and 3D (Figure 4) conditions to reveal the differences in molecular markers upon change in culture dimensionality. *TUBB3*, a mature neuron marker, is upregulated upon differentiation in SH-SY5Y cells encapsulated in both 3D db-ECM hydrogels and conventional 2D culturing. Expression of *CHAT*, a cholinergic neuron marker, was also significantly increased. Unexpectedly, *MAP2*, a gene responsible for neurogenesis, exhibited a small but significant decrease in gene expression upon differentiation in both conditions. Although the expression profile of neuronal markers was correlated for 2D and 3D, another set of genes showed different trends in response to differences in culture dimensionality during the differentiation of SH-SY5Y cells. Expression of *SOX2*, a stemness marker, was significantly decreased in SH-SY5Y cells differentiated on 2D in comparison to the non-differentiated control group (Figure 3). However, in 3D db-ECM hydrogels, cells maintained their stemness despite induction of differentiation and gene expression of *SOX2* remained unaltered (Figure 4). Similarly, the *MAPT* gene was significantly downregulated during differentiation in 2D whereas in 3D, its expression was unchanged. A proto-oncogene involved in neuronal differentiation, *RET*, exhibited a 2.64-fold increase in gene expression in cells following differentiation on 2D while in 3D, differentiation did not affect its expression. Interestingly, differentiation of SH-SY5Y cells in 3D db-ECM hydrogels significantly induced astrocytic (*GFAP*) and synaptogenesis (*SYP*)

markers as opposed to 2D conditions in which expression of these genes did not demonstrate change. On the other hand, the differentiation protocol did not cause any change in the expression of neuropathological markers *APP* and *PSEN1* in either condition.

Evaluation of Neuronal Markers with Immunostaining in Differentiated Cells

To further evaluate the structural and morphological changes in differentiated SH-SY5Y cells in 2D and 3D cultures, protein expression of neuronal nuclei marker NEUN and mature neuron marker beta-tubulin III (TUBB3) was assessed with immunostaining. As shown in Figure 5, in 2D cultures, the number of cells in the differentiation group was reduced distinguishably concomitant with the emergence of elongated axons and TUBB3 expression. On the other hand, in 3D db-ECM hydrogels, a drastic change in morphology was observed (Figure 6). In non-differentiated cells in hydrogels, cell growth demonstrated clump formation, typical for cancerous cell lines. However, in the differentiated cells in 3D, a clear morphological shift was observed with the formation of a neuronal synaptic network alongside the expression of neuronal markers (Figure 6).

DISCUSSION

The neuroblastoma cell line is a preferred model for studying neurodegenerative diseases *in vitro* due to its human origin and ability for expansion and neuronal differentiation. However, the role of culture dimensionality and tissue-specific ECM in the differentiation of neuroblastoma cells has been unknown. A 3D microenvironment offers several advantages such as providing a physiologically relevant matrix that closely mimics the native tissue and enabling cell behavior and functionality observed *in vivo*. Furthermore, mechanical matrix parameters such as stiffness and viscoelasticity can be finely tuned.[5,35−37] In this study,
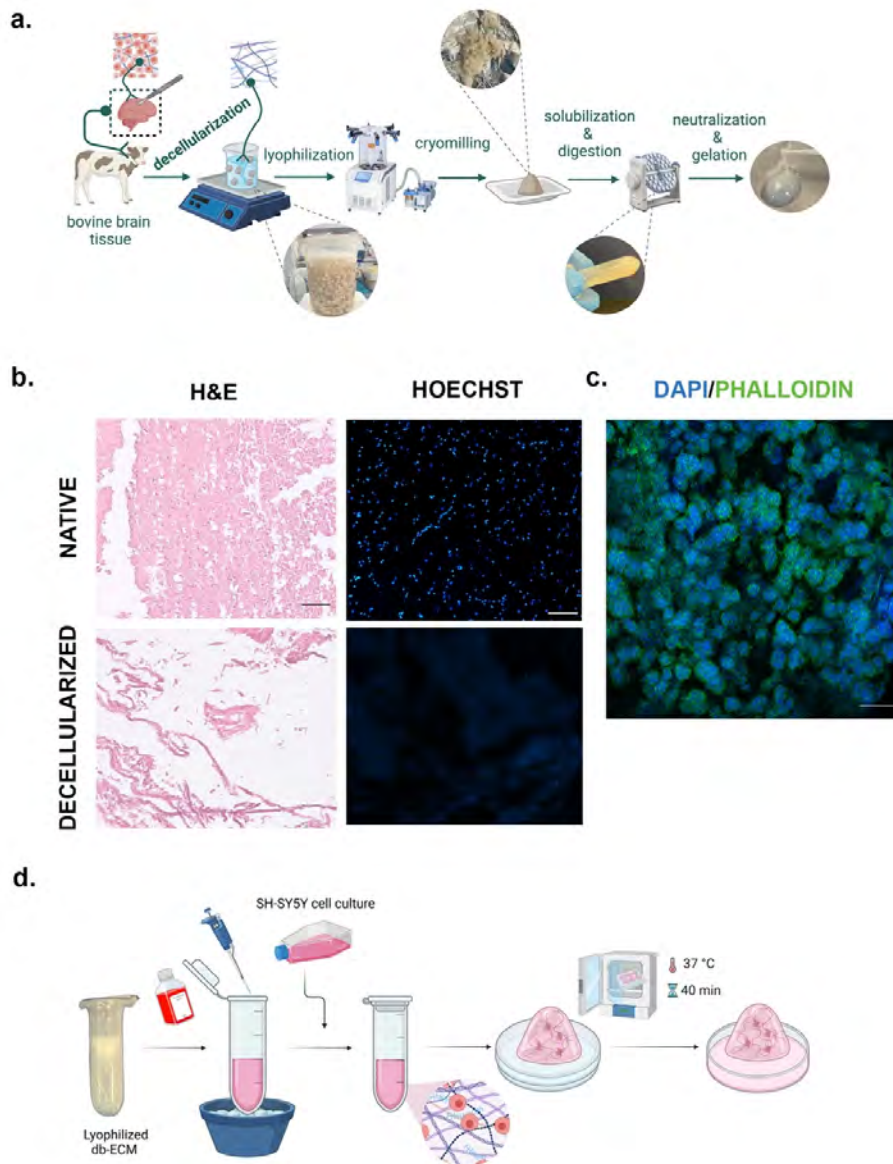
Figure 1. Decellularization of bovine brain tissue and hydrogel generation. a) Schematic description of hydrogel generation derived from decellularized bovine brain tissue (Created with BioRender.com). b) Histological examination of native bovine brain tissue and decellularized bovine brain tissue by H&E staining and Hoechst staining (scale bar: 100μm). c) Phalloidin and DAPI staining applied to SH-SY5Y cells in a 3D microenvironment at day 5 (scale bar: 75μm). d) Pipeline for hydrogel generation (Created with BioRender.com).

we investigated the role of culture dimensionality in neuronal differentiation of SH-SY5Y cells. As a 3D biomimetic model, we fabricated brain ECM hydrogels via decellularization of bovine brain tissues which allowed the culturing of cells within a reconstituted native brain matrix.

Neuroblastoma is a childhood cancer arising from the neural crest which holds the ability to differentiate into mature neuron phenotypes using certain agents.[38] In our work, SH-SY5Y differentiation is induced with a gradual decrease of serum content in the medium, the addition of RA, and neurotrophic

factors. Serum deprivation allows for the elimination of epithelial cells to achieve a homogeneous neuronal cell population in the otherwise heterogeneous SH-SY5Y cells.[39] Until day 9, neuronal cells were selected after which the selected population was supported with neurotrophic factors including N2, B-27, KCl, and RA to induce neuronal maturation. RA plays a major role during neuronal differentiation by administrating complex signaling pathways, such as the protein kinase A-dependent pathway, transcription factors, and extracellular molecules, including Wnt signaling.[40] While N2 and B-27 are expected to

147
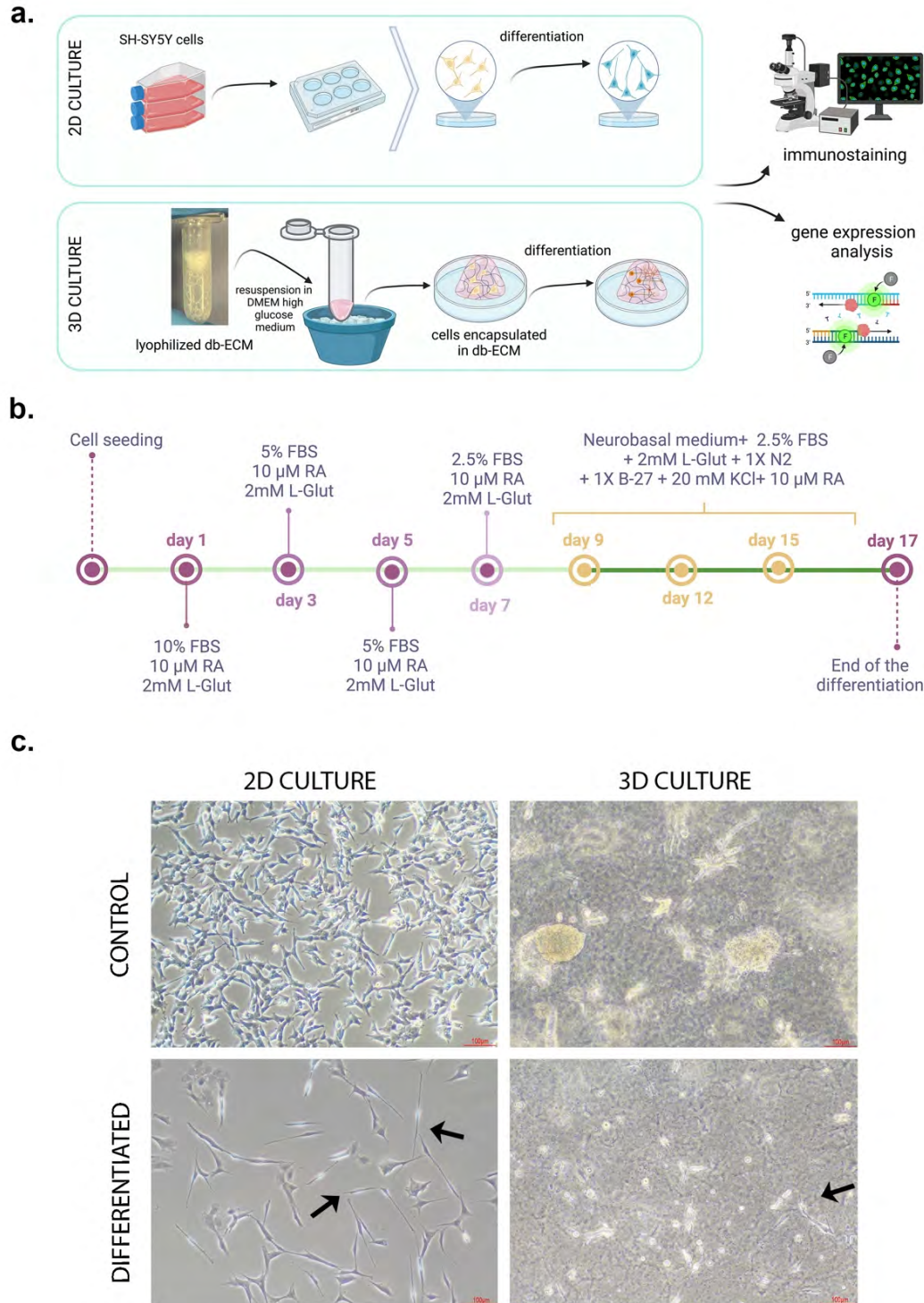
Figure 2. Neuronal differentiation of neuroblastoma cells in 2D and 3D culture. a) Schematic description of neuronal differentiation experiment setup (Created with BioRender.com). b) Neuronal differentiation treatment timeline for 2D and 3D application (Created with BioRender.com). c) Brightfield images of undifferentiated and differentiated neuroblastoma cells in 2D and 3D microenvironments at day 15 (scale bar: 100µm).

promote neurogenesis, KCl is known to induce depolarization of neurons by the activation of potassium channels.[41,42]

During neuronal differentiation, cell proliferation was re-

duced as expected, an important feature of differentiation, the expression of neuronal markers was distinctively changed, and a shift in cell morphology was observed in both 2D and 3D con-
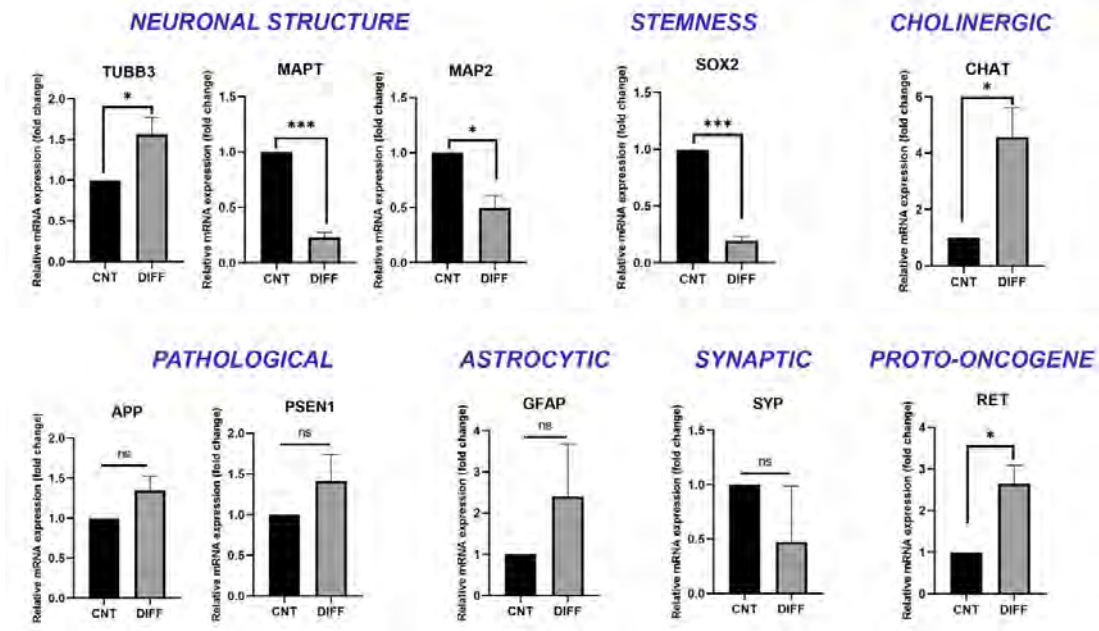
Figure 3. Gene expression analysis of 2D differentiated neuroblastoma cells; the results were normalized to GAPDH expression of the cells.
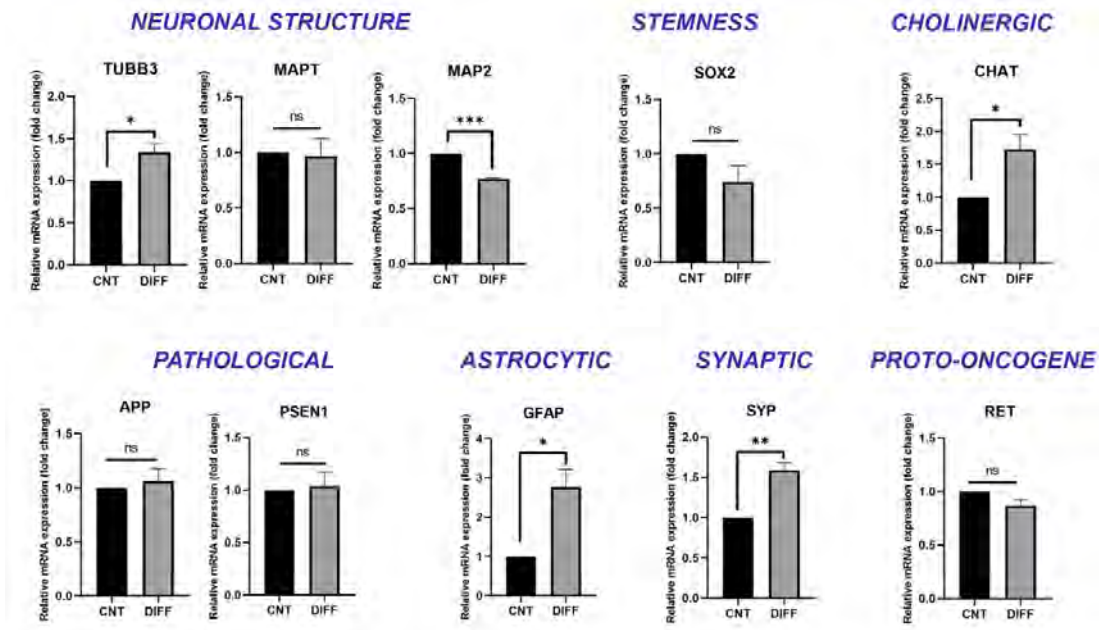
Figure 4. Gene expression analysis of 3D differentiated cells; the results were normalized to GAPDH expression of the cells.

ditions. In 2D culture, cells possessed long axons and formed a synaptic network with nearby cells upon differentiation (Figure 2c). Moreover, there was a significant increase in the mature neuron marker *TUBB3* gene expression and a significant decrease in the stemness marker *SOX2*, indicating neuronal maturation. On the other hand, the expression of the *CHAT* gene was upregulated which hints that cholinergic neuron differentiation

was induced by the applied differentiation protocol. Unexpectedly, the expression of *MAP2* and *MAPT* was significantly reduced in differentiated cells. This might have been due to a lack of matching the timing of sample collection with the stage of differentiation in line with previous studies including Przyborski et al.'s, where it has been shown that upregulated levels of MAP2c mRNA transcripts in the early stages of differentiation
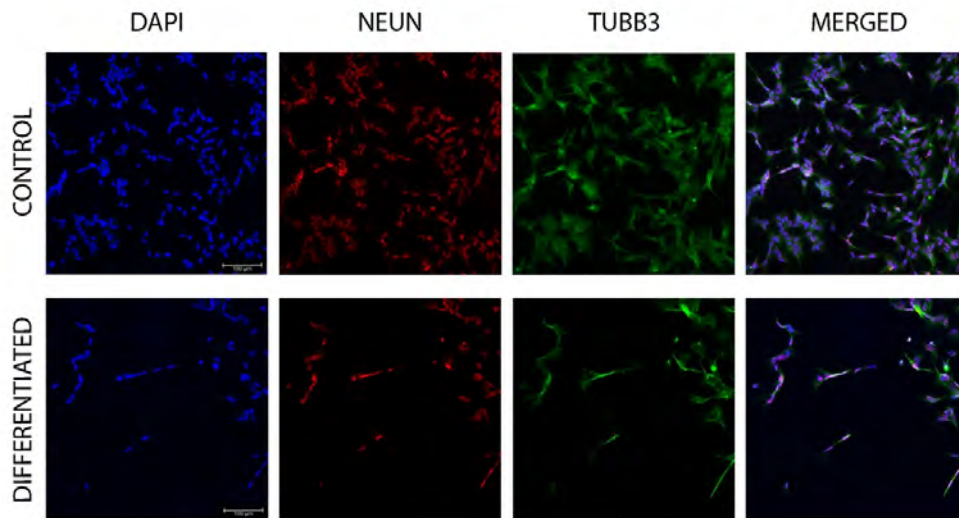
Figure 5. Immunostaining of undifferentiated and differentiated neuroblastoma cells in 2D culture at day 15. Neuronal markers, NEUN:red; Beta-tubulin III, TUBB3:green; Nuclear staining with DAPI:blue. Scale bar:100 µ m.
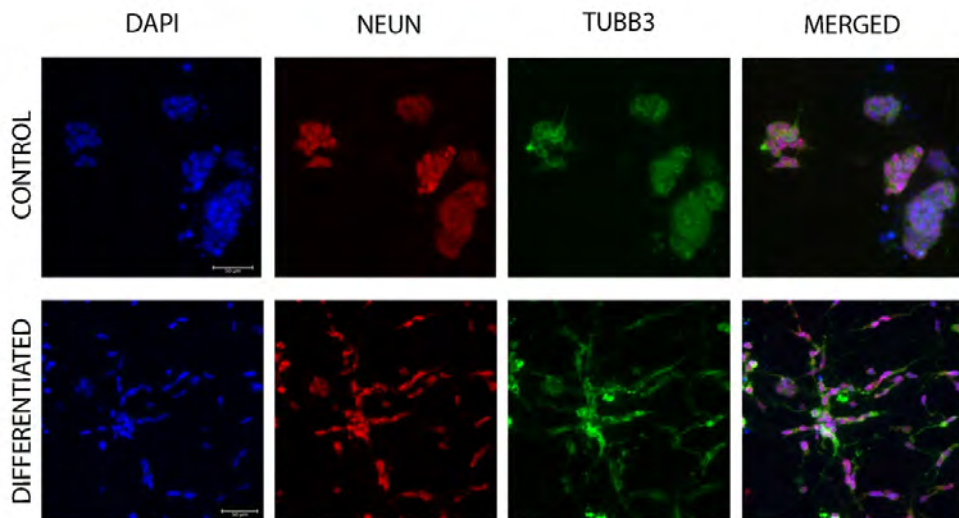
Figure 6. Immunostaining of undifferentiated and differentiated neuroblastoma cells in 3D culture at day 15. Neuronal markers, NEUN:red; Beta-tubulin III, TUBB3:green; Nuclear staining with DAPI:blue. Scale bar:50 µ m.

tended to decrease as developmental progression proceeded.[43] In our study, another gene that was affected by neuronal differentiation in 2D conditions was RET, a proto-oncogene marker. Studies have demonstrated an increased expression of RET starting from day 3 of RA treatment, which was hypothesized to stimulate neuronal differentiation.[29,44] RET expression is more common in dopaminergic neurons, and an increase in this gene is correlated with the promoted neurogenesis in dopaminergic

neurons. Moreover, the elevation of RET expression might be a sign of the completion of early differentiation phases.[14]

SH-SY5Y differentiation in 3D db-ECM hydrogels similarly revealed a morphological shift in cells and neuronal network formation in line with the expression of neuronal markers (Figure 6). On the other hand, non-differentiated neuroblastoma cells exhibited growth in spherical clumps, a behavior common for 3D cancer cell cultures.[45] In response to mechanical stimulus through hydrogels, cells tend to remodel their surroundings and change their cellular shape, behavior, and biological signaling.[46,47] Physical confinement and the presence of brain-specific ECM ligands provided by the 3D hydrogel model used in the study demonstrated distinct changes in gene expression during neuronal differentiation compared to 2D cultures (Figure 4). The expression of the *SYP* gene, a synaptic marker, was significantly increased in 3D matrices in line with neural network formation. Although the functionality of this gene has not been completely clarified, it has important roles in vesicular ion channel activity and endocytosis.[26] Expression profiles of neuronal markers *TUBB3*, *CHAT*, and *MAP2* were unaffected by culture dimensionality and similar in 2D and 3D conditions. On the other hand, SH-SY5Y cells that differentiated in 3D db-ECM hydrogels showed an upregulation of astrocytic marker *GFAP*. Although glial cell formation was not targeted during the differentiation procedure, due to the biomechanical characteristics of the hydrogel, glial cell formation was induced (Figure 4). Similarly, a study by Hu et al. demonstrated increased expression of GFAP in primary rat astrocytes in 3D soft matrices compared to stiff environments which was found to be mediated by the inhibition of Yes-associated protein (YAP), a key transcriptional coregulator of stiffness-induced cellular events.[48]

As opposed to the observed loss of stemness and reduction in *SOX2* gene expression in 2D conditions, neuroblastoma differentiation in 3D hydrogels showed preservation of stemness. This might be due to the presence of ECM components that help cells maintain their stemness characteristics thereby promoting their differentiation capability.[49] Furthermore, matrix properties such as stiffness, viscoelasticity, and degradability were defined as key parameters for regulating the stemness characteristic of stem cells.[50,51] Cells cultured in 3D microenvironments require matrix remodeling to migrate and expand.[52,53] Native tissue matrices are viscoelastic and support such remodeling where differentiation can be induced with instructive ECM ligands.[54]

The expression of neuropathological markers *PSEN1* or *APP* was investigated in different conditions since previous reports have shown that such markers could be upregulated upon differentiation. However, we did not encounter any significant changes in the expression of *PSEN1* or *APP* in either 2D or 3D hydrogels.[11]

CONCLUSION

In this study, we performed a comparative analysis of neuroblastoma cell differentiation within 3D hydrogels constructed from decellularized bovine brain tissue, in comparison to conventional 2D cell cultures. Our investigation focused on evaluating changes in cellular morphology and the expression of molecular markers. In conclusion, the findings of this study reveal that culture dimensionality distinctly affects the neuronal differentiation of neuroblastoma cells. 3D hydrogels with the ability to biomimick the brain microenvironment via reconstitution of native ECM show preservation of stemness, induction of synaptic markers, 3D network formation, and expression of glial markers as opposed to conventional 2D culturing. These hydrogel systems can be adapted to different pathophysiological states by modulating their biophysical and biochemical properties for developing faithful *in vitro* disease models in neuroscience.

ORCID IDs of the authors

Duygu Turan Sorhun   0000-0001-7775-2241
Ece Ozturk   0000-0001-8635-0279

REFERENCES

1. Karamanos NK, Theocharis AD, Piperigkou Z, et al. A guide to the composition and functions of the extracellular matrix. FEBS J. 2021;288(24):6850-6912. doi:10.1111/febs.15776

2. Kim BS, Das S, Jang J, Cho D-W. Decellularized Extracellular Matrix-based bioinks for engineering tissue- and organ-specific microenvironments. *Chem Rev.* 2020;120(19):10608-10661.

3. Badylak SF, Freytes DO, Gilbert TW. Extracellular matrix as a biological scaffold material: Structure and function. *Acta Biomater.* 2009;5(1):1-13.

4. Freytes DO, Martin J, Velankar SS, Lee AS, Badylak SF. Preparation and rheological characterization of a gel form of the porcine urinary bladder matrix. *Biomaterials.* 2008;29(11):1630-1637.

5. DeQuach JA, Yuan SH, Goldstein LS, Christman KL. Decellularized porcine brain matrix for cell culture and tissue engineering

scaffolds. *Tissue Eng Part A*. 2011;17(21-22):2583-2592.

6. Jin Y, Lee JS, Kim J, et al. Three-dimensional brain-like microenvironments facilitate the direct reprogramming of fibroblasts into therapeutic neurons. *Nat Biomed Eng*. 2018;2(7):522-539.

7. Cembran A, Bruggeman KF, Williams RJ, Parish CL, Nisbet DR. Biomimetic materials and their utility in modeling the 3-dimensional neural environment. *iScience*. 2020;23(1):100788. doi:10.1016/j.isci.2019.100788

8. Sood D, Cairns DM, Dabbi JM, et al. Functional maturation of human neural stem cells in a 3D bioengineered brain model enriched with fetal brain-derived matrix. *Sci Rep*. 2019;9(1):17874. doi:10.1038/s41598-019-54248-1

9. Hebisch M, Klostermeier S, Wolf K, et al. The impact of the cellular environment and aging on modeling Alzheimer's disease in 3D cell culture models. *Adv Sci*. 2023;10(8):2205037. doi:10.1002/advs.202205037

10. Jain D, Mattiassi S, Goh EL, Yim EKF. Extracellular matrix and biomimetic engineering microenvironment for neuronal differentiation. *Neural Regen Res*. 2020;15(4):573-585.

11. Nicolas J, Magli S, Rabbachin L, Sampaolesi S, Nicotra F, Russo L. 3D Extracellular matrix mimics: Fundamental concepts and role of materials chemistry to influence stem cell fate. *Biomacromolecules*. 2020;21(6):1968-1994.

12. Biedler JL, Roffler-Tarlov S, Schachner M, Freedman LS. Multiple neurotransmitter synthesis by human neuroblastoma cell lines and clones. *Cancer Res*. 1978;38(11Part1):3751-3757.

13. Kovalevich J, Langford D. Considerations for the use of SH-SY5Y neuroblastoma cells in neurobiology. *Methods Mol Biol*. 2013;1078:9-21.

14. Barth M, Toto Nienguesso A, Navarrete Santos A, Schmidt C. Quantitative proteomics and in-cell cross-linking reveal cellular reorganisation during early neuronal differentiation of SH-SY5Y cells. *Commun Biol*. 2022;5(1):551. doi:10.1038/s42003-022-03478-7

15. de Medeiros LM, De Bastiani MA, Rico EP, et al. Cholinergic differentiation of human neuroblastoma SH-SY5Y cell line and its potential use as an in vitro model for Alzheimer's disease studies. *Mol Neurobiol*. 2019;56(11):7355-7367.

16. Shipley MM, Mangold CA, Szpara ML. Differentiation of the SH-SY5Y human neuroblastoma cell line. *J Vis Exp*. 2016;(108):e53193. doi:10.3791/53193

17. Qiao J, Paul P, Lee S, et al. PI3K/AKT and ERK regulate retinoic acid-induced neuroblastoma cellular differentiation. *Biochem Biophy Res Commun*. 2012;424(3):421-426.

18. Bottenstein JE, Sato GH. Growth of a rat neuroblastoma cell line in serum-free supplemented medium. *Proc Natl Acad Sci USA*. 1979;76(1):514-517.

19. Sünwoldt J, Bosche B, Meisel A, Mergenthaler P. Neuronal culture microenvironments determine preferences in bioenergetic pathway use. *Front Mol Neurosci*. 2017;10:305. doi:10.3389/fnmol.2017.00305

20. Xie H-r, Hu L-s, Li G-y. SH-SY5Y human neuroblastoma cell line: In vitro cell model of dopaminergic neurons in Parkinson's disease. *Chin Med J*. 2010;123(08):1086-1092.

21. Dehmelt L, Halpain S. The MAP2/Tau family of microtubule-associated proteins. *Genome Biol*. 2004;6(1):204. doi:10.1186/gb-2004-6-1-204

22. Kaech S, Ludin B, Matus A. Cytoskeletal plasticity in cells expressing neuronal microtubule-associated proteins. *Neuron*. 1996;17(6):1189-1199.

23. Katsetos CD, Herman MM, Mörk SJ. Class III β-tubulin in human development and cancer. *Cell motil Cytoskelet*. 2003;55(2):77-96.

24. Gusel'nikova VV, Korzhevskiy DE. NeuN As a neuronal nuclear antigen and neuron differentiation marker. *Acta Nat*. 2015;7(2):42-47.

25. Cassiman D, van Pelt J, De Vos R, et al. Synaptophysin: A novel marker for human and rat hepatic stellate cells. *Am J Pathol*. 1999;155(6):1831-1839.

26. White DN, Stowell MHB. Room for two: The synaptophysin/synaptobrevin complex. *Front Synaptic Neurosci*. 2021;13:740318. doi:10.3389/fnsyn.2021.740318.

27. Graham V, Khudyakov J, Ellis P, Pevny L. SOX2 functions to maintain neural progenitor identity. *Neuron*. 2003;39(5):749-765.

28. Bunone G, Borrello MG, Picetti R, et al. Induction of RET proto-oncogene expression in neuroblastoma cells precedes neuronal differentiation and is not mediated by protein synthesis. *Exp Cell Res*. 1995;217(1):92-99.

29. Tahira T, Ishizaka Y, Itoh F, Nakayasu M, Sugimura T, Nagao M. Expression of the ret proto-oncogene in human neuroblastoma cell lines and its increase during neuronal differentiation induced by retinoic acid. *Oncogene*. 1991;6(12):2333-2338.

30. Oda Y. Choline acetyltransferase: The structure, distribution and pathologic changes in the central nervous system. *Pathol Int*. 1999;49(11):921-937.

31. Yang Z, Wang KK. Glial fibrillary acidic protein: From intermediate filament assembly and gliosis to neurobiomarker. *Trends Neurosci*. 2015;38(6):364-374.

32. Müller UC, Deller T, Korte M. Not just amyloid: Physiological functions of the amyloid precursor protein family. *Nat Rev Neurosci*. 2017;18(5):281-298. doi:10.1038/nrn.2017.29

33. Bagaria J, Bagyinszky E, An SSA. Genetics, functions, and clinical impact of presenilin-1 (psen1) gene. *Int J Mol Sci*. 2022;23(18):10970. doi:10.3390/ijms231810970

34. Bayeva N, Coll E, Piskareva O. Differentiating neuroblastoma: A systematic review of the retinoic acid, its derivatives, and synergistic interactions. *J Pers Med*. 2021;11(3): 211. doi:10.3390/jpm11030211

35. Centeno EGZ, Cimarosti H, Bithell A. 2D versus 3D human induced pluripotent stem cell-derived cultures for neurodegenerative disease modelling. *Mol Neurodegener*. 2018;13(1):27. doi:10.1186/s13024-018-0258-4

36. Lovett ML, Nieland TJ, Dingle YTL, Kaplan DL. Innovations in 3D tissue models of human brain physiology and diseases. *Adv Funct Mater*. 2020;30(44):1909146. doi:10.1002/adfm.201909146

37. Roth JG, Huang MS, Li TL, et al. Advancing models of neural development with biomaterials. *Nat Rev Neurosci*. 2021;22(10):593-615. doi:10.1038/s41583-021-00496-y

38. Cai A, Lin Z, Liu N, et al. Neuroblastoma SH-SY5Y cell differentiation to mature neuron by AM580 treatment. *Neurochem Res*. 2022;47(12):3723-3732.

39. Bell N, Hann V, Redfern CPF, Cheek TR. Store-operated Ca^{2+} entry in proliferating and retinoic acid-differentiated N- and S-type neuroblastoma cells. *Biochim Biophys Acta Mol Cell Res*. 2013;1833(3):643-651.

40. Dhara SK, Stice SL. Neural differentiation of human embryonic stem cells. *J Cell Biochem*. 2008;105(3):633-640.

41. Lasher RS, Zagon IS. The effect of potassium on neuronal differentiation in cultures of dissociated newborn rat cerebellum. *Brain Research*. 1972;41(2):482-488.

42. Yang T, Uhler M. KCl-induced depolarization facilitates neuronal differentiation of P19 embryonic carcinoma cells. *UMURF*. 2013; (6): 52-58.

43. Przyborski SA, Cambray-Deakin MA. Developmental regulation of MAP2 variants during neuronal differentiation *in vitro*. *Brain Res Dev Brain Res*. 1995;89(2):187-201.

44. Forster JI, Köglsberger S, Trefois C, et al. Characterization of differentiated SH-SY5Y as neuronal screening model reveals increased oxidative vulnerability. *SLAS Discovery*. 2016;21(5):496-509.

45. Craig BT, Rellinger EJ, Alvarez AL, Dusek HL, Qiao J, Chung DH. Induced differentiation inhibits sphere formation in neuroblastoma. *Biochem Biophys Res Commun*. 2016;477(2):255-259.

46. Long KR, Huttner WB. How the extracellular matrix shapes neural development. *Royal Society Open Biol*. 2019;9(1):180216. doi:10.1098/rsob.180216

47. Ransanz LC, Van Altena PF, Heine VM, Accardo A. Engineered cell culture microenvironments for mechanobiology studies of brain neural cells. *Front Bioeng Biotechnol*. 2022;10:1096054. doi:10.3389/fbioe.2022.1096054

48. Hu Y, Huang G, Tian J, et al. Matrix stiffness changes affect astrocyte phenotype in an in vitro injury model. *NPG Asia Mater*. 2021;13(1):35. doi:10.1038/s41427-021-00304-0

49. Saraswathibhatla A, Indana D, Chaudhuri O. Cell–extracellular matrix mechanotransduction in 3D. *Nat Rev Mol Cell Biol*. 2023;24(7):495-516.

50. Kim HN, Choi N. Consideration of the mechanical properties of hydrogels for brain tissue engineering and brain-on-a-chip. *BioChip J*. 2019;13(1):8-19.

51. Madl CM, LeSavage BL, Dewi RE, et al. Maintenance of neural progenitor cell stemness in 3D hydrogels requires matrix remodelling. *Nature Materials*. 2017;16(12):1233-1242.

52. Chaudhuri O, Gu L, Klumpers D, et al. Hydrogels with tunable stress relaxation regulate stem cell fate and activity. *Nat Mater*. 2016;15(3):326-334.

53. Khetan S, Guvendiren M, Legant WR, Cohen DM, Chen CS, Burdick JA. Degradation-mediated cellular traction directs stem cell fate in covalently crosslinked three-dimensional hydrogels. *Nature Mater*. 2013;12(5):458-465.

54. Ma Y, Han T, Yang Q, et al. Viscoelastic cell microenvironment: Hydrogel-based strategy for recapitulating dynamic ECM mechanics. *Adv Funct Mater*. 2021;31(24):2100848. doi:10.1002/adfm.202100848

How cite this article

RESEARCH ARTICLE

Selenium Toxicity Induced Physiological and Biochemical Alterations in Maize Seedlings

Mustafa Yildiz[1], Emre Pehlivan[1], Hakan Terzi[1]

[1]Afyon Kocatepe University, Department of Molecular Biology and Genetic, Faculty of Science and Literature, Afyonkarahisar, Turkiye

ABSTRACT

Objective: Selenium (Se) is not necessary for plants but alleviates the harmful effects of abiotic stresses. Indeed, high Se levels cause toxicity by inducing oxidative stress and disrupting several metabolic processes. However, the underlying mechanisms remain poorly understood.

Materials and Methods: The effects of Se toxicity on the morphological and physiological attributes of hydroponically grown maize (*Zea mays* L.) seedlings were illustrated. Five-day-old seedlings were subjected to 0 (control), 50, and 100 µM Se. After ten days, the treated seedlings were harvested to analyze growth, cell viability, photosynthetic pigments, lipid peroxidation, reactive oxygen species (ROS) accumulation, and enzymatic antioxidants.

Results: The results indicated that excess Se resulted in phytotoxicity, as demonstrated by reduced seedling growth, root activity, and chlorophyll accumulation but higher malondialdehyde content. Se also increased oxidative stress, as illustrated by the accumulation of ROS, lipid peroxidation, and loss of membrane integrity. The antioxidative system was induced to detoxify ROS through the superoxide dismutase, guaiacol peroxidase, and catalase enzymes. Excess Se increased catalase activity, while the opposite happened in superoxide dismutase and guaiacol peroxidase activities.

Conclusion: These results may improve the understanding of Se phytotoxicity in plants.

Keywords: Antioxidant enzymes, Growth, Oxidative Stress, Phytotoxicity, *Zea mays* L.

INTRODUCTION

Selenium (Se) is a non-metallic element in the soil, occurring in various inorganic forms. Se is essential for human and animal health due to its important role in stress defense systems.[1] Se, which can covalently bond with C, participates in the structural formation of various organic Se-containing compounds, including selenoamino acids and selenoproteins. Selenoproteins are required for maintaining the physiology in a wide variety of prokaryotes, archaea, and eukaryotes; but are absent in fungi or green plants.[2,3] However, Se stimulates the antioxidant mechanism at low concentrations and protects plants from oxidative stress but acts as a heavy metal and an oxidant at high concentrations.[4] Therefore, the beneficial role of Se at low concentrations has been extensively studied.[5]

While selenate, selenite, and organic Se compounds such as selenocysteine and selenomethionine can be quickly absorbed from the soil, the roots cannot take up colloidal elemental Se or selenides.[6] Se is chemically similar to S and shares a similar pathway of uptake and translocation in plants.[7,8] Sele-nate is taken up by sulfate transporters of the root cell plasma membrane.[9] However, excessive Se accumulation can affect amino acid concentrations and alter the levels of nitrogenous compounds and various secondary metabolites[10,11], which can cause phytotoxicity by directly affecting the metabolism.[12] Se-induced toxicity is mediated by increased ROS accumulation and oxidative stress[9] and negatively affects the accumulation of essential nutrients by disrupting the mineral balance in plants.[5] Se toxicity in rice seedlings causes chlorosis, reduced accumulation of photosynthetic pigments, growth inhibition, lipid peroxidation, and enhanced activity of antioxidant enzymes.[4,13] The phytotoxic mechanisms of Se in maize plants have been studied only to a limited extent. Therefore, this research was carried out to obtain information about plant responses to Se-induced toxic effects by investigating seedling growth, root activity, photosynthetic pigments, lipid peroxidation, ROS accumulation, and antioxidant systems in different tissues of maize plants.

MATERIALS AND METHODS

Plant Material and Se Treatment

The seeds of the maize (*Zea mays* L.) cultivar "Capuzi" were surface sterilized using 1% NaOCl and washed five times with sterile distilled water. They were then placed in culture containers with two layers of wetted filter papers and germinated for 48 h in the dark and at 25°C. Homogeneous maize seedlings were transferred to 1 L hydroponic culture pots containing modified Hoagland nutrient solution. They were grown in a growth chamber under a 12 h:12 h photoperiod, 250 µmol m^{-2} s^{-1} light intensity, 25°C ± 1°C, and 60% relative humidity for three days. They were then transferred to a nutrient solution containing 0, 50, and 100 µM of sodium selenite (Na$_2$SeO$_3$) and cultivated for another ten days. The pH of the nutrient solution was adjusted to 6.0 and was renewed every two days.

Determination of Growth Parameters

After exposure for ten days, ~8–10 seedlings were randomly selected from each group treated with a particular concentration of Se and harvested. The shoots and roots of the seedlings were separated, and their fresh weights were determined. The dry weights were determined after 48 h of drying at 80°C.

Determination of Root Activity by TTC Reduction

Root activity was analyzed by determining the activity of dehydrogenases in root tips using the TTC (2,3,5-triphenyl tetrazolium chloride) reduction test.[14] The root tips, ~1 cm long, were exposed to the TTC solution containing 0.8% TTC and 1% Tween-80 in 0.05 M potassium phosphate buffer (pH 7.4) for 2 h. The microscopic images were the taken with a digital camera.

Determination of Total Chlorophyll Content

Total chlorophyll content was determined using the Wellburn method.[15] The second leaves were collected, and ~100 mg were extracted with 10 mL methanol. The supernatants were obtained, OD$_{653}$ and OD$_{666}$ measured, and the chlorophyll content was estimated using the formulae:

Chlorophyll a = 15.65A$_{666}$ - 7.34A$_{653}$
Chlorophyll b = 27.05A$_{653}$ - 11.21A$_{666}$

Determination of Lipid Peroxidation Levels

The level of lipid peroxidation was determined by measuring the malondialdehyde (MDA) content.[16] Leaf tissues, 0.5 g, were homogenized with 0.1% trichloroacetic acid (TCA) and centrifuged at 11,500 × g for 15 min. The supernatant was mixed with 20% TCA containing 0.5% thiobarbituric acid and incubated at 95°C for 30 min. The OD$_{532}$ and OD$_{600}$ were observed, and the MDA content was calculated using the extinction coefficient (155 mM^{-1} cm^{-1}).

Histochemical Detection of Oxidative Damage

Hydrogen peroxide (H$_2$O$_2$) accumulation was determined histochemically using 3,3'-diaminobenzidine (DAB) solution.[17] Superoxide radicals (O$_2^{\bullet-}$) were determined after leaf and root tissues were incubated with 0.1% nitro blue tetrazolium (NBT) solution for 2 h in the dark.[18] Lipid peroxidation in the leaf and root tissues was determined using Schiff's reagent.[19] Membrane integrity at root tips was detected by treating the roots with 0.25% Evans blue solution for 1 h.[19] Leaf and root tissues were photographed using a digital camera.

Extraction and Assay of Antioxidant Enzymes

Fresh leaf and root tissues, 500 mg each, were homogenized separately with 50 mM phosphate buffer (pH 7.0). The homogenates were centrifuged at 14,000 rpm for 20 min. The supernatants were collected and stored for enzyme activity assays, and the total protein level was determined by the Bradford method.[20] Superoxide dismutase (SOD) activity was measured following the method of Beauchamp and Fridovich;[21] catalase (CAT) activity according to the method of Aebi;[22] and Guaiacol peroxidase (GPOX) activity by the method of Mika and Lüthje.[23]

Statistical Analysis

All experiments were carried out twice in triplicates. Statistical analyses were performed by analysis of variance using the SPSS 22.0 software (IBM, NY, USA). Duncan's multiple range test (DMRT) was used to compare the means.

RESULTS

Effect of Se on Seedling Growth

The fresh and dry weights of shoot and root tissues decreased significantly due to increased Se concentration ($P < 0.05$; Table 1). Under 50 and 100 µM Se, the shoot fresh and dry weights were reduced by 29.8% and 64.8%, and by 17.6% and 47.2%, respectively, compared to the control. The root fresh and dry weights decreased by 30.5% and 49.6%, and by 11.8% and 31.7%, respectively. In addition, visual symptoms of toxicity were observed in maize seedlings exposed to Se (Figure 1).

Effect of Se on Root Activity

The root activity in maize seedlings under Se determined by the TTC method revealed an intense red color in the root tips

Table 1. The effects of different Se concentrations on shoot and root fresh (FW) and dry weight (DW) of maize seedlings.

Parameters	Se concentrations (µM)		
	0	**50**	**100**
Shoot FW mg plant $^{-1}$	2893 ± 75.0 [a]	2031 ± 97.4 [b]	1018 ± 92.2 [c]
Shoot DW mg plant $^{-1}$	158.0 ± 2.94 [a]	130.3 ± 11.3 [b]	83.5 ± 6.55 [c]
Root FW mg plant $^{-1}$	351.8 ± 18.2 [a]	244.5 ± 20.2 [b]	177.3 ± 21.6 [c]
Root DW mg plant $^{-1}$	17.4 ± 1.14 [a]	15.4 ± 0.92 [b]	11.9 ± 0.61 [c]

a – c; Different letters indicate significant differences among means according to DMRT analysis (P<0.05). Standard error (±SE).

Figure 1. Visual symptoms of Se toxicity in maize seedlings.

Figure 2. Root activity visualized by the TTC reduction assay in maize seedlings exposed to Se.

Effect of Se on Chlorophyll Content

The total chlorophyll content of leaf tissues reduced markedly by 30.4% and 60.8%, with an increase in Se concentration at 50 and 100 µM, respectively (P < 0.05; Figure 3).
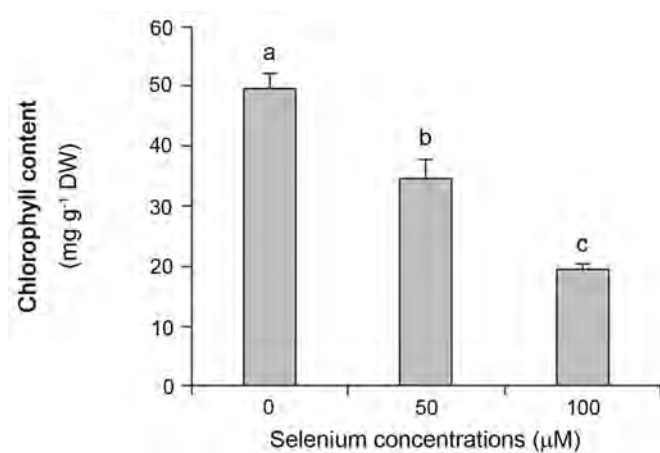
Figure 3. Effect of different Se concentrations on total chlorophyll content in leaf tissues of maize seedlings. Different letters (a – c) indicate significant differences among the means according to DMRT analysis (P<0.05).

Effect of Se on Lipid Peroxidation and ROS Accumulation

A significant increase in the MDA content indicated oxidative stress in plants exposed to Se (P<0.05; Figure 4). The MDA contents elevated by 1.37- and 1.47-fold under 50 and 100 µM Se, respectively. DAB staining detected a higher accumulation of H_2O_2 in the Se-treated seedlings compared to the control (Figures 5 and 6). Se-induced accumulation of $O_2^{\bullet-}$ was confirmed by histochemical staining with NBT. Lipid peroxidation was determined histochemically in leaves but not in roots. Additionally, the roots of maize seedlings treated with Se were stained extensively by Evans blue, indicating a loss of membrane integrity (Figure 6).

Effect of Se on Antioxidant Enzymes

The effects of excess Se on the activities of antioxidant enzymes and protein contents of the leaf and root tissues are depicted in Figure 7. Compared to the control, 50 and 100 µM Se suppressed SOD activity in the root tissues by 40.3% and 31.1%,

of the control seedlings, indicating a high cellular viability or oxidizing ability. Nonetheless, relatively low dehydrogenase activity was also evident in the root tips of Se-treated seedlings (Figure 2).
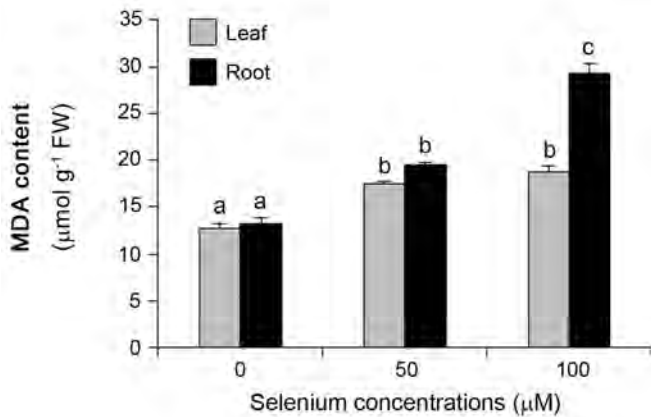
Figure 4. Effect of different Se concentrations on MDA content in leaf and root tissues of maize seedlings. Different letters (a – c) indicate significant differences among the means in each tissue according to the DMRT analysis (P<0.05).
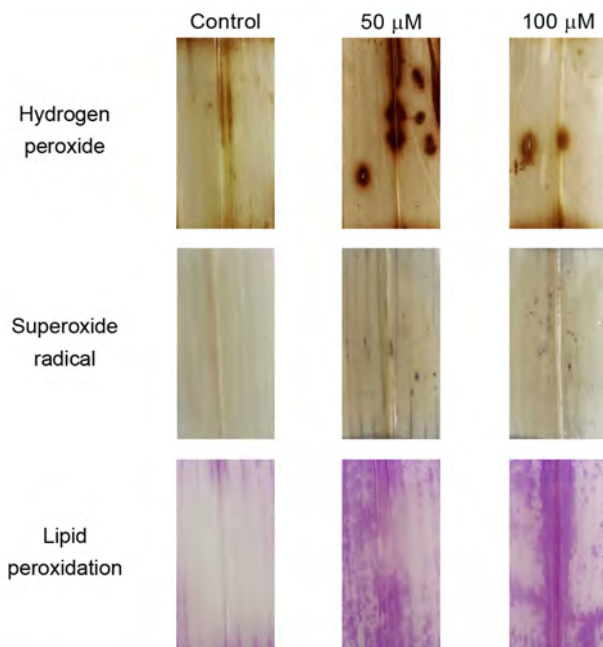
Figure 5. Histochemical analysis of hydrogen peroxide, superoxide radical, and lipid peroxidation accumulation in maize leaves.

respectively; and GPOX activity by 52.9% and 28.2%, respectively. On the other hand, SOD and GPOX activities in the leaf tissues were not significantly affected by Se. Se at 50 and 100 µM enhanced CAT activity in the leaves by 54.9% and 47.4%, respectively, compared to the control plants. However, the root CAT activity was remarkably elevated only at 50 µM Se. Se at 50 and 100 µM reduced the protein content of leaf tissues by 13.7% and 20.6%, but an increase of 21.7% and 34.5% in root tissues, respectively.

DISCUSSION

Although Se is known to have positive effects at low concentrations, it shows toxicity symptoms in plants at high concentrations. One of these symptoms is the reduction in biomass. In this work, an increasing concentration of Se significantly reduced the growth attributes of maize seedlings. Se-induced inhibition of growth was also detected in rice seedlings.[4] Excessive growth inhibition was associated with reduced stomatal density, disrupted stomatal arrangement, and diminished cell viability in *Arabidopsis thaliana*.[24] In a short-term experiment, selenate treatment promoted the Se contents in the rice seedlings grown with 0.1 mM sulfate. This suggested that under the S-limited conditions, plants can absorb selenate more efficiently, inducing toxicity and growth impairment. Excess Se reduced S concentrations in the roots of rice seedlings, indicating a competition between Se and sulfate uptake.[25] Reduced growth in maize seedlings may be related to impaired sulfate availability and damage induced by excessive Se to vital processes such as protein and chlorophyll biosynthesis.[12]

The reduction of colorless TTC to a water-insoluble red formazan depends on the efficient activity of respiratory dehydrogenases and indicates mitochondrial activity and viability in metabolically active cells.[26] The intensity of the red color is proportional to the metabolic activity of the cells, making it a reliable indicator of cell viability. In the present study, suppression in TTC reduction was determined in root cells to indicate cell viability in plants exposed to Se. A reduction in root activity was also reported under metal-induced stress.[27,28] However, low Se concentration (2.5 µM) elevated the TTC reduction capacity in *Phaseolus aureus* roots.[27]

Excess Se negatively affects many physiological and biochemical processes in plants. Among these, chlorosis is one of the most harmful effects due to decreased chlorophyll biosynthesis. A dramatic reduction in chlorophyll contents was observed in Se-treated maize seedlings. In the case of cowpea plants, foliar application of high Se concentrations inhibited photosynthesis and decreased the chlorophyll content, generating leaf chlorosis-related symptoms.[29] Elevated Se accumulation in leaf tissues can destroy chlorophyll molecules and increase oxidative stress.[30,31] Se reduces chlorophyll content in spinach plants by suppressing the activity of δ-aminolevulinate (ALA) dehydratase, which is required for chlorophyll biosynthesis.[32] Similarly, Se reduced ALA content in etiolated maize.[33] However, the Se-induced reduction in chlorophyll concentration may have resulted in lower photosynthetic yields and thus inhibited seedling growth.[13]

Possible mechanisms involved in Se-mediated oxidative stress have been described to explain its harmful effects.[5] Se-induced inhibition in the antioxidant defense system causes the overproduction of ROS.[34] A significant increase in MDA content indicates oxidative stress in plants exposed to Se toxicity due to the overproduction of ROS.[4] Increased oxidative stress
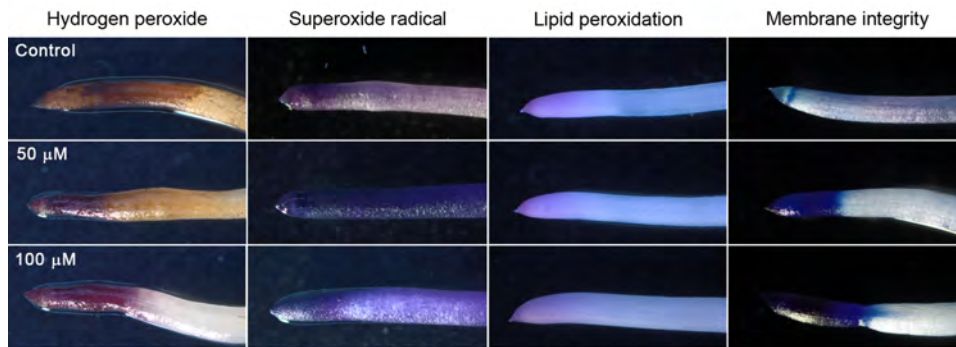
Figure 6. Histochemical analysis of hydrogen peroxide, superoxide radical, lipid peroxidation, and membrane integrity in maize roots.
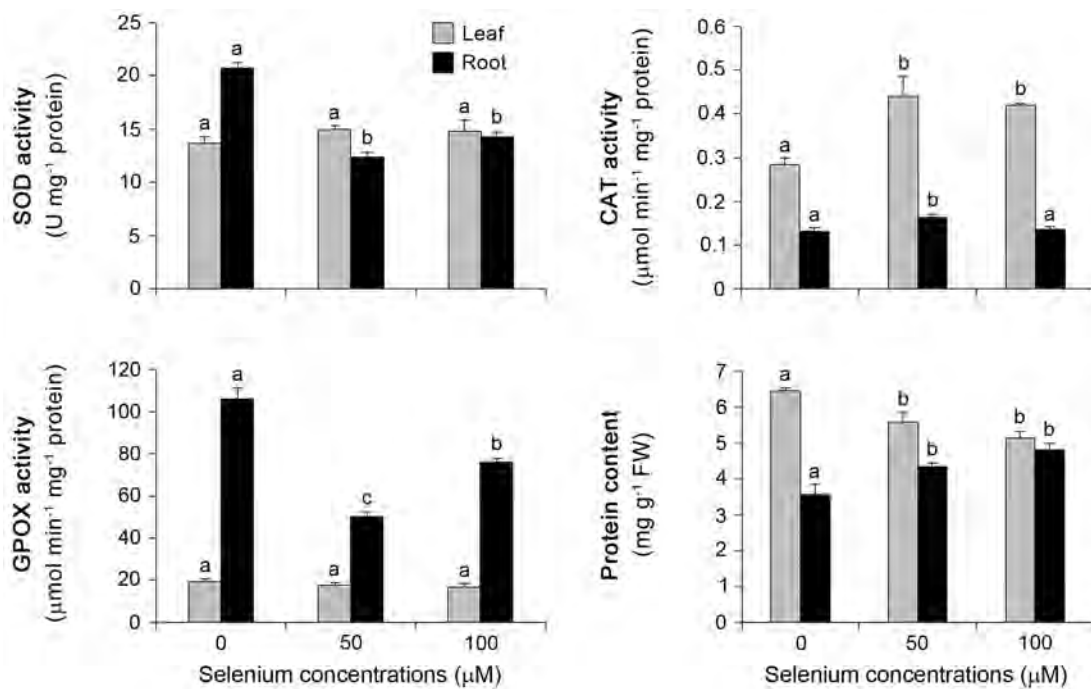
Figure 7. Effects of different Se concentrations on the activities of antioxidant enzymes and protein contents in leaf and root tissues of maize seedlings. Different letters (a – c) indicate significant differences among the means in each tissue according to the DMRT analysis (P<0.05).

and high MDA content in maize leaves due to Se application indicated membrane disruption. Similarly, foliar Se application at high concentrations of 150 g ha^{-1} induced a drastic increase in H_2O_2 concentration and lipid peroxidation in cowpea leaves.[29] On the contrary, foliar application of Se ranging from 20 to 80 ppm in coffee plants decreased lipid peroxidation and H_2O_2 levels, highlighting the antioxidant capacity of Se in combating ROS.[35] Conversely, Se-induced oxidative damage was also demonstrated by the histochemical localization of $O_2^{\bullet-}$, H_2O_2, and lipid peroxidation. In addition, lipid peroxidation severely affected membrane integrity in root cells, as observed through the high uptake of Evans blue reagent by roots. *In vitro* studies have revealed that Se reacts with glutathione, causing excessive $O_2^{\bullet-}$ and, subsequently, H_2O_2 accumulation.[36] Se elevated oxidative stress in rice seedlings, and H_2O_2 accumulation was the

leading cause of Se-related toxicity.[4] Se-induced toxicity disrupted chloroplast and mitochondrial structure and function, leading to the overproduction of ROS.[5]

Plant cells possess a dedicated defense strategy, such as enzymatic antioxidants to detoxify ROS.[37] In the present study, antioxidant enzymes were differentially regulated to scavenge ROS produced under excess Se. For instance, Se decreased SOD and GPOX activities in root tissues, while it did not cause any significant effects in leaf tissues. Se-induced reduction of SOD activity was also observed in wheat and lettuce plants.[38,39] Numerous studies have revealed that excess Se diminished GPOX activity.[40–42] On the other hand, the activity of CAT, another H_2O_2 detoxifying enzyme, increased with Se supplementation, as observed in rice seedlings.[4] However, a reduction was ob-

served in certain plant species.[39,42] Foliar Se application at >100 ppm exceeded the toleration limits of the leaves of coffee plants exercising a pro-oxidant function, as observed by the increased ROS production and decreased activities of SOD, CAT, and APX.[35] However, rice seedlings exposed to Se presented higher CAT and APX activities and higher GSH contents, which probably counteracted the deleterious effects of ROS.[25] Differential regulation of antioxidant enzymes depending on the level of Se exposure suggests that varied mechanisms may play a role in overcoming Se toxicity.

CONCLUSION

Se exposure inhibited the growth of maize seedlings due to reduced photosynthetic pigment content and increased oxidative stress markers. Plants exposed to Se displayed high levels of $O_2^{\bullet-}$, H_2O_2, lipid peroxidation, and loss of membrane integrity. Maize seedlings regulated the antioxidant system to detoxify the Se-induced ROS accumulation, modulated by SOD, GPOX, and CAT. Further research on the impacts of Se on the transcriptome and proteome in plants can provide a better understanding of the effects of Se in maize.

ORCID IDs of the authors

Mustafa Yildiz   0000-0002-6819-9891
Emre Pehlivan   0000-0001-9405-0524
Hakan Terzi   0000-0003-4817-1100

REFERENCES

1. Reis AR, El-Ramady H, Santos EF, Gratao PL, Schomburg L. Overview of selenium deficiency and toxicity worldwide: Affected areas, selenium-related health issues, and case studies. In: Pilon-Smits E, Winkel L, Lin ZQ, eds. *Selenium in Plants: Molecular, Physiological, Ecological and Evolutionary Aspects*. Springer, Cham; 2017:209–230.

2. Castellano S, Novoselov SV, Kryukov GV, et al. Reconsidering the evolution of eukaryotic selenoproteins: A novel nonmammalian family with scattered phylogenetic distribution. *EMBO Reports* 2004;5:71–77.

3. Santesmasses D, Mariotti M, Guigó R. Computational identification of the genomes' selenocysteine tRNA (tRNASec). *PLOS Comput Biol*. 2017;13:e1005383. doi: 10.1371/journal.pcbi.1005383

4. Gouveia GCG, Galindo FS, Lanza MGDB, et al. Selenium toxicity stress-induced phenotypical, biochemical and physiological responses in rice plants: Characterization of symptoms and plant metabolic adjustment. *Ecotox Environ Safe*. 2020;202:110916. doi: 10.1016/j.ecoenv.2020.110916

5. Hasanuzzaman M, Bhuyan MHMB, Raza A, et al. Selenium in plants: Boon or bane? *Environ Exp Bot*. 2020;178:104170. doi: 10.1016/j.envexpbot.2020.104170

6. White PJ. Selenium metabolism in plants. *Biochim Biophys Acta* 2018;1862(11):2333–2342.

7. Golob A, Gadžo D, Stibilj V, Djikić M, Gavrić T, Kreft I. Sulphur interferes with selenium accumulation in Tartary buckwheat plants. *Plant Physiol Bioch*. 2016;108:32–36.

8. González-Morales S, Pérez-Labrada F, García-Enciso EL, Leija-Martínez P, Medrano- Macías J, Dávila-Rangel E. Selenium and sulfur to produce *Allium* functional crops. *Molecules* 2017;22:558. doi: 10.3390/molecules22040558

9. Gupta M, Gupta S. An overview of selenium uptake, metabolism, and toxicity in plants. *Front Plant Sci*. 2017;7:2074. doi: 10.3389/fpls.2016.02074

10. Bielecka M, Watanabe M, Morcuende R, et al. Transcriptome and metabolome analysis of plant sulfate starvation and resupply provide novel information on transcriptional regulation of metabolism associated with sulfur, nitrogen, and phosphorus nutritional responses in Arabidopsis. *Front Plant Sci*. 2015;5:805. doi: 10.3389/fpls.2014.00805

11. Schiavon M, Lima LW, Jiang Y, Hawkesford MJ. Effects of selenium on plant metabolism and implications for crops and consumers. In: Pilon-Smits EAH, Winkel LHE, Lin ZQ, eds. *Selenium in Plants: Molecular, Physiological, Ecological and Evolutionary Aspects*. Springer, Cham; 2017:275–357.

12. Reis AR, Boleta EHM, Alvez CZ, et al. Selenium toxicity in upland field-grown rice: seed physiology responses and nutrient distribution using the μ-XFR technique. *Ecotox Environ Safe*. 2020;190:110147. doi: 10.1016/j.ecoenv.2019.110147

13. Mostofa MG, Hossain MA, Siddiqui MN, Fujita M, Tran LSP. Phenotypical, physiological, and biochemical analyses provide insight into selenium-induced phytotoxicity in rice plants. *Chemosphere*. 2017;178:212–223.

14. Clemensson-Lindell A. Triphenyltetrazolium chloride as an indicator of fine-root vitality and environmental stress in coniferous forest stands: applications and limitations. *Plant Soil* 1994;159:297–300.

15. Wellburn AR. The spectral determination of chlorophylls a and b as well as total carotenoids, using various solvents with spectrophotometers of different resolution. *J Plant Physiol*. 1994;144:307–313.

16. Heath RL, Packer L. Photoperoxidation in isolated chloroplasts I. Kinetics and stoichiometry of fatty acid peroxidation. *Arch Biochem Biophys*. 1968;125:189–198.

17. Deuschle K, Funck D, Forlani G, et al. The role of Δ1-pyrroline-5-carboxylate dehydrogenase in proline degradation. *Plant Cell* 2004;16:3413–3425.

18. Lehotai N, Peto A, Bajkan S, Erdei L, Tari I, Kolbert Z. *In vivo* and *in situ* visualization of early physiological events induced by heavy metals in pea root meristem. *Acta Physiol Plant*. 2017;33:2199–2207.

19. Singh HP, Batish DR, Kaur G, Arora K, Kohli K. Nitric oxide (as sodium nitroprusside) supplementation ameliorates Cd toxicity in hydroponically grown wheat roots. *Environ Exp Bot*.

2008;63:158–167.

20. Bradford MM. A rapid and sensitive method for the quantification of microgram quantities of protein utilizing the principle of protein dye binding. *Anal Biochem*. 1976;72:248–254.

21. Beauchamp C, Fridovich Y. Superoxide dismutase: Improved assays and an assay applicable to acrylamide gels. *Anal Biochem*. 1971;44:276–287.

22. Aebi H. Catalase *in vitro*. *Method Enzymol*. 1984;105:121–126.

23. Mika A, Lüthje S. Properties of guaiacol peroxidase activities isolated from corn root plasma membranes. *Plant Physiol*. 2003;132:1489–1498.

24. Molnár Á, Kolbert Z, Kéri K, et al. Selenite-induced nitro-oxidative stress processes in *Arabidopsis thaliana and Brassica juncea. Ecotox Environ Safe*. 2018;148:664–674.

25. Cardoso AFS, Gomes FTL, Antonio JRR, et al. Sulfate availability and soil selenate adsorption alleviate selenium toxicity in rice plants. *Environ Exp Bot*. 2022;201:104971.

26. Mingji X, Chongling Y, Jing Y, Lily W. Impact of phenanthrene on organic acids secretion and accumulation by perennial ryegrass, *Lolium perenne* L., root. *B Environ Contam* Tox. 2009;83:75–80.

27. Malik JA, Goel S, Kaur N, Sharma S, Singh I, Nayyar H. Selenium antagonises the toxic effects of arsenic on mung bean (*Phaseolus aureus* Roxb.) plants by restricting its uptake and enhancing the antioxidative and detoxification mechanisms. *Environ Exp Bot*. 2012;77:242–248.

28. Hawrylak-Nowak B, Dresler S, Matraszek R. Exogenous malic and acetic acids reduce cadmium phytotoxicity and enhance cadmium accumulation in roots of sunflower plants. *Plant Physiol Biochem*. 2015;94:225–234.

29. Lanza MGDB, Silva VM, Montanha GS, Lavres J, de Carvalho HWP, dos Reis AR. Assessment of selenium spatial distribution using μ-XFR in cowpea (*Vigna unguiculata* (L.) Walp.) plants: Integration of physiological and biochemical responses. *Ecotox Environ Safe*. 2021; 207:111216. doi: 10.1016/j.ecoenv.2020.111216

30. Akbulut M, Çakir S. The effects of Se phytotoxicity on the antioxidant systems of leaf tissues in barley (*Hordeum vulgare L.*) seedlings. *Plant Physiol Biochem*. 2010;48:160–166.

31. Silva VM, Boleta EHM, Lanza MGDB, et al. Physiological, biochemical, and ultrastructural characterization of selenium toxicity in cowpea plants. *Environ Exp Bot*. 2018;150:172–182.

32. Saffaryazdi A, Lahouti M, Ganjeali A, Bayat H. Impact of selenium supplementation on growth and selenium accumulation on spinach (*Spinacia oleracea* L.) plants. *Not Sci Biol*. 2012;4:95–100.

33. Jain M, Panwar M, Gadre R. Influence of selenium supplementation on δ-aminolevulinic acid formation in greening maize leaf segments. *Res J Phytochem*. 2017;11:111–117.

34. Józwiak W, Politycka B. Effect of selenium on alleviating oxidative stress caused by a water deficit in cucumber roots. *Plants* 2019;8:217. doi: 10.3390/plants8070217

35. Mateus MPB, Tavanti RFR, Tavanti TR, Santos EF, Jalal A, dos Reis AR. Selenium biofortification enhances ROS scavenge system increasing yield of coffee plants. *Ecotox Environ Safe*. 2021;209:111772. doi: 10.1016/j.ecoenv.2020.111772

36. Spallholz JE. On the nature of selenium toxicity and carcinostatic activity. *Free Radical Bio Med*. 1994;17:45–64.

37. Mittler R, Vanderauwera S, Gollery M, Van Breusegem F. Reactive oxygen gene network of plants. *Trends Plant Sci*. 2004;9:490–498.

38. Xue T, Hartikainen H, Piironen V. Antioxidative and growth-promoting effect of selenium on senescing lettuce. *Plant Soil* 2001;237:55–61.

39. Łabanowska M, Filek M, Kościelniak J, Kurdziel M, Kuliś E, Hartikainen H. The effects of short-term selenium stress on Polish and Finnish wheat seedlings—EPR, enzymatic and fluorescence studies. *J Plant Physiol*. 2012;169(3):275–284.

40. Nowak J, Kaklewski K, Ligocki M. Influence of selenium on oxidoreductive enzymes activity in soil and in plants. *Soil Biol Biochem*. 2004;36:1553–1558.

41. Kong L, Wang M, Bi D. Selenium modulates the activities of antioxidant enzymes, osmotic homeostasis and promotes the growth of sorrel seedlings under salt stress. *Plant Growth Regul*. 2005;45:155–163.

42. Mroczek-Zdyrska M, Wójcik M. The influence of selenium on root growth and oxidative stress induced by lead in *Vicia faba* L. *minor* plants. *Biol Trace Elem Res*. 2012;147:320–328.

How to cite this article

Investigation into the Usability of the *Maackia amurensis* Lectin in Bacterial Diagnosis with the Help of Transmission Electron Microscope

Yosun Mater[1] (ORCID)

[1]Gebze Technical University, Molecular Biology and Genetics Department, Kocaeli, Turkiye

ABSTRACT

Objective: Glycoconjugates are known to play a crucial role in the attachment-recognition relationship of prokaryotic cells, particularly bacteria. Therefore, understanding the function and properties of these glycoconjugates is of great importance.

Materials and Methods: While various methods have provided significant information in determining the chemical structures and functions of sialic acids, histological methods have remained essential in determining their function and location in living organisms. The discovery of lectins with unique marking ability based on the bond structures of sialic acids and the development of antibodies, which can be microscopically distinguished by adding colloidal silver and gold particles, were significant milestones. In the 1990s, methods were developed to specifically mark the types and locations of sialic acids using immunocytological, histological, and fluorescence microscopy methods with fluorescently labeled lectins and antibodies. These methods still remain valid and important today. Using this information, it is possible to create smart drugs and biomarkers specific to bacteria.

Results: In this study, the unique connections of gold-labeled lectins with different bacteria were demonstrated with the help of transmission electron microscopy.

Conclusion: Our study supports the idea that labeled lectins could be used for rapid and precise bacterial diagnosis.

Keywords: Sialic acid, Bacteria, Biomarkers, Immunocytochemistry, Microscopy

INTRODUCTION

"Glycans", often referred to as oligosaccharides and polysaccharides, are found in all eukaryotic and prokaryotic cells, as well as viruses, including embryonic and pluripotent stem cells. They consist of a basic chain structure with added protein and lipids. When found on cell surfaces, glycans form the "Glycocalyx" layer.[1−5] This layer plays a crucial role in various cellular processes such as cell growth, differentiation, cell migration, disease pathogenesis, and immune system function.[1−3,5] One of the most significant glycans are sialic acids, which were initially discovered in saliva during the mid-1930s and subsequently referred to as sialic acid. In 1941, sialic acid was also identified in nerve cells and termed neuraminic acid. It was later established in the 1950s that sialic acid and neuraminic acid were identical structures consisting of 9-carbon acidic sugar molecules with a pH range of 2-3.[1] N-linked and O-linked glycans, as well as glycosphingolipids, are commonly situated at the outermost ends of biological systems.[1,5,6] When considering the tasks that are solely attributed to their receptor functions, several come to mind. These include primarily the formation of viral and bacterial infections, toxin binding, colony formation of bacteria, determination of serological characteristics, and the preservation of cell shape.[1,5,6]

One of the most commonly utilized methods for labeling surface glycoconjugates and unique sugar sequences is through the use of lectins. Lectins were first discovered in castor bean plant seeds in 1888. These molecules, which have the ability to agglutinate animal red blood cells, have attracted attention with this feature. Although its specific glycan binding properties are known, its biological functions in plants and other organisms are mostly unknown. Different classifications of lectins were later made, such as R-Type, L-Type, P-Type, C-Type, I-Type, Galectins and Bacterial Lectins. The *Maackia amurensis* lectin used in our study is an L-Type lectin and specifically binds to sialylated glycans.[5−7]

Lectins that are utilized to label sialic acids can be obtained from a variety of sources including vertebrates, arthropods, mollusks, protozoa, plants, bacteria, and viruses.[5] Lectins have been found to be useful in the detection of glycoconjugates in complex matrices and body fluids, even in trace amounts.

Additionally, they can be utilized to characterize compounds that bear a specific glycan structure. The mitogenic stimulation of lymphocytes and lectins in cell division can be leveraged due to their distinct and specific binding ability to detect glycostructures, virus and bacteria surfaces, and changes in cancer cells after malignant transformation. These changes may occur in cellular or non-cellular membrane elements or within the cell itself.[8−10]

The *Maackia amurensis* plant lectin (α2-3) utilized in our study is a lectin that specifically recognizes the motif [Siaα2-3Galβ1-4GlcNAc] from bound sialic acids. The *Maackia amurensis* lectin [MAL] demonstrates a unique ability to oligovalently bind (α2-3) sialic acids with high affinity. Conversely, it exhibits a weaker binding affinity towards sialic acids with monovalent (α2-3) linkages.[11]

The identification of bacteria at both the genus and species level was initially performed using morphological characteristics, followed by biochemical tests. However, these traditional methods are time-consuming, taking hours and days to complete. Therefore, molecular biological methods have gained importance in bacterial classification as a result of technological advancements. These methods are based on determining genes and their products and can be categorized into seven main groups. These include DNA-based methods such as 23S, 16S, and 5S rRNA sequence similarity, cataloging of oligonucleotides, analyses for the separation of total soluble proteins that form morphological and biochemical properties, cell wall analysis, serological profiles, and profiles of cellular fatty acids.[7,12,13]

The combined use of traditional and molecular biology-based techniques has facilitated the rapid classification of bacteria and the identification of new microorganism groups. In addition to these methods, automated classification devices such as the VITEK 2 Compact (bioMérieux Diagnostics) microbial identification and API identification systems are commonly used.[12] The VITEK 2 Compact system utilizes colorimetric cards containing 60-65 different tests to determine microorganisms at the species level within 5-8 hours.[13]

In our study, we examined bacterial surface differences using labeled lectins that could make highly specific connections. The feasibility of glycobiology-based bacterial identification was evaluated based on these bacterial cell surface differences. The originality of our work; the aim of this study is to examine the possibility of rapid and accurate bacterial species diagnosis by using the sensitive binding abilities of lectins to glycoconjugates. The method sensitivity was demonstrated by transmission electron microscopy. Based on the results of our study, we believe that the methods developed using labeled lectins can provide more sensitive results than the VITEK and API systems in bacterial species identification.

MATERIALS AND METHODS

In our study, we employed the *Maackia amurensis* lectin, a lectin that selectively recognizes the motif [Siaα2-3Galβ1-4GlcNAc] present on sialic acids (α2-3), as a marker to label bacterial samples from five different strains with three distinct cell morphologies and genera. To achieve this, we conjugated the *Maackia amurensis* lectin with colloidal gold particles measuring 10-12 nm, which were synthesized in our laboratory. The [Siaα2-3Galβ1-4GlcNAc] motif was specifically labeled on the cell membranes of bacteria using the colloidal gold-linked lectin.

To prepare the bacterial samples for microscopy, they were first fixed and embedded in epoxy resin. Thin sections were then obtained using a Reichert OM U3 ultramicrotome and micrographed using a JEOL 1010 transmission electron microscope.

The study employed five bacterial strains of three different cell morphologies and genera, including Gram-negative, coccobacillary strains of *Escherichia coli* ATCC 35860 (K92), ATCC 8739, and ATCC 29998, *Micrococcus luteus* ATCC 9341 in coccal form, and *Bacillus subtilis* ATCC 6634 bacteria in bacillus form.

The *Escherichia coli* ATCC 35860 (K92) strain (BOS12 strain) was isolated from cerebrospinal fluid and is used in sialic acid production and bacteriophage host assays. The *Escherichia coli* ATCC 8739 strain was isolated from feces and is utilized in various microbial tests, including media tests, impact tests, and quality tests. The *Escherichia coli* ATCC 29998 strain is a clinical isolate, particularly used in spectinomycin action spectacin tests and nutritional analysis. The *Micrococcus luteus* ATCC 9341 strain, currently known as the *Kocuria rhizophila* ATCC 9341 strain, is a soil isolate and is frequently used in antibiotic tests. The *Bacillus subtilis subsp. spizizenii* ATCC 6633 strain is a clinical isolate and is also utilized in antibiotic tests.

Bacteria were grown using Luria Broth (LB) and Luria Agar (LA) media. Broth inoculated with a single colony of bacteria grown for appropriate times on solid media was grown at 37 °C until sufficient optical density was achieved and stored in 50% glycerol at -20 °C and 15% glycerol at -80 °C until the marking step.

Preparation of Colloidal Gold

The preparation of colloidal gold followed the procedure outlined in Hayat.[14] To form gold-labeled lectins, a stock colloidal gold solution was first prepared using tetrachlorogold (III). Then, 5 mL of Na-citrate was added to boiling water, followed by the appropriate amount of 0.2% tetrachloroauric acid (gold). The mixture was allowed to boil for 5-10 min, during which red-colored colloidal gold particles were formed. The forma-

tion of the particles was confirmed by spectroscopic scanning $(OD_{400-600})$.

To control the agglutination of colloidal gold, 1% PEG 20,000 and 100 mM K_2CO_3 were added to 5 mL of the gold solution, and the pH of the solution was measured. The amount required for agglutination was determined, and the prepared colloidal gold was then challenged with the *Maackia amurensis* lectin.

Gold-Lectin Conjugation

The gold solution was prepared by adding 100 mM K2CO3 to particle-free glassware on a magnetic stirrer. Then, lectin was added dropwise to the mixture, followed by 1% PEG 20,000. The resulting mixture was centrifuged at 14,000 rpm at 4 °C, and the supernatant was discarded. The precipitates were then diluted with a mixture of PBS and PEG. The conjugates were scanned spectrophotometrically to determine the optimal amount for use.

Exposing the Bacteria to Colloidal Gold-Labeled Lectins

Bacteria were cultured in LB medium at the appropriate temperature. Samples (500 μl) were taken from each bacterial culture and transferred to sterile Eppendorf tubes. The samples were centrifuged at 7,000 rpm for 10 min, and the supernatant was discarded. The obtained precipitates were resuspended in 500 μl of salt solution (PBS pH 7.2/PEG 20,000). A 15 μl part of the samples was separated from the cells, centrifuged at 7,000 rpm for 10 min, and washed by adding 500 μl of salt solution (PBS/PEG 20,000) in sterile Eppendorf tubes.

Salt solution (10 μl) and gold-labeled lectins (10 μl) were added to each tube, and the appropriate storage conditions were observed. The samples were then fixed using TEM fixation steps and embedded in Epoxy resin.[7] Thin sections with a thickness of 250-300 Å were taken using the Reichert OM U3 ultramicrotome and stained with saturated uranyl acetate and 2.66% lead citrate. The samples were examined at 80 kV in a JEOL 1010 electron microscope, and micrographs were taken and evaluated for results.

RESULTS

In this study, we utilized colloidal gold-conjugated *Maackia amurensis* lectin (MAL) to specifically detect the motif [Siaα2-3Galβ1-4GlcNAc] (α2-3). MAL is known to especially bind oligovalently-bound (α2-3) sialic acids.[11] It uniquely marked the [Siaα2-3Galβ1-4GlcNAc] motif observed on the bacterial surfaces following the washing steps (Figures 1-5). When the results of the bacteria used in our study are examined, we see the presence of sialic acids with the [Siaα2-3Galβ1-4GlcNAc] motif in the cell membranes of the coccobacillus *Escherichia coli*

ATCC 35860 (K92) strain (Figure 1), *Escherichia coli* ATCC 8739 strain (Figure 2), and *Escherichia coli* ATCC 29998 strain (Figure 3). It should be noted here that all the bacteria samples examined in this study have the [Siaα2-3Galβ1-4GlcNAc] motif in their membranes, but the densities of oligovalently-bound (α2-3) sialic acids were different even among the various strains of the same bacteria. The *Escherichia coli* ATCC 35860 (K92) strain (Figure 1) and *Escherichia coli* ATCC 8739 strain (Figure 2) specifically exhibited more intense labeling indicating a higher concentration of the [Siaα2-3Galβ1-4GlcNAc] motif. On the other hand, oligovalently-bound (α2-3) sialic acids were found to be quite low in the *Escherichia coli* ATCC 29998 strain (Figure 3).
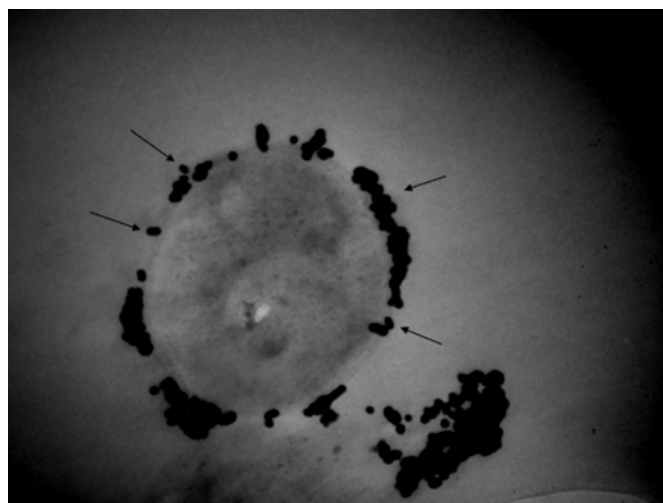
Figure 1. The *Escherichia coli* ATCC 35860 (K92) strain, exhibiting a coccobacillus structure (α2-3) with sialic acids, which were marked with gold-labeled MAL ($\rightarrow$) at a magnification of 100,000X.
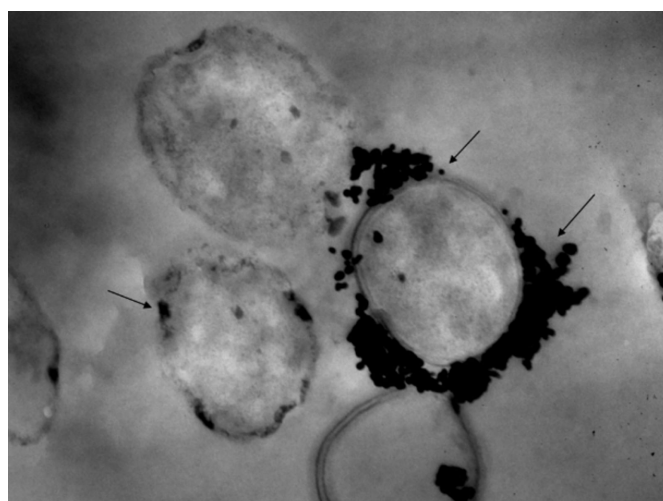
Figure 2. The *Escherichia coli* ATCC 8739 strain, exhibiting a coccobacillus structure (α2-3) with sialic acids, was visualized using gold-labeled MAL ($\rightarrow$) at a magnification of 75,000X.
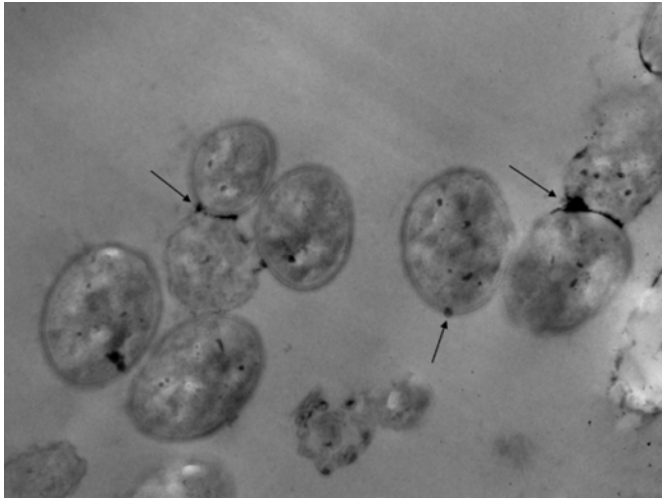
Figure 3. The *Escherichia coli* ATCC 29998 strain, exhibiting a coccobacillus structure (α2-3) with sialic acids, was visualized using gold-labeled MAL (→) at a magnification of 30,000X.

The presence of sialic acid bearing the motif [Siaα2-3Galβ1-4GlcNAc] in the coccus form of *Kocuria rhizophila* ATCC 9341 (formerly known as *Micrococcus luteus* ATCC 9341) is observed to be in a very limited quantity, as depicted in Figure 4.
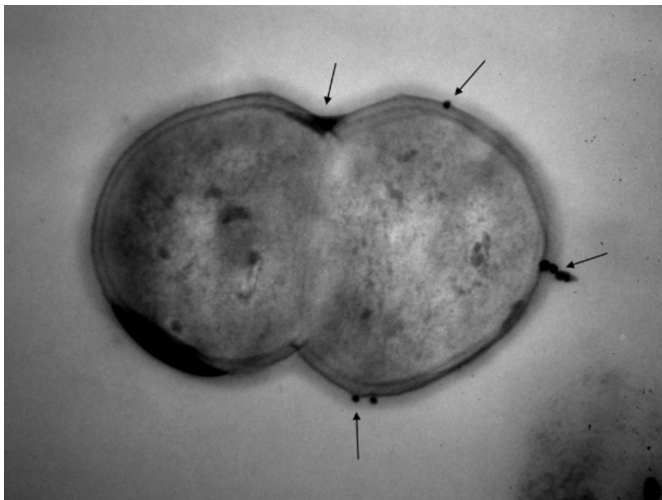
Figure 4. The coccus form of *Micrococcus luteus* ATCC 9341, now classified as the *Kocuria rhizophila* ATCC 9341 strain, displays α2-3 sialic acids labeled with gold using MAL (→) at a magnification of 100,000X.

In the study, it was observed that *Bacillus subtilis* ATCC 6633 cell membrane, in the form of bacillus, contained oligovalently-bound (α2-3) sialic acids which were highly labeled with colloidal gold bound - MAL (Figure 5).

DISCUSSION

The *Maackia amurensis* plant lectin used in our study is a lectin that specifically recognizes the oligovalently-bound
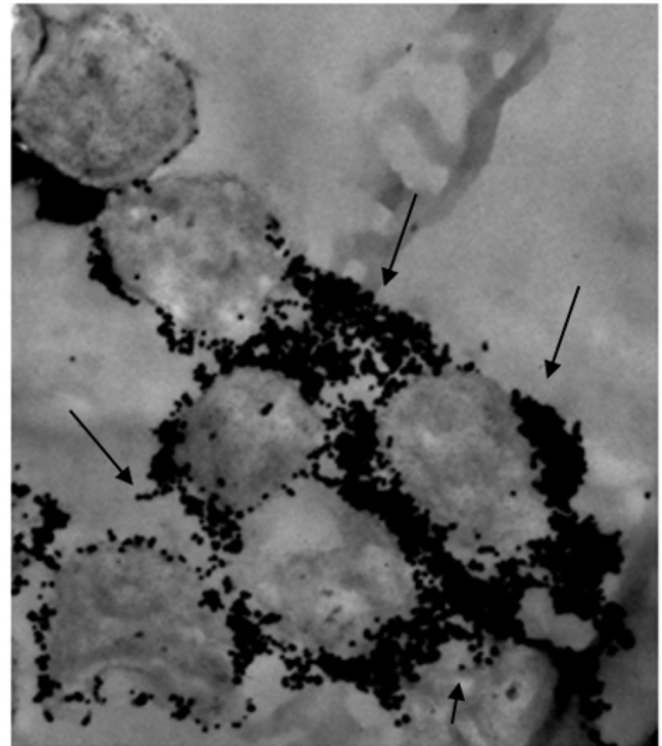
Figure 5. The presence of sialic acids in *Bacillus subtilis* ATCC 6633 strain (α2-3) in its bacillus form was confirmed through gold labeling with MAL (→) at a magnification of 30,000X.

(α2-3) sialic acid motif [Sia2-3Galβ1-4GlcNAc]. The lectin was conjugated with colloidal gold, which was prepared in our laboratory. We investigated bacteria with various cell morphologies, including coccus, coccobacillus, and bacillus forms. The bacterial strains used in this study were Gram-negative coccobacillus *Escherichia coli* strains ATCC 35860 (K92), ATCC 8739, and ATCC 29998, and Gram-positive coccus form *Micrococcus luteus* ATCC 9341, and bacillus form *Bacillus subtilis* ATCC 6634. These morphologies are the most common in bacteria, some of which may have pathogenic properties. These are important species that are frequently encountered in microbiological studies. The lectin-labeling of bacteria was visualized ultrastructurally (Figures 1-5) and quantified to determine the amount of oligovalently-bound (α2-3) sialic acids in different bacterial genera and morphologies (Figures 1, 4 and 5). Specifically, we compared the amount of [Siaα2-3Galβ1-4GlcNAc] sialic acid motif in *Escherichia coli*, *Micrococcus luteus* ATCC 9341, and *Bacillus subtilis* ATCC 6634 strains, as well as in different species of Gram-negative coccobacilli belonging to the same genus (ATCC 35860 [K92], ATCC 8739, and ATCC 29998) (Figures 1-3) of Gram-negative, coccobacillary *Escherichia coli* of different species belonging to the same genus (Figures 1-3). Our results provide serologically sensitive information about the genus and species of bacteria based on the specific labeling of surface glycoconjugates with lectins. The results were verified visu-

ally and ultrastructurally by micrographs (Figures 1-5), which supported previous findings in the literature.[15–17]

Studies on sialic acid and its metabolism in prokaryotes have mainly focused on gene regions associated with capsule synthesis due to their involvement in disease-causing properties.[16–19] Although different bacteria (e.g., *E. coli* K1, K12, K92, O24, O37, O104, O56, O157, O111, BOS12, *Neisseria meningitidis, Haemophilus influenzae, Campylobacter jejuni, Staphylococcus epidermidis, Streptococcus pneumonia, Brucella, etc.*) exhibit striking similarities in determinant organization; the degree of virulence is determined by the existence and type of polysaccharides on the surface of cell membrane.[1,5,7] Based on the findings of our study, we have obtained supportive evidence regarding pathogenicity at the ultrastructural level. Our results indicate that the surface of the selected bacteria contained a higher concentration of sialic acid with an increase in the range of bacteria used. Notably, the *Bacillus subtilis* ATCC 6634 strain demonstrated the most significant labeling, followed by the *Escherichia coli* strains ATCC 35860 (K92), ATCC 8739, and ATCC 29998, which exhibited similar but less pronounced labeling (Figures 1-3 and 5).

This study demonstrates the feasibility of distinguishing between different bacterial species using *Maackia amurensis* lectin, which selectively binds to α2-3 sialic acid units on bacterial surfaces. The observed variations in sialic acid density among strains of the same *Escherichia coli* species suggest that this method can also differentiate between strains within a species. The visual results obtained provide evidence that lectins can provide specific and precise binding, enabling accurate distinction between genera and species. These findings are consistent with previous studies in the literature.[1,5]

CONCLUSION

Transmission electron microscopy has demonstrated that bacterial diagnosis can be achieved at the genus and species level by utilizing specific lectins. This method is based on glycobiology and employs labeled lectins to form unique connections with sialic acid units. These findings suggest that immunofluorescent labeled lectins could be used to develop a practical, rapid, and specific bacterial diagnosis method.

Based on these findings, we aim to develop biomarkers for the genus and species-level diagnosis of bacteria using immunofluorescently-labeled lectins. Additionally, we aim to develop techniques suitable for fluorescent microscopes, which can be considered a faster and easier method for sensitive diagnosis.

ORCID IDs of the author

Yosun Mater   0000-0002-7161-0637

REFERENCES

1. Schauer R, Kamerling JP. Exploration of the sialic acid world. *Adv Carbohydr Chem Biochem*. 2018;75:1-213.

2. Alagesan K, Hoffmann M, Rapp E, et al. Glycoproteomics technologies in glycobiotechnology. *Adv Biochem Eng Biotech*. 2021;175:413-434.

3. Sackstein R, Hoffmeister KM et al. Sialic acids in human health and disease. In Varki A, Cummings RD et al. editors. *Essentials of Glycobiology*. 4th ed. New York, N.Y.: Cold Spring Harbor Laboratory Press; 2022. Chapter 46.

4. Lanctot PM, Gage FH, Varki AP. The glycans of stem cells. *Curr Opin Chem Biol*. 2007;11:373-380.

5. Varki A, Cummings RD, Esko JD, et al. *Essentials of Glycobiology*. 4th ed. New York, N.Y.: Cold Spring Harbor Laboratory Press; 2022.

6. Song Y, Zhang F, Linhardt RJ. Glycosaminoglycans. *Adv Exp Med Biol*. 2021;1325:103-116.

7. Mater Y. The cloning, expression and structure-function relationships of the *Escherichia coli* sialyltransferase gene. Ege University, Graduate School of Natural and Applied Science, PhD Thesis, 2004.

8. Silva M, Luísa S. Lectin biosensors in cancer glycan biomarker detection. *Adv Clin Chem*. 2019;93:1-61.

9. Mater Y, Ozdas S. The analysis of surface saccharide profiles through fluorescein-labelled lectins in a rat pancreatic tissue with established metabolic syndrome model. *Turkish J Biochem*. 2019;44:98-104.

10. Demircan G, Mater Y. Effects of fluorescent marked *Maackia amurensis*-lectin-1 and wheat germ agglutinin on the cell surface glycan profiles in two different breast cancer cell lines. *J Ist Faculty Med*. 2019;82:89-95.

11. Kamerling JP, Gerwig GJ. Strategies for the structural analysis of carbohydrates. *Comprehensive Glycoscience*. 2007;2:1-68. doi:10.1016/B978-044451967-2/00032-5.

12. Biomerieux Diagnostics website. https://www.biomerieux-diagnostics.com/vitek-2-advanced-expert-system. Accessed October 20, 2023.

13. Madigan MT, Bender KS, Buckley DH *Brock Biology of Microorganisms*. 16th ed. New York, N.Y.: Pearson Education Limited; 2021.

14. Hayat MA. *Colloidal Gold Principles, Methods and Applications*. San Diago, California: Academic Press; 1989.

15. Jones CJP, Allen WRT, Wilsher S. A lectin histochemical study to detect variation in glycosylation at the feto-maternal interface in three interbreeding equine species. *Placenta*. 2017;58:115-121.

16. Hu M, Lan Y, Lu A, Ma X, Zhang L. Glycan-based biomarkers for diagnosis of cancers and other diseases: Past, present, and future. *Prog Mol Biol Transl Sci*. 2019;162:1-24.

17. Zhang XL, Qu H. The role of glycosylation in infectious diseases. *Adv Exp Med Biol.* 2021;1325:219-237.

18. Fujitani N, Furukawa J, Araki K, et al. Total cellular glycomics allows characterizing cells and streamlining the discovery process for cellular biomarkers. *Proc Natl Acad Sci USA.* 2013;110(6):2105-2110.

19. Costa AF, Campos D, Reis CA, et al. Targeting glycosylation: A new road for cancer drug discovery. *Trends Cancer*. 2020;6(9):757-766.

How to cite this article

Physiological and Biochemical Changes of Maize (*Zea mays* 'MV500') in Response to Heat Stress under Levels of Salicylic Acid

Esmail Nabizadeh[1], Narges Dolatmand[2], Masoud Haghshenas[3], Khadijeh Ahmadi[4]

[1]Islamic Azad University, Department of Agronomy, Faculty of Agricultural, Mahabad Branch, Mahabad, Iran
[2]Kurdistan University, Department of Agronomy and Plant Breeding, College of Agriculture, Sanandaj, Iran
[3]University of Mohaghegh Ardabili, Department of Horticulture, Faculty of Agriculture, Ardabil, Iran
[4]Shahed University, Department of Agronomy and Crop Breeding, College of Agriculture, Tehran, Iran

ABSTRACT

Objective: Heat stress is a significant factor leading to decreased crop yield. Exceeding the plant's temperature tolerance threshold in ecosystems often results in significant cellular damage and potentially cellular death. Signaling elicitors may mitigate elevated temperatures' detrimental impact and enhance plant defense mechanisms.

Materials and Methods: The present study investigates the influence of varying temperatures (25, 30, 35, 40, and 45°C) and pre-harvest salicylic acid (SA) application (0, 0.5, 1.5, 2.5, 5, and 10 mM) on the morpho-physiological and biochemical attributes of maize. A factorial-based experiment was set up following a completely randomized design and conducted in a growth room.

Results: The findings demonstrated that a 2.5 mM SA treatment at 35°C produced the largest plant leaf area and total chlorophyll content. The temperature and SA application interplay on carotenoid content were maximum at 5 mM. SA treatment under high-temperature conditions effectively elevated proline content, chl a, chl b, chl total, and malondialdehyde compared to untreated plants. The peak stomatal conductance was also observed with a 2.5 mM SA treatment at 30°C. The maximal catalase and peroxidase activities were recorded at 35°C. Furthermore, 2.5 mM SA at 25°C resulted in the highest levels of soluble proteins and RWC. SA (2.5 mM) applied at 30°C was more efficient at decreasing H2O2 production. The highest proline content was observed with 2.5 mM SA at 45°C.

Conclusion: SA (2.5 mM) treatment can have optimal effects on maize plant growth parameters under high-temperature conditions, potentially mitigating the damaging effects of heat stress.

Keywords: Antioxidant, Biological Yield, Heat Stress, Proline, Soluble Protein.

INTRODUCTION

Globally, maize (*Zea mays L.*) ranks second in production per unit area after wheat.[1] As one of the primary crops in temperate and subtropical regions, maize contributes 20-25% to human food sources, 60-75% to animal feed, and 5% to industrial raw materials. This crop has to endure numerous biotic (like herbivores and pathogens) and abiotic (such as radiation, drought, salinity, and temperature) stresses.[2] Heat stress refers to a temperature increase beyond a specific limit long enough to inflict irreversible harm to plant growth and development. Typically, a rise of 10-15°C above the ideal temperature is deemed heat stress. One of the most critical processes adversely affected by heat stress is photosynthesis.[3] Maize, being a C4 plant, requires a higher optimum temperature for photosynthesis, attributable to a CO_2-concentrating system that curbs Rubisco oxygenase activity.[4]

The plant's survival under stress hinges on its ability to detect the stimulus, respond to the perceived signal, and generate biochemical compounds to adapt to the conditions. Several factors, including calcium, ethylene, jasmonic acid, and salicylic acid (SA), have been identified as plant stress signals.[5] SA acts as a signaling molecule, triggering plant responses to environmental stressors. Recent genetic studies have revealed that over 90% of SA is derived from isochorismate. While the role of isochorismate synthases in SA production is well-established, the enzyme responsible for converting isochorismate to SA remains unidentified. The functionality of SA in protecting against various biotic and abiotic stresses is well-documented.[6]

Additionally, SA inhibits ethylene production, respiration, and senescence.

As a plant growth regulator, SA regulates several physiological reactions, including photosynthesis, stomatal closure, transpiration, chlorophyll synthesis, and mineral uptake.[7-9] Furthermore, by influencing catalase (CAT) and peroxidase (POD) activity and boosting the accumulation of osmotic solutes such as proline and glycine betaine, SA mitigates various stresses (like heat, cold, salinity, and heavy metals).[10] Also, SA can impact superoxide dismutase (SOD) enzyme activity, converting free oxygen radicals into hydrogen peroxide. While hydrogen peroxide (H_2O_2) can be harmful, it can also serve as a signaling molecule at low concentrations.[11] The increase in root and shoot dry weight and overall plant biomass is likely connected to the photosynthetic efficiency of SA treatments.[12] The photosynthetic efficiency of plants using SA is tied to increased Rubisco activity and chlorophyll content.[13] The increase in leaf quantity and surface area, which are photosynthetic indicators, could be another benefit of SA treatment.[10] Given the role of SA in enhancing plant tolerance to environmental stressors and considering global warming, this experiment examined whether SA could boost the photosynthetic capacity, antioxidant activity, and biological defense system of maize 'MV500' in response to heat stress.

MATERIALS AND METHODS

Experimental Procedure and Treatment Application

This research assessed the impact of varying temperature degrees (25, 30, 35, 40, and 45°C) and the foliar administration of SA at different concentrations (0, 0.5, 1.5, 2.5, 5, and 10 mM). The experiment focused on maize seedlings' morphological, physiological, and biochemical characteristics. The experimental setup was a factorial structure arranged in completely randomized blocks with three replicates in a growth chamber.

The maize seeds used for the experiment were procured from the Seed and Plant Improvement Institute (SPII). The study was carried out as a pot experiment in 2018 within the research greenhouse of the Islamic Azad University of Mahabad, situated at a latitude of 35° 58'N, a longitude of 44° 3'E, and an altitude of 1354 m above sea level in the West Azerbaijan Province, Iran. The experiments were conducted at the Islamic Azad University of Mahabad.

Maize 'MV500' seeds were sown in loamy clay soil in the growth chamber, which had a light/dark cycle of 16/8 h, a light intensity of 14Klux, a relative humidity (RH) of 65±2%, and a day/night temperature of 23±2/16±2°C (GROUC; Iran). The pots were watered daily.

The treatments were initiated after the maize plants had developed three leaves, a stage that lasted for 3 days. The seedlings were subjected to various temperature degrees for 3 h daily

(Figure 1). The physical and chemical attributes of the farm soil used in the experiment are presented in Table 1.

Stomatal Conductance, Leaf Area Index (LAI), and Photosynthetic Pigments Evaluation

We used a portable probe (1600-LI) to gauge the stomatal conductance of maize leaves. After the experiment, we quantified the plant leaf area using a leaf area meter (A 300; UK). From each test unit, we picked several mature young leaves. Using a Porometer (Leaf Porometer; SN: LP2402; Decagon, US), we computed their average stomatal conductance (mM (H_2O) $m^{-2}s^{-1}$) early in the morning. To determine the photosynthetic pigments (for instance, chlorophyll a, b, and total chlorophyll), we sampled fully matured leaves, dissolved them in 80% acetone, and centrifuged them. We measured each sample's absorption using a spectrophotometer (Perkin Elmer, Lambda 25, UV/VIS Spectrophotometer) at wavelengths of 663.2, 646.8, and 470 nm for chlorophyll a, chlorophyll b, and total chlorophyll content, respectively. The pigments' quantity was subsequently computed based on µg/g fresh weight per the provided formula.[14]

$$Chlorophyll\ a = (12.25 X A_{663.2}) \check{} (2.79 X A_{646.8}) \qquad (1)$$

$$Chlorophyll\ b = (21.21 X A_{646.8}) \check{} (5.1 X A_{663.2}) \qquad (2)$$

$$Total Chlorophyll\ (a+b) = (7.15 X A_{663.2} + 18.71 X A_{646.8}) \qquad (3)$$

$$Carotenoid = ((1000 X A_{470}) - (1.8 X Chla) \qquad (4)$$

$$- (85.02 X Chlb))/198 \qquad (5)$$

$A_{663.2}$: Absorption in wavelength of 663.2; $A_{646.8}$: Absorption in wavelength of 646.8; A_{470}: Absorption in wavelength of 470.

Cell Membrane Stability (Electrolyte Leakage) Assessment

We transferred 1g of fresh leaf tissue into a falcon containing 20 ml of deionized water to evaluate the cell membrane stability. After 24 h at 25°C, we read the samples' electrolyte leakage (L1) using a conductivity meter (Aqualytic Sensdirect, CD24). We autoclaved the samples for 20 min at 120°C, cooled them down, and read the solution's electrical leakage (L2) again. The cell membrane stability percentage was then calculated as per the formula provided.[15]

$$Electrolyte\ leakage(\%) = (L_1/L_2) \times 100 \qquad (6)$$

Relative Water Content (RWC) Measurement

We cut pieces of fully matured leaves into 1 cm^2 and weighed them (FW). Then, we placed the samples in a petri dish filled with distilled water and weighed them in a 4°C incubator after 4 h (TW). Lastly, we put the samples in a 72°C oven for 72 h,
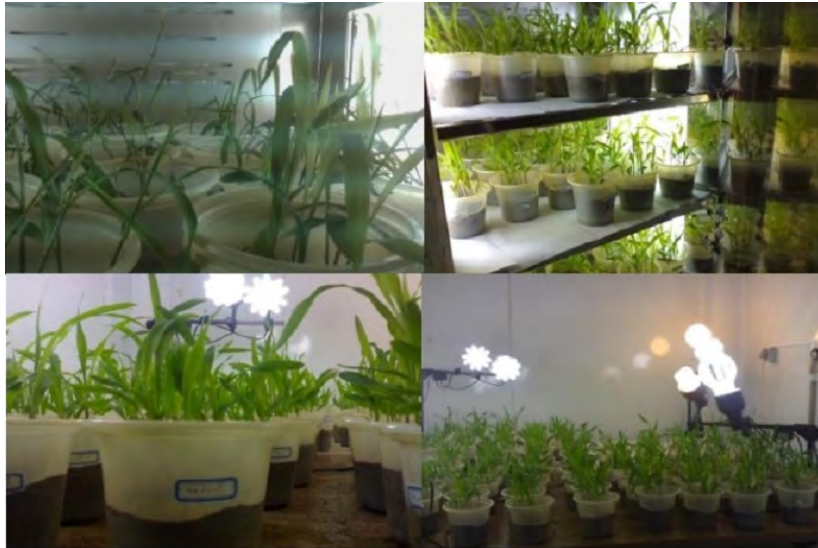
Figure 1. The stages of applying experimental treatments on maize 'Mv500'.

Table 1. Experimental soil analysis results.

pH	N(ppm)	P(ppm)	K(ppm)	Soil Texture (%)	Saturation Percent (%)	Clay (%)	Sand (%)	Silt (%)	Organic Carbon (%)
8.09	0.6	7.40	194.3	Loamy Clay	47.44	38	4-30	22	1.22

weighed them once more (DW), and calculated their relative water content according to the provided formula.[16]

$$RWC = (FW - DW)/(SW - DW) \times 100 \qquad (7)$$

Biological Yield (Biomass) Calculation

After harvest, we measured the leaf, shoot, and stem fresh weights. The plant was then dried in a 70°C oven, and the biomass (dry weight) was measured with 0.001 accuracy.

Enzymatic Extract Preparation

We used the method by Kang and Saltveit[17] with slight modifications. Specifically, we homogenized 0.5 g of leaf fresh weight at 4°C in 3 ml of extraction buffer (50 mM Tris-Hcl buffer, pH 7.5, 3 mM $MgCl_2$, 1 mM Na-EDTA). We then centrifuged the homogenate (Hermle Z 216 MK; Germany) for 20 min at 5000 rpm at 4°C. We used the supernatant as the crude extract to assay CAT, POD, and ascorbate peroxidase (APX) enzyme activity.

Catalase Activity (EC 1.11.1.6) Assessment

We used the method by Aebi.[18] to assay CAT activity. The reaction mixture consisted of 2.5 ml of 50 mM phosphate buffer (pH 7), 0.2 ml of 1% H_2O_2, and 0.3 ml of enzyme extract. We measured the catalase activity as a decrease in absorption at 240 nm and extinction coefficient (0.0436 mM^{-1} cm^{-1}) as per the provided formula.

$$Units\left(\frac{mM}{min}\right) = \frac{\text{dOD}}{\text{min(slope)}} \times \frac{\text{vol of assay (0.0003)}}{\text{Extinction coefficient (0.0436)}}$$

Assessing Peroxidase Activity (EC 1.11.1.7)

The method outlined by Upadhyaya et al.[19] was used to measure POD activity. The reaction mix included 2.5 ml of 50 mM phosphate buffer (pH= 7), 1 ml of 1% H_2O_2, 1 ml of 1% Guaiacol, and 0.1 ml of enzyme extract. One minute was set to monitor the increase in absorbance at 420 nm. The POD activity was then calculated using the extinction coefficient (26.6 mM^{-1} cm^{-1}) in the equation:

$$Units\left(\frac{mM}{min}\right) = \frac{\text{doD}}{\text{min(slope)}} \times \frac{\text{vol of assay(0.0001)}}{\text{Extinction coefficient (26.6)}}$$

Evaluating Ascorbate Peroxidase Activity (EC 1.11.1.11)

The activity of APX enzyme was gauged based on the procedure of Nakano and Asada.[20] This reaction mix contained 2.5 ml 50 mM phosphate buffer (pH 7), 0.1 ml EDTA, 1 mM sodium ascorbate, 0.2 ml of 1% H_2O_2, and 0.1 ml enzyme extract. The APX activity was determined by the decrease in absorption at 240 nm, and the extinction coefficient (2.8 mM^{-1} cm^{-1}) was utilized in the following calculation:

$$Units\left(\frac{mM}{min}\right) = \frac{doD}{min(slope)} \times \frac{vol\ of\ assay\ (0.0001)}{Extinction\ coefficient\ (2.8)}$$

Measuring Protein Content

To estimate the protein levels, a gram of fresh leaf tissue was blended in 5 ml of Tris buffer (0.05 M, pH 7.5). The mixture was centrifuged at 10,000 × g for 25 min at 4°C. The soluble protein concentration was determined using 0.1 ml protein extract and 5 ml of biuret reagent (0.1 g Kumasi Brilliant Blue G250+50 ml of 95% ethanol+100 ml phosphoric acid 85%), which was then diluted to a liter with distilled water. The solution was filtered using a Whatman filter and mixed with a vortex. Absorbance was read at 595 nm by a spectrophotometer (UV/VIS Lambda25 Perkin Elmer) after 2 min, and the concentration was computed based on the bovine serum albumin standard curve.[21]

Quantifying Lipid Peroxidation

In a nutshell, 200 mg of fresh leaf tissue was crushed in 5 ml 0.1% (w/v) TCA. The homogenate was centrifuged (Hermle Z216 MK; Germany) for 5 min at 10,000 × g. Then, 1 ml of the supernatant was added to 4 ml of 20% TCA solution containing 0.5% TBA and boiled for 30 min at 95°C. After cooling in ice, the mixture was centrifuged for 10 min at 10,000 × g. Absorbance was read at 532 nm wavelength. The red complex (malondialdehyde (MDA)-TBA) was targeted for absorption at this wavelength, and non-specific absorption was read at 600 nm and subtracted from the previous value. The extinction coefficient (155 mM^{-1} cm^{-1}) was used to calculate MDA concentration.[22]

Evaluating Hydrogen Peroxide Levels

The method adapted from Velikova et al.[23] was used to measure the H_2O_2 content. A 200 mg leaf tissue sample was homogenized in an ice bath with 3 ml of 0.1% (w/v) TCA. This homogenate was then centrifuged at 12,000 × g for 15 min. One ml of the supernatant was added to 1 ml of 10 mM potassium phosphate buffer (pH= 7.0) and 2 ml of 1 M KI. The absorbance of the supernatant was measured at 390 nm. The H_2O_2 content was determined using the extinction coefficient (0.28 mM^{-1} cm^{-1}).

Proline Measurement Process

The procedure for assessing proline was adapted from Bates et al.[24], but with minor changes. In brief, a 0.1 g of fresh leaf tissue sample was ground up in 10 ml of 3% sulfo-SA. This solution was then spun in a centrifuge (Hermle Z216 MK, Germany) for a quarter of an hour at 4000 revolutions per minute. Following this, 2 ml of the resulting supernatant was combined with 2 mg of ninhydrin reagent and 2 ml of acetic acid. The concoction was then heated in a bath at 100°C for 1 h. The reaction was halted by cooling the mixture in an ice-water bath. Subsequently, 4 ml of toluene was added, which led to the formation of two distinct layers. The proline content was measured using the supernatant. The absorbance was noted at a wavelength of 520 nm, and the proline content was determined using a standard curve.

Statistical Analysis

The data gathered was processed using SAS 9.4 software, and the mean values of the treatments were compared utilizing the Duncan test, with a significance threshold set at 0.05

RESULTS

Growth Metrics

Indicators of photosynthetic capacity (chlorophyll a, chlorophyll b, total chlorophyll content, and carotenoids) were significantly influenced by the treatments (p<0.01). The combined effect of SA at a concentration of 2.5 mM and a temperature of 35°C yielded the highest leaf area, chlorophyll a (5.58 mg/g FW), total chlorophyll content (7.76 mg/g FW). The interaction of SA (10 mM) and a temperature of 35°C resulted in the highest chlorophyll b (2.35 mg/g FW), and the maximum carotenoid content (1.84 mg/g FW) was obtained at a concentration of 5 mM SA and temperature of 35°C. The most excellent stomatal conductance was recorded under the joint treatment of SA (2.5 mM) and a temperature of 30°C (Table 2).

Impact of SA and Temperature on RWC

RWC demonstrated a significant correlation between SA and temperature (p<0.05). The data revealed a decline in RWC across all SA concentrations as the temperature escalated from 25°C to 45°C. The highest RWC was observed at 25°C when the concentration of SA was increased to 2.5 mM. However, as SA concentrations reached 5 and 10 mM, there was a notable reduction in RWC (Table 3).

Lipid Peroxidation

The stability of the MDA was shown to be significantly impacted by both SA and temperature (p<0.01), as well as their combined effect (p<0.05). The most stable cell membranes were

observed at different SA levels at 25°C, whereas the least stable was observed in the control treatment at 45°C. As the temperature rose, electrolyte leakage increased across all SA concentrations. However, SA application at 25°C, 30°C, and 35°C did not significantly impact leaf electrolyte leakage. Contrarily, at 40°C and 45°C, electrolyte leakage decreased with up to 2.5 mM of SA application. This trend reversed with 5 and 10 mM SA concentrations, where electrolyte leakage increased (Table 3).

Impact on Biological Yield

Leaf, stem, and plant dry weight, as measures of plant biomass, were significantly influenced by the interaction of temperature and SA (p<0.01). The lowest weights for leaf, stem, and plant were recorded when the temperature was at 45°C and the SA concentration was at 10 mM. Elevated levels of SA did not alleviate heat stress, but instead exacerbated it. Conversely, SA at a concentration of 2.5 mM moderated heat stress and resulted in the highest leaf, stem, and plant dry weight at 35°C. This led to an increase of 29%, 36.6%, and 31%, respectively, compared to the control treatment (Table 3).

Antioxidant Enzymes Activity

An increase in APX activity was seen with SA (p<0.01). This increase followed the trend of raising SA concentrations to 2.5 mM. The highest APX activity, showing a 10.48% increase compared to the control, was achieved with a SA concentration of 2.5 mM. However, when SA concentration rose from 5 mM to 10 mM, APX activity declined (Figure 2). The effect of temperature on APX activity was less pronounced. APX activity increased at 30°C and 35°C but decreased beyond the plant's tolerance threshold at 40°C and 45°C (Figure 2). Similarly, CAT and POD activity were significantly affected by the interaction of temperature and SA (p<0.05). The highest activity levels of CAT and POD were recorded at 35°C. When the temperature was raised from 35°C to 40°C and 45°C, CAT and POD activities decreased (Figure 3).

MDA and H_2O_2

When the temperature increases, MDA content correspondingly escalates. At 45°C, the MDA content was approximately 62.87% greater than at 25°C (Figure 4). SA (2.5 mM) decreased the MDA content by about 14.92% compared to the control. However, when the concentration of SA rose, there was a corresponding rise in MDA content (Figure 4). Reactive oxygen species (ROSs) play a significant role in lipid peroxidation. In this study, the production of ROSs was affected by the interaction of SA and temperature (p<0.01). The maximum and minimum levels of H_2O_2 were found in the control group at 45°C and the SA (2.5 mM) group at 30°C, respectively (Figure 4).

Soluble Proteins

Both SA and temperature significantly impacted the content of soluble proteins (p<0.01). As the temperature rose by 10-15°C, from 30-35°C, a 60% decrease in soluble protein content was noticed at all tested SA levels. The highest content of soluble proteins was observed when 2.5 mM of SA was applied at 25°C (Figure 5).

Proline

The proline content was significantly influenced by SA, temperature, and the interactive effect of SA and temperature (p<0.01). The maximum proline content (47.13 µmol/g FW) was recorded with a SA (2.5 mM) treatment at 45°C. The minimum proline content (10 µmol/g FW) was noticed in the control SA group at 25°C. When the temperature was raised to 40 and 45°C, an increase in SA concentration up to 2.5 mM increased proline content. However, higher concentrations of SA at 5 and 10 mM led to a decrease in proline content (Figure 6).

DISCUSSION

Heat stress notably impacts maize plants' growth and metabolic activities. Such stress instigates physiological alterations in the plants, which eventually induce morphological modifications. Our study observed that these heat stress effects resulted in a decline in the maize plants' morphological and physiological attributes. However, administering SA in varying concentrations, particularly a concentration of 2.5 mM, enhanced the maize plants' growth and physiological features.

As the temperature increases, the photosynthetic system suffers irreversible damage, particularly the photosynthetic pigments. Yet, SA demonstrated its ability to manage heat stress in temperatures exceeding the plant's tolerance threshold. This allowed for an improvement in the photosynthesis mechanism within the bio-kinetic zone. Photosystem II (PSII), lipid permeability, and rubisco activase are critical components of the photosynthetic apparatus mechanisms affected by heat stress.[25] The photosynthetic capacity of a plant fluctuates significantly under heat-stress conditions. Gradual temperature increases and heat shock factors (HSFs)[12] elicit distinct plant responses. Photosynthesis is a crucial factor influencing maize productivity, particularly within an optimal temperature range of 28-37.5°C. In the course of our study, it was found that chlorophyll a, chlorophyll b, total chlorophyll content, and carotenoid levels declined as temperature increased. However, treatment with 2.5 mM of SA increased the amount of chlorophyll a and total chlorophyll. When the SA concentration was increased to 5 and 10 mM, the chlorophyll b and carotenoid amounts, respectively. A temperature of 35°C and SA treatment in varied concentrations produced beneficial outcomes compared to both high and low temperatures. The reduction in photosynthesis is due to damage to the oxygen-releasing complex, resulting from the

Table 2. The effect of temperature stress and salicylic acid treatments on the photosynthetic capacity of maize (*Zea mays L.*).

	Temperatures	LAI (cm²)	Chl a (mg/g FW)	Chl b (mg/g FW)	Total Chl (mg/g FW)	Carotenoid (mg/g FW)	SC (mM (H_2O) m⁻² s⁻¹)
Control	25°C	162.3±2.9 gh†	3.22±0.11 j	1.42±0.15 d	4.69±0.17 h	0.68±0.02 kl	177.7±1.5 e-g
	30°C	177.4±6.6 ef	3.81±0.08 i	1.55±0.12 d	5.41±0.18 g	0.8±0.06 j-l	179±1.001 e-g
	35°C	177.8±1.9 ef	3.91±0.1 hi	1.59±0.15 d	5.55±0.04 g	0.95±0.2 h-j	176.1±2.01 g
	40°C	89.97±4.5 k	0.87±0.06 n	0.25±0.04 e	1.13±0.19 k	0.23±0.01 o	25.3±0.57 j
	45°C	46.13±5.7 m	0.68±0.9 no	0.13±0.03 e	0.82±0.2 kl	0.2±0.012 o	10.37±0.37 k
SA (0.5 mM)	25°C	170.3±6.9 fg	3.94±0.3 hi	1.54±0.17 d	5.52±0.42 g	0.86±0.06 jk	181.3±1.9 e-g
	30°C	180.3±1.5 ef	4.82±0.01 d-f	1.76±0.1 cd	6.64±0.1 d-f	1.12±0.1 f-h	184±1.73 de
	35°C	183.1±5.1 de	5.15±0.1 b-d	1.85±0.03 b-d	7.1±0.05 b-d	1.29±0.12 d-f	181.3±3.3 e-g
	40°C	106.8±3.44 j	1.43±0.15 m	0.38±0.4 e	1.83±0.15 j	0.36±0.02 no	29.33±1.33 ij
	45°C	65.41±6.81 l	0.92±0.04 n	0.2±0.01 e	1.14±0.05 k	0.25±0.01 no	10.73±0.29 k
SA (1.5 mM)	25°C	182.6±2.6 de	4.48±0.14 fg	1.86±0.2 b-d	6.4±0.01 ef	1.07±0.07 g-i	188.7±2.1 cd
	30°C	198.8±0.7 bc	4.85±0.03 c-f	2.06±0.13 a-c	6.97±0.2 cd	1.22±0.1 e-g	193.1±4.38 c
	35°C	200.3±1.9 bc	5.23±0.2 a-c	2.21±0.2 ab	7.51±0.4 ab	1.47±0.15 cd	190.3±3.76 c
	40°C	104.3±7.37 j	1.37±0.06 m	0.28±0.01 e	1.67±0.06 j	0.45±0.06 mn	34.33±1.45 hi
	45°C	68.9±0.88 l	0.89±0.01 n	0.18±0.01 e	1.08±0.07 kl	0.27±0.22 no	11.77±0.38 k
SA (2.5 mM)	25°C	190.9±5.8 cd	4.92±0.3 c-e	1.86±0.1 b-d	6.84±0.2 c-e	1.21±0.06 e-g	200±3.241 ab
	30°C	206.7±3.2 ab	5.15±0.1 b-d	2.1±0.05 a-c	7.31±0.1 a-c	1.31±0.05 c-f	205.3±3.71 a
	35°C	211.9±2.12 a	5.58±0.18 a	2.12±0.1 a-c	7.76±0.19 a	1.52±0.02 bc	194.7±3.3 bc
	40°C	128.5±3.64 i	1.97±0.79 l	0.4±0.04 e	2.39±0.13 i	0.6±0.01 lm	39.01±1.57 h
	45°C	72.77±2.07 l	0.58±0.5 no	0.09±0.01 e	0.68±0.05 kl	0.22±0.02 o	12.93±0.53 k
SA (5 mM)	25°C	177.6±4.01 ef	4.26±0.2 gh	1.99±0.1 a-c	6.31±0.29 f	1.22±0.06 e-g	181.7±1.2 e-g
	30°C	205.5±5.6 ab	4.79±0.2 d-f	2.06±0.1 a-c	6.91±0.2 c-e	1.39±0.04 c-e	183±1.03 d-f
	35°C	209.1±1.8 ab	5.4±0.17 ab	2.2±0.05 ab	7.67±0.19 a	1.84±0.18 a	183±2.65 d-f
	40°C	119.5±1.05 i	0.71±0.1 no	0.2±0.01 e	0.93±0.05 kl	0.24±0.04 no	34±2.082 hi
	45°C	52.67±2.3 m	0.43±0.01 o	0.08±0.002 e	0.52±0.01 l	0.16±0.012 o	11.7±0.32 k
SA (10 mM)	25°C	155.2±5.01 h	2.64±0.19 k	1.49±0.35 d	4.17±0.28 h	0.89±0.05 i-k	176.7±1.3 fg
	30°C	176.5±4.8 ef	4.63±0.2 ef	2.24±0.4 ab	6.93±0.3 c-e	1.48±0.02 cd	179±0.57 e-g
	35°C	177.1±3.2 ef	5.22±0.1 a-c	2.35±0.19 a	7.64±0.29 a	1.7±0.041 ab	177.3±0.9 e-g
	40°C	83.58±11.9 k	0.68±0.1 no	0.18±0.05 e	0.88±0.15 kl	0.22±0.032 o	31.67±1.20 i
	45°C	32.13±6.47 n	0.54±0.01 no	0.11±0.01 e	0.66±0.01 kl	0.26±0.01 no	11.07±0.37 k

†: (Mean ± S.d, n=3) Values followed by the same letters in a column are not significantly different according to Duncan tests at 5% level; SA: Salicylic acid, LA: Leaf area, Chl a: Chlorophyll a, Chl b: Chlorophyll b, Total Chl: Total Chlorophyll, S.C: Stomatal conductance.

Table 3. The influence of salicylic acid and temperature on select morpho-physiological parameters of maize (*Zea mays L.*) 'MV500'.

	Temperatures	L.D.W (g per plant)	S.D.W (g per plant)	P.D.W (g per plant)	RWC (%)	MP (%)
Control	25°C	0.486±0.06 ij[†]	0.163±0.006 gh	0.65±0.061 j	50.07±1.36e-f	24.79±2.73i
	30°C	0.636±0.03 fg	0.25±0.021 d-f	0.886±0.013h	48.33±0.37g-i	34.29±2.18h
	35°C	0.653±0.01 fg	0.26±0.010 d-f	0.913±0.015h	45.43±1.03 k	46.27±1.85g
	40°C	0.39±0.05 kl	0.123±0.01 h-j	0.513±0.052 l	24.5±0.051 n	89.03±0.3b-d
	45°C	0.223±0.01 no	0.08±0.011 j	0.303±0.016no	10.43±0.21 p	96.48±1.11 a
SA (0.5 mM)	25°C	0.54±0.02 hi	0.223±0.01 ef	0.763±0.029i	51.8±0.72 b	22.23±0.93 i
	30°C	0.783±0.01b-e	0.346±0.01 bc	1.13±0.015de	50.93±0.5 b-e	33.63±1.29h
	35°C	0.796±0.01b-d	0.363±0.02 ab	1.16±0.020 cd	47.83±0.9 hi	44.1±2.19 g
	40°C	0.43±0.001 jk	0.13±0.001 h-j	0.56±0.0001kl	26.23±28 m	86.47±1.1 cd
	45°C	0.27±0.001mn	0.09±0.012 ij	0.363±0.01 mn	11.33±0.3 op	94.45±0.7 ab
SA (1.5 mM)	25°C	0.713±0.04 ef	0.24±0.01 d-f	0.953±0.04 gh	53.4±0.46 a	22.9±0.38 i
	30°C	0.86±0.011ab	0.356±0.003 ab	1.21±0.008 bc	51.5±0.15 bc	33.63±1.61h
	35°C	0.893±0.012 a	0.39±0.052 ab	1.28±0.017 ab	48.03±0.9 hi	43.27±1.21g
	40°C	0.466±0.01 i-k	0.15±0.017 hi	0.616±0.016jk	27±0.46 lm	83.81±1.7 de
	45°C	0.273±0.06 mn	0.106±0.01 h-j	0.38±0.045mn	11.83±0.16op	92.5±0.10 ab
SA (2.5 mM)	25°C	0.763±0.03 c-e	0.296±0.008 cd	1.06±0.021 ef	54.5±0.64 a	22.55±1.66 i
	30°C	0.89±0.005 a	0.38±0.010 ab	1.27±0.011 ab	54±0.3201 a	31.23±1.56 h
	35°C	0.92±0.005 a	0.406±0.012 a	1.32±0.0140 a	49.77±0.9 d-g	40.73±1.06 g
	40°C	0.48±0.011 ij	0.21±0.0050 fg	0.69±0.011 j	27.9±0.62 l	74.6±2.080 f
	45°C	0.296±0.003mn	0.123±0.01 h-j	0.42±0.010 m	12.73±0.17 o	84.68±0.76de
SA (5 mM)	25°C	0.746±0.01 de	0.276±0.003de	1.02±0.012 fg	51.77±0.2 bc	25.87±2.11 i
	30°C	0.84±0.04 a-c	0.37±0.031 ab	1.21±0.061 bc	49.5±0.85 e-h	35.53±0.66 h
	35°C	0.876±0.01 a	0.37±0.012 ab	1.24±0.020 b	47.17±0.57 ij	44.9±1.59 g
	40°C	0.336±0.01 lm	0.166±0.008gh	0.503±0.01 l	27.6±0.15 lm	78.53±3.97 f
	45°C	0.22±0.00 no	0.1±0.0050 ij	0.32±0.005 n	12.23±0.15 o	91.2±2.01 a-c
SA (10 mM)	25°C	0.476±0.018 ij	0.143±0.026hi	0.62±0.015jk	51.3±0.05b-d	24.03±1.86 i
	30°C	0.53±0.015 hi	0.24±0.023d-f	0.77±0.031 i	48.73±0.18f-i	35.13±0.29 h
	35°C	0.593±0.08 gh	0.216±0.021fg	0.81±0.017 i	45.87±0.48jk	44.23±1.36 g
	40°C	0.236±0.02 no	0.113±0.003h-j	0.35±0.03 mn	26.23±0.28m	79.79±4.08ef
	45°C	0.163±0.006 o	0.07±0.0101 j	0.233±0.02 o	11.8±0.21 op	91.2±0.89 a-c

†: Data are shown as the means of three replicates ± S.D. Values followed by the same letters in a column are not significantly different according to Duncan tests at a 5% level; SA: Salicylic acid, L.D.W: Leaf Dry Weight, S.D.W: Stem Dry Weight, P.D.W: Plant Dry Weight, RWC: Relative water content, MP: Cell Membrane stability.
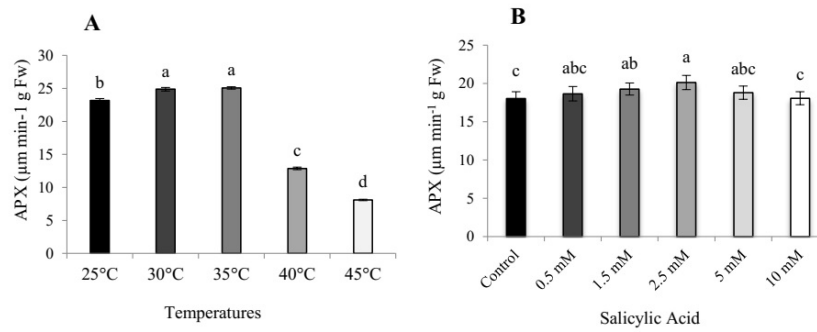
Figure 2. Effect of temperature (A) and salicylic acid (B) on ascorbate peroxidase (APX) activity in maize 'MV500'.
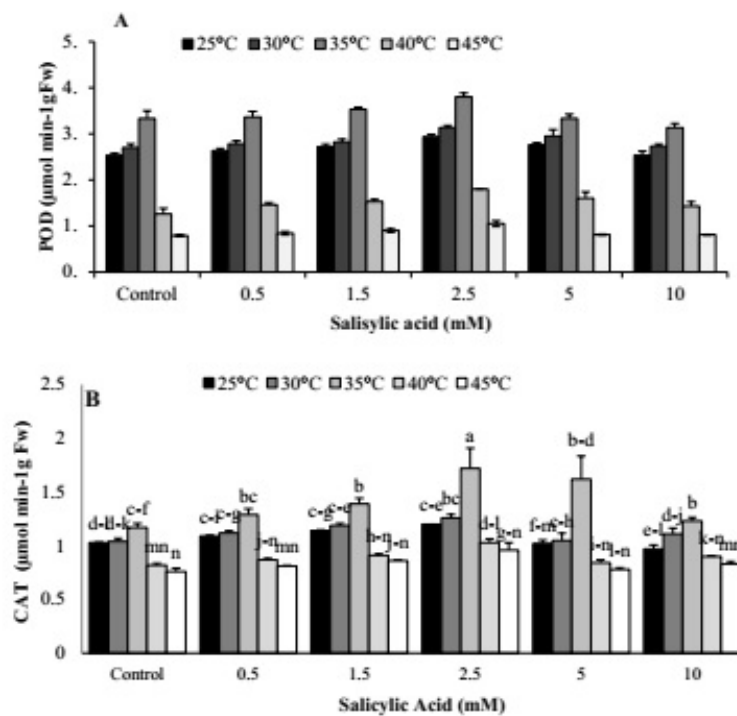
Figure 3. The interaction effect of salicylic acid and temperature on peroxidase (POD) (A) and catalase (CAT) (B) activity in mazie 'MV500'.

limited capacity of the photosynthetic electron transport.[26] An evaluation of 36 genotypes regarding yield traits, phenological traits, plant architectural traits, physiological traits, and stress index under drought, heat, and hybrid stress environments revealed significant losses under heat stress.[27]

An increase in temperature from 25 to 45°C led to a reduction in stomatal conductance. However, treatment with 2.5 mM SA enhanced stomatal conductance under heat-stress conditions. Stomatal closure, a significant factor in heat stress and drought conditions, reduces CO_2 intake into the photosynthetic system. As temperature increases, evaporation and transpiration rates rise, demanding an increased water uptake. The plant responds with stomatal closure if sufficient water is unavailable for absorption. Furthermore, stomatal limitation is attributed to a decrease in Rubisco carboxylation activity and an increase in photorespiration, which results in photosynthetic reduction.[28] SA, a plant growth regulator, positively impacts enzymes involved in photosynthesis, thereby enhancing photosynthetic capacity.[29]

Plant water potential is significantly affected by heat stress. Under such stress, RWC demonstrates a notable decline, with the most prominent increase observed when 2.5 mM of SA was applied at 25°C. As the temperature rises, the evapotranspiration trend escalates, amplifying the water absorption's thermodynamic properties in the root medium. However, when
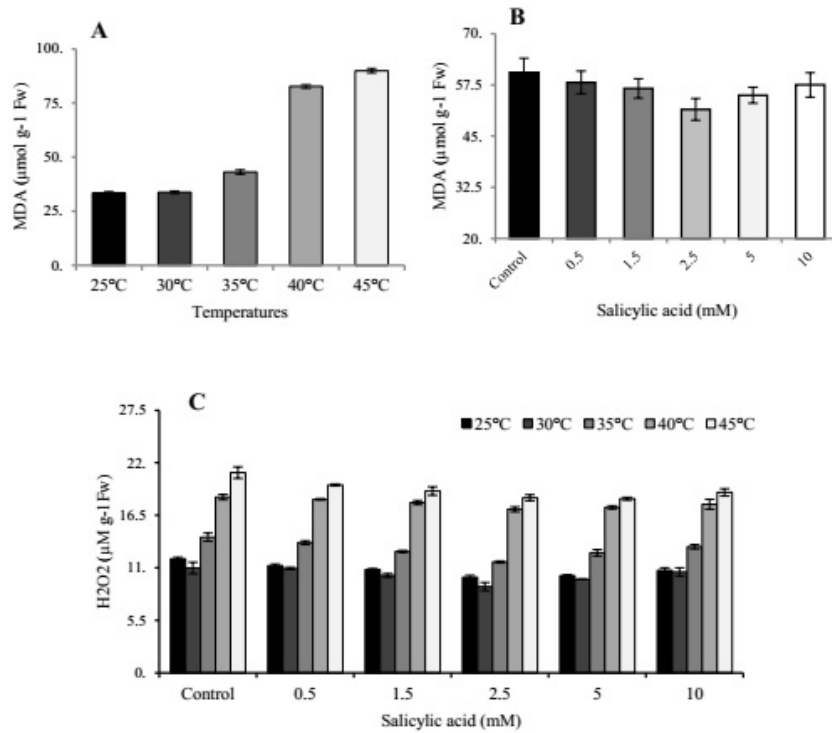
Figure 4. Effect of temperature (A) and salicylic acid (B) on malondialdehyde (MDA) and H_2O_2 (C) in maize 'MV500'.
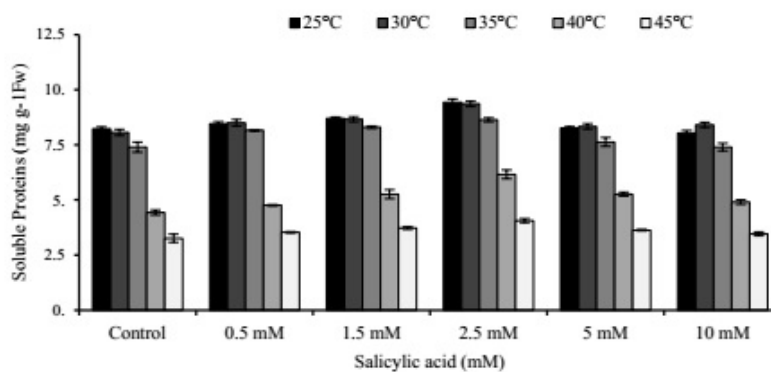
Figure 5. The interaction effect of salicylic acid and temperature on soluble protein content in maize 'MV500'.

temperatures exceed the plant's threshold, the balance between the absorbed and evaporated water (known as the Hydrostatic gradient) is disturbed due to the deterioration of cell structures and self-regulation mechanisms and an increase in electrolyte leakage and stomatal closure. This leads the plant to confront drought-like conditions.[30] In this study, it was observed that a temperature of 45°C, without the application of SA, resulted in the highest level of electrolyte leakage. This may be attributed to the enhanced kinetic energy and movement of molecules across cell membranes, breaking chemical bonds in biological membranes and increasing cell membrane fluidity.[30] Heat stress directly affects proteins and unsaturated fatty acids.[31] The dam-

age inflicted on the cell membrane under heat stress conditions compromises the stability of macromolecules and boosts membrane lipid peroxidation. Given that oxidative stress is common under heat stress conditions, this experiment found that heat stress augmented MDA levels.

The application of SA stimulates antioxidant systems, such as CAT, POD, and APX. It also promotes the accumulation of adaptive osmolytes, including glycine betaine and proline, two primary organic osmolytes that amass in response to environmental stressors. Additionally, the application of SA was found to enhance plant water potential, potentially increasing the re-
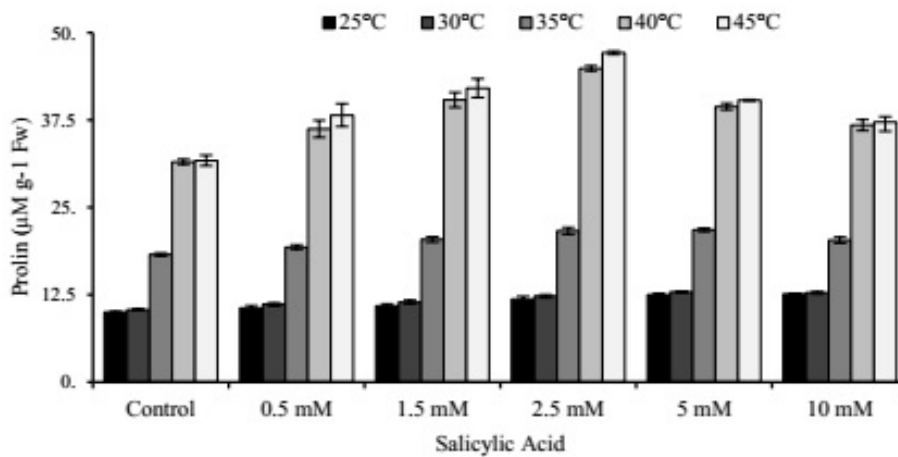
Figure 6. The interaction effect of salicylic acid and temperature on proline content in maize 'MV500'.

sistance of the cell membrane and regulating ROS in plants. This may lead to a decrease in the cell membrane disruption and permeability. In this study, the application of SA increased soluble protein content, cell membrane stability, photosynthetic system efficiency, and antioxidant enzyme activity. As a signaling molecule, SA enhanced gene expression efficacy and HSP-mRNA transcription. Therefore, SA mitigates heat stress in plants and prevents a reduction in soluble protein content. HSFs stimulated the genes responsible for encoding H_2O_2 purification enzymes, such as APX1.[32] The study conducted on rice genotypes observed a significant rise in the activity of antioxidant enzymes, including SOD, APX, and GPX, in both flag leaf and spikelet tissues of the MTU-1010 genotype. Additionally, the MTU-1010 genotype exhibited significantly higher SLW (specific leaf weight) and RWC (relative water content) than the PR-113 genotype across all treatments. This genotype displayed a higher spikelet fertility, a photosynthesis rate, an induced antioxidant system, and improved transpiration, RWC, and SLW, thereby exhibiting greater heat stress tolerance during the flowering stage compared to the PR-113 genotype.[33] Overall, the effect of SA in increasing the activity of antioxidant enzymes under temperature stress is attributed to ROS detoxification. HSFs decrease protein synthesis, particularly as temperatures rise, which triggers the production of a new group of low molecular mass proteins known as heat shock proteins. These proteins act as molecular chaperones within cells.[34] The increase in soluble protein content under SA application may be due to the stimulation of hydrolysis of insoluble proteins, resulting in the accumulation of osmolytes.[35] The protein content decreases as the temperature rises, with the lowest protein content recorded at 45°C. The application of SA increases the soluble protein content, with the highest amount observed at an application of 2.5 mM SA and a temperature of 25°C. Previous reports have also shown that the application of SA increases soluble protein content in Arabidopsis shoots and roots, which aligns with the findings of this research.[35] Furthermore, foliar application of SA has been found to increase carbohydrate content, soluble proteins, free amino acids, and proline content in Basil, supporting the results of this experiment.[36] Proline plays various roles in plants, including regulating osmotic potential, maintaining cell membrane integrity, balancing enzymes/proteins, and the appropriate ratio of $NADP^+/NADPH$ and the scavenging of ROS. The proline accumulation under stress conditions depends on the plant's resistance capacity. A disruption of protein synthesis can result in proline accumulation due to a decreased conversion of proline into protein, leading to reduced growth.[37]

CONCLUSION

The exposure to heat stress led to a decrease in biological yield, RWC, CAT, and POD activity. SA induces a differential antioxidant response in spring maize under high-temperature stress. However, compared to the untreated group, the application of SA to adapt to high temperatures effectively increased proline, chlorophyll, and MDA levels. The utilization of SA exhibited the most significant impact on the growth parameters of maize plants under high-temperature conditions, mitigating the detrimental effects of heat stress on maize.

ORCID IDs of the authors

Esmail Nabizadeh   0000-0002-2449-3984
Narges Dolatmand   0000-0003-1910-825X
Masoud Haghshenas   0000-0001-7379-2107
Khadijeh Ahmadi   0000-0002-2289-9710

REFERENCES

1. Xu N, York K, Miller P, Cheikh N. Co-regulation of ear growth and internode elongation in corn. *Plant Growth Reg*. 2004;44:231–241.

2. Atkinson NJ, Urwin PE. The interaction of plant biotic and abiotic stresses: From genes to the field. *J Exp Bot*. 2012;63:3523–3543.

3. Impa SM, Perumal R, Bean SR, John Sunoj VS, Krishna Jagadish SV. Water deficit and heat stress induced alterations in grain physico-chemical characteristics and micronutrient composition in field grown grain sorghum. *J Cer Sci Technol*. 2019;86:124-131.

4. Crafts-Brandner SJ, Salvucci ME. Sensitivity of photosynthesis in a C4 plant, maize, to heat stress. *Plant Physiol*. 2002;129:1773–1780.

5. Ma M, Wang P, Yang R. UV-B mediates isoflavone accumulation and oxidative-an 460 tioxidant system responses in germinating soybean. *Food Chem*. 2019;275:628-636.

6. Wang LJ, Fan L, Loescher W, et al. Salicylic acid alleviates decreases in photosynthesis under heat stress and accelerates recovery in grapevine leaves. *BMC Plant Biol*. 2010;10:1-10. doi:10.1186/1471-2229-10-34.

7. Sajjad Y, Jaskani MJ, Ashraf MY, et al. Response of morphological and physiological growth attributes to foliar application of plant growth regulators in gladiolus 'white prosperity'. *Pak J Agric Sci*. 2014;51:123–129.

8. Pérez MGF, Rocha-Guzmán NE, Mercado-Silva E, et al. Effect of chemical elicitors on peppermint (*Mentha piperita*) plants and their impact on the metabolite profile and antioxidant capacity of resulting infusions. *Food Chem*. 2014;156:273–278.

9. Karlidag H, Yildirim E, Turan M. Exogenous applications of salicylic acid affect quality and yield of strawberry grown under antifrost heated greenhouse conditions. *J Plant Nutr Soil Sci*. 2009;172:270–276

10. Hayat S, Ali B, Ahmad A. Salicylic acid: Biosynthesis, metabolism and physiological role in plants, In: Salicylic Acid: A Plant Hormone. Springer. 2007; pp:1–14.

11. Dat JF, Lopez-Delgado H, Foyer CH, Scott IM. Effects of salicylic acid on oxidative stress and thermotolerance in tobacco. *J Plant Physiol*. 2000;156:659–665.

12. Souri MK, Tohidloo G. Effectiveness of different methods of salicylic acid application on growth characteristics of tomato seedlings under salinity. *Chem Biol Technol Agric*. 2019;6:26. doi:10.1186/s40538-019-0169-9.

13. Singh B, Usha K. Salicylic acid induced physiological and biochemical changes in wheat seedlings under water stress. *Plant Growth Regul*. 2003;39:137–141.

14. Lichtenthaler HK, Wellburn AR. Determinations of total carotenoids and chlorophylls a and b of leaf extracts in different solvents. *Biochem Soc Trans*. 1983;11:591–592.

15. Lutts S, Kinet JM, Bouharmont J. NaCl-induced senescence in leaves of rice (Oryza sativa L.) cultivars differing in salinity resistance. *Ann Bot*. 1996;78:389–398.

16. Ritchie SW, Nguyen HT, Scott Holaday A. Leaf water content and gas-exchange parameters of two wheat genotypes differing in drought resistance. *Crop Sci*. 1990;30:105–111.

17. Kang HM, Saltveit ME. Chilling tolerance of maize, cucumber and rice seedling leaves and roots are differentially affected by salicylic acid. *Physiol Plant*. 2002;115:571–576.

18. Aebi H. Catalase *in vitro. Methods Enzymol*. 1984;105:121-126.

19. Upadhyaya A, Sankhla D, Davis TD, et al. Effect of paclobutrazol on the activities of some enzymes of activated oxygen metabolism and lipid peroxidation in senescing soybean leaves. *J Plant Physiol*. 1985;121:453–461.

20. Nakano Y, Asada K. Hydrogen peroxide is scavenged by ascorbate-specific peroxidase in spinach chloroplasts. *Plant Cell Physiol*. 1981;22:867–880.

21. Irigoyen JJ, Einerich DW, Sánchez-Díaz M. Water stress induced changes in concentrations of proline and total soluble sugars in nodulated alfalfa (Medicago sativa) plants. *Physiol Plant*. 1992;84:55–60.

22. Bradford M. A Rapid and sensitive method for the quantification of microgram quantities of protein utilizing the principle of protein-dye binding. *Anal Biochem*. 1976;72(1–2):248–254.

23. Heath RL, Packer L. Photoperoxidation in isolated chloroplasts: I. Kinetics and stoichiometry of fatty acid peroxidation. *Arch Biochem Bioph*. 1968;125:189–198.

24. Velikova V, Yordanov I, Edreva A. Oxidative stress and some antioxidant systems in acid rain-treated bean plants: Protective role of exogenous polyamines. *Plant Sci*. 2000;15:59–66.

25. Bates LS, Waldren RP, Teare ID. Rapid determination of free proline for water-stress studies. *Plant Soil*. 1973;39:205. doi:10.1007/BF00018060.

26. Salvucci ME. Association of Rubisco activase with chaperonin-60β: A possible mechanism for protecting photosynthesis during heat stress. *J Exp Bot*. 2008;59:1923–1933.

27. Gupta R. Manganese repairs the oxygen-evolving complex (OEC) in maize (Zea mays L.) damage during seawater vulnerability. *J Plant Nutr Soil Sci*. 2020;20:1387–1396.

28. Yashavanthakumar KJ, Baviskar VS, Navathe S, et al. Impact of heat and drought stress on phenological development and yield in bread wheat. *Plant Physiol Rep*. 2021;26:357–367.

29. Kalaji HM, Schansker G, Brestic M. Frequently asked questions about chlorophyll fluorescence, the sequel. *Photosynth Res*. 2017;132:13-66.

30. Ali F, Waters DLE, Ovenden B, et al. Heat stress during grain fill reduces head rice yield through genotype-dependent increased husk biomass and grain breakage. *J Cereal Sci*. 2019;90:102820.doi:10.1016/j.jcs.2019.102820.

31. Wahid A, Gelani S, Ashraf M, Foolad MR. Heat tolerance in

plants: An overview. *Environ Exp Bot*. 2007;61:199–223.

32. Portis AR, Parry MAJ. Discoveries in Rubisco (Ribulose 1, 5-bisphosphate carboxylase/oxygenase): A historical perspective. *Photosynth Res*. 2007;94:121–143.

33. Khan W, Prithiviraj B, Smith DL. Photosynthetic responses of corn and soybean to foliar application of salicylates. *J Plant Physiol*. 2003;160:485–492.

34. Beney L, Gervais P. Influence of the fluidity of the membrane on the response of microorganisms to environmental stresses. *Appl Microbiol Bio*. 2001;57:34–42.

35. Allakhverdiev SI, Kreslavski VD, Klimov VV, et al. Heat stress: An overview of molecular responses in photosynthesis. *Photosynth Res*. 2008;98(1-3):541-550.

36. Reddy RA, Kumar B, Reddy PS, et al. Molecular cloning and characterization of genes encoding Pennisetum glaucum ascorbate peroxidase and heat-shock factor: interlinking oxidative and heat-stress responses. *J Plant Physiol*. 2009;166:1646–1659.

37. Karwa S, Arya SS, Maurya S, Pal M. Physiological characterization of reproductive stage heat stress tolerance in contrasting rice genotypes. *Plant Physiol Rep.* 2020;25:157–162.

How to cite this article

An Investigation into the Phytochemical Content, Antibacterial Effect, and Antioxidant Capacity of the Ethanol Extract of *Salacca wallichiana* Mart. Peels

Tran Thi Cam Thi[1], Nguyen Trung Quan[1], Hoang Thanh Chi[2], Bui Thi Kim Ly[2]

[1]Vietnam National University, VNU University of Science, Department of Biology and Biotechnology, Ho Chi Minh City, Vietnam
[2]Thu Dau Mot University, Department of Medicine and Pharmacy, Thu Dau Mot, Binh Duong, Vietnam

ABSTRACT

Objective: *Salacca wallichiana* Mart. is a prominent fruit-bearing tree distributed in Southeast Asia and used in treating many diseases and folk remedies. Thus far, only phytochemical composition-related research has been carried out on this plant, while the other bioactivities retarding its applicability in orthodox medicine have been ignored. Screening for the various bioeffects is needed to verify the authenticity of the medicinal activities of plants.

Materials and Methods: Following Ciulei separation, the phytochemical contents of the fruit peel extracts were determined. The antioxidant effect was evaluated by performing the free radical scavenging and potassium ferricyanide-reducing antioxidant power assays. Agar diffusion and broth dilution methods were used to ascertain the antibacterial capacity, and then the minimal inhibitory concentration (MICs) and MBCs were calculated.

Results: The results illustrated a robust free radical scavenging but a weak reducing activity. The MIC against Gram-positive bacteria was <4 mg/mL. The phytochemical composition included tannins and flavonoids, cardiac glycosides, organic acids, and reducing sugars.

Conclusion: The extracts of *S. wallichiana* peels demonstrated a potential antioxidant activity along with lethality against Gram-positive bacteria, which was attributed to the diversity in the contents of secondary metabolites.

Keywords: *Salacca wallichiana*, antioxidant, phytochemicals, antibacterial.

INTRODUCTION

According to ancient Babylonian records, herbs have been used for treating human diseases in the east as far back as 60,000 years ago.[1] Evidence exists for the identification and use of medicinal plants for treating many remedies throughout the history of medicine.[2] The lack of scientific experiment-based evidence is disadvantageous for folk medicine compared to Western medicine. Scientific development has enormously facilitated research on plant-based pharmaceutical products, providing scientific evidence leading to their acceptance and application.[3] Many healthcare and pharmaceutical products derived from plant extracts demonstrated diverse medical applications.[4] Secondary compounds in plants have a great potential for medicinal applications because of their antioxidant, anticancer, and antimicrobial bioactivities.[5,6]

The genus Salacca comprises ~ 20 species, mainly distributed in tropical areas such as Southeast Asia and the east of the Himalayas. *Salacca wallichiana* Mart. grows in many Southeast Asian countries, including Thailand, Vietnam, Malaysia, and Indonesia.[7,8] This plant has many practical applications, such as food, wood, and medicines.[7−9] Contrary to *S. zalacca, S. wallichiana* has not been widely researched, with limited studies and no reports on its bioactivity. Thus, this research aimed to screen the phytochemical composition and evaluate the effects of the peel extracts concerning antioxidant capacity and antibacterial ability through experiments, including qualitative chemical reactions, free radical scavenging, reducing power, disk diffusion, and broth dilution assays.

MATERIALS AND METHODS

Plant Materials and Sample Preparation

The fruits of *Salacca wallichiana* Mart. trees in An Giang province, Vietnam, were harvested (voucher number AG-2018-0150). The fruit peels were collected, washed twice, and oven-dried thoroughly at 40°C. The dried sample was ground into a fine powder, added with ethanol at a ratio of 1:10 (w/v), and extracted for seven days.[10] The crude *S. wallichiana* extract (SWE) was obtained by filtering and rotary evaporating. The crude extract was weighed and dissolved in DMSO to obtain a stock solution of 200 mg/mL, which was stored at -20°C until use.

Phytochemical Detection

The chemical composition of the extract was screened using the method described by Cuilei (1993).[11,12] The SWE was separated into three fractions with different polarities: water, ethanol, and diethyl ether, and the secondary metabolites of each fraction were detected using various reagents and reactions, including Mayer and Wagner reagents for alkaloids;[13] Keller-Kiliani reaction for cardiac glycosides; Fehling's solution for reducing sugars;[14] reducing $FeCl_3$ reaction for polyphenols;[15] gelatin reaction for tannins;[16] foam formation for saponins;[17] and proanthocyanidins with an acidic solution.[18]

Free Radical Scavenging Evaluation

2,2-Diphenyl-1-picrylhydrazyl [DPPH] (Sigma-Aldrich, USA) free radical scavenging assay was performed with a slight modification of the method described by Hatano (1988) to determine the antioxidant effects of SWEs.[19,20] Different extract concentrations were supplemented with the same volume of 0.3 mM DPPH. After 30 min of incubation at 37°C, the OD_{517} of the mixture was recorded.

2,2'-azino-bis-3-ethylbenzothiazoline-6-sulfonic acid [ABTS] (Sigma-Aldrich, USA) radical scavenging assay is based on forming ABTS cation radicals.[21,22] ABTS solution was prepared by adding a triple volume of 7.4 mM potassium peroxydisulfate [$K_2S_2O_8$] (Sigma-Aldrich, USA) into a specific volume of 2.6 mM ABTS for adjusting the reaction solution. It was dark-incubated for 16 h, and the OD_{734} was determined to be 1.00 ± 0.02. For the reaction, 750 µL of the active solution was added to 150 µL of the extract at varying concentrations, and the OD_{734} was ascertained.[20] Then, nonlinear regression equations were developed to determine the EC_{50}. Vitamin C (Sigma-Aldrich, USA) was used as a positive control, and DMSO as the negative control.

Reducing Power Assay

The potassium ferricyanide-reducing antioxidant power (PFRAP) assay was carried out using a modified method.[23] For this, 1 mL of the extract was diluted with 2.5 mL of phosphate-buffered saline [PBS, pH ± 6.6] (TBR Co., Vietnam) and then added with 2.5 mL of 1% potassium ferricyanide (Sigma-Aldrich, USA). After proper mixing and incubation for 20 min at 50°C, the mixture was added with 10% trichloroacetic acid (Sigma-Aldrich, USA), and the reaction was allowed for 10 min at room temperature. The supernatant was collected and diluted with the same volume of water. The solution was supplemented with a-nought-point-1-fold volume of 0.1% $FeCl_3$ (Sigma-Aldrich, USA), and then the OD700 of the teal color solution was determined.[20] The extract at 0 to 800 µg/mL was used for testing. Vitamin C was used as a positive control, and DMSO as the negative control.

Antibacterial Activity

The pathogenic bacteria selected to determine the antibacterial effects of the extracts included *Staphylococcus aureus* (ATCC 25923 and ATCC 6538), *Rhodococcus equi* (ATCC 6939), *Listeria monocytogenes* (ATCC 13932), *Escherichia coli* (ATCC 25922), *Proteus mirabilis* (ATCC 25933), *Shigella sonnei* (ATCC 9290), and *Salmonella enterica* (ATCC 14028). The bacteria were cultured in tryptic soy broth (Acumedia®, Neogen, USA) at 37°C overnight. Then, the agar-well diffusion method was used to determine the sensitivity of the bacterial species.[24] For this, a bacterial solution at 10^8 CFU/mL was prepared and spread out evenly on the surface of MHA [Mueller Hinton Agar] (HiMedia, India). After making 6-mm wells, 50 µL of the extract at different concentrations was loaded into the wells. The plate was incubated at 37°C for 20 h, and the inhibition zones were then measured. Ampicillin was used as the positive control.

Investigation of Antimicroorganism Lethality

The bacteria at a density of 10^5 CFU/mL were co-cultured overnight with varied concentrations of the extract in MHB [Mueller Hinton Broth] (HiMedia, India) in a 96-well plate. Then, 30 µL of 0.02% resazurin (Sigma-Aldrich, USA) was added to each well and incubated at 37°C for 30 min. The MIC (minimal inhibitory concentration) was defined as the lowest concentration of the SWE that maintained the blue color.[25] The bacteria at a concentration < MIC were seeded into TSA plates and incubated for ~ 20 h. The MBC (minimum bactericidal concentration) was identified as the least concentration of SWE at which the bacterial colony was nonostentatious.

Statistical Analysis

The experiments were conducted in triplicates. The data were expressed as mean±SD. The statistical analysis was performed using GraphPad Prism version 9.0.0. The Student's t-test and one-way ANOVA combined with Turkey Post-hoc tests were performed to ascertain the statistical significance of the differences at P<0.05.

RESULTS

The Diversity in the Secondary Metabolite Content of *S. wallichiana*

The medicinal powder was extracted thrice with ethanol. The average crude mass of 40 g of herbal powder was 2.70 ± 0.14 g, with an average extraction yield of 6.72 ± 0.23%. Triterpenoids were identified in the diethyl ether fraction. The ethanol and water fractions revealed a similar composition of polyphenols, including tannins and flavonoids, cardiac glycosides, organic acids, and reducing sugars (Table 1).

SWE Scavenged Free Radicals *In Vitro*

The antioxidant activity was evaluated using an *in vitro* model.[26] The antioxidant effects of the SWEs were investigated by conducting the DPPH and ABTS radical scavenging assays and the ferric-reducing power assay. The proportion of DPPH and ABTS radicals scavenged reached a peak at 100 µg/mL of SWEs with the DPPH assay (Figure 1) and 25 µg/mL with the ABTS assay (Figure 2). The nonlinear regression equation with $R^2 > 0.97$ for the free radical scavenging capacity of SWEs was established as "$Y = 100 \times (X^{1.306})/(17.431.306 + [X^{1.306}])$" and "$Y = 100 \times (X^{1}.712)/(4.511.712 + [X^{1}.712])$" using DPPH and ABTS assays, respectively. The half maximal effective concentration (EC_{50}) was 17.43 ± 0.92 µg/mL for DPPH scavenging and 4.51 ± 0.21 µg/mL for ABTS scavenging.
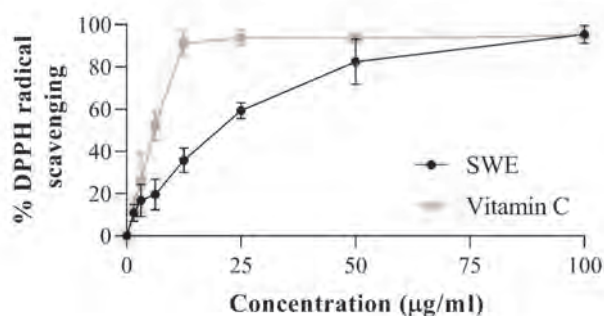
Figure 1. The free radical scavenging ability of the SWEs at 0 to 25 µg/mL as reflected by the proportion of DPPH neutralized. DMSO and Vitamin C were used as negative and positive controls, respectively.
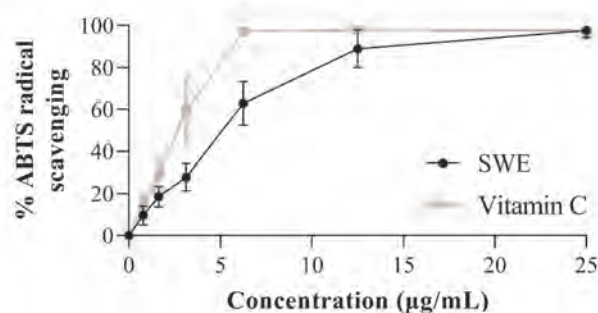
Figure 2. The free radical scavenging ability of the SWEs at 0 to 25 µg/mL was reflected in the proportion of ABTS neutralized. DMSO and vitamin C were used as negative and positive controls, respectively.

SWEs Reduced Fe^{3+} to Fe^{2+}

Fe^{3+} turns to Fe^{2+} under the action of a reducing agent, causing the solution to change from green to yellow. The reducing power of the SWEs was proportional to the concentrations of the extract (Figure 3), which was much lower compared to the control, indicating a limitation in participation in the direct reduction reaction.
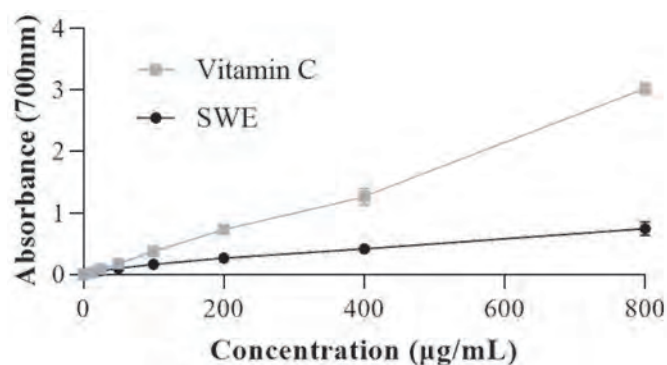
Figure 3. The Fe reduction reaction reflects the electron donor capacity of the SWEs. The reducing power of 0 to 800 µg/mL of the extracts was ascertained by measuring the reduction of Fe3+ to potassium ferricyanide. DMSO was used as blank. Vitamin C was used as a positive control.

SWEs Inhibited Gram-Positive Bacteria

The antibacterial activity of the different concentrations of the SWEs was ascertained using the disk diffusion assay against Gram-positive bacteria.[24] The inhibition zones were measured (Table 2 and Figures 4 A-D) and positively correlated with enhancing SWE concentrations of SWEs. *L. monocytogens* demonstrated the highest resistance to the SWEs.

Table 1. The phytochemical composition of the SWEs.

Phytochemicals	The diethyl eter fraction	The ethanol fraction	The water fraction
Triterpenoid	++	‖	‖
Alkaloid	-	-	-
Anthocyanosid	-	-	-
Proanthocyanidin	-	+++	+++
Polyphenol	‖	+++	+++
Tannin	‖	++	++
Saponin	‖	+	+
Cardiac glycosid	‖	+++	+++
Reducing sugar	‖	+++	+++
Organic acid	‖	++	++

Trace quantity (+); moderate quantity (++); appreciable quantity (+++); absence (-); no need for detection (‖)

Table 2. The antimicrobial activity of the SWEs is indicated by the inhibition zones (mm).

Organism	The SWE concentration (mg/mL) – the inhibition zones (mm)				
	0	25	50	100	200
S. aureus ATCC 25923	0	8.44 ± 0.06	9.83 ± 0.01	11.03 ± 0.17	11.94 ± 0.28
S. aureus ATCC 6538	0	8.11 ± 0.06	9.83 ± 0.17	10.83 ± 0.26	11.78 ± 0.34
R. equi ATCC 6939	0	8.22 ± 0.11	9.50 ± 0.17	10.39 ± 0.34	11.28 ± 0.37
L. monocytogenes ATCC 13932	0	8.50 ± 0.01	8.72 ± 0.15	9.78 ± 0.15	10.64 ± 0.31
S. sonnei ATCC 9290	0	0	0	0	0
E. coli ATCC 25922	0	0	0	0	0
P. mirabilis ATCC 25933	0	0	0	0	0
S. enterica ATCC 14028	0	0	0	0	0

Table 3. The MIC and MBC values of the SWEs and ampicillin.

Organism	The SWE (mg/mL)		Ampicillin (µg/mL)	
	MIC	MBC	MIC	MBC
S.aureus ATCC 6538	1.875	>30	3.125	3.125
S.aureus ATCC 25923	1.875	>30	6.25	12.50
R.equi ATCC 6939	1.563	>30	3.125	6.25
L.monocytogenes ATCC 13932	3.125	>30	3.125	6.25

MIC Values of the SWE-Sensitive Bacteria

The MICs were 1.563–3.125 mg/mL, and MBCs were >30 mg/mL. Ampicillin was used as a positive control (Table 3 and Figure 4E).

DISCUSSION

The primary compounds, such as nucleic acids, proteins, carbohydrates, and lipids, play an essential role in plant sur-
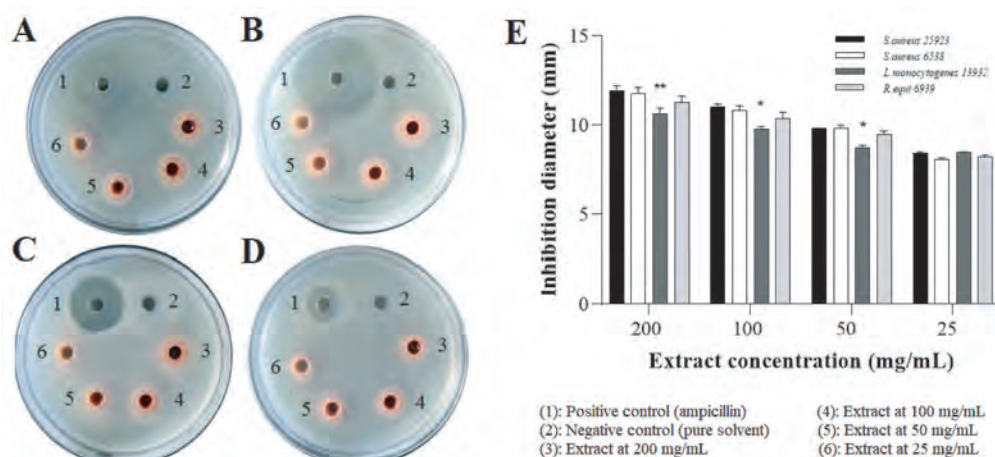
Figure 4. The antibacterial effects of the SWEs against Gram-positive bacteria were determined by the agar diffusion and broth dilution tests. The diameters of the zones of inhibition against *S. aureus* ATCC 25923 (A), *S. aureus* ATCC 6538 (B), *L. monocytogens* ATCC 13932 (C), and *R. equi* ATCC 6939 indicated as a graph (E). **P value < 0.002; ***P value < 0.001.

vival, unlike secondary metabolites, which vary from species to species.[27,28] Many function as cell signaling agents, luring insects or animals for pollination and seed dispersal, and in determining flower color.[28] Based on their chemical structure and functional groups, secondary metabolites directly interact with the cells via cell membranes, proteins including receptors, and nucleic acids, exhibiting a wide range of pharmacological properties such as robust antioxidant activity.[29] The discovery of secondary metabolites in plant extracts holds promise for applying their bioactivities, which can contribute to plant-based medical research.[30] The phytochemicals were extracted into three fractions based on polarity, using diethyl ether, ethanol, and water according to the previous method.[11,12] Based on the solubility of the types of phytochemicals, appropriate chemical reactions were used to detect their presence. Research on the chemical composition of *S. wallichiana* and related plants is limited. One report indicated the presence of flavonoids, alkaloids, tannins, terpenoids, and quinones in *Salacca edulis* fruits, while another detected quercetin and chlorogenic, gallic, cafeic acids in the extracts of *S. edulis* fruit peels.[31,32] Monogalactosyl diacylglycerols, triacylglycerols, β-sitosterol, β-sitosteryl-3β-glucopyranoside-6'-O-fatty acid esters, β-sitosterone, stigmasterol, linoleic acid, lupenone, and taraxerol were isolated from different parts of *S. wallichiana*.[7,9]

The antioxidant capacity of the plant extracts is contributed by the free electrons and atomic H donation by the secondary metabolites.[33] The term "free radical" was first suggested in the 1950s to refer to the oxidizing radicals formed during cellular activity and as the products of certain enzyme-catalyzed reactions.[34] A balance between antioxidants and free radicals in the body is always maintained.[35] However, when the contents of free radicals increase, it causes an imbalance, leading to oxidative-state-related stress.[36] The overaccumulation of free radicals causes various damages to cellular components such as membranes, DNA, and proteins, leading to diseases such as degenerative neurological, heart-related, cancer, and other diseases in humans.[37,38] Secondary metabolites such as polyphenols, flavonoids, and others have potent antioxidant capacity.[39] The EC_{50} values obtained by the two methods were statistically different, and the extracts were much more effective on ABTS radicals than on DPPH. Compared to ABTS radicals, DPPH radicals were less sensitive due to their inability to completely react with slow-acting antioxidant agents and their susceptibility to environmental conditions such as solvents and pH due to phenol oxidizing activity.[40] An EC_{50} of <10 µg/mL for the ABTS radicals suggested that the radical scavenging activity of the total peel extracts was highly efficient; hence, further research is needed.[41] The EC_{50} of the free radical scavenging ability of the peel- and seed-extracts of S. zalacca were 6.4 ± 1.8 µg/mL and 28.9 ± 4.7 µg/mL, which was quite similar to the results obtained in this study.[42] Moreover, the antioxidant capacity of SWEs was higher when compared to other well-known plants, such as green tea (C. sinensis), with EC_{50} values of 3.94 –6.67 µg/mL.[43] During a redox reaction, a reducing agent donates electrons.[44] Hence, an indirect method was used to assess the reducing properties of the extracts to evaluate their antioxidant activity.[45] Fe^{3+} are potent oxidizing agents that readily participate in redox reactions and are often used to qualitatively determine the reducing activities of phytochemicals.[46,47] The PFRAP assay is based on the reduction of Fe^{3+} in potassium ferricyanide to Fe^{2+} catalyzed by an antioxidant agent[23], which demonstrated the reducing ability of the extracts attributed to the presence of secondary metabolites.

The susceptibility of bacteria to treatment with SWEs was determined based on the diameter of the inhibition zones; with a broader diameter indicating an enhanced sensitivity. Phyto-

chemicals possess a potent antibacterial activity, which holds enhanced promise for the applicability of SWEs due to the detection of diverse chemical constituents.[48] This study showed that SWEs were toxic to Gram-positive bacteria. The outer membrane is unique in Gram-negative bacteria, forming a protective barrier that prevents the entry and permeation of hydrophilic agents. Therefore, drug resistance in Gram-negative bacteria is higher than in Gram-positive bacteria.[49] The agar diffusion assay indicated that the species were susceptible to SWEs further used for the broth dilution assay. The broth dilution method was the secondary screening assay that allowed for the determination of the MICs and MBCs. The bacteria cultured in MHB were exposed to the extracts added with 0.02% aniline resazurin and further subcultured on MHA to determine the MBC. Growth inhibition and lethality against bacteria indicated the antimicrobial activity of the SWEs. *S. zalacca* showed moderate antibacterial activity with inhibitory zone diameters of 7.31 ± 0.82 mm and 7.17 ± 0.86 mm for *S. aureus* and *S. typhi*, respectively[50] and also on the Gram-negative bacteria, *E. coli*, with an inhibition zone of 5.96 ± 1.45 to 8.13 ± 0.40 mm.[51,52]

CONCLUSION

The phytochemical screening revealed that the SWEs contained terpenoids and polyphenols, including tannins and flavonoids, cardiac glycosides, organic acids, and reducing sugars, contributing to potent antioxidant and antibacterial effects. The antibacterial effects of SWEs were observed against Gram-positive bacteria with MIC values <4 mg/mL.

ORCID IDs of the authors

Tran Thi Cam Thi   0009-0005-6732-2930
Nguyen Trung Quan   0000-0002-6436-4693
Hoang Thanh Chi   0000-0002-6638-1235
Bui Thi Kim Ly   0000-0002-8433-7035

REFERENCES

1. Nontokozo ZM, Mthokozisi BCS. Herbal Medicine. In: *Philip FB, editor. Herbal Medicine*. Rijeka: IntechOpen; 2018.

2. Petrovska BB. Historical review of medicinal plants' usage. *Pharmacogn Rev.* 2012;6(11):1-5.

3. Schmidt BM, Ribnicky DM, Lipsky PE, Raskin I. Revisiting the ancient concept of botanical therapeutics. *Nat Chem Biol.* 2007;3(7):360-366.

4. Yuan H, Ma Q, Ye L, Piao G. The traditional medicine and modern medicine from natural products. *Molecules.* 2016;21(5):599. doi: 10.3390/molecules21050559

5. Hussein R, El-Anssary A. Plants secondary metabolites: The key drivers of the pharmacological actions of medicinal plants. *Herb Med.* 2019:12-29. doi: 10.5772/intechopen.76139.

6. Seca AML, Pinto D. Biological potential and medical use of secondary metabolites. *Medicines.* 2019;6(2):66. doi: 10.3390/medicines6020066

7. Ragasa C, Ting J, Ramones M, et al. Chemical constituents of *Salacca wallichiana* Mart. *Int J Curr Pharm Res.* 2016;7(4):186-189.

8. Lim T. *Edible Medicinal and Non Medicinal Plants.* Flower. Springer, the Netherlands. 2015.

9. Ragasa C, Ting J, Ramones M, et al. Chemical composition of *Salacca wallichiana. Chem Nat Compd.* 2018;54(4):788-789.

10. Plaskova A, Mlcek J. New insights of the application of water or ethanol-water plant extract rich in active compounds in food. *Front Nutr.* 2023;10:1118761. doi: 10.3389/fnut.2023.1118761

11. Ioan Ciulei EGS, *Plante medicinale , fitochimie si fitoterapie.* Vol. II: Editura medicală; 1993.

12. Ioan Ciulei EGS, U. *Plante medicinale , fitochimie si fitoterapie. Vol. I*: Editura medicală; 1993.

13. Jha D, Panda L, Pandian L, Ramaiah S, Anbarasu A. Detection and confirmation of alkaloids in leaves of *Justicia adhatoda* and bioinformatics approach to elicit its anti-tuberculosis activity. *Appl Biochem Biotechnol.* 2012;168. doi: 10.1007/s12010-012-9834-1

14. Ayoola G, Coker H, Adesegun S, et al. Phytochemical screening and antioxidant activities of some selected medicinal plants used for malaria therapy in Southwestern Nigeria. *Trop J Pharm Res.* (ISSN: 1596-5996) 2008;7(3). doi: 10.4314/tjpr.v7i3.14686

15. MacWilliam IC, Wenn RV. Interpretation of colour tests for polyphenols and melanoidins. *BRI Nutfield Surrey.* 1972;78:309.

16. Baughman IP. The study of the tannin-gelatin reaction. *J Phys Chem.* 1927;31(3):448-458.

17. Edeoga HO, Okwu, DE, Mbaebie, BO. Phytochemical constituents of some Nigerian medicinal plants. *Afr J Biotechnol.* 2005;4(7):685-688.

18. Liu S. Extraction and characterization of proanthocyanidins from grape seeds. *Open Food Sci J.* 2012;6:5-11.

19. Hatano T, Kagawa H, Yasuhara T, Okuda T. Two new flavonoids and other constituents in licorice root: their relative astringency and radical scavenging effects. *Chem Pharm Bull.* 1988;36(6):2090-2097.

20. Ly B, Nguyen Q, Dao L, et al. Evaluation of antimicrobial, antioxidant and cytotoxic activities of *Dialium cochinchinensis* seed extract. *Indian J Pharm Sci.* 2019;81(5): 975-980.

21. Keesey J. Biochemica Information: A revised biochemical reference source: Boehringer Mannheim Biochemicals. *Biochemistry.* 1987.

22. Zheleva-Dimitrova D, Nedialkov P, Kitanov G. Radical scav-

enging and antioxidant activities of methanolic extracts from Hypericum species growing in Bulgaria. *Pharmacogn Mag*. 2010;6(22):74-78.

23. Ponnusamy J, Lalitha P. Reducing power of the solvent extracts of Eichhornia crassipes (Mart.) Solms. *Int J Pharm Pharm Sci*. 2011;3:126-128.

24. Finn RK. Theory of agar diffusion methods for bioassay. *Anal Chem*. 1959;31(6):975-977.

25. Rampersad SN. Multiple applications of Alamar Blue as an indicator of metabolic function and cellular health in cell viability bioassays. *Sensors (Basel, Switzerland)*. 2012;12(9):12347-12360.

26. Alam MN, Bristi NJ, Rafiquzzaman M. Review on in vivo and in vitro methods evaluation of antioxidant activity. *Saudi Pharml J*. 2013;21(2):143-152.

27. Jan R, Asaf S, Numan M, Lubna, Kim K-M. Plant secondary metabolite biosynthesis and transcriptional regulation in response to biotic and abiotic stress conditions. *Agronomy*. 2021;11(5):968. doi: 10.3390/agronomy11050968

28. Pagare S, Bhatia M, Tripathi N, Bansal YK. Secondary metabolites of plants and their role: Overview. *Curr Trends Biotechnol Pharm*. 2015;9:293-304.

29. Velu G, Palanichamy V, Rajan A. Phytochemical and pharmacological importance of plant secondary metabolites in modern medicine. *Bioorganic Phase in Natural Food: An Overview*. 2018:135-156. doi: 10.1007/978-3-319-74210-6_8

30. Kasote DM, Katyare SS, Hegde MV, Bae H. Significance of antioxidant potential of plants and its relevance to therapeutic applications. *Int J Biol Sci*. 2015;11(8):982-991.

31. Kanlayavattanakul M, Lourith N, Ospondpant D, et al. Salak plum peel extract as a safe and efficient antioxidant appraisal for cosmetics. *Biosci Biotechnol Biochem*. 2013;77(5):1068-1074.

32. Afrianti L, Widjaja W, Suliasih N, et al. Anticancer activity of 3-hydroxystigmastan- 5(6)-en (β-sitosterol) compound from Salacca edulis reinw variety Bongkok in MCF-7 and T47D cell line. *J Adv Agric Technol*. 2015;2(2). doi: 10.12720/joaat.2.2.129-133

33. Santos Sánchez N, Salas-Coronado R, Villanueva C, Hernández-Carlos B. Antioxidant compounds and their antioxidant mechanism. *Antioxidants*. 1st ed. London, UK: IntechOpen; 2019: 1-28.

34. Harman D. Aging: A theory based on free radical and radiation chemistry. *J Gerontol*. 1956;11(3):298-300.

35. Pham-Huy L, He H, Pham-Huy C. Free radicals, antioxidants in disease and health. *J Biomed Sci*: IJBS. 2008;4:89-96.

36. Pizzino G, Irrera N, Cucinotta M, et al. Oxidative stress: Harms and benefits for human health. *Oxid Med Cell Longev*. 2017:8416763. doi: 10.1155/2017/8416763

37. Ames BN, Shigenaga MK, Hagen TM. Oxidants, antioxidants, and the degenerative diseases of aging. *Proc Natl Acad Sci USA*. 1993;90(17):7915-7922.

38. Sharifi-Rad M, Anil Kumar NV, Zucca P, et al. Lifestyle, Oxidative stress, and antioxidants: Back and forth in the pathophysiology of chronic diseases. *Front Physiol*. 2020;11:694. doi: 10.3389/fphys.2020.00694

39. Aneklaphakij C, Saigo T, Watanabe M, et al. Diversity of chemical structures and biosynthesis of polyphenols in nut-bearing species. *Front Plant Sci*. 2021;12(440). doi: 10.3389/fpls.2021.642581

40. Danet A. Recent advances in antioxidant capacity assays. *Antioxidants-Benefits, Sources, Mechanisms of Action*. IntechOpen. 2021.

41. Licht O, Weyers A, Nagel R. Ecotoxicological characterisation and classification of existing chemicals. Examples from the ICCA HPV initiative and comparison with other existing chemicals. *Environ Sci Pollut Res Int*. 2004;11(5):291-296.

42. Fitri A, Andriani M, Sudarman A, et al. Screening of antioxidant activities and their bioavailability of tropical fruit byproducts from Indonesia. *Int J Pharm Pharm Sci*. 2016;8:96-100.

43. Paiva L, Lima E, Motta M, Marcone M, Baptista J. Influence of seasonal and yearly variation on phenolic profiles, caffeine, and antioxidant activities of green tea (Camellia sinensis (L.) Kuntze) from Azores. *Appl Sci*. 2021;11(16):7439. doi: 10.3390/app11167439

44. Pietrzyk DJ, Frank CW. Chapter Eleven- Oxidation–reduction titrations. In: Pietrzyk DJ, Frank CW, editors. *Analytical Chemistry: Academic Press*. 1979. p. 245-64.

45. Cheng Z, Li Y. Reducing power: The measure of antioxidant activities of reductant compounds? *Redox Rep*. 2004;9(4):213-217.

46. Murugan M, Kolanjinathan K. Qualitative phytochemical screening and antioxidant activity of elytraria acaulis lindau (Acanthaceae). *Asian J Pharm Clin Res*. 2016;9:1-4.

47. Gülçin İ. Fe$(^{3+})$-Fe$(^{2+})$ transformation method: An important antioxidant assay. *Methods Mol Biol* (Clifton, NJ). 2015;1208:233-246.

48. Wallace RJ. Antimicrobial properties of plant secondary metabolites. *Proc Nutr Soc*. 2004;63(4):621-629.

49. Breijyeh Z, Jubeh B, Karaman R. Resistance of gram-negative bacteria to current antibacterial agents and approaches to resolve it. *Molecules*. 2020;25(6):1340. doi: 10.3390/molecules25061340

50. Sari L, Saputro Z, Utomo M, Prodjosantoso A. The use of *Salacca zalacca* extract as reducing agent to synthesize silver nanoparticles (agnps) and the antibacterial activities. *Orient J Chem*. 2019;35:1557-1564.

51. Wulansari NT, Padmiswari AAIM, Damayanti IAM. The effectiveness probiotic drink of salak bali (salacca zalacca) in inhibiting growth of *Escherichia coli*. *J BiolTropis*. 2022;22(3):934-939.

52. Chiuman L, Sherlyn S, Aritonang NS, Rudy R, Suhartomi S. In vitro study of antibacterial activity of snake fruit extract against extended spectrum beta lactamase (ESBL) Escherichia coli. Jurnal Aisyah: J ILMU Kesehatan (JIKA). 2023. 2023;8(2). doi: 10.30604/jika.v8i2.1962.

How to cite this article

RESEARCH ARTICLE

Bacterial Biodiversity of the Kapova Karst Cave as a Source of Hydrolases Producers

Willam Kurdy[1], Galina Yakovleva[1], Olga Ilinskaya[1]

[1]Kazan Volga-Region Federal University, Kazan, Tatarstan, Russian Federation

ABSTRACT

Objective: Recent studies have revealed the biodiversity of both cultivated and uncultivated microbiomes in extreme environments. It has been shown that terrestrial subsurface ecosystems contain vast metabolic potential. Heterotrophic bacteria living in karst caves with an organic substrate deficit represent a special reserve for the isolation of metabolite producers. Here, we cultivated a bacterial community collected from biofilms in Kapova Cave (Shulgan–Tash Nature Reserve, Bashkortostan), and assessed its ability to synthesize secreted hydrolytic enzymes including RNases, proteases, and amylases.

Materials and Methods: Isolated bacteria were identified by V3-V4 16S rRNA region sequencing. Enzymatic activities were assessed by measuring transparency zones around colonies grown on the appropriate substrate (RNA, casein, starch). Functional profiles of the communities were predicted using the Global Mapper module on iVikodak. Taxonomic, structural, and compositional diversity were calculated using Shannon–Wiener and Bray–Curtis indices.

Results: Eighty-nine percent of 102 bacterial isolates were *Proteobacteria*, whereas other isolates were divided into three other phyla, *Actinobacteria, Firmicutes*, and *Bacteroidetes* that comprised 5%, 4%, and 2% of the isolates, respectively. Genus Pseudomonas was predominant with 42 isolates. Six isolates showed no extracellular enzymatic activity at all, 73 isolates expressed protease, 57 isolates expressed amylase, and 71 isolates had RNase activity. All three extracellular enzymes were expressed by 39 isolates.

Conclusion: The biodiversity of cultivated microbiota from Kapova Cave was characterized. Bacteria that produce large amounts of protease, RNase and amylase were identified as *Stenotrophomonas rhizophila, Lysinibacillus fusiformis*, and *Pseudomonas stutzeri*, respectively.

Keywords: Karst cave, biodiversity, cultivated bacteria, RNase, protease, amylase

INTRODUCTION

Karst caves are underground cavities that encounter the earth's surface or are closed. They form as rainwater seeps into soluble rocks like limestone or gypsum. These nutrient-limited ecosystems feature constant low temperature, high humidity, darkness, low pressure, and low oxygen concentration. Caves create their own microclimatic and physicochemical conditions, giving rise to living organisms that exist in relative isolation from surface ecosystems. Comparative metagenomic analysis shows that cave microbial communities are specialized terrestrial communities that differ from communities found in oceans, soil, or the rhizosphere.[1] The poorly characterized microbial world found in caves is a potential source of antimicrobial and anticancer drugs[2] as well as microorganisms that produce novel agents. However, caves containing fossils, artifacts, Paleolithic paintings, and mineral deposits are prone to microbial damage, particularly during unregulated tourist visits. For example, only tourists have changed Morca Cave in Turkey after only a few years. Once dominated by *Thermoplasmata (Euryarchaeota), Gammaproteobacteria* and *Alphaproteobacteria*, the cave now features more bacteria belonging to *Bacilli* and *Bacteroidia*.[3] Therefore, understanding the microbial diversity in caves is a prerequisite to cave conservation, restoration, and safe cave tourism. It is believed that microbes in caves are most active on rocky surfaces, as most caves lack a significant layer of soil and sediment. In addition, microorganisms constantly move between the walls of the cave and sediments. Removing microbial groups from walls is often futile because soil and sediments are reservoirs of these microbial groups.[4]

These microorganisms not only should be preserved but also

may secrete novel enzymes that can be used in industry, agriculture, and medicine.

Shulgan–Tash (or Kapova) Cave is located in the basin of the Belaya River in the Southern Urals within the Shulgan–Tash State Nature Reserve of the Republic of Bashkortostan; this karst cave is known worldwide for its rock art dating back to the Upper Paleolithic.[5] Seventeen main morphotypes have been identified in Kapova Cave. Communities isolated from the walls of the aphotic part of the cave include prokaryotes (bacteria, including *Actino-* and *Cyanobacteria*) and eukaryotes (yeasts and microscopic fungi).[6] Both metagenomics and traditional culturing methods have been performed to identify representatives belonging to *Proteobacteria, Actinobacteria, Firmicutes, Nitrospirae, Bacteroidetes, Verrucomicrobia* and *Acidobacteria* phyla as well as to isolate new Pseudomonas strains.[7]

Although karst caves present similar oligotrophic habitats, their microbial communities differ and are poorly understood. The bacterial taxa of Kapova Cave and the karst caves of China are dominated by two phyla, *Proteobacteria* and *Actinobacteria*.[8−10] In the Oylat Cave in Turkey, *Proteobacteria* dominate, followed by *Actinobacteria, Acidobacteria*, and *Nitrospirae*.[11] In Pertosa–Auletta Cave in southern Italy, *Proteobacteria* and *Acidobacteria*, dominate, followed by *Actinobacteria*.[12]

Elucidating the biodiversity of karst caves serves will inform the future discovery of useful microbial metabolites. Microorganisms secrete enzymes that benefit industry, agriculture, and medicine. For example, proteases are widely used in the food, leather, and feed industries as well as the production of detergents.[13] As proteases are degradative enzymes with high specificity and selectivity,[14] they can be used to process waste and optimize detergents. Moreover, proteases are widely used in medicine to treat burns, carbuncles, and wounds.[13] Amylase comprises approximately 25% of the world enzyme market[15] and is widely used in food applications like baking and brewing.[16] Extracellular bacterial RNases are also promising antiviral[17−20] and antitumor enzymes.[21−23]

Thus, work aimed to characterize the bacterial community collected by scraping visible colonies or biofilms from the walls of Kapova Cave and assess the ability of isolates to synthesize secreted hydrolytic enzymes, namely RNases, proteases, and amylases.

MATERIALS AND METHODS

Sampling Sites

Kapova Cave is located in the Shulgan–Tash State Nature Reserve of the Bashkortostan Republic; it was formed in a karst massif on the right slope of the river valley and is composed of massive limestones of the Viséan stage of the Lower Car-

boniferous. The cavity lies in the limestones of the lower part of the Carboniferous period. The cave is a weakly branched, three-story, gallery-type cavity that is 3328 m long, of which 782 m are underwater cavities.[5] Here, we used material collected by the Laboratory of Extreme Biology of Kazan Federal University in July 2019. Seven samples of visible colonies or biofilms were sampled from walls of different areas of the cave, whose locations are indicated in Figure 1.
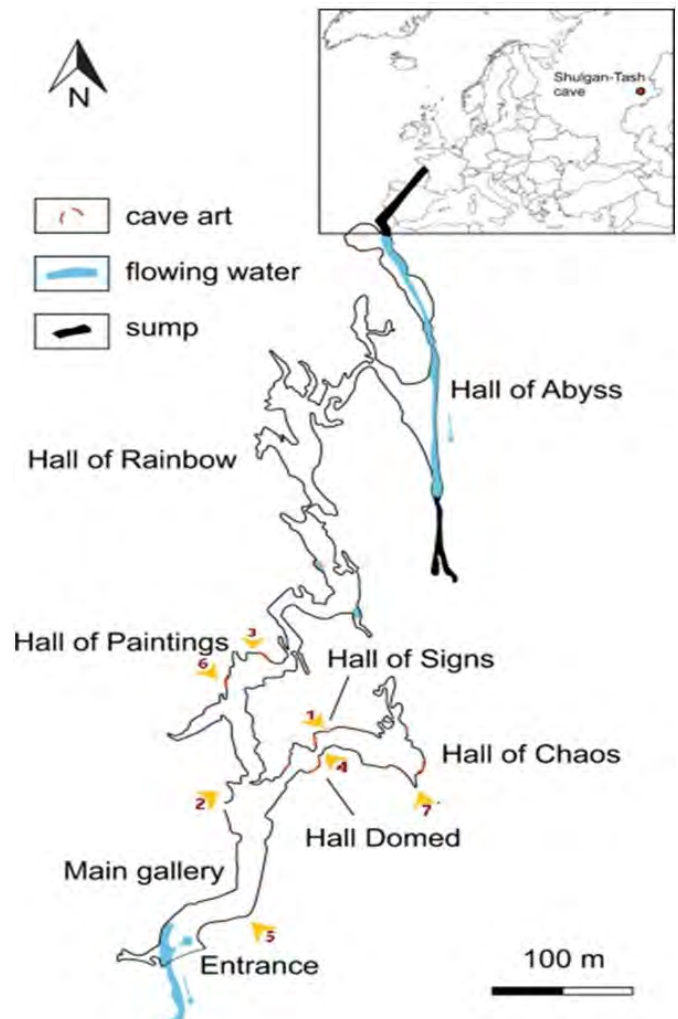
Figure 1. Kapova cave map with sampling locations labeled 1-7.

Pure Bacterial Culture Isolation

Samples were thoroughly mixed in 0.2 ml of a 0.5% NaCl solution and diluted tenfold in triplicate to minimize the bacterial count to use as an inoculation source. To isolate individual bacteria, inoculations, both deep and surface, were sewn on Luria-Bertani (LB), Reasoner's 2A (R2A) medium, and Gauze agar media to capture a spectrum of bacteria from the inoculates. LB is a nutrient-rich medium commonly used to cultivate bacte-

ria, especially members of *Enterobacteriaceae*. R2A Agar is a low-nutrient medium that stimulates the growth of stressed and chlorine-tolerant bacteria at lower incubation temperatures and longer incubation times. Gauze agar media is used to cultivate *Actinomycetes*. Here, microorganisms were cultivated at 30º for 48 h. To obtain pure cultures of microorganisms, colonies with similar morphologies were chosen for subsequent culture using the streak plate method on the appropriate medium twice to check colony purity. Pure cultures were stored in a 10% glycerol solution and frozen at -80°C.

16s rRNA Sequencing

A total of 102 bacterial pure cultures were identified according to their V3-V4 16S rRNA region sequence. Bacterial biomass was collected and placed in a 100°C hot bath for 5 min to disrupt cell integrity. V3 to V4 regions of 16S rRNA genes were then amplified using universal primers (515F and 806R), and an individual index was ligated for labeling isolates. The forward primer sequence was 5'-GTGCCAGCMGCCGCGGTAA-3', and the reverse primer sequence was 5'-GGACTACHVHHHTWTCTAAT-3'.[24] Reaction mixtures (10 µl) comprised 5 µl Hot Start High-Fidelity 2X Master Mix (BioLabs, New England), 0.5 µl primer mix with 5 µM forward and reverse primers, 2 µl gDNA, and 2.5 µl H_2O were used for amplification. The PCR cycles were as follows: (a) 95°C for 5 min; (b) 40 cycles, within each cycle 95°C for 30 s and 60°C for 30 s; and (c) 4°C hold. The concentration of DNA was determined using a Qubit 3.0 fluorometer (Life Technologies, USA) and calibrated to 50 ng/ml. Agencourt AMPure Beads (Beckman Coulter, USA) were used to clean the DNA according to the manufacturer instructions. Sequencing was performed with the MiSeq system (Illumina, USA) using paired-end 2 × 300 (for 16S rRNA genes). Resulting sequences were compared to the NCBI genomic database using the BLAST algorithm for nucleotides (BLASTn).[25] A maximum-likelihood phylogentic tree was created using MEGA-X software.[26]

Isolates with the highest metabolic activity were selected for further sequencing of the nearly full-length 16S rRNA gene following the previously described protocol with some modifications. The V1-V9 regions of the 16S rRNA gene were amplified with the following primers: forward primer (S-D-Bact-0008-c-S-20) with anchor sequence 5'-TTTCTGTTGGTGCTGATATTGCAGRGTTYGATYMTGGCTCAG-3' and reverse primer (1492R) with anchor sequence 5'-CTTGCCTGTCGCTCTATCTTCCGGYTACCTTGTTACGACTT-3'.[24]

Hydrolase Activity Measurement

Bacteria were screened for their ability to synthesize secreted ribonucleolytic, proteolytic and amylolytic enzymes on the following synthetic media, respectively:

(a) Phosphorus-free medium (pH = 8.5, 1L) of the following composition (g/L): Tris basic (hydroxylmethylaminomethane): 6.05; KCl: 5.0; NaCl: 1.0; $(NH_4)_2SO_4$: 2.0; $Na_3C_6H_5O_7$: 1.0; agar-agar: 20.0. Separately prepared: $MgSO_4.7 H_2O$: 2 g/100 ml; yeast extract: 5 g/100 ml. Both solutions were added to the medium under sterile conditions at a rate of 10 ml/L. Before inoculation, a 40% sterile glucose solution was added to the medium at a rate of 12.5 ml/L as well as yeast RNA (Vector, Novosibirsk, Russia) to a final concentration of 5 mg/mL.

(b) A medium containing (g/L): yeast extract: 5.0; casein: 5.0; NaCl: 5.0; agar-agar: 20.0 (pH = 6.5).

(c) Nutrient agar supplemented with 8 g/L starch (pH = 6.8).

Bacterial cultures were sown on Petri dishes with three types of medium (a, b, c) and cultivated for 18 h at 30°C. Hydrolase activities were assessed by measuring the transparent region surrounding the colonies grown on the appropriate substrate (RNA, casein, starch) after the dishes were flooded with a 5% solution of 1 N HCl (colonies grown on medium a), trichloroacetic acid (on medium b), or Lugol's iodine solution (medium c) to visualize the hydrolysis zones. Jeffris et al. [27] used this method to assess RNase activity based on the size of clearance zone corresponding to extracellular enzymes production but not colony size, which we measured to measure different bacterial colonies as described by Price et al. for phospholipase activity detection.[28] Therefore, the hydrolase activity coefficient of a bacterial isolate was calculated as the ratio of the colony radius including the transparent zone surrounding it to the radius of the colony itself. The absence of a lysis zone surrounding colonies corresponds to the absence of secreted hydrolase. Larger transparent zones yield greater hydrolase activity coefficients expressed in conventional units; coefficients of 1, 1.5, and 2 indicate no extracellular hydrolase activity, medium activity, and high activity, respectively.

Prediction of Functional Profiles

Functional profiles of the communities were assessed using the Global Mapper module on iVikodak.[29] Values acquired represent the relative abundance of functional genes according to KEGG.

Statistical Analysis

Alpha diversity was assessed by two measures: taxonomic structural diversity using the Shannon–Wiener index and taxonomic compositional diversity. The Shannon–Wiener Index (H) was calculated using the following formula using Excel software:

H = -å P_i (lnP_i),

where P_i is the proportion of individuals belonging to the i-th genera in the dataset of interest.

To assess compositional taxonomic beta diversity, the Bray–Curtis index[30] was calculated as follows:

$$BC_{ij} = 1 - (2C_{ij}/(S_i + S_j)),$$

where C_{ij} is the sum of values only for common genera between two sampling sites; S_i and S_j are the number of isolates counted at sites i and j individually.

RESULTS

Taxonomic Identification of Bacterial Isolates

Of the 102 bacteria isolated from Kapova Cave, 99 were identified at the genus or family level according to their V3-V4 16S rRNA region sequences. 89% are members of the phylum Proteobacteria, whereas the others comprise three other phyla, *Actinobacteria, Firmicutes*, and *Bacteroidetes*, accounting for 5%, 4%, and 2% of the isolates, respectively (Figure 2). The composition of microbial communities did not significantly differ across sampling points. Two isolates were identified only at the family level as *Burkholderiaceae* and *Enterobacteriaceae* (Figure 3). These isolates are included in the phylogenetic tree at this level (Figure 4). Representatives of the genera *Pseudomonas* were predominant, with 42 isolates (Table 1).
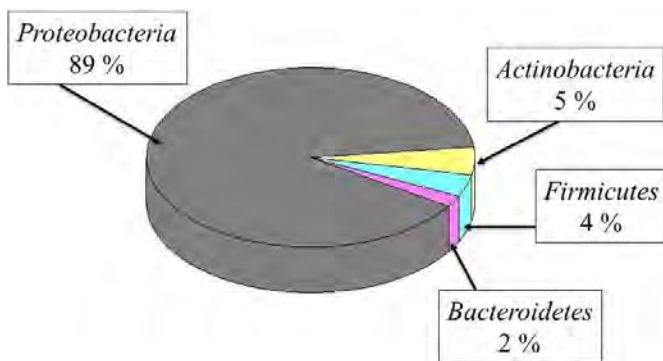
Figure 2. Distribution of bacterial isolates from Kapova cave according to phyla.

Diversity and Potential Functional Activity of Bacteria from Kapova Cave

Sample 7 had the best index of equally represented genera, followed by samples 6 and 1 (Table 2). The Bray–Curtis index of beta diversity ranges from 0 (when communities share the same isolates or phylogenetic lineages) to 1 (when communities do not share common phylogenetic lineages). Table 3 shows that samples 1 and 2 differ significantly from the rest of the samples.

Functional characteristics of the bacterial community from all seven samples were predicted using the Global Mapper module in the iVikodak software. The relative abundance of various metabolic pathways was considered, particularly those related to antimicrobial resistance, xenobiotic destruction, metabolism, and secretory systems. Figure 5 reveals that the community can metabolize different substrates and harbors antibiotic resistance genes.

Enzymatic Activity of Isolates

Six isolates showed no enzymatic activity (amylase, protease, RNase), whereas 73, 57, and 71 isolates expressed protease, amylase, and extracellular RNase activity, respectively. Thirty-nine isolates expressed all three extracellular enzyme activities (Figure 6).

Genera with the highest protease activity were *Pseudomonas, Stenotrophomonas, Bacillus, Acinetobacter*, and *Yersinia*. Genera with the highest RNase activity were *Pseudomonas, Bacillus, Yersinia, Acinetobacter, Lysinibacillus, Polaromonas*, and *Caulobacter*. Genera with the highest amylase activity were *Pseudomonas, Serratia, Yersinia*, and *Acinetobacter*.

Isolate 7 had the highest protease activity and was identified as *Stenotrophomonas rhizophila* (99.5%). Isolate 27 had the highest RNase activity and was identified as *Lysinibacillus fusiformis* (99.3%). Isolate 1 had the highest amylase activity and was identified as *Pseudomonas stutzeri* (99.0%). The genus *Pseudomonas* is a prolific producer of several extracellular enzymes, including amylase,[31,32] which is among the most important enzymes for biotechnology.[15]

DISCUSSION

Karst caves are extreme environments brimming with biodiversity; their food web structure,[33] diverse flora,[34] and influence of heavy metal enrichment are widely studied in China.[35] Furthermore, 40% of Turkey's surface area consists of soluble rocks (limestone, dolomite, and gypsum) suitable for karstification.[36] However, the biodiversity of Kapova Cave in the Urals is poorly characterized. Previous studies have estimated the microbial count (1.4×10^3–2.1×10^5 CFU/mL) in Kapova Cave and the possible origin of its microbiota.[6] Emerging technologies like high-throughput sequencing and bioinformatics have enhanced our understanding of microbial diversity.[37] Recent studies have revealed bacterial diversity in caves in Australia, China, Italy, Spain, Turkey, and the United States,[3,38−42] most of which are dominated by nine groups of domain Bacteria: *Proteobacteria, Acidobacteria, Planctomycetes, Chloroflexi, Bacteroidetes, Gemmatimonadetes, Firmicutes, Nitrospirae*, and *Actinobacteria*, as well as domain Archaea.[38,42−44] The dominant phylum of Kapova Cave, the karst caves in China, and Oylat Cave is *Proteobacteria*,[8−11] whose members are Gram-negative bacteria. Environmental conditions in karst caves such as humidity and the presence of organic nutrient substrates likely promote the development of non-spore-forming bacteria. Yet the predominant species in the Yarık Sinkhole in
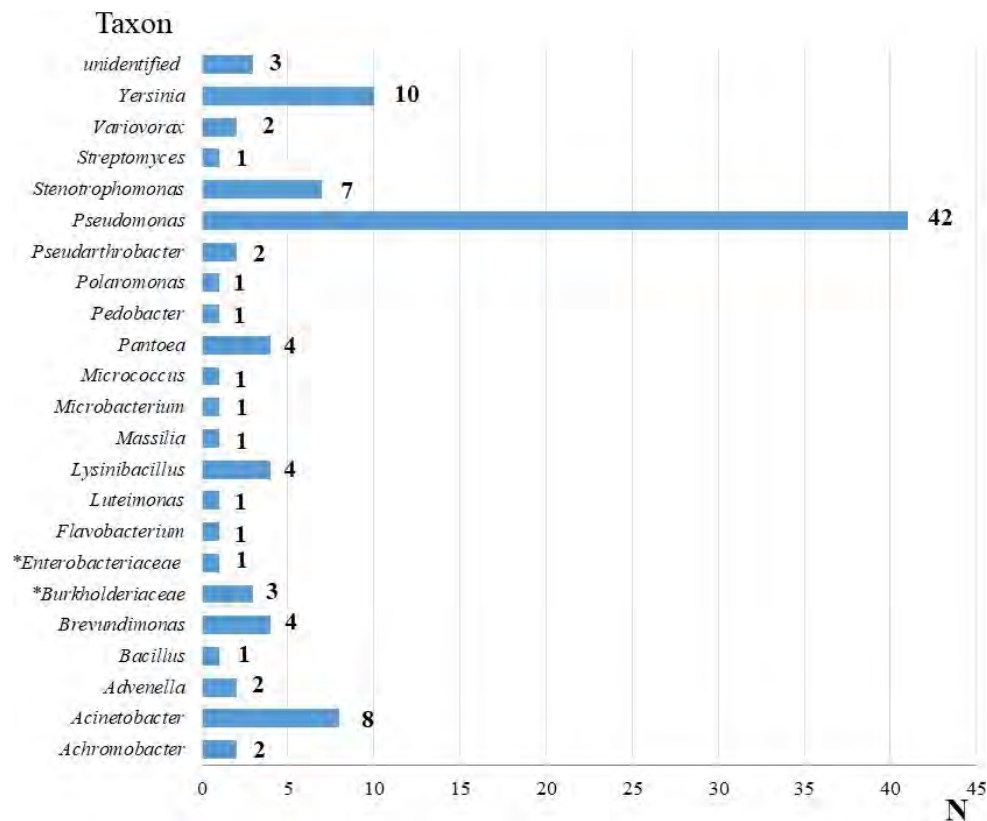
Figure 3. Number (N) of identified bacterial isolates. *Isolate identified only to the family level.

Turkey are *Acinetobacter lwoffii, Methylobacterium tardum*, and *Propionibacterium acnes*.[45] Although the bacteria were sampled during initial exploration, this composition suggests that nearby residents are harming the microbial diversity of the cave. In addition to preserving biodiversity, discovering new and potentially useful bacteria warrants further studies on the diversity of cultivated microorganisms. For example, more than a half of 290 *Actinomycetes* isolates from rock wall and speleothem surfaces of 19 karst caves in Turkey demonstrated antimicrobial activity against antibiotic-resistant bacteria. Strain *Streptomyces* sp. 1492 exhibited bacteriostatic or bactericidal activity against methicillin-resistant *Staphylococcus aureus*, vancomycin resistant *Enterobacter faecium*, and *Acinetobacter baumanii* at bactericidal concentrations lower than that of streptomycin.[46]

Among the isolates collected in this study, *Stenotrophomonas rhizophila* (isolate 7) expressed high levels of protease. This species was also found in the Herrenberg cave in Germany, though it is a plant-associated bacterium[47], as well as in semi-confined caves.[48] *Stenotrophomona* produces keratinases, extracellular proteases, and chitinases.[49] Unlike *S. maltophilia*, *S. rhizophila* cannot proliferate at 37°C and is therefore not pathogenic.

The isolate with the highest RNase activity (isolate 27) was identified as *Lysinibacillus fusiformis*. The *Lysinibacillus* genus, unlike *Bacillus*, contains peptidoglycan with lysine, aspartic acid, alanine, and glutamic acid.[50] Despite sharing many traits with *Bacillus, Lysinibacillus* is poorly characterized. New *Lysinibacillus* strains were recently isolated from a soil in karst caves in Libo County[51] and Xingyi county in China.[52] *In vitro* and *in vivo* assays showed that strain *Lysinibacillus* S4C11 exerts antifungal activity against various pathogens.[53] Similarly, an antifungal protein with RNase activity isolated from *Bacillus subtilis* inhibited mycelial growth in *Magnaporthe griseas, Sclerotinia sclerotiorum, Rhizoctonia solani, Alternaria oleracea, A. brassicae*, and *Botrytis cinerea*.[54] Bacillar RNases are well-known as antitumor [55] and antiviral [56] agents. Our research shows the potential of microbial genera other than bacilli to secrete RNases that may foster the discovery of new RNases to combat tumors, viruses, and pathogenic fungi.

Among bacteria, active producers of amylases include some bacilli like *B. macerans, B. polymyxa, B. subtilis*, and *B. stearothermophilus*.[15] Bacterial extracellular proteases and RNases are also predominantly synthesized by members of the genus *Bacillus*.[57] Although microorganisms including *Bacteroides bivius, Bacteroides melaninogenicus, Bacteroides fragilis, Staphylococcus aureus, Staphylococcus epidermidis, Pseudomonas aeruginosa, Proteus* sp., and *Propionibacterium*
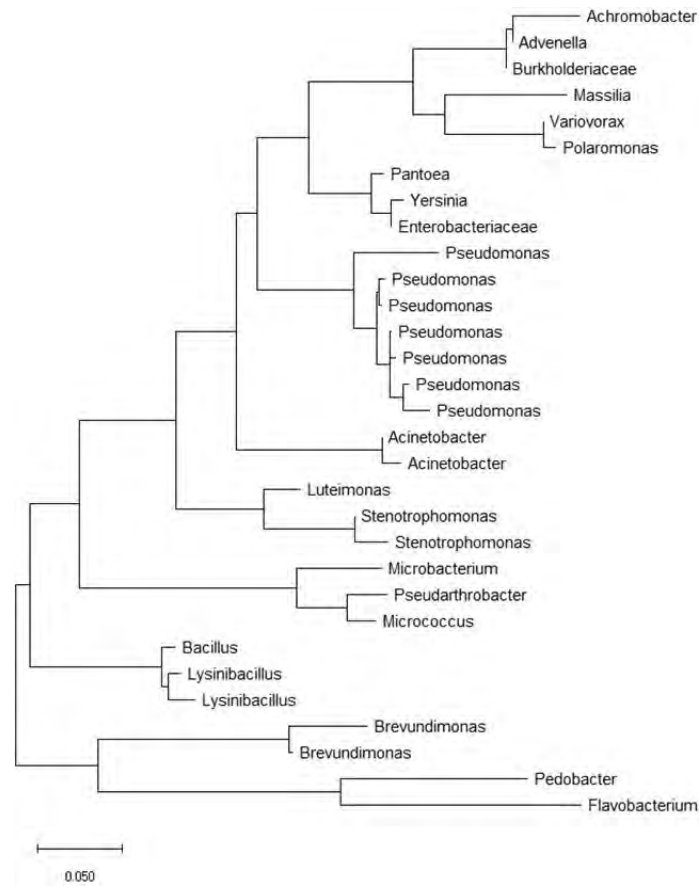
Figure 4. Phylogenetic tree of the isolated bacteria. Isolates with identical 16S rRNA sequences are represented only once.
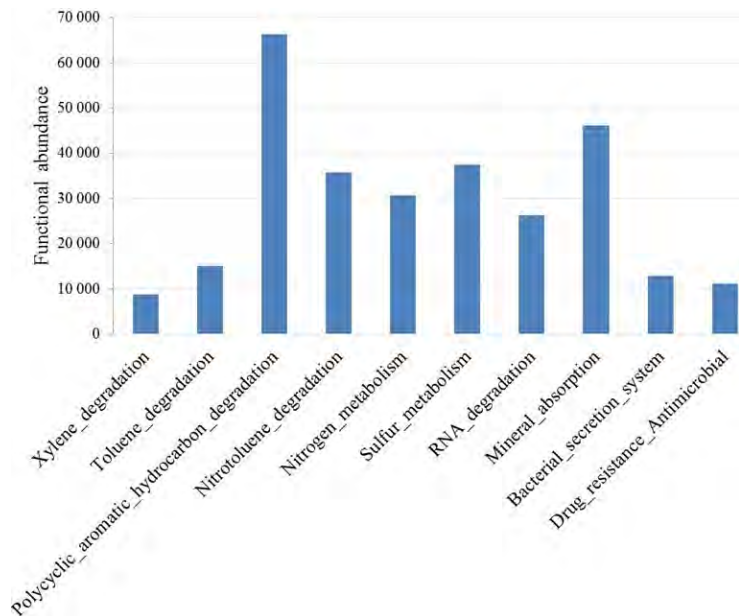
Figure 5. Functional profile of the bacterial community of Kapova cave. Functional abundance represents the number of genes responsible for functions.

Table 1. Identification of analysed isolates based on their 16s rRNA gene sequences.

No	Taxon	No	Taxon	No	Taxon
1	*Pseudomonas stutzeri*	35	*Pseudomonas*	69	*Pseudomonas*
2	*Pseudomonas*	36	*Yersinia*	70	*Pseudomonas*
3	*Pantoea*	37	*Yersinia*	71	*Pseudomonas*
4	*Pseudomonas*	38	Non identified	72	*Pseudomonas*
5	*Pseudomonas*	39	*Pantoea*	73	*Pseudomonas*
6	*Pseudomonas*	40	*Pantoea*	74	*Polaromonas*
7	*Stenotrophomonas rhizophila*	41	*Pseudomonas*	75	*Pseudomonas*
8	*Yersinia*	42	*Brevundimonas*	76	*Pseudomonas*
9	*Yersinia*	43	*Pseudomonas*	77	*Advenella*
10	*Yersinia*	44	*Pantoea*	78	*Pseudomonas*
11	*Achromobacter*	45	*Stenotrophomonas*	79	*Pseudomonas*
12	*Entero bacteriaceae*	46	*Pseudomonas*	80	*Pedobacter*
13	*Pseudomonas*	47	*Stenotrophomonas*	81	*Massilia*
14	*Acinetobacter*	48	*Stenotrophomonas*	82	*Advenella*
15	*Micrococcus*	49	*Yersinia*	83	*Lysinibacillus*
16	*Acinetobacter*	50	*Yersinia*	84	*Stenotrophomonas*
17	*Pseudomonas*	51	*Yersinia*	85	*Stenotrophomonas*
18	*Pseudomonas*	52	*Yersinia*	86	*Stenotrophomonas*
19	*Pseudomonas*	53	*Achromobacter*	87	*Flavobacterium*
20	*Burkholderiaceae*	54	*Acinetobacter*	88	*Pseudomonas*
21	*Burkholderiaceae*	55	*Acinetobacter*	89	Non identified
22	*Pseudomonas*	56	*Acinetobacter*	90	*Pseudarthrobacter*
23	*Pseudomonas*	57	*Acinetobacter*	91	*Pseudomonas*
24	*Bacillus*	57	*Yersinia*	92	*Pseudomonas*
25	*Pseudomonas*	59	*Acinetobacter*	93	*Pseudomonas*
26	*Pseudomonas*	60	*Burkholderiaceae*	94	*Streptomyces*
27	*Lysinibacillus fusiformis*	61	*Pseudarthrobacter*	95	*Brevundimonas*
28	*Pseudomonas*	62	*Microbacterium*	96	Non identified
29	*Pseudomonas*	63	*Acinetobacter*	97	*Pseudomonas*
30	*Pseudomonas*	64	*Pseudomonas*	98	*Pseudomonas*
31	*Lysinibacillus*	65	*Variovorax*	99	*Luteimonas*
32	*Lysinibacillus*	66	*Pseudomonas*	100	*Pseudomonas*
33	*Pseudomonas*	67	*Pseudomonas*	101	*Brevundimonas*
34	*Pseudomonas*	68	*Variovorax*	102	*Brevundimonas*

Table 2. Alpha diversity indices: R is the number of genera, Shannon-Wiener index is genera distribution uniformity.

Sample No	Number of isolates	Richness	Shannon-Wiener index
1	15	4	1.285
2	9	2	0.678
3	11	2	0.678
4	13	3	0.798
5	8	2	0.697
6	26	6	1.36
7	17	6	1.61

Table 3. Bray Curtis index of beta diversity: samples dissimilarity.

Sample No	1	2	3	4	5	6	7
1	0	1	1	1	1	1	1
2	1	0	1	1	1	1	1
3	1	1	0	0.6	0.6	0.83	0.7
4	1	1	0.6	0	0.8	0.63	0.6
5	1	1	0.6	0.8	0	0.82	0.8
6	1	1	0.83	0.6	0.8	0	0.8
7	1	1	0.67	0.6	0.8	0.79	0

acnes produce various proteases,[58] they are pathogenic, and therefore, not suitable for industrial enzyme production. Thus, the isolate *Pseudomonas stutzeri* (number 1) with high amylase activity is promising.
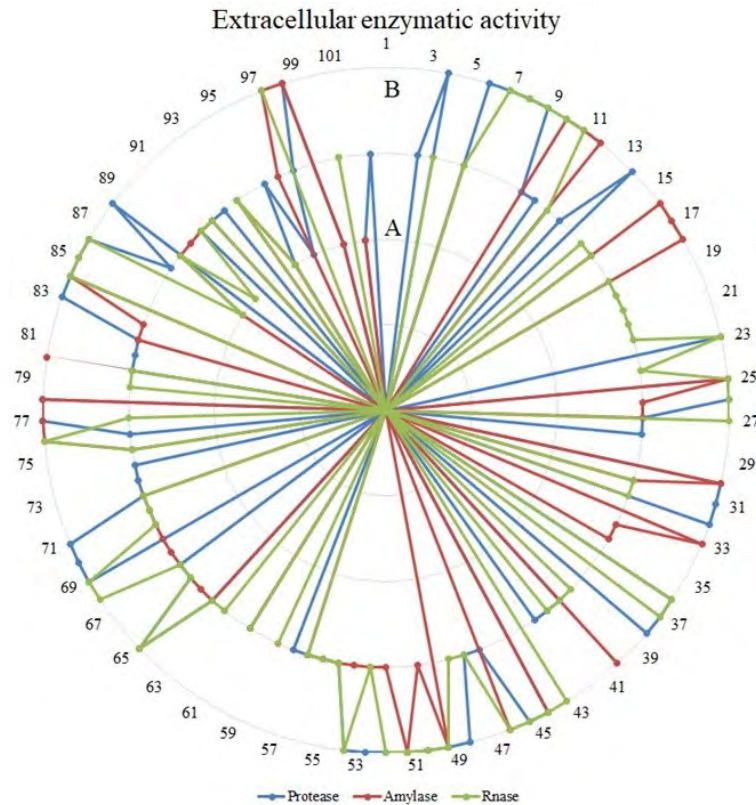
Figure 6. Hydrolytic activity of bacteria isolated from Kapova cave. Hydrolase activity coefficient of a bacterial isolate was calculated as the ratio of colony radius including transparency zone around it to radius of the colony itself. The absence of a lysis zone surrounding colonies indicates the absence of secreted hydrolase. Isolate numbers are circumscribed. Enzymatic activity coefficient value A equals to 1 and is interpreted as isolates not having extracellular hydrolase activity, and value B equals to 2 and is interpreted as possessing high activity.

CONCLUSION

The biodiversity and the ability of bacterial heterotrophic communities harvested from seven biofilms on the walls of Kapova Cave to synthesize secreted hydrolytic enzymes, namely RNases, proteases, and amylases, were explored in this study. Most isolates (89%) belonged to the phylum *Proteobacteria*, and others belonged to three other phyla: *Actinobacteria* (5%), *Firmicutes* (4%), and *Bacteroidetes* (2%). A total of 102 isolates were identified based on sequencing of the V3-V4 16S rRNA gene; among them, 42 belonged to the genus *Pseudomonas*. All three extracellular enzymes were expressed by thirty-nine isolates, and only six of them showed no enzymatic activity. Bacteria producing the highest level of protease, RNase, and amylase were identified as *Stenotrophomonas rhizophila, Lysinibacillus fusiformis, and Pseudomonas stutzeri*, respectively. Overall, these results highlight the importance of discovering microbials that may produce compounds that help develop novel therapeutic and biotechnological agents.

ORCID IDs of the authors

Willam Kurdy	0009-0005-9405-3019
Galina Yakovleva	0000-0002-8504-3434
Olga Ilinskaya	0000-0001-6936-2032

REFERENCES

1. Ortiz M, Legatzki A, Neilson J W, et al. Making a living while starving in the dark: metagenomic insights into the energy dynamics of a carbonate cave. *ISME J*. 2014;8(2):478-491.

2. Zada S, Sajjad W, Rafiq M, et al. Cave microbes as a potential source of drugs development in the modern era. *Microb Ecol*. 2022;84:676-687.

3. Ahamada Rachid N, Doğruöz Güngör N. Major impacts of caving activities on cave microbial diversity: case study of Morca Cave, Turkey. *Int Microbiol*. 2023;26(2):179-190.

4. Adetutu EM, Ball AS. Microbial diversity and activity in caves. *Microb Australia*. 2014;35(4):192-194.

5. Abdullin SR, Kapralov SA, Kuzmina Y. *Biota of the cave Shulgan-Tash (Kapova)*, State reserve "Shulgan-Tash"; 2012. ISBN 5904555415, 9785904555412. (in Russian).

6. Kuzmina LY, Galimzyanova NF, Chervyatsova OY, Sailfullina NM, Kapralov SA, Ryabova AS. Biogenous fouling in Shulgan-Tash cave (Kapova, Southern Urals) and factors influencing on their expansion. *Ecobiotekh*. 2019;2(2):128-142.

7. Galimzianova NF, Gilvanova EA, Ryabova AS, Guvatova ZG, Kudryavtseva AV, Melentiev AI. Phylogenetic diversity of prokaryotes in microbial communities inhabiting rock surfaces of Shulgan-Tash (Kapova) cave, Southern Urals. *Ecobiotekh*. 2020;3(3):298-304.

8. Wang Y, Cheng X, Wang H, Zhou J, Liu X, Tuovinen OH. The characterization of microbiome and interactions on weathered rocks in a subsurface karst cave, Central China. *Front Microbiol*. 2022;13:909494. doi:org/10.3389/fmicb.2022.909494.

9. Zhu HZ, Zhang ZF, Zhou N, et al. Bacteria and metabolic potential in karst caves revealed by intensive bacterial cultivation and genome assembly. *Appl Environ Microbiol*. 2021;87(6):e02440-20. doi.org/10.1128/AEM.02440-20.

10. Cheng XY, Liu XY, Wang HM, et al. USC dominated community composition and cooccurrence network of methanotrophs and bacteria in subterranean karst caves, *Microbiol Spectr*. 2021;9(1): e0082021. doi:org/10.1128/Spectrum.00820-21.

11. Gulecal-Pektas Y. Bacterial diversity and composition in Oylat cave (Turkey) with combined Sanger/pyrosequencing approach. *Pol J Microbiol*. 2016;65(1):69-75.

12. Addesso R, Gonzalez-Pimentel JL, D'Angeli IM, et al. Microbial community characterizing vermiculations from karst caves and its role in their formation. *Microb Ecol*. 2021;81(4):884-896.

13. Razzaq A, Shamsi S, Ali A, et al. Microbial proteases applications. *Front Bioeng Biotechnol*. 2019;7:110. doi:org/10.3389/fbioe.2019.00110.

14. Rao RR, Vimudha M, Kamini N, Gowthaman M, Chandrasekran B, Saravanan P. Alkaline protease production from *Brevibacterium luteolum* (MTCC 5982) under solid-state fermentation and its application for sulfide-free unhairing of cowhides. *Appl Biochem Biotechnol*. 2017;182:511-528

15. De Souza PM, de Oliveira e Magalhães P. Application of microbial *α*-amylase in industry – A review. *Braz J Microbiol*. 2010;41(4):850-861.

16. Gopinath SC, Anbu P, Arshad MK, et al. Biotechnological processes in microbial amylase production. *Biomed Res Int*. 2017:1272193. doi:org/10.1155/2017/1272193.

17. Shah Mahmud R, Efimova MA, Ulyanova V. et al. *Bacillus pumilus* ribonuclease rescues mice infected by double-stranded RNA-containing reovirus serotype 1. *Virus Res*. 2020;286:198086. doi:10.1016/j.virusres.2020.198086.

18. Shah Mahmud R, Mostafa A, Müller C, et al. Bacterial ribonuclease binase exerts an intra-cellular anti-viral mode of action targeting viral RNAs in influenza a virus-infected MDCK-II cells. *Virol J*. 2018;15(1):5. doi:org/10.1186/s12985-017-0915-1.

19. Shah Mahmud R, Müller C, Romanova Y, et al. Ribonuclease from *Bacillus* acts as an antiviral agent against negative- and positive-sense single stranded human respiratory RNA. *Viruses Biomed Res Int*. 2017:5279065. doi:org/10.1155/2017/5279065, 2017.

20. 20. Shah Mahmud R, Efimova M, Mostafa A, Ulyanova V, Ilinskaya O. Antiviral activity of bacterial extracellular ribonuclease against single-, double-stranded RNA and DNA containing viruses in cell cultures. *BioNanoSci*. 2016;6:561-563.

21. Mitkevich VA, Pace CN, Koschinski A, Makarov AA, Ilinskaya ON. Cytotoxicity mechanism of the RNase Sa cationic mutants involves inhibition of potassium current through Ca^{2+}-activated channels. *Mol Biol*. 2015;49:933-938.

22. Ilinskaya ON, Shah-Mahmud RS. Ribonucleases as antiviral agents. *Mol Biol*. 2014;48(5):615-623.

23. Khodzhaeva V, Makeeva A, Ulyanova V, et al. Binase immobilized on halloysite nanotubes exerts enhanced cytotoxicity toward human colon adenocarcinoma cells. *Front Pharmacol*. 2017;8:631. doi:org/10.3389/fphar.2017.00631.

24. Walters W, Hyde ER, Berg-Lyons D, et al. Improved bacterial 16S rRNA gene (v4 and v4-5) and fungal internal transcribed spacer marker gene primers for microbial community surveys. *mSystems*. 2016;1(1):e00009-15. doi:10.1128/mSystems.00009-15.

25. Johnson M, Zaretskaya I, Raytselis Y, Merezhuk Y, McGinnis S, Madden TL. NCBI BLAST: A better web interface. *Nucleic Acids Res*. 2008;36:W5-9. doi:10.1093/nar/gkn201

26. 26. Kumar S, Stecher G, Li M, Knyaz C, Tamura K. MEGA X: Molecular evolutionary genetics analysis across computing platforms. *Mol Biol Evol*. 2018;35(6):1547-1549.

27. 27. Jeffris GD, Holtman WF, Guse D. Rapid method for determining the activity of microorganisms on nucleic acids. *J Bacteriol*. 1957;73:591-601.

28. Price MF, Wilkinson ID, Gentry LO. Plate method for detection of phospholipase activity in *Candida albicans*. *Sabouraudia*. 1982;20(1):7-14.

29. Nagpal S, Haque MM, Singh R, Mande SS. iVikodak – A platform and standard workflow for inferring, analyzing, comparing, and visualizing the functional potential of microbial communities, *Front Microbial*. 2019;9:1-15.

30. Bray JR, Curtis JT. An ordination of the upland forest communities of Southern Wisconsin. *Ecological Monographs*. 1957;27:325-349.

31. Klinfoong R, Thummakasorn C, Ungwiwatkul S, BOONTANOM P, Chantarasirid A. Diversity and activity of amylase-producing bacteria isolated from mangrove soil in Thailand. *Biodiversitas* 2022;23(10):5519-5531. doi:10.13057/biodiv/d231064.

32. Khannous L, Jrad M, Dammak M, et al. Isolation of a novel amylase and lipase-producing *Pseudomonas luteola* strain: Study of amylase production conditions. *Lipids Health Dis*. 2014;13:9. doi:10.1186/1476-511X-13-9.

33. Xu C, Zhao L, Du W, Zhang S, Wu Y, Zhou F. Food sources and trophic levels of terrestrial cave fauna in Yuping Town, Libo County, Guizhou Province. *Biodiv Sci*. 2021;29(8): 1108-1119.

34. Fu L, Monro AK, Wei Y. Cataloguing vascular plant diversity of karst caves in China. *Biodiv Sci*. 2022;30(7):21537. doi:org/10.17520/biods.2021537.

35. Liu R, Zhang Z, Shen J, Wang Z. Community characteristics of

bryophyte in Karst caves and its effect on heavy metal pollution: A case study of Zhijin Cave, Guizhou Province, *Biodiv Sci*. 2018;26(12):1277-1288.

36. Nazik L, Poyraz M, Karabiyikoglu M. Karstic Landscapes and Landforms in Turkey. In book: *Landscapes and Landforms of Turkey*. Chapter: 5. Springer Nature; 2019:181-196. doi:10.1007/978-3-030-03515-0_5.

37. Gao C, Guo L. Progress on microbial species diversity, community assembly and functional traits. *Biodiv Sci*. 2022;30(10):22429. doi:org/10.17520/biods.2022429.

38. Chelius MK, Beresford G, Horton H, et al. Impacts of alterations of organic inputs on the bacterial community within the sediments of wind cave, South Dakota, USA. *Int J Speleol*.2009:38(1):1-10. doi:10.5038/1827-806X.38.1.1.

39. Holmes AJ, Tujula NA, Holley M, et al. Phylogenetic structure of unusual aquatic microbial formations in Nullarbor caves, Australia. *Environ Microbiol*. 2001;3(4):256-264.

40. Macalady JL, Jones DS, Lyon EH. Extremely acidic, pendulous cave wall biofilms from the Frasassi cave system, Italy. *Environ Microbiol*. 2007;9(6):1402-1414.

41. Schabereiter-Gurtner C, Saiz-Jimenez C, Piñar G, Lubitz W, Rölleke S. Phylogenetic diversity of bacteria associated with Paleolithic paintings and surrounding rock walls in two Spanish caves (Llonín and La Garma). FEMS *Microbiol Ecol*. 2004;47(2):235-247.

42. Zhou JP, Gu YQ, Zou CS, Mo MH. Phylogenetic diversity of bacteria in an earth-cave in Guizhou province, southwest of China. *J Microbiol*. 2007;45(2):105-112.

43. Gonzalez JM, Portillo MC, Saiz-Jimenez C. Metabolically active crenarchaeota in Altamira Cave. *Naturwissenschaften*. 2006;93(1):42-45.

44. Leuko S, Koskinen K, Sanna L, et al. The influence of human exploration on the microbial community structure and ammonia oxidizing potential of the Su Bentu limestone cave in Sardinia, Italy. *PLoS One*. 2017;12(7):e0180700. doi:org/10.1371/journal.pone.0180700.

45. Doğruöz-Güngör N, Arslan-Aydoğdu EÖ, Dirmit E, Usuloğlu E. Anthropogenic impacts on the bacterial profile of Yarik Sinkhole in Antalya, Turkey. *J Caves Karst Stud*. 2020;82(2):116-124.

46. 46. Yücel S, Yamaç M. Selection of *Streptomyces* isolates from Turkish karstic caves against antibiotic resistant microorganisms. *Pak J Pharm Sci*. 2010;23(1):1-6.

47. Rusznyák A, Akob DM, Nietzsche S, et al. Calcite biomineralization by bacterial isolates from the recently discovered pristine karstic herrenberg cave, *Appl Environ Microbiol*. 2012;78(4):1157-1167.

48. Cuzman OA, Luvidi L, Colantonio C, et al. Biodiversity and conservation correlation in the case of a Roman fresco located in a semi-confined environment. *Int Biodet Biodeg*. 2023;181:105605. doi.org/10.1016/j.ibiod.2023.105605.

49. Pinski A, Zur J, Hasterok R, Hupert-Kocurek K. Comparative genomics of *Stenotrophomonas maltophilia* and *Stenotrophomonas rhizophila* revealed characteristic features of both species. *Int J Mol Sci*. 2020;21(14):4922. doi:org/10.3390/ijms21144922.

50. Ahmed I, Yokota A, Yamazoe A, Fujiwara T. Proposal of *Lysinibacillus boronitolerans* gen. nov. sp. nov., and transfer of *Bacillus fusiformis* to *Lysinibacillus fusiformis* comb. nov. and *Bacillus sphaericus* to *Lysinibacillus sphaericus* comb. nov. *Int J Syst Evol Microbiol*. 2007;5:1117-1125.

51. Kan Y, Niu XK, Rao MPN, et al. *Lysinibacillus cavernae* sp. nov., isolated from cave soil. *Arch Microbiol*. 2020;202(6):1529-1534.

52. Narsing Rao MP, Dong Z.Y, Niu XK, et al. *Lysinibacillus antri* sp. nov., isolated from cave soil. *Int J Syst Evol Microbiol*. 2020;70(5):3295-3299.

53. Passera A, Rossato M, Oliver JS, et al. Characterization of *Lysinibacillus fusiformis* strain S4C11: *In vitro*, in planta, and in silico analyses reveal a plant-beneficial microbe. *Microbiol Res*. 2021;244:126665. doi:org/10.1016/j.micres.2020.126665.

54. Liu Y, Chen Z, Ng TB, et al. Bacisubin, an antifungal protein with ribonuclease and hemagglutinating activities from *Bacillus subtilis* strain B-916. *Peptides*. 2007;28(3):553-559.

55. Makarov AA, Ilinskaya ON. Cytotoxic ribonucleases: molecular weapons and their targets, *FEBS Lett*. 2003;540(1-3):15-20.

56. Ilinskaya ON, Shah-Mahmud RS. Ribonucleases as antiviral agents, *Mol Biol*. 2014;48(5):615-623.

57. Ulyanova V, Shah Mahmud R, Dudkina E, Vershinina V, Domann E, Ilinskaya O. Phylogenetic distribution of extracellular guanyl-preferring ribonucleases renews taxonomic status of two *Bacillus* strains. *J Gen Appl Microbiol*. 2016;62(4):181-188.

58. McGregor JA, Lawellin D, Franco-Buff A, Todd JK, Makowski EL. Protease production by microorganisms associated with reproductive tract infection. *Am J Obstet Gynecol*. 1986;154(1):109-114.

How cite this article

İSTANBUL
UNIVERSITY
— P R E S S —

Functional Annotation of Uncharacterised Proteins Whose Expression Patterns Affect the Lifespan under Metformin Treatment in Fission Yeast

Cagatay Tarhan[1] , Sumeyra Zeynep Calici[2] , Buse Ozden[2]

[1]Istanbul University, Faculty of Science, Department of Molecular Biology and Genetics, Fatih, Istanbul
[2]Istanbul University, Institute of Science, Program of Molecular Biotechnology and Genetics, Fatih, Istanbul

ABSTRACT

Objective: Metformin, a well-known anti-diabetic drug and a caloric restriction mimetic, seems to attenuate aging through myriad cellular processes, wherein most of its mode of action is still elusive. Thus, bioinformatic analyses that might direct experimental studies are crucial. Moreover, uncharacterised proteins with unknown molecular functions might withhold information regarding metformin's mode of action. Here, we aimed to elucidate genes encoding uncharacterised proteins that are somehow involved in metformin metabolism and elaborate their involvement through functional annotation to reveal novel cellular processes in which metformin interferes.

Materials and Methods: Total RNA isolation was conducted from *Schizosaccharomyces pombe* wild-type cells that were grown in standard and overnutrition conditions. Following the gene expression analysis of the uncharacterised proteins, the bioinformatics analysis of the up- and down-regulated uncharacterised proteins upon metformin treatment in both was conducted using the functional annotator called PANNZER2.

Results: Genes that might be related to cellular processes such as meiosis, protein folding, calcium homeostasis, and heme production are up- and down-regulated upon metformin treatment. Moreover, the up-regulation of apoptosis and antioxidation-related genes and the down-regulation of mitosis, DNA damage, apoptosis, mitochondria, and telomere-capping-related genes were also determined.

Conclusion: We effectively identified associations between metformin and a wide range of cellular processes and genetic mechanisms through the comprehensive annotation of uncharacterised genes. Our findings are consistent with the literature, and many of these uncharacterised proteins could be used as targets for research into aging in the future.

Keywords: Metformin, Aging, Uncharacterized Proteins, *Schizosaccharomyces pombe*

INTRODUCTION

Aging is defined as a gradual deterioration of physiological integrity that diminishes the function at molecular, cellular, tissue, and systemic levels and increases the tendency of mortality. A majority of serious human pathologies, such as cancer, diabetes, cardiovascular problems, and neurological diseases are at high risk owing to this degradation.[1] Although aging is not considered a disease in itself, it is undeniable that it is the main cause of many age-related diseases.

To date, many chemicals and compounds that contribute to the healthy prolongation of the life span of various organisms have been identified. Since they contain unique properties that affect nine hallmarks of aging, one of these compounds, metformin (N,N-dimethylbiguanide), has been identified as ex-

tremely important. Thus, it became the first drug to be tested for its anti-aging effects in the large clinical trial-TAME (Targeting Aging by Metformin) study (visit https://www.afar.org/tame-trial). Since it lowers blood glucose levels, metformin has been used for nearly 65 years to treat type-2 diabetes. In addition to its anti-diabetic properties, it has also been found to be effective in the treatment of cancer, neurological diseases, and biological aging. It is also helpful for treating coronary heart disease by inducing weight loss and improving cholesterol levels.[2–4]

Metformin delays aging by regulating adenosine monophosphate-activated protein kinase (AMPK), endothelial nitric oxide synthase (eNOS)/cyclic guanosine monophosphate (cGMP) and phospho-myosin light chain kinase (p-MLCK) actin remodelling pathways, decreasing

insulin receptor substrate 2 (IRS2) and insulin-like growth factor 1 receptor (IGF1R) in neurons, reducing the buildup of the advanced glycation end products (AGEs), reducing reactive oxygen species (ROS) levels in mitochondria, inhibiting oxidative stress, balancing protein homeostasis, and enhancing autophagy by inhibiting the target of rapamycin (mTOR) signaling pathway.[5] The anti-aging effects of metformin can be used to treat age-related diseases through regulating nutrition sensing. It is effective in treating certain hallmarks of aging, such as DNA damage, the production of ROS, telomere attrition, inflammation, cellular senescence, stem cell depletion, and autophagy.[4] In various model organisms such as mice and *Caenorhabditis elegans*, it has been demonstrated that metformin extends lifespan through interacting with myriad metabolic pathways.[6−8] In a recent study, the autophagy-inducing effect of metformin was shown to delay muscle aging in *Drosophila melanogaster* adults.[9] Şeylan and Tarhan[10] report that metformin significantly extends *Schizosaccharomyces pombe (S. pombe)*'s chronological lifespan (CLS) by mechanisms resembling those identified in mammalian cells and other model organisms. It was demonstrated that metformin increases the production of ROS, glucose uptake, and adenosine triphosphate (ATP) synthesis while decreasing oxidative stress markers such as lipid peroxidation and carbonylated proteins.[10]

Proteins must have accurate functional annotations for biological research to be successful. Unfortunately, functional characterisation or empirically confirmed annotations are absent from the great majority of protein sequences.[11] If a protein's role and relevance in cellular processes are not completely comprehended or annotated, it is said to be uncharacterised.[12] The most accurate technique to characterise proteins with unknown activity is by experimental determination of protein function, however with so many potential uses for a protein, it can be challenging to decide which functional research to prioritise. Several computer methods for protein function prediction have been developed to assist experimentalists.[13] A significant fraction of these proteins lack human analogues and may serve as a valuable source for new antibacterial drug targets.[14]

Sequence homology is a common method for predicting protein function since it assumes that proteins with similar amino acid sequences should have comparable functions. To search a database of known amino acid sequences and their functions, early methods used sequence search tools like BLAST or DIAMOND.[15,16] The main drawback of these approaches is that they are constrained by the databases they use; annotation errors may occur, and it is sometimes challenging to establish a suitable threshold for transferring protein function, leading to low specificity and sensitivity.[17] Researchers have been able to investigate machine learning algorithms that are data-driven because of the improved data availability. In the early days of function prediction, supervised machine learning models like neural networks (NNs), support vector machines (SVMs),

or k-nearest neighbour (KNN) methods were employed to extract characteristics from the sequence of interest.[11,18] Multiple Gene Ontology (GO) predictors are implemented within the Protein ANNotation with Z-scoRE (PANNZER2), and they all are based on enrichment statistics of the sequence neighbourhood that the authors of the publication referred to as scoring functions.[19] Although score calculation differs from one scoring function to another, they all accept the same filtered sequence neighbourhood as an input. The authors state that the PANNZER2 uses the ARGOT scoring function by default, as it performs best. Likewise, the same filtered sequence neighbourhood is clustered according to the description similarity based on word frequencies using hierarchical clustering with average linkage for free text description prediction. The authors use a regression model to select the best cluster, and the output is the most representative description, i.e., the most frequent one within the best cluster.

The discovery of previously unidentified proteins that might be implicated in the aging process is made possible by uncharacterised protein prediction. The creation of thorough networks and pathways involved in aging is made possible by combining prediction algorithms with other high-throughput approaches, including transcriptomics and proteomics. Researchers can find proteins that might act as markers of aging or disease development by identifying uncharacterised proteins and evaluating their expression patterns during aging. These proteins may be used to identify healthy aging biomarkers. Additionally, the identification of targets for therapeutic interventions targeted at slowing down the aging process and age-related disorders can be aided by the prediction of protein function.

In the present study, we focused on uncharacterised proteins that are differentially expressed under metformin treatment in *S. pombe* and estimated their functions using the PANNZER2. In these types of studies, researchers generally focus on the expression pattern of the genes/proteins that have already been characterised, whereas this study focused on genes that have not yet been annotated and we aimed to identify new target genes that may be involved in the life-prolonging effect of metformin. These proteins play roles in many cellular processes such as meiosis, mitosis, DNA damage, protein folding, apoptosis, autophagy, antioxidative effect, mitochondrial changes, heme production, and telomere capping. These results are in line with previous studies. Moreover, most of these non-annotated proteins might serve as targets for further aging studies.

MATERIALS AND METHODS

Organism and Media

S. pombe wild-type strain 972- and Synthetic Dextrose (SD) medium was used in the study. Chen and Runge[20] report that this medium is suitable for chronological lifespan experiments as it recapitulates the evolutionarily conserved response of lifes-

pan shortening due to overnutrition for cells grown in SD with excess glucose. SD medium with 3% glucose (standard condition) and 5% glucose (overnutrition condition) were used in this study. To understand how metformin affects gene expression in these two different conditions, gene expression in cells grown in a 3% glucose medium with metformin was compared with the gene expression profile of cells grown in a 3% glucose medium without metformin (control medium). The same comparison was made for a medium containing 5% glucose. Cells from a single colony with a 5x104 cell/ml density were inoculated in 25 ml SD medium with and without 25 mM Metformin hydrochloride (SIGMA) in a 100 ml flask and orbitally shaken at 180 rpm and at a temperature of 30 °C until respective mid-log phase. Determination of the dose of metformin and its application method were given in our previous study.[10]

Total RNA Isolation

The Hibrigen Total RNA Isolation Kit was used following the manufacturer's instructions for the total RNA isolation from mid-log cells. Briefly, samples were digested and homogenized while exposed to guanidium isothiocyanate, a chaotropic salt protecting RNAs from endogenous RNases. Subsequently, we conducted ethanol precipitation to isolate nucleic acids and transferred the samples into filtered tubes that could selectively withhold RNAs. The attached RNAs were then eluted with DEPC-treated water, and total RNA purity and quantity were assessed using a Nanodrop 2000 spectrophotometer (Nanodrop Technologies, USA). For each sample, three biological replicates were used. Finally, the replicates were pooled for sequencing according to their concentrations.

Library Preparation and RNA Sequencing

Library preparation, fragmentation, adapter binding, RNA sequencing, and bioinformatic analysis of sequence data were performed by Macrogen, Inc. (Seoul, South Korea). Briefly, the contaminating DNAs were eliminated using DNase. TruSeq Stranded Total RNA LT Sample Prep Kit (Gold) was used for the library preparation. The purified RNAs were then randomly fragmented for short-read sequencing, and these fragmented RNAs were reverse transcribed into cDNA. Adapters were ligated onto both ends of the fragments, and those with insert sizes between 200 and 400 base pairs were selected after amplification with PCR. Both ends were sequenced by the read length for paired-end sequencing using the Illumina platform.

Bioinformatic Analysis of Sequence Data

Quality control of the raw sequencing data was conducted using FastQC (ver.0.11.7). Afterward, adapter sequences and bases with a base quality lower than three were removed from the ends using Trimmomatic (ver.0.38). Additionally, bases of reads that do not qualify for window size four and mean quality 15 were trimmed using the sliding window method. Finally, reads shorter than 36 base pairs were dropped to yield trimmed data. The quality of the trimmed data was checked again using FastQC. Subsequently, the trimmed reads were mapped onto the reference genome using HISAT2 (ver.2.1.0), which handles mapping through Bowtie2 (ver.2.3.4.1) aligner. Lastly, transcripts were assembled using StringTie (ver.2.1.3b). After the assembly, the gene/transcript abundance was calculated by using the FPKM (fragments per kilobase per million reads) and TPM (transcripts per kilobase million) for each sample.

Gene Expression Analysis

For the gene expression analysis, TPM values for different conditions (metformin-treated versus control) were rationed. We assumed that changes in gene expression are significant if the ratio is at least twice as high or lower than 1.5-fold for one condition versus the other, a common assumption for such analyses. Among these significantly differentially expressed genes, the uncharacterised ones that lack functional annotation in the literature were filtered, and further research was conducted.

PANNZER2 and the Analysis of the Results

PANNZER2 was used to functionally annotate uncharacterised proteins that the gene expression analysis yielded.[11] PANNZER2 accomplishes functional annotation of uncharacterised proteins by predicting GO classes and free text description lines required for new sequence submission into databases based on enrichment statistics and sequence similarity, respectively. The tool comprises three servers—a web server containing the user interface, the SANSparallel server for homology search, and the DictServer for handling metadata associated with the uncharacterised proteins. First, a sequence similarity search against the UniProtKB database (https://www.uniprot.org/) using SANSparallel is conducted. The output is a subset of sequences called a sequence neighbourhood. Next, the sequence neighbourhood is filtered following several criteria. Finally, the remaining sequences' GO annotations and free text descriptions are gathered using the DictServer.

The sequences of uncharacterised proteins were submitted in FASTA format from the web server and the batch queue option was used to download the results later. For all other parameters, default options were selected. The output is a summary table containing the sequence identifier, description predictions, and GO predictions for biological processes, molecular functions, and cellular components.Color-coded probabilities from green to red that correspond to high-confidence to low-confidence predictions are also provided. After the results were generated, we filtered uncharacterised proteins with at least a GO class or free text description line prediction. Subsequently, we exam-
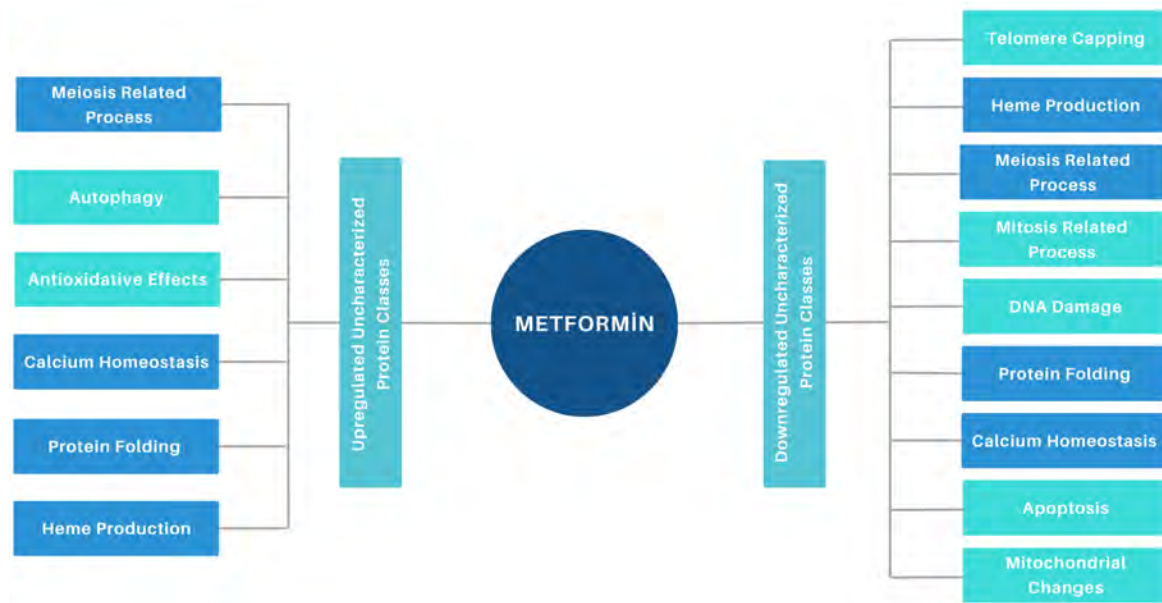
Figure 1. Metformin affects many cellular processes. Boxes with dark blue colours are common uncharacterised genes belonging to both up-regulated and down-regulated classes. Boxes with turquoise colors are uncharacterised genes that belong to only one class. Common cellular processes include meiosis, protein folding, calcium homeostasis, and heme production.

ined the filtered predictions to designate joint GO classes or descriptions, aiming to reveal crucial cellular processes involved in metformin metabolism and to have a more comprehensive perspective.

RESULTS

Based on observations, it appears that metformin treatment can impact the expression of certain genes in various ways. Our gene expression analysis yielded 561 uncharacterised proteins and PANNZER2 predicted at least a GO class or free text description line for 250 of these proteins (44%). Tables 1 and 2 outline the up-regulated and down-regulated proteins, respectively, that were predicted by PANNZER2 and provide details on their molecular and biological functions, as well as their fold changes.

It was found that there are shared up-regulated and uncharacterised genes in standard and overnutrition conditions. These genes play a crucial role in responding to iron ion starvation, as well as in regulating the meiotic cell cycle, and in metabolic processes related to lipids. They also play a role in macroautophagy, in transporting proteins, and in responding to oxidative stress. Proteins named conidiation-specific protein 6 (NP_592798.1), meiotically up-regulated gene 52 protein (NP_593587.1), and meiotically up-regulated gene 144 protein (NP_593215.2) were identified as being commonly expressed in both media. Specifically, the expression of meiotically up-regulated gene 52 protein was found to increase significantly in standard conditions, with a quantitative increase of 636 times.

PANNZER2 predicted myriad biological processes and molecular functions that the uncharacterised down-regulated proteins are involved in and possess, and some of these annotations are crucial to cell viability. We classified these proteins according to their predictions to reveal the cellular processes in which metformin interacts. The classes include meiosis, mitosis, DNA damage, protein folding, apoptosis, mitochondrial changes, heme production, and telomere capping (Figure 1).

DISCUSSION

The primary objective of our study was to illuminate the cellular and molecular repercussions of metformin by establishing associations between the expression profiles of previously uncharacterised proteins. Through the systematic classification of uncharacterised genes predicated on their altered expression patterns, we successfully delineated correlations between metformin and a myriad of cellular processes and genetic mechanisms (Figure 1). Significantly, genes that showed changes in their expression levels held particular importance due to their involvement in pivotal processes, including meiosis, protein folding, and calcium homeostasis.

While we observed alterations in the expression levels of numerous proteins during meiosis, striking ones were meiotically up-regulated genes. One of these genes, meiotically up-regulated gene 52 protein (636.37 fold change in standard condition and 5.1 fold change in overnutrition condition) is up-regulated in both conditions along with conidiation-specific protein 6 (5.46 fold change in standard condition and 5.51 fold change in overnutrition condition). Expressions of meioti-

Table 1. Up-regulated uncharacterised proteins upon metformin treatment both in (3% glucose) standard and (5% glucose) overnutrition conditions.

Query	Description	Biological Process	Molecular Function	Fold Change (3M/3C)	Fold Change (5M/5C)
NP_593587.1 SPAC17H9.18c	Meiotically up-regulated gene 52 protein	No prediction	• GO:0051321 meiotic cell cycle	636.37	5.1
NP_592798.1 SPAC11D3.01c	Conidiation-specific protein 6	No prediction	No prediction	5.46	5.51
NP_593215.2 SPAC30D11.02c	Meiotically up-regulated gene 144 protein	No prediction	• GO:0051321 meiotic cell cycle	3.61	
NP_594740.1 SPAC20G4.05c	Protein adenylyltransferase SelO, mitochondrial	0.64 GO:0016779 nucleotidyltransferase activity 0.56 GO:0005524 ATP binding 0.54 GO:0046872 metal ion binding 0.39 GO:0016209 antioxidant activity 0.36 GO:0016491 oxidoreductase activity	• GO:0018117 protein adenylylation • GO:0045454 cell redox homeostasis • GO:0098869 cellular oxidant detoxification • GO:0034599 cellular response to oxidative stress	2	
NP_592791.1 SPAC1F8.02c	High affinity heme transporter	0.91 GO:0140488 heme receptor activity 0.64 GO:0020037 heme binding	• GO:1904334 heme import across plasma membrane • GO:0010106 cellular response to iron ion starvation • GO:0006897 endocytosis		5.2
NP_592777.1 SPAC977.05c	Velum formation-protein	0.36 GO:0008270 zinc ion binding	No prediction		4.01
NP_595084.1 SPBC660.05	WW domain-containing protein C660.05	No prediction	No prediction		3.57
NP_593689.1 SPAC4G9.07	Meiotically up-regulated gene 133 protein	No prediction	• GO:0051321 meiotic cell cycle		3.38
NP_592814.1 SPAC5H10.01	Hydro-lyase	0.62 GO:0016829 lyase activity 0.39 GO:0009975 cyclase activity	• GO:0006536 glutamate metabolic process		2.93
NP_592939.1 SPAC24H6.13	Phosphate metabolism protein 7	0.81 GO:0005227 calcium activated cation channel activity	• GO:0098655 monoatomic cation transmembrane transport		2.11
NP_587988.1 SPCC16A11.01	Plasma membrane protein	No prediction	• GO:0048017 inositol lipid-mediated signalling • GO:0006629 lipid metabolic process		2.06
NP_594405.1 SPAC27E2.04c	Meiotically up-regulated gene 155 protein	No prediction	• GO:0051321 meiotic cell cycle		2.05
NP_596308.1 SPBC405.05	Autophagy protein 16	0.71 GO:0019776 Atg8 ligase activity	• GO:0016236 macroautophagy • GO:0051321 meiotic cell cycle • GO:0015031 protein transport		2.01
NP_595648.1 SPBC83.16c	Inclusion body clearance protein IML2	No prediction	• GO:0071218 cellular response to misfolded protein • GO:1990748 cellular detoxification		2.01
NP_593616.2 SPAC25A8.03c	Protein arginine methyltransferase NDUFAF7 homolog, mitochondrial	0.85 GO:0035243 protein-arginine omega-N symmetric methyltransferase activity	• GO:0032259 methylation		1.99

Table 2. Down-regulated uncharacterised proteins upon metformin treatment both in (3% glucose) standard and (5% glucose) overnutrition conditions.

Query	Description	Biological Process	Molecular Function	Fold Change (3M/3C)	Fold Change (5M/5C)
NP_596062.1 uncharacterized protein SPBC2G5.01 [Schizosaccharomyces pombe]	0.37 UPF0674 endoplasmic reticulum membrane protein C2G5.01	0.84 GO:0032469 endoplasmic reticulum calcium ion homeostasis 0.62 GO:0045048 protein insertion into ER membrane 0.53 GO:0006457 protein folding	0.69 GO:0005509 calcium ion binding 0.56 GO:0044183 protein folding chaperone	1.484839734	1.244282751
NP_595355.1 uncharacterized protein SPBC216.03 [Schizosaccharomyces pombe]	0.34 NAD(P)-binding domain-containing protein	0.74 GO:0042167 heme catabolic process	0.41 GO:0016829 lyase activity	1.358003583	1.478227884
NP_595087.2 uncharacterized protein SPBC660.08 [Schizosaccharomyces pombe]	0.40 Meiotically up-regulated gene 167 protein	0.79 GO:0016236 macroautophagy 0.67 GO:0051321 meiotic cell cycle	0.56 GO:0005515 protein binding	1.355431673	1.430388762
NP_593856.1 uncharacterized protein SPAC7D4.03c [Schizosaccharomyces pombe]	0.0 Uncharacterized protein	0.85 GO:0051403 stress-activated MAPK cascade 0.80 GO:0043410 positive regulation of MAPK cascade	0.85 GO:0005078 MAP-kinase scaffold activity	1.339964572	1.316245774
NP_587772.3 uncharacterized protein SPCC553.01c [Schizosaccharomyces pombe]	0.0 Uncharacterized protein	0.85 GO:0000712 resolution of meiotic recombination intermediates 0.74 GO:0006302 double-strand break repair		1.310073372	0.900329932
NP_593156.1 uncharacterized protein SPAC821.03c [Schizosaccharomyces pombe]	0.0 Uncharacterized protein	0.88 GO:1903360 protein localization to lateral cortical node 0.88 GO:1903359 lateral cortical node assembly		1.281782062	1.027685654
NP_595544.1 uncharacterized protein SPBC27B12.14 [Schizosaccharomyces pombe]	0.63 Assembly factor cbp4	0.84 GO:0017062 respiratory chain complex III assembly 0.79 GO:0033108 mitochondrial respiratory chain complex assembly		1.16944588	1.416262734
NP_587971.1 uncharacterized protein SPCC1393.13 [Schizosaccharomyces pombe]	0.65 Sugar phosphate phosphatase	0.43 GO:0006974 DNA damage response 0.43 GO:1990748 cellular detoxification	0.85 GO:0103026 fructose-1-phosphatase activity 0.84 GO:0097023 fructose 6-phosphate aldolase activity 0.54 GO:0046872 metal ion binding 0.51 GO:0004427 inorganic diphosphate phosphatase activity	1.155098296	1.409568489
NP_588026.2 uncharacterized protein SPCPB16A4.02c [Schizosaccharomyces pombe]	0.0 Uncharacterized protein	0.88 GO:0031566 actomyosin contractile ring maintenance 0.85 GO:1902410 mitotic cytokinetic process 0.72 GO:1902635 1-phosphatidyl-1D-myo-inositol 4,5-bisphosphate biosynthetic process	0.83 GO:0005546 phosphatidylinositol-4,5-bisphosphate binding 0.79 GO:0140550 phosphatidylinositol-4,5-bisphosphate sensor activity 0.52 GO:0005515 protein binding	1.109540038	1.480591308

Table 2. Continued

NP_593199.1 uncharacterized protein SPAC1A6.07 [Schizosaccharomyces pombe]	0.48 Eisosome protein sle1	0.80 GO:0007009 plasma membrane organization		1.029201593	0.811563261
NP_594986.3 uncharacterized protein SPAC29B12.08 [Schizosaccharomyces pombe]	0.0 Uncharacterized protein	0.86 GO:0030466 silent mating-type cassette heterochromatin formation		1.017425083	0.927726427
NP_587691.1 uncharacterized protein SPCC613.03 [Schizosaccharomyces pombe]	0.18 EF-hand domain-containing protein		0.59 GO:0005509 calcium ion binding	0.985505116	1.090550772
NP_594939.1 uncharacterized protein SPAC11E3.14 [Schizosaccharomyces pombe]	0.0 Uncharacterized protein	0.77 GO:0071218 cellular response to misfolded protein 0.63 GO:1990748 cellular detoxification		0.961099066	1.10032874
NP_588137.1 uncharacterized protein SPCC1322.09 [Schizosaccharomyces pombe]	0.34 Maintenance of telomere capping protein 1			0.953135185	1.161232568
NP_588130.1 uncharacterized protein SPCC1322.02 [Schizosaccharomyces pombe]	0.0 Uncharacterized protein	0.88 GO:0007534 gene conversion at mating-type locus 0.86 GO:0000729 DNA double-strand break processing 0.85 GO:0045002 double-strand break repair via single-strand annealing	0.90 GO:0140656 endodeoxyribonuclease activator activity 0.63 GO:0005515 protein binding	0.933931645	0.926896946
NP_001342866.1 uncharacterized protein SPAC1420.01c [Schizosaccharomyces pombe]	0.0 Uncharacterized protein	0.87 GO:0031930 mitochondria-nucleus signaling pathway 0.78 GO:0000122 negative regulation of transcription by RNA polymerase II 0.77 GO:0006808 regulation of nitrogen utilization		0.914501233	1.073219792
NP_596723.1 uncharacterized protein SPBC1861.06c [Schizosaccharomyces pombe]	0.40 Meiotically up-regulated gene 131 protein	0.77 GO:0051321 meiotic cell cycle		0.893999889	1.15681355
NP_594513.1 uncharacterized protein SPAC2C4.10c [Schizosaccharomyces pombe]	0.0 Uncharacterized protein	0.88 GO:0061509 asymmetric protein localization to old mitotic spindle pole body 0.87 GO:0031030 negative regulation of septation initiation signaling		0.889591019	0.915033714

Table 2. Continued

NP_588087.1 uncharacterized protein SPCC4B3.03c [Schizosaccharomyces pombe]	0.80 Related to MAM3 Protein required for normal mitochondrial morphology	0.83 GO:0010960 magnesium ion homeostasis 0.49 GO:0030026 intracellular manganese ion homeostasis 0.40 GO:0007005 mitochondrion organization 0.37 GO:0006914 autophagy	0.36 GO:0019787 ubiquitin-like protein transferase activity	0.88878451	1.244341597
NP_594906.2 uncharacterized protein SPAC14C4.01c [Schizosaccharomyces pombe]	0.40 Mitophagy receptor atg43	0.85 GO:0000423 mitophagy	0.86 GO:0140580 mitochondrion autophagosome adaptor activity 0.63 GO:0005515 protein binding	0.865426311	1.009510393
NP_594896.1 uncharacterized protein SPAPJ691.03 [Schizosaccharomyces pombe]	0.55 MICOS complex subunit MIC10	0.85 GO:0042407 cristae formation		0.857530553	0.8515606
NP_596357.1 uncharacterized protein SPBC25H2.09 [Schizosaccharomyces pombe]	0.36 MICOS complex subunit mic19	0.85 GO:0042407 cristae formation		0.844529172	0.456016818
NP_596816.1 uncharacterized protein SPBC1539.02 [Schizosaccharomyces pombe]	0.20 Eukaryotic nuclear protein implicated in meiotic chromosome segregation	0.71 GO:0051321 meiotic cell cycle		0.838771377	0.931903577
NP_588164.1 uncharacterized protein SPCC338.02 [Schizosaccharomyces pombe]	0.40 Meiotically up-regulated gene 112 protein	0.77 GO:0051321 meiotic cell cycle		0.82624801	1.121878485
NP_594883.1 uncharacterized protein SPAC26F1.12c [Schizosaccharomyces pombe]	0.0 Uncharacterized protein	0.70 GO:0061077 chaperone-mediated protein folding	0.78 GO:0061770 translation elongation factor binding 0.46 GO:0044183 protein folding chaperone 0.45 GO:0003677 DNA binding	0.818094711	0.839081199
NP_593192.1 uncharacterized protein SPAC1A6.01c [Schizosaccharomyces pombe]	0.96 Thyroid receptor interacting protein	0.60 GO:0045893 positive regulation of DNA-templated transcription 0.54 GO:0006357 regulation of transcription by RNA polymerase II	0.65 GO:0003713 transcription coactivator activity 0.63 GO:0008270 zinc ion binding	0.810588765	0.982837431
NP_593840.1 uncharacterized protein SPAC823.13c [Schizosaccharomyces pombe]	0.61 Sensitive to high expression protein 9, mitochondrial	0.55 GO:0007007 inner mitochondrial membrane organization		0.80229592	0.870844396

Table 2. Continued

NP_596268.1 uncharacterized protein SPBC30D10.17c [Schizosaccharomyces pombe]	0.97 Cell wall biosynthesis/cell cycle regulator	0.68 GO:0070880 fungal-type cell wall beta-glucan biosynthetic process 0.63 GO:0140278 mitotic division septum assembly 0.49 GO:0071555 cell wall organization	0.69 GO:0030674 protein-macromolecule adaptor activity 0.43 GO:0003677 DNA binding	0.800795426	0.702029951
NP_595536.1 uncharacterized protein SPBC27B12.04c [Schizosaccharomyces pombe]	0.94 Eukaryotic protein implicated in cell cycle regulation	0.88 GO:0061509 asymmetric protein localization to old mitotic spindle pole body 0.87 GO:0031030 negative regulation of septation initiation signaling 0.58 GO:0007010 cytoskeleton organization 0.55 GO:0007049 cell cycle		0.769817529	0.810148092
NP_595853.1 uncharacterized protein SPBC18E5.07 [Schizosaccharomyces pombe]	0.0 Uncharacterized protein	0.70 GO:0007015 actin filament organization		0.753490375	0.998961254
NP_588319.1 uncharacterized protein SPCC1442.05c [Schizosaccharomyces pombe]	0.39 MICOS complex subunit	0.85 GO:0042407 cristae formation		0.75240903	0.414149709
NP_596443.1 uncharacterized protein SPBC2G2.14 [Schizosaccharomyces pombe]	0.0 Uncharacterized protein	0.90 GO:0072766 centromere clustering at the mitotic interphase nuclear envelope 0.80 GO:0000070 mitotic sister chromatid segregation	0.63 GO:0005515 protein binding	0.751819481	1.303609909
NP_593089.2 uncharacterized protein SPAC2G11.09 [Schizosaccharomyces pombe]	0.11 Calcium permeable stress-gated cation channel 1	0.61 GO:0098655 monoatomic cation transmembrane transport 0.59 GO:0006816 calcium ion transport 0.51 GO:0098662 inorganic cation transmembrane transport	0.81 GO:0005227 calcium activated cation channel activity 0.60 GO:0015085 calcium ion transmembrane transporter activity 0.52 GO:0003676 nucleic acid binding	0.746571084	1.159343596
NP_593280.1 uncharacterized protein SPAC1565.01 [Schizosaccharomyces pombe]	0.37 Respiratory supercomplex factor 2 homolog C1565.01	0.65 GO:0033617 mitochondrial cytochrome c oxidase assembly		0.723308517	0.745748355

Table 2. Continued

NP_001342840.1 uncharacterized protein SPAC11E3.12 [Schizosaccharomyces pombe]	0.11 NADH-ubiquinone oxidoreductase 24 kDa subunit homolog C11E3.12, mitochondrial	0.60 GO:0017004 cytochrome complex assembly	0.65 GO:0051537 2 iron, 2 sulfur cluster binding 0.54 GO:0046872 metal ion binding 0.52 GO:0016491 oxidoreductase activity	0.715916213	0.850030937
NP_595539.1 uncharacterized protein SPBC27B12.07 [Schizosaccharomyces pombe]	0.0 Uncharacterized protein	0.58 GO:0006560 proline metabolic process		0.704886509	0.868992993
NP_594721.1 uncharacterized protein SPAC11H11.03c [Schizosaccharomyces pombe]	0.49 Smr domain-containing protein	0.71 GO:0070481 nuclear-transcribed mRNA catabolic process, non-stop decay 0.53 GO:0006281 DNA repair	0.69 GO:0046404 ATP-dependent polydeoxyribonucleotide 5'-hydroxyl-kinase activity 0.54 GO:0004519 endonuclease activity	0.698691652	1.228533546
NP_594721.1 uncharacterized protein SPAC11H11.03c [Schizosaccharomyces pombe]	0.49 Smr domain-containing protein	0.71 GO:0070481 nuclear-transcribed mRNA catabolic process, non-stop decay 0.53 GO:0006281 DNA repair	0.69 GO:0046404 ATP-dependent polydeoxyribonucleotide 5'-hydroxyl-kinase activity 0.54 GO:0004519 endonuclease activity	0.698691652	1.228533546
NP_596045.1 uncharacterized protein SPBC365.16 [Schizosaccharomyces pombe]	0.37 Mitochondrial fission process protein 1			0.60030676	0.771552988
NP_593522.2 uncharacterized protein SPAPB1A10.08 [Schizosaccharomyces pombe]	0.67 Meiotically up-regulated protein PB1A10.08			0.550616579	0.784518803
NP_594400.1 uncharacterized protein SPAC11G7.06c [Schizosaccharomyces pombe]	0.40 Meiotically up-regulated gene 132 protein	0.77 GO:0051321 meiotic cell cycle		0.55013418	0.790413974
NP_588079.1 uncharacterized protein SPCC4B3.11c [Schizosaccharomyces pombe]	0.75 BolA-like protein 3	0.79 GO:0106035 protein maturation by [4Fe-4S] cluster transfer		0.540823457	0.643180973
NP_001343089.1 uncharacterized protein SPCC757.15 [Schizosaccharomyces pombe]	0.43 Cytochrome c oxidase assembly protein	0.64 GO:0033617 mitochondrial cytochrome c oxidase assembly		0.508254753	0.612148701

Table 2. Continued

NP_001343011.1 uncharacterized protein SPAC8C9.19 [Schizosaccharomyces pombe]	0.90 ERMES regulator 1	0.84 GO:0007008 outer mitochondrial membrane organization 0.61 GO:0120010 intermembrane phospholipid transfer	0.42 GO:0005515 protein binding	0.338334348	0.444875858
NP_595535.2 uncharacterized protein SPBC27B12.02 [Schizosaccharomyces pombe]	0.40 CENP-A recruiting complex protein mis19	0.85 GO:0051315 attachment of mitotic spindle microtubules to kinetochore 0.85 GO:0071459 protein localization to chromosome, centromeric region 0.66 GO:0051301 cell division	0.63 GO:0005515 protein binding	0.328300005	0.938710618
NP_594342.3 uncharacterized protein SPAC4H3.06 [Schizosaccharomyces pombe]	0.48 Meiotic recombination protein			0.314154011	0.888067929
NP_594483.1 uncharacterized protein SPAC694.03 [Schizosaccharomyces pombe]	0.43 nicotinamide-nucleotide adenylyltransferase	0.75 GO:0034356 NAD biosynthesis via nicotinamide riboside salvage pathway 0.61 GO:0007124 pseudohyphal growth 0.61 GO:0001403 invasive growth in response to glucose limitation 0.55 GO:0030433 ubiquitin-dependent ERAD pathway	0.83 GO:0000309 nicotinamide-nucleotide adenylyltransferase activity 0.53 GO:0016887 ATP hydrolysis activity 0.43 GO:0005524 ATP binding	0.301149026	0.719119844
NP_001018224.1 uncharacterized protein SPAPB17E12.09 [Schizosaccharomyces pombe]	0.67 Meiotically up-regulated protein PB17E12.09	0.77 GO:0051321 meiotic cell cycle		0	0.240788533

cally up-regulated gene 133 protein, 155 protein, and 144 (3.61 fold change in standard condition) proteins also increased in the presence of metformin. PANNZER2 predicted five down-regulated proteins among jointly down-regulated proteins in both conditions: the meiotically up-regulated genes 43, 112, 131, 132, and 167 (1.35 fold change in standard condition and 1.43 in overnutrition condition) are involved in the meiotic cell cycle. Indeed, all five have been reported to be involved in meiosis, although their exact function remains elusive.[21] Meiotic recombination protein, early meiotic induction protein 1, and meiotically up-regulated proteins PB1A10.08 and PB17E12.09 are among other proteins predicted by PANNZER2 to be involved in the meiotic cell cycle. Indeed, a study revealed that the latter two belong to a class of late genes that are stimulated during meiotic divisions and whose expression is high until the end of sporulation.[22]

Nutrition depletion, particularly nitrogen, triggers a switch from a haploid state to a diploid and initiates meiosis in fission yeast.[23] Metformin is a caloric restriction mimetic that recapitulates the beneficial effects of caloric restriction without dietary limitations.[24] Therefore, the drug might induce nutrition depletion conditions, which leads to meiosis initiation. In accordance with this, PANNZER2 predicted that another down-regulated protein (NP_001342866.1 /Mks1) is involved in nitrogen utilisation regulation. The protein shares a high sequence similarity with the Mks1 of *S. cerevisiae*, which inactivates the nitrogen uptake systems upon its under-expression, a possible mechanism for how metformin induces nutrition depletion conditions.[25] Taken together, both the up-regulation and down-regulation of meiosis-related genes suggest metformin's significant role as a calorie restriction mimetic in meiosis.

One of the down-regulated proteins among jointly down-

regulated proteins is UPF0674 endoplasmic reticulum membrane protein (1.48 fold change in standard condition and 1.24 fold change in overnutrition condition), and it is predicted to be involved in ER calcium ion homeostasis, protein insertion into ER membrane, and protein folding. It also has a calcium ion binding and protein folding chaperone activity. The protein shares a high sequence and structure similarity with the PAT complex subunit CCDC47 of *Homo sapiens*.[26] It functions as an intramembrane chaperone that maintains cellular protein. CCDC47 is also reported to regulate calcium ion homeostasis in the ER and is required for the misfolded protein degradation ER-associated degradation (ERAD) pathway.[27,28] Additionally, PANNZER2 predictions for two proteins suggest a role in calcium ion homeostasis. Indeed, the latter shares a high sequence similarity with the calcium permeable stress-gated cation channel 1 of *Homo sapiens*.[29]

ER stress triggers the unfolded protein response (UPR) which reduces unfolded proteins to maintain cell viability and functionality.[30] Conza et al.[31] demonstrated that metformin affects UPR upon ER stress in endometrial cancer cells. One of the thirteen proteins up-regulated in overnutrition conditions, inclusion body clearance protein IML2, is predicted to be involved in the cellular response to misfolded protein and cellular detoxification by PANNZER2. This protein has a significant similarity in sequence with the IML2/YJL082W protein found in *S. cerevisiae*. The latter is essential for removing inclusion bodies, and this protein is known to localise to inclusion bodies that form due to protein misfolding stress.

PANNZER2 predicted that one of the down-regulated proteins (NP_594883.1/Hgh1) is involved in the chaperone-mediated protein folding and has a translation elongation factor binding and protein folding chaperone activity. The protein shares a high sequence similarity with the Hgh1 of *S. cerevisiae,* which is a chaperone involved in the Eukaryotic elongation factor 2 (eEF2) folding.[32] Another down-regulated protein among jointly down-regulated proteins is EF-hand domain-containing protein which is predicted to be involved in the cellular response to misfolded protein and cellular detoxification. The protein shares a high sequence similarity with the inclusion body clearance protein IML2 of *S. cerevisiae*, and this is necessary for inclusion body clearance upon protein folding stress.[33] Thus, both the up-regulation and down-regulation of protein misfolding and calcium homeostasis-related genes indicate metformin's central role in such cellular processes.

Autophagy protein 16 (atg16), is predicted to be involved in the meiotic cell cycle, macroautophagy, and protein transport. Indeed, Gregan et al.[34] report that this protein is required for chromosome segregation during meiosis. PANNZER2 predicted atg16 to be a component of the phagophore (belonging to the autophagy process) assembly site. The autophagosome outer membrane fuses with the vacuole and forms the autophagic body where vacuolar hydrolases degrade cellular

material and permeases release the resulting materials to be recycled in the cytosol.[35] Atg16 interacts with the atg5-atg12 conjugate through atg5, and the atg5-atg12/atg15 complex is required for the atg8 conjugation to phosphatidylethanolamine that leads to the expansion of the phagophore, and atg8 localization to the pre-autophagosomal structure.[36] Autophagy is induced through the AMPK-MTOR-ULK1-mediated signaling or SIRT1-FOXO pathway.[37,38] Metformin is known to activate both AMPK and SIRT1 and, therefore, can induce autophagy.[39]

Protein adenylyltransferase SelO (mitochondrial) is predicted to be involved in protein adenylation, cell redox homeostasis, and cellular response to oxidative stress. The probable protein transfers adenosine 5'-monophosphate (AMP) to Ser, Thr, and Tyr residues of its protein substrates involved in redox homeostasis and, therefore, regulates the cellular response to oxidative stress.[40] Metformin decreases intracellular ROS production, lipid peroxidation, and protein carbonylation in fission yeast.[10] Thus, the up-regulation of Protein adenylyltransferase SelO (mitochondrial) in fission yeast upon metformin treatment suggests that metformin's antioxidative effect might be dependent on this enzyme.

There are at least three types of cortical nodes for distinct cellular processes to take place on the nongrowing middle part of the fission yeast plasma membrane.[41] One type includes the mitotic inhibitor Skb1, a PRMT5-like methyltransferase, which interacts with Slf1 to form the node. Moreover, Skb1 nodes ensure correct cell cycle progression by sequestering Skb1. PANNZER2 predicted that Slf1 is involved in protein localisation to the lateral cortical node assembly. Consequently, Slf1 down-regulation upon metformin treatment might have reduced the cortical node number, which ultimately leads to suppressed mitosis through the freed Skb1. PANNZER2 predicted that another down-regulated protein among jointly down-regulated proteins (NP_596443.1/csi1) is involved in centromere clustering at the mitotic interphase nuclear envelope and mitotic sister chromatid segregation. Indeed, it is reported that csi1 regulates chromosome segregation by positioning the centromeres at the spindle pole body during the interphase and organising the bipolar spindle.[42,43] Another type of cortical node is eisosomes, which regulate phosphatidylinositol (4,5)-bisphosphate levels.[41] PANNZER2 predicted that another protein (NP_588026.2/Opy1) among jointly down-regulated proteins is involved in actomyosin contractile ring maintenance, mitotic cytokinetic process, and 1-phosphatidyl-1D-myo-inositol 4,5-bisphosphate biosynthetic process, and it has a role in phosphatidylinositol metabolism. The precursor of phosphatidylinositol 3,4,5-trisphosphate and actin polymerization regulator phosphatidylinositol 4,5-bisphosphate has a vital role in insulin-stimulated glucose transport.[44] Metformin increases glucose uptake in peripheral tissues, possibly by directly binding to the lipid phosphatase Src homology 2 domain-containing inositol-5-phosphatase 2 (SHIP2).[45] SHIP2 is up-regulated in diabetic rodent models, which leads to insulin resis-

tance and diminished glucose uptake. The down-regulation of Opy1 might be another possible mechanism for how metformin increases glucose uptake as Opy1 binds phosphatidylinositol 4,5-bisphosphate, which leads to reduced cellular amounts of phosphatidylinositol 4,5-bisphosphate.

PANNZER2 predicted that one of the down-regulated proteins (NP_587772.3/Dbl2) is involved in the resolution of meiotic recombination intermediates and double-strand break repair. Indeed, dbl2 gene deletion leads to the failure of homolog chromosome segregation to opposite poles due to DNA double-strand break repair intermediates during meiosis in fission yeast as it is required for Fbh1 DNA helicase foci formation at the DNA double-strand break repair sites that process these intermediates.[46] Another down-regulated protein described as sugar phosphate phosphatase is predicted to be involved in the DNA damage response (DDR) and cellular detoxification. The protein shares a high sequence similarity with the damage-control phosphatase YMR027W of *S.cerevisiae*, according to the UniProt database. Damage-control phosphatase YMR027W is a metal-dependent phosphatase, and its substrates are fructose-1-phosphate and fructose-6-phosphate.[47] The enzyme favors fructose-1-phosphate, which is a strong glycating agent that causes DNA damage, indicating a protective function against such phospho-metabolites in hexose phosphate metabolism.

One of the down-regulated proteins (NP_593856.1, 1.34 fold change in standard condition and 1.32 fold change in overnutrition condition) is involved in the stress-activated mitogen-activated protein kinase (MAPK) cascade. The protein shares a high sequence similarity with the AHK1 of *S. cerevisiae*, according to the PomBase database. Osmotic stress triggers the Hog1 MAPK, which regulates myriad adaptive responses to such stimuli.[48] Moreover, Hkr1 is a putative osmotic sensor of one of the Hog1 upstream pathways called HKR1. Ahk1 binds to the cytoplasmic regulatory domain of Hkr1 (an osmotic sensor), and AHK1 gene deletion partially inhibits osmotic stress-induced Hog1 activation, suggesting that it serves as a scaffold protein. MAPKs can act as apoptosis activators or inhibitors, depending on the cell type and stimulus.[49] Proline dehydrogenase/proline oxidase (PRODH/POX) is a mitochondrial enzyme that degrades proline, producing ROS that induce apoptosis.[50] Metformin increases the expressions of PRODH/POX and AMPK, which also activates PRODH/POX leading to apoptosis. PANNZER2 predicted that another down-regulated protein (NP_595539.1) is involved in the proline metabolic process. The protein shares a high sequence similarity with the PUT7 of *S. cerevisiae*, which acts as a negative regulator of mitochondrial proline uptake.[51] Therefore, its down-regulation upon metformin treatment may lead to increased proline concentration in the mitochondria and subsequent ROS production through PRODH/POX activity and apoptosis.

Down-regulated in overnutrition and normal conditions, cy-

tochrome c oxidase assembly protein COX is predicted to be involved in mitochondrial cytochrome c oxidase assembly by PANNZER2. Since COX is a protein that is entrenched in the mitochondrial membrane, its down-regulation may either be an early apoptotic signaling event or a late effect of apoptotic signaling.[52] HeLa cells were initially exposed to various respiratory chain complex inhibitors for 24 hours before being exposed to hydrogen peroxide for the same amount of time. Here, respiratory complex IV (COX) inactivation significantly increased the susceptibility of cells to treatment with hydrogen peroxide. The same study conclusively demonstrates that COX inhibition accelerates mitochondrial apoptotic response to oxidative stress.[53] This appears to be one of the countless theories explaining how metformin's impacts on energy metabolism prolong life.

Another down-regulated protein, assembly factor cbp4 (1.17 fold change in standard condition and 1.42 fold change in overnutrition condition) is involved in the respiratory chain complex III assembly and mitochondrial respiratory chain complex assembly. The protein shares a high sequence similarity with the assembly factor CBP4 of *S. cerevisiae*, which is essential for the assembly of ubiquinol-cytochrome c reductase with a direct effect on its subunits'.[54] One of the mechanisms by which metformin exerts its anti-aging effects is by selectively inhibiting respiratory chain complex I, consequently causing oxidative phosphorylation. This leads to AMP/ATP and NAD^+/NADH ratio increment that activates AMPK and upregulates SIRT1.[55] The down-regulation of Cbp4 suggests that the drug interferes with oxidative phosphorylation in different stages of the process.

Metformin disrupts the cristae and inner mitochondrial membrane and induces mitochondrial swelling by causing ER stress and subsequently increased calcium influx into the mitochondria.[56] The three down-regulated proteins, MICOS complex subunit MIC10, mic19, and Mic23/26/27 are involved in cristae formation, suggesting a possible mechanism for metformin to disrupt cristae and induce mitochondrial dysfunction. The down-regulated and sensitive to high expression protein 9 (mitochondrial), is also involved in inner mitochondrial membrane organization. The protein shares a high sequence similarity with the sensitive to high expression protein 9 (mitochondrial) (Mdm33) of *S. cerevisiae*. Its overexpression leads to growth arrest, mitochondria aggregation, and unusual inner membrane structure generation, including loss of inner membrane cristae.[57] Related to the MAM3 Protein required for normal mitochondrial morphology this protein was also down-regulated under metformin treatment. The down-regulated ER-MES regulator 1 is predicted to be involved in outer mitochondrial membrane organisation and intermembrane phospholipid transfer. In yeasts, the ER-mitochondria encounter structure (ERMES) complex plays an important role in mediating the formation of ER-mitochondria contact sites.[58,59] In addition to lipid transport, the ERMES complex regulates mitochondrial

fission, mtDNA inheritance, and mitophagy.[60,61] A study reports that the absence of Emr1 leads to abnormal mitochondrial morphology and that Emr1 regulates the number of ERMES foci.[62] The down-regulation of these proteins suggests that metformin interferes with energy metabolism not only through oxidative phosphorylation but also by disrupting mitochondrial structure.

PANNZER2 predicted that one down-regulated protein, mitophagy receptor atg43, is involved in mitophagy and has a mitochondrion autophagosome adaptor and protein binding activity. Indeed, atg43, a mitochondrial outer membrane protein, acts as a mitophagy receptor for selective mitochondria degradation by tethering Atg8 to mitochondria via an Atg8-family-interacting motif.[63] However, it is known that mitophagy contributes to mitochondrial function maintenance, and metformin induces mitophagy.[63,64] Another down-regulated protein Fis1 (mitochondrial fission process protein 1), may influence mitochondrial dynamics by inducing mitochondrial fission through interactions with the enzyme Drp1 or by preventing mitochondrial fusion through inhibition of Mfn2/Opa1. By bringing TBC1D15/17 and Syntaxin17 to the mitochondria, Fis1 takes part in mitophagy. Fascinatingly, Fis1 overexpression may play pathogenic roles in Parkinson's disease and diabetes mellitus, most likely through up-regulating mitochondrial fission and mitophagy. In light of this information, it is quite logical that metformin which is used in Diabetes Mellitus treatment down-regulates the Fis1 gene.[65,66]

Another down-regulated protein among jointly down-regulated proteins is the maintenance of telomere capping protein 1. Telomere attrition is one of the nine hallmarks of aging, and severe telomere uncapping can result from shelterin component deficiencies.[1] Shelterin is a specialized nucleoprotein complex that attracts DNA repair machinery to damaged telomeres through its formation. Metformin treatment prevented telomere attrition in male offspring of mothers with gestational diabetes, suggesting its beneficial effect against telomere attrition.[67]

CONCLUSION

This research concentrated on unannotated genes, aiming to pinpoint novel target genes potentially associated with the life-extending properties of metformin. These proteins are implicated in various cellular processes, including meiosis, mitosis, DNA damage response, protein folding, apoptosis, autophagy, antioxidative effects, mitochondrial changes, heme production, and telomere capping. Many of these unannotated proteins could serve as promising targets for future investigations into aging.

ORCID IDs of the authors

Cagatay Tarhan	0000-0001-5265-4610
Sumeyra Zeynep Calici	0009-0006-0348-1884
Buse Ozden	0009-0009-1415-2420

REFERENCES

1. López-Otín C, Blasco MA, Partridge L, Serrano M, Kroemer G. The hallmarks of aging. Cell. 2013;153(6):1194-1217. doi:10.1016/j.cell.2013.05.039

2. Carlsen SM, Rossvoll O, Bjerve KS, Folling I. Metformin improves blood lipid pattern in nondiabetic patients with coronary heart disease. *J Intern Med.* 1996;239(3):227-233.

3. Podhorecka M, Ibanez B, Dmoszyńska A. Metformin-its potential anti-cancer and anti-aging effects. *Postepy Hig Med Dosw (Online).* 2017;71(0):170-175.

4. Soukas AA, Hao H, Wu L. Metformin as anti-aging therapy: Is ıt for everyone? *Trends Endocrinol Metab.* 2019;30(10):745-755.

5. Zhu Z, Jiang T, Suo H, et al. Metformin potentiates the effects of anlotinib in NSCLC via AMPK/mTOR and ROS-mediated signaling pathways. *Front Pharmacol.* 2021;12:712181. doi:10.3389/fphar.2021.712181

6. Anisimov VN, Berstein LM, Egormin PA, et al. Metformin slows down aging and extends life span of female SHR mice. *Cell Cycle.* 2008;7(17):2769-2773.

7. Cabreiro F, Au C, Leung KY, et al. Metformin retards aging in *C. elegans* by altering microbial folate and methionine metabolism. *Cell.* 2013;153(1):228-239.

8. De Haes W, Frooninckx L, Van Assche R, et al. Metformin promotes lifespan through mitohormesis via the peroxiredoxin PRDX-2. *Proc Natl Acad Sci USA.* 2014;111(24):E2501-E2509. doi:10.1073/pnas.1321776111

9. Suzuta S, Nishida H, Ozaki M, Kohno N, Le TD, Inoue YH. Metformin suppresses progression of muscle aging via activation of the AMP kinase-mediated pathways in Drosophila adults. *Eur Rev Med Pharmacol Sc*i. 2022;26(21):8039-8056.

10. Şeylan C, Tarhan Ç. Metformin extends the chronological lifespan of fission yeast by altering energy metabolism and stress resistance capacity. *FEMS Yeast Res.* 2023;23:foad018. doi:10.1093/femsyr/foad018

11. Törönen P, Medlar A, Holm L. PANNZER2: A rapid functional annotation web server. *Nucleic Acids Res.* 2018;46(W1):W84-W88. doi:10.1093/nar/gky350

12. Alberts B, Johnson A, Lewis J, et al. *Molecular Biology of the Cell.* (Wilson J, Hunt T, eds.). W.W. Norton & Company; 2017. doi:https://doi.org/10.1201/9781315735368

13. Konc J, Hodošček M, Ogrizek M, Trykowska Konc J, Janežič

D. Structure-based function prediction of uncharacterized protein using binding sites comparison. *PLoS Comput Biol.* 2013;9(11):e1003341. doi:10.1371/journal.pcbi.1003341

14. Rosamond J. Harnessing the power of the genome in the search for new antibiotics. *Science.* 2000;287(5460):1973-1976.

15. Altschul SF, Gish W, Miller W, Myers EW, Lipman DJ. Basic local alignment search tool. *J Mol Biol.* 1990;215(3):403-410.

16. Buchfink B, Reuter K, Drost HG. Sensitive protein alignments at tree-of-life scale using DIAMOND. *Nat Methods.* 2021;18(4):366-368.

17. Zhou N, Jiang Y, Bergquist TR, et al. The CAFA challenge reports improved protein function prediction and new functional annotations for hundreds of genes through experimental screens. *Genome Biol.* 2019;20(1). doi:https://doi.org/10.1186/s13059-019-1835-8

18. Jensen LJ, Gupta R, Staerfeldt HH, Brunak S. Prediction of human protein function according to Gene Ontology categories. *Bioinformatics.* 2003;19(5):635-642.

19. Koskinen P, Törönen P, Nokso-Koivisto J, Holm L. PANNZER: High-throughput functional annotation of uncharacterized proteins in an error-prone environment. *Bioinformatics.* 2015;31(10):1544-1552.

20. Chen BR, Runge KW. A new *Schizosaccharomyces pombe* chronological lifespan assay reveals that caloric restriction promotes efficient cell cycle exit and extends longevity. *Exp Gerontol.* 2009;44(8):493-502.

21. Martín-Castellanos C, Blanco M, Rozalén AE, et al. A large-scale screen in S. pombe identifies seven novel genes required for critical meiotic events. *Curr Biol.* 2005;15(22):2056-2062.

22. Mata J, Lyne R, Burns G, Bähler J. The transcriptional program of meiosis and sporulation in fission yeast. *Nat Genet.* 2002;32(1):143-147.

23. Yamashita A, Sakuno T, Watanabe Y, Yamamoto M. Synchronous ınduction of meiosis in the fission yeast *Schizosaccharomyces pombe. Cold Spring Harb Protoc.* 2017;2017(9). doi:10.1101/pdb.prot091777

24. Lee SH, Min KJ. Caloric restriction and its mimetics. *BMB Rep.* 2013;46(4):181-187.

25. Edskes HK, Hanover JA, Wickner RB. Mks1p is a regulator of nitrogen catabolism upstream of Ure2p in *Saccharomyces cerevisiae. Genetics.* 1999;153(2):585-594.

26. Chitwood PJ, Hegde RS. An intramembrane chaperone complex facilitates membrane protein biogenesis. *Nature.* 2020;584(7822):630-634.

27. Morimoto M, Waller-Evans H, Ammous Z, et al. Bi-allelic CCDC47 variants cause a disorder characterized by woolly hair, liver dysfunction, dysmorphic features, and global developmental delay. *Am J Hum Genet.* 2018;103(5):794-807.

28. Yamamoto S, Yamazaki T, Komazaki S, et al. Contribution of calumin to embryogenesis through participation in the endoplasmic reticulum-associated degradation activity. *Dev Biol.* 2014;393(1):33-43.

29. Hou C, Tian W, Kleist T, et al. DUF221 proteins are a family of osmosensitive calcium-permeable cation channels conserved across eukaryotes. *Cell Res.* 2014;24(5):632-635.

30. Hetz C. The unfolded protein response: controlling cell fate decisions under ER stress and beyond. *Nat Rev Mol Cell Biol.* 2012;13(2):89-102.

31. Conza D, Mirra P, Calì G, et al. Metformin dysregulates the unfolded protein response and the WNT/β-catenin pathway in endometrial cancer cells through an AMPK-independent mechanism. *Cells.* 2021;10(5):1067. doi:10.3390/cells10051067

32. Mönkemeyer L, Klaips CL, Balchin D, Körner R, Hartl FU, Bracher A. Chaperone function of Hgh1 in the biogenesis of eukaryotic elongation factor 2. *Mol Cell.* 2019;74(1):88-100.e9. doi:https://doi.org/10.1016/j.molcel.2019.01.034

33. Moldavski O, Amen T, Levin-Zaidman S, et al. Lipid droplets are essential for efficient clearance of cytosolic ınclusion bodies. *Dev Cell.* 2015;33(5):603-610.

34. Gregan J, Rabitsch PK, Sakem B, et al. Novel genes required for meiotic chromosome segregation are identified by a high-throughput knockout screen in fission yeast. *Curr Biol.* 2005;15(18):1663-1669.

35. Levine B, Kroemer G. SnapShot: Macroautophagy. *Cell.* 2008;132(1):162.e1-162.e3. doi:10.1016/j.cell.2007.12.026

36. Sun LL, Li M, Suo F, et al. Global analysis of fission yeast mating genes reveals new autophagy factors. *PLoS Genet.* 2013;9(8):e1003715. doi:10.1371/journal.pgen.1003715

37. Salminen A, Kaarniranta K. AMP-activated protein kinase (AMPK) controls the aging process via an integrated signaling network. *Ageing Res Rev.* 2012;11(2):230-241.

38. Pallauf K, Rimbach G. Autophagy, polyphenols and healthy ageing. *Ageing Res Rev.* 2013;12(1):237-252.

39. Caton PW, Nayuni NK, Kieswich J, Khan NQ, Yaqoob MM, Corder R. Metformin suppresses hepatic gluconeogenesis through induction of SIRT1 and GCN5. *J Endocrinol.* 2010;205(1):97-106.

40. Sreelatha A, Yee SS, Lopez VA, et al. Protein AMPylation by an evolutionarily conserved pseudokinase. *Cell.* 2018;175(3):809-821.e19. doi:10.1016/j.cell.2018.08.046

41. Deng L, Kabeche R, Wang N, Wu JQ, Moseley JB. Megadalton-node assembly by binding of Skb1 to the membrane anchor Slf1. *Mol Biol Cell.* 2014;25(17):2660-2668.

42. Hou H, Zhou Z, Wang Y, et al. Csi1 links centromeres to the nuclear envelope for centromere clustering. *J Cell Biol.* 2012;199(5):735-744.

43. Zheng F, Li T, Jin DY, et al. Csi1p recruits alp7p/TACC to the spindle pole bodies for bipolar spindle formation. *Mol Biol Cell.* 2014;25(18):2750-2760.

44. Strawbridge AB, Elmendorf JS. Phosphatidylinositol 4,5-bisphosphate reverses endothelin-1-induced insulin resistance via an actin-dependent mechanism. *Diabetes.* 2005;54(6):1698-1705.

45. Polianskyte-Prause Z, Tolvanen TA, Lindfors S, et al. Metformin increases glucose uptake and acts renoprotectively by reducing SHIP2 activity. *FASEB J.* 2019;33(2):2858-2869.

46. Polakova S, Molnarova L, Hyppa RW, et al. Dbl2 Regulates Rad51 and DNA joint molecule metabolism to ensure proper meiotic chromosome segregation. *PLoS Genet.* 2016;12(6):e1006102. doi:10.1371/journal.pgen.1006102

47. Huang L, Khusnutdinova A, Nocek B, et al. A family of metal-dependent phosphatases implicated in metabolite damage-control. *Nat Chem Biol.* 2016;12(8):621-627.

48. Nishimura A, Yamamoto K, Oyama M, Kozuka-Hata H, Saito H, Tatebayashi K. Scaffold protein Ahk1, which associates with Hkr1, Sho1, Ste11, and Pbs2, inhibits cross talk signaling from the Hkr1 osmosensor to the Kss1 mitogen-activated protein kinase. *Mol Cell Biol.* 2016;36(7):1109-1123.

49. Yue J, López JM. Understanding MAPK Signaling pathways in apoptosis. *Int J Mol Sci.* 2020;21(7):2346. doi:10.3390/ijms21072346

50. Oscilowska I, Rolkowski K, Baszanowska W, et al. Proline dehydrogenase/proline oxidase (PRODH/POX) is involved in the mechanism of metformin-induced apoptosis in C32 melanoma cell line. *Int J Mol Sci.* 2022;23(4):2354. doi:10.3390/ijms23042354

51. Zulkifli M, Neff JK, Timbalia SA, et al. Yeast homologs of human MCUR1 regulate mitochondrial proline metabolism. *Nat Commun.* 2020;11(1):4866. doi:https://doi.org/10.1038/s41467-020-18704-1

52. Ragno S, Estrada-Garcia I, Butler R, Colston MJ. Regulation of macrophage gene expression by *Mycobacterium tuberculosis:* Down-regulation of mitochondrial cytochrome c oxidase. *Infect Immun.* 1998;66(8):3952-3958.

53. Schüll S, Günther SD, Brodesser S, et al. Cytochrome c oxidase deficiency accelerates mitochondrial apoptosis by activating ceramide synthase 6. *Cell Death Dis.* 2015;6(3):e1691. doi:10.1038/cddis.2015.62

54. Crivellone MD. Characterization of CBP4, a new gene essential for the expression of ubiquinol-cytochrome c reductase in *Saccharomyces cerevisiae. J Biol Chem.* 1994;269(33):21284-21292.

55. Chen S, Gan D, Lin S, et al. Metformin in aging and aging-related diseases: Clinical applications and relevant mechanisms. *Theranostics.* 2022;12(6):2722-2740

56. Loubiere C, Clavel S, Gilleron J, et al. The energy disruptor metformin targets mitochondrial integrity via modification of calcium flux in cancer cells. *Sci Rep.* 2017;7(1):5040. doi:https://doi.org/10.1038/s41598-017-05052-2

57. Messerschmitt M, Jakobs S, Vogel F, et al. The inner membrane protein Mdm33 controls mitochondrial morphology in yeast. *J Cell Biol.* 2003;160(4):553-564.

58. Tamura Y, Kawano S, Endo T. Organelle contact zones as sites for lipid transfer. *J Biochem.* 2019;165(2):115-123.

59. Lang A, John Peter AT, Kornmann B. ER-mitochondria contact sites in yeast: Beyond the myths of ERMES. *Curr Opin Cell Biol.* 2015;35:7-12.

60. Kawano S, Tamura Y, Kojima R, et al. Structure-function insights into direct lipid transfer between membranes by Mmm 1-Mdm 12 of ERMES. *J Cell Biol.* 2018;217(3):959-974.

61. Jeong H, Park J, Jun Y, Lee C. Crystal structures of Mmm1 and Mdm12-Mmm1 reveal mechanistic insight into phospholipid trafficking at ER-mitochondria contact sites. *Proc Natl Acad Sci USA.* 2017;114(45):E9502-E9511.

62. Rasul F, Zheng F, Dong F, et al. Emr1 regulates the number of foci of the endoplasmic reticulum-mitochondria encounter structure complex. *Nat Commun.* 2021;12(1):521. doi:10.1038/s41467-020-20866-x

63. Fukuda T, Ebi Y, Saigusa T, et al. Atg43 tethers isolation membranes to mitochondria to promote starvation-induced mitophagy in fission yeast. *Elife.* 2020;9:e61245.. doi:10.7554/eLife.61245

64. de Marañón AM, Díaz-Pozo P, Canet F, et al. Metformin modulates mitochondrial function and mitophagy in peripheral blood mononuclear cells from type 2 diabetic patients. *Redox Biol.* 2022;53:102342. doi:10.1016/j.redox.2022.102342

65. Shenouda SM, Widlansky ME, Chen K, et al. Altered mitochondrial dynamics contributes to endothelial dysfunction in diabetes mellitus. *Circulation.* 2011;124(4):444-453.

66. Zhang Q, Wu J, Wu R, et al. DJ-1 promotes the proteasomal degradation of Fis1: Implications of DJ-1 in neuronal protection. *Biochem J.* 2012;447(2):261-269.

67. Garcia-Martin I, Penketh RJA, Janssen AB, et al. Met-formin and insulin treatment prevent placental telomere attrition in boys exposed to maternal diabetes. Rosenfeld CS, ed. *PLoS One.* 2018;13(12):e0208533. doi:https://doi.org/10.1371/journal.pone.0208533

How to cite this article

Effects of Phloretin on Bisphenol-A Induced Liver and Kidney Toxicity in Prepubertal Female Rats

Eda Nur Inkaya[1]   Nilufer Coskun Kilic[1],   Nurhayat Barlas[1]

[1]Hacettepe University, Faculty of Science, Department of Biology, Ankara, Turkey

ABSTRACT

Objective: The aim of this study was to investigate the protective effects of phloretin against bisphenol-A (BPA)-induced liver and kidney damage in rats using histopathological and biochemical parameters.

Materials and Methods: This study started on female rats on the postnatal 28th day via subcutaneous injection by dissolving the compounds in corn oil at 30-min intervals, starting with phloretin, and followed by BPA. The dose of BPA was 50 mg/kg bw/day, and the doses of phloretin were 0.5, 5, and 50 mg/kg bw/day. Treatments were administered every day for 15 days. Histopathological, morphometric, and biochemical parameters were analyzed.

Results: Histopathological evaluation revealed tubular degeneration, fibrous tissue formation, congestion, and edema in the kidney tissue and cellular degeneration and congestion in the liver tissue. BPA treatment resulted in a statistically significant increase in serum urea and alanine aminotransferase levels and a decrease in serum glucose and aspartate aminotransferase levels. Against these effects of BPA, a positive effect was detected only on serum urea levels in rats treated with 50 mg/kg bw/day phloretin. There was also no significant change in serum triglyceride, creatinine, and albumin levels in the BPA positive control group. The renal morphometric analysis revealed that treatment with 0.5 mg/kg bw/day phloretin reduced the BPA-induced glomerular damage.

Conclusion: Biochemical parameters and histopathological findings in the kidney and liver tissues revealed no clear evidence of a protective effect of phloretin against the damage caused by BPA. Hence, phloretin exhibits a low level of protection against liver and kidney damage.

Keywords: Bisphenol-A, phloretin, liver, kidney, female rats.

INTRODUCTION

Chemical compounds are indispensable components of our daily life, but many of these compounds, especially endocrine disruptors, can cause harmful effects on endocrine system structures and hormones.[1] However, studies also indicate that endocrine disruptor chemicals negatively affect liver and kidney functions.[2,3] Bisphenol-A (BPA) is a diphenylmethane derivative formed by two phenyl rings attached to two methyl groups. BPA ($C_{15}H_{16}O_2$) is one of the most produced chemicals worldwide.[4] The BPA values recommended by the U.S. Environmental Protection Agency are as follows: lowest-observed-adverse-effect level (LOAEL): 50 mg/kg bw/day, no-observed-adverse-effect level: 5 mg/kg bw/day, and acceptable daily intake: 50 µg/kg bw/day. The average daily exposure in adults is 0.5 µg/kg bw/day.[5] The effects of BPA on animals have been extensively investigated. The liver and kidneys are among the target organs identified in repeated-dose animal studies.[6] Sev-

eral studies on BPA demonstrated that it affects biochemical parameters, exerting a negative effect on antioxidant enzymes and causing damage to liver and kidney tissues.[7,8] In the present study, BPA was used to induce liver and kidney damage.

Sheep that fed on red clover pastures were found to have fertility issues, and therefore the feeding area of the sheep was examined. It was observed that those pastures were denser in terms of phenolic compounds than other pastures. In this manner, phytoestrogens were identified. The possible estrogenic effect of plant-derived compounds was first discussed in the 1940s. Subsequently, interest in plant-derived estrogens increased with the advent of hormone replacement therapy.[9] Phloretin is one of the three chalcone derivatives (butein, marein, and phloretin) of the flavonoid group in the phytoestrogen classification.[10,11] It is a phytopolyphenol found in apples, strawberries, and other fruits and exhibits high antioxidant properties. It is also known to exhibit antitumor and anti-inflammatory properties and al-

leviate liver damage. Moreover, it reduces the risk of serious chronic diseases.[12–14] In the present study, we investigated the protective effects of three doses of phloretin (0.5, 5, and 50 mg/kg bw/day) against BPA-induced liver and kidney damage.

There is no study examining the effects of phloretin against BPA-induced liver and kidney damage. In the present study, the effect of phloretin against BPA-induced liver and kidney damage was firstly examined.

MATERIALS AND METHODS

Chemicals

Phloretin (CAS No. 60-82-2) and BPA (CAS No. 80-05-7) were obtained from Sigma–Aldrich (USA). Creatinine (Cat. No. E-BC-K186), albumin (Cat. No. E-BC-K058), alanine amino-transferase (ALT) (Cat. No. E-BC-K235), aspartate amino-transferase (AST) (Cat. No. E-BC-K236), urea (Cat. No. E-BC-K183), and triglyceride (Cat. No. E-BC-K238) kits were obtained from Elabscience-Biotechnology (China). Glucose kit (Cat. No. E1623R) was obtained from Bioassay Technology Laboratory (China).

Animals and Housing

This study was conducted using 36 Wistar albino (*Rattus norvegicus*) female rats, aged 28 days, and weighing 130–150 g, which were obtained from Hacettepe University Experimental Animals Production Center with the approval number 2018/47-04. The rats were randomly grouped. During the 15-day experiment, the laboratory temperature was set at approximately 23°C ± 2°C, and the relative humidity was 48% ± 3%. The photoperiod was set as 12-h light and 12-h dark. Drinking water and normal pellet feed were provided *ad libitum* during the experiment.

Experimental Protocol

The rats were divided into five groups with six rats in each group, which was based on previous similar toxicological studies, and the smallest sample size was expected to be statistically significant. The five groups were as follows: (1) corn oil-control, (2) 50 mg/kg bw/day BPA positive control, (3) 50 mg/kg bw/day BPA+0.5 mg/kg bw/day phloretin dose, (4) 50 mg/kg bw/day BPA+5 mg/kg bw/day phloretin dose, and (5) 50 mg/kg bw/day BPA+50 mg/kg bw/day phloretin dose. As our aim was to evaluate the protective effect of different doses of phloretin against liver and kidney damage induced by BPA, we did not create a phloretin control group in which BPA was not applied. To ensure that BPA causes damage, we used the LOAEL value of 50 mg/kg bw/day.[5] Phloretin and BPA were dissolved in corn oil and administered to rats. Hence, a separate group was created for the corn oil group used as a vehicle and termed the "corn oil-control group." The purpose of creating this group was to eliminate the doubt that the corn oil exerts any effect on the results. Treatment was started on the rats on the postnatal 28th day. This age range was selected because the effect of chemicals is quite large during the prepubertal period (before puberty) of sexual differentiation (sensitive period) in rodents and humans. All rats were administered at the same age and randomly distributed to the groups, based on their weight. During the study, daily body weight, consumed feed, and water amount were recorded. BPA and phloretin were administered to the rats via subcutaneous injection at 30-min intervals, in the determined doses, starting with phloretin, and followed by BPA. The doses of phloretin were selected according to the phytoestrogen doses that people can take daily. Phloretin is found at rates of 80–420 mg/kg in apple peel, 3–223 mg/L in juice, and 2–5 mg/kg in fresh strawberries.[15] All treatment was administered every day for 15 days. Rats were sacrificed by cervical dislocation 24 h after the final dose under ketamine/xylazine anesthesia.

Liver and Kidney Organ Weights

After sacrificing the rats, the liver and kidney tissues were removed without damage and weighed, and these values were presented as absolute organ weights. To calculate relative organ weights, the organ weights were divided by terminal body weights, and the results were supported by dividing organ weights by brain weight.

Biochemical Analysis

Blood samples collected for biochemical analyses were centrifuged at 3600 rpm for 30 min at 4°C in the Eppendorf Centrifuge 5810R device (Germany), and serum was obtained. The levels of serum ALT, AST, urea, triglyceride, creatinine, albumin, and glucose were determined using kits. Analyses were performed using a BIOTEK uQuant (USA) spectrophotometer device.

Histopathological Analysis

At the end of the experiment, the liver and kidney tissues removed from the rats were fixed in 10% formaldehyde fixative for 24 h, after which they were washed in running water for 24 h. The tissues were blocked in paraffin, and sections of the paraffin blocks were cut at a thickness of 4 μm using a Leica (Germany) microtome. Slides were stained with hematoxylin and eosin. The preparations were examined under the Olympus BX51 system light microscope (Olympus Corporation, Japan) and photographed using Olympus cellSens Entry 4.1.1 program (Olympus Corporation, Japan).

Histomorphometric Measurement of Kidney Tissues

Glomeruli were histomorphometrically measured in all groups. For each group, 100 glomeruli were selected at random. The shortest and longest diameters of glomeruli were measured using the Olympus BX51 system light microscope (Olympus Corporation, Japan) and Olympus cellSens Entry 4.1.1 program (Olympus Corporation, Japan). The glomerular volume was determined using the formula $4\pi(d(G)/2)^3/3$, where d (G) is the arithmetic mean of the long and short diameters.[16]

Statistical Analysis

Data were analyzed using the statistical SPSS IBM-23 program (version 23, USA). Data homogeneity was evaluated using Levene statistics. ANOVA was used when the variances were homogeneous; otherwise, the Welch test was used. Tukey and Games–Howell tests were used as post hoc tests. Fisher's exact test was used to determine the statistical significance of histopathological data. All values were expressed as mean ± SD. $p < 0.05$ was considered statistically significant.

Ethics Committee Approval

Permission required for the studies was obtained from Hacettepe University Experimental Animals Ethics Committee with the number 2018/47-04.

RESULTS

Liver and Kidney Organ Weights

Liver and kidney absolute organ weights, relative organ weights, and final body weights of female rats in the corn oil-control, BPA positive control, and phloretin treatment groups are presented in Table 1. Both initial and final body weights showed a statistically significant difference between the BPA and phloretin dose groups. To determine the accuracy of this difference, we investigated the % weight change but found no significant difference in the results. Overall, BPA positive control and phloretin dose groups showed no significant changes in body weights in this study. However, the absolute kidney weights statistically significantly decreased in the BPA positive control group compared with that in the corn oil-control group, but no difference was detected in the phloretin dose groups. The kidney weights calculated according to body weight significantly reduced in the 50 mg/kg bw/day phloretin dose group compared with that in the BPA positive control group, whereas the relative kidney weights calculated according to brain weight significantly increased compared with that in the 0.5 mg/kg bw/day BPA positive control group. Although no statistically significant change was observed in liver weights in the BPA positive control group, a significant increase was detected in the phloretin dose groups compared with that in the BPA group.

The relative liver weights determined based on body weight showed no significant differences. In the 0.5 mg phloretin dose group, there was a significant reduction in the relative liver weights calculated according to brain weights compared with that in the BPA positive control group.

Biochemical Results

Table 2 shows the biochemical results of the control and experimental groups. Serum ALT levels significantly increased in the BPA positive control group compared with those in the corn oil-control group. Serum ALT values also significantly increased in all phloretin treatment groups compared with those in the corn oil-control group. However, there were no statistically significant differences between the BPA positive control and phloretin treatment dose groups. Regarding serum AST levels, a statistically significant decrease was detected in the BPA positive control group compared with those in the corn oil-control group. Similarly, serum AST values significantly decreased in all the phloretin treatment groups compared with those in the corn oil-control group. With the doses and methods used in this study, we detected no beneficial effect of phloretin on alterations in serum ALT and AST levels caused by BPA. Serum glucose levels statistically decreased in the BPA positive control group compared with those in the corn oil-control group. Similarly, serum glucose levels were significantly lower in the 0.5 and 50 mg/kg bw/day phloretin dose groups than in the corn oil-control group. The decrease in serum glucose levels in the 5 mg/kg bw/day phloretin dose group was not statistically significant compared with that in the corn oil-control group. There was no significant change between the BPA positive control and phloretin dose groups. Serum triglyceride levels also showed no statistically significant differences between the corn oil-control and BPA positive control groups, and the phloretin dose groups also showed no differences triglyceride levels compared with those in the corn oil-control or BPA positive control group. Nevertheless, the 0.5 mg/kg bw/day phloretin dose group showed statistically lower triglyceride levels than the 5 and 50 mg/kg bw/day phloretin dose groups. Regarding serum albumin levels, no statistically significant difference was detected between BPA positive control and corn oil-control groups. Similarly, serum albumin levels in the 0.5 mg/kg bw/day phloretin dose group showed no statistically significant differences compared with those in the corn oil-control and BPA positive control groups. Serum albumin levels in the 5 mg/kg bw/day phloretin dose group were significantly higher than those in the corn oil-control group. Moreover, serum albumin levels statistically significantly decreased in the 50 mg/kg bw/day phloretin dose group compared with those in the BPA positive control group and the 5 mg/kg bw/day phloretin dose group.

Regarding serum creatinine levels, no statistically significant differences were found among the corn oil-control, BPA positive control, and phloretin dose groups. Serum urea levels

Table 1. Absolute and relative organ weights of female rats in the corn oil-control, BPA-positive control and phloretin dose groups.

Measurements	Control Groups			Phloretin Groups		P value
	Corn Oil	BPA (50 mg/kg bw/day)	Phloretin (0.5 mg/kg bw/day) + BPA (50 mg/kg bw/day)	Phloretin (5 mg/kg bw/day) + BPA (50 mg/kg bw/day)	Phloretin (50 mg/kg bw/day) + BPA (50 mg/kg bw/day)	
Initial Body Weights (g)	102 ± 13	90 ± 15 [a,d,e]	117 ± 13 [b]	117 ± 11 [b]	119 ± 18 [b]	0.014
Terminal Body Weights (g)	140 ± 11	120 ± 19 [c,d,e]	157 ± 16 [b]	164 ± 12 [b]	153 ± 15 [b]	0.001
Weight Change (%)	40 ± 23	34 ± 3	35 ± 5	40 ± 5	30 ± 16	0.327
Brain Weights (g)	1.53 ± 0.12	1.5 ± 0.08	1.6 ± 0.07	1.52 ± 0.26	1.6 ± 0.14	0.696
Kidney Weights (g)	1.48 ± 0.15 [b]	1.2 ± 0.07 [a]	1.47 ± 0.18	1.41 ± 0.10	1.26 ± 0.16	0.003
Liver Weights (g)	6.92 ± 0.88	6.09 ± 0.73 [c,d,e]	7.79 ± 0.90 [b]	8.06 ± 0.73 [b]	7.9 ± 0.55 [b]	0.001
Relative Kidney Weights (g/body weight kg)	10.55 ± 0.53 [e]	10.11 ± 1.28	4.42 ± 0.39	9.07 ± 1.64	8.27 ± 0.99 [a]	0.004
Relative Liver Weights (g/body weight kg)	49.22 ± 3.39	51.15 ± 4.45	47.56 ± 2.90	51.32 ± 1.45	52.11 ± 5.64	0.157
Relative Brain Weights (g/body weight kg)	10.96 ± 0.76	12.66 ± 1.39 [c,d]	9.83 ± 0.56 [b]	9.8 ± 2.06 [b]	10.62 ± 1.69	0.012
Relative Kidney Weights (g/brain g)	0.97 ± 0.08 [b]	0.8 ± 0.05 [a,e]	0.96 ± 0.23 [b]	0.92 ± 0.15	0.79 ± 0.10	0.012
Relative Liver Weights (g/brain g)	49.22 ± 3.39	51.15 ± 4.45 [e]	47.56 ± 2.90 [b]	51.32 ± 1.45	52.11 ± 5.64	0.029

Values are given as mean ± SD. [a] Statistically different from the corn oil-control group, [b] statistically different from the BPA-positive control group, [c] statistically different from the 0.5 mg/kg bw/day phloretin dose group, [d] statistically different from the 5 mg/kg bw/day phloretin dose group, [e] statistically different from the 50 mg/kg bw/day phloretin dose group. (Significance level p<0.05). Bisphenol-A (BPA).

Table 2. Biochemical analysis of serum samples of female rats in the corn oil-control, BPA-positive control and phloretin dose groups.

Measurements	Control Groups			Phloretin Groups		
	Corn Oil	BPA (50 mg/kg bw/day)	Phloretin (0.5 mg/kg bw/day) + BPA (50 mg/kg bw/day)	Phloretin (5 mg/kg bw/day) + BPA (50 mg/kg bw/day)	Phloretin (50 mg/kg bw/day) + BPA (50 mg/kg bw/day)	
ALT (IU/L)	5 ± 0.04 [b,c,d,e]	15 ± 0.02 [a]	16 ± 0.01 [a]	19 ± 0.01 [a]	20 ± 0.02 [a]	
AST (IU/L)	164.74 ± 6.39 [b,c,d,e]	121.64 ± 12.33 [a]	126.15 ± 9.67 [a]	121.12 ± 9.09 [a]	123.79 ± 12.55 [a]	
Albumin (g/L)	21.58 ± 0.30 [d]	21.62 ± 0.53 [e]	22.08 ± 0.84	22.92 ± 0.68 [a,e]	20.53 ± 0.68 [b,d]	
Glucose (mg/dL)	84.73 ± 8.8 [b,c,e]	52.46 ± 4.17 [a]	55.26 ± 0.66 [a]	65.26 ± 12.57	53.1 ± 8.91 [a]	
Creatinine (μmol/L)	26.00 ± 3.7	24.15 ± 3.70	24.76 ± 3.02	25.07 ± 6.31	24.15 ± 4.77	
Triglyceride (mmol/L)	0.07 ± 0.02	0.08 ± 0.00	0.04 ± 0.01 [d,e]	0.12 ± 0.01 [c]	0.11 ± 0.06 [c]	
Urea (mmol/L)	1.16 ± 0.26 [b,c,d]	1.82 ± 0.51 [a]	2.40 ± 0.44 [a,d]	2.05 ± 0.30 [a]	1.6 ± 0.17 [c]	

Values are given as mean ± SD. [a]Statistically different from the corn oil-control group, [b]statistically different from the BPA-positive control group, [c]statistically different from the 0.5 mg/kg bw/day phloretin dose group, [d]statistically different from the 5 mg/kg bw/day phloretin dose group, [e]statistically different from the 50 mg/kg bw/day phloretin dose group, (Significance level p < 0.05). Bisphenol-A (BPA), Alanine Aminotransferase (ALT), Aspartate Aminotransferase (AST).

statistically significantly increased in the BPA positive control group compared with those in the corn oil-control group. Serum urea levels in all the phloretin dose groups were also higher than those in the corn oil-control group. This increase was sta-

tistically significantly different in the 0.5 and 5 mg/kg bw/day phloretin dose groups compared with that in the corn oil-control group. Moreover, the 0.5 and 50 mg/kg bw/day phloretin dose groups showed significant differences in serum urea levels.

Histopathological Results

The results of microscopic evaluation of the kidney tissue of the corn oil-control, BPA positive control, and phloretin dose groups are depicted in Figure 1. The incidence of the histopathological findings of the kidney tissues of rats is presented in Table 3. Kidney sections from the corn oil-control group demonstrated healthy kidney tissues. However, kidney sections from the BPA positive control and phloretin treatment groups demonstrated Bowman's capsule dilatation, tubular degeneration, degeneration in the renal parenchyma, congestion, glomerular atrophy, cell expulsion into the lumen, and fibrous tissue formation. No clear protective effect of phloretin against BPA-induced histopathological damage in the kidney tissue was detected. The results of microscopic evaluation of the liver tissue of the corn oil-control, BPA positive control, and phloretin groups are illustrated in Figure 1. The incidence of the histopathological findings of the liver tissues of rats is shown in Table 4. Liver sections from the corn oil-control group revealed healthy liver tissue. However, liver sections from the BPA positive control and phloretin treatment dose groups showed congestion, sinusoidal dilatation, edema, and degeneration in hepatic parenchyma, mononuclear cell infiltration, ballooning in hepatocytes, and steatosis. Ballooning in hepatocytes and congestion in the liver tissue were primarily detected in the BPA positive control group compared with those in the corn oil-control group, but these findings decreased significantly in all the phloretin dose groups compared with those in the BPA positive control group. Although phloretin protected against congestion and ballooning in hepatocytes, no strong protective effect was detected against other BPA-induced liver damage.

Histomorphometric Measurement of Kidney Tissues

The results of kidney morphometric analysis of the corn oil-control, BPA positive control, and phloretin treatment groups are shown in Table 5. A statistically significant decrease was observed in long diameter, short diameter, glomerular diameter, and glomerular volume in the BPA positive control group compared with those in the corn oil-control group. Similarly, the values in the 5 and 50 mg/kg bw/day phloretin dose groups were statistically different from those in the corn oil-control group in all measurements. The values in the 0.5 mg/kg bw/day phloretin dose group were also statistically significantly different from those in the BPA positive control group in all measurements. The 50 mg/kg bw/day phloretin dose group showed highly statistically significant differences in short diameter, glomerular diameter, and glomerular volume from those in the corn oil-control group.

DISCUSSION

Researchers have recently began focusing their attention on the physiological and pharmacological functions of bioactive substances found in plants, such as phloretin. Epidemiological and experimental studies on phloretin have demonstrated that this flavonoid exerts both positive and negative effects, as an exceptionally high-dose of phloretin exerts lethal effects on mice.[17,18] Nevertheless, several studies have demonstrated that phloretin treatment at specific doses exerts numerous protective effects, such as antidiabetic, anticancer, and anti-inflammatory.[17,19] According to the literature, the effects of phloretin differ depending on the type, age, and gender of the experimental animal, the phloretin dose, and the method of administration, and, if the effects against induced damage are being investigated, the substances that cause the damage. Although some of our study findings support the positive findings reported in the literature, our conclusion was that increasing the phloretin dose did not increase the protective effect and would not be safe.

Damage to the structural integrity of the cell membrane, especially in the liver cells, causes the release of ALT and AST in large amounts into the blood, increasing their serum levels.[20] A study in which D-galactosamine was used to cause hepatotoxicity showed an increase in serum ALT and AST levels. In this study, the effects of D-galactosamine on ALT and AST levels were reduced in parallel with increasing doses of phloretin used in the study (0.877 and 1.754 mmol/kg), and hepatic lesions were decreased.[21] Ren et al. investigated choline-induced hepatotoxicity. It was stated that blood ALT and AST levels increased in the choline model group compared to the normal control group. In the experimental groups where phloretin and choline were administered together, it was determined that ALT and AST levels decreased compared to the choline model group. This protective effect occurred in parallel with increasing doses of phloretin (100, 200 and 400 mg/kg/day).[22] In another study on mice, liver damage was induced by CCl_4 and the protective effect of phloretin at doses of 100, 200, and 500 mg/kg/day was evaluated. It was observed that increasing doses of phloretin reduced the excessive increase in serum ALT and AST levels induced by CCl_4.[23] The anticancer properties of phloretin were investigated by Alansari et al.[19] who also showed that the increase in serum ALT and AST levels caused by diethylnitrosamine-induced hepatocellular carcinoma was reduced after treatment with 25 mg/kg/day phloretin. In another study, mice fed on a western diet and high-fructose corn syrup showed increased serum ALT and AST levels, and treatment with 100 and 200 mg/kg/day phloretin significantly decreased the elevated serum ALT levels, whereas 50 mg/kg phloretin dose was ineffective, but the AST levels significantly decreased in all dose groups.[24] In these previous studies, the chemicals
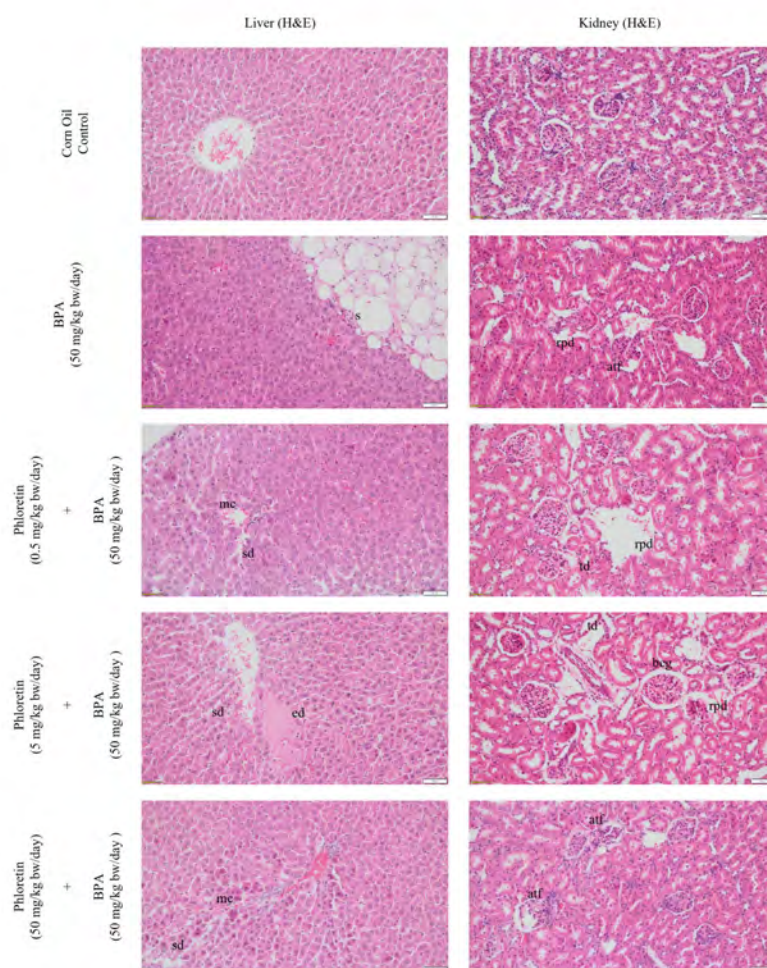
Figure 1. Representative photomicrographs of liver and kidney tissue of the corn oil- control, BPA-positive control and phloretin treatment groups. Normal histology in the kidney tissue of the corn oil-control group; degeneration in renal parenchyma (**rpd**) and glomerular atrophy (**atf**) are shown in BPA-positive control group; tubular degeneration (**td**) and degeneration in renal parenchyma (**rpd**) are shown in 0.5 mg/kg bw/day phloretin dose group; tubular degeneration (**td**), degeneration in renal parenchyma (**rpd**) and bowman capsule dilatation (**bcg**) are shown in 5 mg/kg bw/day phloretin dose group; glomerular atrophy (**atf**) is shown in 50 mg/kg bw/day phloretin dose group. Normal histology in the liver tissue of the corn oil-control group; steatosis (**s**) is shown in BPA-positive control group; minimal congestion (**mc**) and sinusoidal dilatation (**sd**) are shown in 0.5 mg/kg bw/day phloretin dose group; edema (**ed**) and sinusoidal dilatation (**sd**) are shown in 5 mg/kg bw/day phloretin dose group; minimal congestion (**mc**) and sinusoidal dilatation (**sd**) are shown in 50 mg/kg bw/day phloretin dose group; H&E stain, 200X.

used to generate animal models increased serum ALT and AST levels, whereas we used BPA in the present study that decreased serum AST and ALT levels. As we could not detect a significant decrease or increase in the phloretin treatment groups compared with the BPA group, we believe that the decrease in serum AST levels detected in the present study is due to BPA. In contrast, we detected an increase in serum ALT levels, which we again believe is due to BPA. Unlike the previous study, we could not obtain clear information regarding the effect of phloretin on serum ALT and AST levels.

The effects of phloretin on glucose metabolism have been extensively investigated.[25-27] For instance, a study investigating the effects of oral treatment of 5 and 10 mg/kg/day phloretin on body energy and glucose balance in diabetic C57BL BKS-DB mice reported that in parallel to phloretin dosage increases, blood glucose levels considerably lowered and glucose tolerance improved.[25] Shen et al. explored the hypoglycemic effect of phloretin in 8-week-old male rats with streptozotocin-induced diabetes and fed on high fat and high sugar.[26] To determine its protective and therapeutic effects, phloretin was administered to different groups before and after streptozotocin induction at 100 mg/kg daily for 4 weeks, and it was observed that phloretin was protective against diabetes and beneficial in the treatment of glucose and lipid metabolism.[26] Alsenea et al.

Table 3. Incidence of histopathological findings detected in kidney tissues of the corn oil-control, BPA-positive control and phloretin dose groups.

Histopatological Findings	Control Groups		Phloretin Groups		
	Corn Oil	BPA (50 mg/kg bw/day)	Phloretin (0.5 mg/kg bw/day) + BPA (50 mg/kg bw/day)	Phloretin (5 mg/kg bw/day) + BPA (50 mg/kg bw/day)	Phloretin (50 mg/kg bw/day) + BPA (50 mg/kg bw/day)
Bowman Capsule Dilatation	1/6 [c,e]	1/6 [c,d]	6/6 [a,b]	2/6	4/6 [a,b]
Tubular Degeneration	0/6 [b,d,e]	5/6 [a]	3/6	4/6 [a]	4/6 [a]
Degeneration in Renal Parenchyma	0/6	1/6	1/6	1/6	1/6
Minimal Congestion	0/6 [d]	3/6	3/6	4/6 [a]	3/6
Glomerular Atrophy	0/6 [b,d]	4/6 [a]	3/6	4/6 [a]	3/6
Cell Expulsion into the Lumen	0/6	3/6	1/6	1/6	2/6
Mononuclear Cell Infiltration	0/6	1/6	2/6	1/6	2/6
Fibrous Tissue Formation	0/6	1/6	1/6	1/6	2/6

Values are given as the number of rats with histopathological findings/number of rats examined in the group. [a]Statistically different from the corn oil-control group, [b]statistically different from the BPA-positive control group, [c]statistically different from the 0.5 mg/kg bw/day phloretin dose group, [d]statistically different from the 5 mg/kg bw/day phloretin dose group, [e]statistically different from the 50 mg/kg bw/day phloretin dose group. (Significance level p<0.05). Bisphenol-A (BPA)

Table 4. The incidences of histopathological findings detected in the liver tissue of the corn oil-control, BPA-positive control and phloretin dose groups.

Histopathological Findings	Control Groups		Phloretin Groups		
	Corn Oil	BPA (50 mg/kg bw/day)	Phloretin (0.5 mg/kg bw/day) + BPA (50 mg/kg bw/day)	Phloretin (5 mg/kg bw/day) + BPA (50 mg/kg bw/day)	Phloretin (50 mg/kg bw/day) + BPA (50 mg/kg bw/day)
Minimal Congestion	0/6 [b]	4/6 [a,c,d,e]	1/6 [b]	1/6 [b]	1/6 [b]
Sinusoidal Dilatation	0/6 [b,c,d]	4/6 [a]	5/6 [a]	5/6 [a]	3/6
Edema	0/6	0/6	0/6	1/6	1/6
Degeneration in Hepatic Parenchyma	0/6	0/6	0/6	1/6	1/6
Mononuclear Cell Infiltration	1/6	2/6	1/6	2/6	1/6
Ballooning in Hepatocytes	0/6 [b]	4/6 [a,c,d,e]	1/6 [b]	0/6 [b]	0/6 [b]
Steatosis	0/6	1/6	1/6	0/6	0/6

Values are given as the number of rats with histopathological findings / number of rats examined in the group. [a]Statistically different from the corn oil-control group, [b]statistically different from the BPA-positive control group, [c]statistically different from the 0.5 mg/kg bw/day phloretin dose group, [d]statistically different from the 5 mg/kg bw/day phloretin dose group, [e]statistically different from the 50 mg/kg bw/day phloretin dose group, (Significance level p<0.05). Bisphenol-A (BPA).

investigated the preventive and therapeutic effects of phloretin in 10-week-old male C57BL/6 mice with high-fat-diet-induced obesity.[27] Phloretin was administered intraperitoneally at 10 mg/kg twice weekly for 12 weeks, and the results showed that phloretin improved glucose homeostasis and insulin sensitivity and attenuated hepatic lipid accumulation.[27] Furthermore, Mao et al. examined the protective effect of 25 and 75 mg/kg phloretin doses against diabetes-induced endothelial damage through *in vitro* and *in vivo* studies.[28] They observed that both doses of phloretin were protective against endothelial damage in diabetic mice through AMP-activated protein kinase-dependent anti-EndMT (endothelial–mesenchymal transforma-

Table 5. Histomorphometric measurements of glomeruli in the corn oil-control, BPA-positive control and phloretin dose groups.

Measurments	Control Groups			Phloretin Groups			P value
	Corn Oil	BPA (50 mg/kg bw/day)	Phloretin (0.5 mg/kg bw/day) + BPA (50 mg/kg bw/day)	Phloretin (5 mg/kg bw/day) + BPA (50 mg/kg bw/day)	Phloretin (50 mg/kg bw/day) + BPA (50 mg/kg bw/day)		
Long Diameter (μm)	75.07 ± 15.22 [b, d, e]	62.21 ± 13.71 [a, e]	72.01 ± 12.59 [b]	68.08 ± 17.01 [a]	64.46 ± 12.38 [a]		*<0.0001*
Short Diameter (μm)	62.67 ± 12.19 [b, d, e]	48.95 ± 12.44 [a, c, d]	59.89 ± 13.30 [b]	56.3 ± 14.41 [a, b]	48.78 ± 8.67 [a]		*<0.0001*
Glomerular Diameter (μm)	68,87 ± 12.90 [b, d, e]	55.58 ± 12.30 [a, c, d]	65.96 ± 11.95 [b]	62.19 ± 14,93 [a, b]	56.62 ± 9.71 [a]		*<0.0001*
Glomerular Volume (x10⁶ μm³)	0.19 ± 0.10 [b, d, e]	0.1 ± 0.07 [a, c, d]	0.16 ± 0.08 [b]	0.15 ± 0.10 [e, b]	0.1 ± 0.05 [a]		*<0.0001*

Values are given as mean ± SD. [a]Statistically different from the corn oil-control group, [b]statistically different from the BPA-positive control group, [c]statistically different from the 0.5 mg/kg bw/day phloretin dose group, [d]statistically different from the 5 mg/kg bw/day phloretin dose group, [e]statistically different from the 50 mg/kg bw/day phloretin dose group, (Significance level p<0.05). Bisphenol-A (BPA).

tion) activation and reduced procalcification factors and vascular fibrosis.[28] Molecular studies on the effects of phloretin could explain the decrease in glucose levels. Sodium-dependent glucose cotransporter 1 (SGLT1) present in intestinal epithelial cells and glucose transporter protein type 2 (GLUT2) present in the intestinal membrane play a role in glucose absorption. Phloretin inhibits the function of GLUT2 and SGLT1, reducing the basolateral transfer of glucose from intestinal cells to the blood and reducing apical glucose uptake.[17,29,30] Phlorizin (phloretin glycoside) also inhibits the function of SGLT2, which is responsible for renal tubular reabsorption of glucose, increasing its urinary excretion.[17,31,32] Overall, the administration of phloretin reduces glucose levels by decreasing its absorption and increasing its urinary excretion.[17] It is evident that certain doses of phloretin exert curative effects on diabetes and glucose metabolism. In the present study, serum glucose levels decreased in all groups compared with those in the corn oil-control group. However, no significant difference was found between BPA-positive control and phloretin treatment groups. Therefore, phloretin does not appear to have an additional contribution to the decrease in serum glucose levels caused by BPA in all groups. The chemicals used to create a model in the abovementioned studies increased the serum glucose level. Furthermore, some studies have used diabetic animal models. BPA, which was used to induce damage in the present study, decreased the serum glucose level. Therefore, we believe that our results differ from those reported in the literature because BPA and phloretin were administered subcutaneously for 15 days. We believe that it would be valuable to explore the effects of phloretin on hyperglycemia and diabetes.

In mammals, the highest concentrations of creatinine are found in the skeletal muscle, where it plays a significant role in energy metabolism. Experimental data reveal a close relationship between disorders in creatinine metabolism and various muscle diseases. However, creatinine also plays a vital role in kidney metabolism[33] and is produced in the liver as well.[34] Serum creatinine is a biomarker for both the kidney and liver. Studies have demonstrated that treatment with phloretin causes a reduction in serum creatinine levels, which increases the damage caused by different chemicals.[35,36] In a study investigating the toxic effect of phloretin, no effect on serum creatinine level was found.[37] The effect of 50 mmol/kg intraperitoneal phloretin treatment on a sepsis model with cecal ligation and puncture in rats was investigated in another study, which showed that the levels of blood urea nitrogen, tumor necrosis factor-alpha, glutathione, and liver nuclear factor-κB p65 transcription factor increased in the CLP group and decreased in the phloretin treatment groups. However, no significant difference was observed in the levels of serum creatinine and creatinine phosphokinase.[38] Cui et al. investigated the effect of phloretin on kidney damage in mice with adenine/potassium oxonate-induced hyperuricemia.[39] They reported that treatment with 50 mg/kg phloretin significantly decreased the serum urea nitrogen level, which was elevated due to hyperuricemia. In contrast, the creatinine level decreased slightly, but not statistically. In the present study, the slight decrease observed in the BPA group was insignificant. However, no statistically significant difference was observed in serum creatinine levels in the phloretin treatment groups compared with those in the corn oil-control or BPA positive control groups. We concluded that phloretin doses exerted no significant effect no serum creatinine. Urea is a vital parameter to interpret kidney functions.[40,41] Studies have shown that increased serum urea levels due to damage caused by various chemicals are reduced by phloretin treatment.[35,38] In the present study, we detected a significant increase in urea

levels in the BPA group. We also detected a significant increase in urea levels in the phloretin treatment groups compared with those in the corn oil-control group. Nonetheless, the increase in urea levels in the phloretin treatment group was insignificant compared with that in the BPA group. This finding differs from other studies on phloretin. For instance, Un et al. investigated the effect of phloretin and phlorizin against cisplatin-induced damage in Balb/c female mice.[36] They administered 50 and 100 mg/kg phlorizin and phloretin to mice by oral gavage for 3 days and found significant improvement in cisplatin-induced elevated serum urea levels. They also administered phlorizin and phloretin to mice not treated with cisplatin and found no difference in serum urea levels between the phlorizin and phloretin treatment groups and the control group (no treatment).[36] Similarly, Pujari et al. reported that phloretin may not exert a direct increasing or decreasing effect on serum urea levels.[37] Hence, we believe that the phloretin doses we used affect in the present study exerted no effect on serum urea levels and that the statistically significant increase in the 0.5 and 5 mg/kg bw/day phloretin dose groups was caused by BPA.

Triglycerides are esters formed from glycerol and three fatty acids and were previously referred to as triacylglycerols. Triglycerides are essential in metabolism as an energy source and a carrier of dietary fat. Moreover, they are the primary component of low-density lipoprotein and are therefore clinically significant and routinely investigated in serum obtained from human and animal blood samples.[42−45] Studies on phloretin have shown that phloretin treatment individually does not affect serum triglyceride levels.[37] However, phloretin treatment can reduce the increases in serum triglyceride levels caused by chemicals.[24] Chhimwal et al. found that the increased triglyceride levels in rats fed on a western diet and high-fructose corn syrup were significantly reduced by the administration of phloretin at 100 and 200 mg/kg doses.[24] Furthermore, they evaluated the effects of phloretin by creating an *in vitro* model of nonalcoholic fatty liver disease (NAFLD) in Huh7 cells (human hepatoma cells). They found that 50, 100, and 150 µM phloretin doses reduced lipid accumulation by 12%, 31%, and 44% and intracellular triglyceride accumulation by 15%, 30%, and 56%, respectively.[24] However, our study showed no significant differences in serum triglyceride levels.

The most prevalent protein in mammalian plasma is albumin, which is typically considered a multipurpose transport protein.[46] It is believed that phloretin does not exert a toxic effect on serum albumin.[37] However, consistent with other hepatotoxicity and renal toxicity markers, increased serum albumin levels caused by chemical damage were found to decrease with phloretin treatment.[35] In the present study, we observed a significant difference in serum albumin levels in the 5 mg/kg bw/day phloretin treatment group compared with that in the corn oil-control group. We assumed that a statistically significant increase in the 5 mg/kg bw/day dose groups was caused by BPA. The liver is the target organ for endocrine-

disrupting chemicals. The levels of hepatic enzymes may decrease or increase due to BPA, and pathological findings may appear in liver histology. Liver damage caused by BPA can also occur from the accumulation of BPA toxic metabolites and the production of reactive oxygen species in the liver.[20] Congestion, sinusoidal dilatation, edema, degeneration in hepatic parenchyma, mononuclear cell infiltration, ballooning in hepatocytes, and steatosis were detected in the positive control and phloretin treatment dose group. Several studies have indicated that treatment with phloretin decreases the histopathological findings of the liver.[19,24] Chhimwal et al. investigated the effect of phloretin on NAFLD in adult male C57BL/6J mice. They administered phloretin by oral gavage at doses of 50, 100, and 200 mg/kg for 16 weeks to rats that were fed on a western diet and high-fructose corn syrup.[24] Their study results suggested that phloretin effectively reduces the progression of NAFLD and inhibits hepatic inflammation and fibrosis by upregulating autophagy-mediated lipid degradation. Especially at high doses, phloretin has been found to decrease histological damage by reducing hepatic lipogenesis and facilitating fatty acid oxidation. However, our study revealed no evidence that phloretin improves BPA-induced liver injury at oral doses of 0.5, 5, and 50 mg/kg bw/day. A nephrotoxic impact may occur due to the accumulation of BPA and its hazardous metabolites and the kidney's inability to effectively remove these chemicals.[20] In the present study, BPA damage was mostly observed in the kidney. Bowman's capsule dilatation, tubular degeneration, degeneration in renal parenchyma, congestion, glomerular atrophy, cell expulsion into the lumen, and fibrous tissue formation were detected in the positive control and phloretin treatment groups. Several studies have shown that phloretin reduces histopathological findings.[36,39] For instance, treatment with 50 and 100 mg/kg of phloretin was found to significantly improve cisplatin-induced tubular injury, with no abnormalities due to high-dose phloretin administration being identified.[36] In another study, mice with hyperuricemia exhibited tubular atrophy, tubular dilatation, and tubulointerstitial damage with interstitial fibrosis, whereas phloretin administration improved renal morphological lesions and tubular necrosis in mice. Moreover, mice in the phloretin treatment group alone showed no renal histological lesions compared with mice in the control group.[39] Phloretin has also been suggested to exert protective effects against several types of chronic kidney disease.[47] Nevertheless, our study found no statistically significant difference in kidney histopathology. The effects of BPA and phloretin on the kidney in this study were supported by morphometric measurements. As we found in our previous study, BPA exposure led to a statistically significant decrease in all morphometric data.[3] The closest values to those in the corn oil-control group were determined in the 0.5 mg/kg bw/day phloretin dose group, and the data were statistically different from those in the BPA positive control group. In this context, a dose of 0.5 mg/kg bw/day phloretin may protect against BPA-induced kidney damage. However, we observed that with an increase in phloretin dose,

its protective effect against BPA-induced kidney damage decreased. Although some protection might be provided in the 5 mg/kg bw/day phloretin dose group, the results obtained in the 50 mg/kg bw/day dose group were highly similar to those in the BPA positive control group. Overall, no clear evidence was obtained concerning the protective effect of phloretin against BPA-induced kidney damage at oral doses of 5 mg/kg bw/day and especially 50 mg/kg bw/day.

Finally, based on our study results, treatment with 0.5 and 5 mg/kg bw/day phloretin administered as low doses may provide low protection against BPA-induced kidney and liver damage. However, the protective effect of 50 mg/kg bw/day phloretin used as a high-dose was low in this study. Geohagen et al. mentioned that a protective effect does not occur with an increase in phloretin dose; in contrast, it may exert adverse effects.[18] In this study, we did not administer phloretin without BPA. Therefore, we could not obtain information on the negative impact of increased phloretin doses. BPA may have caused the biochemical and histopathological adverse effects in this study. Nevertheless, our results support that increasing the phloretin dose does not increase the protective effect. In the study of Geohagen et al., phloretin was administered via intraperitoneal injection, and the results demonstrated that high-dose (2.40 mmol/kg) phloretin administration did not prevent lethality caused by acetaminophen, whereas low doses (0.2–0.4 mmol/kg) provided moderate hepatoprotection.[18] In another study, the authors concluded that long-term use of high-dose phloretin may cause liver damage.[48] However, there are also studies showing that there are positive effects that increase in parallel with the dose.[49] For instance, Zhao et al. reported protective effects exerted by 25 and 50 mg phloretin doses against cisplatin-induced kidney damage. They observed that phloretin doses increased the levels of serum creatinine, urea, and albumin in a dose-dependent manner, as well as oxidative stress markers in the control group.[35] In a previous study investigating the toxic effect of phloretin, 25 and 50 mg/kg/day doses of phloretin were administered to female and male mice for 28 days. The results of that study revealed no significant difference in the levels of ALT, AST, albumin, triglyceride, creatinine, and glucose compared with those in the control group. The authors of that study concluded that phloretin is safe to use.[37] We did not obtain evidence of a clear protective impact of phloretin in this investigation. Oral administration of phloretin is known to result in low absorption and bioavailability, as phloretin has exceptionally low water solubility.[17,49−51] We administered phloretin subcutaneously for 15 days in the present study; hence, a longer treatment period is recommended to elucidate the protective properties of phloretin. Regarding the data of the phloretin dose groups, the results are quite complex. However, our results revealed that the data of the 0.5 mg/kg bw/day phloretin group were closer to those of the corn oil-control group. To summarize, we could not detect an apparent protective effect of phloretin after 15 days of subcutaneous administration of 0.5, 5,

and 50 mg/kg bw/day doses in female rats against BPA-induced liver and kidney damage.

CONCLUSION

Considering the studies conducted on phloretin, we believe that it would be valuable to investigate its positive effects. However, the results obtained to date are complicated. According to the results of this study and the literature, we can conclude that phloretin is not yet suitable for the development of pharmaceuticals or use as a nutritional supplement. It is necessary to gain a complete understanding of the beneficial or harmful effects of phloretin to take advantage of its benefits. Additional *in vivo* studies are required to confirm the safety of phloretin and clarify its molecular mechanisms.

ORCID IDs of the author

Eda Nur Inkaya   0000-0001-7032-1537
Nilufer Coskun Kilic   0000-0002-2163-1886
Nurhayat Barlas   0000-0001-8657-2058

REFERENCES

1. Monneret C. What is an endocrine disruptor? *C R Biol.* 2017;340(9-10):403-405.

2. Batool S, Batool S, Shameem S, Batool T, Batool S. Effects of dibutyl phthalate and di (2-ethylhexyl) phthalate on the hepatic structure and function of adult male mice. *Toxicol Industrial Health.* 2022;38(8):470-480.

3. İnkaya EN, Barlas N. Investigation of the combined effects of propylparaben and methylparaben on biochemical and histological parameters in male rats. *J Clin Pract Res.* 2023;45(4):360-369.

4. Rutkowska A, Rachoń D. Bisphenol A (BPA) and its potential role in the pathogenesis of the polycystic ovary syndrome (PCOS). *Gynecol Endocrinol.* 2014;30(4):260-265.

5. Diamanti-Kandarakis E, Bourguignon JP, Giudice LC, et al.

Endocrine-disrupting chemicals: An Endocrine Society scientific statement. *Endocr Rev.* 2009;30(4):293–342.

6. International Food Safety Authorities Network (INFOSAN). Bisphenol A (BPA) - Current state of knowledge and future actions by WHO and FAO. 2009;1-6.

7. Abbas MAM, Elmetwally SAF, Mokhtar Abo-Elfotoh, MA. Effect of oral exposure to bisphenol a on the liver and kidney of adult male albino rats. *Int J Med Arts.* 2021;3(1):930-937.

8. Abdulhameed AAR, Lim V, Bahari H, et al. Adverse effects of bisphenol a on the liver and its underlying mechanisms: evidence from *in vivo* and *in vitro* studies. *Biomed Res Int.* 2022;16:8227314. doi:10.1155/2022/8227314

9. İnanç N, Tuna Ş. Fitoöstrojenler ve sağlıktaki etkileri. *Erciyes Üniv Vet Fak Derg.* 2005;2(2):91-95.

10. Shen X, Wang L, Zhou N, Gai S, Liu X, Zhang S. Beneficial effects of combination therapy of phloretin and metformin in streptozotocin-induced diabetic rats and improved insulin sensitivity: *In vitro. Food Funct.* 2020;11(1):392–403.

11. Yang EB, Guo YJ, Zhang K, Chen YZ, Mack P. Inhibition of epidermal growth factor receptor tyrosine kinase by chalcone derivatives. *Biochim Biophy Acta.* 2001;1550(2):144-152.

12. Andrade PB, Barbosa M, Matos RP, et al. Valuable compounds in macroalgae extracts. *Food Chem.* 2013;138(2-3):1819-1828.

13. Nielsen ILF, Williamson G. Review of the factors affecting bioavailability of soy isoflavones in humans. *Nutr Cancer.* 2007;57(1):1-10.

14. Arts ICW, Hollman PCH. Polyphenols and disease risk in epidemiologic studies. *Am J Clin Nutr.* 2005;81(1):317-325.

15. Kabir I, Rahman ER, Rahman MS. A review on endocrine disruptors and their possible impacts on human health. *Environ Toxicol Pharmacol.* 2015;40:241-258.

16. Yıldız N, Barlas N. Hepatic and renal functions in growing male rats after bisphenol A and octylphenol exposure. *Human Exp Toxicol.* 2013;32(7):675-86.

17. Nakhate KT, Badwaik H, Choudhary R, et al. Therapeutic potential and pharmaceutical development of a multi targeted flavonoid phloretin. *Nutrients.* 2022;14(17):3638. doi:10.3390/nu14173638

18. Geohagen BC, Korsharskyy B, Vydyanatha A, Nordstroem L, LoPachin RM. Phloretin cytoprotection and toxicity. *Chem Biol Interact.* 2018; 296:117-123.

19. Alansari WS, Eskandrani AA. The anticarcinogenic effect of the apple polyphenol phloretin in an experimental rat model of hepatocellular carcinoma. *Arab J Sci Eng.* 2020;45:4589-4597.

20. Moselhy W, Ahmed WMS, Moselhy WA, Nabil TM. Bisphenol A toxicity in adult male rats: hematological, biochemical and histopathological approach. *Glob Vet.* 2015;14(2):228-238

21. Zuo AR, Yu YY, Shu QL, et al. Hepatoprotective effects and antioxidant, antityrosinase activities of phloretin and phloretin isonicotinyl hydrazone. *J Chin Med Assoc.* 2014;77(6):290-301.

22. Ren D, Liu Y, Zhao Y, Yang X. Hepatotoxicity and endothelial dysfunction induced by high choline diet and the protective effects of phloretin in mice. *Food Chem Toxicol.* 2016;94:203-212.

23. Lu Y, Chen J, Ren D, Yang X, Zhao Y. Hepatoprotective effects of phloretin against CCl4-induced liver injury in mice. *Food Agric Immunol.* 2017;28(2):211-222.

24. Chhimwal J, Goel A, Sukapaka M, Patial V, Padwad Y. Phloretin mitigates oxidative injury, inflammation, and fibrogenic responses via restoration of autophagic flux in *in vitro* and preclinical models of NAFLD. *J Nutr Biochem.* 2022;107:109062. doi:10.1016/j.jnutbio.2022.109062

25. Shu G, Lu NS, Zhu XT, et al. Phloretin promotes adipocyte dif-

ferentiation in vitro and improves glucose homeostasis *in vivo. J Nutr Biochem.* 2014;25(12):1296-1308.

26. Shen X, Zhou N, Mi L, et al. Phloretin exerts hypoglycemic effect in streptozotocin-induced diabetic rats and improves insulin resistance in vitro. *Drug Des Devel Ther.* 2017;11:313-324.

27. Alsanea S, Gao M, Liu D. Phloretin prevents high-fat diet-induced obesity and improves metabolic homeostasis. *AAPS J.* 2017;19(3):797-805.

28. Mao W, Fan Y, Wang X, et al. Phloretin ameliorates diabetes-induced endothelial injury through AMPK-dependent anti-EndMT pathway. *Pharmacol Res.* 2022;179:106205. doi:10.1016/j.phrs.2022.106205

29. Schulze C, Bangert A, Kottra G, et al. Inhibition of the intestinal sodium-coupled glucose transporter 1 (SGLT1) by extracts and polyphenols from apple reduces postprandial blood glucose levels in mice and humans. *Mol Nutr Food Res.* 2014;58(9):1795-1808.

30. Kellett GL, Helliwell PA. The diffusive component of intestinal glucose absorption is mediated by the glucose-induced recruitment of GLUT2 to the brush-border membrane. *Biochem J.* 2000;350:155–162.

31. Tahrani AA, Barnett AH, Bailey CJ. SGLT inhibitors in management of diabetes. *Lancet Diabetes Endocrinol.* 2013;1:140-151.

32. Osorio H, Bautista R, Rios A, et al. Effect of phlorizin on SGLT2 expression in the kidney of diabetic rats. *J Nephrol.* 2010;23(5):541-546.

33. Wyss M, Kaddurah-Daouk R. Creatine and creatinine metabolism. *Physiol Rev.* 2000;80(3):1107-1213.

34. Beriry HM, Atef K, Gaber AS, Mohi ElDin MM. Ameliorative effect of mushroom extracts against butyl paraben induced toxicity in liver and kidney in female albino rats. *SVU-Int J Vet Sci.* 2022;5(2):11-22.

35. Zhao Y, Dai W. Effect of phloretin treatment ameliorated the cisplatin-induced nephrotoxicity and oxidative stress in experimental rats. *Pharmacogn Mag.* 2020;(16):207-213.

36. Un H, Ugan RA, Gurbuz MA, et al. Phloretin and phloridzin guard against cisplatin-induced nephrotoxicity in mice through inhibiting oxidative stress and inflammation. *Life Sci.* 2021;266:118869. doi:10.1016/j.lfs.2020.118869

37. Pujari NM, Mishra A, Khushtar M. i and histological toxicity profiling of a natural phenol: Phloretin. *Neuroquantology.* 2022;20(16):843-850.

38. Aliomrani M, Sepand MR, Mirzaei HR, Kazemi AR, Nekonam S, Sabzevari O. Effects of phloretin on oxidative and inflammatory reaction in rat model of cecal ligation and puncture induced sepsis. *Daru.* 2016;24(1):15. doi:10.1186/s40199-016-0154-9

39. Cui D, Liu S, Tang M, et al. Phloretin ameliorates hyperuricemia-induced chronic renal dysfunction through inhibiting NLRP3 inflammasome and uric acid reabsorption. *Phytomedicine.* 2020;66:153111. doi:10.1016/j.phymed.2019.153111

40. Galluzzo P, Marino M. Nutritional flavonoids impact on nuclear and extranuclear estrogen receptor activities. *Genes Nutr.* 2006;1(3-4):161–176.

41. Cornwell T. Dietary phytoestrogens and health. *Phytochemistry.* 2004;6(8):995-1016.

42. Washington IM, Van Hoosier G. Clinical Biochemistry and Hematology. In: Suckow MA, Stevens KA, Wilson RP, eds. *In American College of Laboratory Animal Medicine, The Laboratory Rabbit, Guinea Pig, Hamster, and Other Rodents*. Academic Press.2012; 57-116,

43. Ihedioha JI, Noel-Uneke OA, Ihedioha TE. Reference values for the serum lipid profile of albino rats (*Rattus norvegicus*) of varied

ages and sexes. *Comp Clin Path*. 2013;22:93-99.

44. Mesomya W, Hengsawadi D, Cuptapun Y, Jittanoonta P, Thalang VN. Effect of age on serum cholesterol and triglyceride levels in the experimental rats. *Agric Nat Resour*. 2001;35(2):144-148.

45. Christie WW, Han X. Lipid Analysis. *Oily Press Lipid Library Series*. 2012;3-19.

46. Anraku M, Yamasaki K, Maruyama T, Kragh-Hansen U, Otagiri M. Effect of oxidative stress on the structure and function of human serum albumin. *Pharm Res*. 2001;18(5):632-639.

47. Ranich T, Bhathena SJ, Velasquez MT. Protective effects of dietary phytoestrogens in chronic renal disease. *J Ren Nutr*. 2001;11:183-193.

48. Itou da Silva FS, Veiga Bizerra PF, Mito MS, et al.The metabolic and toxic acute effects of phloretin in the rat liver. *Chem Biol Interact.* 2022;364:110054. doi:10.1016/j.cbi.2022.110054

49. Zhao YY, Fan Y, Wang M, et al. Studies on pharmacokinetic properties and absorption mechanism of phloretin: *In vivo* and *in vitro. Biomed Pharmacother.* 2020;132:110809. doi:10.1016/j.biopha.2020.110809

50. Guo D, Liu J, Fan Y, Cheng J, et al., Optimization, characterization and evaluation of liposomes from *Malus hupehensis* (Pamp.) Rehd. Extracts. *J Liposome Res.* 2019;30(4):1-11.

51. Sharifi-Rad A, Mehrzad J, Darroudi M, Saberi MR, Chamani J. Oil-in-water nano emulsions comprising Berberine in olive oil: Biological activities, binding mechanisms to human serum albumin or holo-transferrin and QMMD simulations. *J Biomol Struct Dyn.* 2021;39(3):1029-1043.

How to cite this article

REVIEW ARTICLE

Pseudomonas otitidis: Discovery, Mechanisms and Potential Biotechnological Applications

Gao Jianfeng[1,2], ![ORCID] Rosfarizan Mohamad[1,2], ![ORCID] Murni Halim[1,2], ![ORCID] Mohd Shamzi Mohamed[1,2] ![ORCID]

[1]Universitiy of Putra Malaysia, Department of Bioprocess Technology, Faculty of Biotechnology & Biomolecular Sciences, Selangor, Malaysia
[2]Universitiy of Putra Malaysia, Bioprocessing and Biomanufacturing Research Complex, Faculty of Biotechnology & Biomolecular Sciences, Selangor, Malaysia

ABSTRACT

Pseudomonas otitidis is a species of *Pseudomonas* bacteria discovered in the early 2000s and has been studied systematically by many researchers. *P. otitidis* has been isolated from various infected parts of diseases, such as otitis, recurrent pneumonia, necrotizing fasciitis, peritonitis, foot cleft, or burns. It has been found to produce a variety of enzymes to decompose pollutants in the environment such as petroleum, polycyclic aromatic hydrocarbons, dyes, sodium dodecyl sulfate, zearalenone, etc. Furthermore, it can produce some ingredients for application in agriculture and health industries such as digestive enzymes, melanin, and L-asparaginase. Some scholars used *P. otitidis* as a model organism to investigate environmental degradation, biobattery, plant growth promotion, and biodegradable plastic polyhydroxyalkanoate production. The biofilm of *P. otitidis* consists of rhamnolipid. The research has provided the basis to produce rhamnolipid and the effective removal methods of *P. otitidis*. *P. otitidis* is prone to resistance to lactam antibiotics, and its resistance is caused by its unique metallo-β-lactamase, a polyoxometalate enzyme. In other words, *P. otitidis* is a very interesting bacterium candidate to be used in different research fields. Hence, in this paper, the discovery, mechanisms, and potential biotechnological applications of *P. otitidis* are described.

Keywords: *Pseudomonas* sp., *Pseudomonas otitidis*, Metallo-β-lactamase, Biofilm, L-asparaginase, Biosurfactant

INTRODUCTION

Pseudomonas sp. is a type of Gram-negative strain, which don't possess a cell nucleus and is unable to form spores. It is generally rod-shaped, with one to more flagella. It is easy to culture in vitro conditions, and it can secrete a variety of pigments. Most of the pigments are characteristic of *Pseudomonas* sp. and have antimicrobial properties. *Pseudomonas* sp. is a heterotroph bacterium that can utilize organics and an aerobic bacterium, which metabolizes through respiration. Although it is an obligate aerobe, it can grow anaerobically during nitrate reduction. *Pseudomonas* sp. is present and spread widely in the environment. *Pseudomonas* sp. genus was described as a whole group consisting of more than 100 known species.[1] The rRNA-DNA hybridization method was used to categorize this genus into five groups.[2] Kersters gave a new definition according to its previous classification studies.[3] In the past decades, genetic and molecular techniques played an important role in the classification of Pseudomonas [4] and many species were reclassified again.[5]

The diversity of habitat range, biological shape, and versatile function attracted microbiologists to study it for a long time.[6] Several *Pseudomonas* species can cause disease in humans and animals, like pulmonary infection,[7] respiratory tract infection,[8] bacteremia,[9] and urinary infection.[10] Serious medicine resistance problem exists on *Pseudomonas sp.* The medicine resistance of *Pseudomonas* is related to its ability to produce some enzymes that degrade antibiotics. The enzymes and the relevant genes have been widely studied such as the enzymes *Pseudomonas otitidis* metallo-β-lactamase (POM),[11] Pseudomonas fluorescens metallo-β-lactamase (PFM),[12] or São Paulo metallo-β-lactamase (SPM)[13] that mediate the efficient hydrolysis of carbapenems. Metallo-β-lactamase (MBL) is a kind of enzyme that can cause hydrolysis of carbapenem. It includes the POM enzyme produced by *Pseudomonas otitidis*, the (PAM) enzyme produced by *P. aeruginosa*, L1 enzyme of *Stenotrophomonas maltophilia* et al. Differences in their nucleotide sequences lead to differences in drug resistance and leading to evolutionary diversity.[14] Many functional genes of the *Pseudomonas* genus are similar, it is probably related to the phages that infect them. For example, the pf20 phage derived from Olsen's PX4 is capable of inter-infecting *P. aeruginosa* and *P. putida*.[15] Some phages remain as plasmid-like phages after entering *Pseudomonas*, such as pf16H2 in *P. putida*.[16] It leads to the high similarity between many gene sequences of *Pseudomonas sp*, and the evolution of *Pseudomonas*

sp. Identification of *Pseudomonas* bacteria is usually achieved by 16srDNA sequencing.[17] However, this method can occasionally lead to high similarity between a newly isolated strain and other existing *Pseudomonas* strains. So, it is difficult to determine the attribution of the new strain.[18] For example, *P. aeruginosa* has a strong similarity with *P. otitidis* MrB4, the similarity between them determined by the 16srDNA sequence is 98.6%, but they are in different taxonomic positions.[19] Some studies have analyzed the gyr gene sequence to determine the attribution of new strains.[20] Manivannan et al. isolated a strain and mapped its genome. They proposed that *P. aeruginosa* is a hypothesized species based on sequence homology, which is closest to the homology of *P. otitidis*.[21] In addition to 16SrRNA testing, MALDI-TOF MS Biotyper methods were used by Kačániová et al. for *Pseudomonas*' genotypic identification. It revealed a high discriminatory power of the MALDI-TOF MS Biotyper methods for the identification of *Pseudomonas* sp.[22]

Pseudomonas otitidis

P. otitidis is a novel species of *Pseudomonas sp*, which was discovered in 2002. In clinical studies conducted between 1998 and 2000, 101 researchers in the United States collected microbial samples from 2,039 patients (2,240 diseased ears). A total of 2838 bacteria strains were detected from 2048 ears and clinically diagnosed as acute otitis. Researchers isolated a new strain of *Pseudomonas* genus, closely related to *P. aeruginosa*. It was named *P. otitidis* by Roland et al.[23] In the following years, there were few studies on *P. otitidis* until 2006, when Clark et al. isolated 41 new strains of *P. otitidis* from the affected parts of patients with acute otitis.[24] Using DNA-DNA hybridization, 16S rRNA sequencing, and phenotypic analysis, researchers found that these *Pseudomonas* did not match any other known *Pseudomonas* species except *P. otitidis*. Researchers carried out systematic research about morphological tests, physiological and biochemical tests, drug sensitivity tests, fatty acid identification, and DNA component proportion determination of isolated *P. otitidis*.[24] Due to the systematic study of Clark et al., many researchers also considered that Clark et al. first discovered *P. otitidis* in 2006.[19,25] Clark et al. were the first to study the biochemical and physiological properties of ten *P. otitidis* strains as described below; Nine of ten strains can produce pyocyanin, nine of ten strains can produce fluoroscein, none of the strains can be cultivated at 4 ℃ or 47 ℃, five of ten strains can growth at 7 ℃. None of the strains can produce urease, eight of ten strains can hydrolyze gelatin and no strain can hydrolyze casein. Nine strains can growth on 4% sodium chloride agar, eight stains can grow on 5% sodium chloride agar. Ten strains all can't utilize N-Acetyl-D-glucosamine, D-Arabitol, Glycerol, D-Mannitol, D-Sorbitol, D-Fructose, L-Fucose, D-Galactose, Gentiobiose, Maltose, Sucrose, D-Trehalose, D-Xylose, D-Galacturonic acid, D-Gluconic acid, D-Glucuronic acid, Ita-

conic acid, Itaconic acid, L-Phenylalanine, D-Serine, Cytosine, Acetic acid, Sebacic acid, Inosine and Uridine. They can utilize L-Arginine, L-Histidine, L-Isoleucine, L-Leucine (9/10), L-Ornithine, L-Serine, β-Phenylethylamine, γ-Aminobutyric acid, Phenylethylamine and Putrescine.

Many scholars and doctors have isolated *P. otitidis* strains from infected people. Kim et al. reported two cases of infection in 2016. One is necrotizing fasciitis complications, another is peritonitis.[25] In 2015, researchers isolated 10 strains from the specimens of foot cleft patients, which were identified as *P. otitidis*.[26] In 2020, Japanese researchers sequenced the whole genome of *P. otitidis* TUM18999 from burn patients. The TUM18999 was identified as *P. otitidis*. Other researchers detected a novel specific B3 sub-group BML from this strain. Its similarities with *P. alcaligenes*' PAM-1 and *P. otitidis* TUM18999's POM-1 were 90.24% and 73.14%, respectively.[27] In 2021, Denmark physicians reported a case of known moderate chronic obstructive pulmonary disease with bronchiectasis and recurrent pneumonia. Blood cultures showed growth of *P. otitidis*. Researchers noted in the study that the infection caused by this new pathogen easily causes misdiagnosis.[28] In addition to being isolated from patients, *P. otitidis* also exists widely in nature. At present, some researchers have studied *P. otitidis* isolated from nature. Miyazaki et al. isolated a *P. otitidis* MrB4 strain from Lake Biwa, Japan, and sequenced its whole genome.[19]

P. otitidis can utilize and decompose many pollutants in the natural environment, such as crude oil, polycyclic aromatic hydrocarbons, dyes, sodium dodecyl sulfate (SDS), zearalenone, etc. It also can produce some useful substances, such as digestive enzymes, melanin, and L-asparaginase. Some scholars studied *P. otitidis*' biofilm, including the mechanism of biofilm production and the comparison between *P. otitidis* biofilm and other *Pseudomonas* biofilm. Some researchers used the bacterium to promote plant growth, research on biological batteries, and the production of polyhydroxyalkanoates (PHA). Metallo-β-lactamase produced by *P. otitidis* does not show intrinsic resistance to the carbapenem antibiotics. Figure 1 shows the major research areas of *P. otitidis*. The diagram depicts eight hot areas of research on *P. otitidis* and some achievements have been made in these fields.

Stability of *Pseudomonas otitidis* in Ecosystem

Some researchers are interested in the stability of *P. otitidis* in the ecosystem. García-Ulloa et al. studied *P. otitidis* in Cuatro Cienegas overexploitation of the agricultural wetland ecosystem in Coahuila, Mexico. As the water fades due to overexploitation. *P. otitidis* in the water loses metabolic complexity and diversity. In the following year, *P. otitidis* became extinct in this wetland ecosystem.[29] In addition, the researchers also analyzed the bacterial population history and evolutionary response of bacterial lineages to disturbances by comparing the
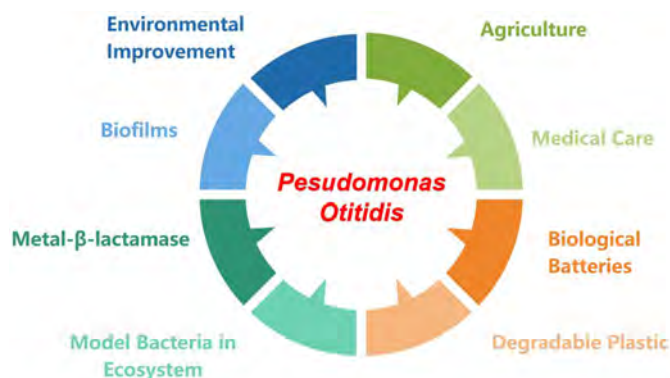
Figure 1. Research areas of *P. otitidis*.

genomes of a population sample.[30] Another study speculated on the eventual decline or possible extinction of *P. otitidis*. They propose that phosphorylation, DNA recombination, changes in small molecule metabolism and transport due to environmental disturbances, and loss of biosynthetic and regulatory genes lead to changes in bacterial populations.[31] Rodríguez-Verdugo et al. investigated the seasonal diversity of culturable *Pseudomonas* bacteria in lagoons of the Chihuahuan Desert, Mexico. They isolated 70 *Pseudomonas* strains collected from lagoons on four independent days. *P. otitidis* and *P. cuatrocienegasensis* accounted for 64% of the total number of isolates. More interestingly, *P. otitidis* was isolated only in summer, while *P. cuatrocienegasensis* was isolated only in winter due to the different growth conditions of *Pseudomonas* sp.[32]

Jun et al. isolated 21 populus-associated *Pseudomonas* isolates from the roots of poplar trees and through genetic analysis, it can be divided into three subgroups. The gene specificity of subgroup 1 includes several sensory systems that play a role in two-component signal transduction and depend on receptors. The gene specificity of the second subgroup included putative genes, and the specific genes of the third group were annotated as having hydrolase activity. The only isolated *P. otitidis* strain was different from the three subgroups.[33] Dahiya and Mohan thought that in the same ecological environment system, different microorganisms could improve and degrade different pollutants, and the addition of external microorganisms with a high degradation rate could significantly improve the process efficiency. In their study, *P. otitidis, Bacillus firmus, Bacillus subtilis* and *Bacillus circulans* were isolated and used to improve chemical oxygen demand (COD) and degrade nitrate, phosphorus, and moldy volatile fatty acids.[34]

Degradation of Organics

The degradation of harmful organics in wastewater and soil is a research focus of *P. otitidis*, such as the degradation of some components of oil pollution. Dasgupta et al. isolated a crude oil-degrading bacteria *P. otitidis*. In their research, the biodegradability of crude oil was evaluated by gas chromatography, and the formation of biofilm near the oil-water interface was quantitatively analyzed by a confocal laser scanning microscope. *Pseudomonas* supported by biofilms was found to degrade crude oil more easily and extensively than plankton. Moreover, *P. otitidis* biofilms formed in the presence of crude oil accumulated higher biomass and thicker biofilms.[35] Gogoi et al. isolated a strain of *P. otitidis* DU-13 capable of degrading oil pollution and water restoration and found that after 7 days of culture and treatment, the biosurfactant produced by the isolated strain could reduce the surface tension of oil-containing medium by 46%.[36] Peng et al. isolated a *P. otitidis* strain (Strain 81F, Accession Number AB698739.1). The degradation activity of polyurethane (PU) was evaluated. Their study describes the activity of *Pseudomonas* to degrade PU at a high level and describes the enzymes involved in this process, a 45 kDa product with PU enzyme activity. It plays an important role in bioremediation and plastic waste treatment.[37] Bestawy et al. investigated the treatment of industrial wastewater by the combination of bacterial consortium and Fe_3O_4 magnetic nanoparticles. Glycine-coated magnetic nanoparticles (Fe_3O_4 NPs) were prepared by reverse coprecipitation and characterized by X-ray diffraction, transmission electron microscopy, scanning electron microscopy, and vibrating sample magnetometer. Exogenous mixers include *Enterobacter cloacae* and *P. otitidis*. The mixture proved to have a good improvement effect on COD, oil, and grease (O&G), and total petroleum hydrocarbons.[38]

Removal of phenolic compounds from waste alkali by *P. otitidis* has been studied.[39] Waste alkali is one of the phenolic industrial pollutants produced by chemical processes in petrochemical plants and refineries. It has high COD, and pH, and contains high salinity and sulfides. The *P. aeruginosa* strain that can degrade phenol was isolated in previous studies. Mohammadi and collegous' study is the first to isolate *P. otitidis* capable of decomposing phenol.[39] Maitra et al isolated and identified phenol-degrading bacteria from soil, identified as *P. otitidis*.[40] Mohanty and Jena isolated a strain (*Pseudomonas* sp. Strain NBM11) from soil samples contaminated with medical waste and wastewater. The degradation capacity of the strain to phenol was up to 1000 mg/L by optimizing the culture conditions.[41]

Poyraz isolated a *P. otitidis* strain capable of degrading toluene from a sewage treatment plant, and researchers measured their tolerance and biotechnological potential.[42] Dados et al. proposed rapid remediation methods for soils heavily contaminated by organics. One of the methods uses contaminated soil as a culture material to enrich strains that degrade soil organic matter and then use those strains for soil remediation. Two *Pseudomonas* strains were isolated, EL20 and EL15 respectively, one of them was *P. otitidis*, which could degrade total petroleum hydrocarbons and N-alkanes *in vitro*.[43] Anwar et al. isolated several novel strains, including *P. otitidis*. The degradation ability of polyvinyl chloride under different cultures and time intervals was studied using scanning elec-

tron microscopy, atomic force microscopy, UV-visible spectroscopy, Fourier transform infrared (FT-IR), gel permeation chromatography, and differential scanning calorimetry.[44] Xu et al. isolated a *P. otitidis* strain W12 using phenanthrene as a carbon source from the activated sludge in the aeration tank of the north Shenyang sewage treatment plant.[45]

Rhamnolipid Content

Rhamnolipid is one of the most characteristic biosurfactants.[46] It is a surface-active molecule produced by *Pseudomonas* using various organic compounds.[47] Biosurfactants are divided into 4 types, they are cationic type, anionic type, zwitterionic type, and non-ionic type separately. Rhamnolipid is an anionic biosurfactant. Its hydrophilic end is composed of 1-2 molecules of rhamnose, and the hydrophobic end is composed of lipid structures.

Rhamnolipid is an important component of *P. otitidis* biofilm formation.[48] Haloi et al. isolated a rhamnolipid-produced *P. otitidis* TMB2 strain and described the process of production of rhamnolipid. They characterized the extracted biosurfactants by Fourier Transformed Infrared Spectroscopy and ^{1}H and ^{13}C nuclear magnetic resonance (NMR) spectroscopy. They used liquid chromatography-mass spectrometry to detect homologs of single and double rhamnolipids. The thermal stability and degradation modes of candidate biosurfactants were tested by thermogravimetry and differential scanning calorimetry to determine their adaptability.[49]

Buonocore et al. reported for the first time the production of RLs using anthracene and benzene as the only carbon sources using 12 different materials such as monosaccharides, polysaccharides, and petroleum industry derivatives as raw materials.[50] Singh and Tiwary isolated a strain of *P. otitidis* P4 from Chirimi Coal Mine in India and determined the structural properties of BS and the glycolipid properties of BS by biochemical tests, thin layer chromatography, FT-IR and NMR analysis.[51] Before characterizing biosurfactants by FT-IR and NMR, they were purified by column chromatography and confirmed by thin-layer chromatography analysis. Furthermore, scanning electron microscope analysis is also used in morphological characterization.

Degradation of Sodium Dodecyl Sulphate

Ibrahim and Abd Elsalam isolated four strains capable of degrading SDS from Taif wastewater in Saudi Arabia. One strain was identified as *P. otitidis*.[52] Chaturvedi and Kumar isolated 24 SDS-degrading strains from Varanasi, India. The isolated NN1 showed 97% homology with the *P. otitidis* strain RW1, which showed 98% homology with *P. otitidis* TNAU45. The degradation rate at 12h was 19.6% to 97.2%.[53] Jovčlć et al isolated a *P. otitidis* strain (*Pseudomonas sp.* ATCC19151). It was found that it contains a gene encoding sdsA, which is in-

volved in the degradation of SDS.[54] Ibrahim et al. isolated *P. otitidis* and *P. aeruginosa* that could degrade SDS and tried to mutate the strains by UV, ethidium bromide, and biological fixation methods. The degradation efficiency of SDS with alginate immobilized strains was higher than free microbial strains.[55]

Degradation of Organic Dyes

Organic dyes are the main pollution component in urban wastewater and industrial wastewater. Ingestion or exposure to dyes can irritate the respiratory, digestive, and nervous systems, leading to acute and chronic poisoning or disease, and in severe cases cancer. The microbial degradation method of dyes is a research focus at present. Many researchers have studied the ability of some strains of *P. otitidis* to remove stains. Wu Jing et al. used *P. otitidis* WL-13 isolated from the sludge of printing and dyeing wastewater treatment plants to degrade triphenylmethane dye in 2009. When the dye concentration is 500 μmol/L, the removal rate of malachite green and brilliant green can reach 95% when shaking cultured for 12 h, the crystal violet degraded 13% under the same conditions.[56] Jing et al. isolated a new dye decolorization strain, which was identified as *P. otitidis* and named CV-1. It can remove various triphenylmethane dyes and methyl red mono azo dyes.[57] Shah et al. isolated a strain with the ability to decolorize triphenylmethane. The decolorization rate was 72%-96% within 24 h. The strain was *P. aeruginosa* ETL-1, but the similarity between the strain and *P. otitidis* 81F reached 98%.[58] Figure 2 shows several common organic dye pollutants.[59−63]

Metal Settlement and Bioelectrochemistry

Bioelectrochemical system is a promising technology for the removal and recovery of metal ions from acid mine drainage wastewater.[64] The discharge of metal ions in water will lead to environmental pollution and human diseases, especially happen of cancer.[65] Martha et al. isolated mercury-resistant bacteria, including *P. otitidis* from Egyptian wastewater, whose mechanism of action may be related to the *merA* gene. It can reduce the soluble mercury ion to the precipitated monomer mercury. All tested strains contained plasmids encoding the *merA* gene.[66] Furthermore, Yeoh found that *P. otitidis* B1 was able to synthesize siderophores, which isolated iron from the environment.[67] Moreover, Ai et al. isolated *P. otitidis* E8 from a microbial fuel cell anode electroactive biofilm. It can effectively recover copper and cadmium ions from acid mine drainage wastewater when inoculated in a bioelectrochemical system.[68] Besides, Modestra and Mohan found that due to the difference in physical and chemical structure of the cell wall, the electron transfer characteristics of Gram-positive and Gram-negative bacteria may also vary.[69] In addition, Thulasinathan et al. isolated *Cronobacter sakazakii* and *P. otitidis* AATB4 from sewage and conducted a comparative study on the two bacteria
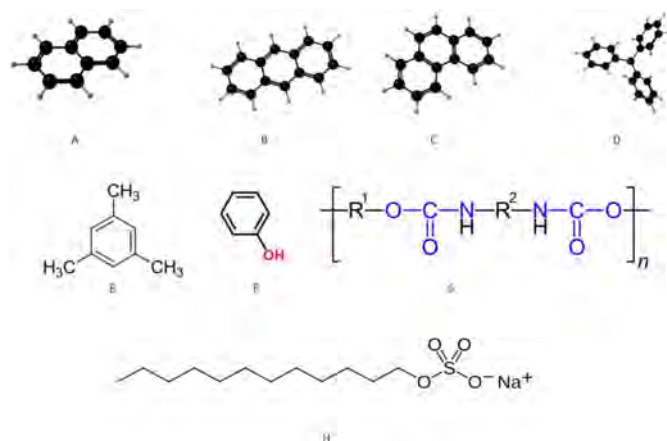
Figure 2. Organic dye pollutants that can be removed by *P. otitidis*. A is naphthaline, B is anthracene, and C is phenanthrene. Phenanthrene is a tricyclic aromatic hydrocarbon with a "bay" region and a "K" region. These two structures are closely related to the carcinogenicity of polycyclic aromatic hydrocarbons. A, B, and C belong to polycyclic aromatic hydrocarbons. Polycyclic aromatic hydrocarbons have toxic, mutagenic, and carcinogenic effects, as well as resistance to biological degradation. Oil spills and environmental pollution impact the food chain in the form of toxic organic materials such as polycyclic aromatic hydrocarbons, posing a major threat to ecosystems including marine life and human beings. Polycyclic aromatic hydrocarbons are potential threats to marine animals and human health because many of them can lead to cancer.[59] D is triphenylmethane. It can be divided into several different categories according to the substituents on the benzene ring. E is toluene. Toluene is an aromatic hydrocarbon that can cause serious social and health problems through the release of petroleum products and the spread of agricultural and industrial activities into the environment.[60] F is phenol, Phenol is an industrial organic compound that can cause gastrointestinal damage and can cause respiratory irritation, and muscle tremor.[61,62] It is very harmful to aquatic ecosystems. Phenol and phenolic wastes must be properly treated before they can be released into nature. G is a polyurethane (PU). Polyurethane is a carbamate polymer. It produces irritating gases at high temperatures. H is sodium dodecyl sulfate (SDS). It is the main raw material of detergent products, with decontamination, emulsification, and excellent foaming power. It is a kind of anionic surface-active agent with certain toxicity to the human body and is a common pollutant in urban water sources.[63]
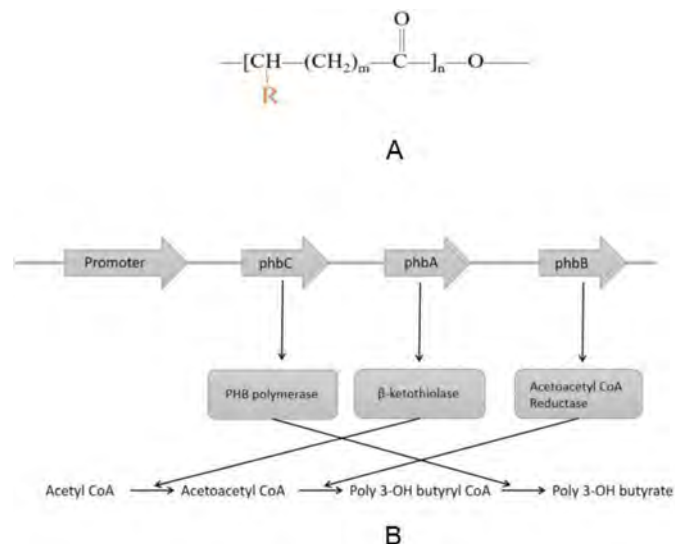

Figure 3. Chemical structure and microbial fermentation pathway of polyhydroxyalkanoates (PHA). A is the chemical structure of PHA. PHA is commonly composed of (R)-β-hydroxy fatty acids. The "R" group varies from methyl (C1) to tridecyl (C13). B is the microbial fermentation pathway of PHA. The promoter upstream of phbC transcribes the entire operon. The phbCAB operon's genes encode three enzymes (PHB polymerase, β-ketothiolase, and Acetoacetyl CoA reductase).[71] These three enzymes are involved in the synthesis of PHA. PHA is polyester produced in nature by numerous microorganisms. They can be either thermoplastic or elastomeric materials, with melting points ranging from 40°C to 180°C.[72] The mechanical properties and biocompatibility of PHA can also be changed by blending, modifying the surface, or combining PHA with other polymers and inorganic materials, making it possible for a wider range of applications. It has broad application prospects in the fields of medicine, agriculture, packaging, and electronics.[73]

and glucose-dehydrogenase 6-phosphate for PHA production in the metabolism of *P. otitidis* LFM046. Analysis revealed that the *gnd* gene, encoding 6-phosphogluconate dehydrogenase, is absent in the LFM046 genome. In LFM046, the *gnd* gene of *P. putidis* KT2440 (NAD+ dependent) and *Escherichia coli* MG1655 (NADP+ dependent) were expressed exogenous, which resulted in delayed cell growth and reduced PHA yield, respectively.[75]

The Synergy between *P. otitidis* and Plants

P. otitidis can promote plant growth and strain colony growth in some cases. Isolated *P. otitidis* and *Bacillus subtilis* strains from the rhizosphere soil of salt-tolerant plants in Pakistan could precipitate free calcium into calcium precipitation. Under salt stress, *P. otitidis* Rhizo SF7 in soil has the potential to produce acetyl-CoA carboxylase which promotes sunflower plant growth.[76] *P. otitidis* JYR27 is a rhizosphere growth bacterium resistant to phytophthora capsici and anthracnose. Researchers conducted three years of field experiments and confirmed that all selected strains significantly reduced pepper blight without affecting the rhizosphere microbial population.[77] *P. otitidis* and *P. alkaline* mixed bacteria were able to induce the expression of biofibril-related genes by corresponding to plant secretions, showing an antagonistic effect against the plant

used in microbial fuel cells for microbial power generation. *P. otitidis* AATB3 achieved the highest bioenergy (power density 280 mW/m^2, current density 800 mA/m^2), with a maximum coulomb efficiency of 15.5% at pH 7. The conclusion is that *P. otitidis* AATB4 can provide stable energy output as a novel biological battery.[70]

Generation of Polyhydroxyalkanoates

Some researchers have studied the production of PHA by *P. otitidis*. Figure 3 shows the structure and preparation process of the PHA.[71−73]

Reddy and Mohan studied the effects of medium selection and different nutrient concentrations on PHA production of *P. otitidis* isolated from sewage.[71] Some synergistic factors can improve PHA yield. An appropriate concentration of molybdenum can promote PHA production.[72,74] There is a negative correlation between enzyme specificity of coenzyme

pathogenic fungus *Rosellinia necatrix*. These two bacteria gathered, and one of their gene (*cmpA*) encodes a GGDEF/EAL domain protein. CmpA plays a role in biofilm formation, and the EAL domain is involved in this function.[78]

Antimicrobial Activity

Some researchers have studied the antagonistic effect of *P. otitidis* on microorganisms under various culture conditions. *P. otitidis* shows a resisting effect on *Naegleria fowleri* through competitive inhibition. The anti-*N. fowleri* activity of *P. otitidis* remains to be further studied.[79] Ahn studied the antibiotic production by *P. otitidis* and action mode. The researchers extracted the antibiotic from *P. otitidis* using ethyl acetate, which produced an orange halo on agar. The activity of *P. otitidis* is germicidal by reactive oxygen species.[80] *P. otitidis* with activity against *Leishmaniasis* was isolated from the midgut of Lutzomyiaevansi, an insect vector of *Leishmaniasis*.[81] *P. otitidis* isolated from cow dung was proved to have nematicidal activity against *Caenorhabditis elegans*.[82] Chellaram and Praveen isolated *P. otitidis* in short-horned grasshopper. It has antagonistic effects on *Candida albicans* and *E. coli*.[83] *P. otitidis* KAF136 (MH393230) has been proven to be a strong probiotic in biosafety, pH resistance, gastric juice resistance, bile salt resistance, and hydrophobicity solvent resistance. It was proved to resist the growth of *Aeromonas hydrophila* in aquaculture.[84] Some protozoa that can be inhibited by *P. otitidis* are shown in Figure 4.[79,85−88]

Microbial Resistance

Microbial medicine resistance is a major problem in clinical medicine and public health, which leads to an increase in medical investment and the emergence of superbugs. Many researchers have studied the resistance of *P. otitidis*, and they found a new carbapenem-resistant gene in this novel *Pseudomonas* gene, which can transcript and translate a new MBL POM-1. MBL produced by *Pseudomonas* can cause many critical diseases, such as septicemia and pneumonia.[89]

Kaur et al. studied tap water from public toilets in Punjab, India, and isolated 25 strains of bacteria, including *P. otitidis*. Drug sensitivity test results showed that cefotaxime, zoltronam, furantoline, cefepime, ceftazidime, and amoxiclaff were mostly ineffective against multiple isolates, and most of them had multiple drug resistance.[90] Nordmann et al. studied the selection medium for screening carbapenem-resistant *Pseudomonas* genus, using the medium containing meropenem (2 mg/L) to screen carbapenem-resistant *Pseudomonas*. Clinical isolates of 29 meropenem-sensitive and 56 meropenem-nonsensitive Pseudomonas strains were evaluated, the latter showing multiple carbapenem-resistance mechanisms.[91] Suzuki et al. studied the penicillin-resistant PAM gene of *P. alkaline*, and the *blaPAM-1* of *P. alcaligenes* strain MRY13-0052 was en-

coded in contig 73 in the chromosome without transposons or integrons around it. The results showed that *blaPAM-1* was a species-specific MBL coding gene inherent in *P. alcaligenes*. Researchers proposed that POM-1, an enzyme in *P. otitidis* is highly conservative.[92] Borgianni et al. systematically studied the biochemical characteristics of POM-1 metallo-β-lactamase from *P. otitidis*.[93]

Some researchers isolated carbapenemase-producing Gram-negative bacilli from American factories and nearby wastewater and identified 13 isolates as *P. otitidis* by the MALDI-TOF method.[94] Miyazaki et al. sequenced the whole genome of *P. otitidis* isolated from Lake Biwa, Japan, they also found a gene coding for POM, its amino acid sequence 99% identity to a similar protein found before.[19] Vieira et al. isolated meropenem-insensitive *P. otitidis* from chicken carcasses and conducted in-depth genomic characterization of the bacterium.[95] The *blaPOM-1* gene carried by *P. otitidis* K_25 encodes a MBL that is resistant to carbapenems. *P. otitidis* is the first pathogenic *Pseudomonas* to be demonstrated to constitutively express MBL and not require inducing MBL coding genes.[95] Carbapenem-resistant *P. otitidis* can be isolated from frozen food. Overexpression of the MBL coding *blaPOM-1* and *ttgABC* in *P. otitidis* is also associated with carbapenem resistance in these organisms.[96] Thaller et al. collected 20 strains of *P. otitidis* and studied the sensitivity of the metallo-β-lactams and MBL production. All strains were sensitive to piperacillin, cefotaxime, ceftazidime, and zoltronam, and occasionally showed sensitivity to carbapenems decreasing. All strains expressed MBL activity and carried a new B3 subclass MBL gene blaPOM, which was highly conserved in this species.[97] Poirel et al. studied B2 MBL, it's a PFM-like enzyme, produced by *Pseudomonas fluorescein*. It is different from B3 MBL produced by *P. otitidis*, which is *P. otitidis*' inherent MBL coding gene.[98] The prevalence and diversity of MBL coding gene containing integrons in MBL producing *Pseudomonas sp*. have been studied. Researchers investigated alleles associated with drug resistance, and analysis of blavim-2 and BLaiMP-1 alleles showed that all *Pseudomonas*, including *P. otitidis*, had BLaiMP-6.[99] Martins et al. discovered that some birds were colonized by *P. otitidis* who have *bla*POM-1 gene that encodes MBL.[100] Kim et al. isolated *P. otitidis* that produced POM-1 MBL from patients with necrotizing fasciitis and peritonitis. They made sure the important feature of *P. otitidis* is the inherent MBL coding gene *bla*POM-1.[25] Although *blaPOM-1* was inherent to the species, only 10% and 35% of isolates were resistant to imipenem and meropenem. Interestingly, the carbapenem-insensitive strains are always sensitive to piperacillin, ceftazidime, or aztreonam. This may be because the catalytic efficiency of POM-1 against carbapenems is higher than that of piperacillin.[93] Some researchers isolated 122 carbapenemase-producing bacterial strains and studied two *P. otitidis* strains' POM-1 coding gene, they confirmed that carbapenase could be produced without induction.[101]
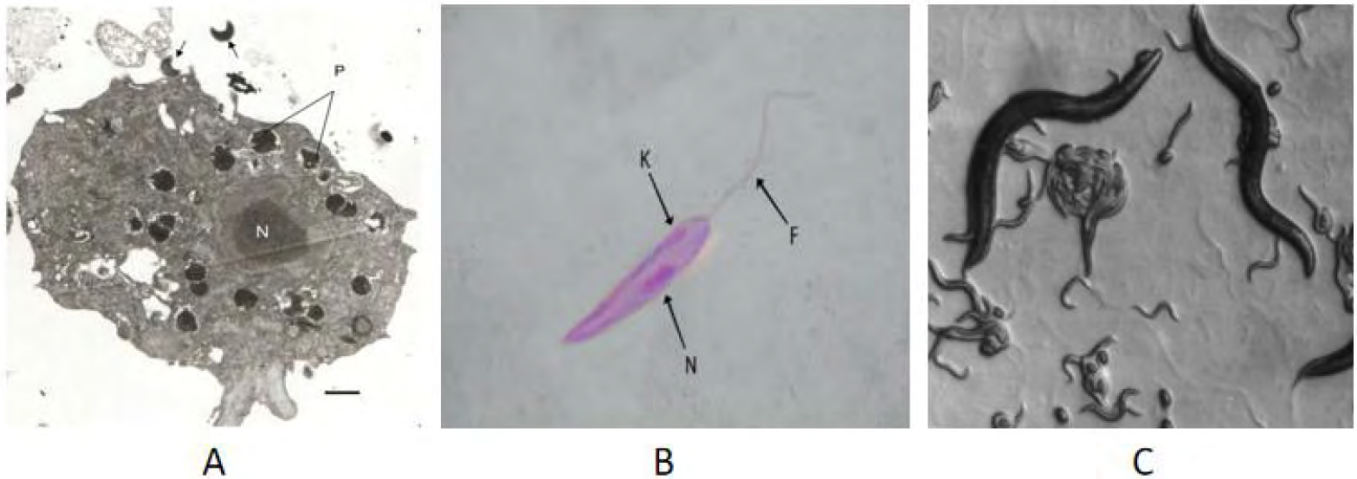
Figure 4. The comparison of three different protozoa from literature. Section A is *Naegleria fowleri*,[85] *Naegleria fowleri* can cause fatal primary amebic meningoencephalitis (PAM) in humans.[79] Section B Promastigote form of *Leishmania sp*. (N-nucleus, K-kinetoplast, F-flagellum),[86] *Leishmaniasis* is a disease caused by the bite of lutzomyia or termites. It can cause host infections in humans, rodents, and dogs.[87] Section C is *Caenorhabditis elegans*. *Caenorhabditis elegans* is a free-living nematode with relatively simple behaviors and structures. A complete life cycle takes three days. The organism is transparent throughout its life cycle, observing its structure and biological processes possible by microscopy.[88]

Usage in Farm

Researchers have studied the use of *P. otitidis* in agriculture and husbandry, such as herbicide resistance or the production of various digestive enzymes. Some researchers used herbicides as a carbon source to isolate *Pseudomonas* from three soil types cultivated corn and cucumber. It was proved that *P. otitidis* could improve soil contaminated with herbicides.[102] Lipase is a carboxyl ester hydrolase that hydrolyses triglycerides into glycerol and fatty acids. It is widely used in the food and feed processing industry. Shaini and Jayasree isolated fat-degraded bacteria WCS1C2 and WCS3C2 from compost. WCS3C2 strain had 91% homology with *P. otitidis*. And, it had a good ability to degrade fat.[103] Ramani et al. isolated a *P. otitidis* strain from sunflower seed oil waste and found that it could produce lipase and hydrolyze sunflower seed oil.[104] Fibriana et al. proposed that the biotransformation of oil-based wastes from the agricultural industry by the production of lipase in the form of solid-state fermentation or submerged fermentation would play a potential role in future biotechnology.[105] Kumar and Vyas isolated one *P. otitidis* strain that showed cellulase activity on the screening medium of carboxymethyl cellulose (CMC).[106] Huang et al studied the degradation of feather powder by isolated *P. otitidis* H11. Feather powder contains a large amount of keratin, which is difficult to hydrolysed by normal proteases to produce oligopeptides. The researchers found that under the optimized fermentation conditions, the feathers were almost completely degraded by *P. otitidis* H11. This kind of hydrolysate can be used as a supplement to feeds and as a source of extraction of functional oligopeptides.[107] Fatoni and Zusfahair isolated a thermophilic protease-producing strain *P. otitidis* WN1 from a hot spring in Indonesia. The protease was separated and partially purified.[108] Protease is one of the most important enzymes used in husbandry and industry. Compared with plant or animal tissues, microorganisms are the most studied source of proteases.[109]

Usage in Healthcare

Zearalenone is a non-steroidal estrogenic mycotoxin produced by a variety of *Fusarium* species, which can cause estrogen increase and related poisoning in livestock and humans.[110] Tan et al. isolated a strain of *P. otitidis* TH-N1 that could degrade zearalenone from the rumen of cattle and evaluated its isolation effect.[111] Uricase is an enzyme that can make uric acid oxidize rapidly, prevent uric acid from being absorbed and excreted by renal tubules, and has ameliorative effects on nodular ventilation, urinary calculus, and hyperuricemia caused by renal failure.[112] Lee et al. isolated a *P. otitidis* SN4 strain and studied the isolation, partial purification, and enzymatic properties of its product, a 33 kDa uricase.[113] Melanin has found great application in various industries due to its unique antioxidant properties.[114] Because of the increasing demand for melanin, scientific researchers are working to find more microbes that have the potential to produce melanin on a large scale. Deepthi et al. studied melanin produced by *P. otitidis* and compared the relevant tyrosinase gene sequences.[115] L-asparaginase is a very important antitumor drug widely used in the treatment of acute lymphoblastic leukemia and other malignant tumors. L-asparagine is a non-essential amino acid, which is an important nutrient for cancer cells. L-asparaginase can be used as an anticancer agent due to its high chemical efficiency in converting asparagine to ammonia and aspartic acid.[116] In the food industry, harmful by-product glutamine may be produced during the fermentation of L-asparaginase. The avoidance of glutamine production is one of the areas of current research.[117]

Shi et al. studied a pH 7.5 L-asparaginase produced by *P. otitidis*. Before this, many rhizobia genes that encode L-asparaginase have been submitted to the NCBI database. Their research is the first *P. otitidis* that can encode the L-asparaginase coding gene (*AnsA*).[118] L-asparaginase is divided into two subtypes, L-asparaginase EI and II, according to its localization in cells.[119] The enzymatic activity of L-asparaginase obtained by fermentation of *P. otitidis* could reach 0.37 IU/ mL.[120] The maximum molecular weight of L-asparaginase produced by *P. otitidis* was 205±3 kDa.[121] The enzyme is a homologous hexamer, and the isoelectric point of the enzyme was 5.5. Purified asparaginase is non-toxic to non-cancerous FR-2 cells or human blood lymphocytes but can induce apoptosis of human leukemia MOLT-4 cells.[122]

PRODUCTS AND MECHANISMS

blaPOM-1 Gene and its Product POM-1 Metallo-β-lactamase

MBL is an enzyme that can change the spatial structure of lactam antibiotics.[123] It belongs to group 3 according to bush classification,[124] while belongs to B group according to Ambler classification.[125] The most characteristic of this enzyme group is that it can hydrolyze carbapenems and other similar antibiotics. It can bind to the β-lactam rings, causing the β-lactam ring cleavage and destruction.[126] MBL had little effect on piperacillin and amtronam. Its activity was not inhibited by clavulanic acid and other β-lactamase inhibitors, but it was inhibited by EDTA.[127] Its enzyme activity center requires the participation of metal zinc ions, so it is called MBL.[123] Carbapenems, a kind of β-lactam antibiotic, are considered the last resort for the treatment of infections caused by multidrug-resistant pathogens.[128]

The β-lactam antibiotics refer to a class of antibiotics with β-lactam ring in the chemical structure, including penicillin and cephalosporin, which are the most used in clinics, as well as other atypical β-lactam antibiotics. These antibiotics have the advantages of strong bactericidal activity, low toxicity, wide indications, and good clinical efficacy.[129] Changes in the chemical structure of this class of antibiotics especially the side chain, lead to many different antimicrobial profiles and actions, as well as a variety of clinical pharmacological properties.[130] Most kinds of β-lactam antibiotics have similar mechanisms of action. All of them can inhibit the cell wall mucin synthase, which is penicillin-binding proteins (PBPs), and thus hinder the synthesis of cell wall mucin, resulting in cell wall defect and cell swelling and cleavage. In addition, the lethal effect on bacteria should include triggering the activity of the bacteria's autolysin, so the mutant lacking autolysin shows drug resistance.[131] Humans and animals have no cell wall, not affected by β-lactam medicines, so this class of drugs has selective bactericidal effects on bacteria with low toxicity to the host.[123] The special

PBPs on bacterial cell membranes are the target of β-lactam. The number, molecular weight, and sensitivity of PBPs to β-lactam antibiotics were different, but taxonomically similar bacteria have similar PBPs types and physiological functions.[131] *E. coli*, for example, has seven PBPs. PBP1A and PBP1B are associated with bacterial lengthening, while PBP2 is associated with membrane tube shape. PBP3 has the same function as PBP1A, but its quantity is small, and it is related to bacterial division. Most penicillin or cephalosporin antibiotics are mainly combined with PBP1 and/or PBP3 to form filamentous and spherical bodies, which cause deformation and atrophy of bacteria and gradually dissolve and die. PBP4, 5, and 6 are related to the activity of carboxypeptidase and have no importance to the survival and reproduction of bacteria.[132]

The genes that produce MBL can be divided into two types according to their level of activity. One is a mobile genetic element carried by plasmids that can move between different bacteria in the same ecological environment.[133–135] Most of the MBL coding genes they expressed were from shuttle plasmids. Some researchers pointed out that some pathogenic genes come from bacteriophages, which do not integrate into chromosomes when they infect bacteria but produce plasmid derivatives that can travel between individuals of different bacteria.[136] Another kind of gene that produces MBL is so conserved that it exists only in one species and cannot move between species or bacteria.[137]

Common resistance mechanisms of *Pseudomonas* include overexpression of the efflux system and AmpC B-lactamase, as well as mutation inactivation of OprD.[138] To date, *P. otitidis* is known to be associated with the endogenous MBL-POM.[139] Studies have shown that *P. otitidis* contains a *blaPOM-1* gene, which can be transcribed and translated into POM-1 enzyme, which is a B3 subgroup MBL. Some scholars have also found that the gene can be expressed without induction. POM is a tetramerase with broad substrate specificity and has higher catalytic activity against penicillin and carbapenems than cephalosporins.[97]

Thaller et al. cloned the POM gene from *P. otitidis*, and the clone producing MBL was named CT-1, carrying about 6 KB of DNA. Sequencing of the inserted fragment revealed the presence of an 859 bp open reading frame (ORF) encoding a protein like B3 subclass MBLs. It was named POM1 (named after *P. otitidis* MBL). The ORF begins with a GTG codon, preceded by an identifiable ribosomal binding site and a putative promoter region.[97] POM-1 enzyme showed the closest similarity to *Stenotrophomonas maltophilia* L1 enzyme (60%-64%), and it has low similarity with other B3 subclass enzymes.[140]

Some researchers sequenced and analyzed the upstream and downstream of the POM gene of *P. otitidis* and found that the region on it was an open reading frame for predicting the production of histamine kinase. Through gene comparison, it was found to be homologous with the PA_2882 pro-

tein gene of *P. aeruginosa*.[141] Downstream of BLAPom-1 is a phosphonate-capable operon protein homologous to *sel*D that is highly conserved.[97] Phylogenesis sketch of subclass B3 MBL enzymes and *bla*POM-1 gene are shown in Figure 5.

Mechanism of Biosurfactant Formation

Biosurfactant is a secondary metabolite synthesized by various bacteria, yeast, and filamentous fungi. It not only has the physicochemical properties of the chemical synthesis of surfactants, but also has the advantages of being non-toxic, biodegradable, and so on. It has a very broad application prospect.[142] Biosurfactant interferes with microbe-host interactions and quorum sensing mechanisms, acting as antimicrobial, insecticidal, antibiofilm, and anti-adhesive agents. Dinache et al. and Myers described the structure and principle of BS.[143,144] The molecular structure of surfactants is amphiphilic: one end is the hydrophilic group; the other end is the hydrophobic (lipophilic) group. Hydrophilic groups are often polar groups, such as carboxylic acid, sulfonic acid, sulfuric acid, amino or amine groups and their salts, hydroxyl, amide group, an ether bond, etc., it can also be used as polar hydrophilic groups. Hydrophobic groups are usually non-polar hydrocarbon chains, such as hydrocarbon chains with more than 8 carbon atoms.[144] BS produced by *P. otitidis* P4 was mainly composed of lipids and carbohydrates. The carbohydrate content was 386.25 µg/mL, and the lipid content was 0.381 mg/g.[51]

Emulsification is one of the main functions of biosurfactants produced by *P. otitidis*, as well as other kinds of biosurfactants. Emulsification refers to the uniform dispersion of one liquid in extremely small droplets in an insoluble liquid. Two insoluble liquids, such as oil and water, are divided into two layers in a container, the less dense oil on the upper layer and the denser water on the lower. If the appropriate surfactant is added under intense agitation, the oil is dispersed in water and forms an emulsion, which is called emulsification.[145] Some researchers have studied the emulsifier formed by *P. otitidis*. The formation of an emulsion is a stable interaction of hydrophobic and hydrophilic phases, largely depending on the solvent used. The biosurfactant formed by *P. otitidis* is an ideal emulsifier in a stable state.[142] Some researchers studied the emulsification of BS produced by *P. otitidis*. Diesel oil and kerosene (55%) were the most effective substrates for emulsification, while sunflower oil (45%) was the matrix with low emulsification efficiency.[146] The results show that the biosurfactants of *P. otitidis* can emulsify different types of hydrocarbon compounds and can improve the utilization rate of insoluble hydrocarbon compounds.

Researchers used different methods to detect surfactants. Ctab-methylene blue agar test is a simple method to detect anionic surfactants. Researchers found isolated *P. otitidis* strain P4 reacted positively on CTAB-methylene blue agar medium, after incubation at 37 ℃ for 48 h. A blue halo appeared around the colony.[51] The relative hydrophobicity of the bacterial surface was measured by the bacterial adhesion to the hydrocarbons method. The results showed that the hydrophobicity of the bacterial surface was up to 69.3% used crude oil for growth.[147]

Submerged fermentation of surfactant-producing *P. otitidis* was carried out to study the amount of biosurfactant produced at different fermentation stages, from the late exponential period to the end of the stationary period.[148] Ron and Rosenberg have also reported that biosurfactants are typically produced during both logarithmic and stationary phases, and that release of cell-bound surfactants into the growth medium results in a reduction in surface tension, even after the stationary phase.[149] The BS produced by *P. otitidis* P4 showed good surface tension reduction ability, reducing the surface tension of the medium from 71.18 mN/m to 33.4 mN/m.[51] This result is comparable to reports of BS production by *P. aeruginosa*.[150,151]

Different carbon and nitrogen sources have important effects on the production of biosurfactants in *P. otitidis*. The preference of microbial carbon sources for biosurfactant production depends on the strain. Different strains produce biosurfactants in different carbon sources, which may be water-soluble or insoluble substances.[152] In *P. otitidis* P4, 2% Sodium acetate was the most effective carbon source, and yeast extract (0.03%) was the most effective nitrogen source to produce biosurfactant. The growth and formation of biosurfactants were not observed in the medium without nitro.[51] *P. otitidis* cannot use ammonium ions to produce biosurfactants under certain nutritional conditions. Maneerat reported that when nitrogen concentration in the medium is depleted, the yield of surface-active compounds increases due to the decreased activity of isocitrate dehydrogenase.[153] Isocitrate dehydrogenase is catalyzed by nicotinamide adenine dinucleotide (NAD) and nicotinamide adenine dinucleotide phosphate (NADP) for the oxidation of isocitrate to 2-oxygen glutaric acid in the citric acid cycle. As isocitrate dehydrogenase activity declines, isocitrate and citrate begin to accumulate. In the cytoplasm, citric acid synthase converts citric acid to oxaloacetate and acetyl-coA, which act as a processor for fatty acid synthesis, thereby increasing biosurfactant production.[154]

Some researchers have found that the biosurfactant produced by *P. otitidis* is heat resistant because heating at 80-100 °C has no significant effect on surface tension and emulsifying activity.[51] However, the surfactants produced by *P. otitidis* are not adapted to all environments. Any decrease or increase in emulsifying activity at extreme temperatures may be due to some structural changes in surfactant molecules.[155] The surface tension and emulsifying activity of biosurfactants remain stable over a wide pH range (3-11).[156] The highest emulsifying activity (68.7%) was observed at neutral pH (pH=7), but significant stable emulsifying activity was also observed at acidic pH (pH=3, 44.4%) and alkaline pH (pH=11, 54.5%). The decrease in emulsification under extreme pH conditions may be due to partial precipitation of biosurfactants.[146] Biosurfactants
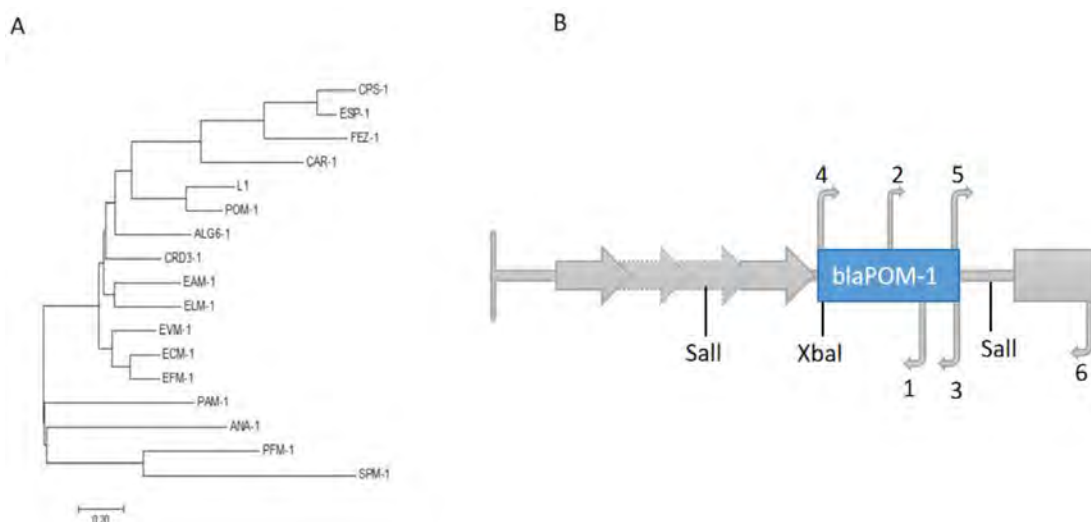
Figure 5. Phylogenesis sketch of subclass B3 MBL enzymes and *blaPOM-1* gene. A is a Phylogenesis sketch of subclass B3 MBL enzymes. The closest match to POM-1 is L1 from *Stenotrophomonas maltophilia*, their similarity is 60%-64%. B is Genetic context of *blaPOM-1*. Numbered arrows show the location of primers used for PCR amplification (Section B): 1, Pom-seq/F; 2, Pom-seq/R; 3, POTSEQ/F; 4, POM948/R; 5, CT1ft/F; 6, CT1Prom/R.[97]

can withstand 2.0% to 10.0% salt concentrations, with maximum emulsifying activity observed at 4% NaCl. Helvaci et al. explained the reasons for stable surface tension at extreme salt concentrations.[157] They describe the presence of electrolytes in the culture medium that directly affects the carboxylic groups of sugar lipids. At alkaline pH, there is a net negative charge in the solution due to the ionization of the carboxylic group. In the presence of NaCl, Na^+ ions shield negative charges in a double electric layer, resulting in the formation of a tightly packed monolayer, followed by a decrease in surface tension. In brief, stability studies showed that biosurfactants remain active at extreme temperatures, pH, and salt concentrations. What needs to be pointed out is that hemolysis, drop-collapse, oil spreading, E_{24}, BATH, and surface tension methods are used to screen the presence of biosurfactants.

CONCLUSION

Pseudomonas sp. is a widely studied bacterial species. It is a new type of *Pseudomonas sp.*, which was first discovered in 2002 and was systematically studied by researchers after 2006. *P. otitidis* can be isolated from the infected site of a patient. It is pathogenic and can cause a single infection or a mixture of multiple infections. *P. otitidis* can also be isolated from natural environments, such as lakes, sludge, and contaminated environments. Research showed that *P. otitidis* can be used and decompose many substances and pollutants that exist in nature, such as crude oil, polycyclic aromatic hydrocarbons, dyes, SDS, and zearalenone. *P. otitidis* can also produce some beneficial substances that can be used, such as digestive enzymes, antibiotic substances, melanin, L-asparaginase, and so on. The unique POM MBL of *P. otitidis* has received much attention. Compared with common plasmid DNA, the POM coding gene

is a conserved intrinsic gene. Functionally, it can decompose Carbapenem antibiotics such as meropenem, leading to the generation of super-resistant bacteria. *Pseudomonas*, including textit*P. otitidis*, can produce a large sum of biofilms. Like other bacteria, *P. otitidis* sticks to material surfaces and secretes many extracellular polymers (glycolipids) that form biofilms. Biofilm can support and protect the whole microflora in a certain area. There is also research on the synergistic effect of plants, the research on biological batteries, and the research on the production of degradable plastic PHA by *Pseudomonas*. Due to the late discovery of *P. otitidis* and the fact that *P. otitidis* is easily confused with other bacteria in species identification, some research fields on *P. otitidis* are not in-depth at present. There are many aspects of genomics, enzymology mechanisms, and clinical research worthy of further investigation. By now, the research on *P. otitidis* is still producing new results and interesting findings continuously as this strain could offer increasing benefits to humans.

ORCID IDs of the authors

Gao Jianfeng	0000-0002-7393-6884
Rosfarizan Mohamad	0000-0001-5672-1905
Murni Halim	0000-0002-5744-2147
Mohd Shamzi Mohamed	0000-0002-9813-2161

REFERENCES

1. Palleroni NJ, Genus I. *Pseudomonas Migula* In Bergey's Manual of Systematic Bacteriology. *Springer*. 1984; 141-199.

2. Palleroni NJ, Kunisawa R, Contopoulou R, Doudoroff M. Nucleic acid homologies in the genus *Pseudomonas. Int J Syst Evol Microbiol*. 1973;23(4):333-339.

3. Kersters K, Ludwig W, Vancanneyt M, De Vos P, Gillis M, Schleifer KH. Recent changes in the classification of the *Pseudomonads*: An overview. *Syst Appl Microbiol*. 1996;19(4):465-477.

4. Romaniuk K, Krucon T, Decewicz P, Gorecki A, Dziewit L. Molecular characterization of the pA3J1 plasmid from the psychrotolerant antarctic bacterium *Pseudomonas sp*. ANT_J3. *Plasmid*. 2017;1(92):49-56.

5. Passarelli-Araujo H, Franco GR, Venancio TM. Network analysis of ten thousand genomes shed light on *Pseudomonas* diversity and classification. *Microbiol Res*. 2022;1(254):126919. doi:10.1016/j.micres.2021.126919

6. Campbell RA, Farlow J, Freyberger HR, et al. Genome Sequences of 17 Diverse *Pseudomonas aeruginosa* phages. *Microbiol Resour Announc*. 2021;10(9):e0003121. doi:10.1128/MRA.00031-21

7. Sundararajaperumal A, Murugan N, Karthick R, Harikrishnan S. Profile of pulmonary infections in renal transplant patients. *J Evid Based Med*. 2018;5(3):260-264.

8. Hillman KM, Twigley A. Aerosol EDTA to eliminate respiratory-tract *Pseudomonas. Lancet*. 1984;324(8394): 99. doi:10.1016/s0140-6736(84)90265-4

9. Beasley KL, Cristy SA, Elmassry MM, et al. During bacteremia, *Pseudomonas aeruginosa* PAO1 adapts by altering the expression of numerous virulence genes including those involved in quorum sensing. *PloS one*. 2020;15(10):e0240351. doi:10.1371/journal.pone.0240351

10. Kalpana Thalava, Vigila J. Urinary infections in pregnancy conditions. *J Pharm Res Int*. 2021;2(17):22-28.

11. Lee K, Kim CK, Yong D, et al. POM-1 metallo-β-lactamase–producing *Pseudomonas otitidis* isolate from a patient with chronic otitis media. *Diagn Microbiol Infect Dis*. 2012;72(3): 295-296.

12. Poirel L, Palmieri M, Brilhante M, Masseron A, Perreten V, Nordmann P. PFM-like enzymes are a novel family of subclass B2 metallo-β-lactamases from *Pseudomonas synxantha* belonging to the *Pseudomonas fluorescens* complex. *Antimicrob Agents Chemother*. 2020;64(2):1700-1719.

13. Silveira MC, Albano RM, Rocha-de-Souza CM, et al. Description of a novel IncP plasmid harboring blaKPC-2 recovered from a SPM-1-producing *Pseudomonas aeruginosa* from ST277. *Infect Genet Evol*. 2022;102:105302. doi:10.1016/j.meegid.2022.105302

14. Lalucat J, Gomila M, Mulet M, Zaruma A, García-Valdés E. Past, present and future of the boundaries of the *Pseudomonas* genus: Proposal of Stutzerimonas gen. Nov. *Syst Appl Microbiol*. 2022;45(1):126289. doi:10.1016/j.syapm.2021.126289

15. Olsen RH, Metcalf ES, Todd JK. Characteristics of bacteriophages attacking psychrophilic and mesophilic *Pseudomonas. J Virol*. 1968;2(4):357-364.

16. Chakrabarty AM. Gunsalus IC. Autonomous replication of a defective transducing phage in *Pseudomonas putida. Virol*. 1969;38(1):92-104.

17. Cornelis, P Ed. *Pseudomonas*: Genomics and molecular biology. *Horizon Scientific Press*; 2008.

18. Anzai Y, Kim H, Park JY, Wakabayashi H, Oyaizu H. Phylogenetic affiliation of the *Pseudomonas* based on 16S rRNA sequence. *Int J Syst Evol Microbiol*. 2000;50(4):1563-1589.

19. Miyazaki K, Hase E, Maruya T. Complete genome sequence of *Pseudomonas otitidis* Strain MrB4, isolated from Lake Biwa in Japan. *Microbiol Resour Announc*. 2020;9(16):e00148-20. doi:10.1128/MRA.00148-20

20. Abed, Wu H, Kareem SM. Molecular detection of *gyrA* and *mexA* genes in Pseudomonas aeruginosa. *Mol Biol Rep*. 2021;48(12):7907-7912.

21. Manivannan B, Mahalingam N, Jadhao S, Mishra A, Nilawe P, Pradeep BE. Draft genome sequence of a clinically isolated extensively drug-resistant *Pseudomonas aeruginosa* strain. *Genome Announc*. 2016;4(2):2-16.

22. Kačániová M, Klūga A, Kántor A, et al. Comparison of MALDI-TOF MS Biotyper and 16S rDNA sequencing for the identification of *Pseudomonas* species isolated from fish. *Microb Pathog*. 2019;132:313-318.

23. Roland PS, Stroman DW. Microbiology of acute otitis externa. *The Laryngoscope*. 2002;112(7):1166-1177.

24. Clark LL, Dajcs JJ, McLean CH, Bartell JG, Stroman DW. *Pseudomonas otitidis sp*. nov., isolated from patients with otic infections. *Int J Syst Evol Microbiol*. 2006;56(4):709-714.

25. Kim D, Hong SK, Seo YH, et al. Two non-otic cases of POM-1 metallo-β-lactamase-producing *Pseudomonas otitidis* infection: Necrotizing fasciitis and pan-peritonitis. *J Glob Antimicrob Resist*. 2016;7:157-158.

26. Balasubramani G, Induja K, Aiswarya D, et al. Isolation and characterization of human foot crack–associated bacterium, *Pseudomonas otitidis*, and its biological propensity. *Smart Science*. 2019;7(2):79-90.

27. Yamada K, Aoki K, Nagasawa T, et al. Complete whole-genome sequence of the novel Pseudomonas species strain TUM18999, isolated from a patient with a burn wound in Japan. *J Glob Antimicrob Resist*. 2021;24:395-397.

28. Adriana LC, Alexandros NV, Ming C, Mats L. *Pseudomonas otitidis* bacteraemia in a patient with COPD and recurrent pneumonia: Case report and literature review. *BMC Infect Dis*. 2021;21:868. doi:10.1186/s12879-021-06569-8

29. García-Ulloa M. II, Souza V, Olmedo-Álvarez G, Eguiarte LE. Can bacterial populations go extinct? Evolutionary biology and bacterial studies in Cuatro Ciénegas shed light on the extinction process. In *Conflicts Between Biodiversity Conservation and Humans*. 2022;143-162.

30. Reddy CSK, Ghai R, Kalia V. Polyhydroxyalkanoates: An overview. *Bioresour Technol*. 2003;87(2):137-146.

31. García-Ulloa MI, Escalante AE, Moreno-Letelier A, Eguiarte LE, Souza V. Evolutionary rescue of an environmental *Pseudomonas otitidis* in response to anthropogenic perturbation. *Front Microbiol*. 2021;11:563885. doi:10.3389/fmicb.2020.563885

32. Rodríguez-Verdugo A, Souza V, Eguiarte LE, Escalante AE. Diversity across seasons of culturable *Pseudomonas* from a Des-

iccation Lagoon in Cuatro Cienegas, Mexico. *Int J Microbiol.* 2012;201389. doi:10.1155/2012/201389

33. Jun SR, Wassenaar TM, Nookaew I, et al. Diversity of Pseudomonas genomes, including populus-associated isolates, as revealed by comparative genome analysis. *Appl Environ Microbiol.* 2015;82(1):375-383. doi:10.1128/AEM.02612-15

34. Dahiya S, Mohan SV. Strategic design of synthetic consortium with embedded wastewater treatment potential: Deciphering the competence of isolates from diverse microbiome. *Front Environ Sci.* 2016; 4:30. https://doi.org/10.3389/fenvs.2016.00030

35. Dasgupta D, Ghosh R, Sengupta TK. Biofilm-mediated enhanced crude oil degradation by newly isolated *Pseudomonas* species. *ISRN Biotechnol.* 2013;2013:250749. doi:10.5402/2013/250749

36. Gogoi B, Das I, Gogoi M, Charingia D, Bandyopadhyay T, Borah D. Bioremediation of motor oil-contaminated soil and water by a novel indigenous *Pseudomonas otitidis* strain DU13 and characterization of its biosurfactant. *3 Biotech.* 2022;3(12):68. doi:10.1007/s13205-022-03133-2

37. Peng YH, Shih YH, Lai YC, Liu YZ, Liu YT, Lin NC. Degradation of polyurethane by bacterium isolated from soil and assessment of polyurethanolytic activity of a *Pseudomonas putida* strain. *Environ Sci Pollut Res Int.* 2014;21(16):9529-9537.

38. Bestawy EE, El-Shatby BF, Eltaweil AS. Integration between bacterial consortium and magnetite (Fe3O4) nanoparticles for the treatment of oily industrial wastewater. *World J Microbiol Biotechnol.* 2020;36(9):141. doi:10.1007/s11274-020-02915-1

39. Mohammadi F, Sepahy A, Naghavi N, Salehi M. Removal of phenolic compounds from Spent caustic wastewater by the isolated and detected *Pseudomonas otitidis. Adv Biores.* 2017; 8(5):123-129. doi: 10.15515/abr.0976-4585.8.5.123129

40. Maitra S, Maity D, Kundu P, Adhikarinee S. Isolation and identification of a bacterial strain from soil for bioremediation of phenol for pollution control. *J Indian Chem Soc.*2020;97(4):607-612.

41. Mohanty SS, Jena HM. Biodegradation of phenol by free and immobilized cells of a novel *Pseudomonas* sp. NBM11. *Braz J Chem Eng.* 2017;34:75-84.

42. Poyraz N. Isolation of novel toluene degrading bacteria from waste water treatment plants and determination of their toluene tolerance and other biotechnological potential. *Pol J Environ Stud.* 2021;30(1):811-821.

43. Dados A, Omirou M, Demetriou K, Papastephanou C, Ioannides IM. Rapid remediation of soil heavily contaminated with hydrocarbons: A comparison of different approaches. *Ann Microbiol.* 2015;65(1):241-251.

44. Anwar MS, Kapri A, Chaudhry V, et al. Response of indigenously developed bacterial consortia in progressive degradation of polyvinyl chloride. *Protoplasma.* 2016;253(4):1023-1032.

45. Xu CB, Wang WY, Li XZ. Identification and characteristics of a phenanthrene degrading bacterium. *Acta Sci.* 2015;35(3):684-691.

46. Soberón-Chávez G, Lépine F, Déziel E. Production of rhamnolipids by *Pseudomonas aeruginosa. Appl Microbiol Biotechnol.* 2005;68(6):718-725.

47. Soberón-Chávez G, Maier RM. Biosurfactants: A general overview. *Biosurfactants.* 2011;1-11.

48. Holland PM, Rubingh DN. Mixed surfactant systems: An overview, 1992. doi:10.1021/bk-1992-0501.ch001

49. Haloi S, Sarmah S, Gogoi SB, Medhi T. Characterization of Pseudomonas sp. TMB2 produced rhamnolipids for ex-situ microbial enhanced oil recovery. *3 Biotech.* 2020;10(3):1-17.

50. Buonocore C, Tedesco P, Vitale GA, et al. Characterization of a new mixture of mono-rhamnolipids produced by *Pseudomonas gessardii* isolated from Edmonson Point (Antarctica). *Mar Drugs.* 2020;18(5): 269. doi:10.3390/md18050269

51. Singh P, Tiwary BN. Isolation and characterization of glycolipid biosurfactant produced by a *Pseudomonas otitidis* strain isolated from Chirimiri coal mines, India. *Bioresour Bioprocess.* 2016;3(1):1-16.

52. Ibrahim AG, Abd Elsalam HE. Biodegradation of anionic surfactants (SDS) by bacteria isolated from waste water in Taif Governate. *Annu Res Rev Biol.* 2018;1-13. doi: 10.9734/ARRB/2018/41436

53. Chaturvedi V, Kumar A. Diversity of culturable sodium dodecyl sulfate (SDS) degrading bacteria isolated from detergent contaminated ponds situated in Varanasi city, India. *Int Biodeterior Biodegradation.* 2011;65(7):961-971.

54. Jovčić B, BegovIć JELENA, Lozo J, Topisirović LJ, Kojić M. Dynamics of sodium dodecyl sulfate utilization and antibiotic susceptibility of strain *Pseudomonas sp.* ATCC19151. *Arch Biol Sci.* 2009;61(2):159-164.

55. Ibrahim AG, Abd Elsalam HE. Enhancement the biodegradation of sodium dodecyl sulfate by *Pseudomonas aeruginosa* and *Pseudomonas otitidis* isolated from waste water in Saudi Arabia. *Annu Res Rev Biol.* 2018; 1-7. doi: 10.9734/arrb/2018/43744

56. Jing WU, Byung-Gil JU, Kyoung-Sook KI, Young-Choon LE, Nak-Chang SU. Isolation and characterization of *Pseudomonas otitidis* WL-13 and its capacity to decolorize triphenylmethane dyes. *J Environ Sci.* 2009;21(7):960-964.

57. Jing W, Kang NY, Kim KS, Sung NC, Lee YC. Isolation and characterization of *Pseudomonas otitidis* Strain CV-1 capable of decolorizing triphenylmethane dye. *In Proceedings of the Korean Society of Life Science Conference.* 2007; 108.

58. Shah MP, Patel KA, Nair SS, Darji AM. Environmental bioremediation of dyes by *Pseudomonas aeruginosa* ETL-1 isolated from final effluent treatment plant of ankleshwar. *Am J Microbiol Res.* 2013;1(4):74-83.

59. Gamboa-Loira B, López-Carrillo L, Mar-Sánchez Y, Stern D, Cebrián ME. Epidemiologic evidence of exposure to polycyclic aromatic hydrocarbons and breast cancer: A systematic review and meta-analysis. *Chemosphere.* 2022;290:133237. doi:10.1016/j.chemosphere.2021.133237

60. Benignus VA. Health effects of toluene: A review. *Neurotoxicology.* 1981;2(3): 567-588.

61. Buckley JP, Quirós-Alcalá L, Teitelbaum SL, Calafat AM, Wolff MS, Engel SM. Associations of prenatal environmental phenol and phthalate biomarkers with respiratory and allergic diseases among children aged 6 and 7 years. *Environ Int.* 2018;115:79-88.

62. Itoh M. The role of brain acetylcholine in phenol-induced tremor in mice. *Arch Oral Biol.* 1995;40(5):365-372.

63. Reynolds JA, Tanford C. The gross conformation of protein-sodium dodecyl sulfate complexes. *J Biol Chem.* 1970;245(19):5161-5165.

64. Sleutels TH, Ter Heijne A, Buisman CJ, Hamelers HV. Bioelectrochemical systems: An outlook for practical applications. *Chem Sus Chem.* 2012;5(6):1012-1019.

65. Carver A, Gallicchio VS. Heavy metals and cancer. In *Cancer Causing Substances.* 2018. doi:10.5772/intechopen.70348.

66. Naguib MM, Khairalla AS, El-Gendy AO, Elkhatib WF. Iso-

lation and characterization of mercury-resistant bacteria from wastewater sources in Egypt. *Can J Microbiol*. 2019;65(4):308-321.

67. Yeoh CC. Production, partial purification and characterization of yellow-green fluorescent siderophores produced by *Pseudomonas otitidis* B1, UTAR, Doctoral dissertation, 2014.

68. Ai C, Hou S, Yan Z, et al. Recovery of metals from acid mine drainage by bioelectrochemical system inoculated with a novel exoelectrogen, *Pseudomonas* sp. E8. *Microorganisms*. 2019;8(1):41. doi:10.3390/microorganisms8010041

69. Modestra, J.A. and Mohan, S.V. Bio-electrocatalyzed electron efflux in Gram-positive and Gram-negative bacteria: An insight into disparity in electron transfer kinetics. *RSC Adv*. 2014;4(64):34045-34055.

70. Thulasinathan B, Nainamohamed S, Samuel JO, et al. Comparative study on *Cronobacter sakazakii* and *Pseudomonas otitidis* isolated from septic tank wastewater in microbial fuel cell for bioelectricity generation. *Fuel*. 2019;248:47-55.

71. Reddy MV, Mohan SV. Effect of substrate load and nutrients concentration on the polyhydroxyalkanoates (PHA) production using mixed consortia through wastewater treatment. *Bioresour Technol*. 2012;114:573-582.

72. Reddy MV, Nikhil GN, Mohan SV, Swamy YV, Sarma PN. *Pseudomonas otitidis* as a potential biocatalyst for polyhydroxyalkanoates (PHA) synthesis using synthetic wastewater and acidogenic effluents. *Bioresour Technol*. 2012; 123 471-479.

73. Wang Y, Yin J, Chen GQ. Polyhydroxyalkanoates, challenges and opportunities. *Curr Opin Biotechnol*. 2014;30:59-65.

74. Venkateswar Reddy M, Chitanya DNSK, Nikhil GN, Venkata Mohan S, Sarma PN. Influence of Co-F actor on enhancement of bioplastic production through wastewater treatment. *Clean–Soil Air Water*. 2014;42(6):809-814. https://doi.org/10.1002/clen.201300105

75. Cardinali-Rezende J, Di Genova A, Nahat RA, et al. The relevance of enzyme specificity for coenzymes and the presence of 6-phosphogluconate dehydrogenase for polyhydroxyalkanoates production in the metabolism of *Pseudomonas sp*. LFM046. *Int J Biol Macromol*. 2020;163:240-250.

76. Idrees N, Liaqat I, Qurashi AW. *Pseudomonas otitidis* and *Bacillus subtilis* from saline soil of Pakistan exhibiting a potential for calcium precipitation. *Inter J Econ Envir Geo*. 2018;9(4):62-67.

77. Sang MK, Shrestha A, Kim DY, Park K, Pak CH, Kim KD. Biocontrol of Phytophthora blight and anthracnose in pepper by sequentially selected antagonistic rhizobacteria against *Phytophthora capsici. Plant Pathol J*. 2013;29(2):154-167.

78. Pintado A, Pérez-Martínez I, Aragón IM, et al. The Rhizobacterium *Pseudomonas alcaligenes* AVO110 induces the expression of biofilm-related genes in response to Rosellinia necatrix exudates. *Microorganisms*. 2021;9(7):1388. doi:10.3390/microorganisms9071388

79. Ruenchit P, Whangviboonkij N, Sawasdipokin H, Phumisantiphong U, Chaicumpa WA. Search for anti-Naegleria fowleri agents based on competitive exclusion behavior of microorganisms in natural aquatic environments. *Pathogens*. 2021;10(2):142. doi:10.3390/pathogens10020142

80. Ahn KJ. Antibiotic production of *Pseudomonas otitidis* PS and mode of action. *Biotechnol Lett*. 2018;46(1):40-44.

81. Vivero RJ, Mesa GB, Robledo SM, Herrera CXM, Cadavid-Restrepo G. Enzymatic, antimicrobial, and leishmanicidal bioactivity of gram-negative bacteria strains from the midgut of *Lutzomyia evansi*, an insect vector of Leishma-

niasis in Colombia. *Biotechnol Rep (Amst)*. 2019;24:e00379 doi:10.1016/j.btre.2019.e00379

82. Lu H, Wang X, Zhang K, Xu Y, Zhou L, Li G. Identification and nematicidal activity of bacteria isolated from cow dung. *Ann Microbiol*. 2014;64(1):407-411.

83. Chellaram C, Praveen MM. Molecular characterization of antagonistic bacteria, *Pseudomonas otitidis* from Insect gut, short horned grasshopper. *J Pure Appl Microbiol*. 2015;9(23):91-96.

84. Husain F, Duraisamy S, Balakrishnan S, Ranjith S, Chidambaram P, Kumarasamy A. Phenotypic assessment of safety and probiotic potential of native isolates from marine fish *Moolgarda seheli* towards sustainable aquaculture. *Biologia (Bratisl)*. 2022;77(3):775-790.

85. Siddiqui R, Ali IK, Cope JR, Khan NA. Biology and pathogenesis of *Naegleria fowleri. Acta Tropica*. 2016;164(3):75-94.

86. Al-Mamary NI, Al-Hayali HL. Effect of synergism of thalidomide and liposomal amphotericin-B on *Leishmania tropica* and *Leishmania donovani* promastigote. *Revis Bionatura*. 2022; 7(2): 59. doi:10.21931/RB/2022.07.02.59

87. Desjeux P. Leishmaniasis: Current situation and new perspectives. *Comp Immunol Microbiol Infect Dis*. 2004;27(5):305-318.

88. Ankeny RA. The natural history of *Caenorhabditis elegans* research. *Nat Rev Genet*. 2001;2(6):474-479.

89. Wang W, Wang X. Prevalence of metallo-β-lactamase genes among *Pseudomonas aeruginosa* isolated from various clinical samples in China. *Lab Med*. 2020;44(4):97-203.

90. Kaur R, Singh D, Kesavan AK, Kaur R. Molecular characterization and antimicrobial susceptibility of bacterial isolates present in tap water of public toilets. *Int Health*. 2020;12(5):472-483.

91. Nordmann P, Fournier C, Poirel L. A Selective culture medium for screening carbapenem resistance in *Pseudomonas* spp. *Microb Drug Resist*. 2021;27(10): 1355-1359.

92. Suzuki M, Suzuki S, Matsui M, Hiraki Y, Kawano F, Shibayama K. A subclass B3 metallo-β-lactamase found in *Pseudomonas alcaligenes*. *J Antimicrob Chemother*. 2014;69(5):1430-1432.

93. Borgianni L, De Luca F, Thaller MC, Chong Y, Rossolini GM, Docquier JD. Biochemical characterization of the POM-1 metallo-β-lactamase from *Pseudomonas otitidis*. *Antimicrob Agents Chemother*. 2015; 59(3):1755-1758.

94. Mathys DA, Mollenkopf DF, Feicht SM, et al. Carbapenemase-producing *Enterobacteriaceae* and *Aeromonas* spp. present in wastewater treatment plant effluent and nearby surface waters in the US. *PloS One* 2019;14(6):e0218650. doi:10.1371/journal.pone.0218650

95. Vieira TR, Sambrano GE, Silva NM, et al. In-Depth genomic characterization of a meropenem-nonsusceptible *Pseudomonas otitidis* strain contaminating chicken carcass. *Acta Sci Vet*. 2020;48. doi:10.22456/1679-9216.103176

96. Wong MHY, Chi Chan EW, Chen S. Isolation of carbapenem-resistant *Pseudomonas* spp. from food. *J Glob Antimicrob Resist* 2015;3(2):109-114.

97. Thaller MC, Borgianni L, Di Lallo G, et al. Metallo-β-lactamase production by *Pseudomonas otitidis*: A species-related trait. *Antimicrob Agents Chemother*. 2011;55(1):118-123.

98. Poirel L, Palmieri M, Brilhante M, Masseron A, Perreten V, Nordmann P. PFM-like enzymes are a novel family of subclass B2 metallo-β-lactamases from *Pseudomonas synxantha* belonging to the *Pseudomonas fluorescens* complex. *Antimicrob Agents Chemother*. 2020;64(2):17-19.

99. Yum JH. Prevalence and diversity of MBL gene-containing inte-

grons in metallo-β-lactamase (MBL)-producing *Pseudomonas spp.* isolates disseminated in a Korean hospital. *Biomed Sci Lett.* 2019;25(4):321-330.

100. Martins WM, Narciso AC, Cayo R, et al. SPM-1-producing *Pseudomonas aeruginosa* ST277 clone recovered from microbiota of migratory birds. *Diagn Microbiol Infect Dis.* 2018; 90(3):221-227.

101. Le Terrier C, Masseron A, Uwaezuoke NS, et al. Wide spread of carbapenemase-producing bacterial isolates in a Nigerian environment. *J Glob Antimicrob Resist.* 2020;21:321-323.

102. El-Bestawy E, Sabir J, Mansy AH, Zabermawi N. Isolation, identification and acclimatization of Atrazine-resistant soil bacteria. *Ann Agric Sci.* 2013; 58(2): 119-130.

103. Shaini VP, Jayasree S. Biochemical characterization and 16S rDNA sequencing of lipolytic bacterial isolates WCS. *Natl Sci.* 2015;11(1):82-90.

104. Ramani K, Saranya P, Jain SC, Sekaran G. Lipase from marine strain using cooked sunflower oil waste: Production optimization and application for hydrolysis and thermodynamic studies. *Bioprocess Biosyst Eng.* 2013;36(3): 301-315.

105. Fibriana F, Upaichit A, Cheirsilp B June. Turning waste into valuable products: Utilization of agroindustrial oily wastes as the low-cost media for microbial lipase production. *In Journal of Physics: Conference Series.* IOP Publishing. 2021;1918(5):28-52.

106. Kumar A, Vyas P. Biochemical and molecular characterization of cellulase producing bacterial isolates from cattle dung samples. *J Adv Res Biotechnol.* 2018;1-6. doi:10.15226/2475-4714/3/1/00132.

107. Huang Y, Liu X, Ran Y, Cao Q, Zhang A, Li D. Production of feather oligopeptides by a newly isolated bacterium *Pseudomonas otitis* H11. *Poult Sci.* 2019.

108. Fatoni A, Zusfahair. Isolation and partial purification of new protease form thermophilic bacteria *Pseudomonas otitidis* WN 1 obtained from Indonesian hot spring. *Conference Paper*; 2016; Jakarta.

109. Shamsi TN, Parveen R, Fatima S. Characterization, biomedical and agricultural applications of protease inhibitors: A review. *Int J Biol Macromol.* 2016;91:1120-1133.

110. Viera-Limón MJ, Morlett-Chávez JA, Sierra-Rivera CA, Luque-Contreras D, Zugasti-Cruz A. Zearalenone induced cytotoxicity and oxidative stress in human peripheral blood leukocytes. *Toxicology.* 2015;1(1):102. doi:10.4172/2476-2067.1000102

111. Tan H, Zhang Z, Hu Y, et al. Isolation and characterization of *Pseudomonas otitidis* TH-N1 capable of degrading Zearalenone. *Food Control.* 2015;47:285-290.

112. Mahler HR, Hubscher Georg, Baum H. Studies on uricase. *J Biol Chem.* 1955; 216:625-641.

113. Lee NSIS, Khosravi HM, Ibrahim N, Shahir S. Isolation, partial purification and characterization of thermophilic uricase from *Pseudomonas otitidis* strain SN4. *Malays J Microbiol.* 2015;352-357.

114. Lerner AB, Fitzpatrick TB. Biochemistry of melanin formation. *Physiol Rev.* 1950;30(1):91-126.

115. Deepthi SS, Reddy MK, Mishra N, Agsar D. Melanin production by *Pseudomonas* sp. and *in silico* comparative analysis of tyrosinase gene sequences. *BioTechnologia (Pozn).* 2021;102(4):411-424.

116. Shrivastava A, Khan AA, Khurshid M, Kalam MA, Jain SK, Singhal PK. Recent developments in L-asparaginase discovery and its potential as anticancer agent. *Crit Rev Oncol Hematol.* 2016;100:1-10.

117. Ehsanipour EA, Sheng X, Behan JW, et al. Adipocytes cause leukemia cell resistance to L-asparaginase via release of glutamine. *Cancer Res.* 2013;73(10): 2998-3006.

118. Shi R, Liu Y, Mu Q, Jiang Z, Yang S. Biochemical characterization of a novel L-asparaginase from *Paenibacillus barengoltzii* being suitable for acrylamide reduction in potato chips and mooncakes. *Int J Biol Macromol.* 2017;96:93-99.

119. Ghosh S, Chaganti SR, Prakasham RS. Polyaniline nanofiber as a novel immobilization matrix for the anti-leukemia enzyme l-asparaginase. *J Mol Catal B Enzym.* 2012;74(1-2):132-137.

120. Sharma A, Husain I. Evaluation of antitumor activity of glutaminase-free periplasmic asparaginase from indigenous bacterial isolates as candidates for cancer therapy. P*roc Natl Acad Sci India Sect B Biol Sci.* 2017;87(3):997-1004.

121. Muneer F, Siddique MH, Azeem F, et al. Microbial L-asparaginase: Purification, characterization and applications. *Arch Microbiol.* 2020;202(5):967-981.

122. Husain I, Sharma A, Kumar S, Malik F. Purification and characterization of glutaminase free asparaginase from *Pseudomonas otitidis*: Induce apoptosis in human leukemia MOLT-4 cells. *Biochimie.* 2016;121:38-51.

123. Wang Z, Fast W, Valentine AM, Benkovic SJ. Metallo-β-lactamase: Structure and mechanism. *Curr Opin Chem Biol.* 1999;3(5):614-622.

124. Bush K, Jacoby GA, Medeiros AA. A functional classification scheme for beta-lactamases and its correlation with molecular structure. *Antimicrob Agents Chemother.* 1995;39(6):1211-1233.

125. Hall BG, Barlow M. Revised ambler classification of β-lactamases. *J Antimicrob Chemother.* 2005;55(6):1050-1051.

126. Khan AU, Maryam L, Zarrilli R. Structure, genetics and worldwide spread of New Delhi metallo-β-lactamase (NDM): A threat to public health. *BMC Microbiol.* 2017;17(1):1-12.

127. Castanheira M, Toleman MA, Jones RN, Schmidt FJ, Walsh TR. Molecular characterization of a β-lactamase gene, bla GIM-1, encoding a new subclass of metallo-β-lactamase. *Antimicrob Agents Chemother.* 2004;48(12):4654-4661.

128. Breilh D, Texier-Maugein J, Allaouchiche B, Saux MC, Boselli, E. Carbapenems. *J Chemother.* 2013;25(1):1-17.

129. Demain AL, Elander RP. The β-lactam antibiotics: Past, present, and future. *Antonie Van Leeuwenhoek.* 1999;75(1):5-19.

130. Hou JP, Poole JW. β-lactam antibiotics: Their physicochemical properties and biological activities in relation to structure. *J Pharm Sci.* 1971;60(4):503-532.

131. Zapun A, Contreras-Martel C, Vernet T. Penicillin-binding proteins and β-lactam resistance. *FEMS Microbiol Rev.* 2008;32(2):361-385.

132. De Sousa Borges A, de Keyzer J, Driessen AJ, Scheffers DJ. The *Escherichia coli* membrane protein insertase YidC assists in the biogenesis of penicillin binding proteins. *J Bacteriol.* 2015;97(8):1444-1450.

133. Yano H, Kuga A, Okamoto R, Kitasato H, Kobayashi T, Inoue M. Plasmid-encoded metallo-β-lactamase (IMP-6) conferring resistance to carbapenems, especially meropenem. *Antimicrob Agents Chemother.* 2001;45(5):1343-1348.

134. Miriagou V, Tzelepi E, Gianneli D, Tzouvelekis LS. *Escherichia coli* with a self-transferable, multiresistant plasmid coding for metallo-β-lactamase VIM-1. *Antimicrob Agents Chemother.* 2003;47(1):395-397.

135. Poirel L, Naas T, Nicolas D, et al. Characterization of VIM-2, a carbapenem-hydrolyzing metallo-β-lactamase and its plasmid- and integron-borne gene from a *Pseudomonas aeruginosa* clinical isolate in France. *Antimicrob Agents Chemother*. 2000;44(4):891-897.

136. Holloway BW, Krishnapillai V, Stanisich V. *Pseudomonas* genetics. *Annu Rev Genet*. 1971;5(1):425-446.

137. Yang Z, Liu W, Cui Q, et al. Prevalence and detection of *Stenotrophomonas maltophilia* carrying metallo-β-lactamase blaL1 in Beijing, China. *Front Microbiol*. 2014;5:692. doi:10.3389/fmicb.2014.00692

138. Quale J, Bratu S, Gupta J, Landman D. Interplay of efflux system, ampC, and oprD expression in carbapenem resistance of *Pseudomonas aeruginosa* clinical isolates. *Antimicrob Agents Chemother*. 2006;50(5):1633-1641.

139. Lee K, Lim JB, Yum JH, et al. bla VIM-2 cassette-containing novel integrons in metallo-β-lactamase-producing *Pseudomonas aeruginosa* and *Pseudomonas putida* isolates disseminated in a Korean hospital. *Antimicrob Agents Chemother*. 2002;46(4):1053-1058.

140. Tickler IA, Shettima SA, Dela Cruz CM, et al. Characterization of carbapenem-resistant gram-negative bacterial isolates from Nigeria by whole genome sequencing. *Diagn Microbiol Infect Dis*. 2021;101(1):115422. doi:10.1016/j.diagmicrobio.2021.115422

141. Frisk A, Schurr JR, Wang G, et al. Transcriptome analysis of *Pseudomonas aeruginosa* after interaction with human airway epithelial cells. *Infect Immun*. 2004;72(9):5433-5438.

142. Reis RS, Pacheco GJ, Pereira AG, Freire DMG. Biosurfactants: Production and Applications [Internet]. Biodegradation-Life of Science. InTech; 2013. Available from: http://dx.doi.org/10.5772/56144)

143. Dinache A, Pascu ML, Smarandache A. Spectral properties of foams and emulsions. *Molecules*. 2021;26(24):7704. doi:10.3390/molecules26247704

144. Myers D. Surfactant science and technology. *Edition, John Wiley & Sons, Inc., Hoboken, NJ*. 2020.

145. McClements DJ, Gumus CE. Natural emulsifiers biosurfactants, phospholipids, biopolymers, and colloidal particles: Molecular and physicochemical basis of functional performance. *Adv Colloid Interface Sci*. 2016;234:3-26.

146. Abouseoud M, Maachi R, Amrane A, Boudergua S, Nabi A. Evaluation of different carbon and nitrogen sources in production of biosurfactant by *Pseudomonas fluorescens*. *Desalination*. 2008;223(1-3):143-151.

147. Thavasi R, Sharma S, Jayalakshmi S. Evaluation of screening methods for the isolation of biosurfactant producing marine bacteria. *J Pet Environ Biotechnol S*. 2011; 1(2): 1-6.

148. Chen CY, Baker SC, Darton RC. Batch production of biosurfactant with foam fractionation. *J Chem Technol*. 2006;81(12):1923-1931.

149. Ron EZ, Rosenberg E. Biosurfactants and oil bioremediation. *Curr Opin Biotechnol*. 2002;13(3):249-252.

150. Mendes AN, Filgueiras LA, Pinto JC, Nele M. Physicochemical properties of rhamnolipid biosurfactant from *Pseudomonas aeruginosa* PA1 to applications in microemulsions. *J Biomater Nanobiotechnol*. 2015;6:64-79.

151. Gudiña EJ, Rangarajan V, Sen R, Rodrigues LR. Potential therapeutic applications of biosurfactants. *Trends Pharmacol Sci*. 2013;34(12):667-675.

152. Dubey K, Juwarkar A. Distillery and curd whey wastes as vi-
able alternative sources for biosurfactant production. *World J Microbiol Biotechnol*. 2001;17(1):61-69.

153. Maneerat S. Biosurfactants from marine microorganisms. *Songklanakarin J Sci Technol*. 2005;27(6):1263-1272.

154. Ray S, Ray, M. Purification and characterization of NAD and NADP-linked alpha-ketoaldehyde dehydrogenases involved in catalyzing the oxidation of methylglyoxal to pyruvate. *J Biol Chem*. 1982;257(18):10566-10570.

155. Aparna A, Srinikethan G, Smitha H. Production and characterization of biosurfactant produced by a novel *Pseudomonas sp*. 2B. *Colloids Surf*. B. 2012; 95:23-29.

156. Ishigami Y, Gama Y, Nagahora H, Yamaguchi M, Nakahara H, Kamata T. The pH-sensitive conversion of molecular aggregates of rhamnolipid biosurfactant. *Chem Lett*. 1987;16(5):763-766.

157. Helvacı ŞŞ, Peker S, Özdemir G. Effect of electrolytes on the surface behavior of rhamnolipids R1 and R2. *Colloids Surf*. B. 2004; 35(3-4):225-233.

How cite this article

Comparison of Fatty Acid Contents of Wild and Cultivated *Arum italicum* Mill. Seed Oils from Kırklareli in Turkey by Gas Chromatography-Mass Spectrometry

Kerim Alpinar[1] , Serap Saglik Aslan[2] , Busra Kulaksiz Piskin[3] , Neset Nesetoglu[2,4] ,
Ibrahim Danis[2,4] , Duri Sehvar Ozer Unal [2,4]

[1]Istanbul Health and Technology University, Faculty of Pharmacy, Pharmacognosy Department, Istanbul, Turkiye
[2]Istanbul University, Faculty of Pharmacy, Analytical Chemistry Department, Istanbul, Turkiye
[3]Jana Kazimierza 53, Warszawa 01-267, Poland
[4]Istanbul University, Drug Research Center, Istanbul, Turkiye

ABSTRACT

Objective: *Arum L.* is the largest genus of Aroids. Tubers, leaves, and fruits of *Arum italicum* Mill. (*Araceae*) are used as a traditional medicine in the treatment of hemorrhoids and in preparing local dishes in Turkey. In this study, the fatty acid contents of the wild and cultivated seed oils of *A. italicum* Mill. species from the Kırklareli region in Turkey were determined and compared by the gas chromatography-mass spectrometry method.

Materials and Methods: Seed oils were obtained via petroleum ether extraction. Fatty acid methyl esters were prepared with boron trifluoride/methanol derivatization and analyzed with TC WAX capillary gas chromatographic column.

Results: The amount of 13-phenyl tridecanoic acid, which is the specific fatty acid of *Arum italicum* Mill. species, was found to be similar in both samples. In addition, 2-hydroxy palmitic acid was identified for the first time in the same species.

Conclusion: This is the first report on the presence of the 2-hydroxy palmitic acid content of *Arum italicum* Mill. seeds from Turkey.

Keywords: *Arum italicum* Mill., Seed, Fatty acids, 13-Phenyl tridecanoic acid, 2-Hydroxy palmitic acid

INTRODUCTION

The *Araceae* family is represented in Turkey by 32 taxa, consisting of five genera, 22 species, five subspecies, and 12 varieties. *Arum* L. is the largest genus among other aroids of Turkey. Representatives of the genus are distributed in Central Asia, Europe, Macaronesia, the Mediterranean, and the Middle East regions. The plant can be found mainly in shady places, near walls, abandoned gardens, cemeteries, and at the base of olive and oak trees. *Arum italicum* Mill. is a well-known species, grown not only for the attractive foliage, but also for rich colored berries that are produced in the autumn in Turkey. The plants sprout in early autumn or early winter from a rhizomatous tuber. It produces arrow or broad hastate or sagittate-hastate deep green leaves, usually with silver or grey blotches, 9–35 (-40) cm long, 2–29 cm wide, and with 15–40 cm long petiole. They produce oblong cylindric fruiting spikes consisting of deep orange or red berries, which are also attractive to birds. The individual fruits contain between two and five seeds. Each seed consists of a leathery, reticulate testa. *Arum* L. taxon has been familiar to Eastern Mediterranean people for centuries and has many vernacular names, such as Serpent knife (*Yılan bıçağı*), Serpent dagger (*Yılan burçağı*), Serpent vetch (*Yılan kaması*), and Serpent pillow (*Yılan yastığı*). Plants have been used as a traditional medicine and food, mostly in rural areas, regardless of the species in the country. The tubers, leaves, and fruits of *A. italicum* Mill. are mainly used as a traditional medicine and in preparing local dishes. In some areas of Turkey, ripe fruits are considered as an effective treatment for hemorrhoids: two or three are swallowed with a glass of water each morning for a week.[1−4]

The aim of this study was to compare the fatty acid contents of the seed oils of wild and cultivated *A. italicum* Mill. from the Kırklareli region of Turkey by gas chromatography-mass spectrometry (GC-MS).

MATERIALS AND METHODS

Samples

Ripe fruit of the wild *A. italicum* Mill. were collected from a field around the Kırklareli region (Northwestern Turkey) when the plants were in the fruiting state and could be identified (July 2018). Ripe fruits of the cultivated specimens were also collected from the same population above, and the seeds were sown for germination, blooming, and growth at the Alfred Heilbronn Botanical Garden, Istanbul University (2015).

Oil Extraction

The dried and crushed seeds were extracted with petroleum ether (40-60 °C) for four hours in a shaker. The solvent was removed and evaporated at 40 °C under nitrogen flow. The obtained oil was kept in a vacuum desiccator with P_2O_5 and then weighed.

Derivatization of Fatty Acids

The dried and crushed seeds were derivatized with 20% BF3/MeOH according to the method of Soukup and Holman.[5] The obtained methyl esters were extracted with petroleum ether (40-60 °C), and the solvent part was evaporated under nitrogen flow at 40 °C.

GC-MS Analysis

The GC-MS model with mass selective detection (ionization energy, 70 eV; source temperature, 300 °C) was used (Agilent 7890B Series GC System). The fatty acid methyl esters were analyzed with TC WAX capillary gas chromatographic column (Capillary column: 30 m x 0.25 mm id, 0.25 mm film thickness; temperature program: 170-210 °C, 1 °C/min) (GL Sciences Inc.). Helium was used as the carrier gas (split ratio 1/20). The injector and detector temperatures were 230 °C and 250 °C, respectively. The fatty acid methyl ester standard mixtures were used for the identification of key fatty acids (Sigma). Calculations were made according to the peak area normalization technique.

RESULTS AND DISCUSSION

In our previous study, we had only determined the fatty acid compositions of *A. italicum* Mill. which grows naturally in Istanbul.6 However, in this study, the fatty acid compositions of the wild and cultivated species were compared, and the naturally grown species from Kırklareli, were investigated for the first time. This is the first report on the 2-hydroxy palmitic acid content of *A. italicum* Mill. seeds from Turkey.

The total oil amounts of wild and cultivated A. italicum Mill. were found to be 4.08 g and 3.57 g/100 g seed, respectively. The fatty acid contents of the wild and cultivated *A. italicum* Mill. seeds from Kırklareli are in Table 1, and the comparison of the fatty acid percentages is illustrated in Figure 1.
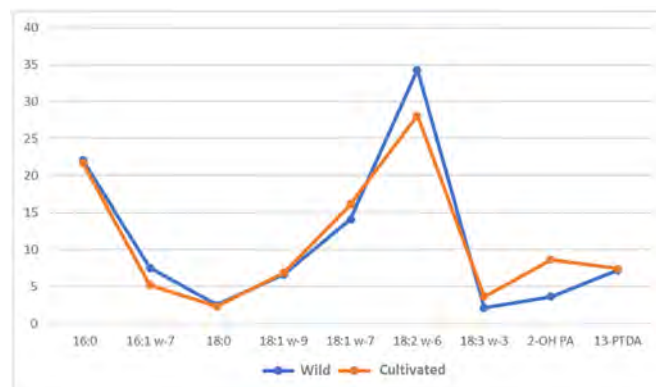
Figure 1. The comparison of fatty acid percentages of the wild and cultivated *Arum italicum* Mill. seed oils.

The main fatty acids were found as palmitic acid, cis-vaccenic acid, and linoleic acid. While the amounts of palmitic acid and cis-vaccenic acid were similar in both samples, the amount of linoleic acid was found to be higher in the wild sample with lower contents in the samples from Istanbul.[6]

It is noteworthy that cis-vaccenic acid, which is an eighteen-carbon monounsaturated fatty acid, is one of the main fatty acids. It is the main fatty acid in bacteria, and it has bacterial biomarker properties. It is found in very small amounts in plant and animal tissues.[7,8]
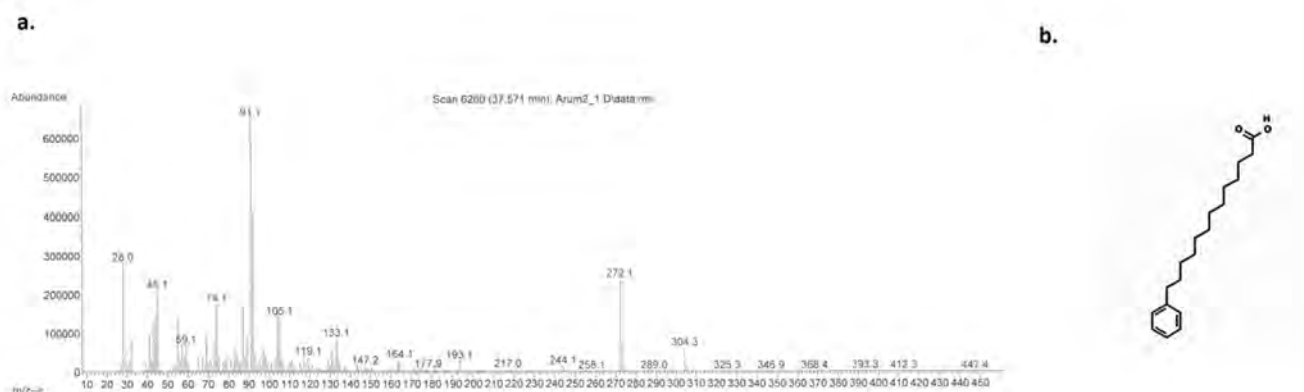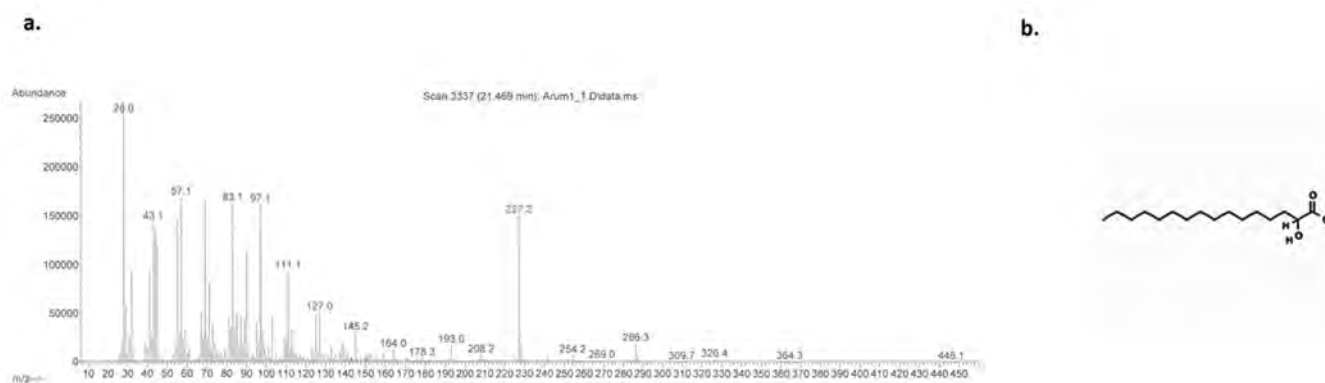
The amounts of 13-phenyl tridecanoic acid, which is a specific fatty acid to *Arum* species, were found to be similar in both samples, which contrasts with the literature findings.[6,8] The mass spectrum and formula of 13-phenyl tridecanoic acid are provided in Figures 2a and 2b, respectively. ω-phenyl fatty acids are cyclic acids with a terminal phenyl group. They are found in seed oils of the *Araceae* especially.[9,10]

The presence of 2-hydroxy palmitic acid (which is effective on inflammation and diabetes)[11] was determined for the first time in *A. italicum* Mill. species. It was found to be approximately three times more in the culture. The mass spectrum and formula of 2-hydroxy palmitic acid are provided in Figures 3a and 3b, respectively. The 2-hydroxy palmitic acid consists of a C16 chain with a hydroxyl group at position 2.

Table 1. Fatty acid contents of the wild and cultivated *Arum italicum* Mill. seed oils (% of total major FAME).

Fatty acid		Retention time (min)	Wild *Arum italicum* (%)	Cultivated *Arum italicum* (%)
Palmitic acid	(C16:0)	7.73	22.05±0.05	21.65±0.05
Palmitoleic acid	(C16:1w-7)	8.33	7.50±0.02	5.21±0.01
Stearic acid	(C18:0)	13.21	2.50±0.01	2.31±0.02
Oleic acid	(C18:1w-9)	13.89	6.63±0.03	6.88±0.04
cis-Vaccenic acid	(C18:1w-7)	14.14	14.10±0.04	16.15±0.07
Linoleic acid	(C18:2w-6)	15.58	34.30±0.05	28.12±0.06
Linolenic acid	(C18:3w-3)	18.17	2.09±0.01	3.62±0.02
2-Hydroxy palmitic acid (2-OH PA)		21.47	3.63±0.02	8.66±0.02
13-Phenyl tridecanoic acid (13-PTDA)		37.57	7.20±0.03	7.40±0.03

The mean values of the results are given as mean ± standard deviation.

Figure 2. Mass spectrum (a) and formula (b) of 13-phenyl tridecanoic acid.

Figure 3. Mass spectrum (a) and formula (b) of 2-hydroxy palmitic acid.

CONCLUSION

In this study, the amount of 13-phenyl tridecanoic acid, is the specific fatty acid of *A. italicum* Mill. species, was found to be similar in the wild and cultivated samples from the Kırklareli region in Turkey. For the first time, 2-hydroxy palmitic acid was identified in this species. It is planned to investigate the fatty acid compositions of other wild and cultivated Aroid species in Turkey for chemotaxonomic and also for therapeutic purposes. Since suitable herbarium specimens could not be prepared from the fruiting plants in this investigation, it is planned to create a herbarium sample by collecting from the same locality in Kırklareli at the appropriate time (when the plant is in bloom). A systematic evaluation can be performed when the oil compositions of the seeds of all *Arum* L. species are revealed.

Peer Review: Externally peer-reviewed.

Author Contributions: Conception/Design of Study- K.A., S.S.A.; Data Acquisition- S.S.A.; Data Analysis/Interpretation- S.S.A.; Drafting Manuscript- K.A.; Critical Revision of Manuscript- S.S.A.; Final Approval and Accountability- K.A., S.S.A., B.K.P, N.N., I.D.,D.O.U.

Conflict of Interest: Authors declared no conflict of interest.

Financial Disclosure: Authors declared no financial support.

ORCID IDs of the authors

Kerim Alpinar	0000-0001-6000-2479
Serap Saglik Aslan	0000-0003-0906-218X
Busra Kulaksiz Piskin	0000-0002-7593-7004
Neset Nesetoglu	0000-0002-2996-8440
Ibrahim Danis	0000-0003-4646-4129
Duri Sehvar Ozer Unal	0000-0003-0754-1240

REFERENCES

1. Alpinar K. The *Araceae* of Turkey. *Aroideana*. 2007;30(1):3-18.

2. Barclay AS, Earle FR. 1974. Chemical analysis of seeds. III. Oil and protein content of 1253 species. *Econ Bot.* 1974;28:178-236.

3. Bown D. Aroids, Plants of the Arum Family (2. Ed) Timber Press Portland, 2000.

4. Boyce P. The genus Arum, The Royal Botanic Gardens, Kew, Stationery Office Books, London, 1993.

5. Soukup VG, Holman RT. Fatty acids of seeds of North American pedicillate *Trillium* species. *Phytochem.* 1987;26(4):1015-1018.

6. Saglik S, Alpinar K, Imre S. Fatty acid composition of the seed oil of *Arum italicum* Miller. *J Food Lipids.* 2002;9(2):95-103.

7. Saglik S, Alpinar K, Imre S. Fatty acid composition of *Dracunculus* vulgaris Schott (*Araceae*) seed oil from Turkey. *J Pharm Pharmaceut Sci.* 2002;5(3):231-233.

8. Mendoza D, Garwin J, Cronan J. Overproduction of cis-vaccenic acid and altered temperature control of fatty acid synthesis in a mutant of *Escherichia coli. J Bacteriol.* 1982;151(3):1608-1611.

9. Schmid PC, Holman RT, Soukup VG. 13-Phenyltridencanoic acid in seed lipids of some aroids. *Phytochem.* 1997;45(6):1173-1175.

10. Christie WW. 13-Phenyltridec-9-enoic and 15-phenylpentadec-9-enoic acids in *Arum maculatum* seed oil. *Eur J Lipid Sci Technol.* 2003;105(12):779-780.

11. Yore MM, Syed I, Moraes-Vieira PM, et al. Discovery of a class of endogenous mammalian lipids with anti-diabetic and anti-inflammatory effects. *Cell.* 2014;159(2):318-332.

How to cite this article

The Effects of Refrigerated Storage Time on Sialic Acid and Nitric Oxide Levels and Oxidant Antioxidant System of Human Milk

Begum Gurel Gokmen[1], [ID] Tugba Akbay[2] [ID]

[1]Marmara University, Institute of Health Science, Department of Biochemistry (Pharmacy), Istanbul, Turkiye
[2]Marmara University, Faculty of Dentistry, Department of Basic Medical Sciences, Istanbul, Turkiye

ABSTRACT

Objective: Human milk (HM) is a marvelous nutrition that serves all the needs of infants in the first six months with the vitamins, minerals, proteins, carbohydrates, and lipids it contains. For the first 4-6 months of a baby's life, Nursing is accepted as the most beneficial and recommended feeding method. The greatest technique for providing nutrition in the absence of breastfeeding is through expressed HM. In this case, milk storage conditions become critical. The proper storage of HM is essential for preserving the nutritional and antioxidant properties of HM. This study aims to examine the effects of storing HM in the refrigerator.

Materials and Methods: The effects of storing HM in the refrigerator were examined for four days with regard to the protein profile oxidant-antioxidant balance and nitric oxide (NO) and sialic acid (SA) levels.

Results: Total protein (TP) levels decreased gradually over the four days. In the SDS-PAGE electrophoresis method, the heavy chain sIgA and κ-casein bands also disappeared in HM. While glutathione-S-transferase and superoxide dismutase activities decreased significantly during the first two days, their activities fell below the detection limit in the last two days. While the glutathione level and catalase activity also decreased gradually over the four days, the malondialdehyde, SA, and NO levels increased significantly.

Conclusion: HM can be safely stored in the refrigerator for two days due to the TP, SA, and NO levels, as well as the antioxidant enzyme activities, remaining unchanged from the first day of expressing HM.

Keywords: Human milk, storage, oxidant-antioxidant system, nitric oxide, sialic acid, SDS-PAGE electrophoresis

INTRODUCTION

Human milk (HM) is a valuable food that contains all the components required for the development and growth of an infant. HM is a liquid that varies depending on the mother's age, medication use, diet, and health and is produced to satisfy the specific needs of each infant.[1] Furthermore, HM serves important functions such as strengthening the immune systems of infants, protecting infection, supporting brain development, and improving digestive system functions.[2]

HM contains many proteins, carbohydrates, lipids, minerals, vitamins, hormones, antioxidant agents, and immunoglobulins that play regulatory and structural roles, as well as antimicrobial peptides, growth factors, and small molecules, and is secreted by mammary epithelial cells.[1] HM proteins consist of up to 70% whey proteins (e.g., α-lactalbumin, lactoferrin, secretory immunoglobulin A) and 30% caseins (α, β, and κ).[3] HM proteins serve many biological functions such as nutrition, nutrient transport, enzymes, intestinal development, im-

mune system regulation, prebiotics, and cognitive functions.[4] The main antioxidant enzymes of HM are superoxide dismutase (SOD), catalase (CAT), and glutathione-s-transferase (GST).[5,6] Glutathione (GSH), a tripeptide that provides the infant with antioxidant protection, is also found in HM.[7]

The sialic acid (SA) bound to oligosaccharides accounts for around 75% of the total SA contained in HM.[8] Human milk oligosaccharides (HMO) are prebiotic components that cannot be digested by the infant but instead stimulate the growth of beneficial bifidobacteria.[9] HMO containing SA is acidic and contains SA in the terminal position of the chain. It constitutes 12-14% of the total HMO content.[10] The trisaccharide sialyllactose, which consists of lactose at the reducing terminus and a Sia residue at the nonreducing terminus, is one of the main sialyloligosaccharides in HMO sialyllactose and a key component of HMO.[11] The SA levels in HM change with the geography, genetics, and diet of the breastfeeding mother. The high sialyloligosaccharide content of HM appears to provide

excellent conditions for the human newborn's absorption and use of the milk Sia to satisfy developmental requirements.[12] SA in HM plays an important role in brain and neural development. Its highest level occurs at the beginning of lactation (5.04 mM) and gradually decreases during the lactation period (1.04 mM).[13,14] Also, another source of SA in HM is κ-casein, a glycoprotein with SA residues.[15]

Nitric oxide (NO) is formed from arginine by the NO synthase enzyme in the endothelial cells and can be found in these cells in the form of a nitrate or nitrite. Recent studies have shown that xanthine oxidase in HM catalyzes the anaerobic reduction of inorganic nitrite to NO.[16] This reaction is thought to be the source of NO in HM. In mammary gland epithelial cells, the xanthine oxidase enzyme bonds to the membrane of milk fat globules.[17] NO is found in HM at around 100 µM. It regulates blood pressure, prevents infections, and regulates the immune system in infants.[18]

The most ideal way to feed HM to a baby is by breastfeeding. However, breastfeeding may sometimes be discontinued due to problems arising from the mother or the infant. Storage conditions and duration are important for the nutritional content, antioxidant capacity, immunological content, and bacterial content of HM.[19] Many studies have shown storing HM in the refrigerator to affect the total protein content and antioxidant-oxidant balance over time.[5−7,20−23] However, no study is found in the literature to have shown the effect of storing HM in the refrigerator with regard to SA and NO levels. Therefore, the results of this study provide a detailed and comprehensive understanding of the changes that occur during the storage of HM, as well as a new perspective to the studies in this field.

MATERIALS AND METHODS

Human Milk Collection

HM collection protocol was approved by the Marmara University School of Medicine Ethics Committee (Approval No. 09.2019.893). Eight breastfeeding mothers signed informed consent forms before donating fresh milk.[24] HM samples were expressed with a pump and stored in milk bags (Lansinoh-Breastmilk Storage Bags). These bags were stored at +4ºC during the four days of the experiment (Figure 1).

Determining the Oxidant Parameter

Malondialdehyde (MDA) levels were determined as an oxidant parameter for measuring the lipid peroxidation level in HM.[25] This method reacts MDA and thiobarbituric acid to produce a pink-colored compound and measures the absorbance of this compound spectrophotometrically. The results are presented as µmol MDA/mL using an extinction coefficient of 1.56×10^5 $M^{-1}cm^{-1}$ to represent the equivalent amount of MDA.

Determining the Antioxidant Parameters

This study investigates the changes over four days regarding GST[26], CAT[27] and SOD[28] activities and GSH level[29] as antioxidant parameters.

In order to determine GSH levels, the study uses a method based on the spectrophotometric detection of the yellow product formed as a result of the reaction of the sulfhydryl groups of GSH with the Elmann reagent (5,5-dithio-bis-2-nitrobenzoic acid). The results are presented as mg% glutathione using an extinction coefficient of 13600 M^{-1} cm^{-1}.

The study investigates GST activity using spectrophotometric detection of the product formed as a result of the reaction of GSH and 1-chloro-2,4-dinitro-benzene at 340 nm. The results are presented as U/mL.

The study determined SOD activity, namely the oxidation of riboflavin sensitized o-dianisidine by the SOD enzyme, spectrophotometrically at 460 nm. The results are presented as U/mL.

The study determined CAT activity by monitoring the conversion reaction of H_2O_2 to H_2O with a decrease in absorbance at 240 nm. The results are presented as U/mL.

Determining the Nitric Oxide and Sialic Acid Levels

To determine the NO levels, vanadium (III) chloride causes the quantitative reduction of nitrate to nitrite. The complex diazonium compound is produced when N-(1-Naphthyl)ethylene diamine dihydrochloride reacts with nitrite in the presence of sulfanilamide. The absorbance of the resulting colored complex is measured spectrophotometrically at 540 nm. The results are presented as µM.[23]

The study identified the SA levels spectrophotometrically at 549 nm through the product formed as a result of the reaction of β-formyl pyruvic acid (resulting from periodic acid oxidation) with thiobarbituric acid. The results are presented as g%.[30]

The Sodium Dodecyl Sulfate-Polyacrylamide Gel Electrophoresis (SDS-PAGE) of HM

The total protein (TP) concentration of HM was determined from skim HM using the Lowry method over the 4 days.[31] The results are presented as g/dL.

The SDS-PAGE method was carried out using the Laemmli system.[32] The molecular weight of the protein bands was determined by comparing the migration rates of the protein standard (BioRad, Rome Italy). The changes in the protein band intensities were examined using ImageJ software. The bands' intensities and peak areas were also calculated in ImageJ software.[33]
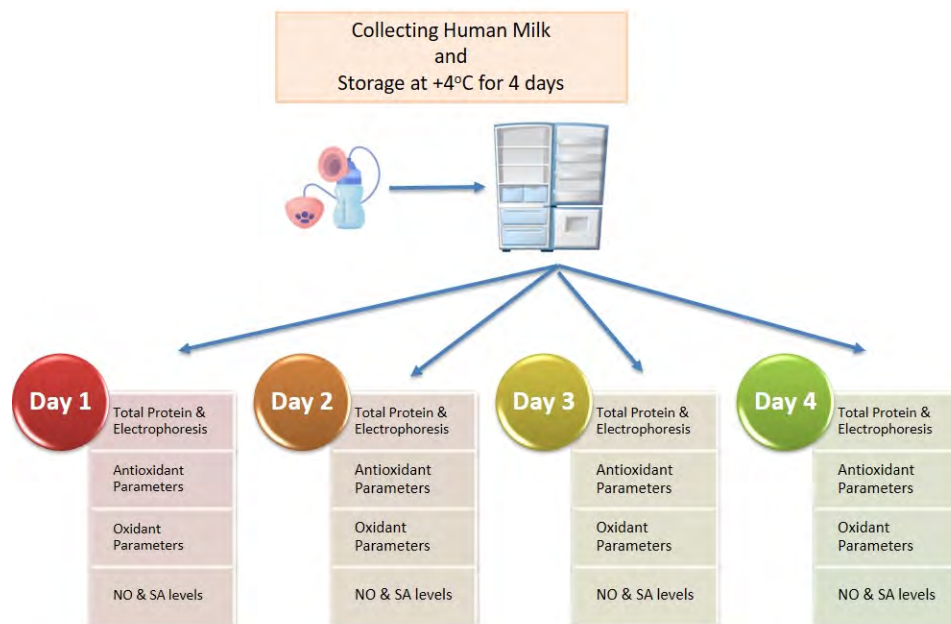
Figure 1. The experimental design.NO = nitric oxide, SA = sialic acid.

Statistical Analysis

The results were evaluated using the GraphPad Prism 6.0 package program (GraphPad Software, San Diego, CA, USA). Data were obtained from at least 10 replicate experiments and presented as means ± standard deviations. Groups of data were analyzed using analysis of variance (ANOVA) followed by Tukey's multiple comparison tests, with a p<0.05 being regarded as significant.

RESULTS

The Oxidant Parameter of HM

The HM MDA level is a final product of lipid peroxidation and therefore a good marker of the degree of the oxidation process. Lipid peroxidation occurs as the result of the direct action of oxygen or other oxidative agents on unsaturated fatty acids and others in the cell membrane. This study saw the MDA level in the HM stored in the refrigerator to increase gradually and significantly over the four days (p<0.05; Table 1).

The Antioxidant Parameters of HM

This study presents the results of the changes in GSH levels and GST, CAT, and SOD enzyme activities as antioxidant parameters of HM over the four days in Table 1. The GSH level and CAT enzyme activity of HM stored in the refrigerator gradually and significantly decreased over the four days (p<0.05). On the other hand, the GST and SOD enzyme activities decreased sig-nificantly on the second day compared to the first day (p<0.05), with no further activity regarding the GST and SOD enzymes in HM being detected on Days 3 and 4.

The Nitric Oxide and Sialic Acid Levels of HM

The NO values of HM increased significantly over the four days (p<0.05; Figure 2). The SA results of HM revealed no significant increase in the first three days, while observing a significant increase on Day 4 (Figure 3).

SDS-PAGE Results of HM

The TP level of HM decreased significantly over the four-day storage period. However, no significant difference occurred in the TP levels between Days 2 and 3 (Figure 4). Significant differences in the SDS-PAGE gel electrophoresis bands of HM were observed to be consistent with the change in TP. Three bands were seen on the electrophoresis gel images around 66 kDa, which belong to lactoferrin (Area 1, band a), serum albumin (Area 1, band b), and the sIgA heavy chain (Area 1, band c) from top to bottom, respectively. The bands around 24 and 36 kDa are the alpha-casein (Area 2, band d), beta-casein (Area 2, band e), kappa-casein (Area 2, band f), and sIgA light chain (Area 2, band g) from top to bottom, respectively. The band at 21 kDa is beta-lactoglobulin (Area 3, band h), and the band at 14 kDa is alpha-lactalbumin (Area 3, band i; Figure 5).

The protein intensity in the lactoferrin, serum albumin, sIgA heavy chain, and κ-casein bands in the gel significantly de-

Table 1. Oxidant-antioxidant parameters of human milk.

Parameters	Day 1	Day 2	Day 3	Day 4
MDA (gmol/mL)	0.058 ± 0.009	0.924 ± 0.064 *	$1.479 \pm 0.087^{*nA}$	$2.239 \pm 0.079^{*n}$
GSH (mg%)	0.469 ± 0.014	$0.259 \pm 0.014^{*A}$	$0.189 \pm 0.001^{*nA}$	$0.103 \pm 0.005*n$
GST (U/mL)	0.059 ± 0.003	0.041 ± 0.005 *	Under the Detection Limit	Under the Detection Limit
CAT (kU/mL)	2.035 ± 0.075	$1.872 \pm 0.027^{*A}$	$1.764 \pm 0.028^{*nA}$	$1.111 \pm 0.132*n$
SOD (U/mL)	4.308 ± 0.083	1.355 ± 0.178 *	Under the Detection Limit	Under the Detection Limit

SD = Standard deviation; * signifies $p<0.05$ compared to Day 1; ^{n} signifies $p<0.05$ compared to Day 2; ^{A} signifies $p<0.05$ compared to Day 4.
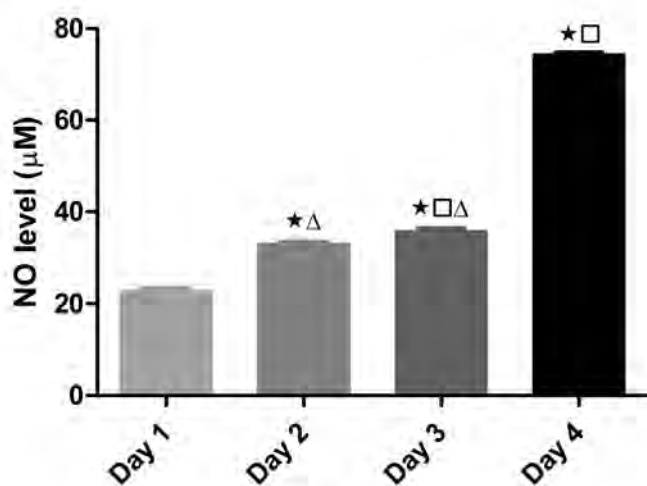
Figure 2. NO levels in human milk. NO = Nitric oxide. * signifies $p<0.05$ compared to Day 1; □ signifies $p<0.05$ compared to Day 2; Δ signifies $p<0.05$ compared to Day 4.

Figure 3. SA levels in human milk. SA = sialic acid. * signifies $p<0.05$ compared to Day 1; Δ signifies $p<0.05$ compared to Day 4.

creased on Days 3 and 4 compared to Days 1 and 2. The α-casein, β-casein, sIgA light chain, β-lactoglobulin, and α-lactalbumin bands in the gel did not change over the four days (Figure 6 and Table 2).

DISCUSSION

HM is a highly nutritious substance that is not only packed with essential nutrients for a growing infant but also contains several chemical substances and antioxidants that play a significant role in promoting infant health. The effect of HM storage conditions on its antioxidant properties mainly involves changes in the antioxidant activity and levels of antioxidant compounds present.[34] HM should be stored at most for 3 hours at room temperature 25ºC, 3 days in a refrigerator +4ºC, or lastly up to 3 months in a freezer -20ºC. [35] The nutritional content of HM has been determined to change when these periods are exceeded.[36,37] Miranda et al. reported a significant increase in MDA values when HM had been stored in the refrigerator for 2 days compared to fresh milk.[23] The current study found the MDA levels of HM to gradually increase over the four days, which is consistent with the literature.
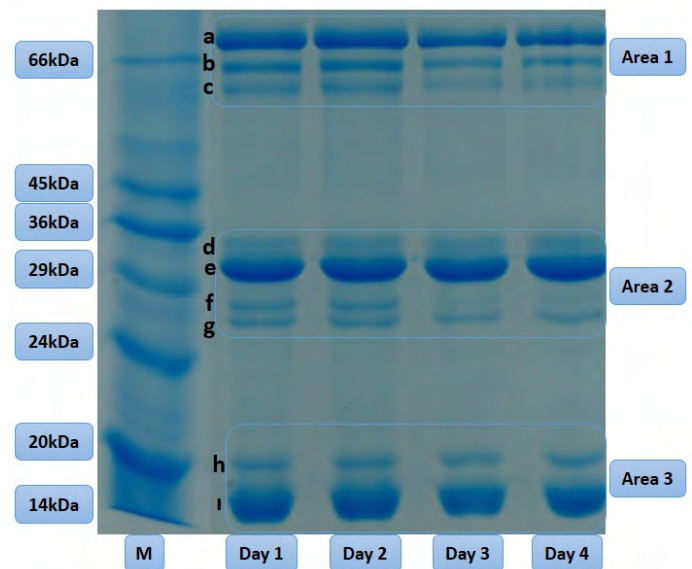
Many studies have examined the change in the antioxidant capacity of HM based on storage conditions. Ankrah et al.'s study found a significant decrease in GSH levels when HM was kept at 4ºC for 2 hours.[7] Marinkovic et al.'s study observed a significant decrease in HM SOD activity when kept at -20ºC

Table 2. Electrophoresis gel band image area analysis.

Area	Protein Bands	Protein	Protein Peaks Areas (cm^2)			
			Day 1	Day 2	Day 3	Day 4
1	a	Lactoferrin	100.2	100.6	69.0	68.9
	b	Serum albumin	40.2	40.4	23.7	21.2
	c	sIgA heavy chain	16.5	16.5	5.6	5.6
2	d	α casein	156.1	158.2	157.1	152.6
	e	β casein	92.7	92.7	92.4	92.3
	f	κ casein	6.59	6.54	0.04	0.04
	g	sIgA light chain	7.6	7.6	7.6	7.5
3	h	β lactoglobulin	19.6	19.7	19.7	19.6
	ı	α lactalbumin	185.3	185.6	185.3	185.2
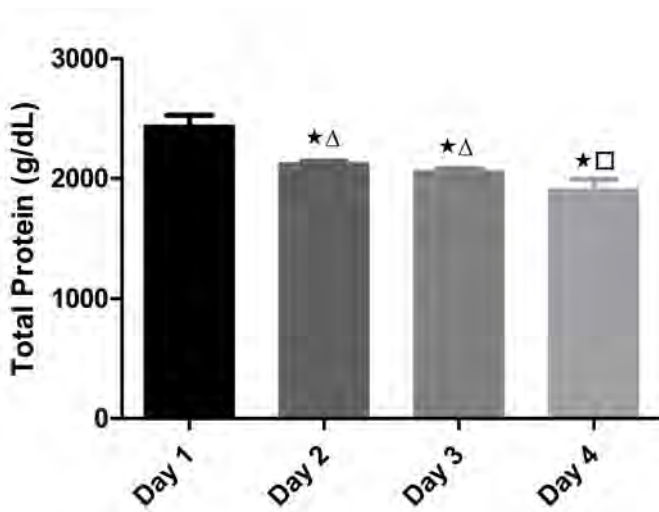
Figure 4. Total protein levels in human milk.* signifies p<0.05 compared to Day 1; □ signifies p<0.05 compared to Day 2; ∆ signifies p<0.05 compared to Day 4.

Figure 5. SDS-PAGE profiles for human milk. a = lactoferrin; b = serum albumin; c = sIgA heavy chain; d = β-casein; e = β-casein; f = κ-casein; g = sIgA heavy chain; h = β-lactoglobulin, i = α-lactalbumin.

for 7 days.[5] These results are also consistent with the findings from the current study. No study is found in the literature to have addressed the changes in GST and CAT activities of HM based on storage conditions. This study saw the GST, SOD, and CAT activities of the HM to gradually decrease during the four days. Even the GST and SOD activities fell under the detection limit after two days of storage. Paduraru et al. showed the total antioxidant capacity of HM to decrease when stored at 4°C for one to three days.[6] Consistent with these studies, the current study detected significant decreases in GSH levels and

antioxidant enzyme activities over the four-day storage period in the refrigerator.

A search of the literature search revealed no findings related to the changes in SA and NO levels in HM during storage in a refrigerator. This is why the current study focused on measuring SA and NO levels in HM. HM contains a significant amount of SA, primarily in the form of N-acetyl neuraminic acid.[14] Wang et al. determined SA levels in colostrum, transi-
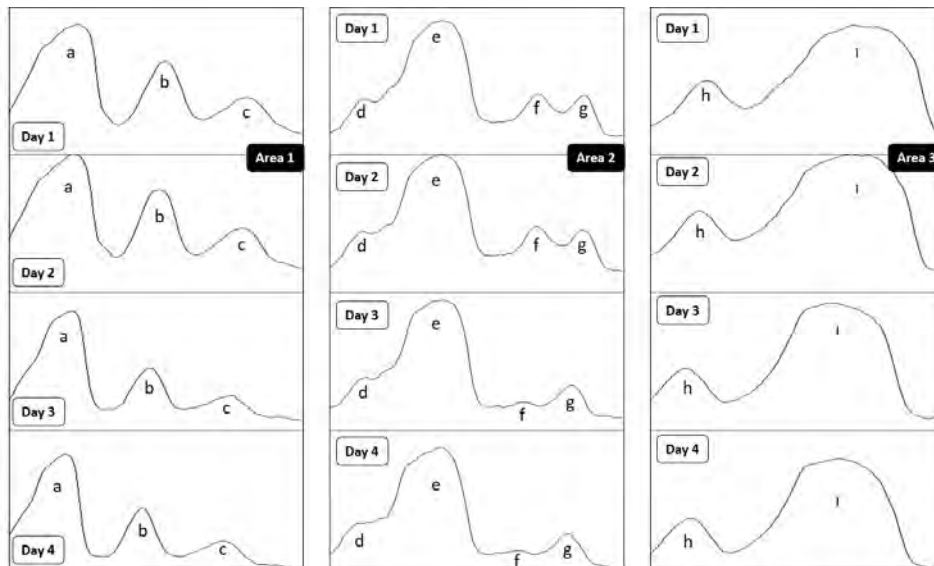
Figure 6. Image J protein band peaks. a = lactoferrin; b = serum albumin; c = sIgA heavy chain; d = α-casein; e = β-casein; f = κ-casein; g = sIgA heavy chain; h = β-lactoglobulin; i = α-lactalbumin.

tion, and mature HM. This current study identified SA levels in mature milk to be at 0.01 g/dL, while Wang et al. found the total SA level in mature milk to be 0.045 g/dL.[38] No study is found in the literature regarding the change in HM SA levels based on storage conditions. Therefore, the SA findings from the current study are novel, which found the SA levels of HM to not change over the first three days of storage in a refrigerator but to increase very sharply on Day 4. In HM, 21%-28% of SA was bound to glycoproteins, with only 3% of SA being found in an unbounded form.[39] The SA levels measured in the first three days are believed to have been the free SA found in HM. Because approximately 12-14% of the total SA in HM is bound to oligosaccharides and 21-28% to glycoproteins, this increase observed on the fourth day may have been due to the release of the SA bound to the oligosaccharide and glycoprotein through the activity of the sialidase enzyme. Because sialylation is important for cell functioning and affects the biological stability of glycoproteins, desialylation in milk is an undesirable reaction as it indicates the oligosaccharides or glycoproteins to which the SA had been attached have lost their function.

This study investigated the NO levels in HM as one of the novel parameters that change with storage in a refrigerator. NO is produced in breast tissue and may stimulate lactation in humans. Fernandes et al. found the nitrate value in HM to range from 42.6 µM to 96.6 µM.[40] Yüksel et al. found the NO value in mature HM to be 93 µM.[18] This study found the NO level of HM to be 22 µM on Day 1 and then to increase on Day 4. The literature search revealed no study to have addressed changes in the NO level of HM based on storage conditions. In this study, the increase in NO concentration of HM on Day 4 can be related to the NO produced by bacterial NO synthase.

If storage exceeding 72 hours is required, cryopreservation is preferred to prevent bacterial growth.[41]

Iqbal et al. found HM protein content to decrease gradually over three days under refrigerated storage conditions.[20] The current study similarly found the protein levels in HM to decrease. Meng et al.'s electrophoretic examination of HM showed the disappearance of sIgA bands after two days and of lactoferrin bands after five days for HM kept at 4°C.[22] Another study on HM electrophoresis determined the β-casein bands to decrease at the end of seven days.[21] The current study found the lactoferrin, serum albumin, sIgA, and κ-casein bands to decrease on Days 3 and 4 compared Days 1 and 2.

CONCLUSION

In conclusion, while storing HM at +4°C for three days did not significantly change the SA and NO levels, these parameters increased significantly on Day 4. Although the SA and NO levels didn't increase until Day 4, storing HM for only two days is considered safer due to the decreased antioxidant capacity and increased lipid peroxidation on Day 2. This is in comparison to the three days of storage recommended in many guidelines.

ORCID IDs of the authors

Begum Gurel Gokmen   0000-0002-3955-1948
Tugba Akbay   0000-0002-2091-9298

REFERENCES

1. Kim JH, Froh EB. What nurses need to know regarding nutritional and immunobiological properties of human milk. *J Obstet Gynecol Neonatal Nurs*. 2012;41(1):122-137.

2. Yi D, Kim S. Human breast milk composition and function in human health: From nutritional components to microbiome and MicroRNAs. *Nutrients*. 2021;13(9):3094. doi:10.3390/nu13093094

3. Hendricks G, Guo M. Bioactive components in human milk. *Human milk biochemistry and infant formula manufacturing technology*. Elsevier; 2014:33-54.

4. Donovan SM. Human milk proteins: Composition and physiological significance. *nestle Nutr Inst Workshop Ser*. 2019;90:93-101.

5. Marinković V, Ranković-Janevski M, Spasić S, et al. Antioxidative activity of colostrum and human milk: Effects of Pasteurization and storage. *J Pediatr Gastroenterol Nutr*. 2016;62(6):901-906.

6. Păduraru L, Dimitriu DC, Avasiloaiei AL, Moscalu M, Zonda GI, Stamatin M. Total antioxidant status in fresh and stored human milk from mothers of term and preterm neonates. *Pediatr Neonatol*. 2018;59(6):600-605.

7. Ankrah NA, Appiah-Opong R, Dzokoto C. Human breast-milk storage and the glutathione content. *J Trop Pediatr*. 2000;46(2):111-113.

8. Nakano T, Sugawara M, Kawakami H. Sialic acid in human milk: Composition and functions. *Acta Paediatr* Taiwan. 2001;42(1):11-17.

9. Ruhaak LR, Stroble C, Underwood MA, Lebrilla CB. Detection of milk oligosaccharides in plasma of infants. *Anal Bioanal Chem*. 2014;406(24):5775-5784.

10. Açar Y, Yassibaş E. Anne sütü oligosakkaritleri ve sağlık üzerine etkileri. *Gazi Sağlık Bilimleri Dergisi*. 2021;6(1):22-33.

11. Newburg DS. Oligosaccharides in human milk and bacterial colonization. *J Pediatr Gastroenterol Nutr*. 2000;30:S8-S17.

12. Liu F, Simpson AB, D'Costa E, Bunn FS, van Leeuwen SS. Sialic acid, the secret gift for the brain. *Crit Rev Food Sci Nutr*. 2022:1-20. doi:10.1080/10408398.2022.2072270

13. Jantscher-Krenn E, Bode L. Human milk oligosaccharides and their potential benefits for the breast-fed neonate. *Minerva Pediatr*. 2012;64(1):83-99.

14. Wang B. Sialic acid is an essential nutrient for brain development and cognition. *Annu Rev Nutr*. 2009;29:177-222.

15. Brignon G, Chtourou A, Ribadeau-Dumas B. Preparation and amino acid sequence of human κ-casein. *FEBS Letters*. 1985;188(1):48-54.

16. Martin HM, Hancock JT, Salisbury V, Harrison R. Role of xanthine oxidoreductase as an antimicrobial agent. *Infect Immun*. 2004;72(9):4933-4939.

17. Stevens CR, Millar TM, Clinch JG, Kanczler JM, Bodamyali T, Blake DR. Antibacterial properties of xanthine oxidase in human milk. *The Lancet*. 2000;356(9232):829-830.

18. Yuksel S, Yigit AA, Cinar M, Atmaca N, Onaran Y. Oxidant and antioxidant status of human breast milk during lactation period. *Dairy Sci & Technol*. 2015;95(3):295-302.

19. Ulukaya B. Storage of human milk: Effect of temperature and storage conditions on microbiota. Karabük University, Institute of Graduate Programs, Department of Midwifery, Master Thesis, 2022.

20. Iqbal M, Lestari LA, Kurdanti W, Mardiyati NL. Effect of temperature and storage duration on lactose, protein and fat content of breast milk. presented at: International Conference on Health and Well-Being; 2016.

21. Li X, Gu Y, He S, et al. Influence of pasteurization and storage on dynamic *in vitro* gastric digestion of milk proteins: Quantitative insights based on peptidomics. *Foods*. 2020;9(8):998. doi:10.3390/foods9080998

22. Meng F, Uniacke-Lowe T, Ryan AC, Kelly AL. The composition and physico-chemical properties of human milk: A review. *Trends Food Sci Technol*. 2021;112:608-621.

23. Miranda KM, Espey MG, Wink DA. A rapid, simple spectrophotometric method for simultaneous detection of nitrate and nitrite. *Nitric Oxide*. 2001;5(1):62-71.

24. Miller EM, Aiello MO, Fujita M, Hinde K, Milligan L, Quinn EA. Field and laboratory methods in human milk research. *Am J Hum Biol*. 2013;25(1):1-11.

25. Ledwozyw A, Michalak J, Stepień A, Kadziołka A. The relationship between plasma triglycerides, cholesterol, total lipids and lipid peroxidation products during human atherosclerosis. *Clin Chim Acta*. 1986;155(3):275-283.

26. Habig WH, Jakoby WB. Assays for differentiation of glutathione S-transferases. *Methods Enzymol*. 1981;77:398-405.

27. Aebi H. Catalase. *Methods of enzymatic analysis*. Elsevier; 1974:673-684.

28. Mylroie AA, Collins H, Umbles C, Kyle J. Erythrocyte superoxide dismutase activity and other parameters of copper status in rats ingesting lead acetate. *Toxicol Appl Pharmacol*. 1986;82(3):512-520.

29. Beutler E. Reduced Glutathione. In: Bergmeyen HV, ed. *Glutathione in red blood cell metabolism: A manuel of biochemical methods*. Grune and Stratton; 1975:112-114.

30. Warren L. The thiobarbituric acid assay of sialic acids. *J Biol Chem*. 1959;234(8):1971-1975.

31. Lowry O, Rosebrough N, Farr A, Randall R. Protein measurement with the Folin phenol reagent. *J Biol Chem.* 1951;193(1):265-275.

32. Laemmli UK. Cleavage of structural proteins during the assembly of the head of bacteriophage T4. *Nature.* 1970;227(5259):680-685.

33. Schneider CA, Rasband WS, Eliceiri KW. NIH Image to ImageJ: 25 years of image analysis. *Nature Methods.* 2012;9(7):671-675.

34. Chang YC, Chen CH, Lin MC. The macronutrients in human milk change after storage in various containers. *Pediatr Neonatol.* 2012;53(3):205-209.

35. Abramovich M. *Human Milk Storage Conditions in regard to safety and optimal preservation of nutritional properties.* University of Manitoba (Canada); 2011.

36. Place M. *Donor Breast Milk Banks: The Operation of Donor Milk Bank Services.* London: National Institute for Health and Clinical Excellence (NICE); February 2010.

37. Aschberger K, Castello P, Hoekstra E, et al. Bisphenol A and baby bottles: Challenges and perspectives. *Luxembourg: Publications Office of the European Union.* 2010;10:5-50.

38. Wang B. Sialic acid is an essential nutrient for brain development and cognition. *Annu Review Nutr.* 2009;29:177-222.

39. Hauser J, Pisa E, Arias Vásquez A, et al. Sialylated human milk oligosaccharides program cognitive development through a non-genomic transmission mode. *Mol Psychiatry.* 2021;26(7):2854-2871.

40. Fernandes JO, Tella SOC, Ferraz IS, Ciampo LAD, Tanus-Santos JE. Assessment of nitric oxide metabolites concentrations in plasma, saliva, and breast milk and their relationship in lactating women. *Mol Cell Biochem.* 2021;476(2):1293-1302.

41. Silvestre D, Löpez M, March L, Plaza A, Martinez-Costa C. Bactericidal activity of human milk: Stability during storage. *Br J Biomed Sci.* 2006;63(2):59-62.

How cite this article

İSTANBUL UNIVERSITY PRESS

RESEARCH ARTICLE

Usnic Acid Exerts Antiproliferative and Apoptotic Effects by Suppressing NF-κB p50 in DU145 Cells

Omer Erdogan[1], Burcin Irem Abas[2], Ozge Cevik[2]

[1]Gaziantep Islam Science and Technology University, Faculty of Medicine, Department of Medical Biochemistry, Gaziantep, Türkiye
[2]Aydın Adnan Menderes University, Faculty of Medicine, Department of Medical Biochemistry, Aydın, Türkiye

ABSTRACT

Objective: Nuclear factor kappa B (NF-κB) is one pathway that controls the expression of genes involved in many cancer events such as proliferation, apoptosis, metastasis, and invasion. Usnic acid is a molecule with many biological effects such as being anticholinergic, gastroprotective, anti-inflammatory, anti-cancerous, and especially antioxidant. This study aims to mechanistically examine the apoptotic behaviors of usnic acid in DU145 prostate cancer cells and the molecules it acts on in the NF-κB pathway.

Materials and Methods: This study investigates the apoptotic changes in DU145 cells after usnic acid administration through JC-1 staining and caspase-3 activity measurements. In addition, it tests the effects of usnic acid on subunit p50 and p65 protein and gene expressions in the NF-κB pathway through the respective Western blot and qPCR measurements.

Results: The IC_{50} values of usnic acid at 24 and 48 h in DU145 cells were calculated as 167.06±12.35 µM and 42.15±3.76 µM, respectively. In addition, JC-1 staining showed usnic acid-treated DU145 cells to trigger apoptosis by increasing the membrane permeability of their mitochondria. NF-κB p50 protein expression was also found to be suppressed after usnic acid administration.

Conclusion: The results of this study show usnic acid administration to suppress proliferation and to induce mitochondrial apoptosis by suppressing the NF-κB pathway in DU145 cells. This effect of usnic acid indicates it to be combinable with chemotherapeutic agents and evaluable as an alternative in cancer treatment.

Keywords: Apoptosis, NF-κB pathway, prostate cancer, usnic acid

INTRODUCTION

Prostate cancer is the second most widespread type of carcinoma in males following lung cancer. According to the latest Globocan data, 375,608 deaths due to prostate cancer have been reported worldwide.[1] The most important risk factors for prostate cancer are genetic predisposition, smoking, excessive red meat diet, and excessive hormonal expression.[2] In particular, men with high serum amounts of insulin-like growth hormone-1 are reported to be 1.7 to 3.4 times more likely to develop prostate cancer than men with low serum levels.[3] Docetaxel, cabazitaxel, mitoxatrone and estramustine are the chemotherapeutics currently used in the treatment of prostate cancer.[4] These types of chemotherapeutics also cause side effects such as nausea, vomiting, and hair loss, which make routine life difficult. Therefore, the discovery of new agents in the treatment of cancer is an urgent necessity.

Nuclear factor kappa-light-chain-enhancer of activated B cells (NF-κB) transcription factor is a pathway that has demonstrated a primary role in the inflammation and initiation of immune response. NF-κB has been emphasized to arrange the expression of genes apoptosis migration and to control cell proliferation in cancer development.[5,6] Due to NF-κB being overexpressed in cancer cells, studies aimed at elucidating this signaling pathway and developing NF-κB-targeted therapy strategies have gained momentum with regard to cancer treatment. Usnic acid is a dibenzofuran-origin compound found abundantly in lichen species.[7] Usnic acid has been reported to have many analgesic, antibiotic, antiviral, antiprotozoal, anti-inflammatory, and cytotoxic pharmacological effects.[8] In addition to these effects, usnic acid has also been reported to have similar activity with existing antioxidant molecules such as trolox and alpha tocopherol in tests regarding antioxidant capacity measurement such as Fe^{3+} and Cu^{2+} reduction, DPPH, $ABTS^+$, $DMPD^+$, and the $O_2.^-$ superoxide anion radical.[9] The phenolic groups present in the structure of usnic acid strengthen its radical scavenging effect, with usnic acid showing greater effects in aqueous media due to being a natural antioxidant.[10]

Usnic acid has also been shown to have a high capacity to scavenge superoxide radicals in methanol extracts of usnic acid isolated from lichen species.[11] Investigating the anti-cancer effects of natural substances with antioxidant properties and high bioactivity and determining their effects on cellular processes are important. This study investigates the proliferative and apoptotic effects of usnic acid application in DU145 cells and additionally examines the possible effects of usnic acid applications on p50 and p65 expression in the NF-κB pathway.

MATERIALS AND METHODS

Chemicals and Cell Culture Equipment

Usnic acid was purchased from the Sigma company (Sigma 329967, Darmstadt, Germany). All equipment and supplements for cell culturation such as Trypsine-EDTA, penicillin-streptomycin, fetal bovine serum, and DMEM medium were bought from Gibco (Billings, MO, USA).

Cell Culture

The DU145 human prostate cancer cell lines were bought from the American Type Culture Collection (ATCC HTB-81, Rockville, MD, USA). Cells were grown in a DMEM medium supplemented with 100 µg/mL streptomycin, 100 U/mL penicillin, 10% fetal bovine serum, and 2 mM L-Glutamine at 37°C and 5% CO_2 ambient conditions. The cell medium was renewed every two days. Once the cells reached 90% occupancy, the stocks were subcultured.

Cytotoxicity Test (MTT Assay)

The DU145 cells were added at a density of $5x10^3$ to 96-well plates in 100 µL of DMEM medium. Cells were incubated for 24 h at 37°C in the CO_2 incubator. Cells were incubated for 24 and 48 h after adding the 5, 10, 25, 50, 100, 250, and 500 µM usnic acid concentrations. At the end of the incubation, 5 mg/mL of MTT (ODC Research and Development Inc., Turkey) were added to the cells, and the cells were incubated for an additional 4 h. After discarding the medium from the cells, 100 µL of DMSO was suffixed to all wells to dissolve the formazan dye that had formed. The intensity of the color that formed was measured spectrophotometrically at 570 nm.[12] The percentage of viable cells was calculated utilizing the following formula:

Cell Viability (%)= (OD test sample/OD control) X 100 (1)

LumiTracker Mito JC-1 Staining

JC-1 is a fluorescent dye used to evaluate mitochondrial membrane potential in apoptotic studies. The DU145 cells were added at a density of $1x10^6$ to 6-well plates. After being incubated for 24 h, 40 µM usnic acid was applied to the cells for another 48 h. The JC-1 dye (ThermoFisher T3168, Waltham, Massachusetts, USA) was added to all wells at a concentration of 10µg/mL, and the cells were incubated at 37°C for 10 min before taking images under a fluorescent microscope.[13]

Caspase-3 Activity Measurement

The DU145 cells were seeded at a density of $1x10^6$ to 6-well plates and then incubated for 24 h. Cells were exposed to 40 µM usnic acid for 48 h, after which the cells were lysed. Caspase-3 activity was measured with the aid of a colorimetric assay kit (Abcam, ab39401, Cambridge, UK).

Protein Expression Analysis (Western Blotting)

The DU145 cells were added at a density of $1x10^6$ to 6-well plates. The cells were incubated for 24 h in a CO_2 oven. Next, the DU145 cells were incubated with 40 µM of usnic acid for 48 h. After the incubation, the cells were collected, and 350 µL of the sample loading buffer (2X) were added to each samples, with the cell proteins underwent denaturation by heating at 95°C.

The stacking and separation gel were prepared utilizing the solutions of pH 6.8 0.5 M Tris, pH 8.8 1.5 M Tris, 10% sodium dodecyl sulphate (SDS), N,N,N,N-tetramethylethylenediamine (TEMED), 30% (w/w) acrylamide-bis-acrylamide, and 10% ammonium persulfate. The samples were then filled onto a gel containing 5-10 µg of protein. The samples underwent electrophoresis with the running buffer (38.4 mM glycine, 1% SDS, 5 mM Tris) for 1-2 h at 100V Following the electrophoresis procedure, immunoblotting was carried out by transferring the gels to the polyvinylidene difluoride membrane. The membrane was respectively washed 3 times using the Tris-buffered saline with 0.1% Tween (TBST) and distilled water. The membrane was blocked with 2.5% bovine serum albumin for 2 h. After washing the membrane 3 times with TBST, it was incubated with the primary antibodies of NF-κB p50 (Santa Cruz SC8414), NF-κB p65 (Santa Cruz SC8008), and β-Actin (Santa Cruz SC47778) overnight at +4°C. The membrane washing process was performed 3 times with TBST for five min each time. After the washings, the membrane was treated with horseradish peroxidase-conjugated secondary antibody for 2 h at room temperature. The membrane washing process was performed again 3 times with TBST for 5 min each time. The chemiluminescence reagent (ECL, Santa Cruz) was suffixed to the membrane for 1 min under dark conditions. Band imaging was performed with the help of an imaging system. Densitometric analysis of the protein blots was carried out with the program ImageJ.[14]

Gene Expression Analysis (qRT-PCR)

The total RNA isolation was drawn out from 5×10^6 DU145 cells as previously described.[15] In accordance with the cDNA Reverse Transcription Kit protocol (Applied Biosytems, Foster City, CA, USA), 1 µg total RNA was utilized for the reverse transcription. Real-time PCR reaction was performed using the *BAX, BCL2, NFKB1*, and *GAPDH* primers with a primer sequence of *BAX*: Forward 5'-GCCCTTTTGCTTCAGGGTTT-3', Reverse 5'-TCCAATGTCCAGCCCATGAT-3'; BCL2: Forward 5'-GACAGAAGATCATGCCGTCC-3', Reverse 5'-GGTACCAATGGCACTTCAAG-3'; *NFKB1*: Forward 5'-GGAGCACTACTTCTTGACCACC-3', Reverse 5'-TCTGTCCTGAGCATTGACGTC-3'; and *GAPDH*: Forward 5'-AGGGCTGCTTTTAACTCTGGT-3', Reverse 5'-CCCCACTTGATTTTGGAGGGA-3'. 100 ng of cDNA were copied using SYBR Green dye with the help of the ABI StepOne Plus detection system. The program characteristics for the amplification reaction involved heating at 95°C for 10 min, then 40 cycles of 95°C for 15 sec, 59°C for 1 min, and 72°C for 30 sec. The qPCR value was calculated utilizing the StepOne Software v2.3 (Applied Biosystems, Foster City, CA, USA), with the the *BAX, BCL2*, and *NFKB1* gene results being normalized to the *GAPDH* gene results.

Statistical Analysis

Statistical analysis was conducted using GraphPad Prism (ver. 7.0) software. The statistical analysis performed data entry for all experiments in triplicate and offered the results as mean ± Standard Deviation (SD) . Alterations between groups were specified by one-way analysis of variance (ANOVA) testing.

RESULTS

Cytotoxic Effects of Usnic Acid on DU145 Cells

The cytotoxic effects of the 5, 10, 25, 50, 100, 250 and 500 µM usnic acid applications on DU145 cells for 24 and 48 h were studied using the MTT method. DU145 cell viability was found to decrease in a dosage-dependent manner at both the 24- and 48-h measurements (Figure 1a; $p<0.05$ and $p<0.001$, respectively). The IC_{50} value of usnic acid regarding the DU145 cells was calculated as 167.06 ± 12.35 µM at 24 h and 42.15 ± 3.76 µM at 48 h. The morphologies of the DU145 cells treated with 40 µM ($\approx IC_{50}$) usnic acid were specified to change compared to the control group, with a decrease in intercellular contact (Figure 1b).

The Effects of Usnic Acids on Apoptosis

The intrinsic apoptotic pathway is known to be triggered by cytochrome c, a protein released as a result of deformation of the mitochondrial membrane. The mitochondrial membrane potentials of DU145 cells treated with 40 µM usnic acid were evaluated through JC-1 staining (Figure 2a). After JC-1 staining, the permeability of the mitochondrial membrane was determined to increase in DU145 cells that had been treated with usnic acid (Figure 2b). In addition, the study also measured caspase-3 activity, which is one of the intrinsic apoptotic molecules affected by cytochrome c released by increasing mitochondrial membrane permeability, and found the caspase-3 activity of DU145 cells treated with 40 µM usnic acid to have increased compared to the control group (Figure 2c).

The study tested the effects of usnic acid applications on *BAX* and *BCL2* gene expressions in the apoptotic pathway of DU145 cells using the qPCR method and found the DU145 cells treated with 40 µM usnic acid to have an increase in proapoptotic *BAX* gene expression and a decrease in anti-apoptotic *BCL2* gene expression compared to the control group (Figures 3a and 3b). In addition, the *BAX /BCL2* expression ratio of DU145 cells treated with 40 µM usnic acid was calculated to have increased by approximately eight compared to the control group (Figure 3c).

The Effects of Usnic Acid on NF-κB Pathways

The study evaluated the effect of usnic acid treatment on p50 and p65 protein expressions in the NF-κB pathway of DU145 cells using the Western blot method (Figure 4a) and found NF-κB p50 protein expression of DU145 cells treated with 40 µM usnic acid to decrease compared to the control group. However, no major change was found regarding p65 expression (Figures 4b and 4c). In addition, the *NFKB1* gene expressions of DU145 cells applied 40 µM usnic acid were found to decrease (Figure 4d).

DISCUSSION

Known as the plague of our age, cancer is the disease that causes the most death after cardiovascular system diseases. Intensive studies have been carried out to elucidate upon the formation mechanism of cancer and its treatment. The NF-κB pathway is known to be overexpressed in cancer cells.[16] The NF-κB transcription factor family includes five members: Rel A (p65), RelB, c-Rel, p105/p50, and p100/p52. Each of these proteins comprises an N-terminal Rel chain that enables nuclear localization, DNA binding, and dimerization. The NF-κB signaling pathway shows its molecular effects in two different ways: canonically and non-canonically. [17] Activation of the canonical pathway occurs with stimuli such as tumor necrosis factor (TNF) and interleukin 1 (IL1). Through pathway activation, IKKα, IKKβ, and IKKγ from the κB protein inhibitors trimerize to form the IκB complex. Under basal conditions, the IκB complex binds to the p65-p50 dimer, allowing the p65-p50 dimer to cross the nuclear membrane. The IκB complex, which
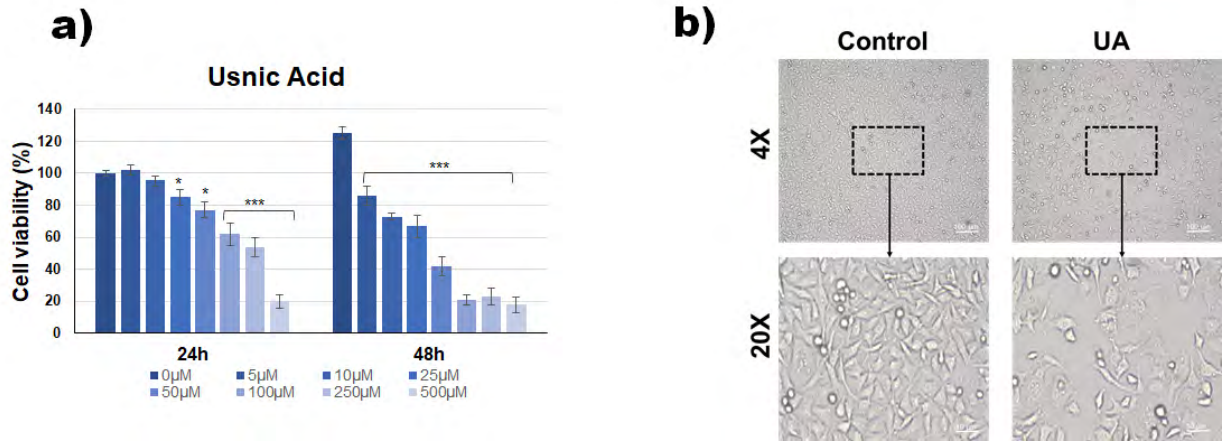
Figure 1. (a) Cell viability graph of DU145 cells treated with usnic acids for 24 and 48 h. **(b)** Inverted microscope images of DU145 cells treated with usnic acids (Scale bar= 100 µm) (*p<0.05; ***p<0.001).
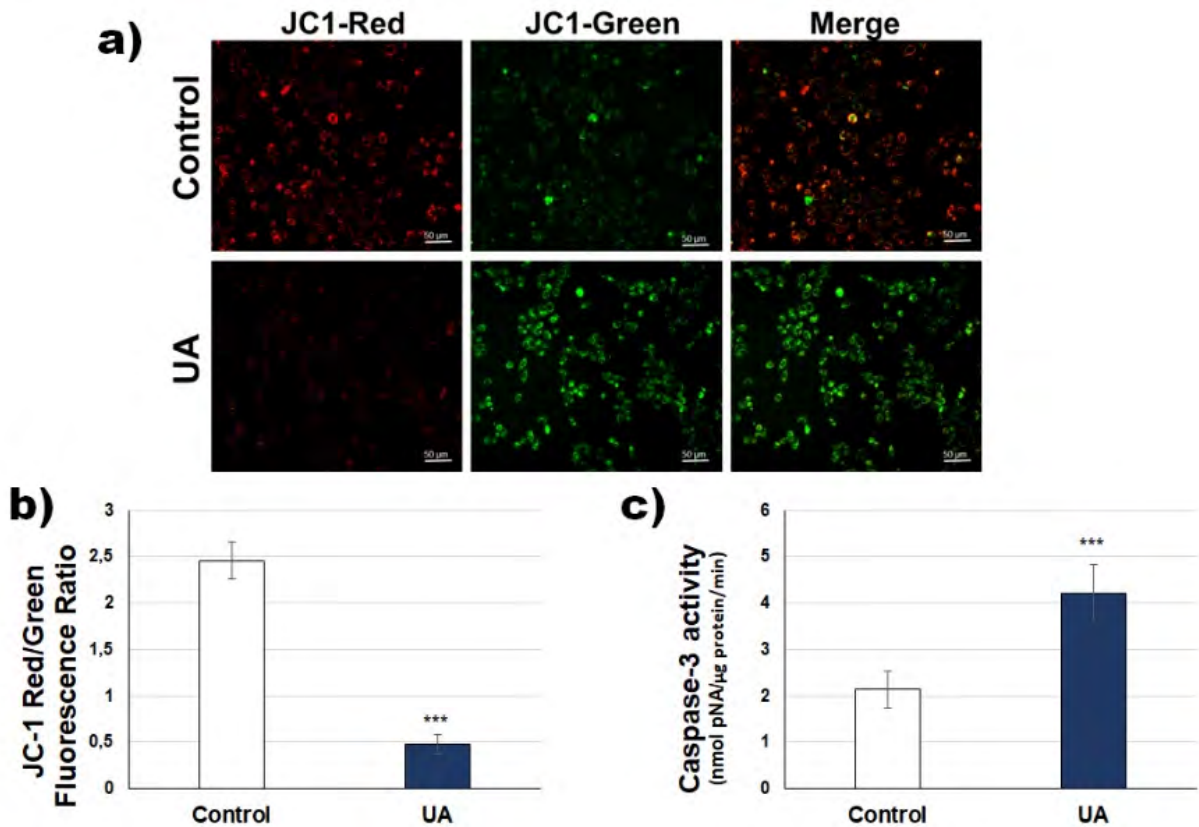

Figure 2. (a) JC-1 staining images of DU145 cells treated with usnic acid (Scale bar= 50 µm) **(b)** Graphical illustration of red/green ratio of DU145 cells treated with usnic acid **(c)** Caspase-3 activity graph of DU145 cells treated with usnic acid (***p<0.001).

returns to the cytoplasm, is degraded by ubiquitination. The p65-p50 dimer activates the transcription of target genes such as anti-apoptotic factors, cytokines (IL6), and proliferation factors (Cyclin D1) in the nucleus.[18,19] Studies are continuously increasing on the discovery of new molecules targeting the destruction of cancer cells by regulating this pathway. Various molecules have been discovered to inhibit the receptors that initiate the NF-κB pathway, such as adalimumab, etanercept, anakinra, brentuximab, and denosumab.[20] Cevik et al. stated a 1 nM cabazitaxel application reduced the expression of NF-κB 50 and led to apoptosis in PC3 cells.[21]

Studies on the isolation and use of plant-derived secondary
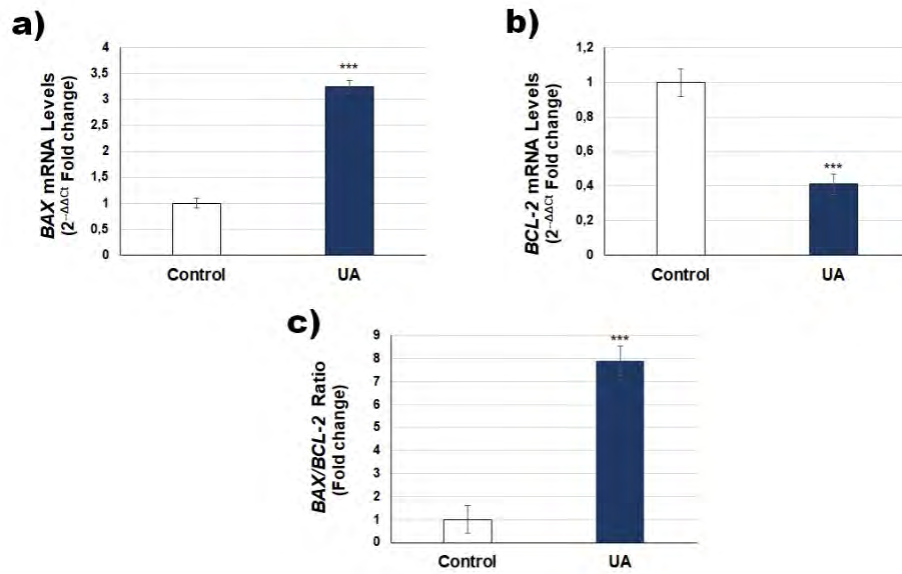
Figure 3. (a) Graphs of *BAX* gene expressions of DU145 cells after administration of usnic acids **(b)** Graphs of *BCL2* gene expressions of DU145 cells after administration of usnic acids **(c)** Graphical illustration of Bax/Bcl-2 ratio of DU145 cells treated with usnic acid (***p<0.001).
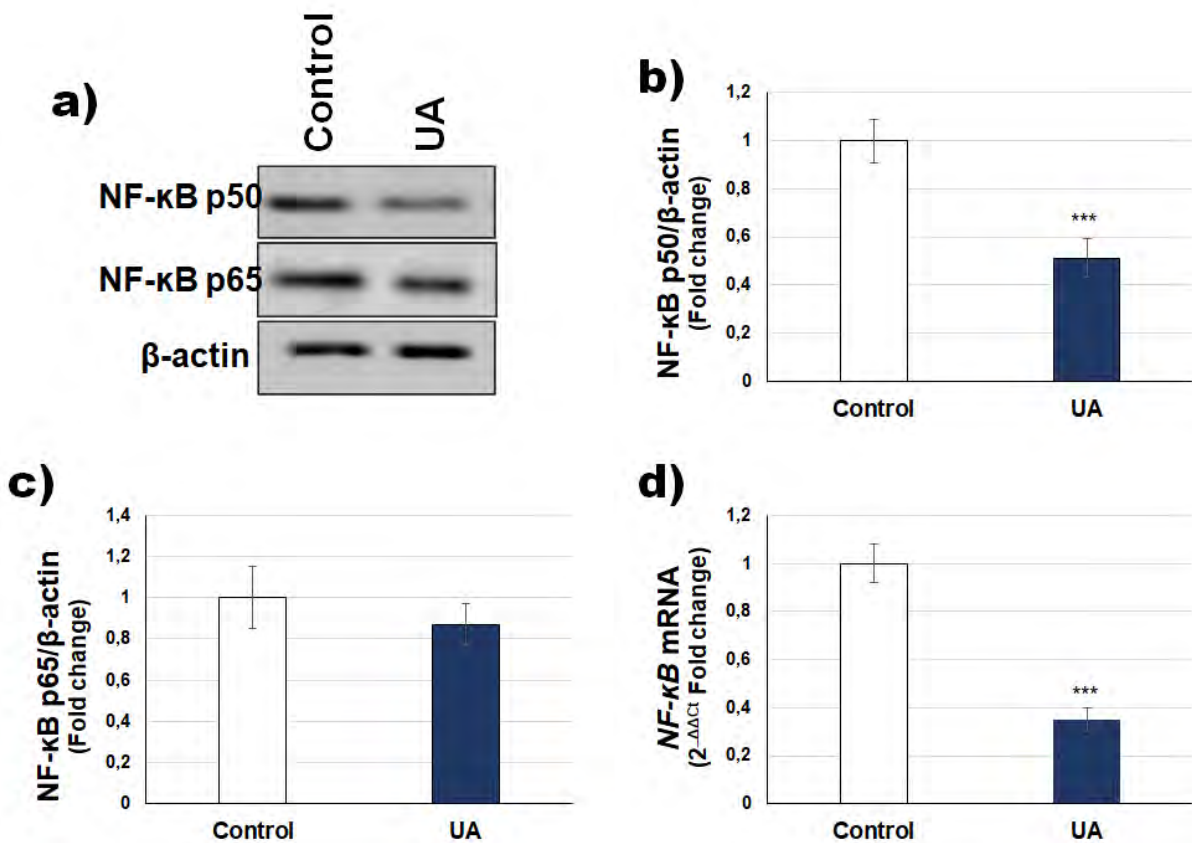
Figure 4. (a) NF-κB p50, NF-κB p65 and β-actin Western blot bands of DU145 cells treated with usnic acid **(b)** Graphs of NF-κB p50 protein expressions of DU145 cells after administration of usnic acid **(c)** Graphs of NF-κB p65 protein expressions of DU145 cells after administration of usnic acid **(d)** Graphs of *NFκB1* gene expressions of DU145 cells after administration of usnic acid (*** p<0.001).

metabolites have increased due to their high compatibility with living systems. Intensive research continueon studying the effectiveness of usnic acid isolated from lichen species.[22] The scavenging effect of reactive oxygen species, especially those produced in large amounts in cancer, has made usnic acid an agent that should be focused on in cancer treatment.[23] Cakmak and Gulcin reported usnic acid to perhaps be a promising agent in pharmaceutical applications due to having antioxidant properties such as high reducing ability, metal chelating, and radical scavenging.[9] On the other hand, usnic acid has been reported to cause free radical production at high doses, as well as mitochondrial stress in healthy hepatocyte cells.[24] A study conducted on healthy hepatocytes reported that usnic acid to cause mitochondrial glutation (GSH) depletion in cells at concentrations of 5 µM or higher and to dysregulate oxidative phosphorylation through adenosine triphosphate (ATP) reduction.[25] In isolated rat hepatocytes, the administration of usnic acid has been shown to cause toxicity and to decrease GSH by increasing lipid peroxidation.[26] Furthermore, when examining this effect over human hepatocellular cancer cells (HepG2), usnic acid was reported to increase cytochrome p450 activity, to cause mitochondrial dysregulation, and to trigger the oxidative stress mechanism.[27] The current study has shown this effect from usnic acid on mitochondria through JC-1 staining in prostate cancer cells to disrupt the mitochondrial membrane potential and lead the cells to apoptosis. Usnic acid decreased the permeability of mitochondria in DU145 cells and disrupted the oxidative phosphorylation balance of the cell. Changes in mitochondrial permeability may also alter transcription factors in cells and increase cellular stress. In addition, NF-κB signaling can regulate the expression of genes involved in mitochondrial function, including those encoding the components of the electron transport chain and antioxidant enzymes. This suggests that NF-κB may affect mitochondrial function beyond permeability.[28] NF-κB, particularly its p50 subunit, can affect mitochondrial permeability and function through various mechanisms, ultimately influencing cellular responses and physiological processes.[29] The current study has found usnic acid administration to suppress the NF-κB's p50 subunit by reducing mitochondrial permeability.

The most studied molecules in the apoptotic pathway regarding cancer treatment are the B-cell lymphoma-2 (BCL-2) for suppressing apoptosis and the Bcl-2-associated X protein (BAX) for promoting apoptosis. Various studies are also found in the literature to have examined the cytotoxic and anti-apoptotic effects of metabolites obtained from lichen species.[8] Takai et al. found usnic acid to exhibit cytotoxic effects regarding the Lewis lung carcinoma test system.[30] Cardarelli et al. found a decrease in the proliferation of K-562, Ishikawa, and HEC50 cells that had been treated with 50 µg/mL usnic acid.[31] Backorova et al. reported A2780 and HT-29 cells that had been treated with usnic acid to increase the Bax protein expression and to decrease p53 and Bcl-2 expression, thus ac-

tivating programmed cell death mechanisms.[32] Dincsoy and Duman emphasized usnic acid as a secondary metabolite of lichen to induce apoptosis by increasing the *BAX* expression and decreasing the *BCL2* expression of HEP2C, RD, and Wehi cells.[33] Similar to these studies, the current article also has found usnic acid to trigger cell death in DU145 cells by activating apoptotic pathways. Jin et al. reported usnic acid to exhibit anti-inflammatory behaviors by suppressing the NF-κB pathway in Raw 264.7 macrophage cells.[34] Although usnic acid is known to suppress the NF-κB pathway, its effects on NF-κB p50 and NF-κB p65 have yet to be clarified. This study has shown usnic acid administration to decrease proliferation by suppressing NF-κB p50 in DU145 human prostate cancer cells.

CONCLUSION

Prostate cancer remains one of the biggest health problems among men, and the need exists to develop new treatment options for prostate cancer. The current study's results have shown usnic acid regarding prostate cancer treatment to suppress NF-κB p50 by reducing mitochondrial permeability in the DU145 prostate cancer cells, thus triggering apoptosis in the cells. The results from this study may shed light on new molecular mechanisms for treating prostate cancer and may offer another treatment option for the use of usnic acid alone or in combination with existing chemotherapeutics used in treatment.

ORCID IDs of the authors

Omer Erdogan   0000-0002-8327-7077
Burcin Irem Abas   0000-0002-1018-5577
Ozge Cevik   0000-0002-9325-3757

REFERENCES

1. Sung H, Ferlay J, Siegel RL, et al. Global cancer statistics 2020: GLOBOCAN estimates of incidence and mortality worldwide for 36 cancers in 185 countries. *CA: Cancer J Clin*. 2021;71(3):209-249.

2. Gandaglia G, Leni R, Bray F, et al. Epidemiology and prevention of prostate cancer. *Eur Urol Oncol*. 2021;4(6):877-892.

3. Rawla P. Epidemiology of prostate cancer. *World J Oncol*. 2019;10(2):63-89.

4. Hurwitz M. Chemotherapy in prostate cancer. *Curr Oncol Rep*. 2015;17:1-10.

5. Erstad DJ, Cusack JC. Targeting the NF-κB pathway in cancer therapy. *Surg Oncol Clin*. 2013;22(4):705-746.

6. Rinkenbaugh AL, Baldwin AS. The NF-κB pathway and cancer stem cells. *Cells*. 2016;5(2):16. doi: 10.3390/cells5020016.

7. Ingolfsdottir K. Usnic acid. *Phytochem*.2002;61(7):729-736.

8. Araújo AA, de Melo MG, Rabelo TK, et al. Review of the biological properties and toxicity of usnic acid. *Nat Prod Res*. 2015;29(23):2167-2180.

9. Cakmak KC, Gulcin I. Anticholinergic and antioxidant activities of usnic acid-an activity-structure insight. *Toxicol Rep*. 2019;6:1273-1280.

10. Hoa NT, Van Bay M, Mechler A, Vo QV. Is usnic acid a promising radical scavenger? *ACS Omega*. 2020;5(28):17715-17720.

11. Maulidiyah M, Rachman F, Mulkiyan OMZ, et al. Antioxidant activity of usnic acid compound from methanol extract of *Lichen usnea* sp. *J Oleo Sci*. 2023;72(2):179-188.

12. Erdoğan Ö, Paşa S, Demirbolat GM, Çevik Ö. Green biosynthesis, characterization, and cytotoxic effect of magnetic iron nanoparticles using *Brassica oleracea var capitata sub var rubra* (red cabbage) aqueous peel extract. *Turk J Chem*. 2021; 45(4):1086-1096.

13. Sivandzade F, Bhalerao A, Cucullo L. Analysis of the mitochondrial membrane potential using the cationic JC-1 dye as a sensitive fluorescent probe. *Bio-protoc*. 2019;9(1):e3128. doi: 10.21769/BioProtoc.3128.

14. Erdogan O, Cevik O. Myricetin can control metastasis and invasion by suppressing ATF2-related signaling pathway in Rapamycin-resistant HepG2 hepatocellular cancer cells. *J Res Pharm*. 2023;27(2):557-565.

15. Pasa S, Erdogan O, Cevik O. Design, synthesis and investigation of procaine based new Pd complexes as DNA methyltransferase inhibitor on gastric cancer cells. *Inorg Chem Commun*. 2021;132:108846. https://doi.org/10.1016/j.inoche.2021.108846.

16. Inoue Ji, Gohda J, Akiyama T, Semba K. NF-B activation in development and progression of cancer. *Cancer Sci*. 2007;98(3):268-274.

17. Sun SC. The non-canonical NF-B pathway in immunity and inflammation. *Nat Rev Immunol*. 2017;17(9):545-558.

18. Naugler WE, Karin M. NF-B and cancer—identifying targets and mechanisms. *Curr Opin Genet Dev*. 2008;18(1):19-26.

19. Yamamoto Y, Gaynor RB. Therapeutic potential of inhibition of the NF-κB pathway in the treatment of inflammation and cancer. *J Clin Invest*. 2001;107(2):135-142.

20. Ramadass V, Vaiyapuri T, Tergaonkar V. Small molecule NF-κB pathway inhibitors in clinic. *Int J Mol Sci*. 2020;21(14):5164. doi: 10.3390/ijms21145164

21. Cevik O, Acidereli H, Turut FA, Yildirim S, Acilan C. Cabazitaxel exhibits more favorable molecular changes compared to other taxanes in androgen-independent prostate cancer cells. *J Biochem Mol Toxicol*. 2020;34(9):e22542. doi: 10.1002/jbt.22542.

22. Odabasoglu F, Cakir A, Suleyman H, et al. Gastroprotective and antioxidant effects of usnic acid on indomethacin-induced gastric ulcer in rats. *J Ethnopharmacol*. 2006; 103(1):59-65.

23. Kohlhardt-Floehr C, Boehm F, Troppens S, Lademann J, Truscott TG. Prooxidant and antioxidant behaviour of usnic acid from lichens under UVB-light irradiation–Studies on human cells. *J Photochem Photobiol B*. 2010;101(1):97-102.

24. Han D, Matsumaru K, Rettori D, Kaplowitz N. Usnic acid-induced necrosis of cultured mouse hepatocytes: Inhibition of mitochondrial function and oxidative stress. *Biochem Pharmacol*. 2004;67(3):439-451.

25. Pramyothin P, Janthasoot W, Pongnimitprasert N, Phrukudom S, Ruangrungsi N. Hepatotoxic effect of (+) usnic acid from Usnea siamensis Wainio in rats, isolated rat hepatocytes and isolated rat liver mitochondria. *J Ethnopharmacol*. 2004;90(2-3): 381-387.

26. Sonko BJ, Schmitt TC, Guo L, et al. Assessment of usnic acid toxicity in rat primary hepatocytes using 13C isotopomer distribution analysis of lactate, glutamate and glucose. *Food Chem Toxicol*. 2011;49(11):2968-2974.

27. Sahu SC, Amankwa-Sakyi M, O'Donnell Jr MW, Sprando RL. Effects of usnic acid exposure on human hepatoblastoma HepG2 cells in culture. *J Appl Toxicol*. 2012;32(9):722-730.

28. Mariappan N, Elks CM, Sriramula S, et al. NF-κB-induced oxidative stress contributes to mitochondrial and cardiac dysfunction in type II diabetes. *Cardiovasc Res*. 2010;85(3):473-483.

29. Elks CM, Mariappan N, Haque M, Guggilam A, Majid DS, Francis J. Chronic NF-κB blockade reduces cytosolic and mitochondrial oxidative stress and attenuates renal injury and hypertension in SHR. *Am J Physiol Renal Physiol*. 2009;296(2):298-305.

30. Takai M, Uehara Y, Beisler JA. Usnic acid derivatives as potential antineoplastic agents. *J Med Chem*. 1979; 22(11):1380-1384.

31. Cardarelli M, Serino G, Campanella L, et al. Antimitotic effects of usnic acid on different biological systems. *Cell Mol Life Sci*. 1997;53:667-672.

32. Bačkorová M, Jendželovský R, Kello M, Bačkor M, Mikeš J, Fedoročko P. Lichen secondary metabolites are responsible for induction of apoptosis in HT-29 and A2780 human cancer cell lines. *Toxicol In Vitro*. 2012;26(3): 462-468.

33. Dincsoy AB, Duman DC. Changes in apoptosis-related gene expression profiles in cancer cell lines exposed to usnic acid lichen secondary metabolite. *Turk J Biol*. 2017;41(3): 484-493.

34. Jin JQ, Li CQ, He LC. Down-regulatory effect of usnic acid on nuclear factor-κB-dependent tumor necrosis factor-α and inducible nitric oxide synthase expression in lipopolysaccharide-stimulated macrophages RAW 264.7. *Phytother Res*. 2008; 22(12):1605-1609.

How to cite this article

Stevioside Improves Brain Oxidant-Antioxidant Status in Overfed Zebrafish

Esra Dandin[1], Ismail Unal[1], Merih Beler[1], Unsal Veli Ustundag[2], Derya Cansiz[2], Perihan Seda Ates Kalkan[3], Ebru Emekli-Alturfan[4]

[1]Marmara University, Institute of Health Sciences, Department of Biochemistry, Istanbul, Turkiye
[2]Department of Biochemistry, Faculty of Medicine, Istanbul Medipol University, Kavacık, Istanbul, Turkiye
[3]Department of Biochemistry, Istanbul Health and Technology University, Istanbul, Turkiye
[4]Marmara University, Faculty of Dentistry, Deparment of Basic Medical Sciences, Istanbul, Turkiye

ABSTRACT

Objective: An excessive buildup of adipose tissue is a defining feature of overnutrition, and a significant fraction of the world's population suffers from obesity. Overnutrition is associated with the deterioration of mitochondrial functions in the brain in the case of obesity. In this study, we evaluated the effects of stevioside (ST) which is a calorie-free, naturally occurring herbal sweetener made from *Stevia rebaudiana* (Bertoni) on the oxidant-antioxidant balance in the brain in cases of overnutrition. Accordingly, the effects of ST consumption on the oxidant-antioxidant balance in the brain was evaluated and determined in a case study of overfeeding adult zebrafish for 15 days.

Materials and Methods: Zebrafish were placed in four groups; the control group (C); overfed group (OF); low-dose (1mg/L) ST treated OF group (OF+LDS); and the high-dose ST (5mg/L) treated OF group (OF+HDS). The levels of lipid peroxidation (LPO) were evaluated together with nitric oxide (NO) to determine the oxidant status. The antioxidant status from the activities of the superoxide dismutase (SOD) and glutathione S-transferase (GST) were determined in brain tissues.

Results: The ST treatment decreased the increased LPO and NO levels in overfed zebrafish and increased SOD and GST activities in a dose-dependent manner.

Conclusion: ST exerted an antioxidant effect on the possible damage mechanisms that could occur in the brain in case of overnutrition by decreasing oxidative stress and improving the antioxidant enzyme activities.

Keywords: Stevioside, overfeeding, brain, oxidant-antioxidant status, zebrafish

INTRODUCTION

Excessive adipose tissue buildup is a defining property of obesity, and a significant fraction of the world's population suffers from obesity related to overnutrition. Overnutrition is linked to elevated chronic diseases risks, including type 2 diabetes, and is a significant cause for premature death and related diseases.[1] Obesity is preventable by physical and nutritional therapies because it is induced by poor diet and insufficient physical activity.[2] A link between obesity and cognitive impairments is reported, as lowered or disrupted mental and/or intellectual functions. In neuroimaging studies, obesity is connected to altered structural and functional features of the brain and linked to increased Alzheimer's disease risk.[3] The brain regulates body weight through its neurotransmitters so obesity and the brain are related. Moreover, obesity-related inflammation and oxida-tive stress may spread to the brain and cause significant changes in the neurotransmitter metabolism and its function.[4]

The substitution of sugars with artificial sweeteners, which provide a sweeter taste without calories, appeared to hold promise for lowering sugar and energy intake. Stevia is a calorie-free, naturally occurring herbal sweetener that is more than 100-300 times sweeter than table sugar. The components that give stevia, its sweet flavor are called steviol glycosides, and they are present on the leaves of *Stevia rebaudiana*, a South American plant.[5] The digestive enzymes found in the gastrointestinal tract are unable to hydrolyze steviol glycosides. But steviol glycosides are broken down by colon microbiota, especially bacteroides.[6] Stevia extracts act as antioxidants and beneficially affect blood pressure and hypertension.[7,8] Stevia leaves contain a diterpenoid called stevioside (ST) and benefi-

cial effects of ST consumption were reported in a diet induced obesity model on parameters related with oxidant-antioxidant balance, inflammation, and insulin resistance and its epigenetic modulation.[8]

Zebrafish are used as model organisms to test pharmacological and toxicological features of novel substances. Both zebrafish larvae and adults are proven to be suitable for analyzing the impacts of novel substances on glucose metabolism.[8] An analysis on the liver and pancreatic tissues RNA-sequence revealed that zebrafish models with type 2 diabetes have pathophysiology that is comparable to that of humans.[8,9]

Although there are reports about the deterioration of mitochondrial functions in the brain in the case of obesity associated with overnutrition, there was no data on the effects of sweeteners, especially ST, on the brain tissue oxidant-antioxidant balance in cases of overnutrition. This current study examined the effects of ST on the oxidant-antioxidant status of brain tissue in the overfeeding model generated in zebrafish.

MATERIALS AND METHODS

Animals and Treatment

All experiments were performed in line with the European Communities Council Directive of 24 November 1986 (86/609/EEC). The methods applied were accepted by the Marmara University Animal Care and Use Committee (98.2018). Wild-type zebrafish were used as the AB/AB strain and fish (4–6 months old) were kept in a special aquarium rack system (ZebTEC, Tecniplast, Italy). The housing conditions included 27-28±1°C, 14/10 h light/dark cycle. Four groups were randomly formed, with 10 fish in each group as the control group (C); overfed group (OF); low-dose (1 mg/L) ST (Tokyo Chemical Industry, S0594) treated OF group (OF+LDS); and the high-dose ST (5 mg/L) treated OF group. The dose of ST was adapted from the study of Chang et al.[10] The OF was induced through feeding 120 mg commercial fish food /fish/day for six feeding intervals daily with an automatic feeding system.[8] The healthy control group was given 20 mg commercial fish food per day. The fish in the OF-LDS and OF-HDS groups were treated with 1 mg/L and 5 mg/L ST correspondingly, which was included to the aquarium water.[8] Every day the water content in the tanks was renewed and the exposure solutions were renewed. After two weeks the zebrafish were anesthetized in tricaine solution prior to the removal of brain tissues.

Biochemical Analyses

The brain tissues were homogenized in physiological saline and 10% (w/v) homogenates were prepared. For the biochemical analyses supernatants obtained from homogenates were used. The total protein levels in the samples were analyzed by Lowry's method[11] in order to give the analyzed parameters

per protein value. The lipid peroxides indicated damage to cell membranes from oxidation and determined the effect of overfeeding on lipid peroxidation (LPO) in the brain. The method of Yagi was applied to determine the malondialdehyde (MDA) levels as the thiobarbituric acid reactive molecules formed in the final LPO products.[12,13] The NO levels were evaluated using the Miranda et al.'s method as a contributing factor to oxidative stress.[14,15] A critical element in the antioxidant mechanism in response to oxidative stress is superoxide dismutase (SOD), and the SOD activity was evaluated as suggested in the method explained by Mylorie et al.[16] The Glutathione S-Transferase (GST) which contributes to the antioxidant defense mechanism by catalyzing the combination of glutathione (GSH) and GST activity in the brain was evaluated by the spectrophotometer at 340 nm.[17] The experiments were performed by researchers' blind to the treatment groups.

Statistical Analysis

The GraphPad Prism 5.0 (GraphPad Software, San Diego, USA) program was used for the statistical analysis of the data obtained. The results are presented as mean±standard deviation (SD). The Shapiro–Wilk test was used for data normality and the Kruskal Wallis test to compare the data among the four groups and then the Dunn's multiple comparison test was applied. When the P levels are lower than 0.05, the differences were considered significant.

RESULTS

The results of the study showed increased LPO in the OF group ($p < 0.01$) and the ST treatment decreased LPO in the OF group both at low and high doses ($p < 0.01$) (Figure 1).
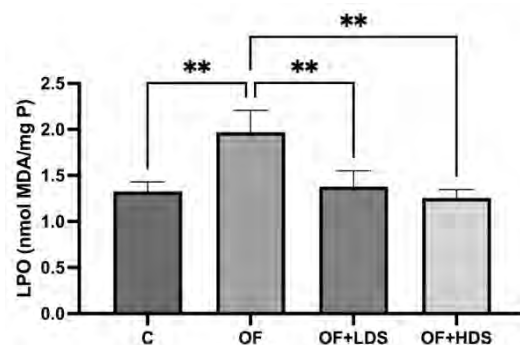

Figure 1. Lipid peroxidation (LPO) levels of the Control (C), overfed (OF), OF+low-dose stevioside (OF+LDS) and OF+high-dose stevioside (OF+HDS) groups. Values are given as means±SD; n= 4, four independent biological replicates were prepared for each treatment. For each biological replicate, three technical replicates were performed. ** $p < 0.01$ significantly different.

Similarly, higher NO levels were determined in the OF group when compared to the control group ($p < 0.0001$) and both low and high doses of ST decreased NO levels significantly in the

OF group (p < 0.001 and p < 0.0001 respectively). The NO levels in the OF+LDS and OF+HDS groups were significantly lower than the Control group (p < 0.0001 and p < 0.001 respectively). In the OF+HDS group the NO levels were found to be significantly lower than that of the OF+LDS group (p < 0.05) (Figure 2).
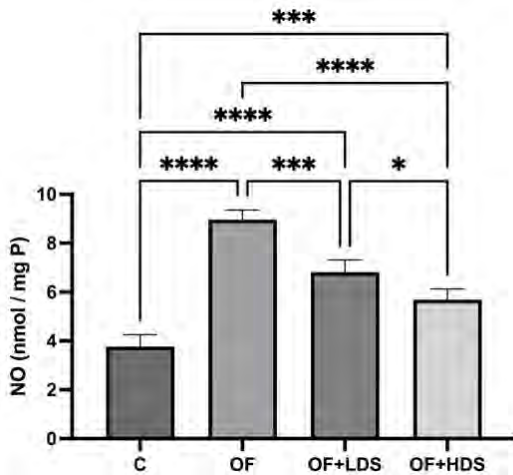

Figure 2. Nitric Oxide (NO) levels of the Control (C), overfed (OF), OF+low-dose stevioside (OF+LDS) and OF+high-dose stevioside (OF+HDS) groups. Values are given as means±SD; n= 4, four independent biological replicates were prepared for each treatment. For each biological replicate, three technical replicates were performed. **** p < 0.0001; *** p < 0.001; ** p < 0.01, * p < 0.05.

The SOD activities decreased significantly in the OF group (p < 0.05). Low dose and high dose ST increased SOD activities significantly in the OF group (p < 0.01 and p < 0.001 respectively) (Figure 3).
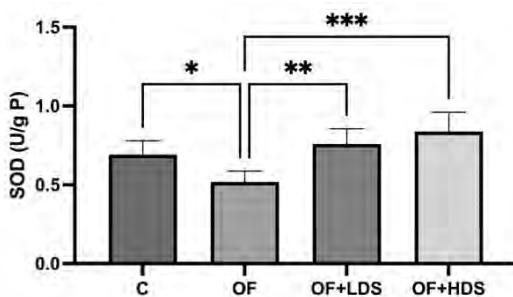

Figure 3. Superoxide dismutase (SOD) activities of the Control (C), overfed (OF), OF+low-dose stevioside (OF+LDS) and OF+high-dose stevioside (OF+HDS) groups. Values are given as means±SD; n= 4, four independent biological replicate were prepared for each biological replicate, three technical replicates were performed. *** p < 0.001; ** p < 0.01, * p < 0.05.

GST activities decreased significantly in the OF group when compared with the Control group (p < 0.05). Low and high doses of ST treatments increased GST activities significantly in the OF group (p < 0.05 and p < 0.0001 respectively). Moreover, there was a significant increase in the GST activity of the

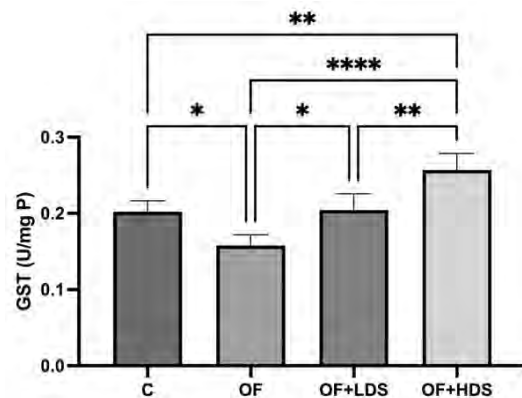OF+HDS group when compared with the OF+LDS group (p < 0.01) (Figure 4).

Figure 4. Glutathione S-transferase (GST) activities of the Control (C), overfed (OF), OF+low-dose stevioside (OF+LDS) and OF+high-dose stevioside (OF+HDS) groups. Values are given as means±SD; n= 4, four independent biological replicates were prepared for each treatment. For each biological replicate, three technical replicates were performed. **** p < 0.0001; ** p < 0.01, * p < 0.05.

DISCUSSION

Imbalanced nutrition is becoming recognized as a significant primary health problem that reduces quality of life due to its related comorbidities, which include diabetes, cardiovascular disease, cancer, hepatic and renal dysfunction, and infertility.[18] It is a multifactorial and complex metabolic condition. Increasing research points to oxidative stress as a crucial link between obesity and its related problems.[19] Through a variety of physiological mechanisms, including the production of superoxide by NADPH oxidases, electron transport chain, and activation of protein kinase C overnutrition can itself cause systemic oxidative stress.[18,19]

Because of its intense and specialized metabolic functions, the brain is especially vulnerable to oxidant injury. High oxygen consumption, almost solely oxidative phosphorylation, lack of energy stores, high quantities of lipids susceptible to oxidation, and high iron levels all operate as pro-oxidants.[20] Because of this, oxidative stress and associated metabolic/ischemic damage to neuronal cells are a serious concern.

The view that diet-induced obesity is associated with deterioration in brain functions has gained importance in recent years. From this point of view, when we examined the effects of overnutrition, which is the leading cause of obesity, on the oxidant-antioxidant status in the brain we found that the oxidant-antioxidant balance was disturbed by overfeeding in zebrafish and ST consumption improved this balance.

Increased lipid levels, deficiencies of vitamin and minerals, inflammation, hyperleptinemia, endothelial dysfunction, impaired mitochondrial function, and hyperglycemia are some

potential causes of oxidative stress in obese people.[18] Traditional plasma, serum, or urine indicators of oxidative stress that include MDA, BMI and oxidative stress indicators are found to correlate significantly and positively.[21]

The primary mechanism of oxidative stress due to reactive oxygen species (ROS) is lipid peroxidation. Since reactive species are not stable, they interact with nearby molecules fast. The sort of injury formed due to oxidant stress is consequently difficult to guess because it is a very quick disease. Microglia and astrocytes are the principal sources of ROS and reactive nitrogen species (RNS).[22] In this study both brain LPO and NO levels increased in overfed zebrafish indicating increased oxidative stress due to overfeeding. It is generally known that metabolic diseases including obesity cause abnormalities in brain structure and function. During white adipose tissue expansion, immune cells, in particular macrophages may infiltrate.[23] Adipose tissue expansion is also related with the activation of proinflammatory cytokines especially IL-6, IL-1β, and TNF-α. Systemic and chronic low-grade inflammation may lead to neuroinflammation and alter certain structures in the brain including the cerebellum and hypothalamus.[24] Since dysfunction of mitochondria is closely associated with oxidant stress and inflammation leading to cellular oxidative damage, disrupted oxidant-antioxidant balance as evidenced in this study with increased LPO, NO and decreased activities of antioxidant enzymes SOD and GST, may be related with mitochondrial dysfunction in brain due to overfeeding. Consistent with the results of this study lower SOD activity was reported in the erythrocytes obtained from obese subjects when compared to those of nonobese subjects.[18] The mRNA transcript levels of GST isoforms were found to be decreased in the livers of diet induced obesity in mice.[25] Continuous inflammatory conditions prevalent in obesity may suppress endogenous antioxidants including SOD as well as GST. This condition is related to adipocytes that generate too many adipokines that increase the generation of ROS, which will eventually result in oxidative stress.

To combat the rising prevalence of obesity, a variety of approaches are advised, including regular exercise, meal replacements, vitamin supplementation, and a diet rich in fruits and vegetables. Losing weight lowers oxidation indicators, boosts antioxidant mechanisms, and lowers the main risk factors linked to obesity.[18] Consuming foods high in antioxidants, vitamins, phytochemicals, probiotics, monounsaturated and omega-3 polyunsaturated fatty acids are shown to help manage body weight and lower the prevalence of metabolic illnesses.[26] As a herbal non-caloric sweetener, stevia is widely used. Glycosides like ST, rebaudioside A, and B are the major ingredients of stevia.[7] Stevia exhibits strong antioxidant potential as a sugar substitute in addition to providing sweetness because of various compounds with therapeutic value, including phenolic compounds, flavonoids, stevioside, tannins, and anthocyanins.[27]

In this study, ST improved the oxidant-antioxidant status in the brain, which was disturbed due to overnutrition, by lowering the LPO and NO and increasing the SOD and GST activities. Increased GST activity could have a significant role in the brain as GSH and GSH-related enzymes are reported to play significant roles in the antioxidant defense in the brain under both normal and obese conditions.[28] Dandin et al. investigated the effects of ST treatment on the epigenetic and metabolic modulators of insulin resistance, glucose tolerance, and oxidant-antioxidant balance in overfed zebrafish.[8] They reported impaired glucose tolerance and increased body weight, glucose levels, *fbf21, lepa, ll21, tnfα* expressions as well as LPO and NO in hepatopancreatic tissues of zebrafish after 15 days of overfeeding.[8] On the other hand, SOD and GST activities, and *dnmt3a* expression as an epigenetic insulin resistance regulator were decreased. Unlike this study, in the current study, it was determined that ST corrected oxidant antioxidant status in brain tissue in the overfeeding model generated in zebrafish. The fact that obesity-related neuropeptides were not examined in the brain in order to reveal the relationship between obesity and the brain more clearly could be considered as a limitation of this study.

CONCLUSION

This study emphasized the significance of oxidative stress in the emergence of various obesity-related health concerns and showed for the first time that ST can exert an antioxidant effect on the possible damage mechanisms that may occur in the brain in case of overnutrition.

ORCID IDs of the authors

Esra Dandin	0000-0003-1096-1553
Ismail Unal	0000-0002-8664-3298
Merih Beler	0000-0002-3828-4630
Unsal Veli Ustundag	0000-0003-0804-1475
Derya Cansiz	0000-0002-6274-801X
Perihan Seda Ates Kalkan	0000-0002-4905-1912
Ebru Emekli-Alturfan	0000-0003-2419-8587

REFERENCES

1. Blüher M. Obesity: Global epidemiology and pathogenesis. *Nat Rev Endocrinol*. 2019;15:288–298.

2. Matikainen-Ankney BA, Kravitz AV. Persistent effects of obesity: A neuroplasticity hypothesis. *Ann N Y Acad Sci*. 2018;1428:221–239.

3. Livingston G, Huntley J, Sommerlad A, et al. Dementia prevention, intervention, and care: 2020 report of the Lancet Commission. *Lancet*. 2020;396:413–446.

4. Labban RSM, Alfawaz H, Almnaizel AT, et al. High-fat diet-induced obesity and impairment of brain neurotransmitter pool. *Transl Neurosci*. 2020; 1:11(1):147-160.

5. Pang MD, Goossens GH, Blaak EE. The impact of artificial sweeteners on body weight control and glucose homeostasis. *Front Nutr*. 2021;7:598340. doi:10.3389/fnut.2020.598340

6. Gardana C, Simonetti P, Canzi E, Zanchi R, Pietta P. Metabolims of stevioside and rebaudioside: A from *Stevia rebaudiana* extracts by human microflora. *J Agric Food Chem*. 2003;51:6618–6622.

7. Goyal SK, Samsher, Goyal RK. Stevia (*Stevia rebaudiana*) a biosweetener: A review. *Int J Food Sci Nutr*. 2010;61(1):1-10.

8. Dandin E, Üstündağ ÜV, Ünal İ, et al. Stevioside ameliorates hyperglycemia and glucose intolerance, in a diet-induced obese zebrafish model, through epigenetic, oxidative stress and inflammatory regulation. *Obes Res Clin Pract*. 2022;16(1):23-29.

9. Zang L, Shimada Y, Nishimura N. Development of a novel zebrafish model for type 2 diabetes mellitus. *Sci Rep*. 2017;7:1461. doi:10.1038/s41598-017-01432-w

10. 1Chang JC, Wu MC, Liu IM, Cheng JT. Increase of insulin sensitivity by stevioside in fructose-rich chow-fed rats. *Horm Metab Res*. 2005;37(10):610–616.

11. Lowry OH, Rosebrough NJ, Farr AL, et al. Protein measurement with the Folin phenol reagent. *J Biol Chem*. 1951;193:265–275.

12. Ayala A, Muñoz MF, Argüelles S. Lipid peroxidation: Production, metabolism, and signaling mechanisms of malondialdehyde and 4-hydroxy-2-nonenal. *Oxid Med Cell Longev*. 2014;360438. doi:10.1155/2014/360438

13. Yagi K. Assay for blood plasma or serum. *Methods Enzymol*. 1981;105:328–337.

14. Lubos E, Handy DE, Loscalzo J. Role of oxidative stress and nitric oxide in atherothrombosis. *Front Biosci*. 2008;1:13:5323-5344.

15. Miranda KM, Espey MG, Wink DA. A rapid, simple spectrophotometric method for simultaneous detection of nitrate and nitrite. *Nitric Oxide*. 2001;5(1):62–71.

16. Mylorie AA, Collins H, Umbles C, Kyle J. Erythrocyte SOD activity and other parameters of copper status in rats ingesting lead acetate. *Toxicol Appl Pharmacol*. 1986;82:512–520.

17. Habig WH, Jacoby WB. Assays for differentiation of glutathione-S-transferases. *J Biol Chem*. 1974;249(22):7130–7139.

18. Manna P, Jain SK. Obesity, oxidative stress, adipose tissue dysfunction, and the associated health risks: Causes and therapeutic strategies. *Metab Syndr Relat Disord*. 2015;13(10):423-44.

19. Savini I, Catani MV, Evangelista D, et al. Obesity-associated oxidative stress: Strategies finalized to improve redox state. *Int J Mol Sci*. 2013;14:10497–10538.

20. Saeed SA, Shad KF, Saleem T, Javed F, Khan MU. Some New Prospects in the Understanding of the Molecular Basis of the Pathogenesis of Stroke. *Exp Brain Res*. 2007;182:1–10.

21. Vincent HK, Taylor AG. Biomarkers and potential mechanisms of obesity-induced oxidant stress in humans. *Int J Obes (Lond)*. 2006;30:400–418.

22. Shirley R, Ord E, Work L. Oxidative stress and the use of antioxidants in stroke. *Antioxidants*. 2014;3:472–501.

23. Sofi F, Abbate R, Gensini GF, et al. Accruing evidence on benefits of adherence to the Mediterranean diet on health: An updated systematic review and meta-analysis. *Am J Clin Nutr*. 2010;92:1189–1196.

24. de Paula GC, Brunetta HS, Engel DF, et al. Hippocampal function is impaired by a short-term high-fat diet in mice: Increased blood-brain barrier permeability and neuroinflammation as triggering events. *Front Neurosci*. 2021;15:734158. doi:10.3389/fnins.2021.734158

25. Ghosh Dastidar S, Jagatheesan G, Haberzettl P, Shah J, Hill BG, Bhatnagar A, Conklin DJ. Glutathione S-transferase P deficiency induces glucose intolerance via JNK-dependent enhancement of hepatic gluconeogenesis. *Am J Physiol Endocrinol Metab*. 2018;1:315(5):E1005-E1018.

26. Schmitt LO, Gaspar JM. Obesity-induced brain neuroinflammatory and mitochondrial changes. *Metabolites*. 2023;5:13(1):86. doi:10.3390/metabo13010086

27. 27. Ghanta S, Banerjee A, Poddar A, Chattopadhyay S. Oxidative DNA damage preventive activity and antioxidant potential of *Stevia rebaudiana* (Bertoni) Bertoni, a natural sweetener. *J Agric Food Chem*. 2007;26:55(26):10962-10967.

28. Del Rosario A, McDermott MM, Panee J. Effects of a high-fat diet and bamboo extract supplement on anxiety- and depression-like neurobehaviors in mice. *Br J Nutr*. 2012;108(7):1143-1149.

İSTANBUL
UNIVERSITY
P R E S S

Effect of Gluten-Free Diet on Serum Antioxidant Levels in Children with Celiac

Mehmet Ali Gul[1], Fatma Betul Ozgeris[2], Nezahat Kurt[3] Burcu Volkan[4], Ali Islek[5], Atilla Cayir[6]

[1] Amasya University, Faculty of Medicine, Department of Medical Biochemistry, Amasya, Turkiye
[2] Ataturk University, Faculty of Healthy Sciences, Department of Nutrition and Dietetics, Erzurum, Turkiye
[3] Erzincan Binali Yildirim University, Faculty of Medicine, Department of Medical Biochemistry, Erzincan, Turkiye
[4] Marmara University, Faculty of Medicine, Department of Pediatric Gastroenterology, İstanbul, Turkiye
[5] Ataturk University, Faculty of Medicine, Department of Pediatric Gastroenterology, Erzurum, Turkiye
[6] Erzurum Regional Training and Research Hospital, Department of Pediatric Pediatric Endocrinology, Erzurum, Turkiye

ABSTRACT

Objective: Celiac disease (CD) is an inflammatory condition of the small intestine triggered by the consumption of gluten. A strict gluten-free diet (GFD) is the only treatment that can eliminate CD complications. It was aimed to evaluate the effect of a gluten-free diet on serum total glutathione (tGSH) level, superoxide dismutase (SOD), myeloperoxida (MPO), paroxanase (PON-1) and aryl esterase (ARE) activity in patients with celiac disease, an autoimmune disease.

Materials and Methods: The study was conducted with 68 participants, 39 of whom were celiac and 29 were healthy. Two groups were formed in patients with celiac disease as newly diagnosed and previously diagnosed and following a gluten-free diet. Blood samples were taken from all participants and tGSH, SOD, MPO, PON-1, and ARE measurements were made spectrophotometrically from serum samples.

Results: While no significant change was observed in tGSH, SOD, and ARE levels, MPO activity was observed to be significantly lower in celiac patients compared to healthy controls, while this decrease was found to be higher in the newly diagnosed group. While PON-1 activity was significantly lower in newly diagnosed patients compared to the control group, it was higher in the gluten-compatible diet group.

Conclusion: Low MPO values in celiac patients may be insufficient to function by creating oxidative stress in inflammation. While PON-1 values are significantly lower in newly diagnosed celiacs, it can be said that they reach normal values with adherence to a gluten-free diet.

Keywords: Antioxidant, Celiac, Gluten-free Diet, Paraoxonase, Superoxide dismutase

INTRODUCTION

Celiac disease (CD) is an autoimmune and multifactorial disease caused by environmental and genetic factors. CD is triggered by gluten proteins especially found in different nutrients such as wheat and barley rye.[1] Toxic and immunogenic pathways are caused by mechanisms of gluten intestinal epithelial damage. The conversion of gluten to immunogenic and toxic peptides occurs by proteolysis. These peptides may adversely affect cells and cause oxidative stress in enterocytes, disrupting cell differentiation and death.[2,3] The incidence of CD is about 1-3% of the population worldwide.[4] Although the incidence

of the disease is different in varied regions of the world, it is increasing day by day.[5]

Unfortunately, there are not many treatment methods for CD. The exclusively effective treatment used today is a gluten-free diet (GFD). Stringent GFD improves parameters of blood biochemistry, clinical signs, some lesions, and other risk of related disease complications in most patients of CD.[6] Gastrointestinal microbiome treatments have also started to be used as alternative treatment methods.[7]

The high-level creation of reactive oxygen species (ROS), which pass over the ability of biologically functional antioxi-

dants, causes oxidative stress.[8] It is thought, that the increase of ROS levels of CD is caused by the entry of gliadin peptides into cells, peptide accumulation in lysosomes, and activation of transduction pathways.[9] Oxidative stress affects numerous physiological conditions, causes damage to proteins and lipids, decreases cell membrane fluidity, and is involved in the disease occurrence of different diseases.[10] Oxidative stress and inflammation associated with decreased antioxidant defense systems and elevated levels of reactive oxygen species may be effective in the molecular mechanism of celiac disease.[11]

Effective antioxidant mechanisms, in reaction to oxidative stress, protect the body against free radical damage for instance glutathione (GSH), serum paraoxanase (PON), superoxide dismutase (SOD), and arylesterase (ARE). GSH defends cells from ROS depredation by responding with hydrogen peroxide (H_2O_2) and organic peroxides and removing H_2O_2 from cells.[12] SOD is an antioxidant enzyme that acts as a central component in defending against oxidative stress.[13] PON is an ester hydrolase that catalyzes the hydrolysis of various organic molecules and can protect low-density lipoproteins against peroxidative reactions.[14] Hydrolysis of toxic metabolites can be carried out by the activity of another hydroloase enzyme, ARE.[15] Myeloperoxidase (MPO) is in excess in phagocytes, it catalyzes oxidative species and H_2O_2 to produce hypochlorous acid (HOCl), and it also reduces nitric oxide activity and increases oxidative stress.[16,17]

Despite being associated with dietary gluten, CD is a genetic disorder and for this reason, keeps going during life. In this way, it is possibly liable for chronic inflammation and oxidative stress. This increases various malignant risks, and oxidative deoxyribonucleic acid damage can cause life-threatening diseases such as cancer.[18] Diets to be applied in daily life are very important in order not to cause more serious problems and to protect living standards.

In the literature, research on children with CD is limited. Due to inflammatory formation and cell damage, oxidant-antioxidant balance is expected to be impaired in patients with CD. In this study, in line with the information between CD and oxidative stress relationship, we aimed to investigate and interpret how a gluten-free diet will affect this situation and its effect on serum GSH, SOD, PON-1, ARE, and MPO levels.

MATERIALS AND METHODS

Patients and Control Group

The present study included 39 children aged 6-15, diagnosed with CD and 29 children without any health problems, who applied to the Pediatrics Diessease polyclinic. The approximative power (1-beta) test value was found as 0.89 with the G-Power program. The diagnosis of CD was made in line with the recommendations of the European Society of Pediatric Gastroenterology, Hepatology, and Nutrition.[19] Newly diagnosed cases and those who have been exposed to a gluten-free diet for at least one year were included in the study group. Individuals with an inflammatory or infectious condition, diabetes mellitus, or any hepatic, metabolic, cardiac, or renal disease were excluded from the study. Moreover, the control group was formed from children of the same age group without any health problems. Informed consent was obtained from the participants. Legal custodian's assent of the children was obtained. The study was approved by the Clinical Ethics Committee of Atatürk University Faculty of Medicine (12/2021 No.B.30.2.ATA.0.01.00/70).

Biochemical Analysis

Blood samples taken for routine biochemistry analysis from patients who agreed to participate in the study were separated into aliquots. Aliquoted samples were transferred to 1.5 mL Eppendorf tubes and stored at -80 °C until the day of analysis.

Serum, SOD, PON-1, ARE, and MPO levels concentrations were analyzed and evaluated using commercial colorimetric kits in a multiplex reader spectrophotometer.

Determination of MPO Activity

The activity of MPO assays is analyzed concerning the method procedures established by Bradley et al.[20] Serum MPO activity was analyzed by transferring 100 mL of serum samples to 1 mL of 1.5 mM o-dianisidine hydrochloride containing 0.0005% (wt/vol) hydrogen peroxide and 1.9 mL of 10 mM phosphate buffer (pH 6.0). Measurements of absorbance changes were made for each sample with an Ultraviolet-vis spectrophotometer at 450 nm.[20]

Determination of SOD Activity

Superoxide Dismutase Assay Kit (Cayman, USA) was performed for analysis of levels of serum SOD. Analyzes were performed according to the directions included in the kit. According to the kit content, superoxide radicals produced by xanthine oxidase and hypoxanthine are determined using tetrazolium salt. The amount of enzyme required to exhibit 50% dismutation of the superoxide radical is defined as one unit of SOD.

tGSH Analysis

tGsh results were analyzed using the methods of Sedlak et al. According to the approach outlined by Sedlak et al.[21] In this method, 5,5'-dithiobis [2-nitrobenzoic acid] disulfide (DTNB), which is chromogenic, is rapidly reduced by sulfhydryl groups. For deproteinization before analysis, 100 µL of meta-phosphoric acid was added to 100 µL of the sample and centrifuged at 1,000 x g for 2 min. A cocktail mixture consisting of 80 mL of 625 U/L Glutathione reductase, 5.85 mL of 100 mM Na-phosphate buffer, 2.8 mL of 1mM DTNB, and 3.75 mL of 1 mM NADPH was prepared for measurement. 150 µL

of the prepared cocktail was mixed with 50 µL of supernatant. At 412 nm, the color formed during reduction is calculated by measuring in the spectrophotometer. A calibration curve was drawn using oxidized L-glutathione (GSSG) and sample results were calculated.

PON-1 and ARE Activity Measurement

Serum PON-1 paraoxonase/ARE activities were analyzed using previously used methods.[22,23] Serum PON-1 activities were analyzed spectrophotometrically in the method with diethyl-p-nitrophenylphosphate as a substrate. 1 nmol 4-nitrophenol/mL serum/min was defined as a unit for PON-1 activity. ARE activity was calculated using phenylacetate as the substrate by measuring the absorbance of the obtained phenol at 270 nm. The activities of PON-1 and ARE were calculated with their absorption coefficients. (17.100 M^{-1} cm^{-1} and 1.310 M^{-1} cm^{-1}, respectively). For ARE activity, as a unit, 1 nmol phenol/mL serum/min was defined.

Statistical Analysis

SPSS for Windows (IBM SPSS Statistics for Windows, Version 20.0. Armonk, NY: IBM Corp. IBM Corp. Released 2012) was used to do data analysis. Shapiro Wilk test was used to evaluate the normal distribution of the data. Accordingly, the Independent-T test was used to compare the patient and control groups for normally distributed data, while the ANOVA test was used to compare patient subgroups with more than two. Data were expressed as mean±standard deviation (Mean±SD) and $p<0.05$ was considered significant.

RESULTS

While 21 of 39 celiac children were girls and 18 boys in the celiac group, there were 17 girls and 12 boys in the control group. The mean age of the 2 groups did not differ. Body mass index (BMI) was lower in children with celiac (Table 1).

MPO activity was observed lower in children in the total celiac group than in the control group, and this decrease was statistically significant ($p<0.001$). PON-1 activity was examined to be lower in the total celiac group, yet this decrease wasn't significant ($p>0.05$). When the two groups are compared, no difference was detected in ARE, SOD activity, and tGSH levels ($p>0.05$). The data of the total celiac group and the control group are demonstrated in Figure 1.

When the three groups were compared, a significant difference was observed in MPO activities. MPO activity was lower in newly diagnosed celiac children compared to the control group and GFD-CD group. However, the observed decrease was statistically significant only compared to the control group ($p<0.05$). MPO activity was higher in the GFD-CD group compared to the newly diagnosed group and lower than the healthy control group. On the other hand, there was no statistically

significant difference between the control group and the GFD-CD groups. When the PON-1 activity between the groups was compared, it was found that it was statistically lower in the newly diagnosed group and higher in the gluten-free diet group compared to the control group ($p<0.05$).

When tGSH level and SOD activity were evaluated, although it was lower in the gluten-free diet group, no statistically significant difference was observed between the three groups ($p>0.05$). On the other hand, while ARE activity was low in the newly diagnosed group, it was close to control in the gluten-free diet group. However, this decrease in the newly diagnosed group was not significant ($p>0.05$). Table 2 presents the data for all three groups.

DISCUSSION

The consequences of the examination were evaluated in our current study to evaluate the antioxidant levels of newly diagnosed CD patients and celiac patients compatible with a gluten-free diet as well as to define the effect of a gluten-free diet on these parameters. When compared with the control group in the same age group, BMI was found lower in the celiac group. This can be explained by the situation caused by the nutrient absorption of celiac patients. Some differences were observed in the gluten-free diet group compared to the newly diagnosed or control group. While this difference was evident in MPO values, no difference was observed in other parameters.

The gastrointestinal symptoms of CD, such as diarrhea, abdominal pain, weight, fatigue, and bloating, are similar to various irritable bowel syndromes, often referred to as diarrhea variant irritable bowel syndromes.[24] Oxidative stress is caused by an impaired antioxidant system or increased levels of ROS.[25] ROS are very dangerous for metabolism due to their high reactivity and production in cells. Nonenzymatic antioxidants such as vitamins, and glutathione and antioxidant enzymes such as glutathione peroxidase/reductase, and superoxide dismutase are antioxidant defense systems that prevent the detrimental effects of ROS. In some cases, the amount of ROS may exceed the volume of the antioxidant defense system, leading to the occurrence of oxidative stress.[26]

Oxidative stress is related to the pathology of many diseases, and CD is one of them. CD is increasing day by day, especially in developing countries, due to modifications in wheat production and processing, heightened awareness of the disease, and changes in diet fluidity.[27] Celiac disease is a genetic disorder, but is affected by dietary gluten and persists throughout life. Due to these properties, it can be a source of chronic oxidative stress and brings various risks for metabolism.[28] Gluten peptides in enterocytes accumulate in lysosomes, altering certain signal transduction pathways and disrupting the oxidation defense balance by raising ROS levels.[29] A recent study on wheat germ peptides indicates that some peptides (WGP2-P7 and WGP11) significantly increased levels of glutathione reduc-

Table 1. Demographic data of celiac and control groups.

	Total Celiac patients n:39; Mean±SD	Control n:29; Mean±SD	P value
Age (year)	11.2±2.8	11.9±1.9	0.250
BMI	15.1±2.1	18.8±2.6	0.045

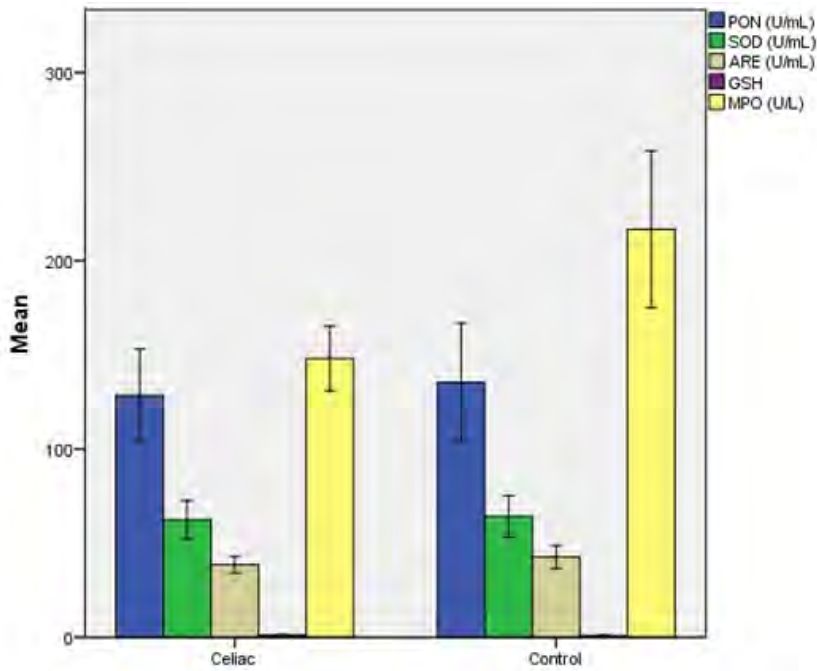BMI: Body mass index

Figure 1. Data of total celiac and control groups.

Table 2. Analysis results of ND-CD, GFD-CD, and control group.

	ND-CD n: 18 Mean±SD	GFD-CD n:21 Mean±SD	Control n:29 Mean±SD	P value
SOD (U/mL)	68.9±36.8	54.9±28.2	64.2±29.7	0.367
MPO (U/mL)	131.5±41.3[a]	167.2±54.4	216.2±112.1	0.003*
tGSH (mol/L)	1.5±1.4	0,98±063	1.3±0.86	0.283
PON-1 (U/mL)	99.1±72.0[a]	162.8±68.4[a,b]	135.4±84.5	0.039*
ARE (U/mL)	35.7±13.3	41.8±14.1	42.6±16.4	0.249

ND-CD: New diagnostic celiac disease group, GFD-CD: Gluten-free diet-celiac disease, SOD: Superoxide dismutase, MPO: Myeloperoxidase, tGSH: Total glutathione, PON-1:Paraoxonase-1, ARE: Arylesterase
*: Statistically significant (among three groups).
a: Statistically significant when compared to the control group.
b: Statistically significant when compared to the ND-CD.

tases and glutathione peroxidase. As a result of this, emphasized that this situation significantly increased the antioxidant level of the cells.[30]

The answer to the question of provided that the use of a gluten-free diet in children with CD is adequate to maintain the balance of serum oxidative/antioxidant in these people is still a subject of research. Rowicka, and et. al. found no differences in the intensity of oxidative/antioxidant between children with celiac disease treated with a gluten-free diet and healthy children.[31]

In their study, Stojiljković et al. found a significant decrease in GSH concentration in the intestinal mucosa of individuals with active CD, and showed that even in patients on a gluten-free diet, the GSH level was 25% lower than in controls. They reported that the GSH concentration was also significantly reduced in the peripheral blood of both active and gluten-free diet patient groups.[32] In our current study, no difference was observed in the newly diagnosed and gluten-free diet patients compared to the control group. Moreover, laboratory studies on the gluten-free diet have also indicated that it allows normalization of bone and mineral metabolism and reverse some abnormalities.[33] GFD is thought to be beneficial not only for people with CD but also for healthy people.[34]

Many functions in the body are adversely affected by ROS-induced oxidative stress. Various studies have been carried out to figure out this process in children with celiac disease. It has been shown that the antioxidant potential of patients newly diagnosed with celiac is lower than that of healthy individuals.[35,36] Studies indicate the importance of a gluten-free diet in CD. Improvements such as improvement of the intestinal mucosa and improvement of clinical features were observed. This situation is considered accompanied by oxidative stress and antioxidant balance.[37] While Rowicka et al. did not find a change in serum total antioxidant capacity levels between CD and control groups, Ferretti et al. found lower compared to controls, Ferretti et al. also showed that it is higher in newly diagnosed patients who don't follow a gluten-free diet.[31,37] Stojiljković et al. showed increased SOD activities and a significant reduction in glutathione content. They stated that antioxidant capacity decreases with consumed glutathione in celiac patients and that dietary antioxidants will be important in the complementary treatment of the disease.[38] In our study, however, no impact of a gluten-free diet on SOD activity was observed in patients with CD.

Previous studies have shown that PON-1, 2, and 3 are expressed in human intestinal cells.[39] In a later study, the relationship of PON-1 with intestinal inflammatory diseases was examined and PON gene expressions were compared in celiac and healthy duodenal tissue biopsies. A severe loss of PON-1 has been reported in celiac patients.[40] Ferretti at all. showed a lower PON-1 and ARE activity in the serum of both groups of CD, (11 at diagnosis, 16 receiving gluten-free diet therapy)

compared to control subjects and they thought that this situation might contribute to gastrointestinal cell damage. Kaplan et al. reported that PON-1 and ARE levels were lower in gluten-sensitive enteropathy patients compared to the control group.[41][37] Similarly, according to our results, PON-1 activity was found low in celiac patients, and a significant increase in PON-1 activity was observed with a gluten-free diet. Moreover, it was found higher in the gluten-free diet group than in the healthy control group. Studies on MPO in celiac patients were limited in the literature. Maluf et al. showed inflammatory marker MPO levels were increased in CD patients compared to controls.[42] However, on the contrary, in our study, a low MPO value was found in newly diagnosed celiac patients, while it was higher in the gluten-free diet-compliant group than in the newly diagnosed group, as well control group had the highest MPO value, which was significant.

One of the limitations of our study is a low number of sample subgroups. Another limitation is that the lipid profile of the sample group could not be included in the study. It would be more meaningful to evaluate the obtained PON-1 values together with HDL.

CONCLUSION

There are many studies in the literature on antioxidant levels in celiac patients, but research on the effects of gluten gluten-free diets on these factors is limited. MPO values in celiac patients may be insufficient to function by creating oxidative stress in inflammation. Although an increase is observed with the gluten-free diet, it remains lower than the control group. Likewise, while PON-1 values are significantly lower in newly diagnosed celiacs, it can be said that they reach normal values with adherence to a gluten-free diet. However, higher PON-1 activity was observed in CD patients on a gluten-free diet compared to the control group, and it is anticipated to investigate the effect of gluten on PON-1 activity in healthy people to better understand this increase.

ORCID IDs of the authors

Mehmet Ali Gul	0000-0002-5849-0116
Fatma Betul Ozgeris	0000-0002-4568-5782
Nezahat Kurt	0000-0002-1685-5332
Burcu Volkan	0000-0002-0528-3826
Ali Islek	0000-0001-6172-7797
Atilla Cayir	0000-0001-9776-555X

REFERENCES

1. Sollid LM, Jabri B. Is celiac disease an autoimmune disorder? *Curr Opin Immunol*. 2005;17(6):595-600.

2. Sayar E, Ozdem S, Uzun G, Islek A, Yilmaz A, Artan R. Total oxidant status, total antioxidant capacity and ischemia modified albumin levels in children with celiac disease. *Turkish J Pediatr*. 2015;57(5):498-503.

3. Ferretti G, Bacchetti T, Masciangelo S, Saturni L. Celiac disease, inflammation and oxidative damage: A nutrigenetic approach. *Nutrients*. 2012;4(4):243-257.

4. Green PH, Lebwohl B. Mesalamine for refractory celiac disease: An old medicine for a new disease. *J Clin Gastroenterol*. 2011;45(1):1-3.

5. King JA, Jeong J, Underwood FE, et al. Incidence of celiac disease is increasing over time: A systematic review and meta-analysis. *Am J Gastroenterol*. 2020;115(4):507-525.

6. Ciacci C, Cirillo M, Cavallaro R, Mazzacca G. Long-term follow-up of celiac adults on gluten-free diet: Prevalence and correlates of intestinal damage. *Digestion*. 2002;66(3):178-185.

7. Wu XX, Qian L, Liu KX, Wu J, Shan ZW. Gastrointestinal microbiome and gluten in celiac disease. *Ann Med*. 2021;53(1):1797-1805.

8. Granot E, Kohen R. Oxidative stress in childhood in health and disease states. *Clin Nutr*. 2004;23(1):3-11.

9. Luciani A, Villella VR, Vasaturo A, et al. Lysosomal accumulation of gliadin p31-43 peptide induces oxidative stress and tissue transglutaminase-mediated PPARgamma downregulation in intestinal epithelial cells and coeliac mucosa. *Gut*. 2010;59(3):311-319.

10. Bagdi E, Diss TC, Munson P, Isaacson PG. Mucosal intraepithelial lymphocytes in enteropathy-associated T-cell lymphoma, ulcerative jejunitis, and refractory celiac disease constitute a neoplastic population. *Blood*. 1999;94(1):260-264.

11. Ferretti G, Bacchetti T, Masciangelo S, Saturni L. Celiac disease, inflammation and oxidative damage: A nutrigenetic approach. *Nutrients*. 2012;4(4):243-257.

12. Pereira B, Costa Rosa LF, Safi DA, Medeiros MH, Curi R, Bechara EJ. Superoxide dismutase, catalase, and glutathione peroxidase activities in muscle and lymphoid organs of sedentary and exercise-trained rats. *Physiol Behav*. 1994;56(5):1095-1099.

13. Genestra M. Oxyl radicals, redox-sensitive signalling cascades and antioxidants. *Cell Signal*. 2007;19(9):1807-1819.

14. Watson AD, Berliner JA, Hama SY, et al. Protective effect of high density lipoprotein associated paraoxonase. Inhibition of the biological activity of minimally oxidized low density lipoprotein. *J Clin Invest*. 1995;96(6):2882-2891.

15. Primo-Parmo SL, Sorenson RC, Teiber J, La Du BN. The human serum paraoxonase/arylesterase gene (PON1) is one member of a multigene family. *Genomics*. 1996;33(3):498-507.

16. Winterbourn CC, Vissers MC, Kettle AJ. Myeloperoxidase. *Curr Opin Hematol*. 2000;7(1):53-58.

17. Eiserich JP, Baldus S, Brennan ML, et al. Myeloperoxidase, a leukocyte-derived vascular NO oxidase. *Science*. 2002;296(5577):2391-2394.

18. Szaflarska-Poplawska A, Siomek A, Czerwionka-Szaflarska M, et al. Oxidatively damaged DNA/oxidative stress in children with celiac disease. *Cancer Epidemiol Biomarkers Prev*. 2010;19(8):1960-1965.

19. Husby S, Koletzko S, Korponay-Szabo IR, et al. European Society for Pediatric Gastroenterology, Hepatology, and Nutrition guidelines for the diagnosis of coeliac disease. *J Pediatr Gastroenterol Nutr*. 2012;54(1):136-160.

20. Bradley PP, Priebat DA, Christensen RD, Rothstein G. Measurement of cutaneous inflammation: Estimation of neutrophil content with an enzyme marker. *J Invest Dermatol*. 1982;78(3):206-209.

21. Sedlak J, Lindsay RH. Estimation of total, protein-bound, and nonprotein sulfhydryl groups in tissue with Ellman's reagent. *Anal Biochem*. 1968;25(1):192-205.

22. Charlton-Menys V, Liu Y, Durrington PN. Semiautomated method for determination of serum paraoxonase activity using paraoxon as substrate. *Clin Chem*. 2006;52(3):453-457.

23. Cayir Y, Cayir A, Turan MI, et al. Antioxidant status in blood of obese children: The relation between trace elements, paraoxonase, and arylesterase values. *Biol Trace Elem Res*. 2014;160(2):155-160.

24. Shahbazkhani B, Forootan M, Merat S, et al. Coeliac disease presenting with symptoms of irritable bowel syndrome. *Aliment Pharmacol Ther*. 2003;18(2):231-235.

25. Halliwell B. How to characterize a biological antioxidant. *Free Radic Res Commun*. 1990;9(1):1-32.

26. Pham-Huy LA, He H, Pham-Huy C. Free radicals, antioxidants in disease and health. *Int J Biomed Sci*. 2008;4(2):89-96.

27. Fasano A, Catassi C. Clinical practice. Celiac disease. *N Engl J Med*. 2012;367(25):2419-2426.

28. Olinski R, Gackowski D, Rozalski R, Foksinski M, Bialkowski K. Oxidative DNA damage in cancer patients: A cause or a consequence of the disease development? *Mutat Res*. 2003;531(1-2):177-190.

29. Stojiljkovic V, Todorovic A, Radlovic N, et al. Antioxidant enzymes, glutathione and lipid peroxidation in peripheral blood of children affected by coeliac disease. *Ann Clin Biochem*. 2007;44(Pt 6):537-543.

30. Wang CF, Cui CX, Li N, et al. Antioxidant activity and protective effect of wheat germ peptides in an *in vitro* celiac disease model via Keap1/Nrf2 signaling pathway. *Food Res Int*. 2022;161.doi:ARTN 11186410.1016/j.foodres.2022.111864

31. Rowicka G, Czaja-Bulsa G, Chelchowska M, et al. Oxidative and antioxidative status of children with celiac disease treated with a gluten free-diet. *Oxid Med Cell Longev*. 2018:1324820. doi:10.1155/2018/1324820

32. Stojiljkovic V, Pejic S, Kasapovic J, et al. Glutathione redox cycle in small intestinal mucosa and peripheral blood of pediatric celiac disease patients. *An Acad Bras Cienc*. 2012;84(1):175-184.

33. Di Stefano M, Miceli E, Mengoli C, Corazza GR, Di Sabatino A. The effect of a gluten-free diet on vitamin D metabolism in celiac disease: The state of the art. *Metabolites*. 2023;13(1).doi:ARTN 7410.3390/metabo13010074

34. Francklin LRD, Dos Santos ACPM, Freitas FEDA, et al. Gluten: Do only celiac patients benefit from its removal from the diet?

Food Rev Int. 2022;doi:10.1080/87559129.2021.2024566

35. Hogberg L, Webb C, Falth-Magnusson K, et al. Children with screening-detected coeliac disease show increased levels of nitric oxide products in urine. *Acta Paediatr*. 2011;100(7):1023-1027.

36. Sayar E, Ozdem S, Uzun G, Islek A, Yilmaz A, Artan R. Total oxidant status, total antioxidant capacity and ischemia modified albumin levels in children with celiac disease. *Turk J Pediatr.* 2015;57(5):498-503.

37. Ferretti G, Bacchetti T, Saturni L, et al. Lipid peroxidation and paraoxonase-1 activity in celiac disease. *J Lipids*. 2012;587479. doi:10.1155/2012/587479

38. Stojiljkovic V, Todorovic A, Pejic S, et al. Antioxidant status and lipid peroxidation in small intestinal mucosa of children with celiac disease. *Clin Biochem*. 2009;42(13-14):1431-1437.

39. Shamir R, Hartman C, Karry R, et al. Paraoxonases (PONs) 1, 2, and 3 are expressed in human and mouse gastrointestinal tract and in Caco-2 cell line: Selective secretion of PON1 and PON2. *Free Radical Bio Med*. 2005;39(3):336-344.

40. Rothem L, Hartman C, Dahan A, Lachter J, Eliakim R, Shamir R. Paraoxonases are associated with intestinal inflammatory diseases and intracellularly localized to the endoplasmic reticulum. *Free Radic Biol Med*. 2007;43(5):730-739.

41. Kaplan M, Ates I, Yuksel M, et al. The Role of oxidative stress in the etiopathogenesis of gluten-sensitive enteropathy disease. *J Med Biochem.* 2017;36(3):243-250.

42. Maluf SW, Wilhelm Filho D, Parisotto EB, et al. DNA damage, oxidative stress, and inflammation in children with celiac disease. *Genet Mol Biol.* 2020;43(2):e20180390. doi:10.1590/1678-4685-GMB-2018-0390

How to cite this article

Measurement of Total Iron in Breast Tissue Samples by Inductively Coupled Plasma-Mass Spectrometry

Mete Bora Tuzuner[1], Burcin Tuzuner[2,3]

[1]Acibadem Labmed Clinical Laboratories, Research and Development Center, Istanbul, Turkiye
[2]Istanbul Gelisim University, Department of Basic Medical Sciences, Biochemistry, Faculty of Dentistry, Istanbul, Turkiye
[3]Istanbul Gelisim University, Life Sciences and Biomedical Engineering Application and Research Centre, Istanbul, Turkiye

ABSTRACT

Objective: Breast cancer is the commonest and the deadliest malignancy among women. Iron is known as an essential element for cell growth and division. The connection between oxidative stress, antioxidants, and progression, aggressiveness, and recurrence of breast cancer, is widely recognized to involve impaired iron metabolism. The purpose of this study was to investigate the connection between the tumor characteristics and the levels of total iron in breast tissues by employing state of the art technology, inductively-coupled plasma/mass spectrometry (ICP-MS) with our in-house analysis methodology for tissue samples.

Materials and Methods: Iron contents were determined in 25 tissue sets (matched tumor and peritumoral tissues) collected from 25 women diagnosed with invasive ductal breast cancer. In addition, three cancer-free breast tissues, obtained from breast reduction surgery, were analyzed as a normal group. Collected samples were digested and introduced to ICP-MS for iron analysis.

Results: Our method showed a low rate of measurement error (<10%). A highly significant (p<0.001) ~3 fold difference of iron concentrations were observed in tumors (24.73±6.15 ppb/mg) as compared to peritumoral tissues (9.10±4.84 ppb/mg). As the grade and stage of the cancer increases, iron levels in tumor tissues were also found to be increased (p=0.006, p=0.022 respectively).

Conclusion: Our ICP-MS based method can be reliably performed at the established conditions for tissue specimens, and also have potential to be used in clinical practice. Understanding the relationship between tissue iron levels and tumor characteristics is essential in identifying potential prevention and treatment strategies.

Keywords: Iron, Breast cancer, ROS, ICP-MS

INTRODUCTION

Breast cancer is a complex and multifaceted disease that continues to pose significant challenges to public health.[1] Extensive research has been dedicated to unraveling the intricate mechanisms underlying its development and progression. Among the various factors implicated in breast cancer, emerging evidence suggests that tissue iron levels play a crucial role in its pathogenesis.[2]

Animal studies conducted so far provide evidence supporting the notion that iron could potentially contribute to the advancement of breast cancer. These studies demonstrate that diets high in iron or subcutaneously injected iron promote the progression of breast cancer at various stages.[3-6] When examining breast epithelial cells at a cellular level, it is widely acknowledged that the malignant state is marked by an imbalance in cellular iron regulation. This is evident through variations in the expression of several iron-related proteins that correlate with indicators of unfavorable prognosis.[7-11]

Iron has been implicated in the development of breast cancer through several proposed pathways. Experimental evidence suggests that iron-induced oxidative stress may result in damage to DNA, proteins, and organelles. This damage arises from the production of hydroxyl radicals and hydrogen peroxide via chemical reactions like the Haber-Weiss and Fenton reactions.[12-14] Moreover, it is hypothesized that prolonged disturbance in the balance of cellular redox processes can influence specific signaling networks associated with the development of cancer.[15] Such disruption may result in the suppression of tumor-inhibiting factors and the heightened expression of oncogenes.[16,17] Considering the vital role of iron in cellular proliferation, it is logical to assume that iron also significantly

contributes to the clonal expansion of malignant cells.[18,19] Furthermore, iron provides a discerning advantage and facilitates the increased proliferation of tumor cells. Interestingly, cancer cells often exhibit a phenotype characterized by iron deficiency, which manifests as increased expression of iron importers and decreased expression of iron exporters.[11,20,21] Therefore, the altered iron metabolism in cancer cells contributes to their growth and survival.

Due to the higher metabolic and proliferation rates of breast tumor cells compared to normal breast cells, their iron demand is substantially greater, resulting in elevated oxidative stress. The use of dietary antioxidants as supplements to alleviate this oxidative stress is a common practice.[22,23] However, the precise and optimal dosage of antioxidants administered in clinical trials remains unclear and insufficiently refined. Moreover, not all tumor types rely on reactive oxygen species (ROS) signaling, which means that the benefits of antioxidants may not be universally applicable.[24] Additionally, it is essential to consider endogenous factors such as genetic variability in enzymes, which can limit the efficacy of antioxidants in reducing ROS levels and protecting cells from oxidative stress by preserving the integrity of lipid membranes.

Increased ROS levels are known to impede cancer cell survival during the initial stages of tumor development and progression. Consequently, dietary supplementation with antioxidants during these stages may inadvertently support cancer cell survival and hasten tumor growth. In fact, studies have revealed that the intake of dietary antioxidants can negatively impact breast cancer prognosis in postmenopausal women and accelerate metastasis while reducing survival rates in mouse models of cancer.[25−29] Although clinical trials have not convincingly demonstrated the effectiveness of antioxidants as standalone therapies, these compounds are gradually being incorporated as supplements or adjuncts to conventional treatments.[30−32]

In addition to its well-known function as a crucial element in cellular growth, division and co-carcinogenesis, iron can contribute to breast carcinogenesis through an alternative pathway. Current scientific understanding suggests a synergistic interaction between iron and estrogen.[33] The connection between estrogen and iron has been suggested as a notable factor in controlling the aggressiveness of breast cancer and the variations in recurrence rates observed in pre- and postmenopausal women.[7] Estrogen and iron have the ability to activate pathways of oxidative stress, leading to the production of ROS. This oxidative stress plays a pivotal role in inducing and sustaining the oncogenic phenotype of cancer cells. Consequently, the combined effects of estrogen and iron may result in elevated ROS production and the occurrence of site-specific or random DNA damage.[34]

In our study, we utilized inductively coupled plasma mass spectrometry (ICP-MS) to quantify tissue iron levels. ICP-MS is a specialized elemental analysis technique, specifically designed for the measurement of elements rather than molecules and compounds, which are typically analyzed using liquid chromatography-mass spectrometry and gas chromatography–mass spectrometry methods. Unlike the qualitative and less sensitive colorimetric approaches used in the past, which relied on the formation of insoluble metal sulfides, ICP-MS provides precise, sensitive, and highly specific quantification of heavy metals, including iron. This technique is applicable to liquid samples or those that can be dissolved or undergo acid digestion to obtain a liquid sample. The versatility of ICP-MS has resulted in its widespread adoption in various industries, including routine environmental monitoring, consumer product testing, food and pharmaceutical safety evaluations, as well as research in life sciences and clinical settings.[35] The popularity of ICP-MS can be attributed to its remarkable capability to achieve remarkably low detection limits for nearly all detectable elements. It can detect numerous elements at levels below 0.1 part per trillion (ppt), surpassing the capabilities of other techniques in terms of broad coverage of elements, low detection limits, and extensive measurement range.[36]

Our study aimed to examine the relationships between various tumor characteristics and the levels of iron in breast tissue using an in-house method using ICP-MS for analyzing iron in breast tissue samples. This method has the potential to be implemented in clinical laboratories for future use.

MATERIALS AND METHODS

Sample Collection

Fresh tumor and peritumoral tissues samples were collected via the Department of Pathology at Istanbul University-Cerrahpasa between June 2018 and December 2020. 50 tissue samples were gathered, comprising 25 pairs of tumor and peritumoral tissues, obtained from 25 women who underwent surgical procedures (mastectomy or breast conservation surgery) due to breast cancer. These women did not receive any additional treatments prior to surgery. Peritumoral tissues were taken at least 1 cm from the tumor boundary. Furthermore, three control samples were procured from premenopausal women who had no previous diagnosis of breast cancer and underwent reduction mammoplasty surgery. Histopathological evaluation was performed independently by two pathologists. The collected samples were rapidly frozen using liquid nitrogen and kept at a temperature of -80°C until they were utilized for iron measurement analysis. Tumor characteristics such as grade, stage, lymphatic invasion status, Ki-67 status and molecular type information were also recorded. The research protocol received approval from the Ethical Committee of Acibadem University (no: 2018-5/9). Prior to their participation, each patient provided informed written consent regarding the study.

Instrumentation

Wet digestion procedure was carried out with an incubator (Nuve EN 400, Turkey) and magnetic stirrer with ceramic heating plate (IKA C-MAG HS 7, China). ICP-MS measurements were performed with a 7700 Series x (Agilent Technologies, Germany) equipped with a third generation Octopole Reaction System (ORS^3) using helium gas. Low matrix was selected as plasma mode. Each measurement was performed with three repetitions. Data acquisition and analysis was performed with MassHunter 4.4 Workstation Software (Agilent Technologies, Germany).

Reagents and Other Materials

Analytical-grade reagents were used throughout the study. Digestion buffer (DB) was prepared via mixing 65% nitric acid (HNO$_3$, Merck, Germany) solution and 30% hydrogen peroxide (H$_2$O$_2$, Merck, Germany) solution (1:1, v/v). Standard iron (56 Fe) solutions were prepared from a 1 g/L stock solution (Trace-CERT Merck, Germany). 5, 10, 25, 50 and 100 ppb standard solutions were prepared in 1% HNO$_3$ solution. Ultra-purified water (Milli-Q Plus® – Millipore, USA) was used for preparation of all solutions. Mineral oil (Sigma-Aldrich, Germany) was used for heating the samples.

Glassware, sample vials, and pipette tips were decontaminated by immersing them in a 10% HNO$_3$ solution for a duration of 4 hours. They were then thoroughly rinsed with water and placed on a plastic tray in an oven at 60°C for drying. Following the drying process, all items were stored in sterilized plastic bags to maintain their decontamination until they were ready for use.

Wet Digestion

The wet digestion method was modified from the work of Badran et al.[37] Approximately 50 mg of breast tissue samples in flat bottom glass sample vials were dried overnight at 37°C, and constant weight was obtained for each sample. 1 mL of DB was added to dry tissue samples and it was allowed to soak thoroughly. Then sample vials were placed into the digestion set up (Figure 1) under the fume hood. The temperature was slowly ramped up until reaching 100°C. 1 mL of DB was added to each vial up to 5 times until a clear solution was obtained. Samples were evaporated to 100 mL and cooled to room temperature. 1% HNO$_3$ solution was added to complete each sample to 1 mL.

Statistical Analysis

All calculations were performed using the SPSS Statistical Program version 24.0 (SPSS Inc. Chicago, IL, USA). The significance of differences in Fe levels was determined by the Wilcoxon signed-rank test (WSR), Mann-Whitney U (MU) or Kruskal Wallis H (KW) test as needed. All reported p values are from two-sided tests, and a value less than 0.05 was considered statistically significant.

RESULTS

Optimization of ICP-MS Analysis

The collision gas utilized in the experiment was helium. Modifying the flow rate of helium gas introduced into the cell resulted in alterations in the production of molecular ions derived from argon gas, specifically ArO and ArN, along with changes in the intensity of the iron signal. To evaluate these alterations, the fluctuations in ArN, ArO and ^{56}Fe signals were quantified at various volume flow rates of helium gas. During each measurement, the instrument settings, such as the ion lens voltage, were optimized to reduce the detection of molecular ions and enhance the detection of iron ions. Optimal instrumental parameters were shown in Table 1.

The instrument was calibrated using aqueous standards of 5, 10, 25, 50 and 100 ppb for Fe. There was a good linear relation between measurements and standard concentrations. Linearity was evaluated by calculating the R-square value, which was 0.999 (Figure 2).

In order to evaluate the % error rates of the method a series of Fe standard samples (300, 600, 800 and 1600 ppb) were digested in triplicate under the optimized conditions and analyzed. All samples were diluted with 1% HNO$_3$ (1:16) before being introduced to the system. The % error of the measured standard concentrations compared to the true value of the standards were calculated by the following equation: % error = [(standard concentration value-calculated value)/ standard concentration value]*100. Our results showed that our method has less than 10% error rate in 300-1600 ppb ranges (Table 2).

Breast Tissue Iron Levels and Alterations within Specific Groups

Tumor, peritumoral and normal breast tissue samples were taken into consideration in order to compare iron concentrations. The levels in tumor (T) tissues were compared to peritumoral (P) tissues as well as to normal (N) tissues (Figure 3). Overall, the lowest iron levels were in N (n=3, 3.72±0.69 ppb/mg) and the highest were in T (n=25, 24.73±6.15 ppb/mg). The difference between T and P (9.10 ±4.84 ppb/mg) tissues was found to be highly significant (WSR, p < 0.001), approximately 3 fold higher in favor of tumor samples. The highest difference between tissues (> 4 fold) was observed in stage II patients' tissues, however, it did not reach statistical significance.

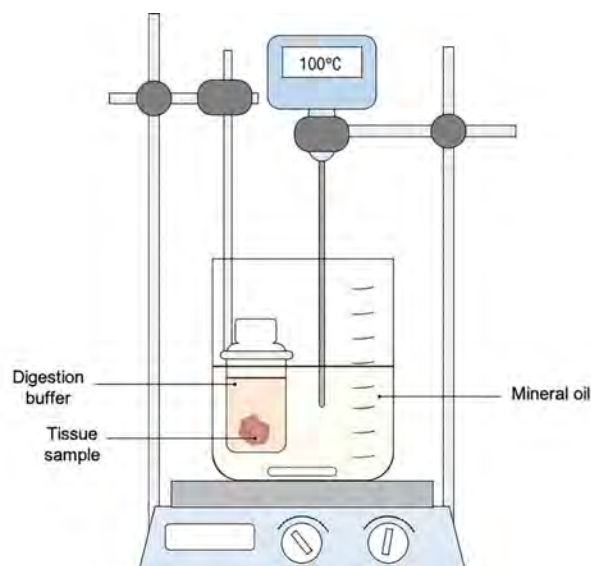When we investigated the iron levels in the same tissue types

Figure 1. Wet digestion set up for breast tissue samples.

Table 1. Operating conditions of the ICP-MS

RF Power (W)	1400
Cooling gas flow rate (L min^{-1})	15
Carrier gas (He) (mL min^{-1})	12.0
Sampling depth (mm)	10
Isotope	^{56}Fe
Replicates	3
Sweeps	100
Acquisition time (s)	55.5

Table 2. Measurement results of iron in standard samples.

Std. Conc.(ppb)	Observed (ppb)	Calculated (ppb)	% Error
300	17.03	272.43	9.19
600	36.25	579.93	3.35
800	48.54	776.57	2.93
1600	94.46	1511.33	5.54

regarding the tumors' characteristics, T tissues that were diagnosed with higher grade had a significant correlation with high tissue iron levels (p = 0.006). On the contrary, P tissues of grade-3 tumors tend to have lower iron levels compared to grade-2 tumors' P tissues (p = 0.054). Iron level difference was also found to be significant between T samples of stage II and III patient group (p = 0.022). There was no statistically significant association between factors such as molecular types, lymphatic invasion and Ki-67 and tissue iron level differences (Table 3).
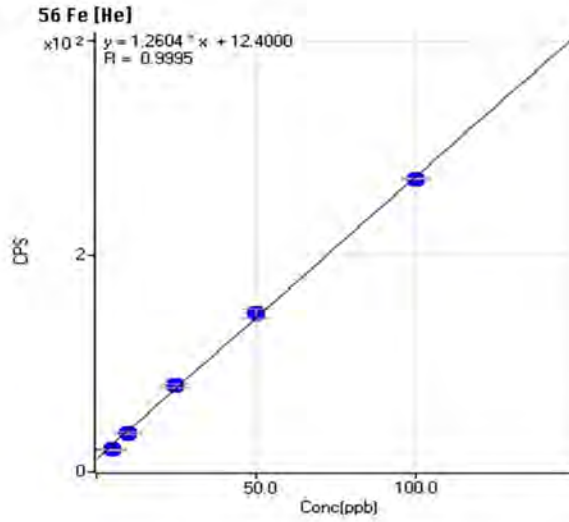
Figure 2. Calibration graph for iron. Blue dots represents 5, 10, 25, 50 and 100 ppb standard solutions measurements respectively. All measurements were triplicates.
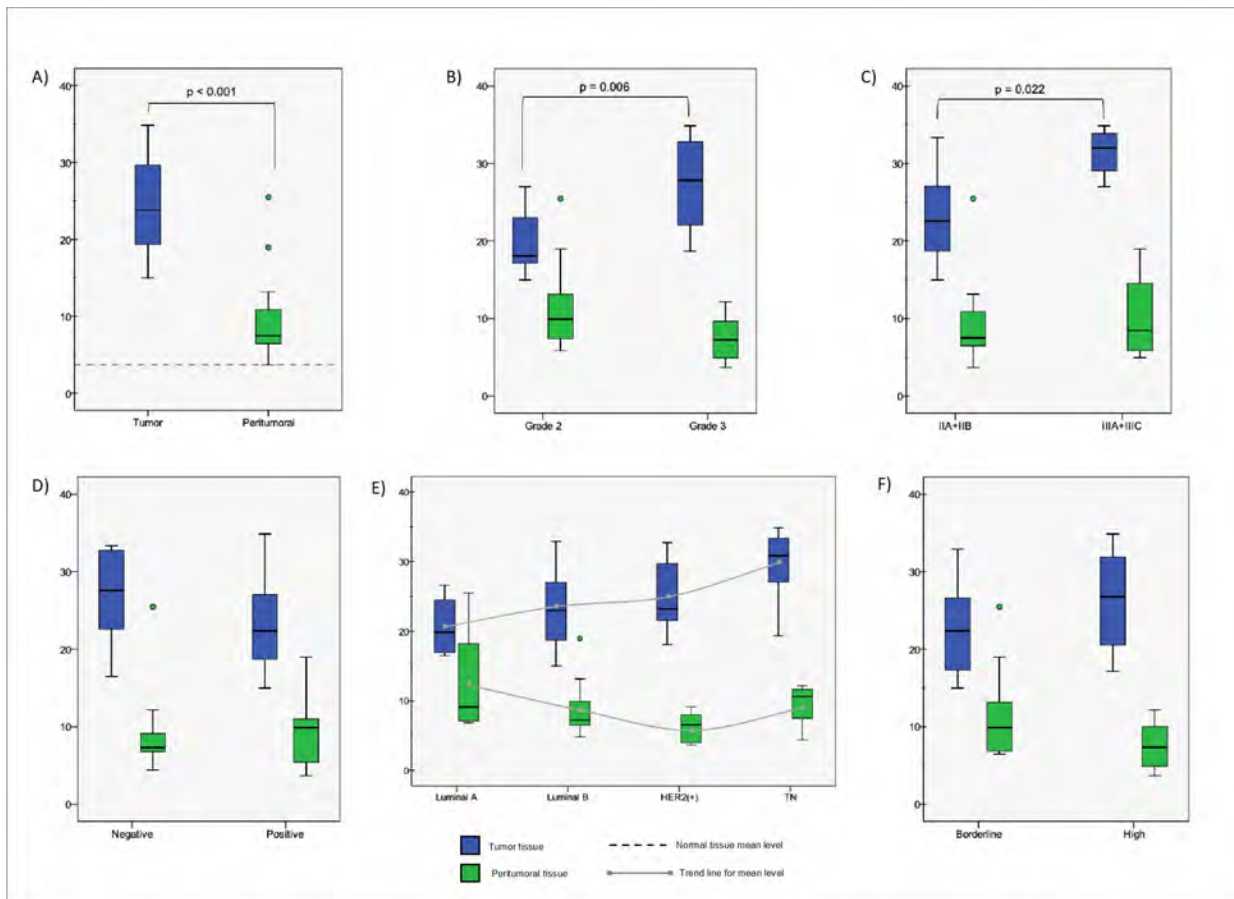

Figure 3. Comparison of iron concentrations among different breast tissue types together with tumor characteristics. Plots represent the difference between A) overall tissue types, B) histological grades, C) stages, D) lymph node status, E) molecular types and F) Ki-67 expression levels respectively. All concentration measurements are presented as ppb per mg tissue.

Table 3. Distribution of iron levels regarding tissue types and tumors' characteristics

Variable (%)	Fe (ppb/mg)		
	T (Mean,SD)	P (Mean,SD)	FC (T/P)
Histological Grade			
Grade 2 (36)	20.33 ±4.50	12.04 ±6.40	1.7
Grade 3 (64)	27.21 ±5.62	7.45 ±2.75	3.7
P value	0.006 (MU)	0.054 (MU)	
Stage			
IIA+IIB (92)	23.46 ±5.74	8.89 ±4.69	4.1
IIIA+IIIC (8)	31.46 ±3.35	10.21 ±6.22	3.1
P value	0.022 (MU)	0.824 (MU)	
Lymphatic invasion			
Negative (40)	26.81 ±5.93	9.43 ±5.98	2.8
Positive (60)	23.35 ±6.10	8.89 ±4.13	2.6
P value	0.222 (MU)	0.868 (MU)	
Ki-67 status			
Borderline (36)	22.16 ±5.89	11.76 ±6.54	1.9
High (64)	26.18 ±5.98	7.60 ±2.83	3.4
P value	0.101 (MU)	0.141 (MU)	
Molecular Type			
Luminal A (16)	20.71-4.72	12.65-8.74	1.6
Luminal B (36)	23.44-6.31	9.13-4.56	2.6
Her2 (+) (24)	24.74-5.44	6.31-2.20	3.9
Triple Negative (24)	29.38-5.76	9.49-2.99	3.1
P value	0.090 (KW)	0.205 (KW)	

T: Tumor tissue P: Peritumoral tissue FC: Fold change, MU: Mann-Whitney Utest, KW: Kruskal Wallis H test

DISCUSSION

The pathways mentioned in the introduction part, which generate ROS and contribute to the development and progression of breast cancer by disrupting iron metabolism, can potentially be restored through the incorporation of antioxidants into patient treatment regimens. This has been proposed as a promising therapeutic strategy to mitigate tissue damage caused by oxidative stress. Importantly, numerous bioactive compounds derived from plants have demonstrated the ability to regulate both iron metabolism and the cellular redox state, possibly through interactive mechanisms.[38] Before considering such treatments, it is essential to measure and assess breast tissue iron levels using a specific method.

Iron is a well-known trace element that plays a significant role in the human body.[39] The study of trace elements in biology and medicine has garnered considerable research attention due to their crucial involvement in the metabolism and growth of living organisms.[40−42] Various methods are currently employed for trace element analysis, including optical spectrometry, atomic mass spectrometry, X-ray Fluorescence Spectrometry, ICP/MS, chromatography, neutron activation, and photon activation techniques.[43−45] Among these methods, ICP-MS is widely recognized as the most accurate technique for determining the content of trace elements in biological samples.[46] Through the optimization of our method, we were able to achieve error rates below 10%. However, the utilization of ICP-MS for trace element analysis necessitates the conversion of solid biological samples, such as breast tissues, into a liquid state through digestion procedures.[47] Therefore, sample digestion, particularly acid digestion, is a crucial and essential process for accurately analyzing the trace element content in biological samples. The elemental analysis of biological samples involves the destruction of organic matter, the primary component of such samples, followed by their dissolution using acid digestion. Various acids and acid mixtures containing nitric, sulfuric, or perchloric acids have been employed for the acid digestion of biological samples to analyze trace elements using ICP-MS.[48−51] Additionally, wet oxidation procedures involving the combination of oxidizing agents such as hydrogen peroxide with nitric, sulfuric, and perchloric acids have been utilized. While most studies investigating breast cancer and iron have been conducted using serum samples, our samples, being derived from breast tissues, possess a more complex matrix. Consequently, we optimized the ratio of nitric acid and hydrogen peroxide in the digestion solution, as well as the temperature, to achieve the most effective dissolution of iron in breast tissue samples.

The causative factors of human breast cancer remain a topic of debate, although various factors such as hormonal influences, toxic substances, oxidative stress, and lipid peroxidation have been proposed as potential contributors to breast cancer development. In biological systems, the concentration of redox-active transition metals, which have the ability to catalyze or generate free radicals like superoxide, hydrogen peroxide, and hydroxyl radical, is typically low. However, in certain pathological conditions such as breast cancer, these transition metals and their transport proteins can accumulate in different target organs, leading to cellular lipid peroxidation and DNA damage. Excessive iron, in particular, is known to facilitate the production of hydroxyl radicals, impair cellular immune functions, and promote tumor growth, as supported by substantial evidence.[52−55]

Several studies have documented alterations in protein expression that may provide insights into the accumulation of iron in breast tumor cells. These investigations have not only focused on ferritin, but also on various other proteins involved in the molecular mechanisms of iron absorption, storage, utilization, and elimination. However, only a limited number of studies have directly measured iron levels in breast tissue. These studies have consistently observed a significant accumulation of iron in breast tumor samples, particularly in postmenopausal women, indicating a correlation between iron accumulation, advancing age, and the cessation of menstrual periods.[56,57] Our analysis aligns with these findings, revealing an overall elevation of iron concentrations in tumor tissues compared to adjacent peritumoral tissues. Furthermore, we observed that iron levels in normal breast tissue were notably lower compared to other tissues.

Although not statistically significant, we observed a 2.5-fold difference between peritumoral and normal breast tissues in terms of iron levels. This finding sheds light on the potential involvement of peritumoral tissue, which encompasses the cells of the tumor microenvironment, in the dysregulation of iron metabolism associated with breast cancer progression. Previous research by Marquez et al. has also identified iron accumulation in stromal inflammatory cells associated with breast cancer, suggesting that these cells could serve as a significant reservoir of iron for the tumor core.[58] Furthermore, their discovery of disrupted iron-related protein expression in infiltrating lymphocytes and macrophages provides further evidence supporting the notion that stromal cell responses within the breast microenvironment play a critical role in tumor progression.[59,60]

In our study, we also explored the potential links between tissue iron levels and factors influencing the prognosis and treatment of breast cancer. The analysis results revealed that the accumulation of iron in tumor tissues was associated with well-known indicators of poor prognosis, such as high histological grade and advanced stage. Although not statistically significant, we also observed an increase in the extent of iron accumulation in tumor tissues compared to peritumoral tissues as the disease exhibited more aggressive characteristics, became resistant to treatment, and showed decreased survival rates (as indicated by Ki-67, molecular type, and lymph node status). Another study, which included the analysis of tumors from 251 breast cancer

patients, explained the relationship between these unfavorable prognostic tumor characteristics and impaired iron metabolism through low expression levels of ferroportin.[61] Overall, it is plausible that the disruption of mechanisms crucial for maintaining a controlled iron balance may contribute to tumor development, increased aggressiveness, metastasis, and higher rates of disease recurrence.[7,62]

Except for normal tissues, all the samples used in our study were obtained from individuals diagnosed with invasive ductal breast cancer. Previous research, including our own, has provided evidence of local estradiol production within breast tissues, particularly in hormone-positive tumors.[63−65] The elevated levels of estrogen in breast tissue disrupt intracellular iron metabolism, causing an excess accumulation of iron. This imbalance in iron levels can trigger the production of superoxide anions and the conversion of Fe^{3+} bound to ferritin to Fe^{2+}, resulting in estrogen-induced oxidative stress on nucleic acids. This oxidative stress can subsequently contribute to the development of cancer.[66−68]

CONCLUSION

In conclusion, our findings indicate a strong correlation between elevated iron levels in breast tumor tissue and the progression and prognosis of the disease. Additionally, we have developed a practical methodology utilizing ICP-MS for accurately measuring iron concentration in breast tissue samples. Iron, as a redox-active metal, possesses the potential to ROS, which can contribute to the development of breast cancer. While cancer cells maintain similar iron metabolism pathways to normal cells, alterations in the expression of proteins and enzyme activities suggest a reprogramming of iron metabolism crucial for tumor cell survival. The upregulation of iron-dependent proteins in cancer cells, accompanied by the avoidance of iron overload-induced damage, leads to an "adjusted iron homeostasis" aligned with tumor metabolism. Furthermore, excess iron and the disruption of intracellular iron metabolism by estrogen play significant roles in breast cancer development and progression. Iron depletion and the use of various antioxidants have the potential to inhibit cancer cell growth and reduce inflammation by suppressing ROS generation. Consequently, antioxidant supplements may complement other therapeutic approaches in managing breast cancer. However, preclinical research, both in vitro and in vivo, is required to elucidate the role of antioxidants in breast cancer initiation and progression, their dual role (antioxidant or oxidant) depending on concentration, and their interaction with other compounds and therapies.

ORCID IDs of the authors

Mete Bora Tuzuner   0000-0001-8924-4850
Burcin Tuzuner   0000-0001-5122-4977

REFERENCES

1. Wilkinson L, Gathani T. Understanding breast cancer as a global health concern. *Br J Radiol.* 2022;95(1130): 20211033. doi:10.1259/bjr.20211033.

2. Guo Q, Li L, Hou S, et al. The role of iron in cancer progression. *Front Oncol.* 2021;11:778492. doi: 10.3389/fonc.2021.778492.

3. Thompson HJ, Kennedy K, Witt M, Juzefyk J. Effect of dietary iron deficiency or excess on the induction of mammary carcinogenesis by 1-methyl-1-nitrosourea. *Carcinogenesis.* 1991;12:111–114.

4. Singh M, Lu J, Briggs SP, McGinley JN, Haegele AD, Thompson HJ. Effect of excess dietary iron on the promotion stage of 1-methyl-1-nitrosourea-induced mammary carcinogenesis: pathogenetic characteristics and distribution of iron. *Carcinogenesis.* 1994;15:1567–1570.

5. Hrabinski D, Hertz JL, Tantillo C, Berger V, Sherman AR. Iron repletion attenuates the protective effects of iron deficiency in DMBA-induced mammary tumors in rats. *Nutr Cancer.* 1995;24:133–142.

6. Diwan BA, Kasprzak KS, Anderson LM. Promotion of dimethylbenz[a]anthracene-initiated mammary carcinogenesis by iron in female Sprague–Dawley rats. *Carcinogenesis.* 1997;18:1757–1762.

7. Huang X. Does iron have a role in breast cancer? *Lancet Oncol.* 2008;9:803–807.

8. Cui Y, Vogt S, Olson N, Glass AG, Rohan TE. Levels of zinc, selenium, calcium, and iron in benign breast tissue and risk of subsequent breast cancer. *Cancer Epidemiol Biomarkers Prev.* 2007;16:1682–1685.

9. Elliott RL, Elliott MC, Wang F, Head JF. Breast carcinoma and the role of iron metabolism. A cytochemical, tissue culture, and ultrastructural study. *Ann N Y Acad Sci.* 1993;698:159–166.

10. Miller LD, Coffman LG, Chou JW, et al. An iron regulatory gene signature predicts outcome in breast cancer. *Cancer Res.* 2011;71:6728–6737.

11. Shpyleva SI, Tryndyak VP, Kovalchuk O, et al. Role of ferritin alterations in human breast cancer cells. *Breast Cancer Res Treat.* 2011;126:63–71.

12. Toyokuni S. Iron-induced carcinogenesis: The role of redox regulation. *Free Radic Biol Med.* 1996;20(4):553-566.

13. Nelson RL. Dietary iron and colorectal cancer risk. *Free Radic Biol Med.* 1992;12(2):161-168.

14. Eaton JW, Qian M. Molecular bases of cellular iron toxicity. *Free Radic Biol Med.* 2002;32(9):833-840.

15. Benhar M, Engelberg D, Levitzki A. ROS, stress-activated kinases and stress signaling in cancer. *EMBO Rep.* 2002;3(5):420-425.

16. Kowdley KV. Iron, hemochromatosis, and hepatocellular carcinoma. *Gastroenterology.* 2004;127(5 Suppl 1):S79-86.

17. Galaris D, Skiada V, Barbouti A. Redox signaling and cancer: The role of "labile" iron. *Cancer Lett.* 2008;266(1):21-29.

18. Cermak J, Balla J, Jacob HS, et al. Tumor cell heme uptake induces ferritin synthesis resulting in altered oxidant sensitivity: possible role in chemotherapy efficacy. *Cancer Res.* 1993;53(21):5308-5313.

19. Omary MB, Trowbridge IS, Minowada J. Human cell-surface glycoprotein with unusual properties. *Nature.* 1980;286(5776):888-891.

20. Brookes MJ, Hughes S, Turner FE, et al. Modulation of iron transport proteins in human colorectal carcinogenesis. *Gut.* 2006;55(10):1449-1460.

21. Boult J, Roberts K, Brookes MJ, et al. Overexpression of cellular iron import proteins is associated with malignant progression of esophageal adenocarcinoma. *Clin Cancer Res.* 2008;14(2):379-387.

22. Gulcin İ. Antioxidants and antioxidant methods: An updated overview. *Arch Toxicol.* 2020;94:651–715.

23. Khurana RK, Jain A, Jain A, Sharma T, Singh B, Kesharwani P. Administration of antioxidants in cancer: Debate of the decade. *Drug Discov Today.* 2018;23:763–770.

24. Athreya K, Xavier MF. Antioxidants in the treatment of cancer. *Nutr Cancer.* 2017;69: 1099–1104.

25. Sarmiento-Salinas FL, Delgado-Magallón A, Cortés-Hernández P, Reyes-Leyva J, Herrera-Camacho I. Breast cancer subtypes present a differential production of reactive oxygen species (ROS) and susceptibility to antioxidant treatment. *Front Oncol.* 2019;9:1–13. doi: 10.3389/fonc.2019.00480.

26. Gill JG, Piskounova E, Morrison SJ. Cancer, oxidative stress, and metastasis. *Cold Spring Harb Symp Quant Biol.* 2016;81:163–175.

27. Satheesh NJ, Samuel SM, Büsselberg D. Combination therapy with vitamin C could eradicate cancer stem cells. *Biomolecules.* 2020;10:79. doi: 10.3390/biom10010079.

28. Mohsin AR, Khan UH, Akbar B. Evaluation of post radiotherapy antioxidants levels in cancer patients. *Asian J Multidiscip Stud.* 2019;7:2348–7186.

29. Jung AY, Cai X, Thoene K, et al. Antioxidant supplementation and breast cancer prognosis in postmenopausal women undergoing chemotherapy and radiation therapy. *Am J Clin Nutr.* 2019;109:69–78.

30. Dastmalchi N, Baradaran B, Latifi-Navid S, et al. Antioxidants with two faces toward cancer. *Life Sci.* 2020;258:118186. doi: 10.1016/j.lfs.2020.118186.

31. Bonner MY, Arbiser JL. The antioxidant paradox: What are antioxidants and how should they be used in a therapeutic context for cancer. *Future Med Chem.* 2014; 6:1413–1422.

32. Ambrosone, C.B. Review article oxidants and antioxidants in breast cancer. *Antioxid Redox Signal.* 2000;2:903–917.

33. Zacharski LR, Ornstein DL, Woloshin S, Schwartz LM. Association of age, sex, and race with body iron stores in adults: Analysis of NHANES III data. *Am Heart J.* 2000;140(1):98-104.

34. Valko M, Rhodes CJ, Moncol J, Izakovic M, Mazur M. Free radicals, metals and antioxidants in oxidative stress-induced cancer. *Chem Biol Interact.* 2006;160(1):1-40. doi: 10.1016/j.cbi.2005.12.009.

35. Whitmire M, Osredkar A, Ammerman J, et al. Full validation of a high resolution ICP-MS bioanalysis method for iron in human plasma with K2EDTA. *J Chromatograph Separat Techniq.* 2011;S4:001. doi:10.4172/2157-7064.S4-001.

36. An introduction to the fundamentals of inductively coupled plasma–mass spectrometry (ICP-MS) facts. Agilent website. https://www.agilent.com/en/product/atomic-spectroscopy/inductively-coupled-plasma-mass-spectrometry-icp-ms/what-is-icp-ms-icp-ms-faqs. Accessed June 8, 2023.

37. Badran M, Morsy R, Soliman H, Elnimr T. Assessment of wet acid digestion methods for ICP-MS determination of trace elements in biological samples by using Multivariate Statistical Analysis. *J Elem.* 2018;23(1):179-189.

38. Imam MU, Zhang S, Ma J, Wang H, Wang F. Antioxidants mediate both iron homeostasis and oxidative stress. *Nutrients.* 2017;9(7): 671. doi: 10.3390/nu9070671.

39. Mertz W. The essential trace elements. *Science.* 1981;213(4514):1332-1338.

40. Malakar R, Kour M, Ahmed A, Malviya SN, Dangi CBS. Trace elements ratio in patients of haemoglobinopathie. *Int J Curr Microbiol App Sci.* 2014;3(6):81-92.

41. Marjania A, kbari FA, Eshghinia S. Association between trace elements and metabolic syndrome among type 2 diabetes mellitus patients in Gorgan. *Asian J Pharm Clin Res.* 2015;8(3): 358-363.

42. Badran M, Morsy R, Soliman H, Elnimr T. Assessment of trace elements levels in patients with Type 2 diabetes using Multivariate Statistical Analysis. *J Trace Elem Med Bio.* 2016;33:114-119.

43. Iyengar VG, Subramanian KS, Joost RW. *Element Analysis of Biological Samples, Principles and Practice.* 1st ed. Woittiez, Boca Raton.;FL:CRC Press. 1998:137.

44. Becker JS, Dietze HJ. State-of-the-art in inorganic mass spectrometry for analysis of high-purity materials. *Int J Mass Spectrom.* 2003;228(2):127-150.

45. McComb JQ, Rogers C, Han FX, Tchounwou PB. Rapid screening of heavy metals and trace elements in environmental samples using portable X-ray fluorescence spectrometer, A comparative study. *Water Air Soil Pollut.* 2014;225(12):1-10. doi: 10.1007/s11270-014-2169-5.

46. Dressler VL, Antes FG, Moreira CM, Pozebon D, Andrei Duarte F. As, Hg, I, Sb, Se and Sn speciation in body fluids and biological tissues using hyphenated-ICP-MS techniques. *Int J Mass Spectrom.* 2011;307(1-3):149-162.

47. Enders A, Lehmann J. Comparison of wet digestion and dry ashing methods for total elemental analysis of biochar. *Commun Soil Sci Plant Anal.* 2012;43(4): 1042-1052.

48. Vanhoe H . A review of the capabilities of ICP-MS for trace element analysis in body fluids and tissues. *J Trace Elem Electrolytes Health Dis*. 1993;7(3):131-139.

49. Takahashi SI, Takahashi H. Sato, Kubota Y, Yoshida S, Muramatsu Y. Determination of major and trace elements in the liver of Wistar rats by inductively coupled plasma-atomic emission spectrometry and mass spectrometry. *Lab Animal*. 2000;34(1): 97-105.

50. Hseu ZY. Evaluating heavy metal contents in nine composts using four digestion methods. *Biores Technol*. 2004;95(1): 53-59.

51. Hansen THK, Laursen H, Persson DP, Pedas P, Husted S, Schjoerring JK. Microscaled high-throughput digestion of plant tissue samples for multi-elemental analysis. *Plant Methods*. 2009;5(1): 5-12.

52. Liu M, Okada S. Induction of free radicals and tumors in the kidney of Wistar rats by ferric ethylendiaminbe-N,N'-diacetate. *Int J Sports Med*. 1996;17: 397–403.

53. Mello FA, Meneghini R. In vivo formation of single-strand breaks in DNA by hydrogen peroxide is mediated by the Haber-Weissreaction. *Biochem Biophys Acta*. 1984;781: 56–63.

54. Okada S. Iron-induced tissue damage and cancer: The role of reactive oxygen species and free radicals. *Pathol Int*. 1996;46:311–332.

55. Weinberg ED. The role of iron in cancer. *Eur J Cancer Prev*. 1996;5: 19–36.

56. Ionescu JG, Novotny J, Stejskal V, Latsch A, Blaurock-Busch E, Eisenmann-Klein M. Increased levels of transition metals in breast cancer tissue. *Neuro Endocrinol Lett*. 2006;27 (Suppl. 1):36-39.

57. Cui Y, Vogt S, Olson N, Glass AG, Rohan TE. Levels of zinc, selenium, calcium, and iron in benign breast tissue and risk of subsequent breast cancer. *Cancer Epidemiol Biomarkers Prev*. 2007;16:1682-1685.

58. Marques O, Porto G, Rêma A, et al. Local iron homeostasis in the breast ductal carcinoma microenvironment. *BMC cancer*. 2016;16(1):1-14. doi: 10.1186/s12885-016-2228-y.

59. Sharma M, Beck AH, Webster JA, et al. Analysis of stromal signatures in the tumor microenvironment of ductal carcinoma in situ. *Breast Cancer Res Treat*. 2010;123:397–404.

60. Ma XJ, Dahiya S, Richardson E, Erlander M, Sgroi DC. Gene expression profiling of the tumor microenvironment during breast cancer progression. *Breast Cancer Res*. 2009;11:R7. doi: 10.1186/bcr2222.

61. Pinnix ZK, Miller LD, Wang W, et al. Ferroportin and iron regulation in breast cancer progression and prognosis. *Sci Transl Med*. 2010;2(43):43ra56. doi: 10.1126/scitranslmed.3001127.

62. Kwok JC, Richardson DR. The iron metabolism of neoplastic cells: alterations that facilitate proliferation? *Crit Rev Oncol Hematol*. 2002;42(1):65-78.

63. Tuzuner MB, Ozturk T, Ilvan S, et al. Local aromatase activity alterations in breast cancer tissues: A potential way of decision support for clinicians. *Exp Mol Pathol*.2021;118:104574. doi: 10.1016/j.yexmp.2020.104574.

64. Simpson ER. Sources of estrogen and their importance. *J Steroid Biochem Mol Biol*. 2003; 86(3-5):225-230.

65. Lonning PE, Haynes BP, Straume AH, et al. Recent data on intra-tumor estrogens in breast cancer. *Steroids*. 2011;76(8):786-791.

66. Bajbouj K, Shafarin J, Abdalla MY, Ahmad I, Hamad M. Estrogen-induced disruption of intracellular iron metabolism leads to oxidative stress, membrane damage, and cell cycle arrest in MCF-7 cells. *Tumor Biol*. 2017;39:1–12. doi: 10.1177/1010428317726184.

67. Cavalieri E, Chakravarti D, Guttenplan J, et al. Catechol estrogen quinones as initiators of breast and other human cancers: Implications for biomarkers of susceptibility and cancer prevention. *Biochim Biophys Acta*. 2006;1766:63–78.

68. Jian J, Yang Q, Dai J, et al. Effects of iron deficiency and iron overload on angiogenesis and oxidative stress—A potential dual role for iron in breast cancer. *Free Radic Biol Med*. 2011;50: 841–847.

How cite this article

In Silico Analysis Determining the Binding Interactions of NAD(P)H: Quinone Oxidoreductase 1 and Resveratrol via Docking and Molecular Dynamic Simulations

Santosh Kumar Behera[1],   Christoffer Briggs Lambring[2],   Albina Hashmi[3]   Sriharika Gottipolu[4]   Riyaz Basha[2]

[1]National Institute of Pharmaceutical Education and Research, Ahmedabad, India
[2]University of North Texas Health Science Center at Fort Worth, Texas, USA
[3]University of Texas at Austion, Austin, Texas, USA
[4]The University of Texas Medical Branch, Galveston, Texas, USA

ABSTRACT

Objective: NAD(P)H: Quinone oxidoreductase1 (NQO1) plays a crucial role in cellular defense against oxidative stress. Overexpression of NQO1 is linked to various cancer pathways. Despite its potential, the actual mechanisms to inhibit NQO1 and increase the efficacy of standard therapeutic options are not yet established. Resveratrol is an anti-cancer polyphenol found in dietary products and red wine. The objective of this investigation is to employ in silico methods to explore how resveratrol interacts with NQO1.

Materials and Methods: Docking analysis of resveratrol against NQO1 was performed using Glide. The most efficiently docked complex was characterized and analyzed by measuring intermolecular (IM) hydrogen (H)-bonds and binding energy values, additional hydrophobic, and electrostatic interactions. IM interaction between complexed protein and compound was demonstrated using LigPlot+ and the Schrödinger ligand interaction module. Molecular dynamics tools were employed to examine the physical movement of molecules to evaluate how macromolecular structures relate to their functions.

Results: The results of this investigation depicted a strong affinity of resveratrol against NQO1 followed by MD simulations (NQO1-resveratrol complex-binding energy: -2.847kcal/mol). Resveratrol's robust binding affinity through docking and molecular dynamic simulations highlights a significant change around 90 ns. The H-bonds number was inversely linked with the resveratrol-NQO1 complex stability. The NQO1-Resveratrol complex displayed dynamic motion, as revealed by porcupine projections, indicating alterations in its movement and flexibility.

Conclusion: The present *in silico* analysis suggests a possible alteration in resveratrol's orientation in the protein binding pocket. The findings encourage further investigation, including validation using *in vitro* and *in vivo* assays.

Keywords: Molecular Dynamic Simulation; NQO1; Resveratrol; Oxidative Stress; *In silico* Analysis

INTRODUCTION

NAD(P)H: Quinone oxidoreductase 1 (NQO1) is a multifunctional enzyme encoded by the NQO1 gene. It functions as an effective cytoprotective agent, a protective antioxidant, and a regulator of the oxidative stressors that cause DNA damage in cancer cells in chromatin-binding proteins.[1–3] Upregulation of NQO1 is observed in numerous human cancers.[4–8] It is established that the elevation of NQO1 levels has been attributed to the cellular defense response against increased oxidative stress associated with cancer. NQO1's induction is driven by transcriptional activation through the Keap1/Nrf2 pathway, which is frequently dysregulated in cancer cells.[9–12] The heightened NQO1 levels in cancer cells confer a survival advantage by enabling better oxidative stress management, facilitating tumor growth, and potentially contributing to treatment resistance.[13–15]

Understanding the intricate relationship between cellular oxidative stress, redox balance, and NQO1's participation in cellular responses holds significant implications for multiple fields.[3,16] Targeting NQO1 and the related pathways could of-

fer novel strategies for therapeutic interventions in cancer treatment, exploiting the dependency of cancer cells on redox adaptation. Multiple iterations of NQO1 regulating or bioactivating methods have already been explored for cancer therapy and diagnostic efforts.[17−19] Further investigations are warranted to decipher the complex interplay between NQO1, ROS generation, and its multifaceted roles in cellular stress responses and carcinogenesis.

Resveratrol, a polyphenol belonging to the stilbenoids family, has two phenol rings joined by an ethylene bridge. Resveratrol (3,5,4-trihydroxy-trans-stilbene) is a polyphenol discovered in dozens of plant species, including the skin and seeds of grapes,[20−22] red wines, and various human diets. Resveratrol exerts its anti-cancer effects through multiple mechanisms. Not only does resveratrol display antioxidant properties, as mentioned above, but it also exhibits more pleiotropic effects, including direct anti-tumor activity. Acting on pathways like Wnt/β-catenin, TGF-β/SMAD, and PI3K/Akt/mTOR, resveratrol can inhibit multiple pathways of tumor progression and metastasis.[23−26]

In this investigation, an *in silico* approach is performed to study the anti-cancerous activity of resveratrol through its inhibitory potential against the NQO1 protein. The *in silico* docking approach depicted a better binding affinity of resveratrol against NQO1, followed by molecular dynamics (MD) simulations, which tracked the trajectory graphs, with a sudden increase in their peaks, particularly at the 90-nanosecond (ns) mark of the MD simulation time period, which is a matter of interest in this investigation. The sudden rise in the peaks may be due to a sudden change in the orientation of resveratrol in the binding pocket of the protein. Therefore, based on the findings, we recommend that the molecule be synthesized and *in vitro* and *in vivo* analyses conducted to corroborate the efficacy seen *in silico* to gauge their potency as anti-cancerous drugs before clinical research.

MATERIALS AND METHODS

In silico Analysis

The information on the 1) structure, 2) sequence, and 3) function of NQO1 was retrieved from the UniProtKB database with ID P15559 (NQO1_HUMAN), Protein Data Bank (PDB) Research Collaboratory for Structural Bioinformatics (RCSB). PDB ID: 1KBQ with resolution 1.80 Å was used in this study. Chain A of NQO1 was found to have 272(2-273) amino acids (aa). Other chains and co-crystallized molecules were evaluated (BIOVIA Discovery Studio 4.5).

Prediction of Binding Site

The active site residues part of the binding site were used to predict the binding site of NQO1 following the published model.[27]

Retrieval of Resveratrol

Resveratrol's structural data was extracted in Structure Data Format (SDF) using the Compound ID: 445154 from the PubChem database.[28] The structure was converted to .pdb format using BIOVIA Discovery Studio 4.5 Visualizer (BIOVIA, San Diego, CA, USA), to use in docking tools.

Molecular Docking

Resveratrol was docked against NQO1 in extra precision (XP) mode using Glide (Grid-based Ligand Docking with Energetics), according to binding energy, IM H-bonds, and hydrophobic and electrostatic interactions, before the most viable docked complexes were analyzed further. Schrödinger's ligand interactions module and LigPlot+ (https://www.ebi.ac.uk/thornton-srv/software/LigPlus/) were utilized to reveal the IM links between the protein-compound complexes.

Molecular Dynamics Simulations

As shown earlier, MD was used to assess the atom and molecule's physical movements.[29] For a set amount of time, the molecules and atoms interact, displaying the system's dynamic "evolution."[30] Drug binding modalities were confirmed through a comprehensive view of the NQO1-resveratrol complex by performing MD simulations of the Apo(NQO1:only protein) and Holo state: NQO1-resveratrol complex using the Desmond program. The top-scoring ligand-protein complexes were analyzed by 100 nanoseconds (ns) MD simulation.

The MD process encompassed several steps: "minimization, heating, equilibration, and run generation."[31] Minimization of protein-ligand complexes utilized the OPLS4 force field, automatically determining topology and atomic coordinates. The ligand was placed within a 15X15X10 orthorhombic box using the SPC solvent model. To achieve physiological pH, neutralization necessitated a concentration of 0.15 M. The Particle Mesh Ewald (PME) boundary condition was employed to establish the water box, ensuring that the solute atoms remained at least 10 Å away from the box's edges. Minimization of the protein-ligand complexes was done with the OPLS4 force field before the topology and atomic coordinates were automatically determined.[32] The ligand was submerged in an orthorhombic 15X15X10 SPC solvent model box. The physiological pH neutralization required 0.15 M. The water box was set up via the PME boundary condition to assure no solute atoms occurred within 10 Å of the border.

Employing the NPT ensemble, the entire system underwent a simulation at 300 K for a duration of 100 ns. Subsequently, graphs depicting the root mean square deviation (RMSD) and root mean square fluctuation (RMSF) were generated. RMSD is used to measure the difference from initial structure conformation compared to its final position. The individual residue flexibility of a protein or complex can be determined by calculating the RMSF.[33] The most likely ligand binding mode at the protein's binding site is demonstrated in the simulated interaction diagram.[34]

Principal Component Analysis (PCA)

By reducing high-dimensional motional sets of data into a manageable subset made up of principal components (PCs) that characterize the collective motion, a PCA or Essential Dynamics (ED) separates collective motions from local dynamics.[35] The ED approach was used to run PCA utilizing the Desmond module of Schrödinger Maestro v 2022.4 to achieve the motions in the Apo and Holo states.

RESULTS

Analysis of Binding Sites and Grid Scores of Targeted Protein NQO1

The consensus results from each web server represented the residues. Active site formation of NQO1 involves the following amino acids: His11, Ser16, Thr15, Phe17, Asn18, Ala20, Pro102, Trp105, Phe106, Leu103, Thr148, Thr147, Gly149, Gly150, Tyr155, Ile192, Arg200, and Leu204. To screen compounds against potential targets, a well-known docking software system called AutoDock tool (ADT) was used.[27] ADT v.1.5 was used to assign Kollman charges to the protein. The dimensions, spacing, and parameters used to build the NQO1 grid were chosen to help the ligand/drug's fully extended conformation. The centering values for the x, y, and z axes were 22.072, 12.323, and 13.297, respectively.

Molecular Docking

The binding energies and other interaction studies of the the NQO1-resveratrol complex (Table 1; Figures 1A and 1B) showed that the drug-target interactions binding energies varied. There were several conformations produced from the docking research analysis utilizing GLIDE, but only the most favorable configuration with the maximum docking score was carefully selected for the IM interaction investigation. The results reflected that -2.847 kcal/mol was the binding energy for the NQO1-resveratrol complex. To comprehend and check the binding modalities of "protein-ligand interaction" for a certain time period, MD simulations of the docked complex were performed.

Trajectory Analysis of MD Simulations

MD was used to analyze atom/molecule physical movements, as described above.[30] A 100 ns MD simulation was used to test the stability of the docked complex with compound and receptor structural rearrangements. In order to comprehend the dynamic behavior and mode of binding, the dynamics and stability of two systems (NQO1: Apo; NQO1-resveratrol complex: Holo) were assessed using the Desmond suite (Schrödinger Release 2022-4: Maestro, Schrödinger, LLC, New York, NY, 2022). The dynamic stability of both systems (Apo and Holo) was assessed using the RMSD profile of the backbone atoms at 100 ns (Figure 2A). After 75 ns of MD simulations, the backbone RMSD graph of the Holo state showed a stable trajectory when compared to the Apo state.

Throughout the MD simulation run, Apo displayed aberrations compared to its Holo condition. In contrast to the Apo state, which showed significant variations over the course of the MD simulations, the Holo state displayed a stable RMSD value between ~1.6 and ~2.8 for the 75 to 100 ns of simulation time. This illustrates how protein can be stabilized by reversing the effects of resveratrol. The RMSD result was further validated by the variation of residues using RMSF. An RMSF graph (Figure 2B) was used to track the movement of specific residues in both states. This could be because resveratrol interaction affected the amino acid residues between 60 and 70, 125 and 130, and 220 and 240, all showing higher changes in their Cα atoms than other sites. The terminal residues, approximately 10 in number, displayed greater fluctuations at both their C- and N-terminal ends across all states, but these variations can be considered negligible. Residues within the protein that engage with the ligand are marked with vertical green bars.

The interactions among amino acids are influenced by their exposure to specific solvents, particularly through hydrophobic interactions. The degree of exposed surface area is inversely correlated with the frequency of these interactions with the solvent and critical protein residues. A decrease in the solvent surface that was accessible in the holo state has been depicted in the SASA graph (Figure 2D).

H-Bond Analysis

Schrödinger Release 2022-4 was used to visualize the IM hydrogen bonds of the Holo state during the MD simulations (Figure 3A to 3C). Variable IM hydrogen bonds were discovered during the modeling of the Holo state. In the case of the Holo state, the post-MD simulation study did not find any H-bonds. The simulation showed that the number of H-bonds was inversely linked with the stability of the resveratrol-NQO1 complex. The Holo state's IM hydrogen bonding was observed. According to the stacked bar chart of Holo in Figure 3A, the amino acid residues Ala20, Arg200, and Glu205 of NQO1 may be necessary for the binding and control of the protein. These residues could be

Table 1. Molecular docking scores of resveratrol against human NQO1.

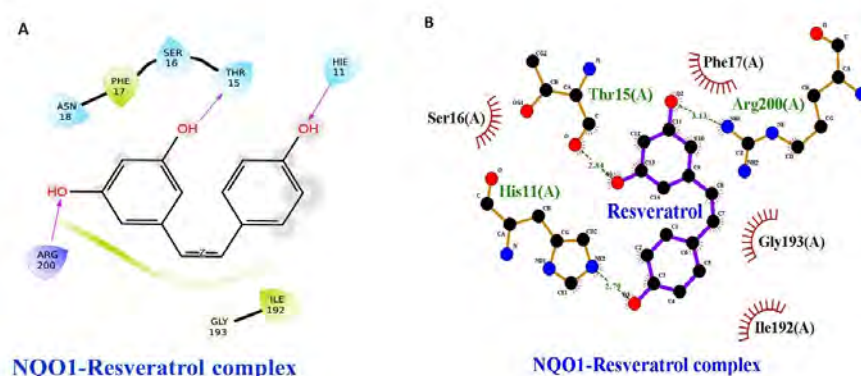| Sl. No.	Target	PubChem CID	Drug	Binding Energy(kcal/Mol)	No. of H-Bonds	H-Bond Forming Residues	Average Distance of H-Bonds (Å)
1.	NAD (P) H dehydrogenase [quinone] 1 (NQO1)	445154	Resveratrol	-2.847	3	His11, Arg200, Thr15	~2.045

Figure 1. Binding energies and other interaction studies of the NQO1-resveratrol complex. (A) The NQO1-resveratrol complex exhibited IM hydrogen bonding, electrostatic interactions, and hydrophobic interactions. The 2D representation was generated using the ligand interactions module of Schrödinger. (B) The NQO1-resveratrol complex displayed its 2D interaction pattern through the utilization of the LigPlot+ tool and BIOVIA Discovery Studio 4.5 Visualizer (BIOVIA, San Diego, CA, USA).
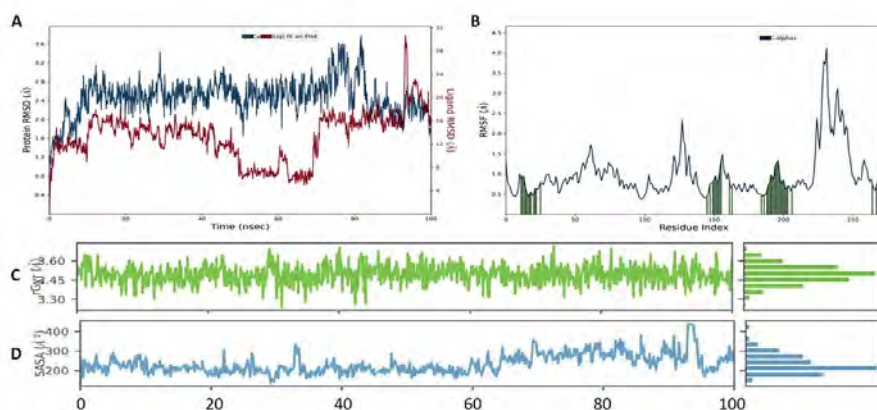

Figure 2. Root mean square deviation of the NQO1-resveratrol complex. The conformational stability of the NQO1 protein's Apo and Holo states was assessed over a 100 nanoseconds (ns) duration of molecular dynamics simulation using the following analyses: (A) Backbone-RMSD of the NQO1-resveratrol complex. (B) Cα-RMSF profile of the NQO1-resveratrol complex. (C) Radius of gyration (Rg) profile of the NQO1-resveratrol complex. (D) Solvent accessible surface analysis (SASA) of the NQO1-resveratrol complex.

the most crucial amino acid residues for binding and protein function. Values exceeding 0.5 in this histogram are achievable due to some protein residues' capacity to produce multiple interactions of the same subtype with resveratrol. The amount of IM hydrogen bonds was consistently reflected in the simulation

of the Holo state (Figure 3B). In the case of the post-MD of Holo, no H-bond was visible (Figure 3C). The H-bond-forming residues of His11, Arg200, and Thr15 broke down during the simulations of Holo but were later made up for by novel hydrophobic interactions and van der Waals interactions.
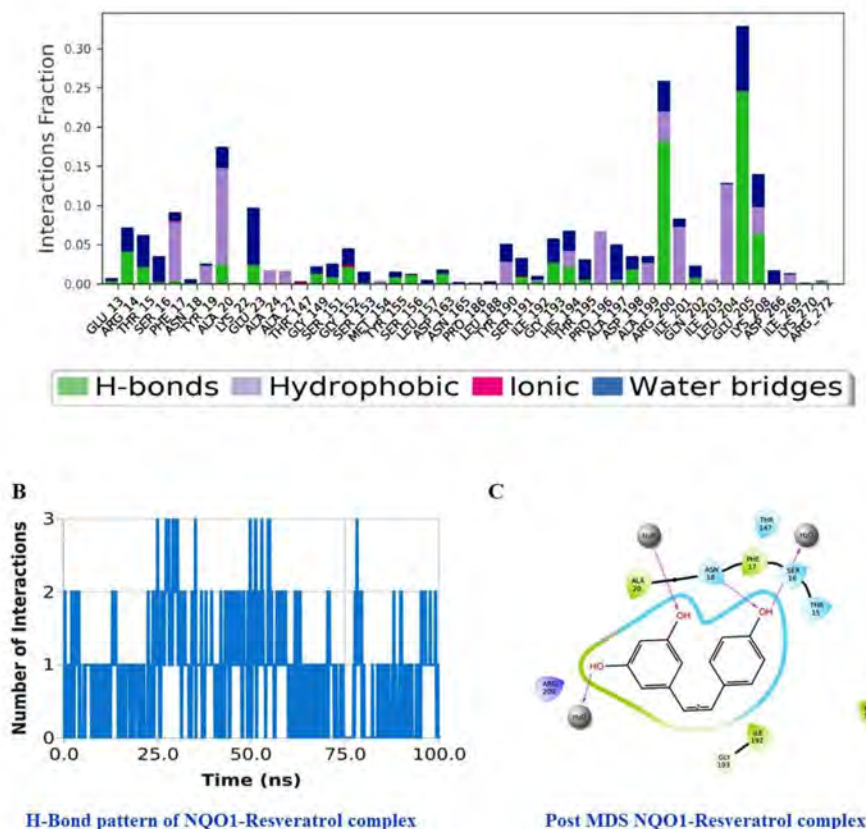
Figure 3. H-bond analysis of the NQO1-resveratrol complex. (A) The protein-ligand contacts within the NQO1-resveratrol complex throughout the 100 ns simulation are visualized through a stacked bar chart. (B) The fluctuations in hydrogen bond interactions within the NQO1-resveratrol complex during the 100 ns simulation are indicated by blue lines. (C) Following the MD simulations, interactions including IM hydrogen bonding, electrostatic, and hydrophobic contacts are depicted within the NQO1-resveratrol complex. This graphical representation was generated using the ligand interaction module of Schrödinger.

Principal Component Analysis (PCA)

The trace values of the covariance matrix for the backbone atoms were instrumental in limiting and characterizing the flexibility of both the apo and Holo states in each simulation protocol. The projections of trajectories along PC1 and PC2 visually depicted how these states moved within the phase space. These trajectories were mapped onto the first two principal components, providing a clear representation of the motion exhibited by the apo and Holo states of the protein-ligand complex (Figure 4A).

Higher flexibility in the Holo: NQO1-resveratrol complex is represented by the scattering cloud of PCA plots. The atom configurations may have moved and moved back during the dual time course of the 100 ns simulation time frame, which could account for the flexibility. The "Cross-correlation matrix" of the Cα- displacement revealed that all of the residues in the "NQO1" protein had motions that were both negatively (Figure 4B, blue shade) and positively (Figure 4B, red shade) linked with them, supporting the protein's erratic movement.

The vectorial representation of its individual components depicted the direction of motion. The majority of internal and external motions were visible in the projection vectors. Sharp porcupine curves were noticed after the graphing (Figure 4C). The NQO1-resveratrol complex was shown by the porcupine projection as inward and outward motion, which signify changes in motion and flexibility. This may result from atom configurations moving and then moving back throughout the 100 ns simulation time frame.

Oxidative stress, originating from the presence of disproportionate reactive oxygen species (ROS) generation and cellular antioxidant defenses, can be mitigated by NQO1's enzymatic activities. Recent studies have highlighted the potential of NQO1 inhibitors to impact cellular responses, particularly in the context of apoptosis induction.
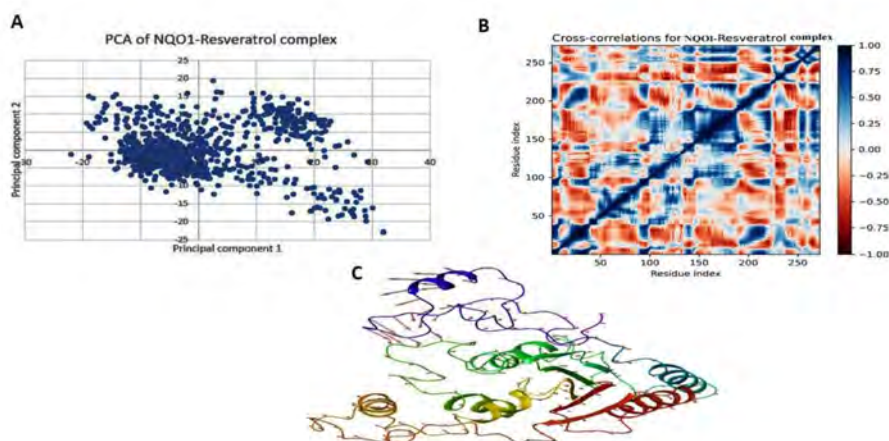
Figure 4. Principal component analysis of the NQO1-resveratrol complex. (A) The projection of trajectories (PC1 and PC2) is symbolized by the cloud. (B) A comparative analysis of cross-correlation matrices for the backbone atoms within the NQO1-resveratrol complex was conducted using PCA. (C) The individual components within the NQO1-resveratrol complex are visually represented through sharp porcupine plot curves in a vectorial manner.

DISCUSSION

The NQO1-resveratrol complex's interaction pattern involving IM hydrogen bonding, electrostatic interactions, and hydrophobic interactions is a crucial aspect of understanding the molecular basis of their binding and potential biological activity. These results have been presented in Table 1 and Figure 1. Hydrogen bonds are critical to stabilize molecular complexes. In the tested NQO1-resveratrol complex, the IM hydrogen bonds form between specific atoms on both molecules, which potentially contribute to the overall stability of the complex.[36,37] Analyzing hydrogen bonding patterns can reveal key binding interactions and help explain the complex's biological activity.[38,39] The electrostatic interactions result from the attraction or repulsion of charged particles, such as positively charged (cationic) and negatively charged (anionic) groups on molecules. In the context of the NQO1-resveratrol complex, electrostatic interactions might involve charged regions on both molecules that come into close proximity during binding. Understanding these interactions is essential for elucidating the electrostatic contributions to the complex's stability and function.[29,40] Hydrophobic interactions can occur between nonpolar or hydrophobic regions of molecules, with such interactions possibly contributing to stabilizing protein-ligand complexes.[41] Resveratrol, being a polyphenolic compound with a hydrophobic core,[42] is likely to engage in hydrophobic interactions with hydrophobic patches on NQO1 or other nearby residues. These interactions can facilitate the binding of resveratrol to NQO1 and influence its biological effects. Schrödinger's Maestro and the Desmond v 2022.4 software suite are commonly used for molecular modeling and simulation studies. In the context of the NQO1-resveratrol complex, it likely offers advanced visualization and analysis capabilities, enabling researchers to produce detailed 2D interaction diagrams that visually represent the specific interactions between NQO1 and resveratrol. This aids in a more comprehensive understanding of the complex's binding pattern.[30,43] Overall, the description of the NQO1-resveratrol complex's interactions and the use of these computational tools reflect a systematic and in-depth approach to studying molecular interactions.[44−46] This knowledge is essential for designing and optimizing drug candidates, understanding biological mechanisms, and potentially developing new therapeutics or interventions based on the NQO1-resveratrol interaction.

The assessment of both the stability of the docked complex involving the compound and any structural rearrangements in the receptor was conducted through MD simulations (Figure 2).

The fluctuation in resveratrol's rGyr within the protein's receptor binding pocket remained consistent, spanning approximately ~3.40 Å to ~3.70 Å. This consistent ligand behavior was evident throughout the 100 ns MD simulation, indicating stability. Notably, this illustrates that the Holo state maintains greater compactness, underscoring the inverse correlation between rGyr values and compactness.[35] The RMSF analysis lends robust validation to the rGyr findings. Hydrophobic interactions influence how amino acids interact with solvents by modulating their exposure. The more an amino acid is exposed to a solvent, the less frequent its interactions with that solvent, with crucial protein residues following this pattern. Figure 2D in the SASA graph illustrates a decrease in solvent-accessible surface area in the Holo state, reflecting this effect. The SASA analysis revealed that resveratrol's binding induced changes in the hydrophilic and hydrophobic interaction regions. This phenomenon could potentially lead to alterations in protein surface orientations, driven by the relocation of amino acid residues from accessible to buried areas. Over the course of a 100 ns MD simulation, the SASA graphs for the Holo state depicted SASA values spanning approximately ~200 to ~360 Å. This

suggests that the protein surface orientation may change due to the amino acid residue moving from the accessible area to the buried area. Taking together all the trajectory graphs, a sudden increase in the peak, particularly at 90 ns MD simulation time period, could be observed, which is a matter of interest in this investigation. The rise in the peak may be due to the sudden change in the orientation of resveratrol in the binding pocket of the protein.[47]

In the study using Schrödinger Release 2022-4, MD simulations were employed to investigate the behavior of IM hydrogen bonds in the Holo state of the resveratrol-NQO1 complex (Figure 3A to 3C). Variable IM hydrogen bonds were observed during the modeling of the Holo state, but interestingly, no hydrogen bonds were found in the post-MD simulation of the Holo state. This suggests that the stability of the resveratrol-NQO1 complex was inversely related to the presence of hydrogen bonds. The stacked bar chart for the Holo state (Figure 3A) highlights specific amino acid residues, namely Ala20, Arg200, and Glu205 of NQO1, which may play a crucial role in the binding and regulation of the protein. These residues appear to be vital for both binding and the protein's overall function. The histogram indicates that values exceeding 0.5 are possible, indicating that specific protein residues have the capacity to form multiple interactions of the same type with resveratrol. This pattern of hydrogen bond behavior was consistently observed throughout the simulation of the Holo state (Figure 3B). However, in the post-MD analysis of Holo, no hydrogen bonds were evident (Figure 3C). During the Holo simulations, specific hydrogen bond-forming residues like His11, Arg200, and Thr15 initially broke their hydrogen bonds but were subsequently compensated by new hydrophobic interactions and van der Waals interactions. This suggests a dynamic and adaptive behavior of the complex during the simulation, where hydrogen bonds were replaced by other types of interactions. Overall, these findings provide insights into the role of hydrogen bonds and other interactions in the stability and dynamics of the resveratrol-NQO1 complex, with specific amino acid residues like Ala20, Arg200, and Glu205 appearing to be critical players in the binding and function of the protein.

The covariance matrix trace values of backbone atoms were critical in governing and defining the flexibility of the apo and Holo states in each simulation protocol. These values provide insights into how atoms within the protein-ligand complex move and interact. Trajectory projections based on PC1 and PC2 illustrated the dynamic behavior of the states within the phase space. This type of analysis helps visualize how the protein and ligand move and evolve during the simulation. In Figure 4A, PC1 and PC2 were used to project the trajectories of the apo and Holo states of the protein-ligand complex. The scattering cloud in the PCA plots for the Holo state suggests higher flexibility in the NQO1-resveratrol complex. This variability in atom configurations may involve movements that

occur and then reverse over the course of the 100 ns simulation, contributing to the overall flexibility observed.

The "Cross-correlation matrix" analysis of C-displacement (Figure 4B) reveals that all residues in the NQO1 protein exhibit both positively (red shade) and negatively (blue shade) correlated motions. This indicates that the protein undergoes complex, coordinated movements during the simulation, with some residues moving in the same direction, while others move in the opposite direction. The vectorial representation of individual components (porcupine plots, Figure 4C) indicates the direction of motion. These plots illustrate both internal and external motions, with sharp curves in the porcupine plots suggesting significant changes in motion and flexibility. In the case of the NQO1-resveratrol complex, the porcupine projection indicates both inward and outward motions, suggesting that atom configurations are not only changing but also returning to previous states during the 100 ns simulation time frame.

Overall, these analyses provide valuable insights into the dynamic behavior of the NQO1-resveratrol complex, highlighting the complex interplay of motions, flexibility, and structural changes that occur during the simulation. These findings can aid in understanding the conformational dynamics of the protein-ligand complex and its functional implications.

CONCLUSION

Oxidative stress, originating from the presence of disproportionate ROS generation and cellular antioxidant defenses, can be mitigated by NQO1's enzymatic activities. Recent studies have highlighted the potential of NQO1 inhibitors to impact cellular responses, particularly in the context of apoptosis induction. Understanding the intricate relationship between cellular oxidative stress, redox balance, and NQO1's participation in cellular responses holds significant implications for multiple fields. Targeting NQO1 and related pathways could offer novel strategies for therapeutic interventions in cancer treatment, exploiting the dependency of cancer cells on redox adaptation. Further investigations are warranted to decipher the complex interplay between NQO1, ROS generation, and its multifaceted roles in cellular stress responses and carcinogenesis.

Cellular oxidative stress, stemming from disruptions in redox equilibrium, is intimately linked to ROS generation, prominently through enzymatic activities involving NQO1. This cytosolic reductase is integral to cellular stress responses and is notably upregulated in various human cancers. Elucidating NQO1's precise functions within the context of oxidative stress and cancer has the potential to unravel novel avenues for therapeutic innovations and deepen our understanding of cellular adaptation to stress conditions. When the Keap1/NRF2 pathways, influenced by cancer-promoting signals, become disrupted in cancer cells, there is a surge in the transcription and translation of NQO1. Resveratrol may bind to NQO1, reduce

its activity, and subsequently raise the levels of intracellular ROS.[48] This process ultimately leads to heightened cancer cell mortality (Figure 5).
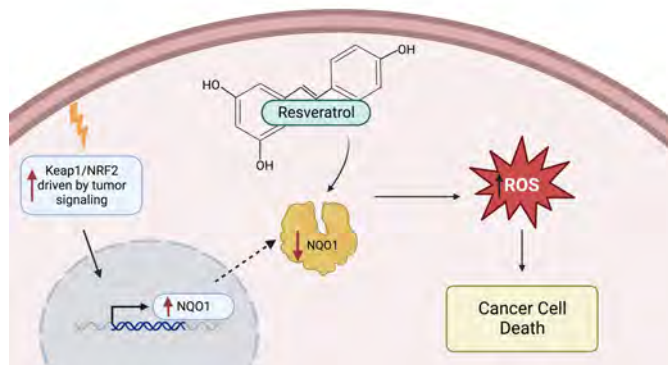

Figure 5. Schematic representation of the mechanism of resveratrol interaction with NQO1 and its implication as a potential cancer therapy. Upon dysregulation of Keap1/NRF2 pathways driven by pro-tumorigenic signaling in cancer cells, NQO1 transcription and translation are increased. We suggest upon binding with resveratrol, NQO1 is downregulated, leading to an elevated level of intracellular ROS resulting in increased cancer cell death.

This investigation utilizing the *in silico* docking approach depicted a strong binding affinity of resveratrol against NQO1. Notably, following the trajectory graphs through MD simulations revealed a sudden increase in the peaks particularly at 90ns MD simulation time period. The rise in the peak may be due to the sudden change in the orientation of resveratrol in the binding pocket of the protein. In addition, the trajectory analysis suggested resveratrol's potential to destabilize protein structure, corroborated by global and local changes in the RMSD and RMSF readings and SASA data. The RMSF values supported the rGyr findings wherein the Holo state was more compact, and multiple residues were identified as potential keys for resveratrol-NQO1 binding interactions. These findings warrant the need for subsequent preclinical studies to verify presented *in silico* results, potentially leading to clinical research involving resveratrol and NQO1 interactions.

Peer Review: Externally peer-reviewed.

Author Contributions: Conception/Design of Study- R.B., S.K.B., C.B.L. ; Data Acquisition- R.B., C.B.L.; Data Analysis/Interpretation- R.B., S.K.B., C.B.L. ; Drafting Manuscript- S.K.B., C.B.L., A.H., S.G.; Final Approval and Accountability- S.K.B., R.B., C.B.L., A.H.S.

Conflict of Interest: Authors declared no conflict of interest.

ORCID IDs of the authors

Santosh Kumar Behera	0000-0001-7915-187X
Christoffer Briggs Lambring	0009-0003-2921-5021
Albina Hashmi	0009-0006-9467-0196
Sriharika Gottipolu	0009-0000-9325-4998
Riyaz Basha	0000-0002-4071-0993

REFERENCES

1. Nishida-Tamehiro K, Kimura A, Tsubata T, Takahashi S, Suzuki H. Antioxidative enzyme NAD(P)H quinone oxidoreductase 1 (NQO1) modulates the differentiation of Th17 cells by regulating ROS levels. *PLoS One*. 2022;17(7):e0272090. doi:10.1371/journal.pone.0272090

2. Preethi S, Arthiga K, Patil AB, Spandana A, Jain V. Review on NAD(P)H dehydrogenase quinone 1 (NQO1) pathway. *Mol Biol Rep*. 2022;49(9):8907-8924

3. Ross D, Siegel D. The diverse functionality of NQO1 and its roles in redox control. *Redox Biol*. 2021;41:101950. doi:10.1016/j.redox.2021.101950

4. Beaver SK, Mesa-Torres N, Pey AL, Timson DJ. NQO1: A target for treating cancer and neurological diseases, and a model to understand loss of function disease mechanisms. *Biochim Biophys Acta Proteins Proteom*. 2019;1867(7-8):663-676.

5. Li X, Liu Z, Zhang A, et al. NQO1 targeting prodrug triggers innate sensing to overcome checkpoint blockade resistance. *Nat Commun*. 2019;10(1):3251. doi:10.1038/s41467-019-11238-1

6. Parkinson EI, Hergenrother PJ. Deoxynyboquinones as NQO1-activated cancer therapeutics. *Acc Chem Res*. 2015;48(10):2715-2723.

7. Lundberg AP, Francis JM, Pajak M, et al. Pharmacokinetics and derivation of an anticancer dosing regimen for the novel anticancer agent isobutyl-deoxynyboquinone (IB-DNQ), a NQO1 bioactivatable molecule, in the domestic felid species. *Invest New Drugs*. 2017;35(2):134-144.

8. Oh ET, Park HJ. Implications of NQO1 in cancer therapy. *BMB Rep*. 2015;48(11):609-617.

9. Liu Y, Jiang M, Zhao Z, Wang N, Wang K, Yuan Y. Cyclic amplification of intracellular ROS boosts enzymatic prodrug activation for enhanced chemo-immunotherapy. *Acta Biomater*. 2023;166:567-580.

10. Yang PW, Xu PL, Cheng CS, et al. Integrating network pharmacology and experimental models to investigate the efficacy of QYHJ on pancreatic cancer. *J Ethnopharmacol*. 2022;297:115516. doi:10.1016/j.jep.2022.115516

11. Xia MH, Yan XY, Zhou L, et al. p62 suppressed VK3-induced oxidative damage through Keap1/Nrf2 pathway in human ovarian cancercells. *J Cancer*. 2020;11(6):1299-1307.

12. Li J, Zhang J, Zhu Y, Afolabi LO, Chen L, Feng X. Natural compounds, optimal combination of brusatol and polydatin promote anti-tumor effect in breast cancer by targeting nrf2 signaling pathway. *Int J Mol Sci*. 2023;24(9). doi:10.3390/ijms24098265

13. Tsai HY, Bronner MP, March JK, et al. Metabolic targeting of NRF2 potentiates the efficacy of the TRAP1 inhibitor G-TPP through reduction of ROS detoxification in colorectal cancer. *Cancer Lett*. 2022;549:215915. doi:10.1016/j.canlet.2022.215915

14. Ramesh PS, Raja S, Udayakumar SH, Chandrashekar S, Nataraj SM, Devegowda D. Role of NRF2 cascade in determining the differential response of cervical cancer cells to anticancer drugs:

An *in vitro* study. *Mol Biol Rep*. 2022;49(1):109-119.

15. Bovilla VR, Kuruburu MG, Bettada VG, et al. Targeted inhibition of anti-inflammatory regulator nrf2 results in breast cancer retardation *in vitro and in vivo. Biomedicines*. 2021;9(9). doi:10.3390/biomedicines9091119

16. Ross D, Siegel D. Functions of NQO1 in cellular protection and CoQ(10) metabolism and its potential role as a redox sensitive molecular switch. *Front Physiol*. 2017;8:595. doi:10.3389/fphys.2017.00595

17. Gong Q, Yang F, Hu J, et al. Rational designed highly sensitive NQO1-activated near-infrared fluorescent probe combined with NQO1 substrates in vivo: An innovative strategy for NQO1-overexpressing cancer theranostics. *Eur J Med Chem*. 2021;224:113707. doi:10.1016/j.ejmech.2021.113707

18. Zhao W, Jiang L, Fang T, et al. Beta-Lapachone selectively kills hepatocellular carcinoma cells by targeting NQO1 to induce extensive dna damage and PARP1 hyperactivation. *Front Oncol*. 2021;11:747282. doi:10.3389/fonc.2021.747282

19. Starcher CL, Pay SL, Singh N, et al. Targeting base excision repair in cancer: NQO1-bioactivatable drugs improve tumor selectivity and reduce treatment toxicity through radiosensitization of human cancer. *Front Oncol*. 2020;10:1575. doi:10.3389/fonc.2020.01575

20. Pervaiz S. Resveratrol–from the bottle to the bedside? *Leuk Lymphoma*. 2001;40(5-6):491-498. doi:10.3109/10428190109097648

21. Soleas GJ, Diamandis EP, Goldberg DM. Resveratrol: A molecule whose time has come? And gone? *Clin Biochem*. 1997;30(2):91-113.

22. Wright JS, Johnson ER, DiLabio GA. Predicting the activity of phenolic antioxidants: Theoretical method, analysis of substituent effects, and application to major families of antioxidants. *J Am Chem Soc*. 2001;123(6):1173-1183.

23. Ji Q, Liu X, Han Z, et al. Resveratrol suppresses epithelial-to-mesenchymal transition in colorectal cancer through TGF-beta1/Smads signaling pathway mediated Snail/E-cadherin expression. *BMC Cancer*. 2015;15:97. doi:10.1186/s12885-015-1119-y

24. Bian P, Hu W, Liu C, Li L. Resveratrol potentiates the anti-tumor effects of rapamycin in papillary thyroid cancer: PI3K/AKT/mTOR pathway involved. *Arch Biochem Biophys*. 2020;689:108461. doi:10.1016/j.abb.2020.108461

25. Hope C, Planutis K, Planutiene M, et al. Low concentrations of resveratrol inhibit Wnt signal throughput in colon-derived cells:Implications for colon cancer prevention. *Mol Nutr Food Res*. 2008;52 Suppl 1(Suppl 1):S52-61.

26. Ren B, Kwah MX, Liu C, et al. Resveratrol for cancer therapy: Challenges and future perspectives. *Cancer Lett*. 2021;515:63-72.

27. Morris GM, Huey R, Lindstrom W, et al. AutoDock4 and AutoDockTools4: Automated docking with selective receptor flexibility. *J Comput Chem*. 2009;30(16):2785-2791.

28. Kim S, Chen J, Cheng T, et al. PubChem in 2021: New data content and improved web interfaces. *Nucleic Acids Res*. 2021;49(D1):388-395.

29. Behera SK, Vhora N, Contractor D, et al. Computational drug repurposing study elucidating simultaneous inhibition of entry and replication of novel corona virus by Grazoprevir. *Sci Rep*. 2021;11(1):7307. doi:10.1038/s41598-021-86712-2

30. Durrant JD, McCammon JA. Molecular dynamics simulations and drug discovery. *BMC Biol*. 2011;9:71. doi:10.1186/1741-7007-9-71

31. Raghu R, Devaraji V, Leena K, et al. Virtual screening and discovery of novel aurora kinase inhibitors. *Curr Top Med Chem*. 2014;14(17):2006-2019.

32. Shivakumar D, Williams J, Wu Y, Damm W, Shelley J, Sherman W. Prediction of absolute solvation free energies using molecular dynamics free energy perturbation and the OPLS force field. *J Chem Theory Comput*. 2010;6(5):1509-1519.

33. Aier I, Varadwaj PK, Raj U. Structural insights into conformational stability of both wild-type and mutant EZH2 receptor. *Sci Rep*. 2016;6:34984. doi:10.1038/srep34984

34. Deniz U, Ozkirimli E, Ulgen KO. A systematic methodology for large scale compound screening: A case study on the discovery of novel S1PL inhibitors. *J Mol Graph Model*. 2016;63:110-124.

35. Behera SK, Mahapatra N, Tripathy CS, Pati S. Drug repurposing for identification of potential inhibitors against SARS-CoV-2 spike receptor-binding domain: An *in silico* approach. *Indian J Med Res*. 2021;153(1 & 2):132-143.

36. Pace CN, Fu H, Lee Fryar K, et al. Contribution of hydrogen bonds to protein stability. *Protein Sci*. 2014;23(5):652-661.

37. Vladilo G, Hassanali A. Hydrogen bonds and life in the universe. *Life (Basel)*. 2018;8(1). doi:10.3390/life8010001

38. Bissantz C, Kuhn B, Stahl M. A medicinal chemist's guide to molecular interactions. *J Med Chem*. 2010;53(14):5061-5084.

39. Chen D, Oezguen N, Urvil P, Ferguson C, Dann SM, Savidge TC. Regulation of protein-ligand binding affinity by hydrogen bond pairing. *Sci Adv*. 2016;2(3):e1501240. doi:10.1126/sciadv.1501240

40. Hamelberg D, Mongan J, McCammon JA. Accelerated molecular dynamics: Apromising and efficient simulation method for biomolecules. *J Chem Phys*. 2004;120(24):11919-11929.

41. Ferenczy GG, Kellermayer M. Contribution of hydrophobic interactions to protein mechanical stability. *Comput Struct Biotechnol J*. 2022;20:1946-1956.

42. Dariya B, Behera SK, Srivani G, Farran B, Alam A, Nagaraju GP. Computational analysis of nuclear factor-kappaB and resveratrol in colorectal cancer. *J Biomol Struct Dyn*. 2021;39(8):2914-2922.

43. Al-Karmalawy AA, Dahab MA, Metwaly AM, et al. Molecular docking and dynamics simulation revealed the potential inhibitory activity of ACEIs against SARS-CoV-2 targeting the hACE2 receptor. *Front Chem*. 2021;9:661230. doi:10.3389/fchem.2021.661230

44. Morris JH, Meng EC, Ferrin TE. Computational tools for the interactive exploration of proteomic and structural data. *Mol Cell Proteomics*. 2010;9(8):1703-1715.

45. Sliwoski G, Kothiwale S, Meiler J, Lowe EW, Jr. Computational methods in drug discovery. *Pharmacol Rev*. 2014;66(1):334-395.

46. Sadybekov AV, Katritch V. Computational approaches streamlining drug discovery. *Nature*. 2023;616(7958):673-685.

47. Du X, Li Y, Xia YL, et al. Insights into protein-ligand interactions: Mechanisms, models, and methods. *Int J Mol Sci*. 2016;17(2). doi:10.3390/ijms17020144

48. Nagaraju GP, Farran B, Farren M, et al. Napabucasin (BBI 608), a potent chemoradiosensitizer in rectal cancer. *Cancer*. 2020;126(14):3360-3371.

How to cite this article

Moringa oleifera Ethanolic Extract Prevents Oxidative Damage on Lens Caused by Sodium Valproate Used in Epilepsy Treatment

Eda Dagsuyu[1], Umar Faruk Magaji[1,2], Ozlem Sacan[1], Refiye Yanardag[1]

[1]İstanbul University-Cerrahpaşa, Faculty of Engineering, Department of Chemistry, Istanbul, Turkiye
[2]Federal University Birnin Kebbi, Department of Biochemistry and Molecular Biology, Kebbi State, Nigeria

ABSTRACT

Objective: Valproic acid/valproate (VPA) is an antiepileptic agent that is structurally a short-chain fatty acid. It triggers the generation of reactive oxidants that can affect lens tissue. *Moringa oleifera* Lam. is a prevalent plant that grows in Asia, Africa and South Africa. The plant has anti-inflammatory, hepatoprotective, nephroprotective and cardioprotective activities.

Materials and Methods: The effect of 70% ethanol extract of the *Moringa oleifera* leaves was examined on VPA-induced lens tissue damage in this study. Experimental rats were grouped into four: the control (C), *Moringa* extract (M), VPA, and VPA+M group. M extract and VPA respectively were administered orally at a dose of 0.3 and 0.5 grams per kg body weight daily for fifteen days. The lens tissues of the rats were taken after sacrifice. Oxidative stress markers including glutathione, lipid peroxidation, and advanced oxidation protein products levels, glutathione reductase, glutathione peroxidase, glutathione-S-transferase, and superoxide dismutase activities, total oxidant status, total antioxidant status, reactive oxygen species, nitric oxide levels and aldose reductase and sorbitol dehydrogenase activities were determined.

Results: Tissue homogenates showed a significant decrease in glutathione and total antioxidants, as well as an altered activity of superoxide dismutase and glutathione-related enzymes in VPA groups. Moreover, a significant rise in the concentration of nitric oxide, reactive oxygen species and total oxidants, coupled with higher aldose reductase and sorbitol dehydrogenase activities were detected. In contrast, changes in the levels of these parameters were offset in the VPA+M group by *Moringa* extract.

Conclusion: This suggests that *Moringa oleifera* leaves are an excellent nutritional composite for mitigating the damaging properties of VPA.

Keywords: Antioxidant enzymes, Lens, *Moringa oleifera*, Oxidative damage, Valproic acid.

INTRODUCTION

Valproic acid/valproate (VPA) is a broad-spectrum agent effective against generalised seizure and other related forms of neurological disorders. It is structurally a short-chain fatty acid. Despite its efficacy and wide acceptance/usage, the administration of VPA is accompanied by a wide range of adverse drug reactions and toxicity. The generation of non-reduced reactive intermediates, reactive oxygen species, as well as peroxides are implicated to be the primary causes of VPA-induced oxidative stress. These intermediates destabilise antioxidant status, deplete glucuronide and CoA levels, disrupt beta-oxidations, and hinder mitochondrial function as well.[1] In addition to the pancreas,[2] heart,[3] intestine,[4] brain,[5] liver,[6] kidney[7] and lungs[8], the functionality of lens tissue is also shown to be affected by VPA.[9] Therefore, the significance of any food-based substance

capable of mitigating the deleterious effect of VPA upon co-administration cannot be over-emphasized.

Moringa oleifera Lam. (Drumstick or Horseradish) is nick-named 'the miracle tree' due to its diverse and multipurpose benefits. The plant is indigenous to Asia, Africa, and South America-regions where epilepsy remains endemic. The leaves of *Moringa oleifera* are rich in vitamins such as vitamin A (as β-carotene), vitamin B, and vitamin C. More so, reasonable concentrations of zinc, calcium, copper, iron, magnesium, and potassium are found in the leaves.[10] Furthermore, studies have shown that *Moringa oleifera* possesses essential fatty acids and some rare essential oils. Besides these, quercetin, kaempferol and myricetin are the conspicuous flavonoids identified in the plant leaves.[11] In addition to enzyme inhibition action,[12] leaf extract of *Moringa oleifera* is verified to

have antioxidant,[13] and anti-inflammatory action.[14] It protects hepatocytes,[15] nephrone,[16] cardiac tissue,[17] and has wound healing effects.[18] Therefore, can be meritoriously engaged in the treatment of multifarious complications and devoid of the fear of toxicity. In the current study, the action of *Moringa* extract against VPA-induced toxicity on the lens tissues of Sprague Dawley rats was investigated.

MATERIALS AND METHODS

Collection and Preparation of Plant Sample

Plant samples were collected, identified, and prepared as earlier reported.[12] Briefly, powdered shade-dried *Moringa oleifera* leaves were extracted using 70% ethanol (Merck KGaA). After boiling and a clear Soxhlet siphon was obtained, the solvent was evaporated, and the residue was weighed and stored at -20°C.

Experimental Protocol

The research protocol (11.2020.mar) for the present experiment has earlier been published.[19] The female Sprague Dawley rats utilised were provided by the Experimental Animals Research and Implementation Centre of Marmara University. Under standard conditions, the rats aged 4-5 months were divided into four experimental groups as follows: The control (C; n=8), *Moringa* extract (M; n=8), VPA (n=15), and VPA+M (n=12) group. All treatments were given orally. *Moringa* extract and VPA (dissolved in normal saline) respectively were given at a dose of 0.3 and 0.5 grams per kg body weight daily for fifteen days. Overnight fasted animals were sacrificed on day sixteen, then lens tissues were collected and homogenised in ice-cold normal saline (at 10% w/v).

Biochemical Analysis

From the homogenates of lens tissue (10% w/v), standard methods were used to determine glutathione (GSH) levels,[20] lipid peroxidation level (LPO) from malondialdehyde (MDA) concentration,[21] the activities of sorbitol dehydrogenase (SDH),[22] aldose reductase (AR),[23] glutathione reductase (GR),[24] superoxide dismutase (SOD),[25] glutathione peroxidase (GPx),[26] and glutathione-S-transferase (GST).[27] The total oxidant status (TOS),[28] total antioxidant status (TAS),[29] concentration of reactive oxygen species (ROS),[30] nitric oxide (NO) levels,[31] advanced oxidation protein products (AOPP),[32] and total protein level[33] of the homogenate were also quantified.

Statistical Analysis

Analysis of variance (ANOVA) from the data expressed as mean ± standard errors (SEM) using GraphPad Prism software version 6.0 (San Diego, CA, USA). Tukey's multiple comparisons test was used to determine significant differences at $p < 0.05$.

The effect of *Moringa* extract against VPA-induced toxicity on the lens tissues of Sprague Dawley rats was further identified by principal component analysis (PCA). This was executed using OriginPro 2022b version 9.95 (Northampton, Massachusetts, USA).

RESULTS

The effect of *Moringa* extract on lens GSH, LPO, and AOPP levels of experimental animals is presented in Figure 1. Statistical analysis revealed a substantial decrease in GSH of the VPA administered group when equated to control groups ($p < 0.0001$). In contrast, levels of LPO, and AOPP were markedly amplified ($p < 0.0001$ and $p < 0.01$ respectively). *Moringa* extract mitigated these defects, keeping GSH, LPO, and AOPP levels of the VPA+M group to a near normal; the GSH level of the VPA+M group was above that of the VPA group ($p < 0.0001$), while levels LPO ($p < 0.0001$) and AOPP ($p < 0.001$) are below that of VPA group.

GR, GPx, GST, and SOD activities are presented in Figure 2. Compared to the control groups, sole treatment with VPA caused a significant alteration in GR ($p < 0.001$), GPx ($p < 0.01$), GST ($p < 0.001$), and SOD ($p < 0.01$) activities. The activity of these enzymes in the VPA+M group was statistically higher than those of animals treated with VPA.

The TAS, TOS, ROS, and NO levels of the experimental animals' lens tissues are depicted in Figure 3. As observed from Figure 3, the TAS of the VPA administered group was below that of the control groups ($p < 0.05$). However, its levels in the VPA+M group were significantly elevated ($p < 0.0001$). On the other hand, TOS, ROS, and NO levels of the VPA group were statistically elevated as compared to the control groups ($p < 0.0001$). These defects were however curtailed by concomitantly administering *Moringa* extract. Thus, resulted in higher levels of TAS ($p < 0.0001$), as well as lower levels of TOS, ROS, and NO ($p < 0.0001$) in the VPA+M group as against the VPA group.

Lens tissue AR and SDH activities are presented in Figure 4. The activities of both AR and SDH were remarkably elevated upon administration of VPA ($p < 0.0001$ and $p < 0.05$ respectively). These defects were significantly reversed upon co-administration of VPA with *Moringa* extracts ($p < 0.0001$) in comparison to VPA.

PCA was used to prove the relationship among biochemical results for each group (Figure 5). PCA analysis revealed that the first two components detailed around 64.23% of the total variation in the experimental data (PC1: 64.23%, PC2: 15.59%). Primarily, in the first component, NO, ROS, AOPP, LPO, TOS, SDH, and AR were collected together. These collected data were highly negatively correlated with GSH, GR, GST, GPx, TAS and, SOD (Figure 5).
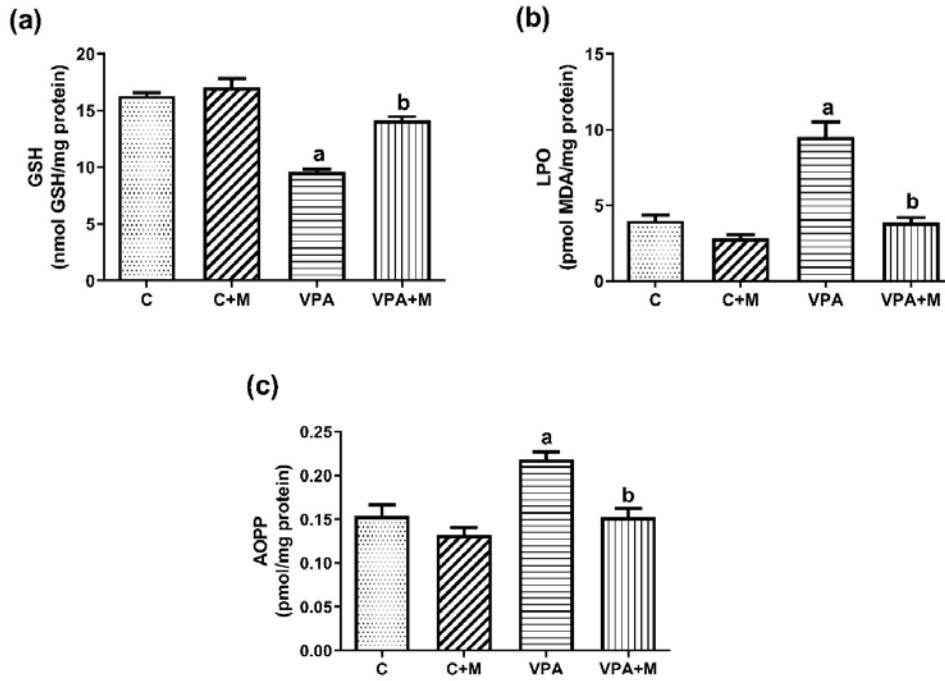
Figure 1. Effect of *Moringa* extract on lens tissue of experimental animals (a) GSH levels; [a]p<0.0001 vs. control; [b]p<0.0001 vs. VPA, (b) LPO levels; [a]p< 0.0001 vs. control, [b]p<0.0001 vs. VPA, (c) AOPP levels; [a]p< 0.01 vs. control; [b]p<0.001 vs. VPA. Values were given as mean and standard error. C: Control group; C+M: Control+*Moringa* extract group; VPA: Valproate group; VPA+M: Valproate+*Moringa* extract group.
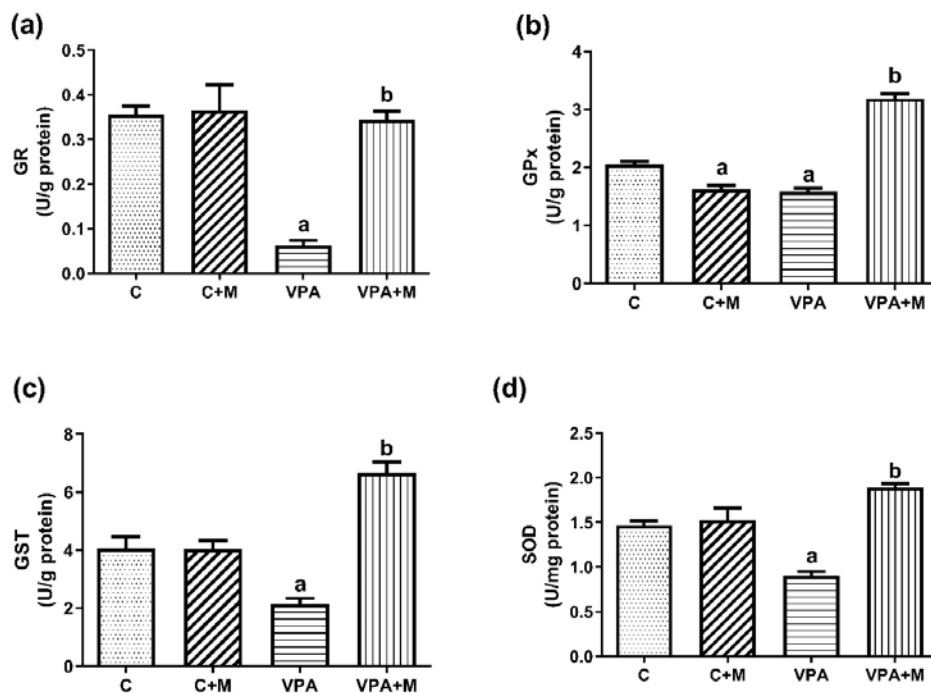

Figure 2. Effect of *Moringa* extract on lens tissue of experimental animals (a) GR activities; [a]p<0.001 vs. control; [b]p<0.0001 vs. VPA, (b) GPx activities; [a]p<0.01 vs. control, [b]p<0.0001 vs. VPA, (c) GST activities; [a]p<0.001 vs. control; [b]p<0.0001 vs. VPA, (d) SOD activities; [a]p<0.01 vs. control; [b]p<0.0001 vs. VPA. Values were given as mean and standard error. C: Control group; C+M: Control+*Moringa* extract group; VPA: Valproate group; VPA+M: Valproate+*Moringa* extract group.
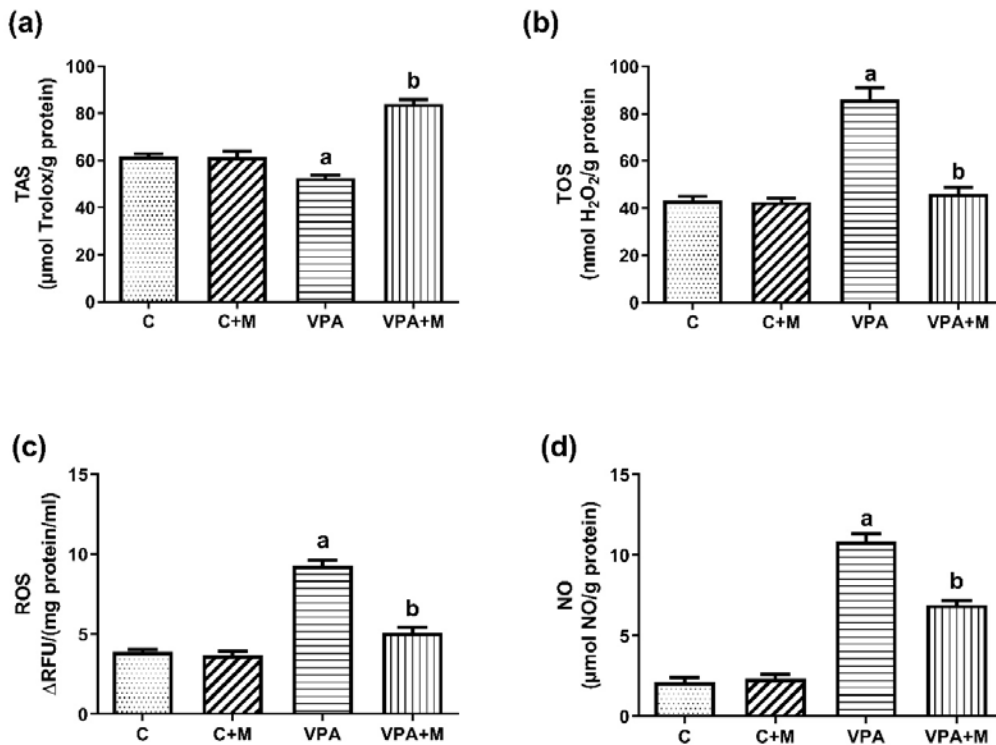
Figure 3. Effect of *Moringa* extract on lens tissue of experimental animals (a) TAS levels; [a]p<0.05 vs. control, [b]p<0.0001 vs. VPA, (b) TOS levels; [a]p<0.0001 vs. control; [b]p<0.0001 vs. VPA; (c) ROS levels; [a]p<0.0001 vs. control; [b]p<0.0001 vs. VPA; (d) NO levels; [a]p<0.0001 vs. control; [b]p<0.0001 vs. VPA. Values were given as mean and standard error. C: Control group; C+M: Control+*Moringa* extract group; VPA: Valproate group; VPA+M: Valproate+*Moringa* extract group.
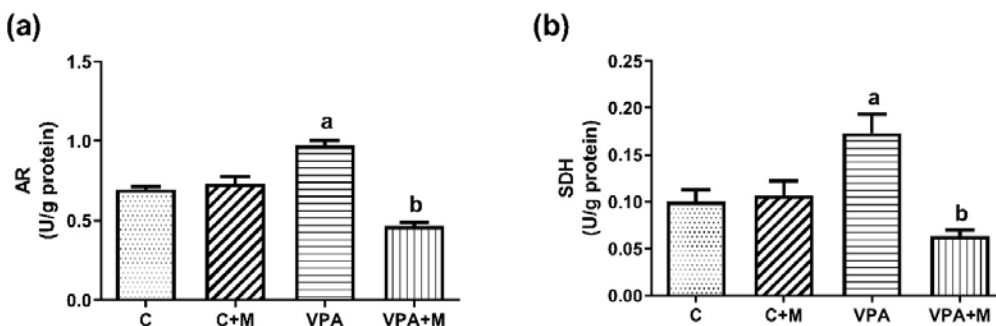

Figure 4. Effect of *Moringa* extract on lens tissue of experimental animals (a) AR activities; [a]p<0.0001 vs. control, [b]p<0.0001 vs. VPA, (b) SDH activities; [a]p<0.05 vs. control; [b]p<0.0001 vs. VPA. Values were given as mean and standard error. C: Control group; C+M: Control+*Moringa* extract group; VPA: Valproate group; VPA+M: Valproate+*Moringa* extract group.

DISCUSSION

Amongst the most widely used anti-epileptic drug is VPA and its corresponding salts. However, this drug has been proven to cause multiple organ damage and subsequently mortality.[2–6,8] Amongst the organs grossly affected is the lens tissue.[34] Findings have shown that VPA exhibits its side effects by destabilising oxidant/antioxidants balance, triggering inflammatory reactions, autoimmune reactions, and lipid peroxidation among other chain reactions.[1] Thus, researching and exploiting molecules as well as food-based substances capable of mitigating the deteriorative effect of VPA is of paramount significance.

The diverse pharmacological effects of *Moringa oleifera* leaves have been proven to be associated with its rich vitamins and antioxidant components. Extracts of the plant leaves are shown to have antioxidant activity,[13] anti-inflammatory,[14] and protective effect on several organs/tissues.[15–17] Consequently, prompting the present study, to evaluate the protective effect of
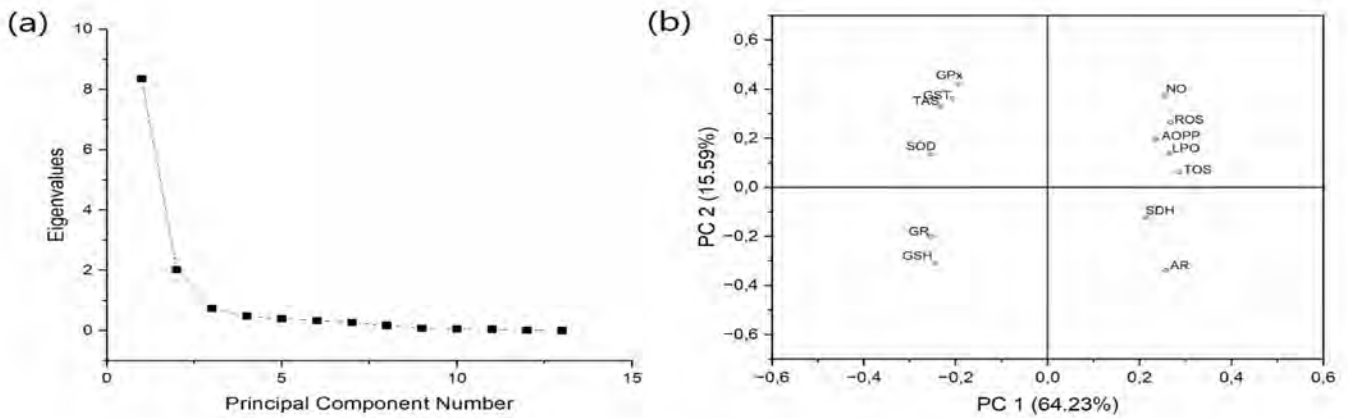
Figure 5. (a) Principal component analysis (PCA) plot, (b) PCA model of biochemical results for all groups. All biochemical results of lens tissues indicator plotted as a function of two first components, principal component 1 (PC1: 64.23%) and principal component 2 (PC2: 15.59%), explaining together 79.92% of information in the obtained dataset.

Moringa extracts against VPA induce lens toxicity in Sprague Dawley rats.

GSH is a substantial antioxidant molecule that participates in a both enzymatic and non-enzymatic process that protect tissues against oxidative stress. It is significant for the protection of proteins, lipids, and important subcellular organelle including mitochondria, and its level is usually high in lens tissue.[35] The present findings suggest that the administration of 0.5 g/kg b.w./day VPA for 15 days resulted in a diminished GSH level in lens tissue. This may be a consequence of the overproduction of free radicals and exhaustive use of the GSH in the lens tissue. Furthermore, the levels of LPO and AOPP-key markers of oxidative stress and contributing risk factors to tissue damage/necrosis were found to significantly increase in the VPA group. This finding is in agreement with the report of Tong et al.,[36] and a clear indication of increased lipid peroxidation and the oxidation proteins, following the accumulation of ROS and/or diminished GSH levels. The present outcomes are in agreement with an earlier report by and Tunali et al.[9] The concurrent administration of VPA with *Moringa* extract prevented the depletion of GSH levels, and as well downregulated the levels of both LPO and AOPP. The ability of *Moringa* extract to exhibit a positive effect on GSH, LPO, and AOPP levels is most likely linked to its antioxidant properties as earlier reported.[13]

Antioxidants enzymes including GR, GPx, GST, and SOD and play a vital role in the antioxidant system. GR is the key enzyme involved in the reconversion of oxidized glutathione (GSSG) to reduced glutathione (GSH) via utilising NADPH. GPx on the other hand is involved in the reduction of hydrogen peroxide to water, as well as the conversion of lipid peroxides to their corresponding alcohols. Thus, GPx protects against oxidative stress and cellular membrane damage.[37] GST catalyses the conjugation of GSH with xenobiotics and other potentially reactive molecules, thereby bringing about their detoxification.[38]

SOD is responsible for the detoxification of superoxide into hydrogen peroxide and oxygen molecules. An alteration in the activity of any of these enzymes (GR, GPx, GST, and SOD) can significantly affect the redox state and the antioxidant mechanism. In the present study, the activities GR, GPx, GST, and SOD in lens tissue were grossly distorted upon administration of only VPA to experimental rats for 15 days. Previous findings indicate that VPA is an inhibitor GR, and chronic administration of VPA can affect the overall activities of antioxidant enzymes.[9] The co-treatment of VPA with *Moringa* extract resulted in a stabilised, non-distorted levels or higher activities of this enzyme. This can be primarily attributed to the strong antioxidant property of the plant extract.

TAS is the measure of the total antioxidants level in a biological system or sample. High TAS levels usually suggest higher antioxidant potential. On the contrary, TOS, ROS, and NO represent the levels of oxidants and oxidants species in a system. The higher their levels, the more likely a system is prone to oxidative stress. In the present study, the administration of VPA resulted in a decline in TAS, as well as a corresponding increase in TOS, ROS, and NO levels. This is a consequence of the excessive production of reactive oxygen species and depletion of antioxidant reserves due to VPA metabolism as earlier suggested.[1] In the VPA+M group, the levels of TAS were markedly elevated even beyond that of the control group, while TOS, ROS and NO levels were kept lower than that of the VPA group. This effect of *Moringa* extract on VPA administered animals is probably due to its rich vitamin composition and antioxidant power. This is in line with earlier studies that proved the ability of antioxidants vitamins to mitigate oxidative stress and mop up radicals.[39]

AR is a key enzyme of the polyol pathway that belongs to the aldoketo reductase superfamily.[40] The activity of AR involves the utilization of NADPH (as reducing equivalents) to

produce sorbitol from glucose. On the other hand, SDH catalyses the conversion of sorbitol to fructose by reducing NAD^+ to $NADH$.[41] Elevated activity of this enzyme will ultimately result in the depletion of NADPH reserve and increased osmotic pressure due to the accumulation of sorbitol in lens tissue. Thus, distorting both GSH levels and the activities of GR, GST, CAT, and other essential antioxidant enzymes. In general, increased tissue activity of AR and SDH could distort the overall antioxidant system by depleting NADPH and inducing osmotic pressure or tissue damage. In the present study, the activities of both AR and SDH (a marker for cellular injury) of VPA-administered rats were significantly elevated. This finding is in agreement with the reports of Tunali et al.[9] The administration of *Moringa* extract together with VPA counterpoises these defects via its antioxidant potential and possible enzyme inhibition effects.

CONCLUSION

The present findings indicate that the co-administration of VPA with *Moringa* extract could mitigate the side effect and deleterious effects of VPA on the lens tissue of experimental animals. This is a positive effect of *Moringa oleifera* leaves is likely due to its antioxidant properties, rich vitamin composition, and antioxidant phytochemical.

ORCID IDs of the authors

Eda Dagsuyu   0000-0003-0395-1058
Umar Faruk Magaji   0000-0002-4009-481X
Ozlem Sacan   0000-0001-6503-4613
Refiye Yanardag   0000-0003-4185-4363

REFERENCES

1. Ghodke-Puranik Y, Thorn CF, Lamba JK, et al. Valproic acid pathway: Pharmacokinetics and pharmacodynamics. *Pharmacogenet Genom*. 2013;23:236–241.

2. Santos BL, Fernandes RM, Neves FF. Valproic acid-induced pancreatitis in an adult. *Arq Neuropsiquiatr*. 2010;68:135–136.

3. Emekli-Alturfan E, Alev B, Tunali S, et al. Effects of edaravone on cardiac damage in valproic acid induced toxicity. *Ann Clin Lab Sci*. 2015;45:166-172.

4. Oktay S, Alev B, Tunali S, et al. Edaravone ameliorates the adverse effects of valproic acid toxicity in small intestine. *Hum Exp Toxicol*. 2015;34:654-661.

5. Turkyılmaz IB, Altas N, Arisan I, Yanardag R. Effect of vitamin B6 on brain damage in valproic acid induced toxicity. *J Biochem Mol Toxicol*. 2021;35:e22855.doi:10.1002/jbt.22847.

6. Celik E, Tunali S, Gezginci-Oktayoglu S, Bolkent S, Can A, Yanardag R. Vitamin U prevents valproic acid-induced liver injury through supporting enzymatic antioxidant system and increasing hepatocyte proliferation triggered by inflammation and apoptosis. *Toxicol Mech Methods*. 2021;31:600-608.

7. Gezginci-Oktayoglu S, Turkyilmaz IB, Ercin M, Yanardag R, Bolkent S. Vitamin U has a protective effect on valproic acid-induced renal damage due to its anti-oxidant, anti-inflammatory, and anti-fibrotic properties. *Protoplasma*. 2016;253:127-135.

8. Bayrak BB, Yılmaz S, Hacıhasanoglu CN, Yanardag R. The effects of edaravone, a free-radical scavenger in lung injury induced by valproic acid demonstrated via different biochemical parameters. *J Biochem Mol Toxicol*. 2021; 35(9): e22847.doi:10.1002/jbt.22847.

9. Tunali S, Kahraman S, Yanardag R. Vitamin U, a novel free radical scavenger, prevents lens injury in rats administered with valproic acid. *Hum Exp Toxicol*. 2014; 34:904-910.

10. Milla PG, Peñalver R, Nieto G. Health benefits of uses and applications of *Moringa oleifera* in bakery products. *Plants*. 2021;10:318. doi:10.3390/plants10020318

11. Sultana B, Anwar F. Flavonols (kaempeferol, quercetin, myricetin) contents of selected fruits, vegetables and medicinal plants. *Food Chem*. 2008;108:879-884.

12. Magaji UF, Sacan O, Yanardag R. Alpha amylase, alpha glucosidase and glycation inhibitory activity of *Moringa oleifera* extracts. *S Afr J Bot*. 2020;128:225-230.

13. Oldoni TLC, Merlin N, Bicas TC, et al. Antihyperglycemic activity of crude extract and isolation of phenolic compounds with antioxidant activity from *Moringa oleifera* Lam. leaves grown in Southern Brazil. *Food Res Int*. 2021;141:110082. doi:10.1016/j.foodres.2020.110082

14. Waterman C, Cheng DM, Rojas-Silva P, et al. Stable, water extractable isothiocyanates from *Moringa oleifera* leaves attenuate inflammation *in vitro*. *Phytochemistry*. 2014;103:114-122.

15. Toppo R, Roy BK, Gora RH, Baxla SL, Kumar P. Hepatoprotective activity of *Moringa oleifera* against cadmium toxicity in rats. *Vet World*. 2015;8:537-540.

16. Ouedraogo M, Lamien-Sanou A, Ramde N, et al. Protective effect of *Moringa oleifera* leaves against gentamicin-induced nephrotoxicity in rabbits. *Exp Toxicol Pathol*. 2013;65:335-339.

17. Saini RK, Sivanesan I, Keum YS. Phytochemicals of *Moringa oleifera*: A review of their nutritional, therapeutic and industrial significance. *3 Biotech*. 2016;6:203. doi:10.1007/s13205-016-0526-3

18. Ali A, Garg P, Goyal R, et al. A novel herbal hydrogel formulation of *Moringa oleifera* for wound healing. *Plants*. 2021;10:25. doi:10.3390/plants10010025

19. Ertik O, Magaji U.F, Sacan O, Yanardag R. Effect of *Moringa oleifera* leaf extract on valproate-induced oxidative damage in muscle. *Drug Chem Toxicol*. 2022.

doi:10.1080/01480545.2022.2144876.

20. Beutler E. Reduced Glutathione (GSH): Red blood cell metabolism: A manual of biochemical methods, In: Bergmeyen, HV ed. New York, Grune & Stratton, 1975, 112-114.

21. Ledwozyw A, Michalak J, Stepien A, Kadziolka A. The relationship between plasma triglycerides, cholesterol, total lipids and lipid peroxidation products during human atteroschlerosis. *Clin Chim Acta*. 1986;155:275-283.

22. Barretto OC, Beutler E. The sorbitol-oxidizing enzyme of red blood cells. *J Lab Clin Med*. 1975;85:645-649.

23. Hayman S, Kinoshita JH. Isolation and properties of lens aldose reductase. *J Biol Chem*. 1965;240:877-882.

24. Beutler E. Red cell metabolism: A manuel of biochemical methods, London, Grune & Stratton, 1971;68-70.

25. Mylroie AA, Collins AH, Umbles C, Kyle J. Erythrocyte superoxide dismutase activity and other parameters of copper status in rats ingesting lead acetate. *Toxicol Appl Pharmacol*. 1986;82:512-520.

26. Wendel A. Glutathione peroxidase. *Methods Enzymol*. 1981;77:325–333.

27. Habig WH, Jakoby WB. Assays for differentiation of glutathione S-transferases. *Methods Enzymol*. 1981;77:398–405.

28. Erel O. A new automated colorimetric method for measuring total oxidant status. *Clin Biochem*. 2005;38:1103–1111.

29. Erel O. A novel automated direct measurement method for total antioxidant capacity using a new generation, more stable ABTS radical cation. *Clin Biochem*. 2004;37: 277–285.

30. Zhang Y, Chen J, Ji H, Xiao ZG, Shen P, Xu LH. Protective effects of Danshen injection against erectile dysfunction via suppression of endoplasmic reticulum stress activation in a streptozotocin-induced diabetic rat model. *BMC Compl Altern Med*. 2018;18:343. doi:10.1186/s12906-018-2414-3

31. Miranda KM, Espey MG, Wink DA. A rapid, simple spectrophotometric method for simultaneous detection of nitrate and nitrite. *Nitric Oxide*. 2001;5:62–71.

32. Witko-Sarsat V, Friedlander M, Capeillère-Blandin C, et al. Advanced oxidation protein products as a novel marker of oxidative stress in uremia. *Kidney Int*. 1996;49: 1304-1313.

33. Lowry OH, Rosebrough NJ, Farr AL, Randall RJ. Protein measurement with the folin phenol reagent. *J Biol Chem*. 1951;193:265–275.

34. Aktas Z, Cansu A, Erdoğan D, et al. Retinal ganglion cell toxicity due to oxcarbazepine and valproic acid treatment in rat. *Seizure*. 2009;18:396–399.

35. Coppola S, Ghibelli L. GSH extrusion and the mitochondrial pathway of apoptotic signalling. *Biochem Soc Trans*. 2000;28:56–61.

36. Tong V, Teng XW, Chang TKH, Abbott FS. Valproic acid I: Time course of lipid peroxidation biomarkers, liver toxicity, and valproic acid metabolite levels in rats. *Toxicol Sci*. 2005;86:427–435.

37. Muthukumar K, Rajakumar S, Sarkar MN, Nachiappan V. Glutathione peroxidase3 of Saccharomyces cerevisiae protects phospholipids during cadmium-induced oxidative stress. *Antonie van Leeuwenhoek*. 2011;9:761–771.

38. Oakley A. Glutathione transferases: A structural perspective. *Drug Metab Rev*. 2011; 43:138–151.

39. Stawiarska-Pieta B, Paszczela A, Grucka-Mamczar E, Szaflarska-Stojko E, Birkner E. The effect of antioxidative vitamins A and E and coenzyme Q on the morphological picture of the lungs and pancreata of rats intoxicated with sodium fluoride. *Food Chem Toxicol*. 2009;47:2544–2550.

40. Wu ZM, Yin XX, Ji L, et al. Ginkgo biloba extract prevents against apoptosis induced by high glucose in human lens epithelial cells. *Acta Pharmacol Sin*. 2008;29:1042–1050.

41. El-Kabbani O, Darmanin C, Chung RP. Sorbitol dehydrogenase: Structure, function and ligand design. *Curr Med Chem*. 2004;11:465–476.

How cite this article

The Effectiveness of Ultrasound-Assisted Extraction on Antioxidative Properties of Bract Leaves of Globe Artichoke

Doruk Akdogan[1,2], Aysegul Peksel[1]

[1]Yıldız Technical University, Faculty of Science and Arts, Department of Chemistry, Istanbul, Turkiye
[2]Istanbul Nisantasi University, Departments of Pharmacy Services, Vocational School of Health Services, Istanbul, Turkiye

ABSTRACT

Objective: The antioxidant-rich artichoke bracts leaves are a particularly waste of the food industry. Thus, it would be possible to utilize a cheap and natural material, which is industrial waste, instead of synthetic antioxidants. The present study aimed to extract from the bract leaves of globe artichoke by ultrasound-assisted extraction and to evaluate their antioxidant activities.

Materials and Methods: In this study, the effect of ultrasound-assisted extraction (UAE) on antioxidative properties was studied. The extracts were obtained from the leaves of the head part of the artichoke by using UAE and evaluated for their antioxidative properties. For this purpose, antioxidant activity methods were investigated for different extraction times. The results obtained were compared with standard antioxidants.

Results: The results obtained from this study showed that the shorter extraction time resulted in higher antioxidative properties. Accordingly, in plant extracts prepared by UAE-1, the highest total phenolic content value (193.80 µg pyrocathecol equivalent/mg extract), the highest total flavonoid content value (254.13 µg catechin equivalent/mg extract), the highest total chlorophyll content value (10.68 µg/mL) and carotenoid (0.57 µg/mL) were found. Similarly, UAE-1 extracts showed the best results in terms of free radical scavenging activity. Also, the 2,2-diphenyl-1-picrylhydrazyl radical scavenging activity of UAE-1 (89.09%) was determined to be higher than the standard antioxidant α-Tocopherol (85.68%) and very close to another standard antioxidant butylated hydroxyanisole (91.98%).

Conclusion: UAE could be preferred instead of the traditional method (Soxhlet) as a shorter, eco-friendly, and low energy cost.

Keywords: Antioxidative properties; Ultrasound-assisted extraction; Plant extract; *Cynara scolymus* L.; Radical scavenging

INTRODUCTION

The increasing interest in the replacement of synthetic antioxidants with natural ones has opened the door to much research, particularly to the study plant sources and new antioxidants contained in these sources.[1,2]

Plant extracts are a generous source of bioactive compounds with medical features.[3] Reactive oxygen species are produced continuously during special metabolic events in the organism, especially various sources such as lipid peroxidation and mitochondrial cytochrome oxidase, or the result of exogenous sources including ultraviolet light, environmental toxins, and anticancer drugs.[4]

It is known that antioxidants have the feature of delaying or preventing bitter and other taste deterioration caused by oxidation when used in foods other than protecting the cell with its defense mechanism.[5] Flavonoids, polyphenolics, tocopherols, and ascorbic acid are the most important natural antioxidant groups. It is known that phenolic compounds have high antioxidant activity and their most important sources are found in plants.

In particular, the extraction of phenolic compounds from agricultural and industrial organic wastes has been one of the most important issues that many researchers are interested in. This is because extraction is the main step in isolating and using biocomponents.

The artichoke (*Cynara scolymus* L.), which grows in Southern Europe and the Mediterranean region and has wild forms in the countries in this basin, is a 50-150 cm tall herbaceous plant that blooms blue-purple flowers of the daisy-family. Artichoke contains some phenolic compounds.[6] The fact that artichoke is nutritious and beneficial to health is due to certain chemi-

cal compositions, including these high levels of polyphenolic compounds and inulin. Previous studies exhibited that the extracts from artichoke have antioxidant[7], antiseptic[8], antibiotic,[9] and anticarcinogenic[10] effects. The antioxidant-rich artichoke bracts leaves are a particularly waste of the food industry. Thus, it would be possible to utilize a cheap and natural material, which is industrial waste, instead of synthetic antioxidants.

Soxhlet extraction, known as the traditional method, has been frequently used to obtain plant extracts containing bioactive compounds. However, situations such as taking a long time and requiring large amounts of toxic and expensive solvents limit the usability of this method. Environmentally friendly and effective extraction techniques are required in order to use bioactive plant extracts in food technology, pharmaceutical, and cosmetic formulations. In recent years, sustainable new extraction techniques have reduced extraction time, reduced solvent consumption, and improved the quality of extracts obtained. However, it has been observed in the literature that studies for extraction of phenolic compounds from various parts of the artichoke are carried out by traditional methods (Soxhlet or maceration).[6] Ultrasound-assisted extraction (UAE) is an important technique used in the pharmaceutical and food industry.[11] Ultrasonic energy produces many tiny bubbles in the liquid medium and causes the particles to break off by causing the solids to mechanically. The sound waves usually provide effective contact between the solid and solvent resulting in good recovery of the analyte. Ultrasonic application mechanically breaks down cell walls. With the mechanical destruction of the cell wall, intracellular components easily exit the cell and pass into the solvent.[12] Long sonication time may cause degradation of the compounds for isolation. Therefore, the processing time of UAE necessarily requires optimization.

The present study aimed to extract from the bract leaves of globe artichoke by UAE during different extraction times and to evaluate their antioxidant activities. For these purposes, different antioxidative properties were studied by optimizing the extraction time.

MATERIALS AND METHODS

Materials

The bract leaves of the artichoke (*Cynara scolymus* L.) plant used as research material in this study were supplied from the Istanbul local market in April 2018 and were thoroughly cleaned with distilled water and dried at room temperature for approximately 7 days in the dark. The leaves were cut into small pieces before extraction. All material was kept in the refrigerator at +4 °C until used.

Reagents and Solvents

All chemicals used in this study are of high-performance liquid chromatography purity and have been obtained from Merck, Sigma Aldrich, Fluka, and Riedel-de Haen companies.

Extraction Procedures: Ultrasound-Assisted Extraction

For UAE, 2.5 g of plant samples were taken into the tared glass beakers and completed with 25 mL of solvent (96% ethanol). Extraction was performed in the ultrasonic bath (Bandelin Electronic 320 w 35 kHz) for different extraction times such as 1, 5, 15, or 30 min, respectively. After this process, the extracts were centrifuged (10,000 rpm for 15 min) (Sigma 3K30). After extraction, the solvent was removed using a fume hood and extracts were obtained. The extracts obtained were kept at +4 °C in the refrigerator.

Determination of Antioxidative Properties

Total phenolic compound content was determined using the method of Slinkard-Singleton.[13] Total flavonoid content was determined by using a colorimetric method according to Zhishen et al.[14] Proline analysis was performed according to the simple modification of the method developed by Bates.[15] Anthocyanin content in dried leaves, has been determined by the modification of the method developed by Padmavati et al.[16] For determination of total chlorophyll and total carotenoid content, used method of Arnon.[17] β-Carotene bleaching method analysis was carried out according to the method developed by Bruni et al.[18] Ferric reducing test was performed according to the method of Oyaizu.[19] Metal chelating activity was determined according to the method of Decker and Welch.[20] 2,2-diphenyl-1-picrylhydrazyl (DPPH) radical scavenging ability of the extracts was determined using the method of Brand-Williams et al.[21] 2,2'-azino-bis(3-ethylbenzothiazoline-6-sulfonic acid) (ABTS) cation radical scavenging ability of the extracts was determined using the method of the Arnao et al.[22] N, N-dimethyl-p-phenylenediamine (DMPD) cation radical scavenging ability was determined according to the method of Fogliano et al.[23] The method of Osawa and Namiki was studied for the measurement of total antioxidant capacity.[24]

RESULTS

Amount of Total Phenolic Compounds

The total phenolic content of the extracts prepared by subjecting the bract leaves of artichokes to different periods in an ultrasonic bath was determined. The results are shown in Table 1. Results are given as µg pyrocatechol equivalent of the phenolic compounds for each mg extract. The highest total phenolic con-

tent value was found in UAE-1 extract (193.80 µg pyrocatechol equivalent/mg extract).

Total Flavonoid Content

The total flavonoid content of the extracts prepared by subjecting the bract leaves of artichokes to different periods in an ultrasonic bath and using ethanol was given in Table 1. The highest flavonoid amount value was found in UAE-1 extract (254.13 µg catechin equivalent/mg extract). Total phenolic compound and flavonoid content results also decreased as the extraction time increased. As a result of the study, the highest antioxidant activity is observed in the extract which was applied for 1 min UAE. Therefore, as a result of the study, it can be concluded that antioxidant activity decreases as long-term ultrasound-assisted extraction can lead to the loss of these phytocomponents which have an antioxidant effect.

Proline Content

The proline content of plants is an indicator of stimulation of the pentose phosphate pathway. The pentose phosphate pathway is controlled by the synthesis of cytosolic proline. High proline content in plants is responsible for high phenolic compounds. For these reasons, proline analysis for edible plants is regarded as an indicator of their antioxidative properties. The total proline contents of the samples obtained from the artichoke leaves are given in Table 1. Among the proline contents of different extracts, the highest amount was found in UAE-30 extract (0.83 µg proline/mg extract). Research on the proline content of plants or food is a newly arising area therefore there is not much data available to compare the results of this study.

Anthocyanin Content

Anthocyanins are dark-coloured pigments extracted from plants. The results obtained from our study, the anthocyanin value of the leaves was 0.065 µmol/g.

Total Chlorophyll and Carotenoid Content

The total chlorophyll and carotenoid contents of the extracts obtained from the artichoke leaves are given in Table 2. The chlorophyll and carotene contents of artichoke leaf extract decreased when the extraction time increased. This situation could be an indication that long-term ultrasound exposure is damaging to these compounds. It was observed that the UAE-1 extract of the plant had the highest total carotenoid content (0.567 µg/mL), and the highest total chlorophyll content (10.68µg/mL).

β-Carotene Bleaching Test Results

The results obtained in the β-carotene bleaching method are given in Table 3. According to the results obtained in this method; two ethanol extracts UAE-15 (1.03), UAE-30 (1.04) of the artichoke leaves were higher than the positive control butylated hydroxyanisole (BHA). It was determined that UAE-1 (0.92) and UAE-5 (0.99) extracts also showed an effect close to BHA.

Ferric Reducing Test Results

In this section, in order to investigate the reduction capacity of the extracts of the bract leaves of artichoke in different concentrations prepared with ethanol to reduce Fe^{3+} to Fe^{2+} added to the tubes, the reducing power was tested by comparing it with standard antioxidants (BHA and α-Tocopherol). Results are shown in Figure 1. The increase in absorbance values is directly proportional to the amount of Fe^{2+} in the reaction medium. In the reducing power assay, the highest reducing power was exhibited by UAE-15 Ethanol extract (0.692 at 700 nm).

Chelating Activity on Ferrous Ion

Metal chelating activities based on inhibition of Ferrozin-Fe^{2+} complex formation in samples and standards are shown in Figure 2. UAE-1 (46.48%) showed the highest metal chelating activity at high concentrations (200 µg/mL). The metal chelating power increased as the extraction time decreased in the extracts created by ultrasound-assisted extraction. On the other hand, increasing the concentration increased the metal chelating power. When comparing extracts with ethylenediaminetetraacetic acid (EDTA), which is known to be a strong chelating agent, it has been observed that EDTA gives higher results compared to all extracts. In addition, according to results the amount of flavonoids and metal chelating activity decreases when the time of ultrasound-assisted extraction increases. Flavonoids, which are from the phenolic family, show strong metal-chelating properties compared to other phenolic compounds. Therefore, the decreasing total flavonoid content also support the results of the metal chelating activity.

DPPH Scavenging Ability

For the determination of DPPH radical scavenging activity in *Cynara scolymus* L. extracts, the extracts were prepared using UAE. The results obtained from samples and standards are shown in Figure 3. UAE-1 extract prepared by the one-min ultrasound-assisted method showed the highest results. According to the results, UAE-1 extract is very close to the standard antioxidant BHA (91.98%) with high antioxidant activity,

Table 1. Total flavonoids, phenolics and, proline amount of artichoke bracts for different extraction times.

Extract	Total Phenolic Content (μg pyrocatechol equivalent/mg extract)	Total Flavonoid Content (μg catechin equivalent/mg extract)	Proline Content (μg proline/mg extract)
UAE-1	193.80	254.13	0.43
UAE-5	188.95	223.30	0.60
UAE-15	182.38	214.97	0.82
UAE-30	182.14	211.08	0.83

UAE-1:Ultrasound-assisted extraction-1 min; UAE-5:Ultrasound-assisted extraction-5 min; UAE-15:Ultrasound-assisted extraction-15 min; UAE-30:Ultrasound-assisted extraction-30 min.

Table 2. Total chlorophyll and carotenoid amounts of bract leaves of artichokes (*Cynara scolymus* L.) for different extraction times.

Extract	Chlorophyll a (μg/mL)	Chlorophyll b (μg/mL)	Total Chlorophyll (μg/mL)	Total Carotenoid (μg/mL)
UAE-1	4.63	6.08	10.68	0.57
UAE-5	3.48	5.88	9.36	0.45
UAE-15	2.19	4.35	5.62	0.38
UAE-30	2.13	4.18	5.55	0.32

UAE-1:Ultrasound-assisted extraction-1 min; UAE-5:Ultrasound-assisted extraction-5 min; UAE-15:Ultrasound-assisted extraction-15 min; UAE-30:Ultrasound-assisted extraction-30 min.

Table 3. β–Carotene bleaching effects of bract leaves of artichoke (*Cynara scolymus* L.) for different extraction times.

Extract	RAA (60 min.)*	RAA (120 min.)*
UAE-1	0.92	0.84
UAE-5	0.99	0.89
UAE-15	1.03	0.96
UAE-30	1.04	0.97
BHA (Positive Control)	1	1
Negative Control (Linoleic Acid Emulsion)	0.14	0.13

UAE-1:Ultrasound-assisted extraction-1 min; UAE-5:Ultrasound-assisted extraction-5 min; UAE-15:Ultrasound-assisted extraction-15 min; UAE-30:Ultrasound-assisted extraction-30 min; RAA*: Relative Antioxidant Activity

while another high antioxidant activity standard, α-Tocopherol (85.68%), has an equally strong antioxidant activity.

ABTS Radical Scavenging Activity

The results of ABTS radical scavenging activities are shown in Figure 4. The ethanol extract UAE-5 (75.04%), which was extracted for 5 min in the studied extracts at a concentration of 200 μg/mL, exhibited the highest ABTS radical scavenging activity. Inhibition values increased in all extracts depending on the concentration. Trolox, a standard with a known antioxidant effect, showed an activity of 99.5% at all concentrations studied.

DMPD⁺ Scavenging Ability

DMPD radical scavenging activities of all samples and standards are shown in Figure 5. At high concentrations (200 μg/mL), in the extracts using UAE 1 minute (UAE-1) has the highest inhibition values (72.02%). DMPD radical scavenging activity increased as the extraction time was shortened. When standard antioxidants were examined, the DMPD radical scavenging activity of ascorbic acid was found to be 98% (200 μg/mL). The synthetic standard antioxidant BHA showed an activity of 65.13% (200 μg/mL). Accordingly, when compared with standard antioxidants, UAE-1 (72.02%) showed higher activity than BHA.
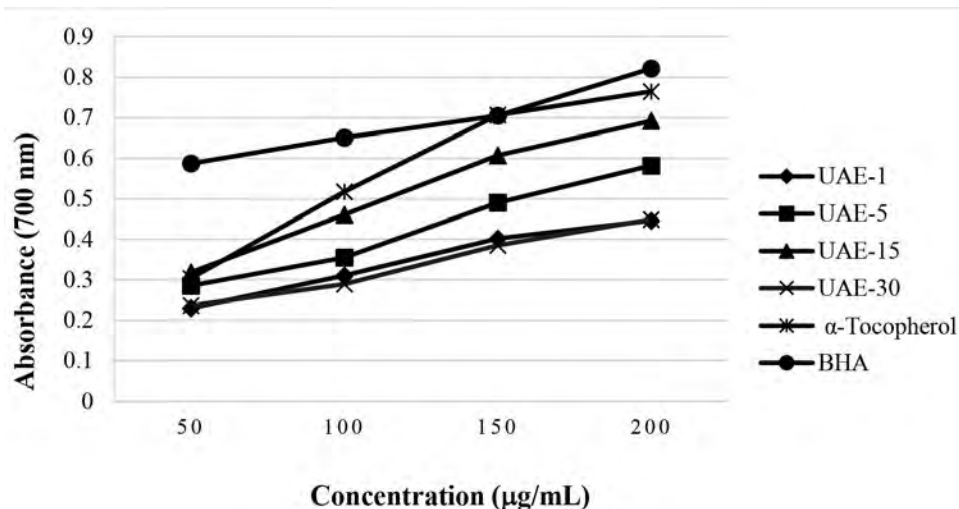
Figure 1. Reducing power of ethanol extracts obtained by UAE methods (1, 5, 15, and 30 min). UAE-1:Ultrasound assisted extraction-1 min; UAE-5:Ultrasound assisted extraction-5 min; UAE-15:Ultrasound assisted extraction-15 min; UAE-30:Ultrasound assisted extraction-30 min; BHA: Butylated hydroxyanisol.
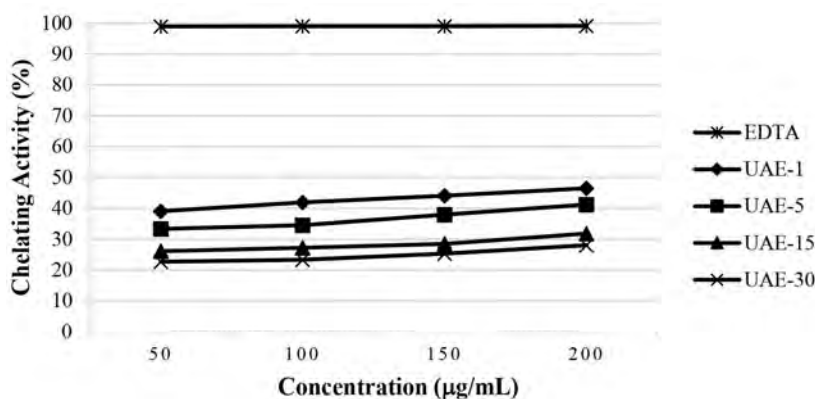

Figure 2. Chelating activities of ethanol extracts obtained by UAE methods (1, 5, 15, and 30 min). UAE-1:Ultrasound assisted extraction-1 min; UAE-5:Ultrasound assisted extraction-5 min; UAE-15:Ultrasound assisted extraction-15 min; UAE-30:Ultrasound assisted extraction-30 min; EDTA: Ethylenediaminetetraacetic acid
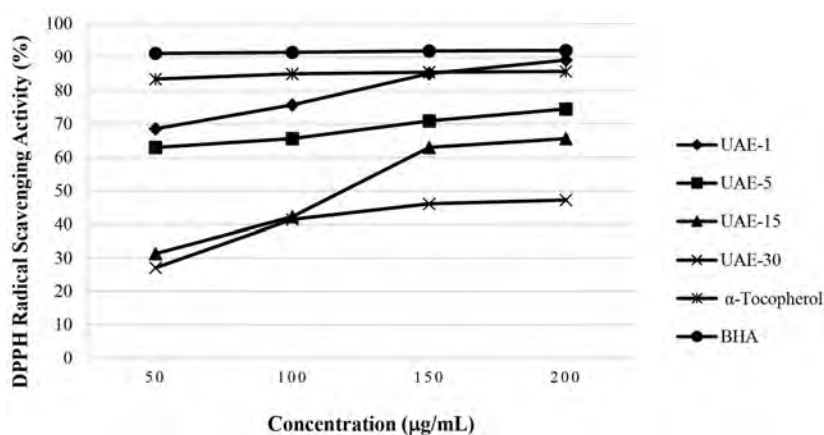

Figure 3. DPPH radical scavenging activities of ethanol extracts obtained by UAE methods (1, 5, 15, and 30 min). UAE-1:Ultrasound assisted extraction-1 min; UAE-5:Ultrasound assisted extraction-5 min; UAE-15:Ultrasound assisted extraction-15 min; UAE-30:Ultrasound assisted extraction-30 min; BHA: Butylated hydroxyanisol.
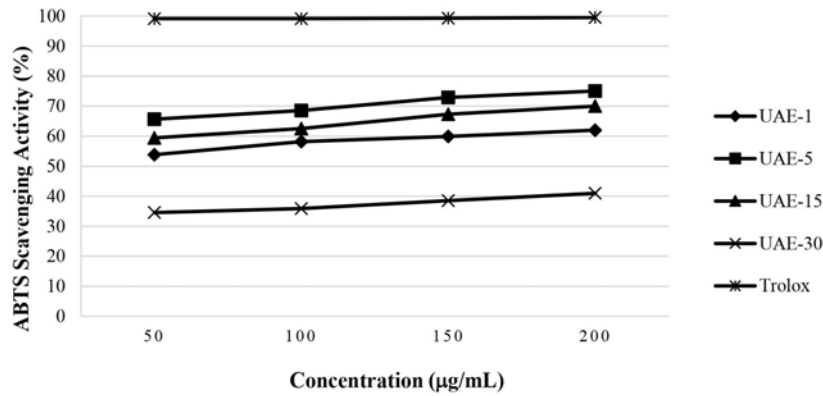
Figure 4. ABTS radical scavenging activities of ethanol extracts obtained by UAE methods (1, 5, 15, and 30 min). UAE-1:Ultrasound assisted extraction-1 min; UAE-5:Ultrasound assisted extraction-5 min; UAE-15:Ultrasound assisted extraction-15 min; UAE-30:Ultrasound assisted extraction-30 min.

Figure 5. DMPD radical scavenging activities of ethanol extracts obtained by UAE methods (1, 5, 15, and 30 min). UAE-1:Ultrasound assisted extraction-1 min; UAE-5:Ultrasound assisted extraction-5 min; UAE-15:Ultrasound assisted extraction-15 min; UAE-30:Ultrasound assisted extraction-30 min; BHA: Butylated hydroxyanisol.
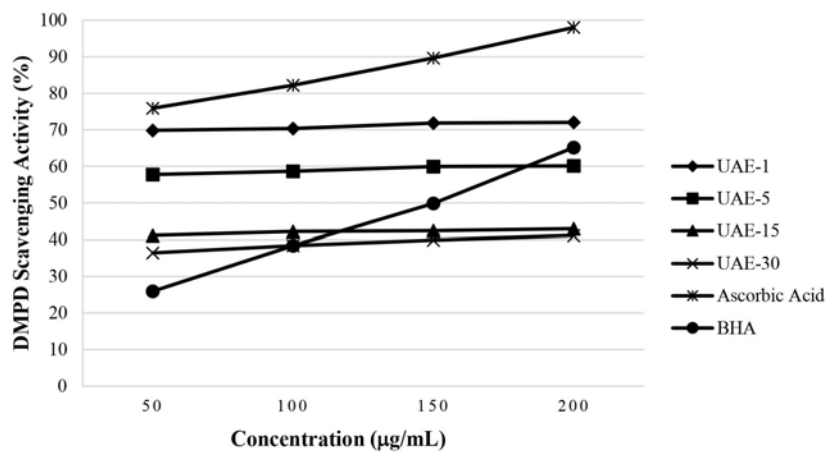

Figure 6. Antioxidative effect of ethanolic samples obtained by UAE (1, 5, 15, and 30 min) at the end of the first 24 h. UAE-1:Ultrasound assisted extraction-1 min; UAE-5:Ultrasound assisted extraction-5 min; UAE-15:Ultrasound assisted extraction-15 min; UAE-30:Ultrasound assisted extraction-30 min; BHA: Butylated hydroxyanisol.
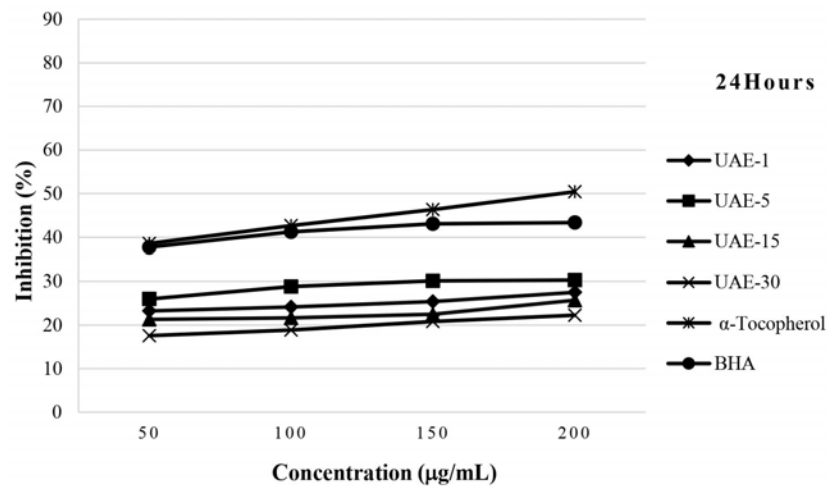
Total Antioxidant Capacity

The total antioxidant activity was determined according to the thiocyanate method with slight modifications. Total antioxidant activity was determined by taking measurements at 24-hour intervals for 3 days. The effects of extracts and standards on linoleic acid peroxidation are shown in Figure 6. It was observed that UAE-5 (30.3%) extract had the highest activity at the end of the first 24 h. The antioxidant activity of this extract is close to the activity of standard antioxidants BHA (43.35%) and α-Tocopherol (50.42%). At the end of 48 h, the total antioxidant activity of the extracts started to decrease due to deterioration in the structure of the extracts over time. After 72 h, ultrasound-assisted extracts and standard antioxidants were no longer active.

DISCUSSION

The antioxidative properties of bract leaves of the artichoke plant (*Cynara scolymus* L.) were investigated using UAE in different antioxidant parameters. According to our results obtained from the study, extracts obtained from the leaves of the artichoke (*Cynara scolymus* L.) bract showed a high antioxidative effect. From these effects, the ethanol extract exhibited high reducing power, noteworthy phenolic content, and DPPH scavenging capability at the same conditions.

The total amount of phenolic compounds was found to be 193.80 µg pyrocatechol equivalent per mg of ethanol extract after one minute of extraction time. There are no studies conducted with bract leaves of artichoke. However, there are studies on the leaves of the artichoke plant. For example, Ben Salem et al.[25] extracted the leaves by maceration method using different increasing solvent polarities (such as hexane, butanol, ethyl acetate, 75% EtOH/H_2O, and aqueous. They found the maximum content of the total phenolic compound by using ethanol extracts. Their result corresponded to 54.54 mg gallic acid equivalent per g dry weight of extract. Our results are higher than the work of Ben Salem et al.[25] Kollia et al.[26] found the phenolic content of artichoke leaves as 1.45 mg GAE/g DW by UAE. All these results comply with our studies in terms of proving the presence of phenolic content in bract leaves of artichoke.

Stumpf et al.[27] prepared extracts from artichoke leaves by using three different extraction methods. The extracts were compared with their total phenolic compounds and total antioxidant capacities. Extraction according to the European Pharmacopoeia or UAE gave similar results when compared. However, the results obtained with hot water extraction are quite inadequate. This study shows us the importance of the UAE-method. Stumpf et al.[27] prepared artichoke leaf extract with 80% methanol by using UAE. All extracts were directly used for the determination of total phenolic concentration and antioxidant capacity. This study was showed that total phenolic

content and total antioxidant capacity are closely related to the extraction method.

Reche et al.[28] performed mathematical modeling of UAE and they studied the kinetics of bioactive compounds obtained from artichoke by-products. In this study, an evaluation of an artichoke by-product rich in bioactive compounds by UAE and ethanol solvent was proposed. The effective diffusion coefficient exhibited temperature dependence, whereas the external mass transfer coefficient and the equilibrium extraction yield depended on both temperature and ultrasound power density. This study also supports our study.

Lavecchia et al.[29] extracted the artichoke residues they prepared using ethanol as a solvent in a thermostated bath at 60°C and determined the phenolic compounds in the stems and bracts by obtaining 51.10±0.74 and 24.58±0.57 mg gallic acid equivalent per g extracts, respectively. These values are very low when compared to our study. Ultrasound-assisted technology is known to act on plant tissues by the cavitational phenomenon induced at the solid/liquid interface. This effect facilitates the release of extractable compounds and enhances mass transport by disrupting the plant cell walls. Pasqualone et al.[30] analyzed the extracts obtained from three artichoke varieties (Opal, Capriccio, and Catanese) in terms of antioxidant parameters; in the UAE of samples, the extract showed a total phenolic content higher than non-ultrasound extraction method. The results were expressed as mg gallic acid equivalent per kg. Zuorro et al.[31] reported total polyphenol content in bracts (24.14 mg GAE/g) using a 50:50 ethanol-water mixture as an efficient extraction method, and solvent-extraction procedure. In our study, UAE-1 extract also exhibited the highest flavonoid amount value with 254.13 µg catechin equivalent per mg of extract. This result was very high when compared the other similar studies. Ben Salem et al.[25] found that ethanol extract had the highest value in terms of total flavonoid content (12±0.83 CE/g DW) by using the maceration method. These studies also determined the flavonoid content of the artichoke leaves, like our study. Petropoulos et al.[3] found very low flavonoid content in the edible head of artichoke. They studied eight different genotypes of artichoke heads and determined the highest value as 7.2 mg/g extract. The chlorophyll and carotenoid contents of our studied samples were also high. In order to make a comparison of chlorophyll and carotenoid contents, no studies were found in the literature with artichoke bracte leaves. Ben Salem et al.[25] measured that the β-carotene bleaching effect of ethanol extract (70.74%) is the highest inhibition rate and higher than butylated hydroxytoluene (BHT) (47.94%).

Flavonoids are a main class of polyphenols in plants. They are known as antioxidants and free radical scavengers. The antioxidant activity of plants has been correlated to the total flavonoid content. For this reason, in our study, especially free or cation radical scavenging capacity was found to be very high. DPPH radical scavenging activity of UAE-1 extract showed similar

activities to the standard antioxidants such as BHA and α-tocopherol, at all concentrations tested. DMPD cation radical scavenging ability of the extract was determined higher than BHA in all the concentrations studied. These results are very pleasing. In addition, in extraction time optimization studies, it is seen that an effective extraction takes place in a very short time such as one minute. Ergezer et al.[32] prepared artichoke bracte leaf extract with 80% ethanol by using the maceration method. They obtained the DPPH radical scavenging activity as 79.91 % after the 7th day of storage. The result we found in our study is that the DPPH radical scavenging activity is 89.09 % for the extract concentration of 200 µg/mL. This result is higher than α-tocopherol (85.68%). Mena García et al.[33] reported lower results of DPPH (26.59 ±0.62 mg TE/g) using a mixture of ethanol/water (50:50 v/v) and a microwave-assisted extraction method from the artichoke. Shallan et al.[34] showed that the antioxidant activity (DPPH) of Globe artichoke bracts extract in ethanolic solution was 6.42 mg/L. Quispe et al.,[35] determined the total phenolic compounds of artichoke bracts between 10.86 mg and 24.82 mg GAE/g in artichoke extracts prepared using ultrasound-assisted extraction and ethanol as solvent. The radical scavenging activity of DPPH was found between 15.49 mM and 38.65 mM trolox, and the trolox equivalent antioxidant capacity from 12.56 to 32.52 mM trolox, respectively.

To investigate the reducing capacity of Fe^{3+} to Fe^{2+}, the reducing power was tested by comparing the extracts with the standards. The increase in absorbance values is directly proportional to the amount of Fe^{2+} in the environment. The best activity among the prepared extracts was UAE-15 (0.692 at 700 nm). The good results obtained from ethanol extracts may suggest that the preparation of artichoke extracts in a moderately apolar solvent such as ethanol will have a more active effect in terms of reducing power than solvents with high polarity or high apolarity. In terms of ultrasound-assisted extraction, it can be argued that the 1-minute and 5-minute extraction times are not fully sufficient to reduce Fe^{3+}, while the 15-minute extraction period provides the necessary optimization for this reduction event. It can be said that in longer extractions such as 30 min, the extract may be damaged by sound waves and cause it to lose its reducing power feature. Ben Salem et al.[25] examined the reducing power parameter in artichoke leaf extracts in their study. For the reducing power test of *Cynara scolymus* L., they measured the absorbance at 515 nm in a UV-VIS spectrophotometer of the ferric reducing antioxidant power mixture prepared with extracts. expressed the antioxidant capacity of artichokes as trolox Equivalent. Among all extracts of artichoke in their work, the ethanol extract demonstrated a favorable iron-reducing capacity (527.79 µmol Fe^{2+}/mg dry extract). Thang et al.[36] studied and compared different extraction techniques to extract cynarine and chlorogenic acid (classical extraction, ultrasound-assisted extraction, enzyme-assisted extraction) from leaves of *Cynara scolymus* L. In addition, the

extracts were also studied for antioxidant activities. The antioxidant activity of the artichoke extract was tested by the ferric-reducing antioxidant power method. They found the highest reducing power of ferric iron in pectinase enzyme extracts from artichoke leaves. The measurement of reducing power of ascorbic acid and artichoke extract from dried artichokes treated with pectinase enzymes was exhibited as 48.0 and 77.8 mg/L, respectively. Artichoke extract hydrolyzed by pectinase enzymes also had a higher radical scavenging capacity (IC_{50}=30 mg/L) compared to ascorbic acid (IC_{50}=11 mg/L). Wioletta Biel et al.[37] reported that the antioxidant capacity of artichoke extract was measured at 1060.8 µmol trolox/1 g dry matter.

UAE-1 (46.48%) showed the highest metal chelating activity at high concentrations (200 µg/mL). It was observed that the percentages of metal chelating activity increased as the extraction time was shortened in the extracts applied ultrasound-assisted extraction. Flavonoids from the phenolic family show strong metal chelating properties compared to other phenolic compounds. Therefore, the decrease in the total flavonoid content due to the increase in the extraction time also supports the results of the metal chelating activity. Among the analyzed extracts, the ethanol extract UAE-5 (75.04%), which was extracted for 5 min at a concentration of 200 µg/mL, exhibited the highest ABTS radical scavenging activity. It can be said that the ultrasonic extraction time, which gives the optimum value and can be considered ideal is 5 min in terms of the high value of ABTS radical scavenging activity of artichoke extracts prepared with ethanol. Kollia et al.[26] found ABTS radical scavenging activity in artichoke leaves as 1.25 mg TE/g DW by UAE in their study with artichoke leaves. Ben Salem et al.[25] also analyzed the scavenging activity of the artichoke extract and found that ethanol extract had a high activity. Sihem et al.[1] also demonstrated that the extracts of the head leaves obtained by using the maceration method had the highest activity. It was observed that UAE-5 (30.3%) extract had the highest total antioxidant activity at the end of the first 24 h. The antioxidant activity of this extract is close to the activity of standard antioxidants BHA (43.35%) and α-tocopherol (50.42%).

It is a very important detail that a waste material can be used instead of synthetic antioxidants in the food, pharmaceutical, or cosmetic industry. It is known that the bract leaves of the artichoke are a waste in local markets and the food industry. The high flavonoid content and high antioxidant activity of these leaves can be evaluated. Thus, the natural antioxidant needs of the food, pharmaceutical, or cosmetic industry can be met. For example, it may be possible for an inexpensive material to replace antioxidants with artificial and toxic properties in the industry by using it for purposes such as preserving properties, extending shelf life, adding nutritional value, flavoring, and coloring in foods. It was determined that extracts (UAE-1) prepared in 1 min in the ultrasound-assisted extraction method had the highest antioxidative properties in most of the parameters studied. Extracts prepared in 30 min (UAE-30) showed

the lowest inhibition values in most of the parameters studied. Therefore, it can be argued that the increase in the extraction time may cause the extract to lose its properties and lead to a decrease in its antioxidative properties.

CONCLUSION

UAE could be preferred instead of the traditional method as a shorter, eco-friendly, and low energy cost. For further studies, it may be recommended to isolate specific compounds from the extracts and optimize extraction methods, especially ultrasound-assisted extraction, through experimental design. Optimization can be achieved by examining the antioxidant activity in conditions where solvent, pH and temperature parameters change.

ORCID IDs of the authors

Doruk Akdogan   0000-0002-3113-9756
Aysegul Peksel   0000-0003-3881-8513

REFERENCES

1. Sihem D, Samia D, Gaetano P, et al. *In vitro* antioxidant activities and phenolic content in crop residues of Tunisian globe artichoke. *Sci Hortic.* 2015;190:128-136.

2. Anwar H, Hussain G, Mustafa I. Antioxidants from natural sources. In: Shalaby E. Azzam GM. ed. Antioxidants in foods and its applications. InTech, London; 2018:1-17.

3. Petropoulos SA, Pereira C, Ntatsi G, Danalatos N, Barros L, Ferreira ICFR. Nutritional value and chemical composition of Greek artichoke genotypes. *Food Chem.* 2018;267:296–302.

4. Marques P, Marto J, Gonçalves LM, et al. *Cynara scolymus* L.: A promising Mediterranean extract for topical anti-aging prevention. *Ind Crops Prod.* 2017;109: 699–706.

5. Lobo V, Patil A, Phatak A, Chandra N. Free radicals, antioxidants and functional foods: Impact on human health. *Pharmacogn Rev.* 2017;4(8):118–126.

6. Pandino G, Lombardo S, Mauromicale G, Williamson G. Profile of polyphenols and phenolic acids in bracts and receptacles of globe artichoke (*Cynara cardunculus var. scolymus*) germplasm. *J Food Compost Anal.* 2011;24(2):148-153.

7. Ben Rejeb I, Dhen N, Gargouri M, Boulila A. Chemical composition, antioxidant potential and enzymes inhibitory proper-

ties of Globe artichoke by-products. *Chem Biodivers.* 2020;17(9): e2000073. doi:10.1002/cbdv.202000073

8. Kukić J, Popović V, Petrović S, et al. Antioxidant and antimicrobial activity of *Cynara cardunculus* extracts. *Food Chem.* 2008;107(2):861–868.

9. Fratianni F, Pepe R, Nazzaro F. Polyphenol composition, antioxidant, antimicrobial and quorum quenching activity of the "Carciofo di Montoro" (*Cynara cardunculus var. scolymus*) Global artichoke of the Campania region, Southern Italy. *Food Nutr Sci.* 2014;5(21): 2053-2062.

10. Shallan MA, Ali MA, Meshrf WA, Marrez DA. In vitro antimicrobial, antioxidant and anticancer activities of globe artichoke (*Cynara cardunculus var. scolymus* L.) bracts and receptacles ethanolic extract. *Biocatal Agric Biotechnol.* 2020;29:101774. doi:10.1016/j.bcab.2020.101774

11. Saleh IA, Vinatoru M, Mason TJ, Abdel-Azim NS, Aboutabl EA, Hammouda FM. A possible general mechanism for ultrasound-assisted extraction (UAE) suggested from the results of UAE of chlorogenic acid from *Cynara scolymus* L. (artichoke) leaves. *Ultrason Sonochem.* 2017;31:330–336.

12. Vilkhu K, Mawson R, Simons L, Bates D. Applications and opportunities for ultrasound assisted extraction in the food industry-A review. *Innov Food Sci Emerg Technol.* 2008;9(2):161–169.

13. Slinkard K, Singleton VL. Total phenol analysis: Automation and comparison with manual methods. *Am J Enol Vitic.* 1977;28:49-55.

14. Zhishen J, Mengcheng T, Jianming W. The determination of flavonoid contents in mulberry and their scavenging effects on superoxide radicals. *Food Chem.* 1999;64: 555-559.

15. Bates SL, Waldren RP, Teare I. Rapid determination of free proline for water stress studies. *Plant Soil.* 1973;39:205-207.

16. Padmavati M, Sakthivel N, Thara TV, Reddy AR. Differential sensivity of rice pathogens to growth inhibition by flavonoids. *Phytochemistry.* 1997;46:449–502

17. Arnon DI. Copper enzymes in isolated chloroplast polyphenoloxidase in *Beta vulgaris. Plant Physiol.* 1949;24: 1–15.

18. Bruni R, Muzzoli M, Ballero M, et al. Tocopherols, fatty acids and sterols in seeds of four Sardinian wild Euphorbia species. *Fitoterapia.* 2004;75:50–61.

19. Oyaizu M. Studies on products of browning reactions: Antioxidative activities of products of browning reaction prepared from glucosamine. *Jpn J Nutr Die*t. 1986;44:307-315.

20. Decker E, Welch B. Role of ferritin as a lipid oxidation catalyst in muscle food. *J Agric Food Chem.* 1990;38:674-677.

21. Brand-Williams W, Cuvelier M, Berset C. Use of a free radical method to evaluate antioxidant activity. *Lebensm Wiss Technol.* 1995;28:25-30.

22. Arnao M, Cano A, Alcolea J, Acosta M. Estimation of free radical-quenching activity of leaf pigment extracts. *Phytochem Anal.* 2001;12(2):138-143.

23. Fogliano V, Verde V, Randazzo G, Ritieni A. Method for measuring antioxidant activity and its application to monitoring the antioxidant capacity of wines. *J Agric Food Chem.* 1999;47:1035-1040.

24. Osawa T, Namiki M. A novel type of antioxidant isolated from leaf wax of eucalyptus leaves. *Agric Biol Chem.* 1981;45(3):735-739.

25. Ben Salem M, Affes H, Athmouni K, et al. Chemicals compositions, antioxidant and anti-inflammatory activity of *Cynara scolymus* leaves extracts, and analysis of major bioactive polyphenols by HPLC. *Evid Based Complement Alternat Med.*

2017; Article ID 4951937:1–14. doi:10.1155/2017/4951937

26. Kollia E, Markaki P, Zoumpoulakis P, Proestos C. ntioxidant activity of *Cynara scolymus* L. and *Cynara cardunculus* L. extracts obtained by different extraction techniques. *Nat Prod Res*. 2016:31(10);1163–1167.

27. Stumpf B, Künne M, Ma L, et al. Optimization of the extraction procedure for the determination of phenolic acids and flavonoids in the leaves of globe artichoke (*Cynara cardunculus var. Scolymus* L.). *J Pharm Biomed Anal*. 2020;177:112879. doi:10.1016/j.jpba.2019.112879

28. Reche C, Rosselló C, Umaña MM, Eim V, Simal S. Mathematical modelling of ultrasound-assisted extraction kinetics of bioactive compounds from artichoke by-products. *Foods*. 2021;10:931. doi:10.3390/foods10050931

29. Lavecchia R, Maffei G, Paccassoni F, Piga L, Zuorro A. Artichoke waste as a source of phenolic antioxidants and bioenergy. *Waste Biomass Valor*. 2019;10:2975–2984.

30. Pasqualone A, Punzi R, Trani A, et al. Enrichment of fresh pasta with antioxidant extracts obtained from artichoke canning by-products by ultrasound-assisted technology and quality characterisation of the end product. *Int J Food Sci Technol & Technolog*. 2017;52(9);2078–2087.

31. Zuorro A, Maffei, G, Lavecchia R. Effect of solvent type and extraction conditions on the recoveryof phenolic compounds from artichoke waste. *Chem Eng Trans*. 2014;39: 463–468.

32. Ergezer H, Serdaroğlu M. Antioxidant potential of artichoke (*Cynara scolymus* L.) byproducts extracts in raw beef patties during refrigerated storage. *J Food Meas Charact*. 2018;12:982–991.

33. Mena-García A, Rodríguez-Sánchez, S, Ruiz-Matute, AI, Sanz ML. Exploitation of artichoke by products to obtain bioactive extracts enriched in inositols and caffeoylquinic acids by microwave assisted extraction. *J Chromatogr A*. 2020;1613:460703. doi:10.1016/j.chroma.2019.460703

34. Shallan MA, Mohamed AA, Meshrf WA, Marrez DA. In vitro antimicrobial, antioxidant and anticancer activities of globe artichoke (*Cynara cardunculus* var. *scolymus* L.) bracts and receptacles ethanolic extract. *Biocatal Agric Biotechnol*. 2020;29:101774. doi:10.1016/j.bcab.2020.101774

35. Quispe MA, Valenzuela JAP, De la Cruz ARH, Silva CRE, Quiñonez GH, Cervantes GMM. Optimization of ultrasound-assisted extraction of polyphenols from globe artichoke (*Cynara scolymus* L.) bracts residues using response surfacemethodology. *Acta Sci Pol Technol Aliment*. 2021;20(3):277-290.

36. Thang NQ, Hoa VTK, Van Tan L, Tho NTM, Hieu TQ, Phuong NTK. Extraction of cynarine and chlorogenic acid from artichoke leaves (*Cynara scolymus* L.) and evaluation of antioxidant activity, antibacterial activity of extract. *Vietnam J Chem*. 2022;60:571-577.

37. Wioletta Biel RW, Piątkowska E, Podsiadło C. Proximate composition, minerals and antioxidant activity of artichoke leaf extracts. *Biol Trace Elem Res*. 2020;194:589-595.

How cite this article

RESEARCH ARTICLE

Potential Therapeutic Effect of Lipoic Acid on Methotrexate-Induced Oxidative Stress in Rat Heart

Sehkar Oktay[1], Sukriye Caliskan[2]

[1]Marmara University Faculty of Dentistry, Department of Basic Medical Science, Biochemistry, Istanbul, Turkiye
[2]Marmara University, Health Sciences Institute, Biochemistry, Maltepe, Istanbul, Turkiye

ABSTRACT

Objective: Methotrexate (MTX), an antifolate and antimetabolite, is used in the treatment of cancer and autoimmune diseases, however, it can cause many adverse events. Lipoic acid (LA) has anticancer and antioxidant activities, and due to these properties, it is effective in curing the complications of various disorders. The study aims to investigate the potential therapeutic effect of LA on MTX-induced oxidative stress in the heart tissues of rats.

Materials and Methods: Eighteen Wistar Albino rats were divided equally into 3 groups as follows: Controls, MT group (MTX was injected with a single dose of 20 mg/kg, i.p.) and MT+LA group (MTX was injected with a single dose of 20 mg/kg, i.p. on the first day and LA (dissolved in saline, 50 mg/kg/day, i.p,) was injected for 5 days). On the sixth day, rats were sacrificed under general anesthesia. Total protein, lipid peroxidation (LPO), nitric oxide (NO), sialic acid (SA), and glutathione (GSH) levels, and also catalase (CAT), superoxide dismutase (SOD) and glutathione-s-transferase (GST) activities were determined in 10% (w/v) heart homogenates.

Results: MTX administration significantly increased LPO and NO levels, and SOD activity and significantly decreased GSH level and CAT activity. LA reversed these parameters by decreasing LPO and NO levels and SOD activity, and increasing GSH levels significantly.

Conclusion: LA has beneficial effects on the impaired oxidant/antioxidant status and is effective in reducing oxidative stress during MTX administration in the heart tissue of rats.

Keywords: Methotrexate, lipoic acid, oxidative stress, heart, rat

INTRODUCTION

Methotrexate (MTX), an antifolate and antimetabolite drug, is used in managing and treating cancer and autoimmune diseases.[1] It was originally designed as an antagonist of the folate pathway in leukemia treatment, and as a folate reductase inhibitor, it has anti-inflammatory, antiproliferative, antipsoriatic, and immunosuppressive effects. In addition to its immunosuppressive effect, MTX fights against neoplastic cells by blocking cell metabolism diseases.[2] As with many chemotherapeutic agents, MTX does not show high selectivity for damaged cells, so it is known to affect healthy cells as well. MTX can cause various toxicological effects and biochemical dysfunctions. In addition, various side effects of MTX, such as teratogenicity, infertility, hepatotoxicity, nephrotoxicity, and neurotoxicity have been reported.[3] Although the exact mechanism of MTX-induced toxicity is unknown, it is thought that it is a result of the formation of reactive oxygen metabolites (ROM) and a decreased antioxidant defense system due to MTX use.[4] Excessive production of ROM and other peroxide radicals increases oxidative stress in the cell and an imbalance between prooxidant and antioxidant defense occurs. Inadequate antioxidant defense mechanisms cannot protect the cell from oxidative damage resulting in cell damage.[5]

One of the alternative treatment methods used to reduce tissue damage during the treatment by chemotherapeutics is the use of antioxidant substances. Dietary antioxidants can enhance the deleterious effects of therapy by reducing or preventing some of the side effects of therapeutic drugs. For this purpose, many antioxidants have been tried and stated to be effective in reducing oxidative stress.[6,7] Lipoic acid (LA) is an endogenous substance found naturally in many common animal and plant foods. It readily crosses the blood-brain barrier and is accepted

as a substrate by human cells. LA has anti-cancer and antioxidant activities, and due to these properties, it is effective in curing the complications of various disorders and has been used as a dietary supplement ingredient for many years.[8,9]

The study aims to investigate the potential therapeutic effect of LA on MTX-induced oxidative stress in the heart tissues of rats.

MATERIALS AND METHODS

The experimental procedures were approved by the Marmara University Animal Care and Use Committee (Protocol Number: 21.2023mar). Eighteen male Wistar Albino rats (200-250gr, 2 months old) were housed under standard laboratory conditions and given water ad libitum and standard rat pellets throughout the study. MTX (50 mg/5 mL) was obtained from Koçak Farma İlaç ve Kimya Sanayi A.S., Turkey, and LA (catalog number: 1077-28-7) was obtained from Sigma-Aldrich Chemical Company (St. Louis, MO, USA).

Study Group

Rats of the experiment were randomly divided into 3 groups as follows: Control group (C) (n=6), MTX administered group (MT) (n=6), and MTX+LA administered group (MT+LA) (n=6). In the MT group, a single dose of MTX was injected (20 mg/kg, i.p.) on the 1st day and saline was injected (0.1 mL/100 g/day, i.p.) for 5 days. In the MT+LA group, a single dose of MTX (20 mg/kg, i.p.) was injected on the 1st day, and LA (dissolved in saline, 50 mg/kg/day, i.p.) was injected for 5 days. On the 6th day of the experiment, all rats were sacrificed under general anesthesia with sodium pentothal (50mg/kg, i.p.), and heart tissues were taken immediately for biochemical examination. Homogenates (10% w/v) were made and kept at -20°C.

Biochemical Parameters

Biochemical parameters; total protein, lipid peroxidation (LPO), nitric oxide (NO), sialic acid (SA), and glutathione (GSH) levels, additionally catalase (CAT), superoxide dismutase (SOD) and glutathione-s-transferase (GST) activities were done in heart homogenates of rats.

Total protein levels of the heart tissues were measured by the method of Lowry et al.[10] and used to express the results of the parameters per protein. LPO level was measured by the method of Yagi[11] and the results were presented as nmol MDA/mg protein. The method of Miranda et al.[12] was used to detect NO levels and the results were expressed as nmol/mg protein. SA levels were determined by the method of Warren[13] and the results were presented as mg/g protein. The method of Beutler[14] was used to determine GSH levels and results were expressed in mg/g protein. CAT activity of the heart tissues was evaluated by the method of Aebi[15] and the results were

presented as U/mg protein. SOD activities of the heart tissues were determined by the method which is based on its ability to increase the effect of riboflavin-sensitized photooxidation of o-dianisidine[16] and the results were expressed in U/g protein. GST activity was evaluated by the method of Habig[17] and the results were expressed as U/g protein.

Statistical Analysis

All data was analyzed by using the program GraphPad Prism 9 (GraphPad Software, San Diego, USA). Shapiro-Wilk test was used to confirm the normal distribution of the data, and the one-way analysis of variance (ANOVA) test and Tukey's multiple comparison tests were applied. Data is presented as mean±standard deviation and a value of $p < 0.05$ indicates that there is a significant difference.

RESULTS

Oxidation Parameters

Heart LPO, NO and SA levels of the groups are shown in Figure 1. LPO and NO levels of the MT group significantly increased compared with the controls, and significantly decreased compared with the MT+LA group ($p < 0.01$, $p < 0.05$, $p < 0.05$, $p < 0.05$, respectively). Besides, heart SA level in the MT group increased compared with the C group, and decreased compared with the MT+LA group, but the results were insignificant.

Antioxidant Parameters

Heart GSH level and CAT, SOD, and GST activities of the groups are shown in Figure 2. In the MT group, a significant decrease in GSH level and CAT activity were found compared with the controls ($p < 0.01$, $p < 0.05$), and GSH level significantly increased compared with the MT+LA group ($p < 0.05$). Besides, a slight increase was noticed in the CAT activity of the MT+LA group compared with the MT group, but the result was insignificant. Heart SOD activity significantly increased in the MT group compared with the C group, and significantly decreased compared with the MT+LA group ($p < 0.01$, $p < 0.05$). Neither MTX administration nor MTX+LA administration changed GST activity in the heart tissue of the rats.

DISCUSSION

MTX is one of the most used antifolate and antimetabolite drug.[1,18,19] However, many adverse events occur due to the use of MTX during treatment. These side effects are generally dose-dependent or related to the usage period.[20] Although the mechanism has not been fully clarified yet, previous studies have put forward excessive ROM production during MTX therapy, and this condition is one of the major causes of MTX-induced side effects.[21,22] MTX inhibits the NAD$^+$-dependent
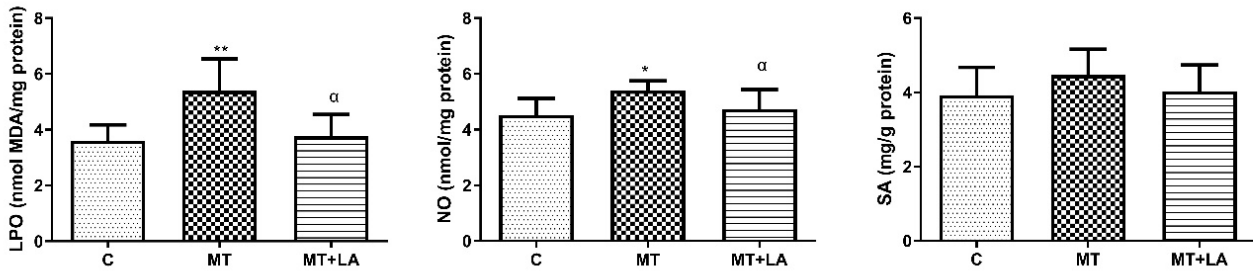
Figure 1. Levels of LPO, NO, and SA in heart tissue. Values are given as mean±standard deviation, C: Control group; MT: Methotrexate given group; MT+LA: Methotrexate and Lipoic acid given group; LPO: lipid peroxidation; MDA: malondialdehite; NO: nitric oxide; SA: sialic acid. *p<0.05, **p<0.01 significantly different from group C; [a]p<0.05 significantly different from group MT.
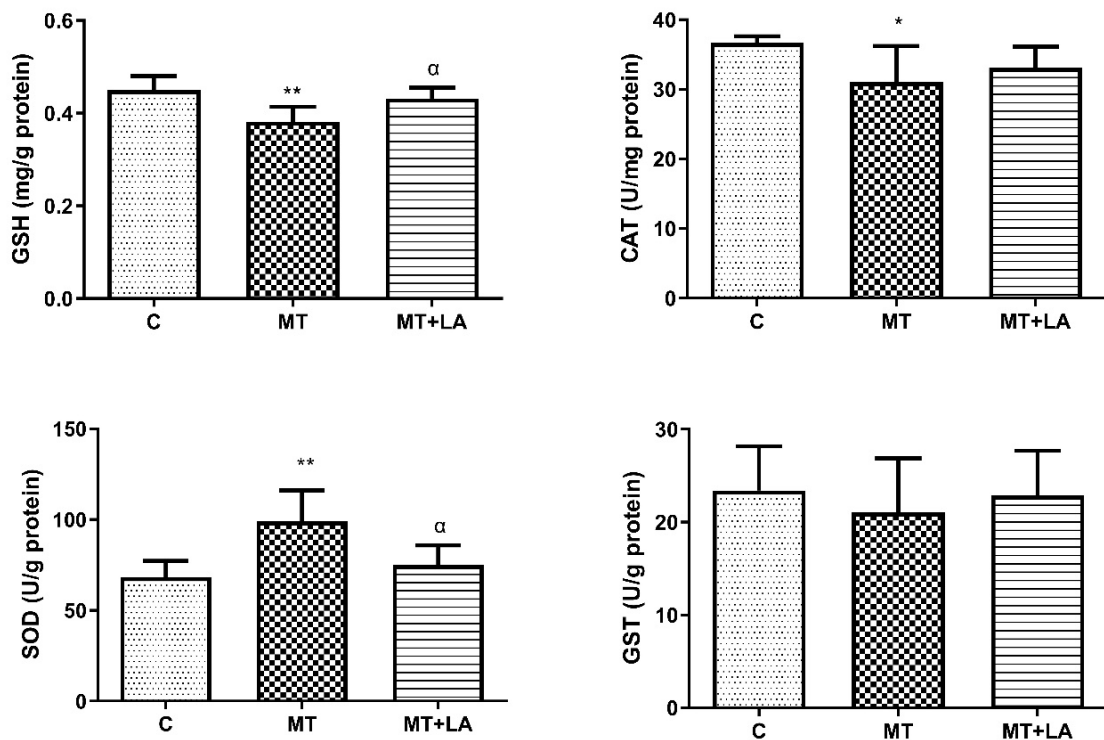

Figure 2. Level of GSH, activities of CAT, SOD, and GST in heart tissue. Values are given as mean±standard deviation, C: Control group; MT: Methotrexate given group; MT+LA: Methotrexate and Lipoic acid given group; GSH: glutathione; CAT: catalase; SOD: superoxide dismutase; GST: glutathione-S-transferase. *p<0.05, **p<0.01 significantly different from group C; [a]p<0.05 significantly different from group MT.

mitochondrial enzymes, impairs the defense system, and thus it causes the cells to be unable to resist free radicals. Besides, MTX depletes protective antioxidant defense molecules and inhibits the activities of free radical scavengers.[23]

Excessive ROM production and increased LPO levels due to radical formation induce cellular injury by damaging the cell membrane. Based on the previous knowledge, 20 mg/kg of MTX was used in the present study to induce MTX-related tissue damage, and LPO level significantly increased in the MT group, by previous data.[24,25] The increase in ROM may have overpowered the antioxidant system and damaged the cell, which could have been detected as an increase in the LPO level. NO is a molecular mediator of various pathological and physiological processes, such as vasodilation and inflammation. Overproduction of NO in the presence of oxidative stress contributes to tissue damage by interacting with superoxide and forming

peroxynitrite, a potent cytotoxic agent.[25] As in elevated LPO level, NO level also increased significantly in the MTX-given group than those of the controls. Other studies also support our findings.[26,27] The increase both in LPO and NO levels of the MT group shows that MTX triggers oxidative stress, exposing cells to radicals and making them prone to cellular damage. SA is one of the terminal sugars in many glycoconjugates and is present in all biological membranes. It has a crucial role in cell protection by increasing in pathological situations. Also, SA is a stable marker of inflammation with less intra-individual variability, and therefore, it can more accurately represent inflammatory status.[28] In the present study, MTX injection elevated SA levels but the result was insignificant, which may be caused by the heart tissue's self-protection against radical damage mediated by MTX administration. The explanation of oxidative stress-induced damage in heart cells may be a reason for the imbalance between antioxidants and oxidants. There may be a loss or insufficiency of antioxidant defense. Depletion of antioxidant enzymes and defense mechanisms in the cell causes mitochondrial dysfunction and induction of endoplasmic reticulum stress due to increased ROM production.

GSH is an important antioxidant due to its involvement in cellular metabolism and reducing properties. In previous studies, MTX-mediated oxidative stress was pointed out as a factor for the depletion of GSH in rats.[25,29] MTX inhibits the activity of malic enzymes and causes a decrease in NADPH. As a result, the activity of GR decreases, which is involved in GSH metabolism and uses NADPH as a cofactor, thus reducing the conversion of GSSG to GSH.[30] In parallel with this information, significantly decreased GSH levels were observed in MTX-injected group, which means MTX may cause a depletion in GSH reservoirs. SOD is an intracellular antioxidant enzyme. It reduces superoxide anion to hydrogen peroxide and protects tissues against reactive metabolites. It is a major defense system against the toxic effects of oxygen radicals.[31] In the present study, MTX injection elevated SOD activity in heart tissues. The result may be a sign that the cell continues to protect itself, since a single dose of MTX injection was not sufficient to deplete the SOD enzyme and the cell may tolerate the dose. CAT and GST enzymes also have antioxidant properties in detoxifying hydrogen peroxide to water. According to previous studies, MTX-induced toxicity decreases the level of antioxidant enzymes in the tissues.[32] MTX injection to the rats caused a significant decrease in CAT activity and a slight decrease in GST activity in heart tissue which may be the result of the depletion of these enzymes or loss of their activity by MTX injection.

There have been several studies regarding the use of antioxidant supplementation to reduce MTX-induced toxicity and its effect on MTX efficacy in diseases.[33] LA is an effective molecule that has a high antioxidant capacity. Both oxidized and reduced forms of LA have antioxidant effects by eliminating and/or reducing reactive metabolites. The disulfide bond of LA reacts with radicals, eliminates radicals that trigger LPO, and then inhibits the initiation and progression of LPO induced by hydrogen peroxide radicals.[34] It has been shown in many studies that LA fights oxidative stress by scavenging free radicals.[8,9,34] In addition to its role in scavenging and eliminating the metabolites of ROM, LA also aids in the formation of other cellular antioxidants, such as vitamins C and E.[35] Given these features of LA, it is useful in reducing cellular MDA and NO dose-dependently.

In the present study, LA administration reduced LPO and NO levels significantly in the MT group, and slightly decreased SA level. Besides, LA increased the level of GSH, which decreased with MTX administration. LA supports the insufficient level of GSH as a result of excessive oxidant formation by reducing cellular damage. Also, the LA administration decreased SOD activity in the MT group. With the reduction of ROM production, the superoxide anion may also have decreased in the medium and the SOD activity may have reversed to the control level. Although LA did not change CAT and GST activities significantly, a slight increase was observed in these parameters, which may be the effect of LA on supporting the antioxidant defense system and reversing the damage in the cell by changing the antioxidant levels.

CONCLUSION

LA has beneficial effects on the impaired oxidant/antioxidant status and is effective in reducing oxidative stress during MTX administration in the heart tissue of rats.

ORCID IDs of the authors

Sehkar Oktay   0000-0002-2878-288X
Sukriye Caliskan   0000-0002-7576-4967

REFERENCES

1. Friedman B, Cronstein B. Methotrexate mechanism in treatment of rheumatoid arthritis. *Jt Bone Spine*. 2019;86(3):301-307.

2. Sentürk N. Metotreksat. *Turkderm*. 2016;50(1):18-21.

3. Ahmed ZSO, Hussein S, Ghandour RA, Azouz AA., El-Sakhawy MA. Evaluation of the effect of methotrexate on the hippocampus, cerebellum, liver, and kidneys of adult male albino rat: Histopathological, immunohistochemical and biochemical studies. *Acta Histochem*. 2021; 123(2):151682. doi: 10.1016/j.acthis.2021.151682

4. Yuksel Y, Yuksel R, Yagmurca M, et al. Effects of quercetin on methotrexate-induced nephrotoxicity in rats. *Hum Exp Toxicol*. 2017;36(1):51–61.

5. Pisoschi AM, Pop A, Iordache F, Stanca L, Predoi G, Serban AI. Oxidative stress mitigation by antioxidants-an overview on their chemistry and influences on health status. *Eur J Med Chem*. 2021;209:112891. doi: 10.1016/j.ejmech.2020.112891

6. Puig L. Methotrexate: New therapeutic approaches. *Actas Dermosifiliogr*. 2014;105(6):583-589.

7. Zwolak I. Protective effects of dietary antioxidants against vanadium-induced toxicity: A review. *Oxid Med Cell Longev*. 2020;1-14. doi:10.1155/2020/1490316

8. Billgren ES, Cicchillo RM, Nesbitt NM, Booker SJ. Lipoic acid biosynthesis and enzymology. *Chem Biol*. 2010;7:181-212.

9. Fayez AM, Zakaria S, Moustafa D. Alpha lipoic acid exerts antioxidant effect via Nrf2/HO-1 pathway activation and suppresses hepatic stellate cells activation induced by methotrexate in rats. *Biomed Pharmacother*. 2018;105:428-433.

10. Lowry OH, Rosebrough NJ, Farr AL, Randall RJ. Protein measurement with the Folin phenol reagent. *J Biol Chem*. 1951;193:265-275.

11. Yagi K. Assay for blood plasma or serum. *Methods Enzymol*. 1984;105:328-337.

12. Miranda K, Espey MG, Wink DA. A rapid, simple spectrophotometric method for simultaneous detection of nitrate and nitrite. *Nitric Oxide*. 2001;5:62–71.

13. Warren L. The thiobarbituric acid assay of sialic acids. *J Biol Chem*. 1959;234:1971-1975.

14. Beutler E. Gluthatione: Red cell metabolism. A manual bio¬chemical methods. New York: Grune and Stratton; 1975.

15. Aebi H. Catalase *in vitro*. In: Methods of enzymatic analysis Bergmeye HU, editor. Wenheim: Verlag Chemie; 1974.

16. Mylorie AA, Collins H, Umbles C, Kyle J. Erythrocyte SOD activity and other parameters of copper status in rats ingesting lead acetate. *Toxicol Appl Pharmacol*. 1986; 82:512-520.

17. Habig WH, Jacoby WB. Assays for differentation of glutathi¬one-s-transferases. *Methods Enzymol*. 1981; 77:398-405.

18. Saibeni S, Bollani S, Losco A, et al. The use of methotrexate for treatment of inflammatory bowel disease in clinical practice. *Dig Liver Dis*. 2012;44(2):123-127.

19. Deo M, Yung A, Hill S, Rademaker M. Methotrexate for treatment of atopic dermatitis in children and adolescents. *Int J Dermatol*. 2014;53(8):1037-1041.

20. 20. Shen S, Yap LM, Prince HM, McCormack CJ. The use of methotrexate in dermatology: A review. *Aust J Dermatol*. 2012;53(1):1-18.

21. Mahmoud AM, Hozayen WG, Ramadan SM. Berberine ameliorates methotrexate-induced liver injury by activating Nrf2/HO-1 pathway and PPARγ, and suppressing oxidative stress and apoptosis in rats. *Biomed Pharmacother*. 2017; 94: 280-291.

22. Malayeri A, Badparva R, Mombeini MA, Khorsandi L, Goudarzi M. Naringenin: A potential natural remedy against methotrexate-induced hepatotoxicity in rats. *Drug Chem Toxicol*. 2020;28:1-8.

23. Mehrzadi S, Safa M, Kamrava SK, Darabi R, Hayat P, Motevalian M. Protective mechanisms of melatonin against hydrogen-peroxide-induced toxicity in human bone-marrow-derived mesenchymal stem cells. *Can J Physiol Pharmacol*. 2017;95:773-786.

24. Uzar E, Koyuncuoglu HR, Uz E, et al. The activities of antioxidant enzymes and the level of malondialdehyde in cerebellum of rats subjected to methotrexate: protective effect of caffeic acid phenethyl ester. *Mol Cell Biochem*. 2006;291:63-68.

25. Kalantar M, Kalantari H, Goudarzi M, et al. Crocin ameliorates methotrexate-induced liver injury via inhibition of oxidative stress and inflammation in rats. *Pharmacol Rep*. 2019;71(4):746-752.

26. Khatab LA, Abdel-Raheem IT, Ghoneim AI. Protective effects of melatonin and L-carnitine against methotrexate-induced toxicity in isolated rat hepatocytes. *Naunyn-Schmiedebergs Arch Pharmacol*. 2022;395:87-97.

27. Owumi SE, Ajijola IJ, Agbeti OM. Hepatorenal protective effects of protocatechuic acid in rats administered with anticancer drug methotrexate. *Hum Exp Toxicol*. 2019;38(11):1254-1265.

28. Rajappa M, Shanmugam R, Munisamy M, et al. Effect of antipsoriatic therapy on oxidative stress index and sialic acid levels in patients with psoriasis. *Int J Dermatol*. 2016;55(8):422-430.

29. Vardi N, Parlakpinar H, Cetin A, Erdogan A, Cetin Ozturk I. Protective effect of β carotene on methotrexate–induced oxidative liver damage. *Toxicol Pathol*. 2010;38:592-597.

30. El-Sheikh AA, Morsy MA, Abdalla AM, Hamouda AH, Alhaider IA. Mechanisms of thymoquinone hepatorenal protection in methotrexate-induced toxicity in rats. *Mediators Inflamm*. 2015; 859383. doi:10.1155/2015/859383

31. Deluao JC, Winstanley Y, Robker RL, Pacella-Ince L, Gonzalez MB, McPherson NO. oxidative stress and reproductive function: Reactive oxygen species in the mammalian pre-implantation embryo. *Reprod*. 2022;164(6):95-108.

32. Quirós Y, Blanco-Gozalo V, Sanchez-Gallego JI, et al. Cardiotrophin-1 therapy prevents gentamicin-induced nephrotoxicity in rats. *Pharmacol Res*. 2016;107:137-146.

33. Dhanesha M, Singh K, Bhori M, Marar T. Impact of antioxidant supplementation on toxicity of methotrexate: An *in vitro* study on erythrocytes using vitamin E. *Asian J Pharm Clin Res*. 2015;8(3):339-343.

34. Selvakumar E, Prahalathan C, Mythili Y, Varalakshmi P.Beneficial effects of DL-α-lipoic acid on cyclophosphamide-induced oxidative stress in mitochondrial fractions of rat testis. *Chem Biol Interact*. 2005;152(1):59-66.

35. Armagan I, Bayram D, Candan IA, et al. Effects of pentoxifylline and alpha lipoic acid on methotrexate-induced damage in liver and kidney of rats. *Environ Toxicol Pharmacol*. 2015;39(3):1122-1131.

How cite this article

RESEARCH ARTICLE

Antioxidant and Anti-inflammatory Activity of Five *Centaurea* Species

Ali Sen[1]

[1]Marmara University, Faculty of Pharmacy, Department of Pharmacognosy, Istanbul, Turkiye

ABSTRACT

Objective: In this study, we examined the anti-inflammatory and antioxidant (ABTS radical scavenging) activity of methanol extracts of aerial parts (except capitula) and capitula of *Centaurea cuneifolia, C. iberica, C. kilaea, C. solstitialis* subsp. *solstitialis* and *C. stenolepis* for the first time comparatively.

Materials and Methods: The antioxidant and anti-inflammatory activity, expressed as IC_{50} values, were determined by 2, 2'-Azino-Bis-3-Ethylbenzothiazoline-6-Sulfonic asit (ABTS) and 5-lipoxygenase methods. The total phenolic content, expressed as gallic acid equivalents, was estimated by Folin-Ciocalteu method.

Results: Methanol extract of capitula of *C. solstitialis* subsp. *solstitialis* (CSSC) with an IC_{50} value of 8.74 µg/mL showed antioxidant activity as strong as standard acarbose (4.41 µg/mL) against ABTS radicals. The IC_{50} values of ABTS radical scavenging activities of other extracts varied between 24.42 and 88.95 µg/mL. CSSC with an IC_{50} value of 122.10 µg/mL displayed moderate inhibitory activity against 5-lipoxygenase enzyme. The IC_{50} values of the antilipoxygenase activities of the other extracts were found to vary between 122.10 and 781.30 µg/mL. Also, the highest amount of total phenolic compounds was found in the CSSC (83.41 mg/g), while the lowest was found in methanol extract of aerial parts of *C. solstitialis* subsp. *solstitialis* (35.20 mg/g).

Conclusion: These results clearly indicate that CSSC has significant antioxidant and anti-inflammatory activity. As far as is known, this paper is the first comparative study on ABTS radical scavenging and lipoxygenase inhibitory activity of five different *Centaurea* species. It is also the first study on the antilipoxygenase activity of *C. iberica* and *C. solstitialis* subsp. *solstitialis*.

Keywords: *Centaurea* species, antioxidant activity, anti-inflammatory activity, total phenolic content

INTRODUCTION

Oxidative stress, an imbalance between reactive oxygen species (ROS) production, acts as significant signaling molecules in the physiological processes, and the antioxidant defenses that protect cells is associated with the development of a number of diseases, including pulmonary hypertension, asthma, cancer, heart disease, autoimmune, metabolic diseases, and others.[1] Antioxidants, known as free radical scavengers, play an important role in preventing cell damage by inhibiting the free radical chain reaction under different physiological conditions.[2] Many antioxidant compounds obtained from plants are identified as free radical inhibitors, reducing agents, or active oxygen scavengers.[3]

Recent substantial evidence suggests that oxidative stress plays a key role in various aspects of acute and chronic inflammation.[4] Inflammation is known as the body's defense mechanism against pathogens and toxic stimuli. An abnormal immune system leads to a chronic immune response, causing inflammatory diseases such as gastritis, cancer, allergies, rheumatoid arthritis, and multiple sclerosis.[5] Medicinal plants have been used in traditional folk medicine for years as anti-inflammatory and antioxidant agents against diseases caused by oxidative stress and/or inflammation.[6] It is therefore important to conduct research on medicinal plants and their secondary metabolites.

The genus *Centaurea* belonging to the family Asteraceae is represented by 159 species and 194 taxa and 110 of these are endemic.[7] These species are used in traditional medicine for the treatment of vaginal yeast infections, menstrual disorders, ulcer, liver and kidney diseases, as well as for anti-diarrhea, stomachic, tonic, appetizer, antidiabetic, antipyretic, diuretic and expectorant treatment.[8] Phytochemical studies on the *Centaurea* species reported that they are rich in sesquiterpene lactones and flavonoids. In addition, it is suggested that these species have other effects such as antimicrobial, antipyretic, antiviral, antimalarial, antiphytoviral, antiulcerogenic, anti-inflammatory, cytotoxic, hypoglycemic, neurotoxic and vasodilator effects.[9,10]

This study aimed to comparatively investigate the anti-inflammatory and antioxidant activity of methanol extracts of aerial parts (except capitula) and capitula of *Centaurea cuneifolia* Sm., *C. iberica* Trev. ex Sprengel, *C. kilaea* Boiss., *C. solstitialis* L. subsp. *solstitialis* L. and *C. stenolepis* A. Kern. [syn. *C. phrygia* subsp. *stenolepis* (Kerner) Gugler] together with their total phenolic contents.

MATERIALS AND METHODS

Plant Material

Aerial parts of *Centaurea cuneifolia, C. iberica, C. kilaea, C. solstitialis* subsp. *solstitialis* and *C. stenolepis* were gathered from different districts of İstanbul, Turkiye in 2009 and identified by Dr. Gizem Bulut, a botanist of the Faculty of Pharmacy, University of Marmara. Voucher specimens were deposited in the Herbarium of the Faculty of Pharmacy, Marmara University (MARE No: 11651, 11712, 11690, 11966 and 11965, respectively).

Extraction

Extracts of the *Centaurea* species were obtained from a previous study.[8] Aerial parts of five *Centaurea* species were separated from the capitula. Next, the aerial parts (except capitula) and capitula of *Centaurea* species were dried and ground, about 15 g each, and macerated with MeOH three times (24 h×180mL). All extracts were filtered and dried in a vacuum. The aerial parts (except capitula) and capitula of *Centaurea cuneifolia, C. iberica, C. kilaea, C. solstitialis* subsp. *solstitialis* and *C. stenolepis* were then coded as CCC, CCA, CIC, CIA, CKC, CKA, CSSC, CSSA, CSC, CSA. Extraction yields were found to be 12.693%, 10.603%, 10.750%, 12.439%, 11.331%, 12.916%, 10.901%, 8.139%, 13.224% and 13.542%, respectively. All extracts were stored at 4°C for further analysis.

2,2'-azinobis-(3-ethylbenzothiazoline-6-sulfonic acid (ABTS) Radical Scavenging Activity

The ABTS radical scavenging capacity was tested as described by Zou et al.[11] The ABTS$^{\bullet+}$radical cation used for the determination of total antioxidant capacity was obtained by mixing 7 mM ABTS (in H_2O) with 2.45 mM potassium persulfate (in H_2O) and then kept in the dark for 12-16 h at room temperature. The ABTS$^{\bullet+}$ solution was diluted with 96% ethanol solvent of analytical purity to give an absorbance value of 0.700±0.050 at 734 nm. Ten µL of each of the solutions was prepared at five different concentrations of the extracts (250-3.91 µg/mL) were transferred to microplate wells and 190 µL of the ABTS$^{\bullet+}$ solution was added. The mixture was kept at room temperature for 30 min and the absorbance at 734 nm was read immediately afterwards. Trolox (250-0.49 µg/mL), an antioxidant molecule, was used as the standard and the results were expressed as an IC$_{50}$ value.

In Vitro Anti-Inflammatory Activity

The anti-inflammatory activity was tested according to the reported procedure.[12,13] Ten µL of each of the samples (extract and standard) were prepared at five different concentrations (250-0.49 µg/mL) and transferred to quartz microplate wells and 20 µL ethanol, 25 µL borate buffer (0.1 M, pH 9) and 25 µL type V soybean lipoxygenase solution (pH 9, 20.000 U/mL) in a buffer were added. The mixture was incubated at 25°C for 5 min, then 100 µL of 0.6 mM linoleic acid solution was added, mixed thoroughly, and absorbance changes at 234 nm were recorded for 6 min. Indomethacin (250 - 0.49 µg/mL) was used as a reference standard and the results were expressed as an IC$_{50}$ value.

Determination of Total Phenolic Contents (TPC)

The total phenolic content was determined according to the reported procedure.[13,14] Ten µL of the solutions prepared from each of the extracts at various concentrations (151.52 – 2.37 µg/mL) were put on microplates and 20 µL of Folin-Ciocalteau solution, 200 µL of ultrapure water and 100 µL of 15% Na_2SO_4 were added. The absorbance of the solutions after 2 h of incubation at room temperature was read at 765 nm in a spectrophotometer. For the standard curve plot, gallic acid (500-0.977 µg/mL) was used as the standard and absorbances corresponding to each concentration were measured at 765 nm. The total phenolic compound amounts of the extracts were calculated from this standard curve plot and the results expressed as mg gallic acid equivalent per gram extract (mg GAE/g plant extract).

Statistical Analysis

All analyses were conducted in triplicate, and the data presented as mean±standard deviation (SD). The data was analyzed by ANOVA followed by the Tukey's multiple comparison tests using the GraphPad Prism 5. Significance was defined at p<0.05.

RESULTS

The CSSC showed the highest antioxidant activity with an IC$_{50}$ value of 8.74 µg/mL, while CSA showed the lowest antioxidant activity with an IC$_{50}$ value of 88.95 µg/mL in the ABTS assay. CSSC demonstrated significant ABTS radical scavenging activity as compared to standard trolox having an IC$_{50}$=4.41 µg/mL (Table 1). From another perspective, CSSC showed a significant effect in inhibiting ABTS radical, reaching up to 78.95% at a concentration of 31.25 µg/mL. However, CIA showed the lowest inhibition against the ABTS radical with a value of 48.64% at a concentration of 31.25 µg/mL (Figure 1).

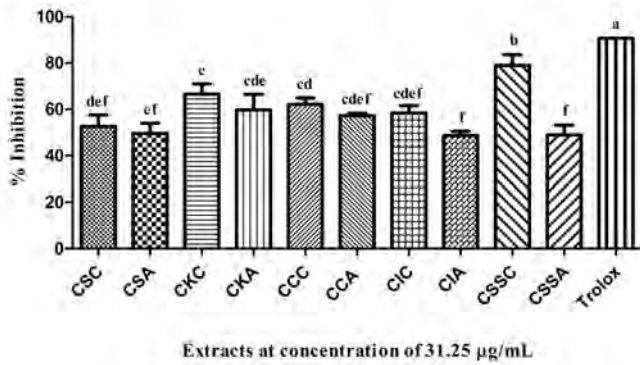In the 5-lipoxygenase inhibitory activity experiment, CSSC exhibited the highest anti-lipoxygenase activity with an IC$_{50}$

Figure 1. Percentage of Inhibition (%) of ABTS radical by various extracts. The aerial parts except capitula and capitula of *Centaurea cuneifolia, C. iberica, C. kilaea, C. solstitialis* subsp. *solstitialis* and *C. stenolepis* coded as CCC, CCA, CIC, CIA, CKC, CKA, CSSC, CSSA, CSC, CSA. The bars represent mean ± standard deviation of triple repetitive analysis. Different and same letters on the error bars indicate statistical significance (p<0.05) and non-significance (p>0.05), respectively.

value of 122.10 µg/mL, while CKA exhibited the lowest antioxidant activity with an IC_{50} value of 781.30 µg/mL. CSSC presented moderate anti-inflammatory activity when compared to the standard indomethacine (23.11 µg/mL) (Table 1). When CSSC was compared against the 5-lipoxygenase enzyme, it displayed a 96.47% inhibition at concentration of 250 µg/mL. However, CKA showed the lowest inhibition against the lipoxygenase enzyme with a value of 21.64% at concentrations of 250 µg/mL (Figure 2).
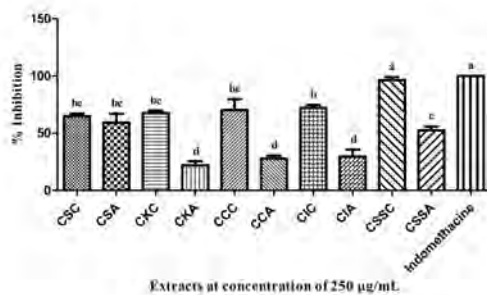

Figure 2. Percentage Inhibition (%) of lipoxygenase enzyme activities of various extracts. The aerial parts except capitula and capitula of *Centaurea cuneifolia, C. iberica, C. kilaea, C. solstitialis* subsp. *solstitialis* and *C. stenolepis* coded as CCC, CCA, CIC, CIA, CKC, CKA, CSSC, CSSA, CSC, CSA. The bars represent mean ± standard deviation of triple repetitive analysis. Different and same letters on the error bars indicate statistical significance (p<0.05) and non-significance (p>0.05), respectively.

The TPC values were obtained from the calibration curve y= 0.127x + 0.075 with R^2= 0.998. Among all the tested extracts, the highest amounts of total phenolic were found in the CSSC (83.41 mg/g). The total phenol contents of other extracts ranged between 35.20 and 79.23 mg GAE per gram extract (Table 1, Figure 3).
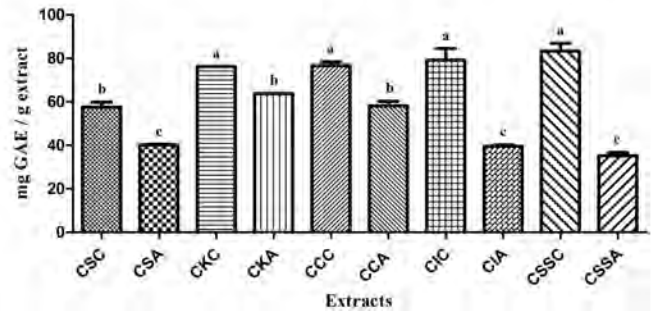

Figure 3. Total phenolic contents of various extracts. The aerial parts except capitula and capitula of *Centaurea cuneifolia, C. iberica, C. kilaea, C. solstitialis* subsp. *solstitialis* and *C. stenolepis* coded as CCC, CCA, CIC, CIA, CKC, CKA, CSSC, CSSA, CSC, CSA. The bars represent mean ± standard deviation of triple repetitive analysis. Different and same letters on the error bars indicate statistical significance (p<0.05) and non-significance (p>0.05), respectively.

DISCUSSION

Oxidative stress and inflammation play an important role in aging and the emergence of chronic diseases.[15] Medicinal plants with antioxidant and anti-inflammatory activity are used in traditional folk medicine for the treatment of chronic disorders caused by oxidative stress and inflammation.[16−18] The antioxidant and anti-inflammatory activity of methanol extracts of aerial parts (except capitula) and capitula of *Centaurea cuneifolia, C. iberica, C. kilaea, C. solstitialis* subsp. *solstitialis* and *C. stenolepis* along with their total phenolic amounts were investigated in the current study.

Among methanol extracts of *Centaurea* species, the CSSC (IC_{50} value: 8.74 µg/mL) had the highest antioxidant activity, followed by CCC (24.42 µg/mL), CKC (25.79 µg/mL), CKA (38.74 µg/mL), CIC (48.20 µg/mL), CCA (48.66 µg/mL), CIA (76.19 µg/mL), CSSA (85.68 µg/mL), CSC (85.74 µg/mL) and CSA (88.95 µg/mL) against the ABTS radical. Necip and colleagues reported that the methanol extract obtained from aerial parts of *C. solstitialis* inhibited the ABTS radical by 21%, 46% and 94% at concentrations of 50, 100 and 250 µg/mL.[19] In our current study, the activity of this species was much better (78.95% inhibition at a concentration of 31.25 µg/mL) than Necip et al. study.[19] This could be due to the difference in the time and place of collection and the part of the plant extracted. In another study, it was reported that C. kilaea (147.2 µg/mL), *C. cuneifolia* (119.5 µg/mL), *C. stenolepis* (129.9 and 146.4 µg/mL) aerial parts chloroform extracts have antioxidant activity against the ABTS radical.[20] Unlike this study, extracts were obtained from the *Centaurea* species using a different solvent (we used methanol) and it revealed that methanol extracts exhibited better antioxidant activity than chloroform extracts.

When comparing the antilipoxygenase activities of the *Centaurea species*, it was observed that the CSSC (IC50 value: 122.10 µg/mL) had the best lipoxygenase inhibitory activity, followed by CIC (169.20 µg/mL), CCC (180.20 µg/mL), CKC

Table 1. Anti-inflammatory/antioxidant activities and total phenolic contents of *Centaurea* extracts.

Extracts / Standards	ABTS radical scavenging activity	5-lipoxygenase inhibitory activity	TPC (mg GAE/g extract)[****]
	IC$_{50}$ (µg/mL)		
CCC	24.42 ± 1.64[c]	180.20 ± 8.63[cd]	76.73 ± 1.78[a]
CCA	48.66 ± 0.30[e]	440.50 ± 2.12[f]	58.16 ± 2.07[b]
CKC	25.79 ± 0.84[c]	184.80 ± 2.76[cd]	76.31 ± 0.00[a]
CKA	38.74 ± 0.83[d]	781.30 ± 8.27[h]	63.79 ± 0.00[b]
CIC	48.20 ± 1.12[e]	169.20 ± 3.96[c]	79.23 ± 5.32[a]
CIA	76.19 ± 0.62[f]	513.80 ± 26.23[g]	39.58 ± 0.59[c]
CSC	85.74 ± 0.32[g]	191.00 ± 5.23[cd]	57.53 ± 2.36[b]
CSA	88.95± 0.17[g]	209.20 ± 8.49[de]	40.21 ± 0.30[c]
CSSC	8.74 ± 0.23[b]	122.10 ± 1.49[b]	83.41 ± 3.54[a]
CSSA	85.68 ± 1.80[g]	233.50 ± 8.13[e]	35.20 ± 1.47[c]
Trolox	4.41 ± 0.17[a]		
Indomethacine		23.11 ± 1.77[a]	

* The aerial parts except capitula and capitula of *Centaurea cuneifolia, C. iberica, C. kilaea, C. solstitialis* subsp. *solstitialis* and *C. stenolepis* coded as CCC, CCA, CIC, CIA, CKC, CKA, CSSC, CSSA, CSC, CSA.

** Each value in the table is the mean of three replicates and was represented as mean±SD.

*** Different and same letter superscripts in the same column show statistical significance (p<0.05) and non-significance (p>0.05), respectively..

**** GAE: Gallic acid equivalent

(184.40 µg/mL), CSC (191.00 µg/mL), CSA (209.20 µg/mL), CSSA (233.50 µg/mL), CCA (440.50 µg/mL), CIA (513.80 µg/mL) and CKA (781.30 µg/mL) against the 5-lipoxygenase enzyme. There has been no study on the antilipoxygenase activity of methanol extracts of these species until the present study. However, chloroform extracts for two species were studied. Sekerler et al. demonstrated that the *C. kilaea* (110.0 µg/mL), *C. cuneifolia* (129.4 µg/mL), *C. stenolepis* (138.5 and 154.4 µg/mL) aerial parts chloroform extracts had anti-inflammatory activities against the 5-lipoxygenase enzyme.[20] Unlike the current study, extracts were obtained using a solvent with lower polarity (chloroform) and it revealed that these extracts (except CSSC) had better anti-inflammatory activity.

The phenolic contents of crude methanol extracts as gallic acid equivalents were found to be highest in CSSC (83.41 mg/g) followed by CIC (79.23 mg/g), CCC (76.73 mg/g), CKC (76.31 mg/g), CKA (63.79 mg/g), CCA (58.16 mg/g), CSC (57.53 mg/g), CSA (40.21 mg/g), CIA (39.58 mg/g) and CSSA (35.20 mg/g). Alper et al. investigated the total phenolic con-

tent of the ethanol extract obtained from the flowers of *C. solstitialis* and found 52.31 mg/g as equivalent to gallic acid in a gram extract.[21] This value was found to be lower than the value in our current study (83.41 mg/g for CSSC). This could be due to the difference in the time and place of collection of the plant. Sekerler et al. reported that the total phenol contents of *C. kilaea, C. cuneifolia* and *C. stenolepis* aerial parts chloroform extracts were found to be 31.57, 55.40, 52.36 and 49.74 mg/g, respectively.[20] Compared to the current study, Sekerler extracts were obtained using a different solvent (chloroform) and the total phenol content of these extracts was found to be lower in general.

The highest total phenolic content with the best antioxidant and anti-inflammatory activity was observed in the methanol extract of *C. solstitialis capitula* (CSSC). Previous studies showed that *C. solstitialis* contains phenolic acids (caffeic acid, chlorogenic acid, cinnamic acid, 2,5-dihydroxybenzoic acid, 3,4-dihydroxybenzoic acid, ellagic acid, ferulic acid, gallic acid, 4-hydroxybenzoic acid, p-coumaric acid, vanil-

lic acid), and flavonoids (epicatechin, naringin, quercetin, rutin) and sesquiterpene lactones (solstitialin A and acetyl solstitialin).[21,22] Phenolic acids and flavonoids were reported to have antioxidant activity.[23,24] It is suggested that sesquiterpene lactones together with these substance groups have anti-inflammatory activity.[25–27] Thus, phenolic acids, flavonoids and sesquiterpene lactones could be responsible for the antioxidant (but not sesquiterpene lactones) and anti-inflammatory activity of CSSC.

CONCLUSION

These findings indicate that the methanol extract of *C. solstitialis* capitula may be a valuable resource in the discovery of antioxidant and anti-inflammatory molecules.

ORCID ID of the author

Ali Sen   0000-0002-2144-5741

REFERENCES

1. Jurčacková Z, Ciglanová D, Mudroňová D, et al. Astaxanthin extract from *Haematococcus pluvialis* and its fractions of astaxanthin mono-and diesters obtained by CCC show differential antioxidant and cytoprotective effects on naïve-mouse spleen cells. *Antioxidants*. 2023;12(6):1144. doi:10.3390/antiox12061144

2. Khan MMR, Susmi TF, Miah M, Reza MA, Rahi MS. Morphological alteration and intracellular ROS generation confirm apoptosis induction on EAC cells by *Leucas indica* bark extract. *J Herbs Spices Med Plants*. 2023;29(1):84-97.

3. Duh PD, Tu YY, Yen GC. Antioxidant activity of water extract of Harng Jyur (*Chrysanthemum morifolium* Ramat). *LWT-Food Sci Technol*. 1999;32(5):269-277.

4. Peake JM, Suzuki K, Coombes JS. The influence of antioxidant supplementation on markers of inflammation and the relationship to oxidative stress after exercise. *J Nutr Biochem*. 2007;18(6):357-371.

5. Kim NY, Kim S, Park HM, et al. *Cinnamomum verum* extract inhibits NOX2/ROS and PKCδ/JNK/AP-1/NF-κB pathway-mediated inflammatory response in PMA-stimulated THP-1 monocytes. *Phytomedicine*. 2023;112:154685. doi:10.1016/j.phymed.2023.154685

6. Chinsamy M, Finnie JF, Van Staden J. Anti-inflammatory, antioxidant, anti-cholinesterase activity and mutagenicity of South African medicinal orchids. *S Afr J Bot*. 2014;91:88-98.

7. Bizim Bitkiler. https://bizimbitkiler.org.tr/v2/hiyerarsi.php?c= *Centaurea* . Accessed June 24, 2023.

8. Şen A, Bitiş L, Birteksöz-Tan S, Bulut G. *In vitro* evaluation of antioxidant and antimicrobial activities of some *Centaurea* L. species. *Marmara Pharm J*. 2013;17(1):42-45.

9. Sen A, Ozbas Turan S, Bitis L. Bioactivity-guided isolation of anti-proliferative compounds from endemic *Centaurea kilaea*. *Pharm Biol*. 2017;55(1):541-546.

10. Reyhan A, Küpeli E, Ergun F. The biological activity of *Centaurea* L. species. *Gazi Univ J Sci*. 2004;17(4):149-164.

11. Zou Y, Chang SKC, Gu Y, Qian SY. Antioxidant activity and phenolic compositions of Lentil (*Lens culinaris* var. *morton*) extract and its fractions. *J Agric Food Chem*. 2011;59(6):2268-2276.

12. Phosrithong N, Nuchtavorn N. Antioxidant and anti-inflammatory activites of *Clerodendrum* leaf extracts collected in Thailand. *Eur J Integr Med*. 2016;8(3):281-285.

13. Yıldırım A, Şen A, Doğan A, Bitis L. Antioxidant and anti-inflammatory activity of capitula, leaf and stem extracts of *Tanacetum cilicicum* (Boiss.) Grierson. *Int J Second Metab*. 2019;6(2):211-222.

14. Gao X, Ohlander M, Jeppsson N, Björk L, Trajkovski V. Changes in antioxidant effects and their relationship to phytonutrients in fruits of Sea buckthorn (*Hippophae rhamnoides* L.) during Maturation. *J Agric Food Chem*. 2000;48:1485-1490.

15. Aleksandrova K, Koelman L, Rodrigues CE. Dietary patterns and biomarkers of oxidative stress and inflammation: A systematic review of observational and intervention studies. *Redox Biol*. 2021;42:101869. doi:10.1016/j.redox.2021.101869

16. Hassan W, Noreen H, Rehman S, et al. Oxidative stress and antioxidant potential of one hundred medicinal plants. *Curr Top Med Chem*. 2017;17(12):1336-1370.

17. Krishnaiah D, Sarbatly R, Nithyanandam, R. A review of the antioxidant potential of medicinal plant species. *Food Bioprod Process*. 2011;89(3):217-233.

18. Oguntibeju OO. Medicinal plants with anti-inflammatory activities from selected countries and regions of Africa. *J Inflamm Res*. 2018;11:307-317.

19. Necip A, Durgun M. Antioxidant properties, total phenolic content and LC-MS/MS analysis of *Mentha pulegium, Lepidium draba* and *Centaurea solstitialis*. *J Inst Sci Technol*. 2022;12(4):2375-2385.

20. Sekerler T, Sen A, Bitis L, Sener A. Anticancer, antioxidant and anti-inflammatory activities of chloroform extracts from some *Centaurea* species. *MDPI-Proceedings*. 2018;2(25):1542. doi:10.3390/proceedings2251542

21. Alper M, Özay C, Güneş H, Mammadov R. Assessment of antioxidant and cytotoxic activities and identification of phenolic compounds of *Centaurea solstitialis* and *Urospermum picroides* from Turkey. *Braz Arch Biol Technol*. 2021;64:e21190530. doi:10.1590/1678-4324-2021190530

22. Akkol EK, Arif R, Ergun F, Yesilada E. Sesquiterpene lactones with antinociceptive and antipyretic activity from two *Centaurea* species. *J Ethnopharmacol*. 2009;122(2):210-215.

23. Croft KD. The chemistry and biological effects of flavonoids and phenolic acids. *Ann N Y Acad Sci*. 1998;854(1):435-442.

24. Rice-Evans CA, Miller NJ, Paganga G. Structure-antioxidant activity relationships of flavonoids and phenolic acids. *Free Radic Biol Med*. 1996;20(7):933-956.

25. Kumar N, Goel N. Phenolic acids: Natural versatile molecules with promising therapeutic applications. *Biotechnol Rep*. 2019;24:e00370. doi:10.1016/j.btre.2019.e00370

26. González R, Ballester I, López-Posadas R, et al. Effects of flavonoids and other polyphenols on inflammation. *Crit Rev Food Sci Nutr*. 2011;51(4):331-362.

27. Matos MS, Anastácio JD, Nunes dos Santos C. Sesquiterpene lactones: Promising natural compounds to fight inflammation. *Pharmaceutics*. 2021;13(7):991. doi:10.3390/pharmaceutics13070991

How to cite this article

Oxidative Stress and Cancer: Harnessing the Therapeutic Potential of Curcumin and Analogues Against Cancer

Christoffer Briggs Lambring[1], Liling Chen[1], Claire Nelson[2], Alyssa Stevens[2], Wynashia Bratcher[3], Riyaz Basha[1]

[1]University of North Texas Health Science Center, Fort Worth, Texas, USA
[2]Missouri Southern State University, Joplin, Missouri, USA
[3]Livingstone College, Salisbury, North Carolina, USA

ABSTRACT

Reactive oxygen species (ROS) are a class of bioactive molecules that are the by-products of many cellular functions. These molecules are present in normal cells at homeostatic levels but have been studied extensively in cancer due to their dysregulation resulting in pro- and anti-tumorigenic environments. Completely understanding the paradoxical nature of ROS in cancer is imperative to fully realize its modulation as cancer therapy. Studies into ROS have shown far-reaching effects in cancer, including how ROS levels regulate signaling, response to treatment, drug resistance, etc. Many drugs were studied with the hopes of regulating the ROS levels in cancer; however, patient response varied. Plant-derived medications offered new avenues of drug treatment over the last few decades, and the phytochemical Curcumin gained ground as an interesting cancer therapeutic. Curcumin is an active phenolic compound used in traditional medicine around the world. Although it suffers from a poor pharmacokinetic profile, Curcumin exerts anti-tumorigenic, as well as ROS-modulating activities. Analogs and derivatives of Curcumin are under development to improve upon its anti-cancer properties and enhance its bioavailability, currently a major limitation of its usage. This review highlights ROS function in cancer treatment focused on ROS, including Curcumin and its analogs.

Keywords: Oxidative Stress, Curcumin, Curcumin analogs, Cancer therapy, ROS-modulating drugs

INTRODUCTION

Reactive Oxygen Species

Reactive Oxygen Species (ROS) are chemically reactive species containing diatomic oxygen, including peroxides, superoxide, hydroxyl radicals, and singlet oxygen.[1] ROS is an over-arching term for derivatives of molecular oxygen that were originally thought to be purely by-products of metabolic activities, such as aerobic respiration, in cells. ROS can include radicals, molecules with an unpaired electron, such as superoxide and hydroxyl radicals, or non-radical molecules, like hydrogen peroxide and hypochlorite. ROS are thought to be tumor-suppressing agents since they are produced as a result of the administration of most chemotherapeutic drugs to activate cell death. However, in some cases they exert pro-tumorigenic functions.[2−4] ROS are generated at the plasma membrane level by nicotinamide adenine dinucleotide phosphate (NADPH) or at the mitochondrial level by nicotinamide adenine dinucleotide (NAD) dependent reactions. The evaluation of molecular interactions between certain ROS molecules and particular targets in redox signaling pathways is the focus of research, as their manipulation can result in a wide range of physiological effects. As a result, significant progress has been made in our understanding of how these oxidants affect physiology and disease, including the neurological, cardiovascular, and immunological systems, skeletal muscle, metabolism, aging, and cancer.[5] Using drugs to simply increase or decrease ROS levels has had mediocre results. More targeted approaches were developed, and ROS-modulating drugs are being investigated in many diseases, including cancer.

Generation of ROS

ROS levels are maintained in a healthy cell via various detoxifying processes controlled by antioxidant enzymes. As a result, ROS homeostasis is successfully regulated which helps maintain the redox balance in healthy cells. Numerous endogenous and exogenous biological functions produce ROS, which lead to over- or under-production in response to various stimuli,

and result in cellular responses ranging from normal signaling mechanisms to cell death and DNA damage (Figure 1). At the mitochondrial level, specifically the inner mitochondrial membrane, where most ROS are generated during oxidative phosphorylation, there are three major complexes that result in the bulk of ROS production. Complex I (CI) of the electron transport chain (ETC) generates ROS during electron transfer from NADH to Coenzyme Q (CoQ), while CII produces ROS through potential electron leakage. CIII can result in ROS through leaking of a single electron that moves freely through CIII, resulting in non-enzymatic ROS production.[6]

Due to the action of multiple antioxidant systems, which regulate ROS generation by altering metabolic and signaling pathways, normal cells can maintain oxidative equilibrium.[3] Antioxidant defense mechanisms encourage cell death when ROS levels are continually elevated.[7] However, oxidative stress causes harm to numerous molecules and cell structures, resulting in the emergence of pathological conditions like inflammation, aging, cancer, and neurological diseases. Further, ROS are strongly associated with carcinogenesis. To understand the mechanisms of tumor initiation and progression, as well as the development of treatments, it is crucial to summarize the most recent evidence on ROS biology.

Antioxidant Defense and Redox Homeostasis

Oxidative stress is generated when there is an imbalance between the production and elimination of ROS. As mentioned, low levels of ROS promote signal transduction to help the cancer cells proliferate, differentiate, migrate, and invade.[8−10] At high levels, however, ROS induces lipid peroxidation, DNA and RNA damage, protein backbone damage, and alteration of enzyme activity.[11] As such, it is vital for cell survival to prevent accumulation of ROS and maintain redox homeostasis. Various mechanisms, including hypoxia, metabolic defects, ER stress, and oncogenes affect basal levels of ROS.[5] Fortunately, there are several mechanisms by which cells deploy endogenous and exogenous antioxidants or free radical scavengers.[12]

Within many cells, activation of the transcription factor, nuclear factor erythroid 2-related factor 2 (NRF2), plays a pivotal role in regulating antioxidant functions.[3,7,13] Under resting conditions, NRF2 is bound to and constitutively degraded by Kelch-like ECH-associated protein 1 (KEAP1)-Cullin 3 (CUL2) E3 ligase complex. However, when cells experience oxidative stress, NRF2 dissociates from KEAP1 and translocates to the nucleus. In the nucleus, NRF2 binds to and activates the antioxidant response element (ARE) in various antioxidant target genes.[4,14,15] AREs are enhancer sequences found in the promoter region of genes encoding for various antioxidant enzymes. These antioxidants include superoxide dismutases (SODs), catalase (CAT), glutathione reductase, glutathione peroxidases (GPx), UDP-glycosyltransferases (UGTs), NADPH quinone oxidoreductase 1 (NQO1), heme oxyge-

nase (HMOX1), peroxiredoxins (PRx), thioredoxin (TRx), and thioredoxin reductase (TRxR).[16,17] SODs provide the first line of defense against free radicals through the conversion of O_2^- to H_2O_2. The H_2O_2 is neutralized to yield water and O_2 by CAT. Non-enzymatic molecules play a key role in ROS maintenance including glutathione, flavonoids, and vitamins C and E. Overall, the antioxidant defense of tumor cells play a major role in their ability to survive, as there is a delicate balance between the production and neutralization of ROS.

CANCER and ROS

Cancer is a disease in which the body's cells divide uncontrollably and spread throughout the body. Cancer remains one of the leading causes of death globally, second only to cardiovascular disease. Approximately 1,958,310 new cases and 609,829 deaths are projected to occur in the United States in 2023.[18] Numerous research studies and trials are conducted to better understand and develop new treatment for this deadly disease.

For decades, the activation of oncogenes and inactivation of tumor suppressor genes were thought to be the main cause of cancer development and progression– a phenomenon known as the 'oncogene addiction'.[19] However, recent studies emphasized the importance of the metabolic changes that cancer cells undergo, as these changes help to evade normal cellular limitations and aid in cancer cell proliferation.[20] Most notable is the increase in aerobic glycolysis, known as the Warburg effect. Cancer cells typically exhibit higher metabolic rates than normal cells, and the amount of ROS production is increased as a result.[7] This increase in ROS is countered by the cells' ability to upregulate their antioxidant mechanisms.[3] There is a delicate balance between the production and neutralization of ROS, resulting in a paradoxical effect on cancer cells. Previous research showed that at moderate to low levels, ROS promoted signal transduction to help the cancer cells proliferation, differentiation, migration, and invasion.[8,10,19] At high levels, however, ROS is detrimental to cancer cells survival due to DNA, lipid, and protein damage. Increased levels of ROS induced apoptosis in multiple myeloma and colorectal cancer cells in previous studies.[21,22] Therefore, inducing a high concentration of ROS in cancer cells provides a potential strategy for cancer therapy.

In the early stages of cancer, ROS has pro-oncogenic actions, and antioxidant levels are decreased. Increased ROS production due to elevated metabolic function leads to constitutive activation of various signaling pathways. PI3K/Akt/mTOR mediated survival signaling is commonly seen upon increases of ROS in cancer cells and results in tumor growth and progression.[23,24] ROS also contributes to tumor progression through action against proteins such as PTEN and PTP1B to downregulate apoptosis and inhibit anti-growth signaling.[25,26] However, high levels of ROS present in cancer cells is harmful to tumor progression and tumor cell viability. Abnormal
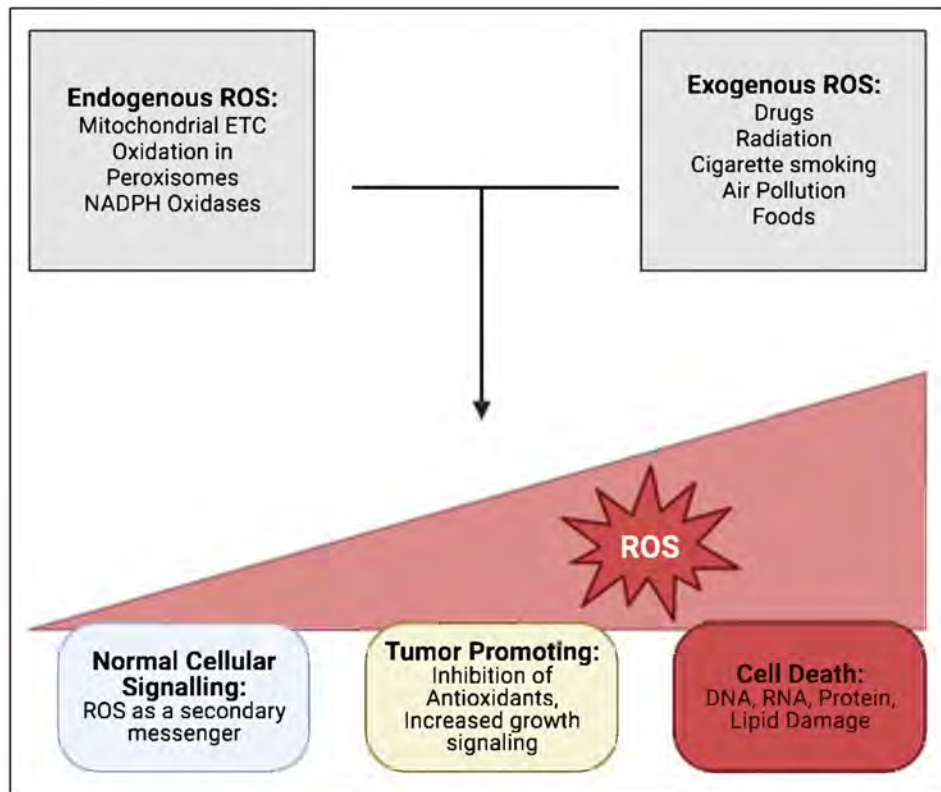
Figure 1. ROS sources and implication in cancer. There are multiple endogenous and exogenous sources of cancer. All can increase the amount of ROS contributing to the sliding scale of ROS-cancer interaction. This can lead to pro-tumorigenic environment under the right circumstances; however, high levels of ROS are toxic to normal and cancerous cells alike. Created in biorender.com.

levels of antioxidative enzymes are often found among cancer patients along with elevated levels of ROS and increased oxidative stress.[12,27] Lowering the amounts of ROS within cells through antioxidants is used to prevent the proliferation of cancer cells from occurring.[28] However, raising intracellular levels of ROS leaves cells with lower defenses and increases the chances of death caused by oxidative stress. Increasing levels of ROS may potentially result in cell death for cancer cells while saving normal cells. However, increasing ROS levels could lead to elevated mutational burden in cancer cells, warranting pro-tumorigenic effects.[28]

ROS and CANCER THERAPY

The sliding scale of ROS involvement in cancer makes ROS an interesting target of cancer therapies. New research suggested that instead of solely targeting oncogenes or tumor suppressor genes, the strengthened immune surveillance, aneuploidy, and increased metabolism in cancer cells that ensure survival should also be targeted. Manipulation of ROS pathways is a potential step to provide effective forms of cancer therapy.[29,30]

In the early stages of cancer, it is beneficial to maintain low ROS levels to reduce the survival of tumor-initiating cells (TICs) due to TICs' ability to survive in high levels of ROS

through an upregulation of antioxidant levels.[31] If high levels of ROS are present in the early stages of tumor development, then pre-neoplastic cells develop strong antioxidant mechanisms, allowing for the development of drug-resistant tumor cells.[30] Targeting these antioxidant mechanisms allow for cancer cell-specific therapies.

Oncogenes and tumor suppressor genes heavily impact the initiation and progression of tumorigenesis. Studies showed that oncogenes affect NRF2 regulation, and FOXO transcription factors enhanced oncogenic functions due to oncogenic factors like b-catenin.[5] Tumor suppressors were found to activate or suppress antioxidant gene expression.[5] For example, BRCA1 is a required regulator of NRF2 if an efficient antioxidant response is to be produced. But, ataxia telangiectasia mutate (ATM), another tumor suppressor gene that regulates ROS levels, is found to cause bone marrow failure in mice.[5] PKM2 functions as an oncogene and plays a significant role when ROS levels are high, leading to increased NADPH synthesis, allowing for solid tumors to detach from their matrix.[5,32]

ROS scavengers present a potential anticancer therapeutic strategy. Numerous studies have been conducted in which antioxidants, often Vitamin E, C, and selenium were implemented and found to have positive results, such as reduced mortality

rates. Another potential anti-cancer therapy focuses on increasing ROS by using drugs that target two of the three major antioxidant pathways. Currently, chemotherapy induces oxidative stress leading to cell death from potential excessive ROS levels in cancer cells. Platinum conjugated complexes and anthracyclines are also used to produce excess levels of ROS.[5] Arsenic trioxide and 2-methoxyestradiol showed positive results against different cancers through increased levels of ROS.[33,34] Another effective method for killing cancer cells is using an agent that increases oxidative stress and inhibits HSP90. Inhibiting the enzyme poly (ADP-ribose) polymerase (PARP) is effective in treating breast cancer, and ionizing radiation is found to dramatically increase ROS levels, especially through the activation of NADPH oxidase via radiation exposure.[5] Taking advantage of multiple aspects of ROS manipulation in cancer therapy has led to multiple treatments, including a variety that were successful in a clinical trial setting (Table 1).

ROS Therapy Clinical Trials

Vitamin C or ascorbic acid was involved in various clinical trials; however, the ongoing clinical trial NCT03418038 is observing deeper exploratory effects. Aside from safety and response rates, TET2MT allele, DNA methylation, and plasma cytokine activity are also being studied. Mangafodipir is a traditional MRI contrast agent, however it exhibits antioxidant properties through manganese superoxide dismutase mimetic activity.[35] Clinical trial NCT00727922 aimed to show Mangafodipir's neuroprotective properties in cancer patients who underwent oxaliplatin treatment. Mangafodipir showed significant results with 77% of patients treated with both oxaliplatin and Mangafodipir exhibiting improved or stabilized neuropathy.[36] A study that aimed to show the relationship between resectable colon cancer patients and Niclosamide treatment (NCT02687009) was opened for recruitment in 2016. The phase 1 study was canceled due to low recruitment, however recent evidence suggests Niclosamide, an effective Wnt signaling pathway regulator, as a candidate for colon cancer management as Wnt signaling is heavily upregulated in most patients.[37,38] Besides its' antioxidant properties, Quercetin exhibited the ability to regulate various cancer signaling pathways including PI3K/Akt/mTOR, MAPK/ERK, and Wnt signaling showing anti-metastatic, anti-angiogenic, and anti-proliferative potential.[39] Quercetin is part of clinical trial NCT04733534, an ongoing study aimed at improving the quality of life in adult survivors of childhood cancers. Improvement of frailty and markers observing senescence, inflammation, bone resorption, insulin resistance, and cognitive function are under study. Dimethyl Fumarate was studied in concert with Temozolomide and radiation therapy for patients with glioblastoma multiforme in clinical trial NCT02337426. A maximum tolerated dose was recommended at 240 mg three times daily, and patients saw varying degrees of progression-free survival with a median of 8.7 months and a median survival rate of 13.8 months was

noted.[40] Clinical trial NCT04566328 observed Bortezomib in combination with dexamethasone, daratumumab, and lenalidomide for patients with multiple myeloma. The study is still recruiting, and primary endpoints include overall survival with secondary endpoints aimed at adverse events, including neurotoxicity, recovery rate, and non-hematologic adverse events. Arsenic Trioxide is an interesting anti-cancer candidate that was tested with a variety of cancers for its ability to affect cancer stem-like cells, induce cell cycle arrest and apoptosis, chemo-sensitize, and decrease angiogenic potential.[41] Many clinical trials involving arsenic trioxide were undertaken, one recruiting trial (NCT04897490) evaluates first line arsenic trioxide and all trans retinoic acid treatment for patients with acute promyelocytic leukemia. Primary outcomes include evaluation of overall survival and event free survival with secondary measures observing molecular remission rate, toxicity, and FLT3 as a prognostic marker. Curcumin (Cur) is involved in a plethora of clinical trials (Table 1) touching on a wide range of cancers. Taking advantage of Cur's innate antioxidant and anti-cancer abilities clinical trials are observing improvements in recurrence-free survival in pancreatic cancer (NCT02064673), safety and tolerability in metastatic treatment-resistant colorectal cancer (NCT01490996), tumor-induced inflammation reduction in endometrial carcinoma (NCT02017353), and efficacy and bioavailability in glioblastoma (NCT01712542).[41] The mechanisms by which Cur affects this array of systems and cancers are discussed in detail below.

CURCUMIN in CANCER THERAPY

Phytochemicals are plant metabolites that possess innate antioxidant properties. Plant by-products offer a unique approach to cancer therapeutics, and multiple drugs like vincristine and paclitaxel are already used in various cancers.[42] There is a high demand for medicines from plant origins; most have relatively low toxicity levels toward normal cells and offer safer alternatives over traditional chemically derived drugs.[43]

Cur is a phytochemical derived from *Curcuma longa*. A commonly used spice originating from Asia, Cur received attention as an anti-cancer therapy. Cur has a history of use in medicines in Asian countries where it was used as an anti-inflammatory and anti-dysenteric, and has recently shown antioxidant properties in the context of various disease instances.[44,45] Cur has become a popular drug for cancer therapy over the last few decades and multiple analogs have arisen based on Cur structure. Mechanistically, Cur has shown the ability to regulate a plethora of molecular targets lending to its anti-cancer properties (Figure 2). The transcription factor NF-kB is one of the longest known targets of Cur and its suppression in a variety of cancers including leukemia and melanoma.[46,47] NF-kβ suppression from Cur interaction led to the identification of Cur's immunomodulatory effects on various cytokines and immune related proteins such as IL-6, TNF-α, and PD-L1 and is suggested as a potential adjuvant treatment for immunotherapy.[48-50] Regulation

Table 1. List of ROS modulating drugs in cancer treatment.

| ROS Modulating Drug	Cancer Type	Clinical Trial Phase	NCT Identifier
Vitamin C (Ascorbic Acid)	Relapsed/Refractory Lymphoma	Phase II – Ongoing	**NCT03418038**
Mangafodipir	Multiple, required mild oxaliplatin neuropathy	Phase II – Concluded	**NCT00727922**
Niclosamide	Resectable Colon Cancer	Phase I – Terminated	**NCT02687009**
Quercetin	Childhood Cancers	Phase II – Ongoing	**NCT04733534**
Curcumin	Endometrial Carcinoma, Glioblastoma, Prostate, Colorectal	Multiple Phases	**NCT02064673, NCT01490996, NCT02017353, NCT01712542**
Dimethyl Fumarate	Glioblastoma Multiforme	Phase I – Concluded	**NCT02337426**
Bortezomib	Multiple Myeloma	Phase III – Ongoing	**NCT04566328**
Arsenic Trioxide	Acute Promyelocytic Leukemia	Observational-Recruiting	**NCT04897490**
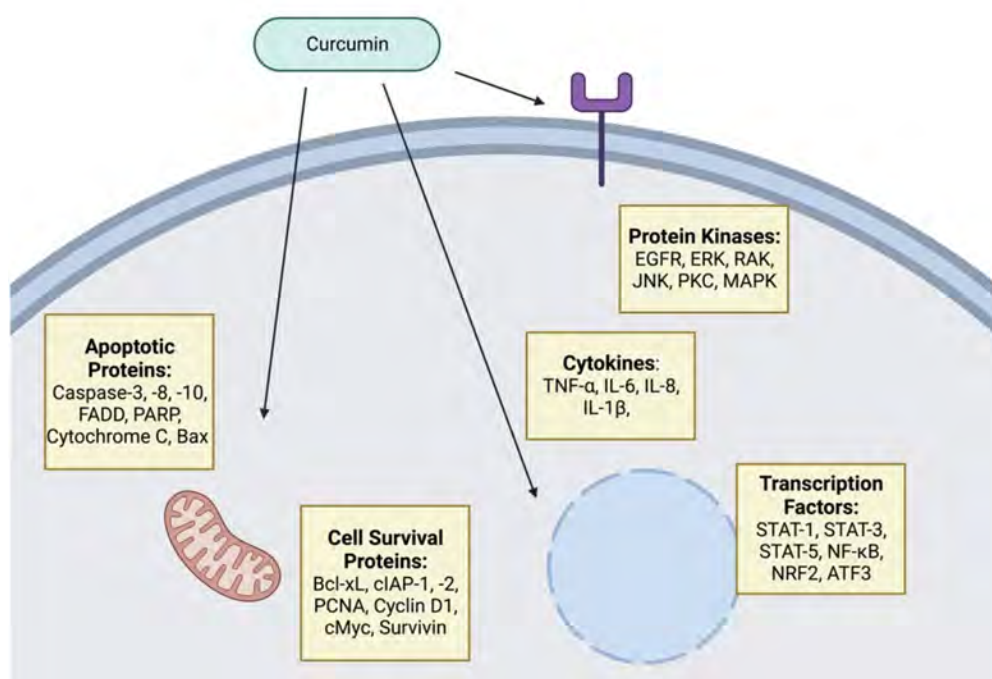
Figure 2. Curcumin molecular targets. EGFR- epidermal growth factor receptor, ERK- extracellular signal related kinases, JNK- c-Jun N-terminal kinase, PKC-protein kinase C, MAPK- mitogen-activated protein kinase, STAT- signal transducer and activator of transcription, NF-kB- nuclear factor-kappa-light-chain-enhancer of activated B cells, NRF2- nuclear factor erythroid 2-related factor 2, ATF3- activating transcription factor 3, Bcl-xL- B-cell lymphoma-extra-large, cIAP- cellular inhibitor of apoptosis protein, PCNA- proliferating cell nuclear antigen, TNF- tumor necrosis factor, IL- interleukin, FADD- FAS-associated death domain protein, PARP- Poly (ADP-ribose) polymerase. Created in biorender.com.

of several signaling pathways is evidence of the wide range of effects by Cur. PI3K/Akt, MAPK, and JAK/STAT regulation were noted in a variety of cancers with a long list of downstream target modulation occurring as a result of upstream Cur interference.[51]

The ROS interacting effects of Cur and its analogs were realized as important mechanisms in their ability to combat cancers. At a mechanistic level, multiple explanations are given for Cur and its capacity to perform ROS modulation. Both the keto-enol and phenolic group of Cur are thought to be the site responsible for radical scavenging, and other groups have suggested that hydrogen cleavage is the preferred ROS interaction mechanism of Cur.[52] In clinical trials, Cur is shown to increase total antioxidant capacity (TAC) and decrease malondialdehyde.[53] It also affects energy metabolism and increases overall ROS accumulation in SiHa cervical cancer cells resulting in increased autophagy and G2/M phase cell cycle arrest.[54] Cur targets multiple enzymes in ROS metabolic pathways. In leukemic cells, Cur showed an inhibition of CBR1/3, NQO1/2, PRDX1, and ADH1A some of which were also upregulated in patient leukemia samples.[55] Through induction of ROS in colorectal cancer cell lines Cur was able to activate KEAP1/NRF2/ARE pathways and serve as an effective therapeutic especially in combination with 5-FU.[56] Cur is an option for resensitization of chemo-resistant cancer cells. Against drug resistant MCF7/TH, A549/ADR, and HCT116R Cur modulated oxidative stress and increased apoptosis through multiple mechanisms including increases in SOD and CAT and an upregulation of SIRT1.[57]

Cur has the ability to overcome carboplatin resistance in triple negative breast cancer cell lines. Recently, Cur demonstrated its ability to overcome carboplatin resistance through increased ROS production leading to downregulation of RAD51 and an upregulation of γH2AX.[58] Wu et al. demonstrated that Cur had a similar result against chemo-resistant lung cancer cells. There was a drastic increase in apoptosis of A549/D16 cells due to ROS guided p38 MAPK phosphorylation.[59] This affect was exaggerated when used in combination with Docetaxel and Vincristine with little toxicity arising upon the Cur addition, suggesting that Cur has a role in enhancing chemotherapeutic effectiveness.[59]

Curcumin Derivatives and Cancer

Several Cur analogs can increase their antioxidant ability. The presence of Cu^{2+}, Pb^{2+}, and Fe^{2+} increased the chelating effect of Cur derivatives and O-methoxy substitution also exhibited increased antioxidant activity in comparison to regular Cur.[60,61] Pyridine and sulfone derivatives in prostate cancer, glucoside and heterocyclic Cur derivatives in breast cancer, and mono-carbonyl and various methoxy and hydroxy derivatives of Cur in colon cancer have increased its effectiveness when compared to Cur.[62] C7-curcuminoids, which have the same framework as Cur, and C5-curcuminoids, Cur derivatives

with a removed ethylene group, were found to be more effective than base Cur against K562 leukemic cells and resulted in ROS upregulation.[63] A novel Cur derivative, 1g, was effective against colon cancer cells. The administration of 1g resulted in ROS production, G1 cell cycle phase arrest, and increased ER-stress which was reversed upon addition of NAC, an ROS scavenging agent.[64] Recently, Liu et al. demonstrated the effectiveness of a series of Cur analogs and showed the effectiveness of a mono-carbonyl analog. Non-small cell lung cancer cell lines showed marked increases in apoptosis and ferroptosis driven by the analogs ability to generate ROS through TrxR inhibition.[65] The analog WZ26 increased ROS and cell death in cholangiocarcinoma via STAT3 inhibition and L48H37 was found to have similar results and induced ER-stress in human lung cancer cells.[66,67] An allylated mono-carbonyl Cur analog (CA6) showed effectiveness against gastric cancer cells through TrxR1 inhibition and ROS-dependent apoptotic death.[68] Another Cur analog, WZ37, induced ROS-dependent ER stress and mitochondrial injury, resulting in an increase in cell death and G2/M phase cell cycle arrest along with decreased Akt/mTOR phosphorylation and an upregulation of BAD and PTEN in head and neck squamous cell carcinoma.[69] Continued development of Cur derivatives will hopefully lead to not only increased targeting of tumorigenic factors such as ROS, but also continued improvement over base Cur formulations.

Multiple limitations surround Cur and its analogs usage including poor bioavailability and cellular uptake which decrease the therapeutic potential of the compound. Studies with doses as high as 12 g/day still resulted in small amounts of traceable plasma Cur, mostly due to low absorption in the small intestine and rapid elimination in the body via the gall bladder.[70−72] Efforts to improve the pharmacokinetic profile of Cur involve nanoparticle formulation and increased analog development. Cur nanoparticles not only increase its ability to attack many of its targets mentioned above, but also show increased antioxidant potential and exhibit improved distribution and absorption by target cells.[73−75]

CONCLUSION

The paradoxical nature of ROS made for a difficult target in the hope for its use in cancer therapy. Relying solely on decreasing or increasing ROS in either direction is still a questionable approach for treatment. However, taking advantage of the antioxidant abilities of drugs shows some promise in terms of its inclusion in treatment regimens. Natural compounds like Cur are especially advantageous in this aspect due to their low toxicity towards healthy cells. Its natural antioxidant ability including its targeting of various protein kinases, transcription factors, and growth factors makes Cur an attractive alternative despite its pharmacokinetic limitations. Further studies into Cur's mechanistic abilities to alter ROS and change antioxidant potential, chemical analogs, and nanoparticle formulation will

improve the chances for successful Cur adaptation into cancer treatments.

Utilizing antioxidants in cancer therapy is a delicate balance and the research is still evolving. Since antioxidant activity can protect cancer cells, novel approaches such as modulation of oxidative stress for the implications in therapeutic application is challenging. Rigorous preclinical and clinical studies are essential to ensure safety and efficacy. Clinical testing utilizing antioxidant mechanisms for cancer therapy is ongoing. New discoveries and clinical trials can provide more insights and potential strategies beyond what is currently known.

ORCID IDs of the authors

Christoffer Briggs Lambring	0009-0003-2921-5021
Liling Chen	0009-0006-0191-1887
Claire Nelson	0009-0008-9256-4634
Alyssa Stevens	0009-0005-6799-0090
Wynashia Bratcher	0009-0004-2385-6685
Riyaz Basha	0000-0002-4071-0993

REFERENCES

1. Sahoo BM, Banik BK, Borah P, Jain A. Reactive oxygen species (ROS): Key components in cancer therapies. *Anticancer Agents Med Chem*. 2022;22(2):215-222.

2. Reczek CR, Chandel NS. ROS Promotes cancer cell survival through calcium signaling. *Cancer Cell*. 2018;33(6):949-951.

3. Schafer ZT, Grassian AR, Song L, et al. Antioxidant and oncogene rescue of metabolic defects caused by loss of matrix attachment. *Nature*. 2009;461(7260):109-113.

4. Weinberg F, Ramnath N, Nagrath D. Reactive oxygen species in the tumor microenvironment: An overview. *Cancers (Basel)*. 2019;11(8). doi:10.3390/cancers11081191

5. Gorrini C, Harris IS, Mak TW. Modulation of oxidative stress as an anticancer strategy. *Nat Rev Drug Discov*. 2013;12(12):931-947.

6. Zhao RZ, Jiang S, Zhang L, Yu ZB. Mitochondrial electron transport chain, ROS generation and uncoupling (Review). *Int J Mol Med*. 2019;44(1):3-15.

7. Perillo B, Di Donato M, Pezone A, et al. ROS in cancer therapy: The bright side of the moon. *Exp Mol Med*. 2020;52(2):192-203.

8. Sena LA, Chandel NS. Physiological roles of mitochondrial reactive oxygen species. *Mol Cell*. 2012;48(2):158-167.

9. Wiseman H, Halliwell B. Damage to DNA by reactive oxygen and nitrogen species: Role in inflammatory disease and progression to cancer. *Biochem J*. 1996;313 (Pt 1)(Pt 1):17-29.

10. Okon IS, Zou MH. Mitochondrial ROS and cancer drug resistance: Implications for therapy. *Pharmacol Res*. 2015;100:170-174.

11. Nakamura H, Takada K. Reactive oxygen species in cancer: Current findings and future directions. *Cancer Sci*. 2021;112(10):3945-3952.

12. Jelic MD, Mandic AD, Maricic SM, Srdjenovic BU. Oxidative stress and its role in cancer. *J Cancer Res Ther*. 2021;17(1):22-28.

13. Ishimoto T, Nagano O, Yae T, et al. CD44 variant regulates redox status in cancer cells by stabilizing the xCT subunit of system xc(-) and thereby promotes tumor growth. *Cancer Cell*. 2011;19(3):387-400.

14. Taguchi K, Motohashi H, Yamamoto M. Molecular mechanisms of the Keap1-Nrf2 pathway in stress response and cancer evolution. *Genes Cells*. 2011;16(2):123-140.

15. Kansanen E, Kuosmanen SM, Leinonen H, Levonen AL. The Keap1-Nrf2 pathway: Mechanisms of activation and dysregulation in cancer. *Redox Biol*. 2013;1(1):45-49.

16. Ma Q. Role of nrf2 in oxidative stress and toxicity. *Annu Rev Pharmacol Toxicol*. 2013;53:401-426.

17. Li W, Kong AN. Molecular mechanisms of Nrf2-mediated antioxidant response. *Mol Carcinog*. 2009;48(2):91-104.

18. Siegel RL, Miller KD, Wagle NS, Jemal A. Cancer statistics, 2023. *CA Cancer J Clin*. 2023;73(1):17-48.

19. Weinstein IB, Joe A. Oncogene addiction. *Cancer Res*. 2008;68(9):3077-3080. doi:10.1158/0008-5472.CAN-07-3293

20. Hanahan D, Weinberg RA. Hallmarks of cancer: The next generation. *Cell*. 2011;144(5):646-674. doi:10.1016/j.cell.2011.02.013

21. Arihara Y, Takada K, Kamihara Y, et al. Small molecule CP-31398 induces reactive oxygen species-dependent apoptosis in human multiple myeloma. *Oncotarget*. 2017;8(39):65889-65899.

22. Nakamura H, Takada K, Arihara Y, et al. Six-transmembrane epithelial antigen of the prostate 1 protects against increased oxidative stress via a nuclear erythroid 2-related factor pathway in colorectal cancer. *Cancer Gene Ther*. 2019;26(9-10):313-322.

23. Shiau JP, Chuang YT, Cheng YB, et al. Impacts of oxidative stress and PI3K/AKT/mTOR on metabolism and the future direction of investigating fucoidan-modulated metabolism. *Antioxidants (Basel)*. 2022;11(5). doi:10.3390/antiox11050911

24. Wen C, Wang H, Wu X, et al. ROS-mediated inactivation of the PI3K/AKT pathway is involved in the antigastric cancer effects of thioredoxin reductase-1 inhibitor chaetocin. *Cell Death Dis*. 2019;10(11):809. doi:10.1038/s41419-019-2035-x

25. Wang Y, Qi H, Liu Y, et al. The double-edged roles of ROS in cancer prevention and therapy. *Theranostics*. 2021;11(10):4839-4857.

26. Assi M. The differential role of reactive oxygen species in early and late stages of cancer. *Am J Physiol Regul Integr Comp Physiol*. 2017;313(6):R646-R653.

27. Zalewska-Ziob M, Adamek B, Kasperczyk J, et al. Activity of antioxidant enzymes in the tumor and adjacent noncancerous tissues of non-small-cell lung cancer. *Oxid Med Cell Longev*. 2019;2901840. doi:10.1155/2019/2901840

28. Reczek CR CN. The two faces of reactive oxygen species in cancer. *Annu Rev Cancer Biol*. 2017;1:79-98.

29. Luo J, Solimini NL, Elledge SJ. Principles of cancer therapy: Oncogene and non-oncogene addiction. *Cell*. 2009;136(5):823-837.

30. Li Y, Zhang X, Wang Z, Li B, Zhu H. Modulation of redox homeostasis: A strategy to overcome cancer drug resistance. *Front Pharmacol*. 2023;14:1156538. doi:10.3389/fphar.2023.1156538

31. Aggarwal V, Tuli HS, Varol A, et al. Role of reactive oxygen species in cancer progression: Molecular mechanisms and recent advancements. *Biomolecules*. 2019;9(11). doi:10.3390/biom9110735

32. Yu G, Sun W, Shen Y, et al. PKM2 functions as a potential oncogene and is a crucial target of miR-148a and miR-326 in thyroid tumorigenesis. *Am J Transl Res*. 2018;10(6):1793-1801.

33. Huang W, Zeng YC. A candidate for lung cancer treatment: arsenic trioxide. *Clin Transl Oncol*. 2019;21(9):1115-1126.

34. Massaro RR, Faiao-Flores F, Rebecca VW, et al. Inhibition of proliferation and invasion in 2D and 3D models by 2-methoxyestradiol in human melanoma cells. *Pharmacol Res*. 2017;119:242-250.

35. Karlsson JO, Kurz T, Flechsig S, Nasstrom J, Andersson RG. Superior therapeutic index of calmangafodipir in comparison to mangafodipir as a chemotherapy adjunct. *Transl Oncol*. 2012;5(6):492-502.

36. Coriat R, Alexandre J, Nicco C, et al. Treatment of oxaliplatin-induced peripheral neuropathy by intravenous mangafodipir. *J Clin Invest*. 2014;124(1):262-272.

37. Wang J, Ren XR, Piao H, et al. Niclosamide-induced Wnt signaling inhibition in colorectal cancer is mediated by autophagy. *Biochem J*. 2019;476(3):535-546.

38. Disoma C, Zhou Y, Li S, Peng J, Xia Z. Wnt/beta-catenin signaling in colorectal cancer: Is therapeutic targeting even possible? *Biochimie*. 2022;195:39-53.

39. Lotfi N, Yousefi Z, Golabi M, et al. The potential anti-cancer effects of quercetin on blood, prostate and lung cancers: An update. *Front Immunol*. 2023;14:1077531. doi:10.3389/fimmu.2023.1077531

40. Shafer D, Tombes MB, Shrader E, et al. Phase I trial of dimethyl fumarate, temozolomide, and radiation therapy in glioblastoma. *Neurooncol Adv*. 2020;2(1):vdz052. doi:10.1093/noajnl/vdz052

41. Howells LM, Iwuji COO, Irving GRB, et al. Curcumin combined with FOLFOX chemotherapy is safe and tolerable in patients with metastatic colorectal cancer in a randomized phase IIa trial. *J Nutr*. 2019;149(7):1133-1139.

42. Talib WH, Alsalahat I, Daoud S, Abutayeh RF, Mahmod AI. Plant-derived natural products in cancer research: extraction, mechanism of action, and drug formulation. *Molecules*. 2020;25(22). doi:10.3390/molecules25225319

43. Hashem S, Ali TA, Akhtar S, et al. Targeting cancer signaling pathways by natural products: Exploring promising anti-cancer agents. *Biomed Pharmacother*. 2022;150:113054. doi:10.1016/j.biopha.2022.113054

44. Hatcher H, Planalp R, Cho J, Torti FM, Torti SV. Curcumin: From ancient medicine to current clinical trials. *Cell Mol Life Sci*. 2008;65(11):1631-1652.

45. Choudhari AS, Mandave PC, Deshpande M, Ranjekar P, Prakash O. Phytochemicals in cancer treatment: From preclinical studies to clinical practice. *Front Pharmacol*. 2019;10:1614. doi:10.3389/fphar.2019.01614

46. Singh S, Aggarwal BB. Activation of transcription factor NF-kappa B is suppressed by curcumin (diferuloylmethane). *J Biol Chem*. 1995;270(42):24995-5000.

47. Marin YE, Wall BA, Wang S, et al. Curcumin downregulates the constitutive activity of NF-kappaB and induces apoptosis in novel mouse melanoma cells. *Melanoma Res*. 2007;17(5):274-283.

48. Paul S, Sa G. Curcumin as an adjuvant to cancer immunotherapy. *Front Oncol*. 2021;11:675923. doi:10.3389/fonc.2021.675923

49. Kim GY, Kim KH, Lee SH, et al. Curcumin inhibits immunostimulatory function of dendritic cells: MAPKs and translocation of NF-kappa B as potential targets. *J Immunol*. 2005;174(12):8116-8124.

50. Giordano A, Tommonaro G. Curcumin and cancer. *Nutrients*. 2019;11(10). doi:10.3390/nu11102376

51. Wang H, Zhang K, Liu J, et al. Curcumin regulates cancer progression: Focus on ncRNAs and molecular signaling pathways. *Front Oncol*. 2021;11:660712. doi:10.3389/fonc.2021.660712

52. Sadatsharifi M, Purgel M. Radical scavenger competition of alizarin and curcumin: A mechanistic DFT study on antioxidant activity. *J Mol Model*. 2021;27(6):166. doi:10.1007/s00894-021-04778-1

53. Jakubczyk K, Druzga A, Katarzyna J, Skonieczna-Zydecka K. Antioxidant Potential of curcumin-a meta-analysis of randomized clinical trials. *Antioxidants (Basel)*. 2020;9(11). doi:10.3390/antiox9111092

54. Wang T, Wu X, Al Rudaisat M, Song Y, Cheng H. Curcumin induces G2/M arrest and triggers autophagy, ROS generation and cell senescence in cervical cancer cells. *J Cancer*. 2020;11(22):6704-6715.

55. Larasati YA, Yoneda-Kato N, Nakamae I, Yokoyama T, Meiyanto E, Kato JY. Curcumin targets multiple enzymes involved in the ROS metabolic pathway to suppress tumor cell growth. *Sci Rep*. 2018;8(1):2039. doi:10.1038/s41598-018-20179-6

56. Liu C, Rokavec M, Huang Z, Hermeking H. Curcumin activates a ROS/KEAP1/NRF2/miR-34a/b/c cascade to suppress colorectal cancer metastasis. *Cell Death Differ*. 2023;30(7):1771-1785.

57. Gabr SA, Elsaed WM, Eladl MA, et al. Curcumin modulates oxidative stress, fibrosis, and apoptosis in drug-resistant cancer cell lines. *Life (Basel)*. 2022;12(9). doi:10.3390/life12091427

58. Wang G, Duan P, Wei Z, Liu F. Curcumin sensitizes carboplatin treatment in triple negative breast cancer through reactive oxygen species induced DNA repair pathway. *Mol Biol Rep*. 2022;49(4):3259-3270.

59. Wu MF, Huang YH, Chiu LY, Cherng SH, Sheu GT, Yang TY. Curcumin induces apoptosis of chemoresistant lung cancer cells via ROS-Regulated p38 MAPK phosphorylation. *Int J Mol Sci*. 2022;23(15). doi:10.3390/ijms23158248

60. Dairam A, Limson JL, Watkins GM, Antunes E, Daya S. Curcuminoids, curcumin, and demethoxycurcumin reduce lead-induced memory deficits in male Wistar rats. *J Agric Food Chem*. 2007;55(3):1039-1044.

61. Ravindran J, Subbaraju GV, Ramani MV, Sung B, Aggarwal BB. Bisdemethylcurcumin and structurally related hispolon analogues of curcumin exhibit enhanced prooxidant, anti-proliferative and anti-inflammatory activities *in vitro*. *Biochem Pharmacol*. 2010;79(11):1658-1666.

62. Mbese Z, Khwaza V, Aderibigbe BA. Curcumin and its derivatives as potential therapeutic agents in prostate, colon and breast cancers. *Molecules*. 2019;24(23). doi:10.3390/molecules24234386

63. Nakamae I, Morimoto T, Shima H, et al. Curcumin derivatives verify the essentiality of ROS upregulation in tumor suppression.

Molecules. 2019;24(22). doi:10.3390/molecules24224067

64. Wang H, Xu Y, Sun J, Sui Z. The novel curcumin derivative 1g induces mitochondrial and ER-stress-dependent apoptosis in colon cancer cells by induction of ROS production. *Front Oncol.* 2021;11:644197. doi:10.3389/fonc.2021.644197

65. Liu X, Cui H, Li M, et al. Tumor killing by a dietary curcumin mono-carbonyl analog that works as a selective ROS generator via TrxR inhibition. *Eur J Med Chem.* 2023;250:115191. doi:10.1016/j.ejmech.2023.115191

66. Chen M, Qian C, Jin B, et al. Curcumin analog WZ26 induces ROS and cell death via inhibition of STAT3 in cholangiocarcinoma. *Cancer Biol Ther.* 2023;24(1):2162807. doi:10.1080/15384047.2022.2162807

67. Feng C, Xia Y, Zou P, et al. Curcumin analog L48H37 induces apoptosis through ROS-mediated endoplasmic reticulum stress and STAT3 pathways in human lung cancer cells. *Mol Carcinog.* 2017;56(7):1765-1777.

68. Rajamanickam V, Yan T, Wu L, et al. Allylated curcumin analog CA6 inhibits TrxR1 and leads to ROS-dependent apoptotic cell death in gastric cancer through Akt-FoxO3a. *Cancer Manag Res.* 2020;12:247-263.

69. Zhang Z, Lin R, Liu Z, et al. Curcumin analog, WZ37, promotes G2/M arrest and apoptosis of HNSCC cells through Akt/mTOR inhibition. *Toxicol In Vitro.* 2020;65:104754. doi:10.1016/j.tiv.2019.104754

70. Anand P, Kunnumakkara AB, Newman RA, Aggarwal BB. Bioavailability of curcumin: Problems and promises. *Mol Pharm.* 2007;4(6):807-818.

71. Heger M, van Golen RF, Broekgaarden M, Michel MC. The molecular basis for the pharmacokinetics and pharmacodynamics of curcumin and its metabolites in relation to cancer. *Pharmacol Rev*. 2014;66(1):222-307.

72. Lao CD, Ruffin MTt, Normolle D, et al. Dose escalation of a curcuminoid formulation. *BMC Complement Altern Med*. 2006;6:10. doi:10.1186/1472-6882-6-10

73. Sandhiutami NMD, Arozal W, Louisa M, Rahmat D, Wuyung PE. Curcumin nanoparticle enhances the anticancer effect of cisplatin by inhibiting PI3K/AKT and JAK/STAT3 pathway in rat ovarian carcinoma induced by DMBA. *Front Pharmacol.* 2020;11:603235. doi:10.3389/fphar.2020.603235

74. Adahoun MA, Al-Akhras MH, Jaafar MS, Bououdina M. Enhanced anti-cancer and antimicrobial activities of curcumin nanoparticles. *Artif Cells Nanomed Biotechnol*. 2017;45(1):98-107.

75. Basniwal RK, Khosla R, Jain N. Improving the anticancer activity of curcumin using nanocurcumin dispersion in water. *Nutr Cancer.* 2014;66(6):1015-1022.

How cite this article

Correction Notes

Due to a technical error in the layout process, it has been discovered that the informed consent statement was inadvertently added to the end of some articles. The consent statement has been removed from the articles below.

VOLUME 82, ISSUE 1, 2023

Karakaya-Cimen FB, Macit C, Goksun Sivas G, Tunali Akbay T, Sener G, Ercan F. Morphological and Biochemical Investigation of the Protective Effects of *Panax ginseng* on Methotrexate-Induced Testicular Damage. Eur J Biol 2023;82(1):31-37.DOI: 10.26650/EurJBiol.2023.1271825

Kanbur E, Seker S, Budak F, Yerlikaya A. The Senescence Program is Reduced in Proteasome Inhibitor Bortezomib-Resistant PC3 Prostate Cancer Cell Line. Eur J Biol 2023;82(1):49-58. DOI: 10.26650/EurJBiol.2023.11240253

VOLUME 81, ISSUE 2, 2022

Kanpalta Mustafaoglu F, Ertas B, Sen A, Akakin D, Sener G, Ercan F. *Myrtus communis* L. Extract Ameliorates High Fat Diet Induced Kidney and Bladder Damage by Inhibiting Oxidative Stress and Inflammation. Eur J Biol 2022; 81(2): 217-230. DOI: 10.26650/EurJBiol.2022.1111191

Acikel Elmas M, Ozgun G, Bingol Ozakpinar O, Guleken Z, Arbak S. Effects of Apocynin against Monosodium Glutamate-Induced Oxidative Damage in Rat Kidney. Eur J Biol 2022; 81(2): 231-239. DOI: 10.26650/EurJBiol.2022.1148934

Dalbayrak B, Dogukan Metiner M. Personalized Medicine: A Solution for Today and Tomorrow. Eur J Biol 2022; 81(2): 267-273. DOI: 10.26650/EurJBiol.2022.1110344

VOLUME 81, ISSUE 1, 2022

Kayabas A, Yildirim E. Chemical Profiling and Wetting Behaviors of Endemic *Salvia absconditiflora* Greuter & Burdet (Lamiaceae) Collected from Gypsum Areas. Eur J Biol 2022; 81(1): 1-10. DOI: 10.26650/EurJBiol.2021.1011530

Vidya P, Sebastian CD. Yeast Diversity in the Mangrove Sediments of North Kerala, India. Eur J Biol 2022; 81(1): 50-57. DOI: 10.26650/EurJBiol.2022.1027475

Corresponding Author: Author name **E-mail:** Author email

21 December 2023